WASTE WATER - TREATMENT AND REUTILIZATION

Edited by **Fernando S. García Einschlag**

Waste Water - Treatment and Reutilization
Edited by Fernando S. García Einschlag

Contents

Preface

The steady increase in industrialization, urbanization and enormous population growth are leading to production of huge quantities of wastewaters that may frequently cause environmental hazards. Raw or treated waste water is very often discharged to freshwaters and results in changing ecological performance and biological diversity of these systems. About 70% of water supplied ends up as wastewater and several natural water reservoirs are being contaminated by untreated sewage/industrial effluents. This makes waste water treatment and waste water reduction very important issues.

The problem of water pollution is very complex. The major sources of wastewater can be classified as municipal, industrial and agricultural. Therefore, effluents may have high contents of harmful organic compounds, heavy metals and biohazards that may have serious health implications. Thus, according to the nature of the waste water, different treatment strategies should be used. Available techniques are used to reduce the amount of effluents as well as the impact on the environment, but threats on the ecosystem continue and fresh water resources are limited. Although wastewater treatments have reduced contamination and improved the quality of rivers, the generated waste product or sludge remains difficult to eliminate and poses serious safety and quality aspects of environmental concern.

The reuse of municipal wastewater for land irrigation constitutes a practical method of disposal which is expected to decisively contribute to the handling and minimization of environmental problems arising from the disposal of wastewater effluents on land and into aquatic systems. Water reuse is of vital importance, mostly in water scarce regions, hence, marginal-quality water will become and increasingly important component of agricultural water supplies. In addition, many waste waters contain relatively high concentrations substances with commercially important applications, thus, such waste waters may be used as potential sources of added-value molecules.

The book offers an interdisciplinary collection of studies and findings concerning waste water treatment, minimization and reuse. An attempt has been made through this book to provide a gist of current, relevant and comprehensive information on various aspects of waste water treatment technologies and waste water reutilization strategies. The book chapters were invited by the publisher and the authors are responsible for their statements. The accuracy of each chapter was checked by the authors through proof reading stages. Most of the chapters are based upon the ongoing research in the field. The book, which covers a wide spectrum of topics about waste water treatment technologies and waste water minimization strategies, is grouped in

three different sections. The first section are related to bioremediation methods for waste water, the second section is focused on physicochemical methods for waste water treatment and the last section covers different issues concerning waste water reuse and minimization.

We hope that this book will be helpful for graduate students, environmental professionals and researchers. I especially appreciate the support and encouragement from Prof. Katarina Lovrecic throughout the whole publishing process and I would also like to thank the authors for their contributions to the book.

Fernando García Einschlag
La Plata University
Argentina

Part 1

Bioremediation of Waste Water

Anaerobic Treatment of Industrial Effluents: An Overview of Applications

Mustafa Evren Ersahin, Hale Ozgun,
Recep Kaan Dereli and Izzet Ozturk
Istanbul Technical University,
Turkey

1. Introduction

Anaerobic treatment is an energy generating process, in contrast to aerobic systems that generally demand a high energy input for aeration purposes. It is a technically simple and relatively inexpensive technology which consumes less energy, space and produces less excess sludge in comparison to the conventional aerobic treatment technologies. Net energy production from biogas makes the anaerobic treatment technology an attractive option over other treatment methods.

Increasing industrialization trend in the worldwide has resulted in the generation of industrial effluents in large quantities with high organic content, which if treated appropriately, can result in a significant source of energy. Anaerobic digestion seems to be the most suitable option for the treatment of high strength organic effluents. Anaerobic technology has improved significantly in the last few decades with the applications of differently configured high rate treatment processes, especially for the treatment of industrial wastewaters. High organic loading rates can be achieved at smaller footprints by using high rate anaerobic reactors for the treatment of industrial effluents.

This chapter intends to bring together the knowledge obtained from different applications of the anaerobic technology for treatment of various types of industrial wastewaters. The first part of the chapter covers brief essential information on the fundamentals of anaerobic technology. The remainder of this chapter focuses on various anaerobic reactor configurations and operating conditions used for the treatment applications of different industrial wastewaters. Examples of applications that reflect the state-of-the-art in the treatment of industrial effluents by high rate anaerobic reactors are also provided.

2. Fundamentals of anaerobic digestion

Anaerobic digestion is a complex multistep process in terms of chemistry and microbiology. Organic material is degraded to basic constituents, finally to methane gas under the absence of an electron acceptor such as oxygen. The basic metabolic pathway of anaerobic digestion is shown in Fig. 1. To achieve this pathway, presence of very different and closely dependent microbial populations is required.
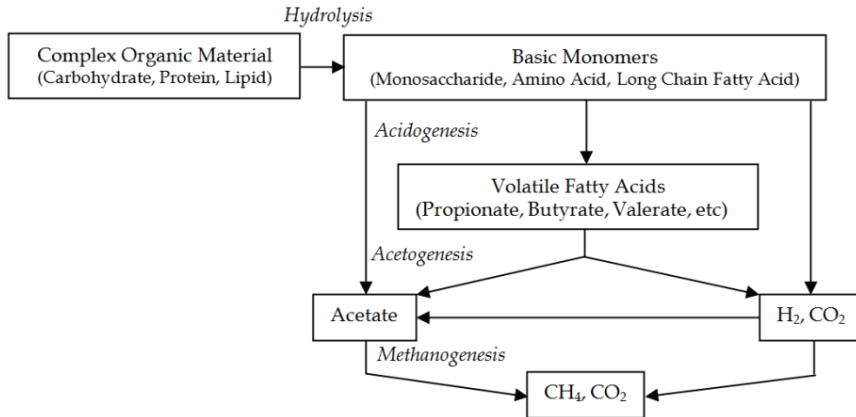
Fig. 1. Steps of anaerobic digestion process

The first step of the anaerobic degradation is the hydrolysis of complex organic material to its basic monomers by the hydrolytic enzymes. The simpler organics are then fermented to organic acids and hydrogen by the fermenting bacteria (acidogens). The volatile organic acids are transformed into acetate and hydrogen by the acetogenic bacteria. Archael methanogens use hydrogen and acetic acid produced by obligate hydrogen producing acetogens to convert them into methane. Methane production from acetic acid and from hydrogen and carbon dioxide is carried out by acetoclastic methanogens and hydrogenotrophic methanogens, respectively. Thermodynamic conditions play a key role in methane formation. Therefore, appropriate environmental conditions should be provided in order to carry out acetogenesis and methanogenesis, simultaneously (Rittmann & McCarty, 2001).

3. Reactor types

Many reactor configurations are used for the anaerobic treatment of industrial wastes and wastewaters. Among them, the most common types are discussed here and illustrated in Fig. 2.

3.1 Completely mixed anaerobic digester

The completely mixed anaerobic digester is the basic anaerobic treatment system with an equal hydraulic retention time (HRT) and solids retention time (SRT) in the range of 15-40 days in order to provide sufficient retention time for both operation and process stability. Completely mixed anaerobic digesters without recycle are more suitable for wastes with high solids concentrations (Tchobanoglous et al., 2003). A disadvantage of this system is that a high volumetric loading rate is only obtained with quite concentrated waste streams with a biodegradable chemical oxygen demand (COD) content between 8000 and 50000 mg/L. However, many waste streams are much dilute (Rittmann & McCarty, 2001). Thus, COD loading per unit volume may be very low with the detention times of this system which eliminates the cost advantage of anaerobic treatment technology. Typical organic loading rate (OLR) for completely mixed anaerobic digester is between 1-5 kg COD/m^3.day (Tchobanoglous et al., 2003).

3.2 Upflow anaerobic sludge blanket reactor

One of the most notable developments in anaerobic treatment process technology is the upflow anaerobic sludge blanket (UASB) reactor invented by Lettinga and his co-workers (Lettinga et al., 1980) with its wide applications in relatively dilute municipal wastewater treatment and over 500 installations in a wide range of industrial wastewater treatment including food-processing, paper and chemical industries (Tchobanoglous et al., 2003). Influent flow distributed at the bottom of the UASB reactor travels in an upflow mode through the sludge blanket and passes out around the edges of a funnel which provides a greater area for the effluent with the reduction in the upflow velocity, enhancement in the solids retention in the reactor and efficiency in the solids separation from the outward flowing wastewater. Granules which naturally form after several weeks of the reactor operation consist primarily of a dense mixed population of bacteria that is responsible for the overall methane fermentation of substrates (Rittmann & McCarty, 2001). Good settleability, low retention times, elimination of the packing material cost, high biomass concentrations (30000-80000 mg/L), excellent solids/liquid separation and operation at very high loading rates can be achieved by UASB systems (Speece, 1996). The only limitation of this process is related to the wastewaters having high solid content which prevents the dense granular sludge development (Tchobanoglous et al., 2003). Design OLR is typically in the range of 4 to 15 kg COD/m^3.day (Rittmann & McCarty, 2001).

3.3 Fluidized and expanded bed reactors

The anaerobic fluidized bed (AFB) reactor comprises small media, such as sand or granular activated carbon, to which bacteria attach. Good mass transfer resulting from the high flow rate around the particles, less clogging and short-circuiting due to the large pore spaces formed through bed expansion and high specific surface area of the carriers due to their small size make fluidized bed reactors highly efficient. However, difficulty in developing strongly attached biofilm containing the correct blend of methanogens, detachment risks of microorganisms, negative effects of the dilution near the inlet as a result of high recycle rate and high energy costs due to the high recycle rate are the main drawbacks of this system. The expanded granular sludge bed (EGSB) reactor is a modification of the AFB reactor with a difference in the fluid's upward flow velocity. The upflow velocity is not as high as in the fluidized bed which results in partial bed fluidization. (Rittmann & McCarty, 2001). OLR of 10-50 kg COD/m^3.day can be applied in AFB reactors (Ozturk, 2007) .

3.4 Anaerobic filters

The anaerobic filter (AF) has been widely applied in the beverage, food-processing, pharmaceutical and chemical industries due to its high capability of biosolids retention. In fact clogging by biosolids, influent suspended solids, and precipitated minerals is the main problem for this system. Applications of both upflow and downflow packed bed processes can be observed. Prevention of methanogens found at the lower levels of the reactor from the toxicity of hydrogen sulfide by stripping sulfide in the upper part of the column and solids removal from the top by gas recirculation can easily be achieved in downflow systems in comparison to upflow systems. However, there is a higher risk of losing biosolids to the effluent in the downflow systems. Design OLR is often in the range of 8-16 kg COD/m^3.day which is more than tenfold higher than the design loading rates for aerobic processes (Rittmann & McCarty, 2001).
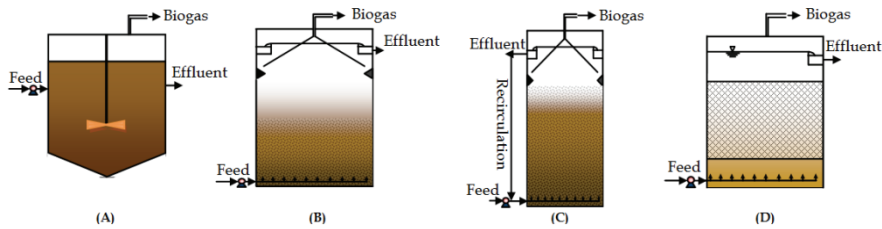
Fig. 2. Most commonly used anaerobic reactor types: (A) Completely mixed anaerobic digester, (B) UASB reactor, (C) AFB or EGSB reactor, (D) Upflow AF

4. Industrial applications

4.1 Corn processing industry
4.1.1 Process description

Corn is an important agricultural product that in the period of 2008-2009, nearly 789 million tons of corn was produced throughout the world (CRAR, 2009). Corn processing industries take corn apart and purify its different constituents and condition these constituents to be used in food and other industries (Anderson & Watson, 1982). Starch, gluten, dextrin, glucose and fructose are the main products produced by corn processing. Corn based glucose products are significant ingredients in major international markets (food, biochemical, pharmaceutical). Intermediate products, such as vegetable oil, protein or/and whole-wheat and fructose obtained from starch are utilized as raw material in catering factories, stockfarming facilities, and processing industries for sweeteners and beverages, respectively (Ersahin et al., 2007).

There are two distinct processes for corn processing; wet-milling and starch slurry derivatives production (refinery) and each process generates unique co-products. A simplified product flow diagram for a typical corn processing industry is given in Fig. 3 (Eremektar et al., 2002; Ersahin et al., 2007).

Wet milling is the breakdown of the corn into its components to provide starch slurry of very high purity and by products, incorporating with process water in countercurrent flow. Steeping is the most important process that is used to soften the grains for grinding, to break down the protein matrix to leave starch, and to remove the soluble matter from germ. Separated soluble proteins can be added to fiber and/or sold as protein. Steeped corn is passed through grinding mills to liberate germ from the corn kernel with as little damage as possible. The remaining material including starch slurry, gluten and fiber is screened by a fine screen and then passed through a squeezer. By this way, fiber is separated, washed, purified, and dewatered. The remaining slurry including starch and gluten is retained in a thickener and then gluten is concentrated by a centrifuge, thus lighter gluten is separated. (Ovez et al., 2001; Ersahin et al., 2006; Ersahin et al., 2007).

The starch slurry is further processed to produce dry starch, glucose, fructose and dextrin in the starch slurry derivatives units. Starch slurry is passed through centrifuge and then some of the starch is dried to get dry starch and malt sugar and marketed. Most of the remaining starch is converted into corn syrups and dextrose. In glucose refinery step, chemical and mechanical breakdown of starch slurry are carried out by acidification, mechanical breakdown unit and enzyme treatment tank. Then demineralization and evaporation processes are applied as the last step of glucose production. After evaporation, isocolumns are used in order to convert dextrose to fructose. (Ovez et al., 2001; Ozturk et al., 2005).
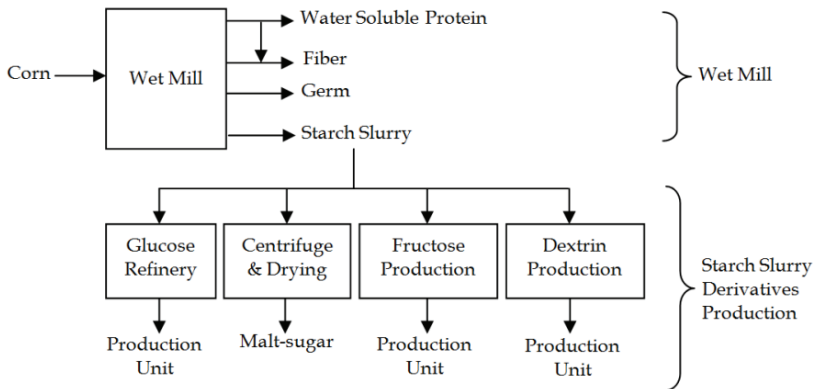
Fig. 3. Process flow diagram for a typical corn processing industry

4.1.2 Wastewater sources and characterization

Effluent from the corn milling industry is known as a high strength wastewater due to its high protein and starch content. The wastewater has a high COD, mainly of soluble and biodegradable character, with an initial inert COD content of less than 15%. The biodegradability of corn processing wastewaters is high in comparison to most of the other industrial effluents (Howgrave-Graham et al., 1994; Eremektar et al., 2002).

Typically, wastewater generation is mainly originated from evaporator vapor condensate, evaporator cleaning water and grinding mill cleaning water for wet milling process. Generally, the wastewater generated in germ and fiber washing and dewatering processes is recycled within the system (e.g. used for steeping). For starch slurry derivatives production, the wastewater sources are mainly consisting of cooler condensate, vacuum filter filtrate, activated carbon recovery water, and demineralization unit cleaning water from dextrose and fructose refinery (Ersahin et al., 2006). Table 1 includes the summary of characterization studies derived from different studies.

Parameter[1]	Unit	Reference				
		(Blanchard, 1992)	(Ovez et al., 2001)	(Eremektar et al., 2002)	(Johnson & May, 2003)	(Ersahin et al., 2006)
COD_{total}	mg/L	-	4850	3800	-	2810
$COD_{soluble}$	mg/L	-	3850	3230	-	-
BOD_5	mg/L	1000-3000	3000	2800	1000-2000	-
TKN	mg/L	-	174	84	-	60
NH_4-N	mg/L	-	-	23	-	-
TP	mg/L	-	125	33	-	-
TSS	mg/L	500	650	400	-	-
pH	-	-	5,2	-	-	-

[1] BOD5: Biochemical oxygen demand; TKN: Total Kjeldahl Nitrogen; TP: Total phosphorus; TSS: Total suspended solids

Table 1. Comparison of different studies from the literature for the characterization of corn processing wastewaters

Wet milling process generates more pollution in terms of COD than refinery process. A pollution profile study for a corn processing industry conducted by Ersahin et al. (2007) indicated that refinery process produced more wastewater than wet milling process, however wet milling process generated wastewater with more COD load than refinery process. In this study the specific wastewater flows from wet mill and refinery processes were determined as 0,64 m^3/ton corn processed and 0,80 m^3/ton product, respectively. They also indicated that specific COD loads from wet mill and refinery processes were 2,65 m^3/ton corn processed and 1,41 m^3/ton product.

4.1.3 Anaerobic treatment applications for the treatment of corn processing wastewaters

High strength and biodegradable character of the corn processing wastewaters makes biological treatment systems appropriate for the treatment of this type of effluents (Howgrave-Graham et al., 1994). Generally two stage biological treatment, an anaerobic stage followed by an aerobic stage, is applied for the treatment of corn processing effluents.

The presence of sufficient amount of macronutrients and trace elements is required for the granulation and stability of anaerobic reactors (Speece, 1996; Ozturk, 2007). However, some agro-industrial effluents that are generated from industries such as corn processing may not contain these elements in the required amounts for the optimum growth of microorganisms. In these situations, trace elements may be supplemented prior to anaerobic processes for an effective treatment. For an optimum methane yield, the optimum Carbon/Nitrogen/Phosphorus (C:N:P) ratio was reported as 100:2,5:0,5 (Rajeshwari et al., 2000).

EGSB reactor system is one of the most appropriate anaerobic treatment process alternatives for the treatment of corn processing wastewaters. A full-scale application of EGSB reactor for the treatment of corn processing industry effluents was evaluated by Ersahin et al (2007). The industry had a three-stage advanced wastewater treatment plant (WWTP) including an EGSB reactor, intermittently aerated activated sludge system for biological nitrogen removal and chemical post treatment unit for phosphorus removal. The first stage is an anaerobic EGSB reactor with an effective volume of 1226 m^3. The average OLR and HRT values were 3,57 kg COD/m^3.day and 18,5 hours, respectively. Average influent COD concentration and pH value of the reactor were 2750 mg COD/L and 6,9, respectively. SRT in the anaerobic reactor was above 100 days in general and the ratio of volatile suspended solids (VSS)/TSS for the granular biomass averaged 80%. Methane production potential was reported as 850-1540 m^3/day for the investigated EGSB reactor for one year operating period. COD removal rates of the anaerobic and aerobic units were same at 85%. By this combination of biological treatment processes, the quality of the final effluent met the discharge limits of European Union (EU) Urban Wastewater Directive for Sensitive Regions (EU 91/271/EEC, 1991).

A lab-scale AFB reactor using cultivated polyvinyl alcohol gel beads with a diameter of 2–3 mm, to treat corn steep liquor was investigated by Zhang et al. (2009). The effective volume of the reactor was 3,9 L. Influent COD concentration varied in a range of 2100-12900 mg/L. COD removal efficiencies of 96% and 91% were achieved at OLRs of 27,5 and 25 kg COD/m^3.day with HRTs of 10 h and 6 h, respectively. 610 g/L of biomass concentration was achieved by the biomass attachment of 1,02 g VSS/g PVA-gel beads.

Duran-deBazua et al. (2007) evaluated two stage biological treatment system consisting of anaerobic and aerobic processes for the treatment of effluents from a corn processing industry manufacturing tortillas, one of the Mexican traditional corn (maize) products. 500 ton corn/day was processed and an average wastewater flow of 2500 m^3/day was generated in the industry. They proposed high rate anaerobic reactors such as packed bed type or UASB reactors depending upon the availability of the granular anaerobic biomass for the treatment of the effluents generated from corn processing industries. They indicated that 9,6-16,8 m^3 biogas per ton of corn processed could be obtained by anaerobic treatment of these type of wastewaters.

ADUF (anaerobic digestion ultrafiltration), a membrane-assisted process for the separation of biomass from the treated effluent, was also investigated for the treatment of corn processing wastewaters (Ross et al., 1992). Both pilot (3 m^3) and full scales (2610 m^3) of completely mixed reactors were operated at mesophilic conditions with HRTs of 1,6 and 5,2 days and OLRs of 5 and 2,9 kg COD/m^3.day, respectively. Pilot reactor provided 90% COD removal at an influent concentration of 8000 mg COD/L, although 97% COD removal was obtained by the full scale reactor with an influent COD concentration of 15000 mg/L. 8-37 L/m^2.h flux was achieved in a pilot scale ADUF process.

A mass balance for a two-staged wastewater treatment plant of a corn processing industry was presented in Fig. 4. The COD removal efficiencies of the anaerobic and aerobic stages of the treatment plant were 89% and 85%, respectively (Ozturk et al., 2001).
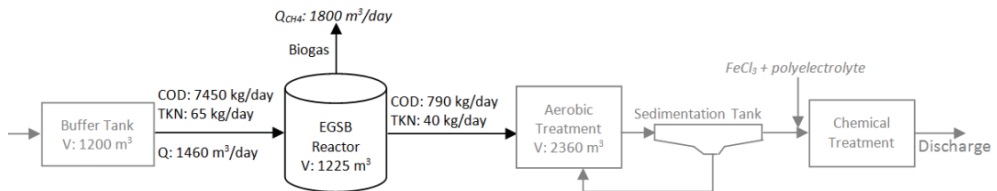
Fig. 4. Mass balance study for a wastewater treatment plant of the corn processing industry

4.2 Baker's yeast industry
4.2.1 Process description

Baker's yeast, which is one of the main products in the preparation of breadbaker, is manufactured through the aerobic fermentation of the selected strains of *Saccharomyces cerevisiae* according to their special qualities relating to the needs of the baking industry (Catalkaya & Sengul, 2006). The production of baker's yeast includes the processes, such as cultivation, fermentation, separation, rinsing and pressurized filtration as shown in Fig. 5.

The most common raw material of baker's yeast industry is molasses which is a by-product of sugar production due to its low cost and high content of sugar (Liang et al., 2009). After the dilution, clarification and sterilization, the molasses, which is commonly referred to as mash or wort, is fed to the fermentation vessels with nutrients. The grown cells at the early stages of fermentation are transferred into a series of progressively larger seed and semi-seed fermentors. At these stages of fermentation; molasses, nutrients and minerals are fed to the yeast at a controlled rate. At the end of the semi-seed fermentation, the content of the

tank at about 5 percent solids is concentrated to about 18-22 percent solids. The concentrated yeast which is called yeast cream is then washed with cold water and pumped to a semi-seed yeast storage tank where it is stored at 4 ^{0}C until it is used to inoculate the commercial fermentation tanks. The commercial fermentors are the final step in the process. After commercial fermentation, the yeast is pumped to the rotary drum filters and dewatered to a cake-like consistency with 30-33% yeast solids content. Depending on the market demands, the solids content of the yeast can be increased to 90–98% by drying and marketed as dry or instant baker's yeast (Ersahin et al., in press).
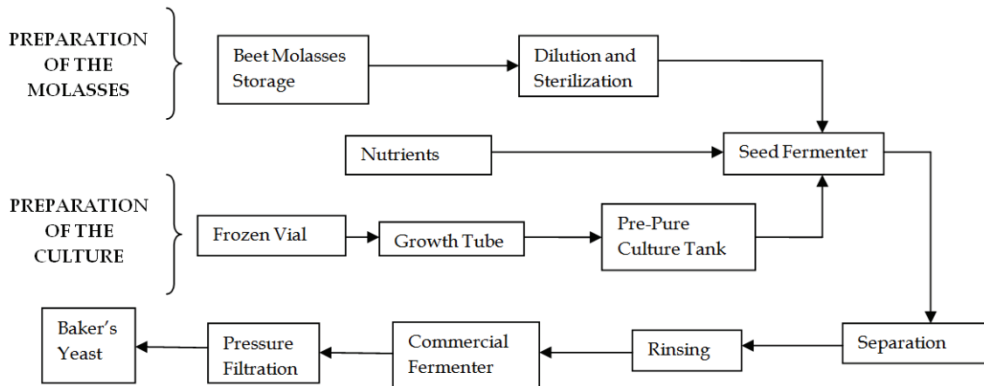
Fig. 5. Process flow diagram for a baker's yeast industry

4.2.2 Wastewater sources and characterization

During the fermentation process of the baker's yeast industry, large quantity of wastewater with high organic content, dark colour, high concentrations of total nitrogen, trimethylglycine and sulphate, variable phosphorus content and non-biodegradable organic pollutants are generated (Liang et al., 2009; Blonskaja et al., 2006). Colour is one of the most problematic parameters at the baker's yeast industry as a result of the presence of melanoid in the molasses which gives a brownish colour to the wastewater (Buyukkamaci & Filibeli, 2002). Molasses is the source of the most of contaminants in the wastewater with its content of 45-50% residual sugars, 15-20% non-sugar organic substances, 10-15% ash (minerals) and about 20% water. Yilmaz and Ozturk (1995) determined the initial soluble inert COD fraction of soluble COD in baker's yeast industry wastewaters between 10-15% under aerobic conditions.

The wastewater originated from baker's yeast industry can be classified into two groups as high strength process wastewater and low-medium strength process wastewater. The former one is generated from the yeast separators and processes such as centrifuges and rotary vacuum filters, whereas the latter one mainly constitutes the floor washing and equipment cleaning water (Catalkaya & Sengul, 2006). Table 2 presents some examples of baker's yeast industry wastewater characterization studies from the literature. Unlike from the other studies, Ozturk et al. (2010) reported a considerable decrease in the concentration of pollutant parameters such as COD, total nitrogen, sulphate, potassium, BOD$_5$ and colour for a baker's yeast industry after the installation of evaporation process.

Parameter[1]	Unit	Reference				
		(Ersahin et al., in press)	(Krapivina et al., 2007)	(Blonskaja et al., 2006)	(Altinbas et al., 2003)	(Gulmez et al., 1998)
pH	mg/L	6,5	-	-	6,2	5,9
COD	mg/L	6090	14400-25700	25020	15848	17100
TOC	mg/L	-	-	-	-	-
Magnesium	mg/L	-	-	-	30,7	-
Ferrous	mg/L	-	-	-	4,9	-
PO_4-P	mg/L	2,3	-	-	6,6	-
TSS	mg/L	583	-	-	835	-
VSS	mg/L	475	-	-	810	-
Alkalinity	mg $CaCO_3$/L	1475	-	-	2349	1675
Soluble COD	mg/L	4980	-	23420	15193	-
TKN	mg/L	274	-	-	1196	1185
NH_3-N	mg/L	132	-	-	206	250
TN	mg/L	-	250-350	1470	-	-
TP	mg/L	3	17,3-48,2	100	20,1	21
Sulphate	mg/L	485	3500-5300	2940	-	-

[1] TOC: Total organic carbon; TN: Total nitrogen

Table 2. Characterization of the effluent from the baker's yeast industry

4.2.3 Anaerobic treatment applications for the treatment of Baker's yeast wastewaters

Anaerobic processes appears to be economically more attractive in comparison to aerobic processes for the treatment of high strength wastewaters with the achievement of simultaneous organic matter and sulphate removal, low sludge production and low energy requirement. However, the effluents of the anaerobic treatment stages should be further treated by the other treatment technologies in order to fulfill the discharge requirements for baker's yeast industries.

Kalyuzhnyi et al. (2005) studied the anaerobic treatment of baker's yeast industry effluent by an UASB reactor as a pre-treatment followed by aerobic-anoxic biofilter and coagulation processes. According to the results, the UASB reactor was found to be quite efficient for both raw and diluted samples with COD removal efficiencies between 52-74% for the OLRs of 3,7-16 g COD/L.day. A stepwise increase in the OLR from 3,7 to 10,3 g COD/L.day during the treatment of the raw sample didn't make a significant effect on COD removal which was in the range of 60-67%. However, further increase in OLR to 16 g COD/L.day in the treatment of the diluted sample led to a drop in the COD removal to 52%. Complete removal of sulphate which was transformed into soluble sulphide was observed in the UASB reactor. In fact, the observed sulphide concentrations were not inhibitory for anaerobic sludge. Colour was not generally removed during the anaerobic treatment stage.

Gulmez et al. (1998) investigated the feasibility of anaerobic treatment technology for baker's yeast industry wastewater which was combined with the wastewater generated from pharmaceutical industry. The study was performed at a lab-scale UASB reactor with

an effective volume of 10,35 L and a sedimentation volume of 6,05 L at mesophilic conditions. The experimental study was carried out for 333 days. The first 198 days the system was only fed with baker's yeast industry wastewater. After the achievement of the steady-state operating conditions at the 140th day, COD removal rates of 62% and 64% were observed between 140th and 198th day at the OLRs of 2,4 kg COD/m³.day and 4,8 kg COD/m³.day, respectively. After the 198th day, the system was fed with the combination of baker's yeast and pharmaceutical industry wastewaters at different dilution ratios between 1/50 and 1/1000 (pharmaceutical industry wastewater volume/the total wastewater volume). The combination of pharmaceutical industry wastewater with baker's yeast industry wastewater at the lower dilutions resulted in a decrease in terms of COD removal.

Ciftci & Ozturk (1995) presented the performance of a full-scale two-staged UASB reactors (acid reactor+methane reactors) treating baker's yeast industry effluents. Long-term (nine years) average COD removal efficiency, biogas flow and methane conversion yield were reported as 75%, 18000 m³/day and 0,45 m³/kg COD$_{removed}$, respectively. However, a decrease in the biogas flow has been observed in the study of Ozturk et al. (2010) that was derived from a baker's yeast industry with an evaporation process as a result of a decrease in the pollutant loads.

Hybrid reactor, which combines an UASB reactor in the lower part with a filter in the upper part and promotes the advantages of both reactor types, was tested in order to overcome the disadvantages of fully packed anaerobic filters. The performance of hybrid upflow anaerobic filters depends on the contact of the wastewater with both the attached biofilm in the media and suspended growth in the sludge part (Buyukkamaci & Filibeli, 2002). A laboratory scale hybrid reactor with a fixed bed at the upper two-third of the reactor was used in this study. The reactor was operated at mesophilic conditions with three different types of wastewater sources including synthetic wastewater containing molasses, baker's yeast industry wastewater and meat processing industry wastewater. HRT was kept constant at 2 days and the OLR was approximately 9 kg/m³.day during the study. Average COD, TOC, and colour removal efficiencies were 78%, 76%, and 12% respectively.

Krapivina et al. (2007) studied the treatability of sulphate-rich high strength baker's yeast industry wastewater by using anaerobic sequencing batch reactor technology. Three different treatment schemes including anaerobic sequencing batch reactor with or without a polymeric filler and coupled micro-aerophilic/anaerobic sequencing batch reactor were investigated with an optimal sludge concentration of 17300 mg/L and an optimal reaction time of 22 hours in the reactor. The third treatment alternative prevented sulphate formation by the oxidation of the sulphide formed in the anaerobic stage of the process and left sulphur in the form of elemental sulphur which was a colloid, inert solid and could be removed from the wastewater easily by keeping the level of oxygen content in the micro-aerophilic reservoir at 0,1-0,15 mg/L. The solution of sulphate and sulphide removal problems resulted in an alleviation for sulphide inhibition of both methanogenesis and sulphate reducing bacteria and made the third alternative preferable for the treatment of sulphate-rich yeast wastewaters.

A mass balance study for the wastewater treatment plant of a baker's yeast industry which had an evaporation process was presented in Fig. 6 (Ozturk et al., 2010).
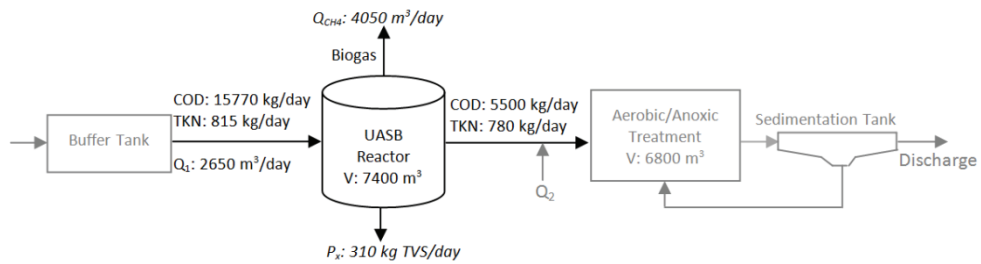
Fig. 6. Mass balance study for a wastewater treatment plant of the baker's yeast industry

The main problems encountered in the anaerobic treatment of the baker's yeast industries are the accumulation of the inorganic matter (i.e. $CaSO_4$, $MgNH_4PO_4$) in the reactor, ammonia toxicity due to high pH values (>8) and high hydrogen sulphur content in the biogas.

4.3 Confectionery industry
4.3.1 Process description
Confectionery industry is an important branch of food sector. The confectionery industry can be classified into three main segments: chocolate confectionery, sugar confectionery and flour confectionery. Chocolate confectionery, which has four category including chocolate bars, chocolate blocks, boxed chocolate and other chocolate, is the predominant category covering items made out of chocolate. Flour confectionery is obviously things made out of flour, whereas sugar confectionery covers the rest of confectionery (Edwards, 2000).
There is a wide range of products with different production schemes in the confectionery industry. Chocolate confectionery was selected to provide a flow diagram and process description (Fig. 7).
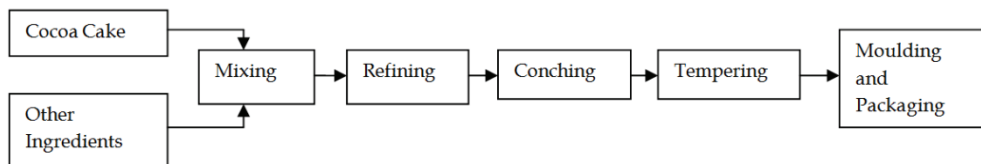
Fig. 7. Process flow diagram for a chocolate confectionery industry

Chocolate, which is made from the fruit of the cacao tree, is used as an ingredient for beverages and various kinds of confectionery. The cocoa cake is mixed in a heated kneading machine with the other ingredients such as sugar, cocoa butter, milk powder or crumb, vegetable fats, lecithin, condensed milk and flavourings. Refining machinery consists of cooled metal rollers which run at a higher speed to assist the crushing process. As the chocolate passes through the refiners the particles are crushed by the pressure between the rollers. After refining process, the chocolate is transferred to the conche-refiner for further processing. Heat is introduced to this process by mechanically working the mix by vigorous slapping agitation for several hours. The aim of this process is to ensure that the liquid is evenly blended. Conches are heated normally by a water jacket and can be continuous or batch design. Following conching, the liquid chocolate is tempered for several hours in

order to stabilize the cocoa butter crystals and make them more uniform in size. It also gives the chocolate a bright lustre and a sharp snap. The tempering process involves heating the chocolate liquor and then cooling it in several stages. The final steps in the process are moulding the chocolate, allowing it to cool and harden, and then finally packaging it (Aesseal Environmental Technology, 2003).

4.3.2 Wastewater sources and characterization

Confectionery industry generates high amounts of wastewater which contains high concentrations of readily biodegradable organic materials characterized with high COD and BOD (Beal & Raman, 2000; Diwani et al., 2000). Orhon et al. (1995) determined the initial soluble inert COD percentage of confectionary industry wastewaters between 1,5-7,1% under aerobic conditions. Some examples from the literature for the characterization of the wastewater discharged from the confectionery industry were provided in Table 3.

Parameter	Unit	Reference			
		(El-Gohary et al., 1999)	(Orhon et al., 1995)	(Diwani et al., 2000)	(Ozturk & Altinbas, 2008)
COD	mg/L	4475	2840-6220	5000	19900
COD$_{soluble}$	mg/L	-	2500-5400	-	-
BOD	mg/L	2200	1840-4910	3200	-
TKN	mg/L	100	33-55	-	-
TP	mg/L	17,2	8,6-65	-	-
TSS	mg/L	649	260-440	177	1050
VSS	mg/L	490	-	-	-
pH	-	-	4-5,1	6	-
Oil and grease	mg/L	367	-	-	-

Table 3. Characterization of the wastewater discharged from the confectionery industry

4.3.3 Anaerobic treatment applications for the treatment of confectionery wastewaters

An UASB reactor may be a viable alternative for the primary treatment of the confectionery wastewater as this technology is designed to make the upflow velocity of the wastewater much lower than the settling velocity of the granules. In this way, the settling process uncouples HRT from SRT that results in the retaining of the biomass in the reactor (Beal and Raman, 2000).

El-Gohary et al. (1999) compared the performance of laboratory-scale aerobic and anaerobic systems treating confectionery wastewater. The experiments were conducted at a laboratory-scale one-phase UASB reactor with a sludge content kept around 22 g/L. The results showed that UASB system with a HRT of 12 hours and OLR of 4,4 kg BOD/m³.day achieved COD and BOD removal efficiencies of 92,4% and 91,5%, respectively. Mean COD, BOD, TSS and oil and grease values analyzed in the effluent were all in agreement with the standards set by the regulatory authorities.

Berardino et al. (2000) provided the experimental results of semi-continuous tests of the anaerobic digestion of confectionery wastewater, carried out at different residence times and organic loads in a laboratory-scale upflow anaerobic filter at mesophilic conditions with

a working reactor volume of 10 L. COD removal rates didn't fall below 80% under the whole range of conditions, while a maximum removal rate of 92% was achieved.

Ozturk & Altinbas (2008) evaluated the treatment performance of one of the main confectionery industries in Turkey. The treatment plant of the investigated industry involved physical treatment system including screens, dissolved air flotation, equalization tank and two-staged biological system including anaerobic and aerobic reactors. The anaerobic stage of the industry included an EGSB reactor with 1200 m³ volume operated at mesophilic conditions. Average OLR was 3 kg COD/m³.day, however it could increase to 7,5 kg COD/m³.day at shock loadings. COD removal rate at the anaerobic stage of the system was 91% with a biogas generation of 1880±640 m³/day.

Single-reactor processes are sometimes insufficient for the treatment of the effluents with high COD loads due to the extensive treatment requirements to meet the strict discharge limits. In this situation, various types of anaerobic processes can be applied in order to enhance the treatment performance. The study of Beal and Raman (2000) both evaluated the feasibility of high-rate anaerobic treatment for the confectionery wastewater and examined the possibility of using a second-stage anaerobic reactor. The treatment system included an UASB reactor operated at 35 °C followed by a downflow anaerobic filter operated at ambient temperature (25 °C). The UASB reactor consistently achieved COD removal rate of 98% at the highest organic loadings, whereas COD removal efficiencies achieved by downflow anaerobic filter are above 50%. The COD treatment efficiency of the whole system is 99% at a total OLR of 12,5 kg/m³.day with an effluent COD concentration below 400 mg/L that was not yet dischargeable but more amenable to aerobic treatment than the raw wastewater.

Moody & Raman (2001) investigated the performance of two dual-reactor high-rate anaerobic systems in the treatment of confectionery wastewater. Diluted wastewater from a confectionery plant, which had a COD concentration of 8000 mg/L, was fed to the primary reactors at a constant flow rate. Primary reactors, which were downflow anaerobic filter and UASB reactor, were operated at constant HRT of 1,6 day and achieved COD removal rate of 94% and 88%, respectively. Effluents from the primary reactors were combined and fed to the secondary reactors which were both downflow anaerobic filters with different packing media including brick pieces and plastic rings at different HRTs of 0,8, 1,6 and 3,2 days. The results showed that a brick media downflow anaeobic filter with a 1,6 day HRT, placed down-stream of a functional high-rate anaerobic reactor, achieved the best removal efficiency of 89% for COD parameter in comparison to the other HRTs and packing media.

A COD mass balance study for a two-staged wastewater treatment plant of a confectionery industry was presented in Fig. 8 (Ozturk & Altinbas, 2008).
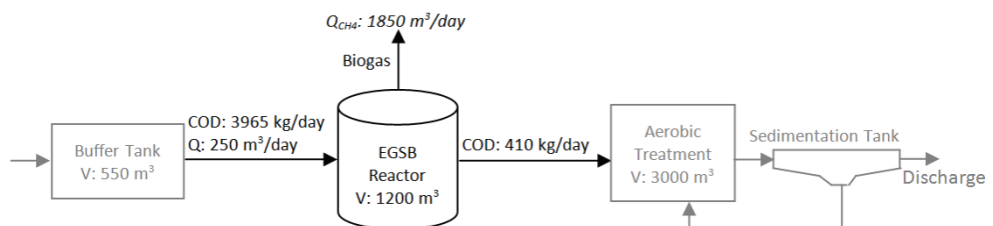
Fig. 8. Mass balance study for a wastewater treatment plant of the confectionery industry

4.4 Potato processing industry
4.4.1 Process description

Food processing industry has grown rapidly parallel to the world population growth as a result of the inevitable necessity of the food to feed billions of people. Potato is a very important and popular vegetable in human diet and its worldwide production has reached to 314,2 million by 2008 (FAOSTAT, 2008). Various types of products such as potato chips, frozen French fries and other frozen food, dehydrated mashed potatoes, dehydrated diced potatoes, potato flake, potato starch, potato flour, canned white potatoes, prepeeled potatoes are processed from potato. Due to the wide range of the products, the potato processing industries can differ in their process lines. Although the type of processing unit depends upon the product selection, the major processes in all products are storage, washing, peeling, trimming, slicing, blanching, cooking, drying, etc. The process line of a potato chips manufacturing plant is given in Fig. 9.
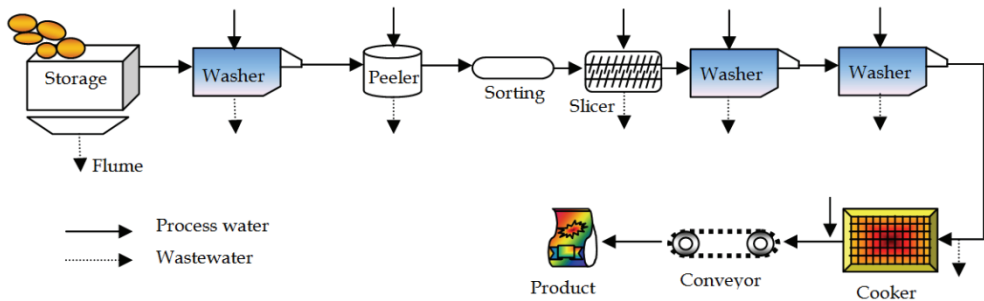
Fig. 9. Process flow diagram for a potato chips industry

4.4.2 Wastewater sources and characterization

Potato processing wastewater contains high concentrations of biodegradable components such as starch and proteins, in addition to high concentrations of COD, TSS and TKN. Therefore, wastewater production and composition of potato processing plants depend on the processing techniques to a large extent (Senturk et al., 2010a). Raw potatoes must be washed thoroughly to remove sand and dirt prior to other processes. Water consumption for fluming and washing varies from 18,5 to 7,9 liters per ton of potatoes. Peeling of potatoes contributes the major portion of the organic load in potato processing waste. Among three different peeling methods (abrasion peeling, steam peeling and lye peeling), lye peeling is the most popular peeling method used today. Therefore, lye peeling wastewater is the most troublesome potato waste due to very high pH (11–12), high organic content mostly in colloidal form (Hung et al., 2006). The wastewater flows from different potato processing industries were reported as 17 m^3/ton potato processed (Hung et al., 2006), 5-8 m^3/ton potato processed (Guttormsen & Carlson, 1969), 3,9 m^3/ton potato processed (Austerman-Houn & Seyfried, 1992) and 5,8 m^3/ton potato processed (Cooley et al., 1964). Several publications on the characteristics of wastewaters resulting from various types of potato processing plants are summarized in Table 4.

Parameter[1]	Unit	Reference				
		(Senturk et al., 2010b)	(Wang et al., 2009)	(Kalyuzhnyi et al., 1998)	(Hadjivassilis et al., 1997)	(Austerman-Houn & Seyfried, 1992)
Industry	-	Potato chips[2]	Potato starch	Potato maize	Potato chips	Potato chips[3]
COD	mg/L	5250 – 5750	1100 – 4500	5500 – 18100	4000 – 7000	389 – 5899 (3638)[4]
Soluble COD	mg CaCO$_3$/L	2500 – 3000	-	3200 – 7400	-	-
BOD$_5$	mg/L	4000 – 5000	-	-	2000 – 3000	155 – 3465 (1977)
Alkalinity	mg/L	2000 – 2500	-	-	-	-
pH	-	7,0 – 8,0	5,0 – 8,5	6,0 – 11,0	-	-
TKN	mg/L	200 – 250	-	-	-	88 – 509 (296)
Ammonia	mg/L	50 – 60	8,9 – 48,5	-	-	-
Sulphate	mg/L	40 – 50	-	-	-	-
TP	mg/L	90 – 100	-	-	-	6 – 51 (25)
TS	mg/L	4800 – 5000	-	-	-	-
TVS	mg/L	4400 – 4500	-	-	-	-
TSS	mg/L	-	-	2700 – 7100	1000 – 3000	-
VSS	mg/L	-	-	1400 – 6600	-	-

[1] TS: Total solids; TVS: Total volatile solids

[2] Potato peeling and cutting process wastewater

[3] Process wastewater which is a mixture of potato washing water after sand separation and potato fruit water after starch recovery

[4] Values in paranthesis represent the average values

Table 4. Characteristics of wastewaters resulting from various types of potato processing

4.4.3 Anaerobic treatment applications for the treatment of potato processing wastewaters

Senturk et al. (2010a) investigated the mesophilic anaerobic treatment of potato processing wastewater obtained from a factory producing potato chips, maize chips and other snacks. They used a laboratory scale mesophilic anaerobic contact reactor which had similar features with activated sludge systems. The reactor was operated at different OLRs and HRTs ranging from 1,1–5,0 kg COD/m^3.day and 5,11–1,06 day, respectively, and it achieved COD removal efficiencies between 78–92%. Furthermore, various kinetic models such as Monod first order model, Stover–Kincannon model, Grau second-order and Michaelis–Menten models have been applied to the experimental data in order to determine substrate balance, maximum utilization rate and volumetric methane production. The applied models showed good agreement ($R^2 > 0,98$) with the experimental data and methane yield was determined as 0,394 L CH$_4$/g COD$_{removed}$.

A novel anaerobic–aerobic integrative baffled bioreactor supplied with porous burnt-coke particles was developed for the treatment of potato starch wastewater by Wang et al. (2009). This bioreactor was found to be effective for the removal of COD (88,4–98,7%) and NH$_3$–N (50,4 to 82,3%), in high-strength starch wastewater.

Musluoglu (2010) studied the co-digestion of potato chips production industry waste with the waste activated sludge from two different full-scale facilities. Average biogas potentials in both completely mixed reactors were between 600-650 m^3/ton VS$_{added}$.

The performances of laboratory scale UASB (0,84 L) and anaerobic packed-bed reactors (APB) (0,7 L) treating high strength potato leachate were compared by Parawira et al. (2006).

The maximum OLRs that could be applied to the UASB and APB reactors for stable operation were approximately 6,1 and 4,7 g COD/L day, respectively. More than 90% COD removal efficiency was reported for both type of reactors. On the contrary to the results obtained by Linke (2006) at an anaerobic completely mixed reactor treating solid potato waste, the methane yield increased with increasing organic loading rate up to 0,23 L CH_4/g $COD_{degraded}$ in the UASB reactor and 0,161 CH_4/g $COD_{degraded}$ in the APB reactor.

The effect of recirculation rate on packed bed reactors (1 L) treating potato leachate at different OLRs ranging between 4–12 kg COD/day was studied by Mshandete et al. (2004). The methane yield for the bioreactor with the lower recirculation flow rate (10 mL/minute) ranged between 0,10-0,14 m^3 CH_4/kg $COD_{removed}$, while for the other bioreactor it was between 0,14–0,20 m^3 CH_4/kg $COD_{removed}$. Lower methane yields were achieved at higher OLRs. While the methane yield of the reactor operated at high recirculation rate was more than the other bioreactor, in terms of process stability the reactor operated at low recirculation rate was superior. Process failure, indicated by low pH, high volatile fatty acid (VFA) concentration, was experienced at an OLR of 12 kg COD/m^3.day in the reactor operated at high recirculation rate. This was attributed to the high recirculation flow rate which provided rapid mixing and fast diffusion of the accumulated VFAs into the biofilm where microbes were accumulated.

The efficiency of the UASB process for the treatment of raw and pre-clarified potato maize waste up to the OLR of about 13-14 g COD/L.day was illustrated by Kalyuzhnyi et al. (1998). Although the reactor performed high COD removal efficiencies (63-81%) for raw potato maize waste (PMW), some problems such as excessive foaming and sludge flotation were experienced due to the accumulation of undigested ingredients at high OLR (> 10 g COD/L.day) and moderate HRT (> 1 day). These problems were eliminated by the application of shorter HRTs in order to enable better washout of light ingredients that were accumulated in the reactor, or by temporarily decreasing OLR. Methane yield varied from 0,24 to 0,44 L/g $COD_{removed}$ for raw PMW and from 0,30 to 0,37 L/g $COD_{removed}$ for pre-clarified PMW.

The anaerobic treatability of potato processing effluents by an anaerobic contact reactor operated at thermophilic conditions was studied by Senturk et al. (2010b). The OLR of the reactor was gradually increased from 0,6 kg COD/m^3.day to 8,0 kg COD/m^3.day by decrementing the HRT from 9,2 days to 0,69 days. The reactor could be operated at high OLRs without process failure and the average COD removal efficiency obtained at 8,0 kg COD/m^3.day was 86%. The average methane gas production was reported as 0,42 m^3 CH_4/kg $COD_{removed}$ and the methane content in the biogas ranged between 68–89%.

The performance of two-stage anaerobic digestion of solid potato waste under mesophilic and thermophilic conditions was evaluated by Parawira et al. (2007). A solid bed reactor was used as the hydrolytic stage of the two staged process. An UASB reactor fed with the leachate obtained from the hydrolysis reactor was used in the second step of the two-stage system with three different temperature combinations (mesophilic+mesophilic, mesophilic+thermophilic, thermophilic+thermophilic). They found that the methane yield of the mesophilic system (0,49 m^3 CH_4/kg $COD_{degraded}$) was significantly higher than the thermophilic system (0,31 m^3 CH_4/kg $COD_{degraded}$). However, thermophilic operation reduced the complete digestion period of the waste (from 36 to 25 days) and higher OLRs up to 36 kg COD/m^3.day could be applied to the UASB reactor.

The biogas yield of a completely stirred reactor treating solid potato waste at thermophilic conditions was found as 0,85–0,65 L/g TVS for the OLRs in the range of 0,8–3,4 g TVS/L.day, respectively (Linke, 2006). The results indicated a gradual decrease in the biogas

yield and methane content (from 58% to 50%) of the biogas depending on the increase in the OLR of the reactor.

The performance of two types of two-stage systems, one consisting of a solid-bed reactor connected to an UASB reactor, and the other consisting of a solid-bed reactor connected to a methanogenic reactor packed with wheat straw biofilm carriers, were investigated by Parawira et al. (2005). While the performance in terms of methane yield was the same (0,39 m^3 CH_4/kg VS_{added}) in the straw packed-bed reactor and the UASB reactor, the packed-bed reactor degraded the potato waste in a shorter time due to the improved retention of methanogenic microorganisms in the process.

4.5 Opium alkaloid industry
4.5.1 Process description
Opium is known to contain about 26 types of alkaloids such as morphine, narcodine, codein, papvarine and thebain (Sevimli et al., 1999). There are many different methods for the extraction of alkaloids from natural raw materials. Most of the methods depend on both the solubility of the alkaloids in organic solvents and solubility of their salts in water (Hesse, 2002). The process flow scheme of a wet-mill opium alkaloid industry, which mainly consists of grinding, solid-liquid and liquid-liquid extraction and crystallization processes, was given in Fig. 10.
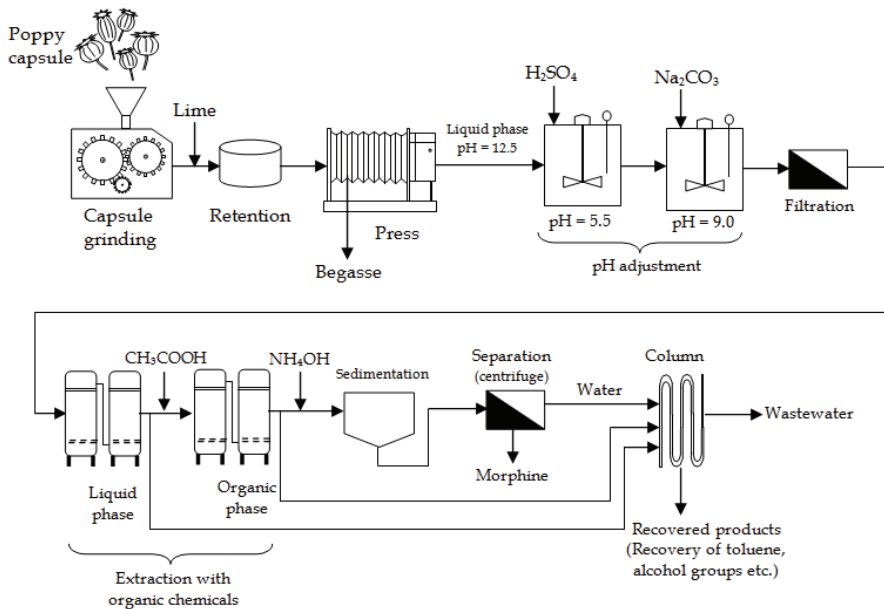
Fig. 10. Process flow diagram for an opium alkaloid industry

Firstly opium poppy capsules are grinded and treated with an alkaline solution (lime), and then the slurry is pressed to extract the liquid that contains the alkaloids. The pH of the liquid is adjusted to 9,0 and the impurities are separated by a filtration process. In the extraction process, the alkaloids are extracted with acetic acid solution and other organic solvents such as toluene and butanol. The morphine is crystallized by adding ammonium

and separated from the solution by centrifuges. The used solvents and the water are sent to the distillation column in order to recover toluene, alcohol groups and the remaining wastewater is treated in a wastewater treatment plant (Sevimli et al., 1999).

4.5.2 Wastewater sources and characterization

Opium alkaloid industry wastewaters are highly polluted effluents characterized with high concentrations of COD (mainly soluble), BOD_5 and TKN, dark brown colour and low pH. Alkaloid industry wastewaters are generally phosphorus deficient; therefore phosphorus addition might be required for biological treatment. Soluble COD content and acetic acid related COD of the wastewater can be as high as 90% and 33%, respectively (Aydin et al., 2010). Sevimli et al. (1999) determined the initial soluble inert COD percentage of opium alkaloid industry wastewaters as 2%. Aydin et al. (2010) reported the initial soluble and particulate inert COD content of opium alkaloid industry wastewaters under anaerobic conditions as 1,64% and 2,42%, respectively. Although no available data could be found in the literature for the sulphate content of the alkaloid industry wastewaters, it may be present at high concentrations due to the addition of sulphuric acid at the pH adjustment stage. Ozdemir (2006) reported a sulphuric acid usage of 48,3 kilograms per ton of opium processed. Furthermore, the alkaloid wastewaters might contain some toxic organic chemicals such as N,N-dimethylaniline, toluene which are inhibitory for biological treatment (Aydin et al., 2010). The general characteristics of opium alkaloid plant effluents given in the literature are presented in Table 5.

Parameter	Unit	Reference					
		Bural et al. (2010)	Aydin et al. (2010)[1]	Ozdemir (2006)	Sevimli et al. (1999)	Timur & Altinbas (1997)	Deshkar et al. (1982)
COD	mg/L	30000-43078	18300–42500(25560)	22000-34780	36500	21040	18800
Soluble COD	mg $CaCO_3$/L	28500-40525	17050–39470	-	-	-	-
BOD_5	mg/L	16625-23670	4250–22215(12000)	21250	32620	12075	15000
Alkalinity	mg/L	-	315–4450 (1290)	144-1050	-	4450	-
pH	-	4,5–5,36	4,9–6,3 (5,4)	-	4,95	5,1	8,4
TKN	mg/L	396–1001	550–841(673)	1001	1030	380	1870
NH_3-N	mg/L	61,6–259	73–141(98)	61,6-172,5	140	110	35
TP	mg/L	4,0–5,21	3,1–15,0	4-5,21	65	2,0	1,3
TS	mg/L		27235–29750	-	-	27235	15475
TSS	mg/L	555–2193	565–2295	1120-1700	1400	1005	38
TVS	mg/L	382–1395	320–1775	580-990	-	805	-
Color	Pt-Co	4375–4750[2]	2150–2550	4750	-	-	-

[1] Numbers in parenthesis represent the median values.

[2] After coarse filtration

Table 5. Characteristics of opium alkaloid industry effluents

4.5.3 Anaerobic treatment applications for the treatment of opium alkaloid wastewaters

Sevimli et al. (2000) investigated the mesophilic anaerobic treatment of opium alkaloids industry effluents by a pilot scale UASB reactor (36 L) operated at different OLRs (2,8 – 5,2

kg COD/m^3.day) at a HRT of 2,5 days. Although they experienced some operational problems, COD removal efficiency of 50–75% was achieved throughout the operational period. One of the most detailed and long termed study on the anaerobic treatability of effluents generated form an opium alkaloids industry was presented by Aydin et al. (2010). The treatment performance of a lab-scale UASB reactor (11,5 L) was investigated under different HRTs (0,84–1,62 days) and OLRs (3,4–12,25 kg COD/m^3.day) at mesophilic conditions. Although, the COD removal efficiency slightly decreased with increasing OLR and decreasing HRT, the reactor performed high COD removal efficiencies varying between 74%–88%. Furthermore, a severe inhibition caused by N,N-dimethylaniline, coming from the wastewater generated in the cleaning operation at the derivation unit tanks of the industry, was experienced in the study. During the inhibition period the treatment efficiency and biogas production dropped suddenly, even though the OLR was decreased and HRT was increased as a preventive action. Despite these interventions, the reactor performance could not be improved and the reactor sludge had to be renewed due to the irreversible inhibition occurred for four months. The reactor could easily reach to the same efficiency level after the renewal of the sludge. Average methane yield of the opium alkaloids industry wastewater was reported as 0,3 m^3 CH_4/kg $COD_{removed}$. Dereli et al., (2010) applied Anaerobic Digestion Model No.1 (ADM1), a structured model developed by IWA Task Group (Batstone et al., 2002), for the data obtained by Aydin et al. (2010). ADM1 was able to simulate the UASB reactor performance in terms of effluent COD and pH, whereas some discrepancies were observed for methane gas predictions.

Ozdemir (2006) investigated the co-digestion of alkaloid wastewater with acetate/glucose by batch experiments, therefore the usage of these co-substrates did not improve removal efficiency significantly but acclimation period of microorganisms was reduced. Continuous anaerobic treatment of alkaloid industry wastewater was further investigated by Ozdemir (2006) using three lab scale UASB reactors (Reactor 1: fed with alkaloid wastewater after hydrolysis/acidification, Reactor 2: fed with raw alkaloid wastewater, Reactor 3: fed with alkaloid wastewater together with sodium acetate as co-substrate) operated at different OLRs (2,5–9,2 kg COD/m^3.day) and a HRT of 4 days. Although all of the reactors performed well at low OLRs (~80% COD removal efficiency), process failure was experienced in R1 and R2 reactors at the OLR of 9,2 kg COD/m^3.day.

Ozturk et al. (2008) studied the anaerobic treatability for the mixture of wastewater generated from the distillation column and domestic wastewater of an alkaloid industry by a full-scale anaerobic Internal Cycling (IC) reactor with an OLR of 5 kg COD/m^3.day. COD and VFA removal efficiencies were 85 and 95%, respectively. Biogas production rate of 0,1-0,35 m^3 CH_4/$COD_{removed}$ was obtained. The main problems stated in this study were high salinity and sulphate concentrations.

4.6 Other industries
4.6.1 Anaerobic treatment applications for the treatment of other industrial wastewaters

A large quantity of wastewaters has generated from many different industries which, especially including high organic contents, if treated by anaerobic technology, a remarkable source of energy can be gained. Considerable attention has been paid to high rate anaerobic digesters such as UASB and EGSB reactors in order to provide possibility to treat industrial wastewaters at a high OLR and a low HRT (Rajeshwari et al., 2000). Application of anaerobic digestion for the industrial effluents is not limited with the industries discussed in

Wastewater Type	Reactor Type/Operating Temperature (°C)	Capacity (m³)	OLR (kgCOD/m³.day)	COD removal (%)	Methane yield (m³/kg COD)	Reference
Pulp and Paper	Baffled/35	0,01	5	60	0,141-0,178	(Grover et al., 1999)
Pulp and Paper	Anaerobic Contact/-	-	-	80	0,34	(Rajeshwari et al., 2000)
Slaughterhouse	UASB/-	450	2,1	80	-	(Del Nery et al., 2001)
Slaughterhouse	AF/-	21	2,3	85	-	(Johns, 1995)
Cheese Whey	Baffled/35	0,015	-	94-99	0,31	(Antonopoulou et al., 2008)
Cheese Whey	Upflow Filter/35	0,00536	-	95	0,55 (biogas)	(Yilmazer & Yenigun, 1999)
Textile	UASB/35	0,00125	-	>90	-	(Somasiri et al., 2008)
Textile	Fluidized Bed/35	0,004	3	82	-	(Sen & Demirer, 2003)
Coffee	Hybrid (UASB + AF)/23	10,5	1,89	77,2	-	(Bello-Mendoza & Castillo-Rivera, 1998)
Coffee	UASB/35	0,005	10	78	0,29	(Dinsdale et al., 1997)
Brewery	Sequencing Batch/33	0,045	1,5-5	>90	0,326	(Xiangwen et al., 2008)
Brewery	AF/34-39	5,8	8	96	0,15	(Leal et al., 1998)
Brewery	AF Fluidized Bed/35	0,06	8,9-14	75-87	0,34	(Anderson et al., 1990)
Olive Oil	UASB/37	-	12-18	70-75	-	(Azbar et al., 2010)
Olive Oil	Hybrid (UASB +AF)/35	-	17,8	76,2	-	(Azbar et al., 2010)
Sugar Mill	UASB/33-36	0,05	16	>90	0,355	(Nacheva et al., 2009)
Sugar Mill	Fixed Bed/32-34	0,06	10	90	-	(Farhadian et al., 2007)
Distillery	Granular bed-Baffled/37	0,035	4,75	80	-	(Akunna & Clark, 2000)
Distillery	Fixed Film/37	0,001	23,25	64	-	(Acharya et al., 2008)

Table 6. Anaerobic treatment applications for different industrial wastewaters

the previous sections. Besides, it has a wide potential for wastewater treatment applications of many industries such as pulp and paper, slaughterhouse, cheese whey, textile, coffee, brewery, olive oil, sugar mill, distillery, etc. It is not possible to present all industrial wastewater treatment application examples of anaerobic digestion in a chapter; instead, examples from a number of selected studies were given in Table 6.

5. Conclusions and future perspectives

Anaerobic biotechnology has a significant potential for the recovery of biomethane by the treatment of medium and/or high strength wastewaters especially produced in agro-industries. By using this technology, ~ 250-300 m³ biomethane can be recovered per ton COD$_{removed}$ depending on the inert COD content of the substrate. COD removal rates are generally between 65-90% in these systems. Anaerobic biotechnology, when used in the first

treatment stage, provides the reduction of aeration energy and excess sludge production in the followed aerobic stage, thus increasing the total energy efficiency of the treatment plant. Besides, it contributes to the increase in the treatment capacity of the aerobic stage. Also it is possible to obtain a considerable increase of production capacity for an industry if an anaerobic first stage treatment is applied before aerobic stage in an industrial wastewater treatment plant treating medium strength organic waste. In case of nitrogen removal in a two-stage (anaerobic+aerobic) biological wastewater treatment process, it may be necessary to bypass some of the influent stream from anaerobic to aerobic stage in order to increase the denitrification capacity. Autotrophic denitrification with H_2S in the biogas is an important option that should be kept in mind to reduce organic carbon requirement for denitrification in two-stage treatment process treating wastewaters that contains high organic matter and high nitrogen (Baspinar, 2008). It is more appropriate to apply pre-treatment as phase-separation (two-staged) for industrial wastewaters containing high sulphate concentration.

There are many full-scale applications for the operation of anaerobic processes under sub-mesophilic (27-30 ^{0}C) and high pH conditions, especially for the treatment of high strength wastewaters with high nitrogen content. In such conditions, full nitrification but partial denitrification at aerobic stage or an innovative nitrogen removal technology, Sharon/Anammox process, may be applied.

Another option for the pre-treatment of wastewater streams containing high COD (>40000 mg/L), total dissolved solids (TDS), TKN and potassium is an evaporation process that useful material can be recovered and residual condensate may be further treated by an anaerobic process.

Recently, co-digestion applications of treatment sludge with other organic wastes have increased dramatically due to the subsidies for renewable energy produced from wastes. In this respect, organic solid wastes and biological treatment sludge can be co-digested by installation of anaerobic co-digesters at the same location with available industrial-scale anaerobic bioreactors or near the sources of wastes to be digested.

6. References

Acharya, B. K.; Mohana, S. & Madamwar, D. (2008). Anaerobic treatment of distillery spent wash-A study on upflow anaerobic fixed film bioreactor. *Bioresource Technology,* 99, 4621-4626

Aesseal Environmental Technology. (2003). Guide to Sealing the Chocolate Confectionery Industry, http://www.arthomson.com/Literature/brochures/MechSeals/AESSEAL/IndustrySealingGuides/L_UK_CHOC.pdf, Accessed: 10 September 2010

Akunna, J. C. & Clark, M. (2000). Performance of a granular-bed anaerobic ba.ed reactor (GRABBR) treating whisky distillery wastewater. *Bioresource Technology,* 74, 257-261

Altinbas, M.; Aydin, A. F.; Sevimli, M. F.; Ozturk, I. (2003). Advanced Oxidation of Biologically Pretreated Baker's yeast industry effluents for high recalcitrant COD and color removal. *Journal of Environmental Science and Health*, A38, 10, 2229-2240.

Antonopoulou, G.; Stamatelatou, K.; Venetsaneas, N.; Kornaros, M. & Lyberatos, G. (2008). Biohydrogen and methane production from cheese whey in a two-stage anaerobic process. *Industrial & Engineering Chemistry Research*, 47, 5227-5233

Anderson, G. K., Ozturk, I. & Saw, C. B. (1990). Pilot-Scale experiences on anaerobic fluidized-bed treatment of brewery wastes. *Water Science and Technology*, 22(9), 157-166.

Anderson, R. A. & Watson, S. A. (1982). The corn milling industry, In: *Handbook of Processing and Utilization in Agriculture*, Wolff, I. A. (Ed.), 31-78, CRC Press, ISBN: 0-8493-3872-7, Florida, USA

Austerman-Houn, U. & Seyfried, C.F. (1992). Anaerobic-aerobic wastewater treatment plant of a potato chips factory. *Water Science and Technology*, 26(9), 2065 – 2068

Aydin, A. F.; Ersahin, M. E.; Dereli, R. K.; Sarikaya, H. Z. & Ozturk, I. (2010). Longterm anaerobic treatability studies on opium alkaloids industry effluents. *Journal of Environmental Science and Health, Part A: Toxic / Hazardous Substances and Environmental Engineering*, 45(2), 192-200

Azbar, N.; Bayram, A.; Filibeli, A.; Muezzinoglu, A.; Sengul, F. & Ozer, A. (2010). A review of waste management options in olive oil production. *Critical Reviews in Environmental Science and Technology*, 34, 3, 209-247

Baspinar A.B. (2008). *Hydrogen Sulphide Removal from Biogas With Nitrate Coming from An Industrial Wastewater Treatment Plant*, M.Sc. Thesis, Istanbul Technical University, Istanbul

Batstone, D. J.; Keller, J.; Angelidaki, I.; Kalyuzhnyi, S. V.; Pavlostathis, S. G.; Rozzi, A.; Sanders, W. T. M.; Siegrist, H. & Vavilin, V. A. (2002). *Anaerobic Digestion Model No.1, Scientific and Technical Report No.13*, IWA Publishing, ISBN: 9781900222785, London

Beal, L. J. & Raman, D. R. (2000). Sequential Two-Stage Anaerobic Treatment of Confectionery Wastewater, *Journal of Agricultural Engineering Research*, 76, 2000, 211-217.

Bello-Mendoza, R. & Castillo-Rivera, M. F. (1998). Start-up of an anaerobic hybrid (UASB/Filter) reactor treating wastewater from a coffee processing plant. *Anaerobe*, 4, 219-225

Berardino, S. D.; Costa, S. & Converti, A. (2000). Semi-continuous anaerobic digestion of a food industry wastewater in an anaerobic filter. *Bioresource Technology*, 71, 2000, 261-266

Blanchard, P. H. (1992). *Technology of Corn Wet Milling and Associated Processes*, Elsevier, ISBN-10: 0-4448-8255-3, USA

Blonskaja, V.; Kamenev, I. & Zub, S. (2006). Possibilities of using ozone for the treatment of wastewater from the yeast industry. *Proceedings of the Estonian Academy of Sciences*, 55, 1, 29-39

Bural, C.B.; Demirer, G.N.; Kantoglu, O. & Dilek, F.B. (2010). Treatment of opium alkaloid containing wastewater in sequencing batch reactor (SBR)—Effect of gamma irradiation. *Radiation Physics and Chemistry*, 79, 519–526

Buyukkamaci, N. & Filibeli, A. (2002). Concentrated wastewater treatment studies using an anaerobic hybrid reactor. *Process Biochemistry*, 38, 2002, 771-775

Catalkaya, E. C. & Sengul, F. (2006). Application of Box-Wilson experimental design method for the photodegradation of bakery's yeast industry with UV/H_2O_2 and $UV/H_2O_2/Fe(II)$ process. *Journal of Hazardous Materials*, B128, 2006, 201-207

Ciftci, T. & Ozturk, I. (1995). Nine years of full-scale anaerobic-aerobic treatment experiences with fermentation industry effluents. *Water Science and Technology*, 32(12), 131-139

Cooley, A.M.; Wahl, E.D. & Fossum, G.O. (1964). Characteristics and amounts of potato wastes from various process stream, *Proceedings of the 19th Industrial Waste Conference*, pp. 379–390, Purdue University, West Lafayette, IN

CRAR (2009). *Corn Refiners Association 2009 Annual Report*,
     http://www.corn.org/CRAR2009.pdf. Accessed 10 August 2010

Del Nery, V.; Damianovic, M. H. Z. & Barros, F. G. (2001). The use of upflow anaerobic
     sludge blanket reactors in the treatment of poultry slaughterhouse wastewater.
     Water Science&Technology, 44, 4, 83-88

Dereli, R.K.; Ersahin, M.E.; Ozgun, H.; Ozturk, I. & Aydin, A.F. (2010). Applicability of
     Anaerobic Digestion Model No.1 (ADM1) for a Specific Industrial Wastewater:
     Opium alkaloid effluents. *Chemical Engineering Journal,* 165, 1, 89-94

Deshkar, A. M.; Saxena, K.L.; Charrabarti, T. & Subrahmanyam, P.V.R. (1982).
     Characterization and treatment of opium alkaloid processing wastewater. *IAWPC
     Tech. Annual.,* 9, 64–72

Dinsdale, R. M.; Hawkes, F. R. & Hawkes, D. L. (1997). Comparison of mesophilic and
     thermophilic upflow anaerobic sludge blanket reactors treating instant coffee
     production wastewater. *Water Research*, 31, 1, 163-169

Diwani, G. E.; Abd, H. E.; Hawash, S.; Ibiari, N. E. & Rafei, S. E. (2000). Treatment of
     Confectionery and Gum Factory Wastewater Effluent. *Adsorption Science and
     Technology*, 18, 9, 813-821

Duran-deBazua, C.; Sanchez-Tovar, S. A. ; Hernandez-Morales, M. R. & Bernal-Gonzalez, M.
     (2007). Use of anaerobic-aerobic treatment systems for maize processing
     installations: applied microbiology in action, In: *Communicating Current Research
     and Educational Topics and Trends in Applied Microbiology*, Mendez-Vilas, A., (Ed.), 3-
     12, Formatex, ISBN-13: 978-84-611-9422-3, Spain

Edwards, W. P. (2000). *The Science of Sugar Confectionery*, The Royal Society of Chemistry,
     ISBN: 0-85404-593-7, Cambridge, UK.

El-Gohary, F. A.; Nasr, F. A. & Aly, H. I. (1999). Cost-Effective Pre-treatment of Food-
     Procesing Industrial Wastewater. *Water Science and Technology,* 40, 7,17-24.

Eremektar, G. ; Karahan-Gul, O. ; Babuna, F. G. ; Ovez, S. ; Uner, H. & Orhon, D. (2002).
     Biological treatability of a corn wet mill. *Water Science and Technology*, 45, 12, 339–
     346

Ersahin, M. E.; Dereli, R.K; Ozgun, H.; Donmez, B.G.; Koyuncu, I.; Altinbas, M. & Ozturk, I.
     (in press). Source based characterization and pollution profile of a baker's yeast
     industry. *Clean-Soil Air Water*.

Ersahin, M. E. ; Insel, G. ; Dereli, R. K. ; Ozturk, I. & Kinaci, C. (2007). Model based
     evaluation for the anaerobic treatment of corn processing wastewaters. *Clean-Soil
     Air Water*, 35, 6, 576-581

Ersahin, M. E. ; Tezer, B. H. ; Ozturk, I. & Bilge, C. (2006). Pollution profile and waste
     minimization study for a corn processing industry. *Journal of ITU/e*, 16, 1-3, 25-35 (in
     Turkish)

EU 91/271/EEC. (1991). European Union Directive: Council Directive 91/271/EEC of 21
     May 1991 concerning urban waste-water treatment

Farhadian, M.; Borghei, M. & Umrania, V. V. (2007). Treatment of beet sugar wastewater by
     UAFB bioprocess. *Bioresource Technology*, 98, 3080-3083

Food and Agriculture Organization of The United Nations (FAOSTAT) (2008).
     http://faostat.fao.org/site/567/DesktopDefault.aspx?PageID=567#ancor,
     Accessed: 13 August 2010

Grover, R.; Marwaha, S. S. & Kennedy, J. F. (1999). Studies on the use of an anaerobic baffled
     reactor for the continuous anaerobic digestion of pulp and paper mill black liquors.
     Process Biochemistry, 39, 653-657

Gulmez, B.; Ozturk, I.; Alp, K. & Arikan, O. A. (1998). Common Anaerobic Treatability of Pharmaceutical and Yeast Industry Wastewater. *Water Science and Technology*, 38, 4-5, 37-44

Guttormsen, K.G. & Carlson, D.A. (1969). *Current Practice In Potato Processing Waste Treatment*, Water Pollution Research Series, Report No. DAST-14, Water Pollution Control Federation, U.S. Department of the Interior, Washington, DC

Hadjivassilis, I.; Gajdos, S.; Vanco, D. & Nicolaou, M. (1997). Treatment of wastewater from the potato chips and snacks manufacturing industry. *Water Science and Technology,* 36(2-3), 329–335

Hesse, M. (2002). *Alkaloids: Nature's Curse or Blessing?* Wiley – VCH, ISBN: 3-906390−24-1, Zurich

Howgrave-Graham, A. R.; Isherwood, H. I. & Wallis, F. M. (1994). Evaluation of two upflow anaerobic digesters purifying industrial wastewaters high in organic matter. *Water Science and Technology,* 29, 9, 225–229

Hung, Y.T.; Lo, H.H.; Awad, A. & Salman H. (2006). Potato wastewater treatment, in: *Waste Treatment in the Food Processing Industry*, Wang, L.K.; Hung, Y.T.; Lo, H.H. & Yapijakis C., (Eds.), 193–254, CRC Press, Taylor and Francis Group, ISBN: 0-8493-7236-4, Florida

Johns, M. R. (1995). Development in wastewater treatment in the meat processing industry: a review. *Bioresource Technology*, 54, 3, 203-216

Johnson, L. A. & May, J. B. (2003). Wet milling: the basis for corn biorefiners, In: *Corn Chemistry and Technology*, White P. J. & Johnson L. A., (Ed.), 449-494, American Association of Cereal Chemists Inc., ISBN: 1-891127-33-0, Minnesota, USA

Kalyuzhnyi, S.; Santos, L.E. & Martinez, J.R. (1998). Anaerobic treatment of raw and preclarified potato-maize wastewaters in a UASB reactor. *Bioresource Technology,* 66, 195–199

Kalyuzhnyi, S.; Gladchenko, M.; Starostina, E.; Shcherbakov, S. & Versprille, A. (2005). Combined biological and physico-chemical treatment of baker's yeast wastewater. *Water Science and Technology*, 52, 1-2, 175-181.

Krapivina, M; Kurissoo, T.; Blonskaja, V.; Zub, S. & Vilu, R. (2007). Treatment of sulphate containing yeast wastewater in an anaerobic sequence batch reactor. *Proceedings of the Estonian Academy of Sciences*, 56, 1, 38-52.

Leal, K.; Chacin, E.; Behling, E.; Gutierez, E.; Fernandez, N. & Forster, C. F. (1998). A mesophilic digestion of brewery wastewater in an unheated anaerobic filter. *Bioresource Technology*, 65, 51-55

Lettinga, G.; van Velsen, A. F. M.; Hobma, S. W.; de Zeeuw, W. & Klapwijk, A. (1980). Use of the upflow sludge blanket (USB) reactor concept for biological wastewater treatment, especially for anaerobic treatment. *Biotechnology and Bioengineering*, 22, 4, 699-734

Liang, Z.; Wang, Y.; Zhou, Y. & Liu, H. (2009). Coagulation removal of melanoidins from biologically treated molasses wastewater using ferric chloride. *Chemical Engineering Journal*, 152, 2009, 88-94

Linke, B. (2006). Kinetic study of thermophilic anaerobic digestion of solid wastes from potato processing. *Biomass and Bioenergy,* 30, 892–896

Moody, L. B. & Raman, D. R. (2001). A Dual-reactor Anaerobic system for Complete Treatment of a Food Processing Waste. *Journal of Agricultural Engineering Research*, 80, 3, 293-299

Mshandete, A.;Murto, M.; Kivaisi, A.K.; Rubindamayugi, M.S.T & Mattiasson, B. (2004). Influence of recirculation flow rate on the performance of anaerobic packed-bed bioreactors treating potato-waste leachate. *Environmental Technology*, 25, 929-936

Musluoglu, A. (2010). Biogas and energy recovery from industrial organic wastes, Frito Lay case study, *Proceedings of Compost and Renewable Energy Production from Organic Wastes Workshop (ORAK 2010)*, pp. 195–202, 08-09 June, Istanbul, Turkey (in Turkish).

Nacheva, P. M.; Chavez, G. M.; Chacon, J. M. & Chuil, C. (2009). Treatment of cane sugar mill wastewater in an upflow anaerobic sludge bed reactor. *Water Science and Technology*, 60, 5, 1347-1352

Orhon D.; Yıldız G.; Cokgor E. U. & Sozen, S. (1995). Respirometric Evaluation of the Biodegrability of Confectionery Wastewaters. *Water Science and Technology*, 32, 12, 11-19.

Ovez, S.; Eremektar, G.; Germirli-Babuna, F. & Orhon, D. (2001). Pollution profile of a corn wet mill. *Fresenius Environmental Bulletin*, 10, 12, 539-544

Ozdemir R.T. (2006). *Anaerobic Treatment of Opium Alkaloid Wastewater and Effect of Gamma-Rays on Anaerobic Treatment*, M.Sc. Thesis, Middle East Technical University, Ankara

Ozturk, I.; Altinbas, M. & Okten, H. E. (2001). *Performance Evaluation of Cargill Orhangazi Wastewater Treatment Plant*, Istanbul Technical University, Istanbul, Turkey (in Turkish)

Ozturk, I.; Ersahin, M. E. & Tezer, B. H. (2005). *Pollution Profile Report of Cargill Orhangazi Corn Processing Factory*, Istanbul Technical University, Istanbul, Turkey (in Turkish)

Ozturk, I. (2007). *Anaerobic Treatment and Applications*, Water Foundation Press, ISBN: 978-975-6455-30-2, Istanbul, Turkey (in Turkish)

Ozturk, I. & Altinbas, M. (2008). *The Project of Process Improvement in the Treatment Plant of Kent Food Factory*, Istanbul Technical University, Istanbul, Turkey.

Ozturk, I.; Aydin, A. F. & Koyuncu, I. (2008). *Technical Evaluation Report for Upgrading of Bolvadin Alkaloid Industry Wastewater Treatment Plant*, Istanbul Technical University, Istanbul, Turkey.

Ozturk, I.; Koyuncu, I.; Altinbas, M.; Ozgun, H.; Ersahin; M. E. & Dereli, R. K. (2010). Process and Pollution Profile of Pak Gida A.S. Facility and Evaluation of Treatment Plant Performance Report, Istanbul Technical University, Istanbul, Turkey.

Parawira, W.; Murto, M.; Read, J.S & Mattiasson, B. (2005). Profile of hydrolases and biogas production during two-stage mesophilic anaerobic digestion of solid potato waste. *Process Biochemistry*, 40, 2945–2952

Parawira, W.; Murto, M.; Zvauya, R. & Mattiasson, B. (2006). Comparative performance of a UASB reactor and an anaerobic packed-bed reactor when treating potato waste leachate. *Renewable Energy*, 31, 893–903

Parawira, W.; Murto, M.; Read, J. S. & Mattiasson B. (2007). A study of two-stage anaerobic digestion of solid potato waste using reactors under mesophilic and thermophilic conditions. *Environmental Technology*, 28, 1205-1216

Rajeshwari, K. V.; Balakrishnan, M.; Kansal, A.; Lata, K. & Kishore, V. V. N. (2000). State-of-the-art of anaerobic digestion technology for industrial wastewater treatment. *Renewable and Sustainable Energy Reviews*, 4, 135-156

Rittmann, B. E. & McCarty, P. L. (2001). *Environmental Biotechnology: Principles And Applications*. McGraw-Hill, ISBN: 0072345535, New York, The United States of America.

Ross, W. R.; Barnard, J. P.; Strohwald, N. K.; Grobler, C. J. & Sanetra, J. (1992). Practical application of the ADUF process to the full-scale treatment of maize-processing effluent. *Water Science and Technology,* 25, 10, 27-39

Sen, S. & Demirer, G. N. (2003). Anaerobic treatment of real textile wastewater with a fluidized bed reactor. *Water Research*, 37, 1868-1878

Senturk, E.; Ince, M. & Onkal Engin, G. (2010a). Kinetic evaluation and performance of a mesophilic anaerobic contact reactor treating medium-strength food-processing wastewater. *Bioresource Technology,* 101, 3970-3977

Senturk, E.; Ince, M. & Onkal Engin, G. (2010b). Treatment efficiency and VFA composition of a thermophilic anaerobic contact reactor treating food industry wastewater. *Journal of Hazardous Materials,* 176, 843–848

Sevimli, M. F.; Aydin, A. F.; Ozturk, I. & Sarikaya, H. Z. (2000). Evaluation of the alternative treatment processes to upgrade an opium alkaloid wastewater treatment plant. *Water Science and Technology*, 41(1), 223-230

Sevimli, M. F.; Aydin, A. F.; Sarikaya, H. Z. & Ozturk, I. (1999). Characterization and treatment of effluent from effluent from opium alkaloid processing wastewater. *Water Science and Technology*, 40(1), 23-30

Somasiri, W.; Li, X. F.; Ruan, W. Q. & Jian, C. (2008). Evaluation of the efficacy of upflow anaerobic sludge blanket reactor in removal of colour and reduction of COD in real textile wastewater. *Bioresource Technology*, 99, 3692-3699

Speece, R. E. (1996). *Anaerobic Biotechnology for Industrial Wastewaters*, Archae Press, ISBN: 0-9650226-0-9, USA

Tchobanoglous, G.; Burton, F. L. & Stensel, H. D. (2003). *Wastewater Engineering Treatment and Reuse*, Metcalf and Eddy, Inc., 4th ed. Revised, Mc-Graw-Hill, ISBN: 0-07-041878-0, New York, USA

Timur, H. & Altinbas U. (1997). Treatability studies and determination of kinetic parameters for a high-strength opium production wastewater. *Environmental Technology,* 18, 339-344

Wang, R.; Wang, Y.; Ma, G.; He, Y. & Zhao, Y. (2009). Efficiency of porous burnt-coke carrier on treatment of potato starch wastewater with an anaerobic–aerobic bioreactor. *Chemical Engineering Journal*, 148, 35–40

Xiangwen, S.; Dangcong, P.; Zhaohua, T. & Xinghua, J. (2008). Treatment of brewery wastewater using anaerobic sequencing batch reactor (ASBR). *Bioresource Technology*, 99, 3182-3186

Yilmaz, G. & Ozturk, I. (1995). The effect of anaerobic pre-treatment on the inert soluble COD of fermentation industry effluents. *Water Science and Technology,* 32, 12, 35-42

Yilmazer, G. & Yenigun, O. (1999). Two-phase anaerobic treatment of cheese whey. *Water Science and Technology*, 40, 1, 289-295

Zhang, W.; Xie, Q.; Rouse, J. D.; Qiao,S. & Furukawa, K. (2009). Treatment of high-strength corn steep liquor using cultivated Polyvinyl alcohol gel beads in an anaerobic fluidized-bed reactor. *Journal of Bioscience and Bioengineering*, 107, 1, 49–53

Removal of Endocrine Disruptors in Waste Waters by Means of Bioreactors

Nadia Diano and Damiano Gustavo Mita

Department of Experimental Medicine, Second University of Naples,
Via S. M. di Costantinopoli 16, 80138 Naples
Institute of Genetics and Biophysics, CNR, Via Pietro Castellino,
111, 80131 Naples
National Institute of Biostructures and Biosystems (INBB),
Viale Medaglie d'Oro, 305, 00136 Rome
Italy

1. Introduction

The presence of Endocrine Disrupting Chemicals (EDCs) represents an area of concern in the environmental field. An EDC is defined as "an exogenous substance that causes adverse health effects in an intact organism, or its progeny, in consequence to the induced changes in endocrine functions" (EU Commission, 1996). A large number of chemical compounds have been recognized as EDCs. Among these, natural and synthetic steroid hormones, phytoestrogens, alkylphenols, phthalates, pesticides, surfactants and polychlorinated biphenyls (Soto et al., 1995, Jobling et al., 1995; Routledge & Sumpter, 1997). EDCs are not defined on the basis of their chemical nature, but by their biological effects. They exhibit agonistic or antagonistic properties depending on the kind of interaction with the receptors. As estrogenic receptors have similar structure between different animals, including humans, EDCs can affect the endocrine functions of many living species. The main mechanisms through which they interfere with the endocrine system are: i) the simulation of the activities of physiological hormones, thereby participating in the same reactions and causing the same effects; ii) the inactivation, with competitive action, of hormone receptors and, consequently, the neutralisation of their activity; iii) the interference with the synthesis, transport, metabolism and secretion of natural hormones, altering their physiological concentrations and therefore their corresponding endocrine functions.
EDCs enter the environment from a variety of sources, such as effluent discharge pipes, agricultural runoff, landfills, atmospheric deposition and aerosols (Campbell et al., 2006). In particular aquatic ecosystems have been studied for the effect of wastewater treatment plant (WWTP) effluents, which are continuously discharged to the receiving water bodies (Jobling et al., 1998; Routledge et al., 1998; Tilton et al., 2002). Due to their incomplete removal during the waste treatment process, synthetic and natural estrogens are considered as the major responsible for the estrogenic activity associated with WWTP effluents (Gutendorf & Westendorf, 2001). So natural steroid hormones and the synthetic ethynylestradiol, alkylphenols, bisphenol A and phthalates are EDCs identified in sewage effluents (Desbrow

et al., 1998; Körner et al., 2000; Lye et al., 1999; Spengler et al., 2001). In consequence reproductive disorders and feminization of fish populations are alarming signs of endocrine disruption. Adverse effects have been also observed in humans, such as the increasing number of endocrine responsive cancers and the decreasing reproductive fitness of men (Daston et al., 1997).

Owing to these noxious effects remediation processes are requested in order to remove these pollutants. Conventional approaches (e.g. landfilling, recycling, pyrolysis and incineration) to the remediation of contaminated sites are inefficient and costly and can also lead to the formation of toxic intermediates (Dua et al., 2002; Spain et al., 2000). Thus, biological decontamination methods are preferable because whole microorganisms or enzymes degrade numerous environmental pollutants without producing toxic intermediates (Furukawa, 2003; Pieper & Reineke, 2000).

To reduce the harmful effects due the EDCs presence in aqueous systems we will report here in the following some our results obtained with a biotechnological approach based on their enzymatic bioremediation as an alternative technology to the classical membrane processes.

In particular our attention will be focused on the bioremediation of Bisphenol A (BPA) and some of its congeners, such as Bisphenol B (BPB), Bisphenol F (BPF) and Tetrachlorobisphenol A (TCBPA), taken as model of EDCs of phenolic origin, and of Dimethylphthalate (DMP), taken as model of phthalates.

Bisphenol A (BPA) is an industrial raw material for polycarbonate and epoxy resins, unsaturated polyester-styrene resins and flame retardants. The final products are used as coatings on cans, powder paints, additives in thermal paper and in dental fillings, and as antioxidants in plastics. Several studies demonstrated that BPA is an EDC. It mimics or interferes with the action of endogenous hormones (Gaido et al. 1997; Kim et al. 2001; Krishnan et al. 1993; Matthews et al. 2001; Synder et al. 2003; Tinwell et al. 2000), causing adverse alterations in reproductive and developmental processes as well as metabolic disorders. Like BPA, also BPB, BPF and TCBPA are used as materials for epoxy resins and polycarbonates lining large food containers and water pipes. Coatings can also be made from mixtures of BPA congeners. All show estrogenic activity, but the activities varied markedly from compound to compound (Kitamura et al., 2005).

Phthalates are plasticizers used in polymer industry to improve their flexibility, workability and handling properties. They are used in films, in tubing, in liners of bulk liquid holding tanks or in conveyor belt material (Kirkpatrick et al., 1989). Phthalates, as bisphenols, are not bound chemically in the plastics and can consequently migrate into food that comes into contact. The presence of phthalates in packaging materials and their migration into packaged foods have been confirmed by a number of authors (Castle et al., 1988; Nerin et al., 1993; Page & Lacroix, 1992; Petersen, 1991).

This chapter has been written in order to promote the technology of waste bioremediation by means of bioreactors, in particular with our innovative process based on non-isothermal bioreactors. To this aim some of our published results have been selected and discussed. New perspectives will be also indicated.

2. Bioremediation versus remediation

For problems of water treatment in ecosystems the traditional membrane-based processes are not useful since they alter the life conditions. Ultrafiltration and reverse osmosis, for example, allow endocrine disruptors removal, but since the filtrate consists in pure water its

intake in the ecosystem alters the concentrations of salts and bioelements necessary for the life. On the contrary, the selective removal of endocrine disruptors by enzyme treatment (bioremediation) appears more suitable, since the treatment is effective only towards the target harmful chemical remaining unchanged the other components present in the water. For this reason to bioremediate polluted waters in small ecosystems we propose, in place of reactors, the use of bioreactors, i.e. reactors where a biological element is operating. In particular we have suggested the use of non-isothermal bioreactors (Attanasio et al., 2005; Diano et al., 2007; Durante et al., 2004; Georgieva et al., 2008; Georgieva et al., 2010; Ignatova et al., 2009; Mita et al., 2010). With these apparatuses we have found that 1°C of temperature difference across the catalytic membrane increases the enzyme reaction rate from 30% to 80% in comparison to the same reaction rate measured under comparable isothermal conditions. The increase of enzyme activity has been found to depend upon: i) the substrate concentration, ii) the average temperature in the bioreactor, and iii) the temperature difference across the catalytic membrane. The main advantage on using non-isothermal bioreactors is the reduction in the treatment times that is proportional to the size of the temperature difference applied across the catalytic membrane.

3. The catalytic systems

Laccase from *Trametes Versicolor* and tyrosinase from mushroom have been employed to biodegrade the phenol compounds, whereas Lipase from *Candida Rugosa* for removing the phthalates.
Laccase and tyrosinase were immobilized on polyacrylonitrile (PAN) beads employed into a fluidized bed bioreactor working under isothermal conditions.
Lipase was immobilized on a Polypropylene (PP) membrane from GE Osmonics (GE Labstore-Osmonics, Minnetonka, Minnesota), with a thickness of 150 µm and a nominal pore diameter of 0.22 µm. When made catalytic, the membrane was employed in a planar membrane reactor working under isothermal or non-isothermal conditions.

3.1 Carrier functionalitation
3.1.1 PAN bead preparation and activation
PAN powder (18 g), $LiNO_3$ (1 g) and glycerin (3 g) were dissolved in 78 mL of dimethylformamide. The homogenized mixture was pipetted and precipitated in water. The beads obtained were water-washed and immersed for 24 hr in a 30% (v/v) glycerin aqueous solution. After this step the beads were dried in an oven at 70°C for a time sufficient to reach a constant weight.
20 cm³ (12 g) of PAN beads were activated at 50°C for 60 min by treatment with 15% (w/v) NaOH aqueous solution. After washing in distilled water, the beads were treated with a 10% (v/v) aqueous solution of 1,2-diaminoethane (15 mL) at room temperature for 60 min. Then the beads were washed once more in distilled water.

3.1.2 Polypropylene membrane activation
Polypropylene is a non-polar material that lacks reactive groups for enzyme immobilization. Consequently, functional groups have been created on the PP membrane by means of a plasma reactor. Plasma was powered by a mixture of acrylic acid (Sigma–Aldrich, 99%) and He according to the ratio of 3:20 sccm (standard cubic centimetres per minute). The experimental conditions (power = 80W, pressure = 400 mTorr, time = 10min) gave rise to a

very stable coating on the membrane, showing the following abundance of reactive groups: COOH< CO<COH< CC.

3.2 Immobilization techniques
3.2.1 Laccase immobilization

Laccase immobilization was carried out through a diazotation process, involving the phenolic group of tyrosine residues far from the catalytic site. The PAN beads were treated at room temperature for 1 hr with a 2.5% (v/v) glutaraldehyde (GA) aqueous solution (15 mL). GA was used as the coupling agent. After washing at room temperature with double distilled water, the beads were treated, at room temperature for 90 min, with a 2% (w/v) Phenylendiamine (PDA) solution in 0.1 M sodium carbonate buffer, pH 9.0. PDA was used to obtain aminoaryl derivatives on the supports. Once water-washed, the beads were treated at 0°C for 40 min with an aqueous solution containing 2M HCl and 4% $NaNO_2$. At the end of this treatment, the beads were washed at room temperature in 0.1 M citrate buffer solution, pH 5.0, and then treated at 4 °C for 16 hr with the same buffer solution containing laccase at concentration of 3 mg/mL. At the end, in order to remove the unbound enzymes, the beads were washed in 0.1 M citrate buffer solution, pH 5.0.

The amount of immobilized enzyme was determined by measuring, through the Lowry protein assay method (Lowry et al. 1951), the initial and final concentrations of protein in the solution used for the immobilization and taking into account also the protein amount found in the washing solutions. Under the experimental conditions reported above, and using 12g (20 cm^3) of activated PAN beads, the amount of immobilized laccase resulted to be 3.56±0.40 mg. When not used, the beads were stored at 4°C in 0.1 M citrate buffer pH 5.0.

3.2.2 Tyrosinase immobilization

Tyrosinase was immobilized by using glutaraldehyde in a condensation process involving its NH_2-groups. For this purpose, the PAN beads were treated at room temperature for 1 hr with a 2.5% (v/v) GA aqueous solution (15 mL). After washing at room temperature, the beads were incubated at 4°C for 16 hr in a 0.1M phosphate buffer solution, pH 6.5, containing tyrosinase at concentration of 3 mg/mL. At the end of this step, in order to remove the unbound enzyme, the beads were washed in the phosphate buffer solution. The amount of immobilized tyrosinase, measured by Lowry protein assay method, resulted to be 3.21±0.60 mg. When not used, the beads were stored at 4°C in 0.1M phosphate buffer pH 6.5.

3.2.3 Lipase immobilization

Lipase was immobilized on the activated PP membrane through a diazotation process involving the phenolic groups of tyrosine residues. This procedure was chosen because the tyrosine residues are far from the catalytic site. To generate aminoaryl derivatives on the plasma activated PP membranes, the membranes were treated for 90 min with a 2% (w/v) PDA aqueous solution of 0.1M sodium carbonate buffer, pH 9.0. Later, the membranes were washed with double distilled water. The obtained aminoaryl derivatives were treated for 40 min at 0°C with an aqueous solution containing 4% (w/v) $NaNO_2$ and 2M HCl, in a ratio of 1:5. At the end of this treatment the membranes were washed at room temperature in a buffer solution (0.1M phosphate, pH 7.0), and then treated for 16 h at 4°C with 30mL of the same buffer solution containing 20mg/mL of enzyme power. After this step the membranes were washed with 0.1M phosphate buffer, pH 7.0, to remove the material not bound. Under

the experimental conditions above reported, the amount of immobilized protein on PP membranes, measured by Lowry protein assay method, was 3.26±0.2 mg. When not used, the membranes were stored at 4°C in 0.1M phosphate buffer pH 7.0.

4. The bioreactors

4.1 The fluidized bed bioreactor

A fluidized bed reactor (Figure 1) was used for the continuous removal of the single bisphenols from the buffered solution by laccase or tyrosinase immobilized on PAN beads. The bed reactor was constituted by a polystyrene pipe (1.7 cm inner diameter, 20 cm length) packed with 12 g ($20cm^3$) of PAN catalytic beads. The bioreactor was fed with 40 mL of bisphenols substrate solution, at concentration 1mM and thermostated at 25°C, recirculating at a flow rate of 140 mL/min by means of a peristaltic pump.

The amount of enzymatic degradation was calculated after 90 min of enzyme treatment considering the initial and final bisphenols concentration in the reaction solution.
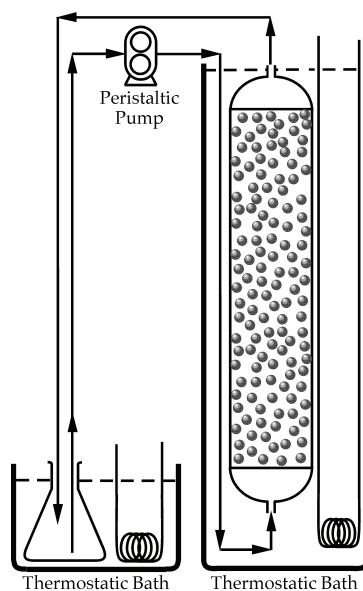
Fig. 1. Schematic (not to scale) representation of the fluidized bed bioreactor.

4.2 The planar membrane bioreactor

The bioreactor (Figure 2a) consists of two metallic flanges in each of which it is bored a shallow cylindrical cavity, 70 mm in diameter and 2.5 mm depth, constituting the working volume filled with the aqueous solutions containing BPA. The catalytic membrane is clamped between the two flanges so as to separate and, at the same time, to connect the solutions filling the half-cells. Solutions are circulated in each half-cell by means of two peristaltic pumps through hydraulic circuits starting and ending in a common glass container. By means of independent thermostats, the two half-cells are maintained at predetermined temperatures. Thermocouples, placed 1.5 mm away from the membrane

surfaces, measure the local temperature of the solutions in each half-cell. These measures allow the calculation of the temperature profile into the whole bioreactor and across the catalytic membrane.
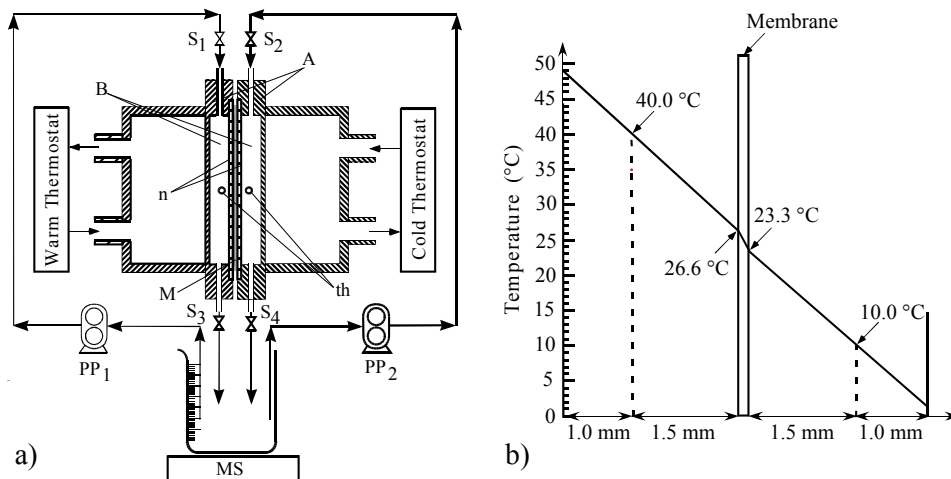
Fig. 2. a) Schematic representation of the planar bioreactor. Half-cells (A); internal working volumes (B); membrane (M); supporting nets (n); thermocouples (th); stopcocks (Si); thermostatic magnetic stirrer (MS); peristaltic pumps (PPi); b) Temperature profile in a non-isothermal bioreactor under the following experimental conditions: $\Delta T=30°C$, $T_{av}=25°C$.

To estimate the real effects of temperature gradients on the activity of immobilized enzymes, the actual temperatures on the surfaces of the catalytic membrane (T_W^* and T_C^*) must be known. The subscripts "w" and "c" stay for warm and cold side, respectively. Being impossible to measure the temperatures on each membrane face, these were calculated from those measured at the position of the thermocouples (T_W and T_C), because the solution motion in the two half-cells was laminar. Indeed, in each half-cell the solution motion is constrained by two fins with rounded tips, at a flow rate of 3.5 mL min^{-1}. Under these conditions, the Reynolds number Re is lower than Re^{crit}, being Re lower than 10 (Diano et al., 2000). It follows that heat propagation through the bioreactor occurs by conduction between isothermal liquid planes perpendicular to the direction of the heat flow. By knowing the thermal conductivities and thickness of both filling solutions and membrane (Lide 1990; Touloukian 1970), it is possible to calculate the temperatures on the membrane surfaces by means of the heat flux continuity principle. It was found that the correlation between the temperatures read at the thermocouple positions, T, and the ones on the surfaces of the catalytic membranes, T*, is given by:

$$\begin{cases} T_w^* = T_w - a\Delta T \\ T_c^* = T_c + b\Delta T \end{cases} \qquad (1)$$

where a and b are numerical constants. Being our system symmetric, a=b and, hence

$$\Delta T^* = (1-2a)\ \Delta T = const\ \Delta T \qquad (2)$$

$$T_{av} = \frac{T_W + T_C}{2} = T_{av}^* = \frac{T_W^* + T_C^*}{2} \tag{3}$$

T_{av} and T_{av}^* being the average temperatures of the bioreactor and membrane, respectively. With the PP membrane, we have found a = b = 0.445 and therefore $\Delta T^* = 0.11\ \Delta T$. It follows that in non-isothermal experiments $T_W^* < T_W$; $T_C^* > T_C$; and $\Delta T^* < \Delta T$. Figure 2b shows the actual temperature profile in the bioreactor, when $T_W = 40°C$ and $T_C = 10°C$, i.e. under the conditions $\Delta T = 30°C$ and $T_{av} = 25°C$.

The functioning of this bioreactor is based on the application of the process of thermodialysis (Mita et al., 1992; Gaeta et al., 1992; Diano et al., 2000). Thermodialysis is the selective matter transport across a hydrophobic porous membrane separating two thermal solutions maintained at different temperatures. The driving force is the differential radiation pressure associated to the heat flux acting on the solvent and on the solute particles confined in the membrane pores. Each pore constitutes a microscopic Soret cell into which a modified thermal diffusion occurs, the modifications being on the water structure owing to its interaction with the pore walls.

When all fluxes (water and solutes) are allowed, as in Figure 3 where is illustrate the case of a two components solution, three matter fluxes are observed: a macroscopic volume flux, J_{vol}, from the warm to the cold side of the reactor; a drag solute flux, $J_{S,\ drag}$, associated to the volume flux, and a thermodiffusive solute flux, generally from the cold to the warm side.
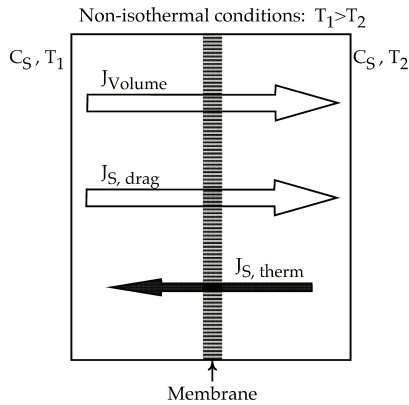
Non-isothermal conditions: $T_1 > T_2$

Fig. 3. Water and solutes fluxes

The expressions for each of the three fluxes are:

$$J_{vol} = \frac{cm^3}{cm^2 s} = D_{H_2O}^* \frac{\Delta T}{\Delta x} \tag{4}$$

$$J_{S,drag} = \frac{mol}{cm^2 s} = \sigma\, J_{vol} C_s \tag{5}$$

$$J_{S,th} = \frac{mol}{cm^2 s} = D_{th}^* C_s \frac{\Delta T}{\Delta x} \tag{6}$$

where, ΔT is the temperature difference measured in the two half cell, Δx is the membrane thickness, C_S is the solute concentration expressed in moles cm^{-3}, σ is a Staverman coefficient related to selectivity of the membrane, $D^*_{H_2O}$ and D^*_{th} are the modified thermal diffusion coefficients, in cm^2 s^{-1} K^{-1}, for water and solute, respectively. If the solute is an appropriate pollutant, the enzymes immobilized on the membrane in the unit of time will encounter a number of substrate molecules higher than that encountered under the isothermal condition, where alone isothermal diffusion occurs, so that the enzyme reaction rate in the former case is increased in respect to the latter case in a manner proportional to the size of the temperature gradient.

5. Bioremediation quantification

The quantification of pollutant removal, and hence the enzyme reaction rate, is followed by measuring during the time by HPLC the changes in the substrate concentration in the common glass container. To show the followed methodology in Figure 4 two typical experimental models of pollutant degradation are reported.
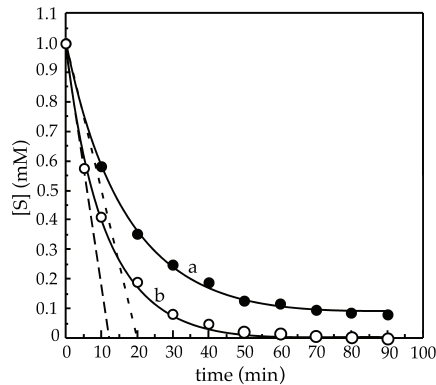
Fig. 4. Pollutant concentration decreases as function of time.

In particular curve "a" represents the case in which the enzyme activity, after a certain time, is inhibited by the substrate concentration or by a "suicide" effect. Curve "b", instead, represents the case in which enzyme inhibition does not occur. In the figure the pollutant concentration, expressed in mM, is reported as a function of time. Curve "a" is represented by an analytical expression given by:

$$C(t) = C_\infty + (C_0 - C_\infty)\ e^{-kt} \tag{7}$$

where C_∞ and C_0 are the BPA concentrations at $t=\infty$ and $t=0$, respectively, and k is a time constant (min^{-1}) related to the rate by which the enzyme reaction occurs. Curve "b" is expressed by the expression:

$$C(t) = C_0\ e^{-kt} \tag{8}$$

In both cases, the initial reaction rate, measured as µmoles min^{-1}, is obtained from the value of $\left(\dfrac{dC}{dt}\right)_{t=0}$ multiplied by the solution volume in which the enzyme reaction is occurring.

When, instead, the pollutant decrease is linear, as it will be seen in the case of phthalates, the $\left(\dfrac{dC}{dt}\right)_{t=0}$ is coincident with the slope of the line best fitting the experimental results.

The removal efficiency (RE$_t$) at any time "t" is obtained in percentage by the expression:

$$RE_t(\%) = \frac{C(t) - C_0}{C_0} x100 \tag{9}$$

6. Results

6.1 With the fluidized bed bioreactor

In order to determine the catalytic power of the catalytic PAN beads towards the single bisphenols, it has been investigated the rate of removal of each bisphenol at a concentration 1 mM in citrate buffer at pH 5.0 and at T=25°C. 1 mM was chosen considering that this concentration is higher than the effective concentrations in ecosystems (see log K_{ow} in the Table 1) and that the enzyme removal rate of a substrate decreases with increase of the substrate concentration. This means that the observed effects at 1 mM concentration are lower than those observable at smaller (and more natural) concentrations. Indeed, in the literature BPA measurements showed low concentrations: from 0.0005 to 0.41 mgL^{-1} in surface water, from 0.018 to 0.702 mg L^{-1} in sewage effluents, from 0.01 to 0.19mg kg^{-1} in sediments and from 0.004 to 1.363 mgkg^{-1}dw in sewage sludge. Measured concentrations of BPF result lower than those of BPA in all environmental media.
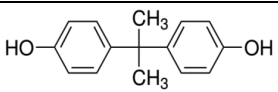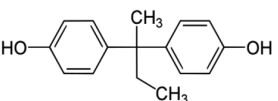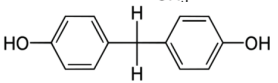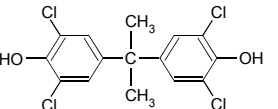
Substrate	Structural formula	Molecular weight	Water solubility	Log K_{ow}
BPA		228.29 g/mol	280 mg L^{-1}	3.32
BPB		242.31 g/mol	220 mg L^{-1}	3.90
BPF		200.23 g/mol	360 mg L^{-1}	3.06
TCBPA		366.07 g/mol	200 mg L^{-1}	4.02

Table 1. Schematic representation of the structure of studied bisphenols and some of their chemical and physical characteristics.

In Figure 5 the decreases of BPA, BPB, BPF and TCBPA concentrations are reported as function of time when immobilized laccase (●) or tyrosinase (○) are used. The substrate concentrations decrease with the enzyme treatment time following an exponential curve of

the type $C(t) = C_0\ e^{-kt}$, where C(t) and C_0 are the pollutant concentration at t and zero time, and k (min⁻¹) is a rate constant which depends on the C_0 value or, better, on the ratio between substrate molecules and available enzyme active sites.
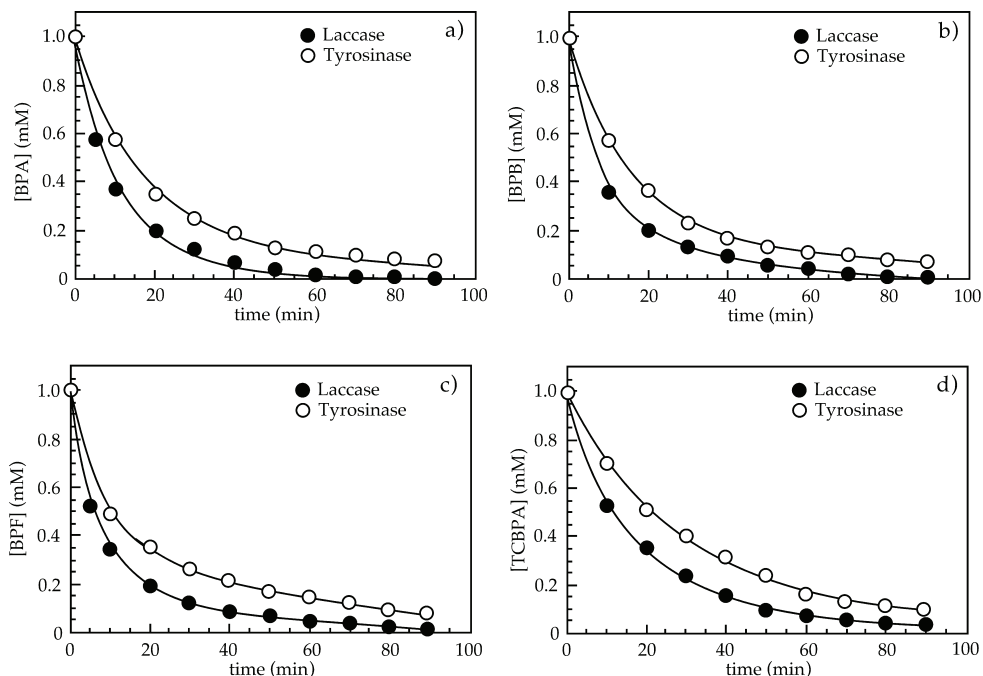
Fig. 5. Decreases of pollutant concentration as function of time. (●) laccase; (○) tyrosinase. The k values for each substrate are reported in Table 2.

Substrate	Laccase			Tyrosinase		
	k (min⁻¹)	τ_{50} (min)	RE₉₀ (%)	k (min⁻¹)	τ_{50} (min)	RE₉₀ (%)
BPA	0.087	8.0	100	0.059	13.0	92
BPB	0.083	7.5	100	0.054	13.4	93
BPF	0.117	5.0	100	0.070	10.0	94
TCBPA	0.057	11.5	96	0.033	21.0	91

Table 2. Rate constant (k), τ_{50} and removal efficiency (RE₉₀) of laccase and tyrosinase immobilized on PAN beads towards the studied bisphenols.

The k values relative to BPF, BPA, BPB and TCBPA have been found to decrease in this order, from 0.117 to 0.057 min⁻¹ for laccase and from 0.070 to 0.033 min⁻¹ for tyrosinase. For each pollutant the k values of laccase are higher than the corresponding values of tyrosinase. The k values for tyrosinase follow the same order than those found for laccase.

Moreover, looking at the results in Figure 5, two other efficiency factors can be calculated: τ_{50} and RE₉₀. τ_{50} is the time required to obtain, under our experimental conditions, the 50% of

substrate biodegradation. The obtained τ_{50} and RE_{90} values are also listed in Table 2. By comparing the time to obtain the 50% of initial concentration reduction, it is interesting to observe that by using the tyrosinase that time is quite doubled compared to that calculated for the laccase. Also interesting is the observation that, at least under our experimental conditions, 90 min of treatment with the enzyme laccase are sufficient to obtain the complete biodegradation of BPA, BPB and BPF. For TCBPA, a 96% reduction of its initial concentration has been calculated. Instead, 90 min of treatment with the enzyme tyrosinase are sufficient to obtain a biodegradation of all substrates near 90%.

Additionally, for both enzymes, the BPF is the substrate towards which the enzymes have the greatest biodegradation ability. In any case the biodegradation power of both enzymes is interesting for practical application.

6.2 With the planar membrane bioreactor

As reported in the introduction, lipase from *Candida rugosa* was used to biodegrade DMP. Lipase, like the other esterases, catalyses the hydrolysis and transesterification of ester groups. However, while esterases act on water soluble substrates, lipases catalyse reactions of water insoluble substrates. The presence of a water/lipid mixture is an essential prerequisite for an efficient catalysis reaction.

According to scheme 1, DMP hydrolysis by lipase may involve both methyl groups getting phthalic acid (PA) and two molecules of methanol, or may cause the rupture of a single bond thus producing monomethylphthalate (MMP) and methanol.

Scheme 1. Possible mechanism of DMP oxidation.

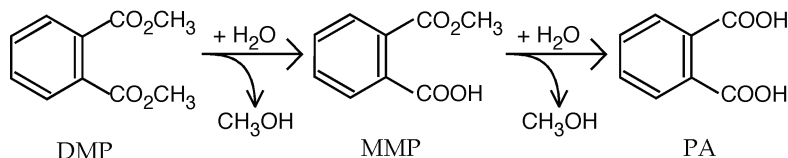To ascertain the mechanism involving our enzyme, preliminary experiments have been carried out using MMP as substrate. It was found that our lipase did not catalyze this substrate, at least in any detectable amount after four hours of incubation. Incidentally it is important to stress the circumstance that MMP does no exhibit the same toxicological properties of DMP, as found by us with the MTT test, a rapid and sensitive method for screening the assessment of cytotoxicity of materials.

In each experiment, after the first ten minutes, subsequent points indicate that the sum of the moles of substrate and reaction product give a constant value equal to the initial value of DMP moles, as the stoichiometry of the reaction is 1:1 (Scheme 1 and Fig. 6). However, this sum is lower by about 10% with respect to the moles corresponding to the initial value of the substrate concentration. This difference is attributed to an initial substrate adsorption on either the membrane or the tubing of the hydraulic circuits. This percentage lost of DMP was constant in each experiment performed, regardless of the initial DMP concentration values. It must be noted that the bioreactor with the catalytic membrane was washed after each run with the 0.1 M phosphate buffer, pH 7.0.

The enzyme activity, expressed as μmoles min^{-1}, is given by the slope of the lines that best fit the experimental points showing the decrease in DMP moles or the increase in MMP moles. No significant differences were found in the two calculations. Just to give an example for the
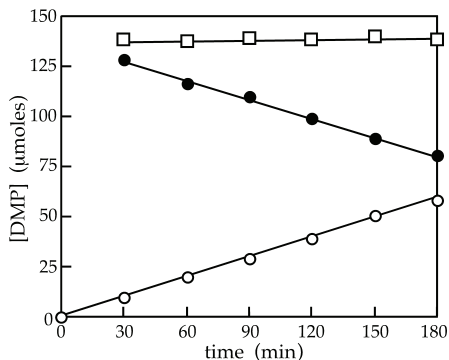
Fig. 6. Variation of DMP (○), MMP (●) and DMP + MMP (□) in function of time.

followed methodology in Figure 6 it has been reported the case of an experiment carried out with a 5 mM DMP initial solution. The DMP concentration has been converted in μmoles by multiplying the measured concentration for the volume of the treated solution.

We now examine the behaviour of the catalytic membranes in the presence of temperature gradients. Figure 7 shows the results obtained under non-isothermal conditions by varying the DMP concentration from 1 to 15 mM. For comparison, the data obtained under isothermal conditions ($\Delta T=0$) have also been added.
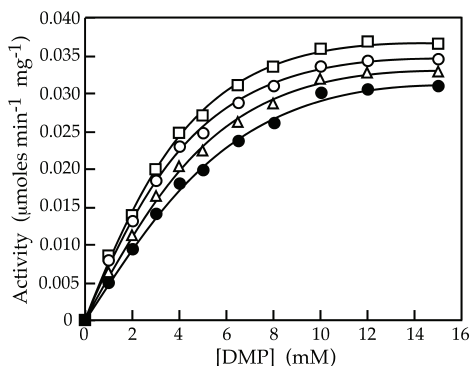
Fig. 7. Enzyme activity as function of DMP concentration. $T_{av}=25°C$. ●:$\Delta T=0°C$; Δ:$\Delta T=10°C$; ○:$\Delta T=20°C$; □:$\Delta T=30 °C$.

Data in figure indicate that: i) the dependence of the reaction rate on the substrate concentration shows a behaviour described by a Michaelis-Menten equation either under isothermal or non-isothermal conditions; ii) for each DMP concentration the reaction rate under non-isothermal conditions is higher than the corresponding reaction rate under isothermal conditions; iii) at each substrate concentration, the reaction rate increases with the increase in the applied ΔT. From the curves in Figure 7, the kinetic parameters reported in Table 3 have been calculated. These values show that: i) the K_m values obtained under non-isothermal conditions are lower than those obtained under the corresponding isothermal condition, thus demonstrating that the non-isothermal conditions increase the affinity of immobilized lipase for DMP; ii) under non-isothermal conditions the V_{max} values

for the immobilized lipase increase with the increase in the value of ΔT, compared to those obtained under isothermal conditions, and approach the value (0.063 μmoles min^{-1}mg^1 of enzyme) obtained for the free enzyme in the course of another experimentation (private communication), thus proving the effectiveness of non-isothermal bioreactors.

T_{av} (°C)	ΔT(°C)	K_M (mM)	V_{max} (μmoles min^{-1} mg^{-1} of enzyme)
	0	5.5	0.031
	10	5.1	0.033
25	20	4.7	0.035
	30	4.2	0.037

Table 3. Kinetic parameters calculated at T_{av}=25°C and ΔT=0, 10, 20, 30°C.

As reported in the section 4.2, the obtained results are explained by considering that, in the presence of a temperature gradient, the immobilized enzymes in the unit of time "encounter" more substrate molecules, since additional thermodiffusive fluxes add to the diffusive ones (Diano et al., 2000). This means that under non-isothermal conditions the immobilized enzymes "see" in the microenvironment around the catalytic site a substrate concentration that is higher than in the bulk solution. This is a new kind of "partitioning effect" that is related to the presence of the temperature gradient.

Let us consider again Figure 7 where it is possible to observe that at each DMP concentration the enzyme reaction rate increases with the increase of the size of the applied temperature gradient. To verify the type of dependence, it is appropriate to plot, at each substrate concentration, the enzyme reaction rate as a function of the applied ΔT. This has been done, as one example, in Figure 8 for the case of 5 mM DMP. From this figure, it is possible to observe that the lipase catalytic activity linearly increases with the applied ΔT. The best line interpolating the experimental points is described by the equation:

$$y_{\Delta T \neq 0}\left(T_{av}\right) = y_{\Delta T = 0}\left(T_{av}\right)\left(1 + \frac{\alpha}{100}\Delta T\right) \tag{10}$$

where $y_{\Delta T \neq 0}(T_{av})$ and $y_{\Delta T = 0}(T_{av})$ are the catalytic activity values measured under non-isothermal ($\Delta T \neq 0$) or isothermal ($\Delta T = 0$) conditions, respectively, at a fixed value of T_{av}. From the above equation one obtains:

$$\alpha = \frac{y_{\Delta T \neq 0}\left(T_{av}\right) - y_{\Delta T = 0}\left(T_{av}\right)}{y_{\Delta T = 0}\left(T_{av}\right)}\frac{100}{\Delta T} = \frac{P.A.I.}{\Delta T} \tag{11}$$

where the α coefficient (%, °C^{-1}) represents the Percentage Activity Increase (P.A.I.), when a macroscopic temperature difference ΔT=1°C is read at the position of the thermocouple.

Following the procedure described above, the values of the P.A.I., calculated for each substrate concentration, have been reported in Figure 9a as a function of DMP concentration. The curve parameter is the applied ΔT. Figure 9a shows that the P.A.I. values decrease with the increase in substrate concentration. This is explained by considering that when the immobilized enzyme works at substrate concentrations close to saturation, the addition of further substrate fluxes driven by the temperature gradients is less effective in increasing the enzyme activity. Alternately, when the enzymes work at low concentrations, far from the saturation value, any additional substrate flux effectively increases the enzyme activity.
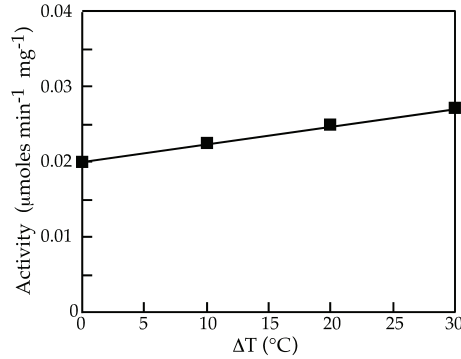
Fig. 8. Activity in function of temperature gradient ΔT.
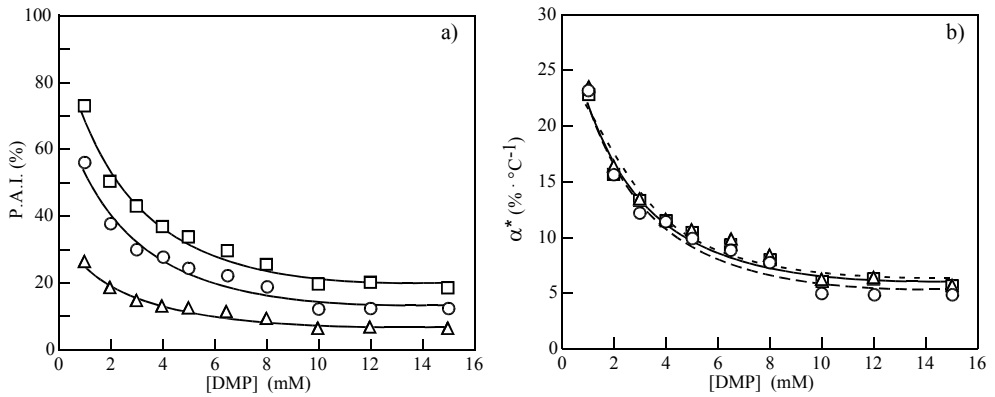
Fig. 9. (a): Percentage Activity Increase in function of DMP concentration. (b): α* coefficient in function of DMP Concentration. Symbols: Δ: ΔT=10°C; O: ΔT=20°C; □: ΔT=30°C.

Another interesting parameter for the process is $\alpha*$ ($\%$, $°C^{-1}$), the percentage activity increase of the enzyme reaction rate for ΔT*=1°C, i.e., when an actual temperature difference of 1°C is applied across the catalytic membrane. The expression for $\alpha*$ is:

$$\alpha^{*} = \frac{\text{P.A.I.}}{\Delta T^{*}}$$

(12)

Figure 9b shows, as a function of DMP concentration, the $\alpha*$ values obtained from the results in Figure 9a. Because this process is similar to a normalization process, overlapping curves are present. It is interesting to observe that at low concentrations of DMP (1 mM) the $\alpha*$ value amounts to 24%, while at high DMP concentrations (10÷15 mM) the $\alpha*$ values amounts to 6%. From the applied point of view, these results indicate that at concentrations of DMP lower than those used by us, such as those actually existing in the environment, a temperature difference of 1°C across the catalytic membrane is enough to obtain increases of over 20% in the removal of DMP concentration. Looking at our similar publications, it is possible to see that the α^* values for lipase are smaller than those found for other catalytic systems, may be because the aqueous system is not completely suitable for lipase activity.

From the industrial point of view, the results discussed above indicate a substantial reduction in the processing times to bioremediate water polluted by DMP and thus a reduction in the process's costs. In fact, it is possible to correlate the parameters α or P.A.I., which are functions of ΔT, with the reduction in the bioremediation time, τ_r, defined as

$$\tau_r \; (\%) \; = \; \frac{\tau_{iso} \, - \, \tau_{non-iso}}{\tau_{iso}} \; \times 100 \tag{13}$$

where τ_{iso} and $\tau_{non\text{-}iso}$ are the time required to obtain the same percentage of DMP biodegradation under isothermal and non-isothermal conditions, respectively. To correlate τ_r with the applied ΔT^* it is necessary to calculate the time required to obtain the same amount of DMP removal under isothermal and non-isothermal conditions. This calculation can be done graphically or analytically.
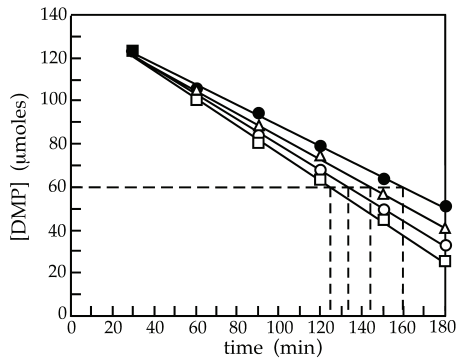
Fig. 10. DMP in function of reaction time. ●: $\Delta T=0°C$; Δ: $\Delta T=10°C$; O: $\Delta T=20°C$; □: $\Delta T=30°C$.

As one example of the graphical calculation let us see Figure 10, where we has been reported as a function of the time of enzyme treatment, the DMP decrease in the case of $T_{average} =25°C$, with $\Delta T=0$ or 10 or 20 or 30°C. The initial DMP concentration was 5 mM. To obtain the same biodegradation of DMP, for example a 50% reduction, 161 minutes are needed for the isothermal condition, while 145 or 134 or 125 minutes are required for $\Delta T=10°C$, $\Delta T=20°C$, $\Delta T=30°C$, respectively. It follows that a value of $\tau_r =9.9\%$ is obtained with a $\Delta T=10°C$, a $\tau_r =16.8\%$ with a $\Delta T=20°C$, and a $\tau_r =25\%$ with a $\Delta T=30°C$. The τ_r values increase with an increase in the applied ΔT and therefore with the P.A.I.

The analytical approach is based on the consideration that the same DMP degradation is obtained when $RR_{C,\Delta T=0} \cdot \tau_{iso} = RR_{C,\Delta T\neq0} \cdot \tau_{non\text{-}iso}$, where RR stands for the reaction rate. By recalling that

$$RR_{C, \, \Delta T=0} \; \tau_{iso} = RR_{C, \, \Delta T=0} \; \left(1+\frac{\alpha}{100}\Delta T\right)\tau_{non\text{-}iso} \tag{14}$$

after a series of mathematical steps one obtains

$$\tau_r(\%) =\left(\frac{\alpha\Delta T}{\alpha\Delta T + 100}\right)100 =\left(\frac{\alpha^*\Delta T^*}{\alpha^*\Delta T^* + 100}\right)100 =\left(\frac{P.A.I.}{100 + P.A.I.}\right)100 \tag{15}$$

In Figure 11a, the τ_r values obtained at different DMP concentrations with $\Delta T=30°C$ have been reported as a function of the P.A.I. calculated for each DMP concentration. As expected, the reduction in bioremediation time is an increasing function of the percentage increase in the enzyme activity (P.A.I.) and, consequently, in the temperature difference applied across the membrane. Highlighted in black is the case for a DMP concentration equal to 5 mM, for which the P.A.I. is 33.4% and the τ_r is 25%.
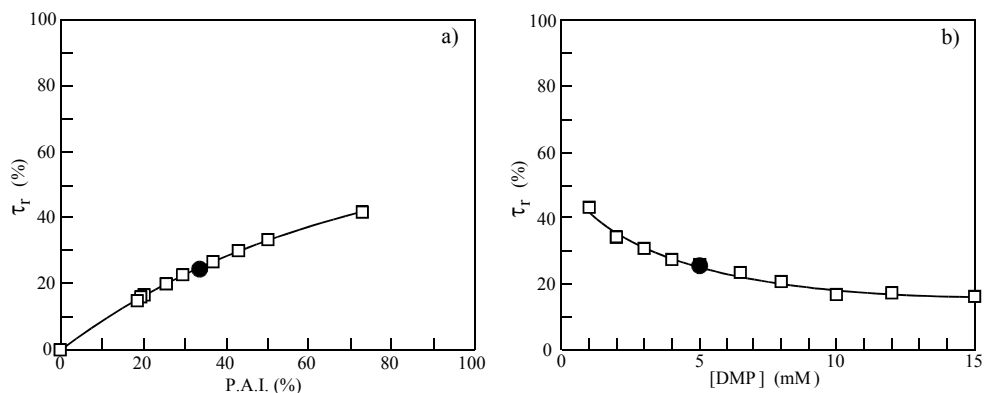
Fig. 11. (a): Percentage reduction of the productions time (τ_r) in function of Percentage Activity Increase. (b): τ_r in function of DMP concentration.

Because the P.A.I. is related to the substrate concentration, we have reported the reduction in biodegradation time as a function of the DMP concentration in Figure 11b. Again, highlighted in black is the result relative to the DMP concentration of 5 mM. As is evident from Figure 11b, the reduction in the biodegradation time decreases with the increase in the DMP concentration. Also, this result is interesting for practical applications, because the concentrations used by us are higher than those actually found in polluted water, owing to DMP's small solubility in water.

From the above results, it follows that the decrease in DMP concentration is a linear function of the applied temperature difference and is inversely proportional to the initial DMP concentration. To quantify this observation, in Table 4 we have reported the percentage decreases of DMP concentration after 180 minutes of enzyme treatment.

T_{av} (°C)	ΔT (°C)	[DMP]			
		1 mM	3 mM	5 mM	8 mM
	0	68.5 %	63.0 %	58.1 %	43.4 %
	10	84 .0 %	72.5 %	66.1 %	47.7 %
25	20	100.0 %	82.7 %	72.9 %	51.9 %
	30	100.0 %	89.5 %	79.3 %	55.1 %

Table 4. Percentage decreases of DMP concentration after 180 minutes of enzyme treatment.

7. Conclusions

The obtained results have shown that the laccase from *Trametes versicolor* and the tyrosinase from mushrooms immobilized on PAN beads filling a fluidized bed bioreactor are able to

oxidize different bisphenols. In particular, the BPF is the substrate towards which the immobilized enzymes have the highest bioremediation power. Moreover the higher removal efficiencies (≈100%) for all bisphenols were obtained with immobilized laccase. The immobilized tyrosinase, under the same experimental conditions, showed smaller removal efficiency (~90%), notwithstanding the specific activity of this enzyme results to be 1500U/mg, about 75 time that of laccase.

Coming to the experiments carried out in planar membrane bioreactors working under non-isothermal conditions, the results have shown the possibility of using the enzyme lipase from *Candida rugosa* in the pathway for the biodegradation of phthalates to bioremediate water polluted by these compounds. The use of non-isothermal bioreactors proved the utility of this technology in solving some of the pollution problems affecting human life and wildlife. Moreover, our studies may increase the limited knowledge regarding the direct exploitation of purified enzymes in the hydrolysis of phthalates, since the literature exhibits very few papers in this field.

8. Perspectives

Our results encourage new studies in order to bioremediate waters polluted by EDCs. By considering that in real samples EDCs are present in mixture, it will be interesting for the future to coimmobilize different enzymes able to hydrolyze different pollutants. But a more intriguing observation can be advanced by considering the meaning of the word "cleaning up". From the analytic point of view "cleaning up" means to "reduce or eliminate" the pollutant concentration. From the biological point of view, indeed, and particularly in the case of EDCs, besides "the reduction or elimination" of the pollutant concentration, "cleaning up" means the removal of the endocrine effects observed before the enzyme treatment. So, tests on cell line and on living organisms are request to assess the toxicity or the endocrine power of the reaction products. If these tests will result negative, only in this case we can speak of occurred "cleaning up".

9. References

Attanasio, A.; Diano, N.; Grano, V.; Sicuranza, S.; Rossi, S.; Bencivenga, U.; Fraconte, L.; Di Martino, S.; Canciglia, P. & Mita, D.G. (2005). Non-isothermal bioreactors in the treatment of vegetation waters from olive oil: laccase versus syringic acid as bioremediation model. *Biotechnology Progress*, 21, 806-815

Campbell, C.G.; Borglin, S.E.; Green, F.B.; Grayson, A.; Wozei, E. & Stringfellow, W.T. (2006). Biologically directed environmental monitoring, fate, and transport of estrogenic endocrine disrupting compounds in water: a review. *Chemosphere*, 65, 1265–1280

Castle, I.; Mercer, A.J.; Startin, J.R. & Gilbert, J. (1988). Migration from plasticised films into foods. Migration of phthalate, sebacate, citrate and phosphate esters from film used for retail food packaging. *Food Additives and Contaminants*, 5, 9-20

Daston, G.P.; Gooch, J.W.; Breslin, W.J.; Shuey, D.L.; Nikiforov, A.I.; Fico, T.A. & Gorsuch, J.W. (1997). Environmental estrogens and reproductive health: a discussion of the human and environmental data. *Reproductive Toxicology*, 11, 465–481

Desbrow, C.; Routledge, E.J.; Brighty, G.C.; Sumpter, J.P. & Waldock, M. (1998). Identification of estrogenic chemicals in STW effluent. 1.Chemical fractionation and in vitro biological screening. *Environmental Science and Technology*, 32, 1549–1558

Diano, N.; El-Masry, M.M.; Portaccio, M.; Santucci, M.; De Maio, A.; Grano, V.; Castagnolo, U.; Bencivenga, U.; Gaeta, F.S. & Mita, D.G. (2000). The process of thermodialysis and the efficiency increase of bioreactors operating under non-isothermal conditions *Journal of Molecular Catalysis B: Enzymatic*, 11, 97-112

Diano, N.; Grano, V.; Fraconte, L.; Caputo, P.; Ricupito, A.; Attanasio, A.; Bianco, M.; Bencivenga, U.; Rossi, S.; Manco, I.; Mita, L.; Del Pozzo, G. & Mita, D.G. (2007). Non-isothermal bioreactors in enzymatic remediation of waters polluted by endocrine disruptors: the BPA as model of pollutant. *Applied Catalalysis B: Environmental*, 69, 252-261

Dua, M.; Singh, A.; Sethunathan, N. & Johri, A.K. (2002).Biotechnology and bioremediation: successes and limitations. *Applied Microbiology Biotechnol*ogy, 59, 143–152

Durante, D.; Casadio, R.; Martelli, L.; Tasco, G.; Portaccio, M.; De Luca, P.; Bencivenga, U.; Rossi, S.; Di Martino, S.; Grano, V.; Diano, N. & Mita, D.G. (2004). Isothermal and non-isothermal bioreactors in the detoxification of waste waters polluted by aromatic compounds by means of immobilized laccase from *Rhus veinicifera*. *Jounal Molecular Catalalysis B: Enzymatic*, 27, 191-206

European Commission. European workshop on the impact of endocrine disrupters on human health and wildlife. Report *of the Proceedings*. pp 125, Weybridge, UK, 2–4 December 1996, vol. 17549. Report EUR

Furukawa, K. (2003). 'Super bugs' for bioremediation. *Trends Biotechnology*, 21, 187–190

Gaeta, F.S.; Ascolese, E.; Bencivenga, U.; Ortiz de Zarate, J.M.; Pagliuca, N.; Perna, G.; Rossi, S. & Mita, D.G. (1992). Theories and experiments on non-isothermal matter transport in porous membranes. *Journal of Physical Chemistry*, 96, 6342-6359

Gaido, K.W.; Leonard, L.S.; Lovell, S.; Gould, J.C.; Babai, D.; Portier, C.J. & McDonnell, D.P. (1997). Evaluation of chemicals with endocrine modulating activity in a yeast-based steroid hormone receptor gene transcription assay. *Toxicology and Applied Pharmacology*, 143, 205-212

Georgieva, S.; Godjevargova, T.; Portaccio, M.; Lepore, M. & Mita, D.G. (2008). Advantages in using non-isotermal bioreactors in bioremediation of water polluted by phenol by means of immobilized laccase from Rhus *vernicifera*. *Journal of Molecular Catalysis B: Enzymatic*, 55 177-184

Georgieva, S.; Godjevargova, T.; Mita, D.G.; Diano, N.; Menale, C.; Nicolucci, C.; Romano Carratelli, C.; Mita, L. & Golovinsky, E. (2010). Non-isothermal bioremediation of waters polluted by phenol and some of its derivatives by laccase covalently immobilized on polypropylene membranes. *Journal of Molecular Catalysis B: Enzymatic*, 66, 210-218

Gutendorf, B. & Westendorf, J. (2001). Comparison of an array of in vitro assays for the assessment of the estrogenic potential of natural and synthetic estrogens, fytoestrogens and xenoestrogens. *Toxicology*, 166, 79–89

Ignatova, M.; Stoilova, O.; Manolova, N., Mita, D.G., Diano, N.; Nicolucci, C. & Rashkov, I. (2009). Electrospun microfibrous poly(styrene-alt-maleic anhydride)/poly(styrene-co-maleic anhydride) mats tailored for enzymatic remediation of waters polluted by endocrine disruptors. *European Polymer Journal*, 45, 2494-2504

Jobling, S.; Reynolds, T.; White, R.; Parker, M.G. & Sumpter, J.P. (1995). A variety of environmentally persistent chemicals, including some phthalate plasticizers, are weakly estrogenic. *Environmental Health Perspective*, 103, 582–587

Jobling, S.; Nolan, M.; Tyler, C.R.; Brighty, G. & Sumpter, J.P. (1998). Widespread sexual disruption in wild fish. *Environmental Science and Technology,* 32, 2498–2506

Kim, H.S.; Han, S.Y.; Yoo, S.D.; Lee, B.M. & Park, K.L. (2001). Potential estrogenic effects of bisphenol-A estimated by in vitro and in vivo combination assays. *Journal of Toxicology Science*, 26, 111-118

Kirkpatrick, D.C.; Ripley, R.A. & Pelletier, M.A. (1989). Food packaging materials: health implications. *Nutritional Toxicology*, 3, 1-20

Kitamura, S.; Suzuki, T.; Sanoh, S.; Kohta, R., Jinno, N.; Sugihara, K.; Yoshihara, S.; Fujimoto, N.; Watanabe, H. & Ohta, S. (2005). Comparative study of the endocrine-disrupting activity of bisphenol A and 19 related compounds. *Toxicology Science* , 84, 249-259

Körner, W.; Bolz, U.; Sussmuth, W.; Hiller, G.; Schuller, W.; Hanf, V. & Hagenmaier, H. (2000). Input/output balance of estrogenic active compounds in a major municipal sewage plant in Germany. *Chemosphere* 40, 1131–1142

Krishnan, A.V.; Stathis, P.; Permuth, S.F.; Tokes, L. & Feldman, D. (1993). Bisphenol-A: an estrogenic substance is released from polycarbonate flasks during autoclaving. *Endocrinology,* 132, 2279-2286

Lide, D.R. (1990). *Handbook of Chemistry and Physics*, Press C Editor, Boka Raton

Lowry, O.H.; Rosebrough, N.J.; Farr, A.L. & Randall, R.J. (1951). Protein measurement with the Folin phenol reagent. *Journal of Biological Chemistry,* 193, 265-275

Lye, C.M.; Frid, C.L.J.; Gill, M.E.; Cooper, D.W. & Jones, D.M. (1999). Estrogenic alkylphenols in fish tissues, sediments, and waters from the U.K. Tyne and Tees estuaries. *Environmental Science and Technology*, 33, 1009–1014

Matthews, J.B.; Twomey, K.; Zacharewski, T.R. (2001). In vitro and in vivo interactions of bisphenol A and its metabolite, bisphenol A glucuronide, with estrogen receptors alpha and beta. *Chemical Research in Toxicology*, 14, 149-157

Mita, D.G.; Bellucci, F.; Cutuli, M.G. & Gaeta F.S. (1982). Non-isothermal matter transport in sodium chloride and potassium chloride aqueous solutions. 2. Heterogeneous membrane system (thermodialysis). *Journal of Physical Chemistry*, 86, 2975-2982

Mita, L.; Sica, V.; Guida, M.; Nicolucci, C.; Grimaldi, T.; Caputo, L.; Bianco, M.; Rossi, S.; Bencivenga, U.; Mohy Eldin, M.S.; Tufano, M.A.; Mita, D.G. & Diano, N. (2010). Employment of immobilized lipase from *Candida rugosa* for the bioremediation of waters polluted by dimethylphthalate, as a model of endocrine disruptors. *Journal Molecular Catalysis B: Enzymatic*, 62, 133-141

Nerin, C.; Cacho, J. & Gancedo, P. (1993). Plasticisers from printing inks in a selection of food packagings and their migration to food. *Food Additives and Contaminants*, 10, 453-460

Page, B.D. & Lacroix, G.M. (1992). Studies into transfer and migration of phthalate esters from aluminium foil-paper laminates to butter and margarine. *Food Additives and Contaminants*, 9, 197-212

Petersen, J.H. (1991). Survey of di-ethyl hexyl phthalate plasticiser contamination of Danish milks. *Food Additives and Contaminants*, 8, 701-706

Pieper, D.H. & Reineke, W. (2000). Engineering bacteria for bioremediation. *Current Opinion in Biotechnology*, 11, 262–270

Routledge, E.J.; Sheahan, D.; Desbrow, C.; Brighty, G.C.; Waldock, M. & Sumpter, J.P. (1998). Identification of estrogenic chemicals in STW effluent. 2. In vivo responses in trout and roach. *Environmental Science Technology*, 32, 1559–1565

Routledge, E.J. & Sumpter, J.P. (1997). Structural features of alkylphenolic chemicals associated with estrogenic activity. *Journal of Biological Chemistry,* 272, 3280–3288

Snyder, R.W.; Maness, S.C.; Gaido, K.W.; Welsch, F.; Sumner, S.C. & Fennell, T.R. (2000). Metabolism and disposition of bisphenol A in female rats. *Toxicology and Applied Pharmacology*, 168, 225-234

Soto, A.M.; Sonnenschein, C.; Chung, K.L.; Fernandez, M.F.; Olea, N. & Serrano, F.O. (1995). The E SCREEN assay as a tool to identify estrogens: an update on estrogenic environmental pollutants. *Environental Health Perspective*, 103, 113–122

Spain, J.C.; Hughes, E.J. & Knackmuss, H-J. (2000). *Biodegradation of Nitroaromatic Compounds*, Lewis Publishers, Washington DC

Spengler, P.; Körner, W. & Metzger, J.W. (2001). Substances with estrogenic activity in effluents of sewage treatment plants in southwestern Germany. 1. Chemical analysis. *Environmental Toxicology and Chemistry*, 20, 2133–2141

Tilton, F.; Benson, W.H. & Schlenk, D. (2002). Evaluation of estrogenic activity from a municipal wastewater treatment plant with predominantly domestic input. *Aquatic Toxicology*, 61, 211–224

Tinwell, H.; Joiner, R.; Pate, I.; Soames, A.; Foster, J. & Ashby, J. (2000). Uterotrophic activity of bisphenol A in the immature mouse. *Regulatory and Toxicology Pharmacology*, 32, 118-126

Touloukian, Y.S.; Liley, P.E. & Saxena, S.C. (1970). In: Thermophysical Properties of Matter, Touloukian, Y.S. (Ed.), IFI, Plenum, New York.

Evaluation of Anaerobic Treatability of Between Cotton and Polyester Textile Industry Wastewater

Zehra Sapci-Zengin[1,2] and F. Ilter Turkdogan[1]
[1]Yildiz Technical University, Department of Environmental Engineering
[2]Norwegian University of Life Sciences, Department of Mathematical
Sciences and Technology
[1]Turkey
[2]Norway (current address)

1. Introduction

Recently, the fast increase in the cost of energy and the decrease in the used economic fossil fuel reserves cause an increase in the interest to the energy production from wastes using anaerobic biotechnology (Speece, 1996). The anaerobic treatment is defined as the biological separation of organic wastes in anaerobic conditions and also the production of their last products, such as CH_4, CO_2, NH_3, and H_2S (biogas). The processes, employed by anaerobic bacteria, have been widely used in treatment of municipal wastewaters and varying types of industrial wastewaters for removal of organic material in the wastewaters and also produce biogas as energy from the wastewaters. Treatment capacity of an anaerobic digestion system is primarily determined by the amount of active microorganism population retained within the system dependent on wastewater composition, system configuration and operation of anaerobic reactor (Zainol et al., 2009).

2. Important

Textiles and apparel sector, one of the important industries in the world, is a vital contributor to Turkey's economy, accounting for approximately 10 percent of the country's gross domestic product. It is the largest industry in the country, constituting approximately 15 percent of manufacturing and about one-third of manufactured exports. Nowadays, the country produces the eighth-largest volume of man-made fibers in the world, at 1.2 million tons per year (Pelot, n.d.). Therefore, textile industries are vitally distributed in the country. The variety of raw materials, chemicals, processes and also technological variations applied to the processes cause complex and dynamic structure of environmental impact from the textile industry (Sapci & Ustun, 2003). The textile industries as pretreatment (desizing - scouring - bleaching) and dyeing processes generate large quantity of wastewater containing unreacted dyes, suspended solids, dissolved solids, and biodegradable and non-biodegradable other auxiliary chemicals (Raju et al., 2008, Somasiri et al., 2008, Georgiou et al., 2005, Isik & Sponza 2004). For example, polyester is a material produced on a large scale

as a component of textile fiber, which results in a great deal of discharge wastewater with various additives and detergents, including wetting agents, softening agents, antioxidant, surfactant, detergent, antiseptic and dyes (Yang, 2009). Cliona et al. (1999) reported that the dyes can be classified on their chemical structure (azo, anthraquinone, azine, xanthene, nitro, phthalocyanine, etc.) or application methods used in the dyeing process (acid, basic, direct, reactive, etc) (Somasiri et al., 2008). Therefore, these industries have also shown a significant increase in the use of synthetic complex organic dyes as coloring material. The discharge of these textiles is viewed to have negative effect on the environment in this area, also damaging the quality of water sources and may be toxic to treatment processes, to food chain organisms and to aquatic life (Talarposhti et al., 2001). Therefore, it is of paramount importance to know its exact nature, in order to implement an appropriate treatment process (Marmagne & Coste, 1999). For the foregoing reasons, textile industries wastewater was selected for the research.

On the other hand, the country has around 1.9 million employees in the textile and apparel sector (Pelot, n.d.). Therefore, wastewater of these industries has generally been a combination of textile and municipal wastewater. If the municipal wastewater mixes with the other kind of wastewater, it has lost its domestic property, and is considered to be process wastewater. Biological treatment may be a good alternative as the operational costs are relatively low when compared to most of the physical/chemical technologies. Although recent studies of anaerobic treatment of textile wastewater using several high-rate up-flow anaerobic sludge blanket reactors were conducted, however studies about anaerobic treatment of mixture wastewater (both textile and municipal wastewater) are deficient. For the foregoing reasons, between textile industries wastewater and municipal wastewater were applied for the research.

The aim of this work was to study the treatment of textile wastewater using an up-flow anaerobic sludge blanket (UASB). Textile wastewater was selected for the research due to its total volume (53.5% of all types of industry in Turkey). In this study, firstly, treatability of textile polyester wastewater diluted with a municipal one is examined in an UASB system according to organic loading rate (OLR), hydraulic retention time (HRT), as well as important anaerobic operating parameters. Three reactors were operated at mesophilic conditions (37±0.5 °C) in a temperature-controlled water-bath with hydraulic retention times (HRTs) of 5 days, and with organic loading rates (OLR) between 0.314(±0.03) – 0.567(±0.05) kg COD/m^3/day. Three different dilution ratios (45%, 30% and 15%) of municipal with real polyester textile wastewater are employed. Secondly, the effects of glucose and lactose selected as a co-substrate, with constant HRT values of 5 days, on the systems with same dilution ratios for each reactor (30%) were examined. All these results evaluated in the manuscript. Thirdly, to show a difference of anaerobic treatability between polyester wastewater diluted with municipal wastewater and cotton textile wastewater diluted with municipal wastewater, all these results compared with previous study (Zengin & Aydinol, 2007). The previous study about real cotton textile wastewater treatment were run two hydraulic retention times (HRTs) of 4.5 and 9.0 days, and with organic loading rates (OLR) between 0.087(±0.016) – 0.517(±0.090) kg COD/m^3/day. Three different dilution ratios (15%, 30% and 40%) of municipal with textile wastewater were employed at same mesophilic conditions. Fourthly, regarding mixed wastewater, co-substrate effect on anaerobic treatment evaluated according to COD removal efficiency. For this reason, assessment of anaerobic treatment results from previous experiments which were used glucose (as co-substrate) with varied dilution ratios (60%, 40%, 45%, 30%, and 15%) of municipal with

cotton textile wastewater experiments and these trials which were used same co-substrate with different dilution ratios (45%, 30% and 15%) of municipal with real polyester textile wastewater were examined.

The results showed that the municipal wastewater rate in both the polyester wastewater and the cotton wastewater did not have a substantial change in COD removal efficiency. Textile polyester wastewater diluted with different ratio of municipal one was not treated in UASB as a satisfied for COD removal efficiency even though values of alkalinity, SS and pH are founded optimum range for successful operation of the digester. In addition, even if when either glucose or lactose as a co-substrate was added mixed wastewater; it was not seen positive effect for anaerobic treatment of polyester wastewater. However, addition of co-substrate (glucose) in cotton wastewaters had a positive effect on the COD removal efficiency. Therefore, COD removal efficiency of textile wastewater on anaerobic digestion change especially depends on textile wastewater types. Before the anaerobic treatment of polyester wastewater, it should be treated via advance technology.

3. Information

3.1 Sampling

In this study, original wastewater samples were obtained from the knit fabric wastewater and polyester process wastewater of two different industries located in Istanbul, Turkey. First industry, knit fabric industry, dyed of fiber, wool yarn and fabric (before knit process) or texture (after the unit). This industry wastewater was used during the start-up period of anaerobic treatment in the study. Second industry uses only polyester fabrics which are dyed using dispersive dyes. Used cotton textile wastewater for comparing of anaerobic treatment results in the study was taken from another industry in Istanbul, which detail information was given previous study (Zengin & Aydinol, 2007). In addition, municipal wastewater used for dilution was supplied from a municipal wastewater plant in Istanbul. All samples were delivered to the laboratory cooled and kept 4 °C during the experimental study.

3.2 Experimental set-up

Three reactors, made of serum bottles similar to studies cited in literature (Tang et al., 1999, Sacks & Buckley, 1999, Cordina et al., 1998, Fang & Chan, 1997, Madsen & Rasmussen 1996, Soto et al., 1993, Guiot et al, 1986) were used, each having a volume of 1.2 L and operated for 80 days at mesophilic conditions (37±0.5 °C) in a temperature-controlled water- bath (Ben-Marie device) with two hydraulic retention times (HRTs) of 4.5 and 9.0 days (Fig 1). The upper side of the reactors (14% of reactor volume) had a slope similar to a gas collection funnel. The biogas collected here was measured by the method of volume displacement.

Prior to experiments, 3 UASB reactors were inoculated with granular biomass (25% of the working volume) obtained from Tekel Brewery Inc. (Istanbul, Turkey) and N_2 gas passed through them. The reactors then were filled to their respective volumes with textile wastewater (61% of the total volume). After the start-up period, the real textile wastewater obtained from effluent of textile houses in Istanbul, Turkey fed to the reactors with domestic wastewater. The treatment process was monitored and components of wastewater samples were analyzed in the Environmental Engineering Laboratory at Yildiz Technical University (YTU), Istanbul, Turkey. A detailed schematic diagram of the experimental set-up is shown in Fig. 1.
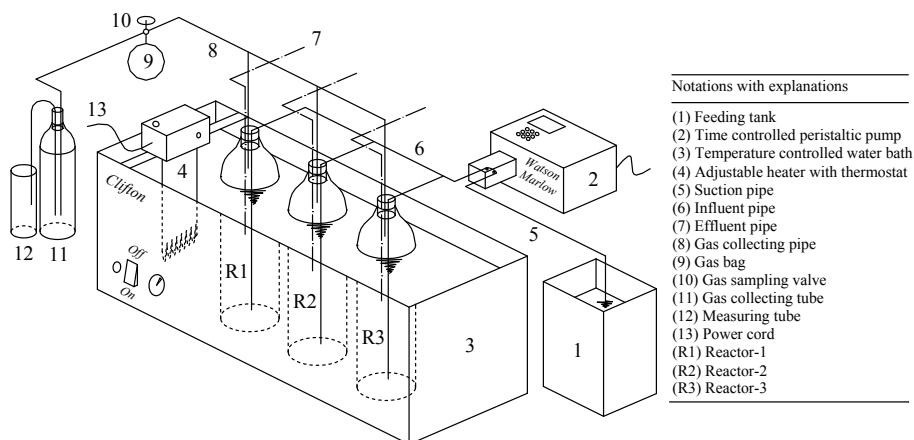
Fig. 1. Detailed schematic of the experimental set-up

3.3 Analytical methods

The temperature, pH, biogas volume (ml) and COD removal efficiency (%) were measured daily. Alkalinity (mg/L as CaCO$_3$), TSS (Total Suspended Solids) (mg/L), and VFA (Volatile Fatty Acids) were measured three times a week according to Standard Methods of APHA-AWWA (1995) (Table 1). During the study, the operational temperatures of the reactors were monitored with a digital thermometer, and pH was measured by a Jenway 3040 Ion Analyzer. The other parameters were determined by the procedures described in Method Numbers 5220-B (Open Reflux Method for COD), 2320-B (Titration Method for Alkalinity), 2540-D (Total Suspended Solids Dried at 103-105 °C) and 5560-C (Distillation Method for VFA) respectively. Concentration of heavy metals (Table 1) were analyzed by the procedure described in Method Number 3111-B (Direct Air Acetylene Flame Method) with an ATI Unicam 929AA-Spectrometer.

Hydraulic retention time (HRT) is a measure of the amount of time the digester liquid remains in the digester. Organic loading rate (OLR) is a measure of the biological conversion capacity of the anaerobic treatment system. COD removal efficiency (COD$_{RE}$) of UASB reactors being output parameter was considered as a measure of treatment performance. COD$_{RE}$ value is defined as follows:

$$COD_{RE} (\%) = (COD_i - COD_e) / COD_i * 100 \qquad (1)$$

where COD$_i$ is the influent COD concentration and COD$_e$ is the effluent COD concentration. Six anaerobic reactors having a total volume of 200 ml were also operated to determine COD fractions of wastewater samples. These reactors were conducted for about 1800 hours at mesophilic conditions (37±0.5 °C), maintained by an adjustable aquarium heater with thermostat (Otto Aquarium Company, Taiwan). Each of them was seeded with 30 mg/L as Mixed Liquor Volatile Suspended Solids (MLVSS) of acclimated granular sludge and homogenized with 100 ml of textile and municipal wastewater. Filtrates of samples obtained from vacuum filtration by means of glass microfibre filters having a pore size of 0.45 µm (Whatman glass microfibre filter) were defined as "soluble fractions". Filter wastewaters and raw wastewaters were fed in the different COD fraction reactors.

4. Results and discussion

4.1 Start-up period

The system was fed by the knit fabric textile wastewater for the adaptation of bacteria. In this study, the start- up period was conducted by the original wastewater (Table 1) which did not have much pollution. Knit fabric is used in textile industry work for all kinds of printing

Characterization of parameters	Knit fabric wastewater	Polyester process wastewater	Cotton process wastewater (Zengin & Aydinol, 2007, Sapci, 2002)
pH	6.4	8.72	9.4
COD (mg/L)	640	3218	1757
TKN (mg/L)	43	204	16
Total P (mg/L)	5	21	34
Alkalinity (mg/L asCaCO$_3$)	1200	230	1750
Sulphate (mg/L)	300	130	760
Detergent (mg/L)	2	2	10
Oil-Grease (mg/L)	-	10	50
Color (Pt-Co)	175	-	520
TSS (mg/L)	47	250	95
Mg(mg/L)	<0.03	3.7	2.2
Fe(mg/L)	0.45	2.1	1.8
Mn(mg/L)	<0.03	0.23	0.3
Zn (mg/L)	1.11	0.8	10
Pb (mg/L)	0.03	<0.03	0.3
Cr (mg/L)	0.68	0.45	3
Ni (mg/L)	<0.01	<0.01	0.4
Co (mg/L)	<0.01	-	<0.03
Cu (mg/L)	0.03	<0.01	0.3

Table 1. Characterization of the studied textile wastewater (cotton process, polyester process and knit fabric)

and sizing. For example, fiber, wool, yarn and cloth print are produced. The sector is an integrated foundation that can produce everything needed with woven workbenches.

In the start-up period, three reactors were fed the same characterized wastewater for HRT for 9 days. Each reactor was fed with 0.071 kg COD/m^3/day of organic loading rate (OLR) without co-substrate. In the next step, glucose used as co-substrate was increased up to 0.245 kg COD/m^3/day of OLR, step by step. Variations of pH and COD parameters observed in the start-up period are given in Fig. 2 (HRT=9 days). During the start-up period, COD efficiency increased step by step, and also the value of pH was determined to be stable (Fig.2). Operating temperature in the systems was carefully maintained between 38±2 °C. During this period, some fluctuations were recorded for the values of biogas (between 25 and 170 mL/day) and SS (between 20 and 55 mg/L). In 2nd reactor and 3rd reactor, fluctuations of them showed a similar behavior.
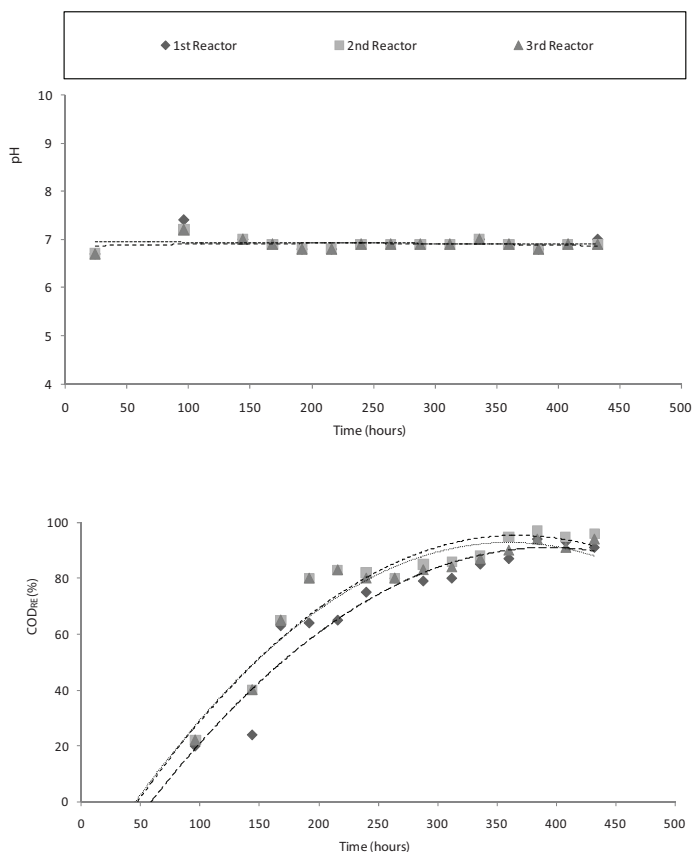
Fig. 2. Variation of pH and COD_{RE} (%) during the start-up period (HRT=9 days).

4.2 Treatment of polyester textile wastewater with municipal wastewater (HRT 5 days) (1st system)

Before, three UASB reactors are fed with diluted polyester textile industry wastewater with municipal wastewater and glucose for helping acclimatization period of bacteria. After the acclimatization period, the process are fed the different ratios mixed wastewaters (without co-substrate), operated for 504 hours, and fed under batch mode for period 24 hours. During the first 145 hours period, COD removal efficiency is drastically decreased from 30 to 5 % for each reactor. Values of alkalinity, SS and pH are founded optimum range of literature required for successful operation of the digester (Metcalf & Eddy, 2003, Kalogo et al., 2001). After the 145 hours, COD removal efficiencies are investigated in the effluent waters of all reactors. No differences have been observed. Hence, graphs of operational parameters changes of a representative anaerobic digestion are not given in the manuscript. Yang (2009) reported that antioxidants used in textile industry to inhibit the oxidation of the fiber could resist the oxidation of contaminations in wastewater treatment and antiseptic take negative effect on growth of bacteria. Therefore, these pollutants discharged from various stages of

the polyester manufacturing process are characterized by hard oxidation, toxicity and poor biodegradation. Additionally, the wastewater resources are dying units of polyester products. Some of dyes are toxic and carcinogenic and require separation and advanced treatment of textile effluents before discharge into treatment plant (Georgiou et al., 2005). Hsieh et al. (2007) emphasized that traditional treatment methods were often ineffective in reducing COD of dyes which were highly complex and varied chemical structures

4.3 Treatment of polyester textile wastewater with municipal wastewater and glucose as co-substrate (HRT 5 days) (2nd system)

The effects of glucoses as co-substrate are researched in the reactors. Mixed wastewater charges including 45, 30 and 15% of municipal wastewater with real polyester textile wastewater are studied for the treatability in UASB systems.

Before the trial, the reactors fed with knit wastewater with co-substrate due to adaptation of bacteria. When finding approx. 80% COD removal efficiency, the three reactors are fed the mixed wastewater with an OLR of 0.166(±0.03), 0.178(±0.02), 0.227(±0.04) kg COD/m3/day for HRT of 5 days, respectively. Fig. 3 denotes that COD removal efficiency, pH an alkanility of all effluent water give parallel behaviour, even though different mixtures used. It indicates that COD removal efficiency of three reactors sluggishly decreased approx. from 75% to 40% (in first 300th hours), even with the feeding of co-substrate, easily decomposable monosaccharides, such as glucose. At the same time, the VFA values from the beginning to the end value of the effluents increase. These differences from beginning to end of the trial are calculated almost 125 mg/L. This sluggish reduction in COD removal efficiency and increasing VFA value result in toxic conditions for methane production bacteria. On the other hand, even though VFA values of effluent in all reactors enhance during the digestion period, the pH values are slowly increased approx from 7 to 7.5. Similarly, the alkalinity also increased approx from 1000 mg/L to 1750 mg/L, expressed as $CaCO_3$. Kalogo et al. (2001) reported that VFA values must be below 100-1500 mg/L, and alkalinity between 1000-4000 mg/L. Therefore, during this period, buffer material is not used because there is neither decrease in alkalinity nor passes limit value of VFA. In the study, this change in the parameters may be caused by instability, even though the values were under the limits for anaerobic systems.

Biogas production has some fluctuations, although it is observed that values of pH, alkalinity and VFA, and COD removal efficiency in the effluents are almost parallel for the whole study period. Kalogo et al. (2001) found that COD removal was not in agreement with biogas production. In the study, biogas fluctuations are caused by gas bubbles which could not overcome partial pressure. Bubbles occur due to result of internal biological activities in anaerobic reactors. The bubble formation process and gas production rate in the bioreactors are greatly influenced hydrodynamic conditions existing in the reactor (Pauss et al., 1990). In the past decade, it has become apparent that many potential applications of dynamic anaerobic models can be cited for gas production under dynamic condition. A description of mass transfer for the major gaseous products carbon dioxide (CO_2) and methane (CH_4) from the liquid into the gas phase under dynamic substrate loading conditions showed that gas solubility as in the case of CO_2 and H_2S more often a liquid phase transport resistance has a flux equation (Merkel & Krauth, 1999). The 3 reactors containing polyester wastewater with 45, 30, and 15% of municipal wastewater and glucose showed similar downward COD removal efficiencies (Fig. 3). Therefore, it can be concluded that municipal mixture ratio and added glucose as a co-substrate in the polyester wastewater does not have a substantial change in COD removal efficiency.

Fig. 3. Mixed wastewater charges including 45, 30 and 15% of municipal wastewater with co- substrate (glucose)

4.4 Treatment of polyester textile wastewater with municipal wastewater and two different co-substrates (HRT 5 days) (3rd system)

Previous chapter indicated that municipal mixture ratio and added glucose as a co-substrate in the polyester wastewater does not have a substanti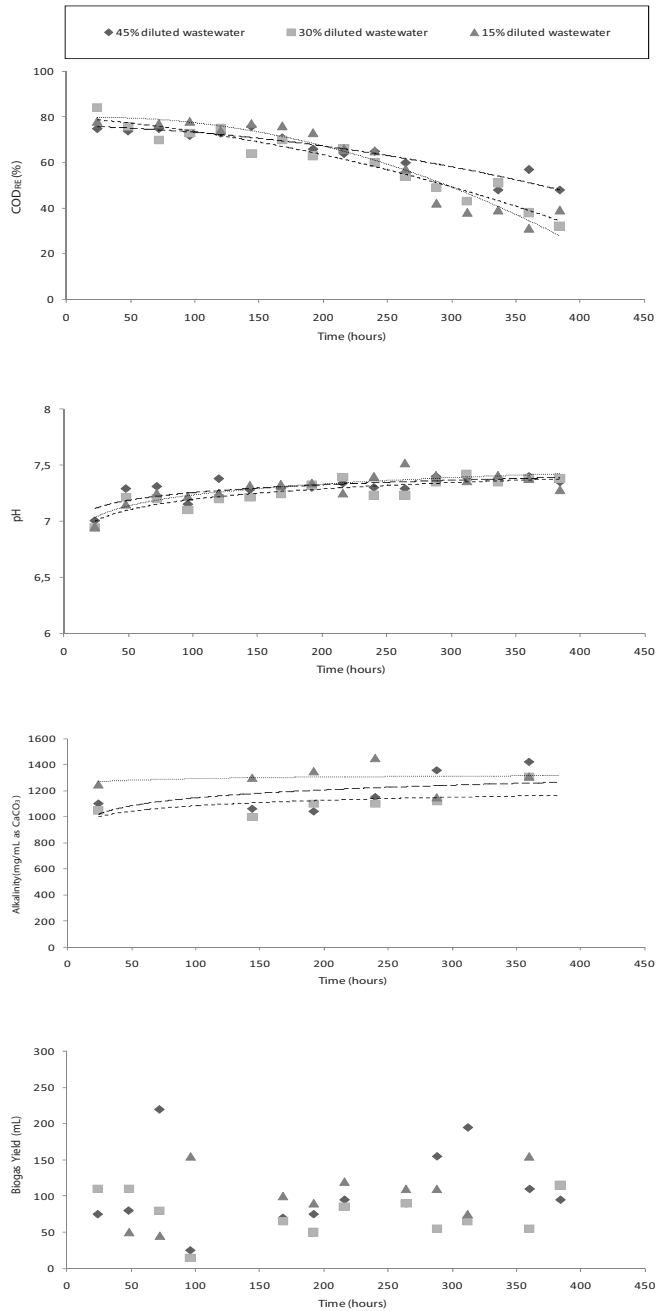al change in COD removal efficiency. Therefore in this part, distinct effects of glucose and lactose as co-substrate, called 3rd system, were researched in the reactors. Mixed wastewater charges including 30% of municipal wastewater with real polyester textile wastewater are studied for the treatability in two UASB systems.

Even with the feeding of two different co-substrates such as glucose and lactose, Fig. 4 indicates that ratios of the COD removal efficiencies in both reactors decreased during the trial. For example, the efficiencies in the both effluents decrease consistently between beginning time and 265th hours in the trial approx. from 75% to 50%. This result is also similar the previous trial (Fig. 3).

In both reactors, it was observed that values of pH, alkalinity and VFA were almost parallel during the 735 hours trial period. The values of VFA in the effluents of mixed wastewater with glucose reactor and with lactose reactor are measured 700 mg/L and 900 mg/L, respectively. This change in parameters may be caused by instability, even though the values were under the limits for anaerobic systems.

4.5 General evaluation of polyester wastewater and cotton wastewater

In this section, anaerobic treatability of polyester wastewater with domestic wastewater is compared the treatability of cotton wastewater in the same condition. This last process of cotton is changed depending on the type and amount of cloths in the batch process. Used cloth types are knit, viscose rayon, cotton, polyester, polyamide knit fabrics together with cotton/polyester, polyester/viscose rayon and viscose rayon/knit blends. The type used most is cotton knit fabrics cloths (60%).

The characteristic of each raw wastewater sample is given in Table 1. Table 1 shows that the raw polyester wastewater has a high COD, TKN, TSS concentration than other textile wastewaters. Table 2 reveals that total dissolved COD ratios of real cotton textile wastewater and raw polyester textile wastewater has almost similar ratio, 82% and 84% respectively. On the other hand, the total COD consisted of inert microbial products and ratio of inert COD in the influent of polyester wastewater have founded two times bigger ratio than cotton last process wastewater textile wastewater. The fractions of easily biodegradable and rapidly hydrolysable are found high ratio the cotton wastewater (72%) than the polyester wastewater (64%). The total active biomass and the total particular biodegradable COD of both textile wastewaters are found to be equal after the measurements. The particular inert fraction of influent COD for both textile wastewaters and particulate inert microbial products are measured almost same ratio, 15% for cotton wastewater and 13% for polyester wastewater. Because the inert part is not biodegradable, this COD fraction is measured as the same value in effluent water. Total (particular and soluble) inert COD and total (particular and soluble) inert microbial product are measured as 25% for the cotton and 33% for the polyester wastewater. Therefore, 75% of COD in cotton wastewater and 66% of COD in the polyester wastewater are biodegradable in the process. The fraction of total COD in municipal wastewater was obtained to be 35%. Total particulate COD for the municipal wastewater was found to be 65%.

COD Fractions	Polyester process wastewater		Cotton process wastewater (From Sapci (2002))		Municipal wastewater	
	Total (mg/L)	Fraction (%)	Total (mg/L)	Fraction (%)	Total (mg/L)	Fraction (%)
C_T	3218	100	1757	100	925	100
ST1	2708	84	1440	82	325	35
SI1+SP	636	20	180	10	231	25
SS1+SH1	2072	64	1260	72	94	10
XT1	510	16	317	18	600	65
XH+XP	409	13	265	15	403	44
XH1+XS1	101	3	52	3	197	21

CT: total COD in the influent, ST1: total dissolved COD, SI1: inert COD in the influent, SP: dissolved inert microbial products, SS1: easily degradable COD, SH1: rapidly hydrolysable COD, XT1: total particulate COD, XH: particulate inert COD in the influent, XH1: active heterotrophic biomass, XP: particulate inert microbial products, XS1: particular degradable COD.

Table 2. COD fractions of textile industries wastewater and municipal wastewkoater

The fraction of total biodegradable and active biomass was found to be 31% for the used municipal wastewater. On the other hand, Cokgor et al. (1998) reported that the total ratio of total biodegradable COD and COD of active biomass were found to be 94 % for municipal wastewater having a COD concentration of 670 mg/L, and 93% for municipal wastewater having a COD concentration of 315 mg/L. This difference may be caused by several chemicals, such as cleaning materials, having high COD values and also anaerobic granular sludge.

4.6 Comparison of anaerobic treatability between polyester wastewater with municipal wastewater (1st system) and cotton last process wastewater with municipal wastewater (4th and 5th system)

After the acclimatization period, the process are fed the different ratios mixed wastewaters, 45, 30 and 15 % diluted polyester wastewater with municipal wastewater, operate for 504 hours, and fed under batch mode for period 24 hours (HRT 5 days) which is called as 1st system. For the previous study (Zengin & Aydinol, 2007), 3 different dilution rates of municipal wastewater (40, 30 and 15%) and raw cotton textile wastewater are used which is called here as 4th system. The 4th system was run according to HRT of 4.5 days. 1st and 4th systems were employed on the same conditions (except HRT), such as temperature, reactor type.

Values of alkalinity, SS and pH in effluents of both system exhibited similar behavior and they founded optimum range of literature required for successful operation of digester (Metcalf & Eddy, 2003, Kalogo et al., 2001). Therefore, during the trial periods, buffer material was not used because there is neither decrease in alkalinity nor increase in VFA.

During the first 145 hours period at the 1st system, COD removal efficiency is drastically decreased from 30 to 5 % for each reactor and after the 145 hours it did not show any differences. On the other hand, even though COD removal efficiency was found unstable at the same period for 4th system, COD removal increased after the first 145 hours. The three reactors containing 40, 30, and 15% of municipal wastewater in the 4th system showed similar COD removal efficiencies of 53, 46 and 40%, respectively. As a result, it was observed that the municipal wastewater rate in both the polyester wastewater and the cotton wastewater
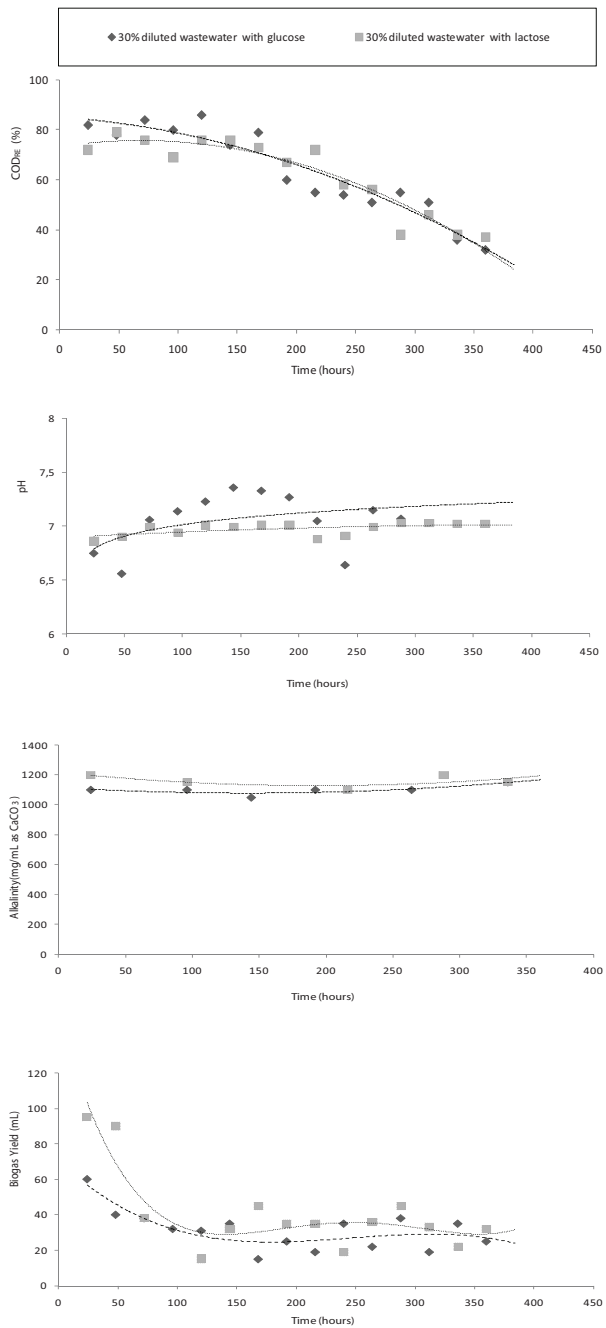
Fig. 4. Mixed wastewater charges including 30 % of municipal wastewater with two different co- substrates (glucose and lactose)

did not have a substantial change in COD removal efficiency. On the other hand, when the ratio of municipal wastewater in 4th system was increased, COD removal efficiency slightly increased (COD of effluent wastewater 630-635 mg/L) for the cotton wastewater treatment. Additionally, when the 3 reactors were fed with same mixed wastewater (40, 30, and 15 % diluted cotton wastewater) under 9-days batch mode (HRT) (5th system), they showed a parallel COD removal efficiency but also this efficiency was slightly higher than 4th system. Therefore, it can be said that different HRTs did not affect COD removal efficiency for cotton textile wastewater treatment.

4.7 Comparison of anaerobic treatability between polyester wastewater and municipal wastewater with co-substrate (2nd system) and cotton last process wastewater and municipal wastewater with co-substrate (6th and 7th system)

Results of anaerobic treatability of both 2nd system (mixed wastewater charges including 45, 30 and 15% of municipal wastewater with real polyester textile wastewater) and 6th system (60, 45 and 30% of municipal wastewater with real cotton textile wastewater) are evaluated according to COD removal efficiency as a result of that the effects of co-substrate were determined. 3rd system indicates that using glucose or lactose as a co-substrate give similar result in effect of treatability. Therefore, in this part of the study, glucose is chosen as a co-substrate. HRT of 2nd and 6th system are run 5 and 4.5 days, respectively.

It is observed that values of pH, alkalinity, VFA, and COD removal efficiency in effluents of the both systems are found almost similar for the whole study period (Table 3). Buffer material was not added during the studies because of that the values of alkalinity and pH were under the limits for anaerobic systems. Biogas productions of both systems also showed fluctuations. Therefore, it can be concluded that municipal mixture ratio and added glucose as a co-substrate does not have a substantial change in COD removal efficiency for neither the polyester wastewater treatment under 5 days nor the cotton textile wastewater treatment under 4.5 days. However, when HRT was increased, the ratio of COD removal efficiency increased in the 7th system. Therefore, it can be said that HRT are important in the treatment systems, in case of cotton wastewater as a feed source for anaerobic digester.

5. Conclusions

Anaerobic treatability of a real polyester textile wastewater diluted with municipal wastewater under various operating conditions is investigated in 3 UASB reactors. The main findings obtained can be outlined as follows:

- Firstly, values of alkalinity, SS, VFA and pH in each experiment are founded optimum range of literature required for successful operation of the reactor. Although it is observed that values of the process parameters in the effluents are almost parallel for the whole study period, biogas production has some fluctuations. In the study, biogas fluctuations are caused by gas bubbles which could not overcome partial pressure. The bubble formation process and gas production rate in the bioreactors are greatly influenced by hydrodynamic conditions existing in the reactor.
- Secondly, even though the municipal wastewater rate is increased, the COD removal rates in each reactor are not increased during the 400 hours trial period. On the country the efficiency is slowly decreased.
- Thirdly, the 3 reactors containing polyester wastewater with 45, 30, and 15% of municipal wastewater and glucose (easily decomposable monosaccharide) showed

System no	Type of textile ww	Rate of municipal ww (%)	Co-substrate	HRT (days)	OLR (kgCOD/m3/d)	COD_{RE} (%)	pH	VFA (mg/L)	Alkalinity (mg/L as CaCO3)	SS (mg/L)	Biogas average yield (mL/day)
1	Polyester	45	Not added	5	0.411±0.01	5	7.05±0.4	465±87	1005±25	147±8	-
	Polyester	30	Not added	5	0.498±0.005	5	7.05±0.6	467±65	1065±75	158±6	-
	Polyester	15	Not added	5	0.567±0.005	5	7.35±0.8	475±40	1075±75	177±7.5	-
4	Cotton	40	Not added	4.5	0.175±0.02	53	7.1±0.6	565±85	1475±125	152±8	67±33
	Cotton	30	Not added	4.5	0.175±0.02	46	7.35±0.8	565±65	1475±125	189±6	77±22
	Cotton	15	Not added	4.5	0.224±0.06	40	7.35±0.8	575±50	1475±125	223±7.5	70±20
5	Cotton	40	Not added	9	0.088±0.003	53	7.7±0.2	565±25	1510±90	170±1	67±33
	Cotton	30	Not added	9	0.089±0.007	50	7.7±0.1	585±15	1475±125	185±1	72±22
	Cotton	15	Not added	9	0.087±0.016	46	7.7±0.2	570±40	1525±75	195±15	68±22
2	Polyester	45	Glucose	5	0.319±0.05	~45	7.3±0.1	281±124	1187±160	30±12	107±55
	Polyester	30	Glucose	5	0.314±0.03	~35	7.2±0.1	323±54	1113±105	34±16	75±29
	Polyester	15	Glucose	5	0.408±0.14	~30	7.3±0.1	313±30	1302±99	67±21	101±38
6	Cotton	60	Glucose	4.5	0.468±0.082	36	7.2±0.2	525±75	1625±225	99±31	53±14
	Cotton	45	Glucose	4.5	0.494±0.077	28	7.2±0.3	475±25	1600±200	101±19	75±30
	Cotton	30	Glucose	4.5	0.517±0.090	32	7.3±0.3	510±10	1650±130	81±12	75±30
7	Cotton	40	Glucose	9	0.313±0.052	76	6.7±0.4	605±5	1375±25	131±54	69±50
	Cotton	30	Glucose	9	0.313±0.051	75	7.0±0.1	610±110	1425±25	188±86	67±43
	Cotton	15	Glucose	9	0.311±0.620	69	7.0±0.2	635±15	1475±25	202±115	80±35

Table 3. Operating conditions and specific outcome parameters

similar decaying COD removal efficiencies. Therefore, it can be concluded that municipal mixture ratio and added glucose as a co-substrate in the polyester wastewater does not have a substantial change in COD removal efficiency.

- Fourthly, even with the feeding of two different co-substrates such as glucose and lactose, the COD removal efficiencies in both reactors decreased continuously during the trial. This result can be concluded that during approx. 400 hours trial period, addition of either glucose or lactose in polyester wastewater does not affect positively on the performance of UASB reactor. However, addition of co-substrate (glucose) in cotton wastewaters had a positive effect on the COD removal efficiency. Therefore, it depends on the textile wastewater prosperities, not only physicochemical parameters but also biologic parameters should be investigated in lab condition before starting the treatment.

6. References

APHA-AWWA (American Public Health Association), (1995). Standard methods for the examination of Water and wastewater, 19th Ed., Washington, DC.

Cordina, J.C., Munoz, M.A., Cazorlaf, M., Perez-Garcia, A., Morinigo, M.A. & De Vincentea, A. (1998) Technical Note; The Inhibition of Methanogenic Activity From An-aerobic Domestic Sludge's as a Simple Toxicity Bioassay. Water Research 32, 1338-1342.

Cokgor, E. U.; Orhon, D. & Sozen, S. (1998). COD Fractions in Municipal and Industrial Wastewaters. ITU, 6th Industrial Pollution Control Symposium'98, June, 3-5, Istanbul, (in Turkish).

Fang, H.H.P. & Chan, O. (1997) Toxicity of Phenol to-wards Anaerobic Biogranules. Water Research 31, 2229- 2242.

Georgiou D., Hatiras, J. & Aivasidis, A. (2005). Microbial Immobilization in a Two-Stage Fixed-Bed-Reactor Pilot Plant for On-Site Anaerobic Decolorization of Textile Wastewater, Enzyme and Microbial Technology 37, 597-605.

Guiot, S. R., Gorur, S.S. & Kennedy, K.J. (1986). Nutritional and Environmental Factors Contributing to Microbial Aggregation During Upflow Anaerobic Sludge Bed-Filter (UBF) Reactor Start-Up, In: Proc. Of the 5th Int. Symp. On Anaerobic Digestion, Pergamon Press, pp. 47-53.

Hsieh, L.-L.; Kang H.-J. & Shyu H.-L. (2007). Optimization of a Ultrasound-Assisted Nanoscale Fe/Fenton Process for Dye Wastewater Through a Statistical Experiment Design Method, Environmental Informatics Archives, Volume 5, 664-673.

Isik, M. & Sponza, D.T. (2004). Anaerobic/Aerobic Sequential Treatment of a Cotton Textile Mill Wastewater. Journal of Chemical Technology and Biotechnology 79, 1268-1274.

Kalogo, Y., Mbouche, J.H. & Verstraete, W. (2001). Physical and Biological Performance of Self-Inoculated UASB Reactor Treating Raw Domestic Sewage, Journal of Environmental Engineering Feb., pp 179-183.

Madsen, T. & Rasmussen, H.B. (1996) A Method for Screening the Potential Toxicity of Organic Chemicals to Methanogenic Gas Production. Water Science Technology 33, 213-220.

Marmagne, O. & Coste, C. (1999). Color Removal from Textile Plant Effluents, American Dyestuff Reports. 85, 15- 21.

Merkel W. & Krauth K., (1999). Mass Transfer of Carbon Dioxide in Anaerobic Reactors under Dynamic Substrate Loading Conditions, Wat. Res. Vol. 33, No. 9, pp. 2011-2020.

Metcalf & Eddy (2003). wastewater engineering treatment and reuse, the McGraw Hill series in Civil and Environmental Engineering, Fourth edition

Sacks, J. & Buckley, C.A. (1999) Anaerobic Treatment of Textile Size Effluent. Water Science and Technology, 40, 177-182.

Sapci, Z. (2002). Investigation of Anaerobic Treatibility of Textile Wastewaters. Master Thesis. Yildiz Technical University, Institute of Science, Istanbul, Turkey.

Sapci, Z. & Ustun, B. (2003). The Removal of Color and COD from Textile Wastewater by Using Waste Pumice, Electron. J. Environ. Agric. Food Chem. (2) 2, 286-290.

Somasiri, W.; Li, X.-F.; Ruan, W.-Q. & Jian, C.; (2008). Evaluation of the Efficacy of Upflow Anaerobic Sludge Blanket Reactor in Removal of Colour and Reduction of COD in Real textile wastewater, Bioresource Technology 99, 3692–3699.

Soto, M.; Mendez, R. & Lema, J.M. (1993). Methanogenic and Non-Methanogenik Activity Tests Theoretical Basis and Experimental Set-up. Water Research 27, 1361-1376.

Speece, R. E. (1996). Anaerobic Biotechnology for Industrial Wastewaters. Archae Press. USA.

Pauss ,A.; Andre, G.; Perrier, M. & Guiot S. R. (1990). Liquid-To-Gas Mass Transfer In Anaerobic Processes:Inevitable Transfer Limitations Of Methane And Hydrogen In The Biomethanation Process, Applied And Environmental Microbiology, June, vol. 56 (6), 1636-1644.

Pelot, S. (n.d.). Turkey Textile Industry Profile:Turkey maintains its role as a diverse textile manufacturing country.
http://www.textileworldasia.com/Articles/2009/June_Issue/
Features/Turkey_Textile_ Industry _Profile.html

Raju, G. B.; Karuppiah, M. T.; Latha, S. S.; Parvathy, S. & Prabhakar, S. (2008). Treatment of Wastewater from Synthetic Textile Industry by Electrocoagulation–Electrooxidation, Chemical Engineering Journal 144, 51–58.

Talarposhti, A.M., Donnelly, T. & Andersonm, G.K. (2001). Colour Removal from a Simulated Dye Wastewater Using a Two-Phase Anaerobic Packed Bed Reactor, Water Research 35, 425-432.

Tang, H.N., Blum, D.J.W. & Speece, E.R. (1999). Comparison of Serum Bottle Toxicity Test with OECD Method, Joun. of Env. Eng. 116, 1076-1085.

Yang, X. (2009). Interior Microelectrolysis Oxidation of Polyester Wastewater and Its Treatment Technology, Journal of Hazardous Materials 169, 480–485.

Zengin, Z. S. & Aydinol, F. I. T. (2007). Treatment of Textile Industry Wastewater In Anaerobic Conditions; Subcategory: Cotton Industry, Fresenius Environmental Bulletin, Volume 16, No 12, 1593-1599.

Zainol, N., Salihon, J. &Abdul-Rahman, R. (2009). Biogas Production from Waste using Biofilm Reactor: Factor Analysis in Two Stages System, World Academy of Science, Engineering and Technology 54.

Fungal Decolourization and Degradation of Synthetic Dyes Some Chemical Engineering Aspects

Aleksander Pavko
University of Ljubljana, Faculty of Chemistry and Chemical Technology
Slovenia

1. Introduction

There are more than 100,000 different synthetic dyes available on the market, produced in over 700,000 tons annually worldwide. They are used in the textile, paper, cosmetics, food and pharmaceutical industries. Some of them are dangerous to living organisms due to their possible toxicity and carcinogenicity. About 10% of the above mentioned amount is lost in wastewater, which justifies the concern about the environment. Among the numerous water-treatment technologies, research interest in the fungal bioremediation, i.e. decolourization and degradation of synthetic dyes, has increased significantly in the last three decades.

The physico-chemical methods of dye degradation have already been well recognized from the chemical engineering point of view and also widely applied on the industrial scale. In the last few decades, research in the dye bioremediation technologies has gained its significance. From the available literature, it can be seen that the majority of research has been performed from the biochemical and microbiological point of view on a laboratory scale, while there is a lack of chemical engineering approach to the research of this serious problem. The purpose of this work is to review the chemical engineering principles, which should be applied during the research and transfer of dye bioremediation technologies to a large scale. Accordingly, a brief review of research results from bioreactors of volumes larger than 1.0 L is presented.

2. Alternative technologies

The dyes in wastewaters present a significant problem in the wastewater treatment, due to the complex and varied chemical structure of these compounds along with other residual chemical reagents and impurities. Generally, organic contents are high, while the BOD/COD ratios are low due to the not easily degradable nature of dyes. In addition, the degradation of products may be toxic. According to the latter, no universal method is known for their treatment. The degradation of synthetic dyes in waste streams can be performed with various technologies, which can be subdivided into four main groups: 1) physical, 2) chemical and photochemical, 3) electrochemical, and 4) biological processes. The processes are presented in Table 1 and briefly described below (Robinson et al, 2001; Joshi et al, 2004; Singh, 2006).

Regulatory agencies, esp. in developed countries, are concerned with environmental and public health, and with the imposition of the stringent environmental legislation, which is increasingly causing problems for the textile and dyestuff industry. The legislation and colour standards for waste discharge vary in different states. In addition, there are several standard methods for determining the colour standards, which aggravates a comparison of different colour degradation methods from various sources (Hao et al, 2000; Singh, 2006).

2.1 Physical methods

Adsorption has gained a favourable interest due to the efficient pollutant removal, quality product and economical feasibility. It is influenced by many physico-chemical factors, e.g. dye-sorbent interaction, adsorbent surface area and particle size, temperature, pH and contact time. Materials, like activated carbon, peat, wood chips, fly ash and coal, silica gel, microbial biomass, and other inexpensive materials (e.g. natural clay, corn cobs, rice hulls), are used, since they do not require regeneration. *Sedimentation* is a solid-liquid separation method. In the case of dye solutions, it is used in a combination with chemical or biological methods producing particles containing dye or dye degradation products with coagulation/precipitation or with some other chemical methods, or adsorption on various materials. The rate of sedimentation of particles suspended in a fluid can be described with Stoke's law and is influenced by many physico-chemical factors. The disadvantage here is a high sludge production. *Flotation* is a foam separation technique. Generally, it is performed by adding a surface active ion of the opposite charge to the ion to be separated from the solution. The solid product which appears on the gas-liquid surface is levitated to the surface of the solution by means of a gentle stream of fine gas bubbles. *Coagulation* can be induced by an electrolytic reaction at electrode surface or by changing pH or adding coagulants (Shakir et al, 2010). Furthermore, *membrane filtration* can be used to remove dye molecules. The classification of membranes is conducted on the basis of their pore size to retain solutes with different molecular weights. The membrane parameter is called molecular weight cut off (MWCO). In the case of dye separation, reverse osmosis (MWCO < 1000), nanofiltration (500 < MWCO < 15000) and ultrafiltration (1000 < MWCO < 100000) membranes can be used according to the dye characteristics. In addition to the dye solution separation, membranes can be used also for the separation of particles after the adsorption or coagulation/precipitation instead of the sedimentation (Hao et al, 2000). The *radiation* itself can be classified as a physical method. However, in the case of dye degradation, the radiation dose in aqueous media leads to the formation of strong oxidizing species such as *OH radicals, which are able to react with dye molecules, degrade them and consequently,

Physical	Chemical	Electrochemical	Biological
Adsorption	H_2O_2 oxidation	Electrocoagulation	Bacterial aerobic
Sedimentation	Fenton oxidation	Electroflotation	Bacterial anaerobic
Flotation	Ozonization	Electrooxidation	Algae
Coagulation	Chlorination	Electroreduction	Fungi
Membrane filtration	Photochemical oxidation		Yeast
Radiation	Wet air oxidation		
	Reduction		

Table 1. Methods for dye degradation and decolourization in waste streams

enhance the degradation process. Therefore, radiation methods are usually included in the advanced oxidation processes (AOPs) (Rauf et al, 2009). During *ultrasonic irradiation*, the propagation of an ultrasound wave leads to the formation of cavitation bubbles. The collapse of these bubbles spawns high temperatures and pressures, which leads to the production of radical species and in consequence, to the chemical reaction of dye degradation (Vinodgopal et al, 1998). In general, solid waste disposal is required after the physical methods of separation.

2.2 Chemical and electrochemical methods

Chemical oxidation is the most commonly used method of decolourization, mainly due to its simplicity of application. The oxidising agent is usually hydrogen peroxide, which needs to be activated due to its stability in the pure form. Methods vary according to the way in which H_2O_2 is activated. It removes the dye from the effluent with an aromatic ring cleavage of dye molecules. A well known activator is Fe(II) salt known as Fenton's reagent. The result of sorption or bonding of dissolved dyes is a sludge generation through the flocculation of reagent and dye molecules, which needs disposal and is therefore disadvantageous. H_2O_2 can be activated also with ozonization. A major drawback is a short half-life of ozone in water and its cost – it degrades in about 20 minutes and has to be applied continuously. In addition, its stability is affected by the presence of dyes, salts, pH and temperature. Hydrogen peroxide can be activated also with UV radiation. The major advantage of H_2O_2/UV treatment is that the use of no other chemicals is required. The wet air oxidation (WAO) process presents a hydrothermal treatment of dissolved and suspended components in water, and has been successfully used also for several azo dyes (Kusvuran et al, 2004; Rodriguez et al, 2009). Chlorination, using chlorine gas or sodium hypochloride, is an inexpensive and effective method. It has become less frequent due to the generation of toxic and carcinogenic compounds. In addition, the use of chemicals containing chlorine is restricted due to environmental reasons. As already mentioned, photochemical methods are based on the use of UV light, which activates the chemicals and consequently, enhances the chemical reaction and makes the process more efficient.

The principle of electrochemical methods is to charge the electric current through electrodes made of different materials (e.g. iron or aluminium) resulting in the oxidation process at anode and reduction at the cathode with H_2 production. The resulting processes are known as electrocoagulation, electroflotation, electrooxidation and electroreduction. The majority of the above mentioned methods are the so-called 'advanced oxidation processes' (AOP), and are essentially based on the generation of highly reactive radial species (Hao et al, 2000; Slokar & Majcen, 1998; Joshi et al, 2004).

2.3 Biological methods

A biological treatment presents a degradation of organic substances by microorganisms under aerobic or anaerobic conditions, and has been widely used and researched. The dyes themselves are generally resistant to oxidative biodegradation. In addition, toxicity, as well as the acclimating ability is a drawback of using microbial cultures. It has been demonstrated that mixed bacterial cultures are capable of decolourizing textile dye solutions. Nevertheless, several studies show that little biodegradation actually occurs and that the primary mechanism is adsorption to the microbial biomass (Slokar, 1998; Robinson et al, 2001; Knapp, 2001).

A continuous aerobic or anaerobic treatment can be conducted in a variety of bacterial bioreactors, e.g. reactors with activated sludge, reactors with biofilm in the form of fixed bed, rotating discs or rotating drum. An aerobic and anaerobic treatment can also be combined. It has also been reported that few species of algae are capable of degrading azo dyes and utilize them as a sole source of carbon. Some articles on yeasts capable of dye decolourization can also be found in the literature (Joshi et al, 2004). Several fungal systems have been demonstrated to degrade various classes of dyes. A particular interest was devoted to the white-rot fungi and azo dyes, the largest class of commercial dyes. A fungal treatment of dyes is an economical and feasible alternative to the present treatment technologies (Knapp, 2001; Singh, 2006).

3. Dyes

The main common property of dyes is to absorb light due to the chromophore, a part of the molecule responsible for its colour. The colour arises when a molecule absorbs certain wavelengths of visible light and transmits or reflects the others. However, the variation in the structure is enormous and many thousand different dyes are produced for commercial use. In general, dyes can be classified according to their chemical structure, particularly chromophore, and the method of application. The classes of dyes from the textile industry together with some of their typical representatives are presented in Table 2 (Corbmann, 1983; Hao et al, 2000).

Classification according to chemical structure and/or chromophore	Classification according to method of application
azo anthraquinone triphenylmethane phthalocyanine indigo sulphur	acid basic direct reactive disperse vat mordant sulphur

Table 2. Main groups of dyes according to chemical structure and method of application

Among 12 different chromophores, azo and anthraquinone dyes are the major units. *Azo dyes*, characterized by nitrogen to nitrogen double bonds account for up to 70% of all textile dyestuff produced and are the most common chromophore of reactive dyes. *Anthraquinone dyes* derive from anthraquinone with a quinoid ring acting as the chromophore and either hydroxyl groups or amino groups attached to the general structure. *Triphenylmethane dyes* are synthetic organic dyes with a molecular structure based on the hydrocarbon triphenylmethane, used in textile applications where lightfastness is not important. The *phthalocyanine dyes* derive from the macrocyclic compound which forms a coordination complex with most elements of the periodic table. They are few in number, but commonly used. *Indigo* is an organic dye with a distinctive blue colour. Historically, it was extracted

from plants; however, nearly all indigo produced today is synthetic. *Sulphur* dyes are a group of sulphur-containing complex synthetic organic dyes (Hao et al, 2000).

Acid dyes are water soluble anionic dyes with different chromophore groups substituted with acidic functional groups such as nitro-, carboxyl- and sulphonic acid, for the dye to become soluble. *Basic dyes* are cationic types with chromophores typically having amino groups. *Direct dyes* are highly water-soluble salts of sulphonic acid of azo dyes. *Reactive dyes* are highly water-soluble anionic dyes with wet fastness and binding to textile fibres via covalent bonds. *Disperse dyes* are substantially water-insoluble non-ionic dyes for the application to the hydrophobic fibres from aqueous dispersions. *Sulphur dyes* are dyes applied in two parts. The initial bath consists of the yellow or pale chartreuse colour, which is aftertreated with a sulphur compound in place to produce dark black. *Mordant dyes* require a mordant (usu. potassium dichromate), which improves dyestuff fastness on a dyeing material in water media. Many mordants can be hazardous to health. *Vat dyes* are essentially insoluble in water and incapable of direct dyeing of fibres. A reduction in alkaline liquor makes them water soluble and attachable to textile fibres, while a subsequent oxidation reforms the originally insoluble dye (Corbmann, 1983).

4. Fungal decolourization and degradation of dyes

4.1 White-rot fungi

White-rot basidiomycetes are a group of fungi capable of depolymerizing and mineralizing otherwise not easily degradable lignin with their extracellular and non-specific ligninolytic enzymes. In the 1980s, this fact stimulated research on the ability of ligninolytic fungi to degrade organic pollutants (Pointing, 2001; Gao et al., 2010). It was established that *Phanerochaete chrysosporium* is capable of biodegrading various pollutants and it soon became a model white-rot fungus with most of the research done up to now. The enzymes produced with this fungus are lignin peroxidase (LiP) and manganese peroxidise (MnP)(Podgornik et al, 2001; Faraco et al, 2009). In the next decade, a few new species of white-rot fungi like *Pleurotus ostreatus* and *Trametes versicolour* (Heinfling et al, 1997; Sukumar et al, 2009; Pazarlioglu et al, 2010) were characterized for the dye degradation. A more intense research with *Irpex lacteus* (Novotny et al, 2009) and *Bjerkandera adusta* (Robinson et al, 2001; Eichlerova et al, 2007) started in the last decade, while the interest in the decolourization capability of *Ceriporiopsis subvermispora* (Babič & Pavko, 2007; Tanaka et al, 2009) and *Dichomites squalens* (Eichlerova et al, 2006; Pavko & Novotny, 2008) has increased in the last few years.

Organism	Enzyme activities	Reference
Bjerkandera adusta	MnP, Lac, LiP	Robinson et al, 2001; Eichlerova et al, 2007
Ceriporiopsis subvermispora	MnP,Lac	Babič & Pavko, 2007; Tanaka et al, 2009
Dichomitus squalens	MnP, Lac	Eichlerova et al, 2006; Pavko & Novotny, 2008
Irpex lacteus	MnP, Lac, LiP	Novotny, 2009
Phanerochaete chrysosporium	LiP, MnP	Podgornik et al, 2001; Faraco et al, 2009
Pleurotus ostreatus	LiP, Lac	Heinfling et al,1997; Sukumar et al, 2009; Pazarlioglu et al, 2010
Trametes versicolour	Lac, LiP	Heinfling et al,1997; Sukumar et al, 2009; Pazarlioglu et al, 2010

Table 3. Some white-rot fungi used in biodegradation/decolourization studies and their most commonly expressed enzyme activities

Some white-rot fungi used in the biodegradation/decolourization studies and their most commonly expressed enzyme activities are presented in Table 3. The data are collected from numerous research articles, where the cultivation conditions varied and it is thus possible that an activity would or would not occur under different cultivation conditions, esp. nitrogen contents (Knapp, 2001; Singh, 2006).

4.2 Mechanisms of fungal dye degradation and decolourization

The mechanisms of fungal dye decolourization and degradation are listed in Table 4. The accumulation of chemicals with the microbial biomass is termed *biosorption*, and can take place on living or dead biomass. Waste and/or dead microbial biomass can be used as an efficient adsorbent, especially if containing a natural polysaccharide chitin and its derivative chitosan in the cell walls. Chitosan, a cell wall component of many industrially useful fungi, has a unique molecular structure with a high affinity for many classes of dyes (Joshi et al, 2004).

Adsorption (biosorption)
Biodegradation
Adsorption and biodegradation
Mineralization
Utilization as carbon source

Table 4. Mechanisms of fungal dye degradation and decolourization

It is known that most of the white-rot fungi produce at least two of the three highly nonspecific enzymes like LiP, MnP and Lac, which enable the generation of free radicals when conducting a variety of reactions (Pointing, 2001; Knapp, 2001). The structure of dyes strongly influences their degradability by pure cultures and isolated enzymes. Numerous data about biodegradation of various synthetic dyes with selected white-rot fungi have been published. Nevertheless, a limited number of data are available on systematic studies about the relation between the structure and biodegradability, esp. for commercial dyes with a complex structure. According to the above mentioned, in the presence of biomass in the dye solution, it has to be distinguished between the dye depletion due to adsorption and the one due to enzymatic degradation. The fungal action rarely leads to the mineralization of dyes and very much depends on the chemical structure. A higher mineralization occurs with dyes containing substituted aromatic rings in their structure compared to the unsubstituted rings. A better mineralization is observed also under nitrogen limited conditions. Some reports on the utilization of dyes as a carbon source have been published in the last decade. Certain bonds in the dye molecule are cleaved and utilized as a carbon source, the chromophore not being affected. This mechanism occurs preferably in the consortium of microorganisms (Knapp, 2001; Singh, 2006).

4.3 Factors affecting fungal decolourization and degradation of dyes

The fungal growth and enzyme production, and consequently, decolourization and degradation are influenced by numerous factors, e.g. media composition, pH value, agitation and aeration, temperature and initial dye concentration. Their effect is briefly presented and discussed below.

4.3.1 Media composition

There is no doubt that media composition has an enormous effect on fungal growth and production of their decolourization systems. It must be noted that real industrial effluents vary with location and time, not to mention the often very complex composition with a lack of nutrients, compared to the usually well defined media used in the research. Therefore, attention has to be focused on the supply of carbon and nitrogen sources together with mineral nutrients and other additives (Hao et al, 2000; Knapp, 2001; Singh, 2006).

Carbon source. A carbon source is necessary for fungal growth and to provide the supply for oxidants, the fungus requires for decolourization. Glucose has been used in the majority of research studies. Alternatives are fructose, sucrose, maltose, xylose and glycerol, while also starch and xylan seem to be useful. Surprisingly, cellulose and its derivatives were not effective. For initial experiments, glucose at 5–10 g/L is a good choice. Effluents from dyeing or chemical/dye production usually do not contain usable carbon substrates, while others from distilling or paper pulping may have a range of carbohydrates as useful substrates for certain white-rot fungi. The need to add carbon source depends on the organism and type of the dye to be treated.

Nitrogen source. The nitrogen demand for growth and especially enzyme production differ markedly among fungal species. It is well known that the production of ligninolytic enzymes with *P. chrysosporium* is much more effective under the conditions of nitrogen limitation. On the other hand, *B. adusta* produces more LiP and MnP in nitrogen-sufficient media. White-rot fungi can use inorganic as well as organic nitrogen sources. Inorganic nitrogen, in most cases ammonium salts, has been used during the research of fungal growth and enzyme production, since the organic nitrogen seems not to be advantageous. In the case of effluents, the presence of usable nitrogen sources should be considered.

Other media components. Many studies have been using growth factors. However, considering their expense, it is not economical to use them in the decolourization technologies. All microbes have certain requirements for mineral nutrients, e.g. white-rot fungi need iron, copper and manganese. They can be a part of the effluent or must be added to the media. A variety of other materials, like veratryl alcohol, tryptophan and aromatics, e.g. phenol and aniline, can act as low molecular mass redox mediators of ligninolytic activities and therefore promote the decolourization (Knapp, 2001; Singh, 2006). It is interesting that some components in wood and straw induce the enzyme production with white-rot fungi. For example, the enzyme activity ratio Lac/MnP can be regulated using beech wood as the immobilization support and inducer together with a combination of various concentrations of additional nitrogen and carbon source in the liquid media during the cultivation of *Ceriporiopsis subvermispora* (Babič & Pavko, 2007). The ligninolytic enzyme production by *Dichomitus squalens* can be substantially induced by adding beech wood and straw particles to the liquid media (Pavko & Novotny, 2008).

4.3.2 pH

Most of the research on growth and enzyme production has been performed in batch cultures, usually without the pH control during the cultivation, for the influence of initial pH value, sometimes with adequate buffering, to be investigated. The majority of filamentous fungi together with white-rots grow optimally at acidic pH values. Depending on the used substrate, pH changes during cultivation. The growth on carbohydrate-containing media generally causes acidification of the media, which depends on the carbon source and present buffering. The decolourization can be conducted with a whole

fermentation broth (mycelium and enzymes) or with isolated enzymes. It has to be distinguished between the optimum pH for growth and enzyme production, the optimum pH for the action of isolated enzymes and the optimum pH for dye degradation. Therefore, optimum pH depends on the medium, fungus and its enzyme system, as well as on the decolourization under consideration. The majority of researchers suggest that the optimum pH values are likely to be in the range 4–4.5 (Knapp, 2001).

4.3.3 Temperature
Temperature has to be considered from various viewpoints: its influence on the growth and enzyme production, the enzymatic decolourization rate and the temperature of the waste stream. Most white-rot fungi are mesophiles with the optimal cultivation temperature 27–30 °C. The optimal temperatures for enzyme reactions are usually higher, but the enzyme instability and degradation has to be taken into account at temperatures approaching for example 65 °C. Various textile and dye effluents are produced at temperatures 50–60 °C. The optimal decolourization process temperature for a particular process has to be thus selected from case to case according to the mentioned parameters (Knapp, 2001; Singh, 2006).

4.3.4 Agitation and aeration
Ligninolytic fungi are obligate aerobes and therefore need oxygen for growth and maintenance of their viability. In addition, lignin degradation also requires oxygen, either for the mycelial generation of H_2O_2 for peroxidases or for the direct action of oxidases. Oxygen could also act directly on lignin fragments. The oxygen demand depends on the fungus and its ligninolytic system.

The oxygen supply to the culture media during the cultivation has been an interesting research topic for decades and has been covered in numerous articles. The major problem is its low water solubility, which is only 8 mg/L at 20 °C. To satisfy the microbial oxygen requirements during the cultivation and to enhance the oxygen gas-liquid mass transfer, the aeration and agitation are necessary. This might affect the morphology of filamentous fungi and lead to the decreased rate of enzyme synthesis (Žnidaršič & Pavko, 2001). As a result, various bioreactor types generally divided into static and agitated configurations were invented to provide enough oxygen. The choice of the reactor depends on the particular system although an appropriate agitation gives as good or even better results as those from static conditions. Particular studies on the effect of agitation and aeration only on the decolourization process were not found in the literature (Knapp, 2001).

4.3.5 Initial dye concentration
It is important to optimize the initial dye concentration for colour removal. Dyes are namely usually toxic to microorganisms, while the toxicity depends on the type of dye. Higher dye concentrations are always toxic. The range of initial dye concentrations studied in the literature generally varies from 50–1000 mg/L, and depends on the investigated microorganism and type of dye (Singh, 2006).

5. Reactor design considerations

The reactor design uses information, knowledge and experience from various areas, e.g. thermodynamics, chemical kinetics, fluid mechanics, mass and heat transfer, and economics.

To select a proper reactor configuration and size, it is necessary to know how materials flow and contact in the reactor, and how fast is the process. Usually, the conversion of the reactant should be as high and as fast as possible at the lowest costs (Levenspiel, 1999).

In our case, two different processes are taking place. The first one is the fungal growth and enzyme synthesis with fungal biomass, and the second one is the decolourization and degradation of dyes caused by the produced enzymes. Fungal enzymes can be intracellular or extracellular products, synthesized during the growth or after the growth phase. The colour depletion in wastewater can take place due to the enzymatic degradation or only adsorption on the biomass. The enzyme production and decolourization must be simultaneously optimized to get the best dye conversion in the shortest time. According to this, two main strategies can be pursued, i.e. (1) the direct transformation of dye with the active biomass in one reactor, or (2) the use of extracted enzymes from the culture medium.

The biomass growth and enzyme production as well as dye degradation take place in the liquid phase. Under aerobic conditions, the aeration of the reactor is necessary, while under anaerobic conditions, methane is produced. The microbial biomass, especially when immobilized, can be treated as a solid phase; therefore, the reactor can be considered as a gas-liquid-solid system with all its liquid flow and mass transfer characteristics.

For a successful design of the process with a given capacity, the reactor type, i.e. shape and size, as well as the operation mode of the reactor must be selected at the beginning. Moreover, the operating conditions such as concentrations, flow rates, temperature and pH must be defined. One of the most important data for the design is the reaction rate, which allows the calculation of time in the batch mode or flow throughput in a continuous mode for the necessary reactant conversion – in our case, dye degradation or decolourization degree. Frequently, pilot plant experiments in addition to laboratory data are necessary to establish the proper scale up method for the transfer of the process from the laboratory to industrial scale. Finally, an economical evaluation is crucial before the realization of the project. All these facts are briefly described in the continuation of this chapter.

5.1 Reaction rate

In the chemical reactor design, chemical reactions can be usefully classified into homogeneous and heterogeneous reactions according to the present gas, liquid and solid phases. In addition, a distinction can be made between non-catalytic and catalytic reactions. The reaction rate of the reaction component is usually based on the unit volume of reaction fluid (mol/Ls); however, it can be based on the unit mass of catalyst, unit interfacial surface in the heterogeneous system etc. On the other hand, a chemical reaction follows the stoichiometric equation. In the simplest case of a homogenous reaction of components A and B in a liquid phase:

$$aA + bB \rightarrow products \tag{1}$$

the expression for the reaction rate of disappearance of the component A can be written as follows:

$$dC_A / dt = -r_A = k\, C_A^a C_B^b = k\, C_A^a\, (b/a)^b C_A^b = kC_A^{a+b} = kC_A^n \tag{2}$$

where $k = k(b/a)^b$ is the reaction rate constant, a and b are the reaction order with respect to A and B – the power to which the concentration is raised, while n is the overall reaction order. The integrated form of the equation allows the calculation (prediction) of time

required to achieve the desired degradation level or conversion for the component A (e.g. dye) in a batch reactor for a given concentration at the beginning (C_{A0}) and the end (C_A) of the process:

$$t = -\int_{C_{A0}}^{C_A} dC_A / (-r_A)$$

(3)

For elementary reactions, the correlation between the stoichiometric and rate equation is simple, while with non-elementary reactions, the reaction mechanism must be known to write down the correct rate equation. The enzyme-substrate reactions are a typical case (Levenspiel, 1999). With heterogeneous reactions, the oxygen transfer from air bubbles to the liquid phase or the transport of dye from the bulk solution inside the biomass particle and its degradation has to be considered. In this case, the rate expression and the design equation to predict the conversion in the reactor of selected size and operating conditions are much more complicated.

Figure 1 shows that the shape of the concentration vs. time curve varies with the reaction order (n = 0 : k = 1.2 mg/Lh; n = 1 : k = 0.1 h^{-1}; 0 < n < 1 : k_1 = 1 h^{-1}, k_2 = 1 mg/L). A mathematical analysis of the experimental data allows the determination of the kinetic Equation 2.
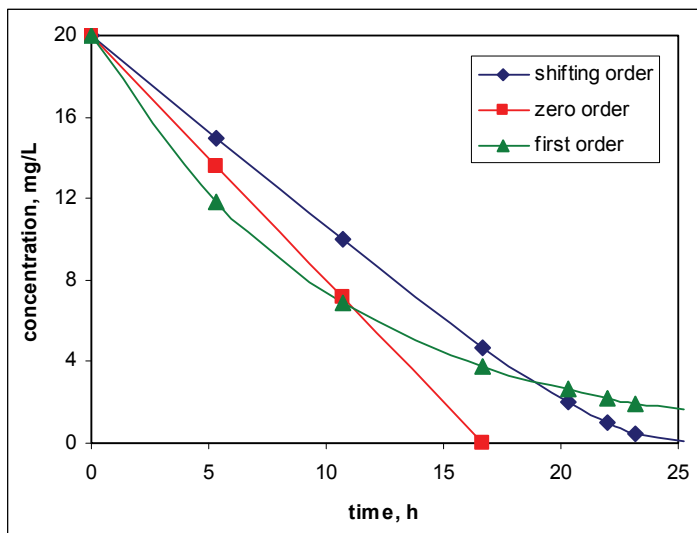
Fig. 1. Concentration profile of reactant following reaction of zero and first order, and for shifting order (enzyme catalysed reaction following Monod kinetics) in batch reactor

5.2 Fluid flow

Ideal reactors have three ideal flow or contacting patterns. In a well mixed batch reactor, a uniform composition is everywhere in the reactor, but the composition and consequently, the reaction rate changes with time. For a continuous operation, two types of ideal flow can be achieved. In a mixed flow, the same composition is everywhere within the reactor and

also at the exit. Furthermore, the reaction rate is the same at any point in the reactor. Therefore, the performance equation can be written for the reactor as a whole:

$$\tau = V/F = (C_{A0} - C_A)/(-r_A) \tag{4}$$

where τ (s) is the space time or time required to process one reactor volume of feed measured at specified conditions, V (m³) is the fluid volume in the reactor, F is the volumetric flow (m³/s), C_{A0} and C_A are the concentrations of reactant in the inlet and outlet stream, while $-r_A$ (g/m³s) is the expression for the reaction rate of disappearance of the reactant – in our case dye.
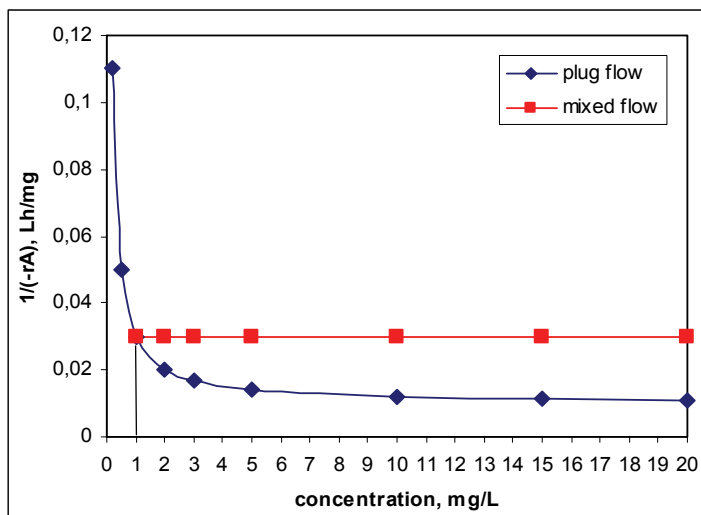

Fig. 2. Effect of ideal fluid flow on reactor performance: for same inlet and outlet concentrations, and fluid flow rate, volume of plug flow reactor is smaller

In the reactor with a plug flow, the composition of the fluid varies from point to point along the flow path. To obtain the performance equation for the whole reactor, an integration of differential mass balance equation for a differential volume element is necessary.

$$\tau = V/F = -\int_{C_{A0}}^{C_A} dC_A / (-r_A) \tag{5}$$

In the above equation, τ (s) is the space time or time required to process one reactor volume of feed measured at specified conditions, V (m³) is the fluid volume in the reactor, F is the volumetric flow (m³/s), C_{A0} and C_A are the concentrations of reactant in the inlet and outlet stream, while $-r_A$ (g/m³s) is the expression for the reaction rate of disappearance of the reactant, in our case dye.

Typical shapes of reactors where the plug flow can be achieved are tubular reactors or long columns. A consequence of the type of flow is that the reactor volume for mixed flow and plug flow (for reaction order not equal zero) is different for the same fluid throughput and reactant inlet concentrations and its conversion at the exit. This very important fact has to be

considered in the reactor selection and design. Figure 2 shows the case for the Michaelis-Menten enzyme kinetics (v_{max} = 100 mg/Lh, K_m = 2.0 mg/L, C_{A0} = 20 mg/L, C_A = 1 mg/L). It can be seen that the space time and consequently, the volume for the mixed flow reactor is proportional to the area below the horizontal line (cf. Equation 4), while for the plug flow reactor, the space time is proportional to the area below the curve (cf. Equation 5). In consequence, the required volume of plug flow reactor is by 50% lower (Doran, 1995; Levenspiel, 1999).

Real reactors always deviate from an ideal flow due to stagnant regions, fluid channelling, or short-circuiting. To predict the behaviour of a continuous reactor, the velocity distribution of fluid elements or their residence time distribution (RTD) has to be considered. This information can be obtained easily and directly with stimulus-response experiments. In a two phase reactor, stirred tank with aeration or bubble column for example, each phase can have its own flow characteristics (Levenspiel, 1999).

5.3 Types of operation

In general, two basic modes of reactor operation are known. A constant volume batch operation is a typical non-steady state process. Here, the final concentration of the produced biomass and enzyme and/or degraded dye and degradation products in the reactor are achieved after a certain process time. During the constant volume continuous process, the biomass growth and enzyme production as well as dye degradation take place in the reactor with the reactant inflow, in our case substrate and/or dye, and liquid outflow with the products of the process. The outflow may contain biomass, produced enzyme, non-used substrate, non-degraded dye and dye degradation products. The type of flow must be considered and a steady state can be achieved. To increase the process performance, biomass and/or enzymes can be immobilized and kept in the reactor. Extracellular enzymes can be retained in the reactor by using a membrane, which permeates the dye with its degradation products. The concentrations at the liquid outflow mainly depend on the kinetics of growth, enzyme production and dye degradation as well as space time, defined as the reactor volume divided by volumetric feed rate. An inverse value of space time is dilution rate, a well known parameter in biotechnology of continuous processes. Other types of operation are also known, i.e. fed batch, repeated fed batch and recycle (Doran, 1995).

5.4 Productivity and throughput

The simplest case, a direct transformation of dye with active biomass in one reactor is considered here. The productivity of biomass during the batch fermentation can be simply defined as an increase in the biomass concentration at the point of productivity estimation from the point of inoculation divided by the process time. The productivity is shown in Figure 3 as the slope of the line. The maximum biomass productivity is achieved earlier than the maximum biomass concentration. For the process time, growth time after inoculation as well as 'dead' periods like cleaning, sterilizing and harvesting are taken into account. It should be noted that the maximum biomass productivity is not always at the point of maximum biomass concentration. In the case of batch dye decolourization/degradation, productivity should be redefined as dye degradation or dye decolourization capacity according to a specific case. For example, if the growth and enzyme production is followed by the dye degradation process in a batch reactor, the dye concentration drop from the point

of dye addition till the end of degradation process should be divided with the whole process time for growth, enzyme production, decolourization, plus dead time. For such a definition, the decolourization capacity very much depends on the initial and final dye concentrations, and the decolourization/degradation rate around the final dye concentration.
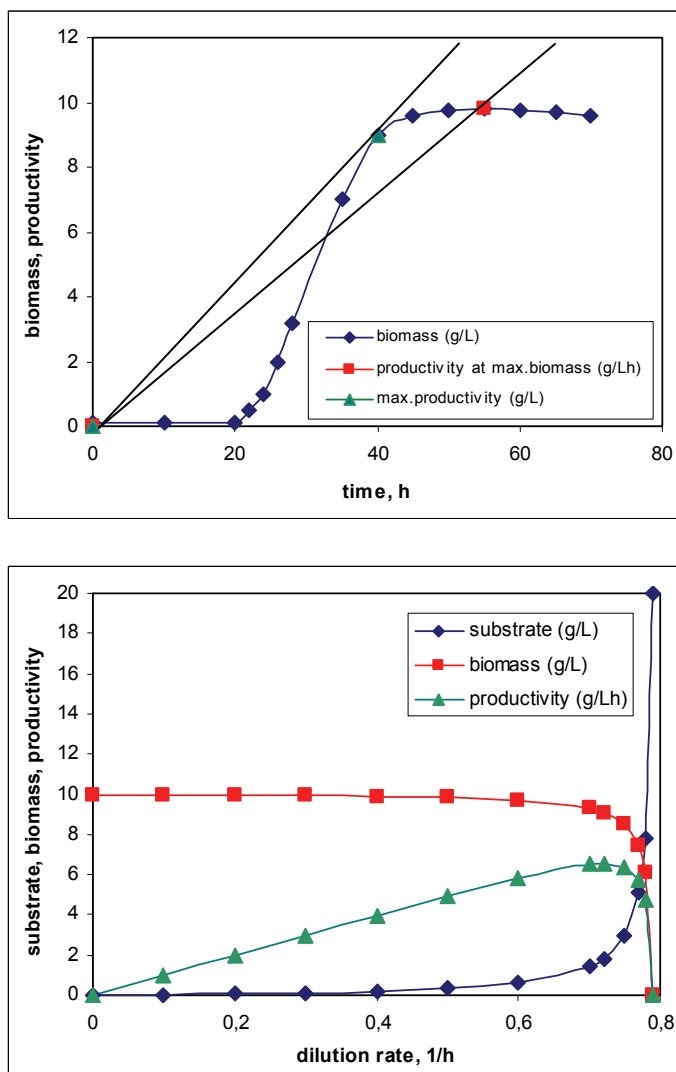

Fig. 3. Biomass productivity during batch (above) and continuous operation (below) of stirred tank reactor

The steady state concentrations during a continuous fermentation in a constant volume ideal stirred tank bioreactor are dependent on the dilution rate D = F/V, i.e. the ratio between the liquid volumetric flow rate and liquid volume in the reactor. Here, the variables like substrate, dye, enzyme, biomass and product concentrations can be considered. The critical operating point is the value of dilution rate, where the biomass and fermentation products are washed out from the reactor and the inlet stream with its components simply flows through the reactor, since there is no chemical reaction within the reactor. Figure 3 demonstrates the case of continuous biomass production for Monod growth kinetics (So = 20 g/L; $Y_{x/s}$ = 0.5; K_s = 0.2 g/L; μ_{max} = 0.8 h^{-1}). The biomass productivity here is defined as a product between biomass concentration (X) and dilution rate (D). It can be seen that it has its maximum at a certain dilution rate; therefore, the dye degradation should be controlled around this point (around 0,7 h^{-1} in our case). The dosing of dye to the reactor can be performed separately or together with the substrate inflow (F). The dye flow into the reactor with a given volume (V) must correspond to the requested dye conversion and degradation rate according to Equation 4 (Doran, 1995).

5.5 Mathematical modelling

Mathematical modelling is a useful tool for chemical engineers, which leads to better understanding of the process and reduces the number of experiments. It helps designing experiments and it is successfully used for the process regulation and control. Mathematical simulations can also be a very good enrichment for the teaching process. Briefly, it means writing down an idea of a process in the mathematical language. It consists of several steps. The system with its boundaries has to be defined first, where a chemical reaction can occur, and then the mass and energy exchange can take place. In bioremediation, the reactor is a typical system. Afterwards, the process variables and parameters have to be defined, e.g. biomass, enzyme and dye concentrations. The analysis of process dynamics gives useful information, which of the process variables considerably changes with time, or which remains constant. One of the main steps is the formulation of the mathematical model on the basis of previous steps. The type of fluid flow and various physical and chemical laws have to be considered. Equations describing mass and heat transfer, reaction rate and correlations for various coefficients are written and solved for the corresponding initial and boundary conditions. On the basis of parametric sensitivity analysis which follows, the effect of various parameters on process variables is seen and the model can be simplified. The crucial step is the verification of the mathematical model, which means a comparison of the calculated results with the model and experimental results. If the results agree within the expected deviation, the model is good and useful. If not, previous steps must be repeated by including new data (Snape et al, 1995).

5.6 Scale up

The development of a microbiological process is usually conducted in three scales, i.e. 1) laboratory scale, where a basic screening and growth conditions are investigated; 2) pilot plant, where an optimization of environmental factors is studied; and 3) plant scale, where the process is brought to an economic function. Environmental conditions involve chemical factors (e.g. media composition, pH) and physical factors (e.g. mixing, aeration, shear). They are crucial for the successful aerobic growth and enzyme production in an aerobic bioreactor, which is considered a two phase system. The transport phenomena like gas-

liquid oxygen transfer, heat transfer and mixing, as well as the chemical reactions in a liquid phase like oxygen and substrate consumption, the biomass growth and enzyme production take place simultaneously during the cultivation. On the basis of regime analysis, it must be established which of the above mentioned processes is the slowest, and therefore controls the microbial growth and enzyme production. During the transfer from the laboratory to larger scale, an optimization of this process must be considered. Historically, keeping a constant gas-liquid oxygen transfer rate in a small and large scale was mostly used, proving as a successful scale up criteria. Namely, the low rate of this process compared to other previously mentioned is characterized by low oxygen solubility in water, and can be improved with increased mixing and aeration. Usually, the geometrical similarity of both reactors was ensured and the maximum allowed impeller tip speed to avoid cell damage was taken into account. According to the above mentioned, a general scale up criteria for the microbial cultivation is to keep the optimal environmental conditions as much as possible on all scales to obtain the necessary productivity (Wang et al., 1979).

The dye degradation and/or decolourization reactions at a given enzyme activity in the solution take place in a liquid phase, and do not depend on oxygen gas-liquid mass transfer. According to the literature data, these reactions are mostly slow. The scale up of this process needs the expression of the reaction rate at a given dye concentration range, as well as the optimal pH and temperature. On the basis of the reactor type, its operation mode, rate equation and given dye conversion, the necessary degradation time in a large batch reactor of a given volume can be estimated. Similarly, the dye feed rate in a large continuous reactor can be calculated (cf. Equations 3–5).

In the case of biodegradation or decolourization in the presence of the biomass, the situation is much more complex, since the dye transport from the liquid to the active site inside the biomass has to be taken into account. Here, the degradation and/or adsorption can take place. Generally, proper mixing or fluid flow, as well as the biomass thickness can affect the dye depletion rate in the solution. For a successful scale up, a detailed investigation of the effect of the mentioned parameters on the reaction rate is necessary on the laboratory and pilot plant scale. The scale up principle may vary from case to case. Unfortunately, no research data covering this topic were found in the available literature.

5.7 Costs

Costs fall into two categories, i.e. capital costs and operating costs. Capital costs generally include initial and periodic expenses and consist of 1) design and construction, 2) equipment and installation, 3) buildings and structures, and 4) auxiliary facilities. The costs for a start up have to be taken into account in this category as well. Operating costs generally cover 1) labour, 2) equipment maintenance and parts, 3) expendable supplies and materials, 4) utilities (e.g. electricity, water, steam, gas, telephone etc), 5) ongoing inspection and engineering, and 6) laboratory analyses (Freeman, 1998).

The degradability of the dye strongly depends on its chemical structure. This fact plays an important role during the bioremediation. In addition, the fungal cultivation is done under sterile conditions, which increases the costs of the process. The dye removal efficiency is usually better with one of the chemical oxidation methods, where it can exceed 90%. The time required for oxidative decolourizations are much shorter (in minutes) compared to those needed for the adsorption or biodegradation (in hours or days) (Slokar & Majcen Le Marechal, 1998).

Practically no data on the costs of dye removal can be found. Only the evaluation of water reuse technologies for the spent dyebath wastewater containing three reactive dyes from a jig dyeing operation was found in the literature. With several methods, e.g. electrochemical oxidation, oxidation with ozone, reduction with sodium borohydride and adsorption on activated carbon, the colour removal was 78–98%, while the operating costs were estimated to be 10–94 \$ per 1,000 gallons treated. Unfortunately, the dyes were toxic to the tested microorganisms and the biodegradation method was unsuccessful (Sarina, 2006).

Therefore, from this point of view, chemical methods seem for the time being more economical than the fungal bioremediation.

6. Bioreactors for fungal degradation and decolourization of dyes

A variety of reactor configurations has been used, similar to those for the fungal cultivation under submerged conditions. Gentle mixing and aeration have usually been the necessary prerequisites for a successful biomass growth and enzyme production. The immobilization of fungal mycelia also showed useful results. Batch and continuous operations were shown to be effective – both having advantages and disadvantages. Several papers have reported the repeated use of mycelia over several cycles of decolourization lasting from several weeks to a few months. Most of the studies were performed under aseptic conditions, while some were effective also during non-aseptic conditions. The toxicity of the dye highly affects the dye degradation and decolourization. Selected references from the last decade for laboratory reactors with volumes larger than 1.0 L are briefly presented below.

Type of reactor	Volume	Organism	Dye	Removal	Duration	Reference
Stirred tank	5 L	*B. adusta*	Black 5	95%	20 d	Mohorčič, 2004
Stirred tank	3.5 L	*T. versicolour*	R. Black 5	91–99%	8 d/200 d	Borchert, 2001
			R. Red 198			
			Brilliant Blue R			
Stirred tank	4.0 L	*T. versicolour*		90%	10 d	Libra, 2003
Stirred tank	1.0 L	*T. versicolour*	Poly R-478	80%	19 d	Leidig, 1999
Bubble column	1.5 L	*T. versicolour*	Orange G	97%	20 h	Casas, 2007
Bubble column	1.5 L	*T. versicolour*	Grey Lanaset G	90%	42 d	Blanquez, 2004
Packed bed	2.0 L	*Strain F29*	Orange I	95%	3.5 d HRT/60 d	Zhang, 1999
Trickle bed	1.0 L	*I. lacteus*	RO16	95%	6 d	Tavčar, 2006
Rotating discs	1.7 L	*C. versicolour*	Everzol T Blue G	80%	2 d/12 d	Kapdan, 2002
Rotating discs	1.6 L	*P. Sordida*	Basic Blue 22	80%	2 d/12 d	Ge, 2004
Rotating discs,	1.0 L	*I. lacteus*	RO16	95%	10 d	Tavčar, 2006
Rotating discs	1.0 L	*D. squalens*	RBBR,	99%	6 h	Trošt, 2010
			Azure B	92%	8 d	
			Methylene blue	59%	30 h	
Biofilm	1.0 L	*Fungal consortium*	RB5, AR249, RR M-3BE	70–90%	12 h/96 d	Yang, 2009
Biofilm	10.0 L	*C. versicolour*	Everzol T Blue G	82%	50 h	Kapdan, 2002
Membrane	11.8 L	*C. versicolour*	Acid Orange II	97%	1 d/62 d	Hai, 2008
Membrane	5.0 L	*P. chrysosporium*	RBR X-3B	90%	1 d/65 d	Gao, 2009

Table 5. Fungal bioreactors for degradation and decolourization of dyes

6.1 Stirred tank bioreactor

The decolourization of the diazo dye Reactive Black 5 with *Bjerkandera adusta* was conducted in a 5-L aerated stirred tank bioreactor. The fungus was immobilized on a plastic net in the form of a cylinder inside the vessel. The decolourization of the dye in an initial

concentration of 0.2 g/L from black-blue to intense yellow (95% removal) was reached in 20 days. Initially, lignin peroxidases and subsequently manganese dependent peroxidases were responsible for the decolourization (Mohorčič et al, 2004).

The white-rot fungus *Trametes versicolour* proved to be capable of decolourizing Reactive Black 5, Reactive Red 198 and Brilliant Blue R. in a 3.5-L aerated stirred tank bioreactor during a sequencing batch process. The decolourization activity was related to the expression of extracellular nonspecific peroxidases, which could be continuously reactivated by sheering the suspended microbial pellets. Under sterile conditions, 12 cycles of decolourization were performed, while under non-sterile conditions, only 5 cycles of decolourization could be achieved. One cycle lasted for 5–20 days. 91–99% of colour removal was achieved in the experiments which lasted up to 200 days (Borchert & Libra, 2001).

Various strategies for the decolourization of Reactive Black 5 with *Trametes versicolour* in a 4-L aerated stirred tank reactor with two flat-blade impellers under non-sterile conditions were compared. To obtain poor growth conditions for bacterial contamination, medium pH and nitrogen source were reduced during the cultivation of *T. versicolour* in two separate experiments. The enzyme, produced during the fungus cultivation and then isolated, was used alone for the decolourization. These three strategies were not as successful as the fourth one, where the fungus was grown on lignocellulosic solids as a sole substrate, such as straw and grain. Here, more than 90% degree of decolourization was achieved under non-sterile conditions in 10 days (Libra et al, 2003).

The mycelia of *Trametes versicolour* were aseptically encapsulated in the PVAL hydrogel beads 1–2 mm in diameter to be protected against the microbial contamination and mechanical stress. The encapsulated fungi, which were grown in a 1.0-L aerated stirred tank bioreactor under non-sterile conditions, expressed the ligninolytic enzymes which were capable of decolourizing polyvinylamine sulphonate anthrapyridone (Poly R-478). The average dye elimination of 80% was achieved in 19 days (Leidig et al, 1999).

6.2 Bubble column bioreactor

The white-rot fungus *Trametes versicolour* in the form of pellets was cultivated in a 1.5-L bioreactor, where the fluidization of biomass was achieved with a pulsating introduction of air at the bottom. The reactor was filled with separately cultivated microbial pellets, media with glucose and Orange G synthetic dye. The obtained percentage of decolourization was 97% in only 20 h. As high as 3500 AU/L of laccase was determined, while no MnP activity was detected. Better results were obtained this way compared to *In Vitro* experiments with commercial purified laccase from *T. versicolour* (Casas et al, 2007).

The batch and continuous operation mode of a 1.5-L bubble column bioreactor were used for the cultivation of *T. versicolour* in the pellet form and degradation of Grey Lanaset G metal-complex dye. A six days long batch operation was followed by a 36-day continuous operation. In both experiments, the decolourization was efficient (90%), but could not be correlated with extracellular laccase activities. The degradation occurs in several steps including the initial adsorption of the dye onto the biomass, followed by its transfer into the cells, where the degradation occurs due to the enzymes attached to the membrane (Blanquez et al, 2004).

6.3 Packed bed bioreactor

A vertical glass jar of 2.0-L working volume with an open-ended stainless wire mesh cylinder as support for mycelia growth was used for the cultivation of the fungal strain F29,

assuming to be white-rot fungus and capable of producing lignin peroxidase, manganese peroxidase and laccase. In the first 7 days of the submerged batch cultivation under aeration, the mycelium grew on the wire mesh rather than in suspension. Afterwards, the reactor was operated in a continuous mode by pumping nitrogen limited media with dye Orange II to study the decolourization process. At the retention time 3–3.5 days, the decolourization remained high (95%) for two months (Zhang et al, 1999).
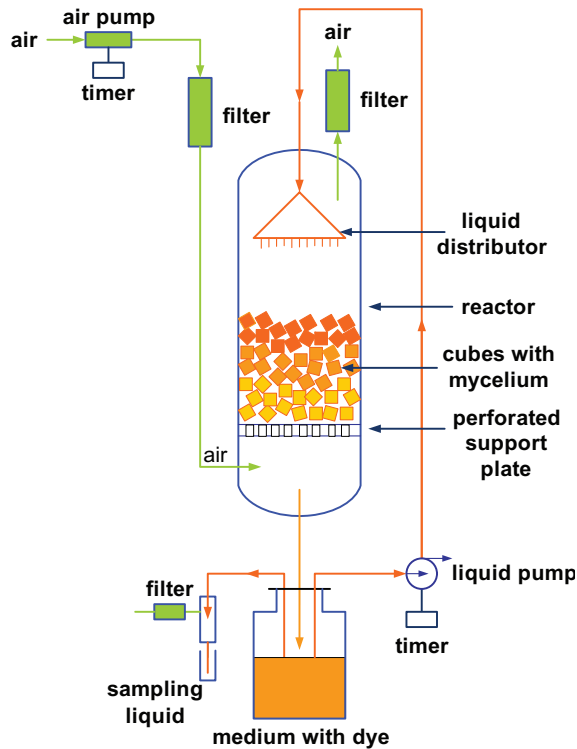

Fig. 4. Trickle bed reactor for decolourization of RO 16 with *Irpex lacteus*

The trickle bed reactor was constructed using a 10-cm ID glass cylinder, where 2-cm PUF cubes were used for the *Irpex lacteus* immobilization support. A special liquid distributor was used to uniformly distribute the liquid over the culture surface from the top of the reactor. A 2-L Erlenmeyer flask was used as a reservoir containing 1.0 L of the growth medium together with Reactive orange 16 (initial concentration 0.3 g/L), which circulated in the reactor by the means of a peristaltic pump. The reactor was also aerated through the bottom. The inoculation was done with the 10-day old fungal biomass grown on PUF. A successful decolourization due to the extracellular activities of MnP and laccases as well as the mycelium-associated laccase was performed in six days (Tavčar et al, 2006).

6.4 Rotating discs bioreactor
The biodiscs reactor consisted of 13 plastic discs with 13 cm in diameter in a horizontal cylinder with a liquid volume of 1.7 L. The rotation speed was 30 rpm. For the first three

days, the fungi *Coriolus versicolour* was cultivated in a nitrogen limited media for the biofilm formation. Then the media was replaced with fresh media with nutrients and dyestuff Everzol Turquoise Blue G. The reactor was operated in a repeated-batch mode by removing the liquid media, reloading the coloured fresh media every two days for the 12 days of operation. The decolourization efficiency was around 80% for 50–200 mg/L and 33% for 500 mg/L of initial dye concentration (Kapdan & Kargi, 2002).

The biological decolourization of Basic Blue 22 by *Phanerochaete sordida* was studied in a 1.6-L biodiscs reactor with 15 plastic discs with a 15-cm diameter at various rotational speeds 10–50 rpm. During the first 3 days, fungi were cultivated in the reactor for the biofilm formation. After that, the reactor operated in a repeated-batch mode in 2-day cycles for 12 days. A metal mesh covering the discs gave the best results, while the highest decolourization efficiency was obtained at the rotational speed 40 rpm. The TOC removal efficiency was around 80% for 50–200 mg/L and 52% for 400 mg/L of dyestuff concentration (Ge et al, 2004).

The rotating discs reactor with six 1-cm thick and 8-cm OD PUF plates was used to study the decolourization of Reactive orange 16 with *Irpex lacteus*. The liquid volume in the reactor was 1.0 L. The reactor was also aerated. First, the growth media in the reactor was inoculated with a culture homogenate and after 10 days of cultivation, when the fungus colonized the discs, the liquid in the reactor was replaced with 1.0 L of fresh medium containing 0.3 g/L of the dye. A successful decolourization due to extracellular activities of MnP and laccases, as well as mycelium-associated laccase was conducted in ten days (Tavčar et al, 2006).
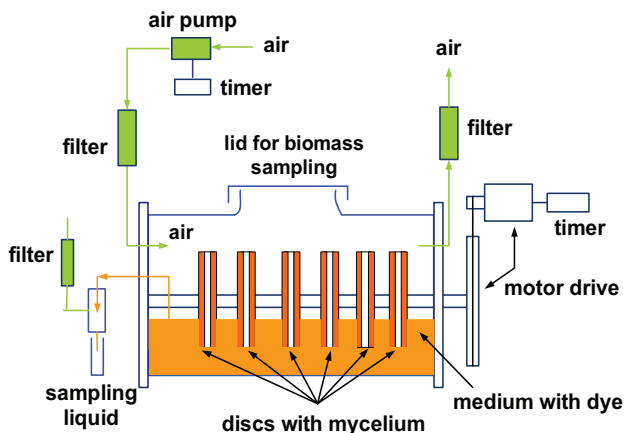
Fig. 5. Rotating discs reactor for decolourization of RO 16 with *Irpex lacteus*

Dichomitus Squalens was grown on 8.0 cm beech wood discs in a 3.0-L laboratory rotating-disc reactor (RDR) with 1.0 L of cultivation media. Three cultivations were done and the produced enzymes were used to decolourize three types of synthetic dyes, each in separate experiments: anthraquinone dye Remazol Brilliant Blue R (RBBR), thiazine dye Azure B (AB) and phenothiazine dye Methylene Blue (MB). The dye solution to obtain the initial dye concentration 50 mg/L was added to the reactor after 5 days and the following final decolourization efficiencies were obtained: 99% for RBBR after 6 h, 92% for AB after 200 h, and 59% for MB after 30 h (Trošt & Pavko, 2010).

Fig. 6. Decolourization of various dyes in rotating discs reactor

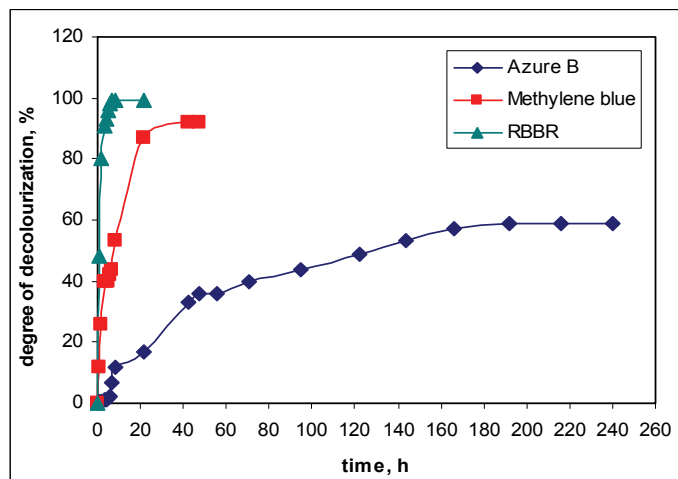## 6.5 Biofilm reactor

A biofilm reactor was made up of a plastic column filled with polyethylene fibre wads with a 4.5-L effective volume. 1.0 L of selected microbial consortium (obtained from rotten wood soil samples and a textile wastewater treatment plant) together with 3.0 L of growth medium were introduced into the reactor and gently aerated for the biofilm to culture under non-sterile conditions. The growth medium was replaced several times until a complete biofilm was formed. Fungi were the dominant population in the biofilm. Then, various synthetic azo dyes (Reactive Black RB5, Acid Red AR 249 and Reactive Red RR M-3BE) and textile wastewater were continuously fed into the reactor. The whole process lasted for 96 days at hydraulic retention time (HRT) of 12 h. The colour removal efficiencies were 70–80% for 100 mg/L of dye solutions and 79–89% for textile wastewaters (Yang et al, 2009).

The white-rot fungus *Coriolus versicolour* in the form of a biofilm on surfaces of inclined plates immersed in the aeration tank together with the activated sludge culture and wood ash particles as adsorbents were used for simultaneous adsorption and degradation of the textile dyestuff Everzol Turquoise Blue G. The major process variables such as dyestuff and adsorbent concentrations and sludge retention time on decolourization efficiency were studied. HRT was 50 h in all experiments. The highest colour removal efficiency was 82% at 200 mg/L of dyestuff concentration, 150 mg/L of adsorbent concentration and sludge age of 20 days (Kapdan & Kargi, 2002).

6.6 Membrane reactors

In a membrane reactor, the biocatalyst is retained within the system with a semi-permeable membrane, allowing a continuous operation with a substrate feed and product withdrawal (Lopez et al, 2002).

A cylindrical PVC bioreactor with an 11.8-L working volume was used in the study of Acid Orange II decolourization with the white-rot fungus *Coriolus versicolour*. A hollow fibre membrane module (pore size 0.4 μm) was submerged into the reactor. The system was first inoculated with the fungus and kept under aeration for 2 weeks to obtain the necessary

enzyme and biomass concentration. Afterwards, a continuous operation started by adding the nutrient sufficient synthetic wastewater with 100 mg/L of dye at HRT of 1 day under non-sterile conditions. During 62 days of successful operation, 97% of decolourization in the permeate was achieved. Later, the bacterial contamination ceased the enzymatic activity and consequently, the process efficiency (Hai et al, 2008).

A membrane bioreactor with an effective volume of 5.0 L comprised of the membrane reaction zone and hollow fibre membrane separation zone. In the reaction zone, *Phanerochaete chrysosporium* was cultivated in the form of a biofilm on the fibrous inert material. The polyvinylidene fluoride membrane (pore size 0.2 μm) was used for the separation of the permeate. The reactor was aerated during operation. After the inoculation, the reactor was operated under aeration for 8 days for the biofilm formation. Then, the dye wastewater with the dye concentration 100 mg/L was fed to the reactor, in order to achieve 24 h of the retention time. The decolourization efficiency was between 79.3% and 90.2% for the 65 days of operation, when the peroxidase isoenzyme activities were high enough. Afterwards, the biofilm retrogradation occurred and the enzyme activities decreased (Gao et al, 2009).

7. Conclusions

An enormous number of articles published in the last two decades cover the 'fungal dye decolourization'. This proves that great attention has been paid by researchers to use the lignin degrading enzymatic system of white-rot fungi for solving this serious pollution problem. A considerable amount of work in the fungal decolourization studies has been conducted on a laboratory scale to find fungal strains with effective enzymes. The main fungal enzymes have been indicated and various mechanisms have been explained, however, several studies show that unknown enzymes or mechanisms, respectively, are still present. The studies mainly cover chemically defined dyes, while the research with wastewater from dyestuff industry is rare. White-rot fungi as a group can decolourize a wide range of dyes. Nevertheless, the chemical and physical decolourization and/or degradation processes are usually faster than the processes using fungal cultures. In addition, a fungal cultivation takes place under sterile conditions, which increases the cost of bioremediation technology and additionally lowers the economics of the process. Unfortunately, there are not many results of dye degradation during the cultivation under non-sterile operation conditions available yet. Therefore, the research of screening or genetic manipulation of fungi to be more resistant, to be capable of faster dye degradation, to reach higher mineralization degree or to use dyes as sole substrates would also be of great interest.

The experiments in various types of bioreactors on a laboratory and pilot plant scale present an engineering approach to the scale up of the process, which leads to some interesting results. From the economical point of view in general, the process should be fast and effective. There are several descriptions of degradation kinetics with isolated enzymes and a few with the whole mycelia, but for the industrialization of fungal bioremediation, more attention should be paid to the degradation kinetics studies. The studies of pilot plant reactors with volumes 10–100 L for the transfer to a larger scale could be more intense. There is a lack of comparative data to indicate the best reactor configuration. On the other hand, the research in the last decade shows that the membrane reactors have an interesting potential. There is practically no data about the bioremediation costs; it would be very interesting to compare this promising technology with alternative processes for the treatment of effluents with synthetic dyes.

Moreover, the mathematical modelling of the decolourization process has not gained such significance here, as it has in other fields of biotechnology.

8. References

Babič, J. & Pavko, A. (2007). Production of ligninolytic enzymes by *Ceriporiopsis subvermispora* for decolourization of synthetic dyes. *Acta Chim. Slov.*, 54, 730 -734, ISSN 1318-0207

Blanquez, P.; Casas, N.; Font, X.; Gabarrell, X.; Sarra, M.; Caminal,G. & Vicent, T. (2004). Mechanism of textile metal dye biotransformation by *Trametes versicolor*, *Water Research,* 38, 2166 – 2172, ISSN 0043-1354

Borchert, M. & Libra, J. A. (2001). Decolorization of reactive dyes by the white rot fungus *Trametes versicolor* in sequencing batch reactors, *Biotechnology and Bioengineering,* 3, 312-321, ISSN 0006-3592

Casas, N.; Blanquez, P.; Gabarrell, X.; Vicent, T.; Caminal, G. & Sarra, M. (2007). Degradation of orange G by laccase: Fungal versus enzymatic process, *Environmental Technology*, 28, 1103-1110, ISSN 0959-3330

Corbman, B. P. (1983). *Textiles: Fiber to fabric*, pp. 201-222, McGraw-Hill, ISBN 0-07-066263-3, New York

Doran, P. M. (1995). *Bioprocess engineering principles*, pp. 352-377, Academic Press, ISBN 0-12-220855-2, London NW1 7DK

Eichlerova, I.; Homolka, L. & Nerud, F. (2006). Synthetic dye decolorization capacity of white rot fungus *Dichomites squalens. Bioresource Technology*, 97, 2153-2159, ISSN 0960-8524

Eichlerova, I.; Homolka, L. & Nerud, F. (2007). Decolorization of high concentrations of synthetic dyes by the white rot fungus *Bjerkandera adusta* strain CCBAS 232. *Dyes and Pigments,* 75, 38-44, ISSN 0143-7208

Ergas, S. J., Therriault, B. M. & Rechkow, D. A. (2006), Evaluation of water reuse technologies for textile industry. *Journal of Environmental engineering,* March 2006, 315-323. ISSN 0733-9372.

Faraco, V.; Pezzella, C.; Miele, A.; Giardina, P. & Sannia, G. (2009). Bio-remediation of colored industrial wastewaters by the white-rot fungi *Phanerochaete chrysosporium* and *Pleurotus ostreatus* and their enzymes. *Biodegradation,* 20, 209-220, ISSN 0923-9820

Freeman, H. M. (Ed), (1998). *Standard Handbook of hazardous Waste Treatment and Disposal*, pp. 10.28-10.29, Mc Graw Hill, ISBN 0-07-0212044-1, New York.

Gao, S.; Chen, C.; Tao, F.; Huang, M.; Ma, L.; Wang, Z. & Wu, L. (2009). Variation of peroxidise isoenzyme and biofilm of *Phanerochaete chrysosporiom* in continuous membrane bioreactor for Reactive Brilliant Red X3-B treatment. *Journal of Environmental Sciences,* 21, 940-947, ISSN 1819-3412

Gao, D.; Du, L.; Yang, J.; Wu, W.M. % Liang, H. (2010). A critical review of the application of white rot fungus to environmental pollution control. *Critical Reviews in Biotechnology*, 30, 70-77, ISSN 0738-8551

Hai, F. I.; Yamamoto, K.; Nakajama, K. & Fukushi, K. (2008). Factors governing performance of continuous fungal reactor during non-sterile operation – The case of a membrane reactor treating textile wastewater. *Chemosphere,* 74, 810- 817, ISSN 0045-653

Hao, O. J.; Hyunook, K.; Chiang P. (2000). Decolorization of wastewater. *Critical reviews in environmental science and technology*, 30, 449-505, ISSN 1064-3389

Heinfling, A.; Berghauer, M. & Szewzyk, U. (1997), Biodegradation of azo and phthalocyanine dyes by *Trametes versicolor* and *Bjerkandera adusta. Appl Microbiol Biotechnol,* 48, 261-266, ISSN 0175-7598

Joshi, M.; Bansal, R. & Purwar, R. (2004). Color removal from textile effluents, *Indian Journal of Fibre & Textile research*, 29, 239-259, ISSN 0971-042

Kapdan, I. K. & Kargi, F. (2002). Biological decolorization of textiledyestuff containing wastewater by *Coriolus versicolor* in a rotating biological contactor. *Enzyme Microb. Technol.*, 30, 195-199, ISSN 0141-0229

Kapdan, I. K. & Kargi, F. (2002). Simultaneous biodegradation and adsorption of textile dyestuff in an activated sludge unit. *Process Biochemistry*, 37, 973-981, ISSN 0032 -9592

Knapp, J. S.; Vantoch-Wood, E. J. & Zhang, F. (2001). Use of Wood – rotting fungi for the decolorization of dyes and industrial effluents, In: *Fungi in Bioremediation*, G. M. Gadd(Ed.), pp.253-261, Cambridge University Press, ISBN 0 521 78119 1, Cambridge

Kusvuran E.; Gulnaz, O.; Irmak, S.; Atanur, O. M., Yavuz, H. I. & Erbatur, O. (2004). Comparion of several advanced oxidation processes for the decolorization of Reactive red 120 Azo dye in aqueous solution. *Journal of Hazardous Materials*, B109, 85-93, ISSN 0304-8394

Leidig, E.; Prusse, U.; Vorlop, K.D. & Winter, J. (1999). Biotransformation of poly R-478 by continuous cultures of PVAL-encapsulated *Trametes versicolor* under non-sterile conditions. *Bioprocess Engineering*, 21, 5-32, ISSN 1226-8372

Levenspiel O. (1999). *Chemical Reaction Engineering*, pp.13-22, John Wiley & Sons, ISBN 0-471-25424-X, New York

Libra, J. A.; Borchert, M. & Banit, S. (2003). Competition strategies for the decolorization of a textile reactive dye with the white-rot fungi *Trametes versicolor* under non-sterile conditions. *Biotechnology and Bioengineering*, 6, 736-744, ISSN 0006-3592

Lopez, C.; Mielgo, I.; Moreira, G.; Feijoo, G. & Lema, J. M. (2002). Enzymatic membrane reactors for biodegradation of recalcitrant compounds. Application to dye decolourisation. *Journal of Biotechnology*, 99, 249-257, ISSN 0168-1656

Mohorčič, M.; Friedrich, J. & Pavko, A. (2004). Docoloration of the diazo dye reactive black 5 by immobilised *Bjerkandera adusta* in a stirred tank bioreactor. *Acta Chim. Slov.*, 51, 619-628, ISSN 1318 -0207

Novotny, Č.; Cajthaml, T.; Svobodova, K.; Šušla, M. & Šašek, V. (2009), *Irpex lacteus*, a white-rot fungus with biotechnological potential – review. *Folia Microbiol*, 54, 375-390, ISSN 0015-5632

Pavko, A. & Novotny, Č. (2008). Induction of ligninolytic enzyme production by *Dichomitus squalens* on various types of immobilization support. *Acta Chim. Slov.*, 55, 648-652, ISSN 1318-0207

Pazarlioglu, N. K.; Akkaya, A.; Akdogan, H. A. & Gungor, B. (2010). Biodegradation of direct blue 15 by free and immobilized *Trametes versicolor. Water Environment Research*, 82, 579-585, ISSN 1061-4303.

Podgornik, H.; Poljanšek, I. & Perdih, A. (2001). Transformation of Indigo carmine by *Phanerochaete chrysosporium* ligninolytic enzymes. *Enzyme and Microbial Technology*, 29, 166-172, ISSN 0141-0229

Pointing, S.B. (2001). Feasibility of bioremediation by white-rot fungi. *Appl Microbiol Biotechnol*, 57, 20-33, ISSN 0175-7598

Qingxiang, Y; Chunmao, L.; Huijun, L.; Yuhui, L. & Ning, Y. (2009). Degradation of synthetic reactive azo dyes and treatment of textile wastewater by a fungi consortium reactor. *Biochemical engineering Journal*, 43, 225-230, ISSN1369-703X

Rauf, M. A. & Ashraf, S.S. (2009). Radiation induced degradation of dyes. *Journal of hazardous materials*, 166, 6-16, ISSN 0304-3894

Robinson, T.; Chandran, B. & Nigam, P. (2001). Studies on the production of enzymes by white-rot fungi for the decolourisation of textile dyes. *Enzyme and Microbial technology,* 29, 575-579, ISSN 0141-0229

Robinson, T.; McMullan, G.; Marchant, R. Nigam, P. (2001). Remediation of dyes in textile effluent: a critical review on current treatment technologies with a proposed alternative. *Bioresource technology,* 77, 247-255, ISSN 0960-8524

Rodrigues, A.; Garcia, J.; Ovejero, G. & Mestanza, M. (2009). Wet air and catalytic wet air oxidation of several azo dyes from wastewaters: the beneficial role of catalysis. *Water Science and technology,* 60, 1989-1999, ISSN 0273-1223

Shakir, K.; Elkafrawy, A. F.; Ghoneimy, H. F.; Behir, S. G. E. &Refaat, M. (2010). Removal of rhodamine B (a basic dye) and thoron (an acidic dye) from dilute aqueous solutions and wastewater simulants by ion flotation. *Water research*, 44, 1449-1461. ISSN 0043-1354

Singh, H. (2006). *Mycoremediation-Fungal Bioremediation*, pp. 421-471, Wiley Interscience, ISBN-13: 978-0-471-75501-2, Hoboken

Slokar Y. M.; Majcen Le Marechal, A. (1998). Methods of decoloration of textile wastewaters. *Dyes and Pigments,* 37, 335-356, ISSN 0143-7208

Snape, J. B.; Dunn, I. J.; Ingham, J. & Prenosil, J. E. (1995). Dynamics of environmental bioprocesses. Modelling and simulation. pp. 1-6. VCH Publishers, ISBN 3-527-28705-1, New York

Sukumar, M.; Sivasamy, A. & Swaminathan, G. (2009). In situ biodecolorization kinetics of Acid Red 66 in aqueous solutions by *Trametes versicolor. Journal of hazardous materials,* 167, 660-663, ISSN 0304-8394

Tanaka, H.; Koike, K.; Itakura, S. & Enoki, A. (2009). Degradation of wood and enzyme production by *Ceriporiopsis subvermispora. Enzyme and Microbial Technology,* 45, 384-390, ISSN 0141-0229.

Tavčar, M.; Svobodova, K., Kuplenk,J.; Novotny, Č. & Pavko A. (2006). Biodegradation of azo dye RO16 in different reactors by immobilized *Irpex lacteus*. *Acta Chim. Slov.,* 53, 338-343. ISSN 1318-0207

Trošt, N. & Pavko, A. (2010). Ligninolytic enzyme production by *Dichomitus squalens* immobilized on beech wood, Proceedings: Slovenski kemijski dnevi 2010, pp. 25, ISBN 978-961-248-241-1, September 1010, Slovensko Kemijsko Društvo, Ljubljana, Slovenia

Vinodgopal K.; Peller, J.; Makogon, O.; Kamat P.V. (1998) Ultrasonic Mineralization of a reactive textile azo dye Remazol Black B. *Water research*, 32, 3646-3650, ISSN 0043-1354

Wang, D.I.C.; Cooney, C.L.; Demain, A.L.; Dunhill, P.; Humphrey, A.E & Lilly, M.D. (1979). *Fermentation and enzyme technology,* pp. 194-212, John Wiley and Sons, ISBN 0-471-91945-4, New York

Yang, G.; Liu, Y. & Kong Q .(2004). Effect of environmental factors on dye decolorization by *P. sordida* ATCC90872 in an aerated reactor. *Process Biochemistry*, 39, 1401 – 1405, ISSN 0032-9592

Zhang, F; Knapp, J. S. & Tapley K.N. (1999). Development of bioreactor systems for decolorization of Orange II using white rot fungus. *Enzyme Microb. Technol.*, 24, 48-53, ISSN 0141-0229

Žnidaršič, P. & Pavko, A. (2001). The morphology of filamentous fungi in submerged cultivations as a bioprocess parameter. *Food technol. biotechnol.,* 39, 237-252, ISSN 1330-9862

Anaerobic Ammonium Oxidation in Waste Water - An Isotope Hydrological Perspective

Yangping Xing and Ian D. Clark
Department of Earth Science, University of Ottawa
Canada

1. Introduction

Excess nitrogen components must be removed from wastewater to protect the quality of the water bodies that it will be eventually discharged to. A conventional wastewater treatment system for nitrogen removal is often involved with two processes, nitrification and denitrification. Nitrification is mostly achieved by complete oxidation of ammonium (NH_4^+) to nitrite (NO_2^-) by the appropriate aerobic bacteria and then oxidation of the nitrite to nitrate ion (NO_3^-) by another variety of aerobic bacteria. Subsequently, the formed nitrate will be reduced to dinitrogen gas under anoxic conditions at the expense of organic carbon and released into the atmosphere as a harmless product (van Dongen et al., 2001). The introduction of oxygen into wastewater for nitrification requires a large amount of energy. Furthermore, the carbon source is often limited in wastewater, so purchasing of carbon source (typically methanol) is necessary too. A newly discovered anaerobic ammonium oxidation (anammox) may circumvent the limitations and open up a new possibility for nitrogen removal from wastewater. The alternative approach is a microbiological involved activity which requires less energy and enables more efficiency on N removal.

2. The history and physiology of anammox

The discovery of anammox activity and anammox bacteria is quite recent. Even though Richards (1965) has noticed NH_4^+ deficits in anoxic marine basins, and proposed that the missing NH_4^+ was anaerobically oxidized to N_2 by some unknown microbe using nitrate as an oxidant, which was coined one of two "lithotrophs missing in nature" by Broda (1977). Because there was no known biological pathway for this transformation, biological anaerobic ammonium oxidation received littler further attention (Arrigo, 2005). It was not until mid-1990s, work with bioreactors designed to remove NH_4^+ from wastewater provided direct evidence for anaerobic ammonium oxidation, and the process was termed "anammox" by Mulder and his colleagues (1995). A series of ^{15}N-labellling experiment were carried out to study the metabolic mechanism and intermediates of anammox reaction (van de Graaf et al., 1995; 1997). It is a chemolithotrophic process in which 1 mol of NH_4^+ is oxidized by 1 mol of NO_2^- to produce N_2 gas in the absence of oxygen (Strous et al., 1999).

$$NH_4^+ + NO_2^- \rightarrow N_2 + 2H_2O \tag{1}$$

The pathway of N_2 formation clearly distinguishes anammox from denitrification which combines N from two NO_3^- molecules to form N_2 and presents as an elegant shortcut in the natural nitrogen cycles (Fig 1.) Physical purification of the anammox microbes from the multispecies biofilms yielded a 99.6% pure culture that was capable of carrying out PCR amplification of the DNA. The microbes responsible for anammox process were identified as members of the bacterial order Planctomycetales (Strous et al., 1999). The first genome sequence of a representative anammox bacterium was published in 2006 (Strous et al., 2006). To date, five anammox genera have been described, *Candidatus* Brocadia, *Candidatus* Kuenenia, *Candidatus* Scalindua, *Candidatus* Anammoxoglobus and *Candidatus* Jettenia.

A range of studies have been conducted for the detection of anammox bacteria and activities in variable environments from natural to man-made ecosystems (Risgaard-Petersen et al., 2003; Schmid et al., 2005). Anammox activity was found in marine environments, such as the Black Sea, the coast of Namibia, Chile, Peru and some freshwater and estuarine systems like, Lake Tanganyika and mangroves (Kuypers et al. 2003; 2005; Risgaard-Petersen et al., 2004; Meyer et al., 2005; Thamdrup et al., 2006; Schubert et al., 2006; Hamersley et al., 2009).In addition to widespread distribution, the activity of anammox bacteria in the environments also be substantial. The maximum reported contribution of anammox is 67-79%, occurring in sediments at a depth of 700m of the Norwegian Trench (Engström et al., 2005). Considerable supporting evidences have confirmed that anammox has global importance (Kuene, 2008).

Owing to the availability of laboratory enrichment cultures, the physiology of anammox bacteria has been relatively well characterized (Jetten et al, 2005). Anammox is characterized by slow growth and its cell doubles only once per 11 days under optimum conditions and 2-3 weeks on average (Strous et al., 2006). The low growth rate of anammox bacteria is not caused by inefficient energy conservation but by a low substrate-conversion rate. Furthermore, anammox bacteria are obligate anaerobes and their metabolism is reversibly inhibited when oxygen concentration is above 2 µM and nitrite is higher than 10 mM (Strous et al., 1997a). The temperature range suitable for anammox bacteria has been reported between -2℃ (sea ice, Rysgaard & Glud, 2004) and 43℃ (Strous et al., 1999). A recent study has observed anammox activity at temperature from 60℃ to 85℃ at hydrothermal vents located along Mid-Atlantic Ridge (Byrne et al., 2008). At optimal condition, anammox biomass could be enriched from activated sludge within hundred days. Enriched anammox bacteria in active sludge or biofilm present as brownish or red granule (Fig 2.). Under the microscope, the bacteria are observed as small coccoid cells with diameter of approximately 800 nm. They all possess one anammoxosome, a membrane bound compartment inside the cytoplasm which is the locus of anammox catabolism. Further, the intracytoplasmic is surrounded by unique lipids, called ladderanes (Sinninghe Damsté et al., 2004). Due to their unique characteristics, ladderane lipids have also been used as a biomarker for the presence of anammox bacteria (Kuypers et al., 2003). Besides, an interesting special feature is the turnover of hydrazine (normally used as a high-energy rocket fuel and poisonous to most living organisms) as an intermediate.

In addition, anammox bacteria have been found to be metabolically flexible, exhibiting alternative metabolic pathways. For instance, anammox can subsequently reduce NO_3^- to NO_2^- to NH_4^+, followed by the conversion of NH_4^+ and NO_2^- to N_2 through anammox pathway, allowing anammox bacteria to overcome NH_4^+ limitation. Anammox bacteria are also a potential source of N_2O production by nitric oxide detoxification (Kartal et al., 2007). Apart from NO_2^- and NO_3^-, anammox bacteria also employ Fe^{3+}, manganese oxides as electron acceptors (Strous et al., 2006), which further expended the metabolic diversity of the anammox bacteria.
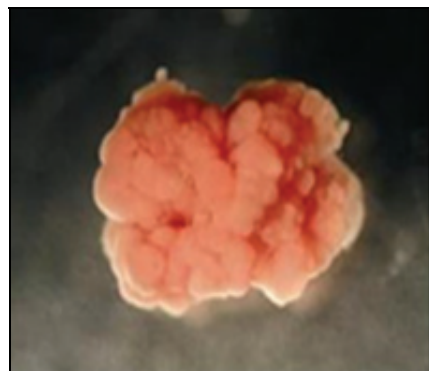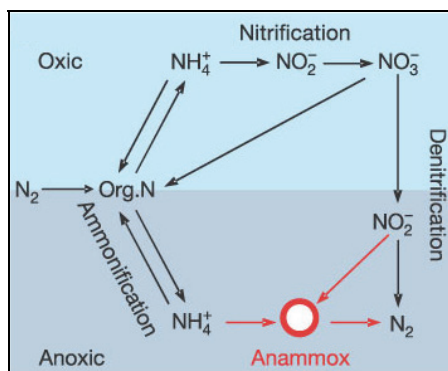
Fig. 1. Anammox in the context of nitrogen cycle (Modified from Kuyper, et al., 2003).

Fig. 2. Typical anammox granular sludge (Photo modified from Van Loosdrecht, 2006).

3. The application of anammox in waste water

Since anammox was discovered in a denitrifying fluidized bed reactor for wastewater treatment, it was realized that having a great potential for the removal of undesired NH_4^+ from wastewater from the beginning. The introduction of anammox process to N-removal would lead to a 90% reduction in operation costs because by using anammox process, nitrification process normally employed in wastewater treatment can be stopped at the nitrite level which can save aeration and carbon sources. For this reason, Mulder and colleagues patented the process immediately, even without direct proof and understanding of its biological nature (Mulder, 1992). In recent years, many research efforts dedicated to the application aspects of anammox reaction. The feasibility of the anammox process for the removal of NH_4^+ from sludge digester effluents was evaluated. Experiments with a laboratory-scale (2L) fluidized bed reactor showed that the anammox process was capable to remove NH_4^+ and NO_2^- (externally added) efficiently from the sludge digester effluent. And anammox biomass could be enriched from activated sludge within 100 days (Strous et al., 1997 b; Jetten et al., 1997). The possible reactors are sequencing batch reactors (SBR), moving bed reactor, blanket reactor or gas-lift-loop reactor. In these studies, NO_2^- was supplied from a concentrated stock solution. However, for application in real wastewater practice, a suitable system for biological NO_2^- has to be developed. One such system is the combination of the anammox process and SHARON (Sustainable high rate ammonium removal over nitrite) process. The principle of the combined process is that the NH_4^+ in the sludge digester effluent is oxidized in the SHARON reactor to NO_2^- for only 50% in the reaction I. The mixture of NO_2^- and NH_4^+ is ideally suited as influent for the anammox process in reaction II. With this system sludge digester effluent can be treated independently. In the study, the SHARON process was operated stably for more than 2 years. During the test period the overall NH_4^+ removal efficiency was 83% (Van Dongen et al., 2001). In the earlier design, reactions I and II were carried out in consecutive reactors, but these were later combined in a single oxygen-limited reactor where nitrite-producing bacteria and anammox bacteria coexist. However, anammox bacteria grow slowly and because of the low specific conversion rates of one reactor process, the bottleneck in this combination has been insufficient biomass retention (Kartal et al., 2010). A granular-sludge reactor is developed to achieve a high volumetric conversion rate due to a large surface area for mass transfer (Kartal

et al., 2010). The selective production of granules has been successfully applied on nitrifying/anammox sludge in a sludge blanket reactor, which substantially improved the energy management of wastewater facilities. Granular-sludge system not only overcome the limit of conversion rate, but also offers the possibility for application of anammox for wastewater treatment at low temperature and concentrations. The upper limits of nitrogen loading to anammox process were explored in gas lift reactors. The results showed that anammox bacteria were able to remove 8.9 kg N m^{-3} reactor day^{-1} (Jetten et al., 2004). Due to extensive explorations of anammox process and combinations with other processes in the practices of application, there are numerous developed systems from SHARON-anammox, OLAND (Oxygen-limited autotrophic nitrification-denitrification, Kuai & Verstraete, 1998) to CANON (Completely autotrophic nitrogen removal over nitrite, Third et al., 2001) and DEAMOX (Denitrifying ammonium oxidation, Kalyuzhnyi et al., 2006). Van der Star et al., (2007) have made an overview and suggested that a uniform naming of these process as shown in table 1.

Process name proposed by van der Star et al., (2007)	Source of nitrite	Alternative process name	Reference
Two reactor Nitritation-anammox process	Nitritation of NH_4^+	SHARON[a,b]-anammox Two stage OLAND	Van Dongen et al., 2001 Wyffels et al., 2004
One- reactor Nitritation-anammox	Nitritation of NH_4^+	OLAND[c] CANON[d] Aerobic/anoxic deammonification SNAP[e] DEMON[f] DIB[f,g]	Kuai and Verstraete, 1998 Third et al., 2001 Hippen et al., 2001 Lieu et al., 2005 Wett, 2006 Ladiges et al., 2006
One reactor denitrification-anammox process	NO_3^- of denitrification	Anammox[h] DEAMOX[i]	Mulder et al., 1995 Kalyuzhnyi et al., 2006

[a] Sustainable high rate ammonium removal over nitrate; the name only refers to nitritation when nitrite oxidation is avoided by choice of residence time and operation at elevated temperature.
[b] Sometimes the nitrification-denitrification over nitrite is addressed by this term.
[c] Oxygen-limited autotrophic nitrification denitrification.
[d] Completely autotrophic nitrogen removal over nitrite.
[e] Single-stage nitrogen removal using the Anammox and partial nitritation.
[f] Name refers to the deammonification process in an SBR under pH-control.
[g] Deammonification in Interval-aerated Biofilm systems.
[h] System where Anammox was found originally. The whole process was originally designated as Anammox.
[i] Denitrifying ammonium oxidation: this name only refers to denitrification with sulphide as electron donor.

Table 1. Process names for nitrogen removal systems involving the anammox process (modified from van der Star et al., 2007).

To date, there are several full-scale installations of anammox applications in the wastewater treatment plants. The first full scale reactor was built in Netherlands in 2002. The prototype has been set up as part of a municipal wastewater treatment plant in Rotterdam and is performing well. The internal circulation type reactor used in Rotterdam is especially suited for use of granular sludge. As of 2006, three full scale processes intended for the application of anammox have been built in Europe. In addition, anammox bacteria have been found that can be enriched from various types of wastewater sludge, indicating that anammox bacteria are indigenous in many treatment plants throughout the world (Op den Camp et al., 2006). Therefore, the ubiquitous characteristic of anammox bacteria makes no real limit to its application at normal wastewater treatment plants.

4. Tracing anammox in contaminated ground water- a case study

Groundwater contamination by NH_4^+ typically occurs because of surface activities such as composting, landfilling (Erksine, 2000), disposal of animal wastes and animal carcasses (Ritter & Chirnside, 1995; Umezawa et al., 2008), fertilizer storage (Barcelona& Naymik, 1984), and septic system effluent (Aravena & Robertson, 1998). NH_4^+ contaminated groundwater is a likely site for anammox activity. NH_4^+ enters the groundwater system and competes for exchange sites on soil particle surfaces; then nitrifying organisms in the oxic zone oxidize NH_4^+ to NO_2^- and then to NO_3^-. Movement of the groundwater through the soil matrix carries the products of partial nitrification (NH_4^+ and NO_2^-/NO_3^-) as the plume spreads due to the effects of retardation by aquifer material (Erksine, 2000). It is expected that contaminated groundwater environments will favor the anammox reaction when both NO_2^- and NH_4^+ are present in areas of low oxygen. In landfills, NH_4^+ is rarely detected over a few hundred meters away from the source, suggesting that attenuation of NH_4^+ is occurring along the flowpath (Erksine, 2000), and this is likely to be the case regardless of the source of NH_4^+. We think that groundwater provides anammox organisms with an ideal environment for growth. Isotope evidence for anammox in groundwater has been shown by Clark and colleagues (Clark et al., 2008), but the presence and activity of anammox organisms has yet to be confirmed. In the case study, a series of geochemical, isotopic, labelling experiments and microbiological techniques including FISH, PCR, are used to assess whether anammox organisms are present and active in NH_4^+-contaminated groundwater sites.

4.1 Isotopic evidence of anammox

Tracing the fate of NH_4^+ and NO_3^- in ground water is greatly aided by measurement of ^{15}N and ^{18}O, which can be used to characterize sources of these compounds and the reaction pathways they may have followed (Delwiche & Steyn, 1970; Hübner, 1986; Kendall, 1998). The reactions of nitrogen species in the environment are associated with characteristic fractionations that provide additional insights to subsurface processes and fate. Transformation of NO_3^- to N_2 by denitrifying bacteria is accompanied by a ^{15}N fractionation on the order of $\varepsilon^{15}N_{N_2-NO_3}$ = -15‰ to -20‰ (Wada et al., 1975; Böttcher et al. 1990). Böttcher et al. (1990) also showed that [18]O is also enriched in the residual NO_3^- product, with $\varepsilon^{18}O_{N_2-NO_3}$ = -8‰. Accordingly, stable isotopes provide important constraints on plausible reaction pathways for nitrogen species in the subsurface. Within the context of tracing anammox in ground water through the use of stable isotopes, a detailed investigation was undertaken at the site of a municipal water supply aquifer contaminated by the activities of

a chemical plant and fertilizer blending operation (Fig 3.). Wastewater contribution comes from the chemical company and fertilizer blending company with ammonium approaching 840 ppm N and nitrate up to 350 ppm N.

4.1.1 Field and analytical work

A program of field sampling and analytical work was carried out in 2003 and again in 2004, involving sampling ground water from 62 piezometers and extraction wells both on two companies sites. Total NH_4^+ concentrations were analyzed on unfiltered samples by distillation and titration with sulphuric acid. NO_3^- and NO_2^- concentrations were measured by liquid chromatography. The 2004 series of samples were analyzed for isotopes of NH_4^+ (^{15}N) and NO_3^- (^{15}N and ^{18}O) in the G.G. Hatch Isotope Laboratory in University of Ottawa. ^{15}N-NH_4^+ was measured by a diffusion procedure. The sample was first distilled at high pH into a sulphuric acid solution, and concentrated to ammonium sulphate salt by evaporation. The salt precipitation was analyzed as N_2 gas by continuous flow isotope ratio mass spectrometry using a Finigan MAT Delta Plus directly interfaced with a Carlo Erba elemental analyzer (EA). Isotopes in NO_3^- were analyzed by quantitative conversion of NO_3^- to N_2O gas according to the bacterial denitrifier method (Sigman et al. 2001; Casciotti et al. 2002). The bacterial N_2O was analyzed for both ^{15}N and ^{18}O by injection through a gas bench interfaced with a Finnigan MAT Delta Advantage continuous flow mass spectrometer. The
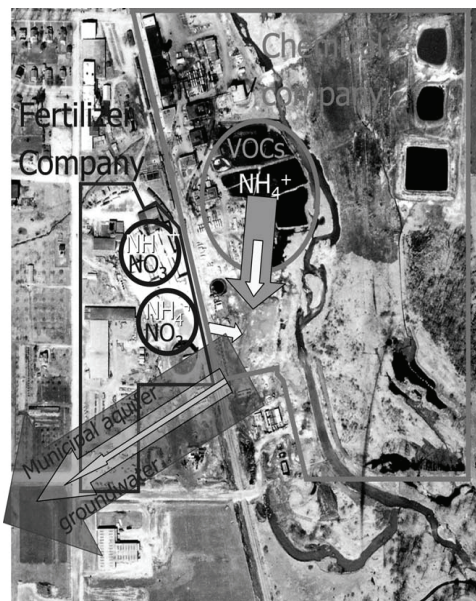

Fig. 3. Air photo of study area showing the direction ground water flow from the waste water ponds from chemical company and fertilizer company to the confined municipal aquifer.

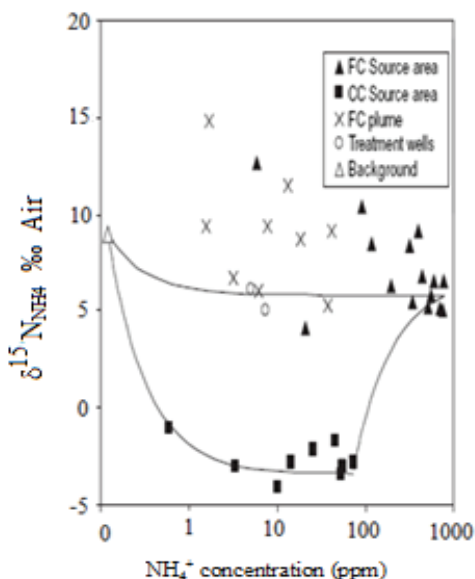Fig. 4. $\delta^{15}N_{NH4}$ vs. total NH_4^+ for waste of water source area and treatment well ground water. Conservative mixing envelope shown with black line.

N_2 gas concentrations were measured in ground water sampled in septum vials by purging with Helium (He) and direct injection into a Finnigan MAT Delta Advantage mass spectrometer.

4.1.2 Isotope results and discussion

The regional background geochemistry of the confined municipal upper aquifer was measured in two wells. The concentrations of NH_4^+ and NO_3^- of background water is lower than 1 ppm N, and the redox conditions are considered to be moderately reducing, with dissolved oxygen less than 1 mg L^{-1} and Eh of 137mV. Ground water at fertilizer company source area was dominated by NH_4-NO_3 with an average NH_4^+ 632 ppm N and 250ppm NO_3^- ppm N. The NH_4^+ concentration at chemical company source area was lower with an average value of 40.6ppm N and this water has no detectable NO_3^-. However within municipal upper aquifer, concentration of NH_4^+ was highly diluted with a maximum of 7.3 ppm N in the water treatment wells. The comparison between the really measured NH_4^+ and the predicted concentration of NH_4^+ by a conservative mixing model indicated that a significant loss of NH_4^+ in ground water aquifer. The missing NH_4^+ was calculated to be 30.7 and 21.2 ppm N in treatment well 1 and treatment well 2, respectively. In the same way, NO_3^- was found a loss of 8.0 and 3.2 ppm N from the two wells. These values are minimum estimate because NO_3^- is not retarded by sorption in the aquifer like NH_4^+ (For more information, please refer to the publication (Clark et al., 2008).

The missing of NH_4^+ was believed as a reactive loss involved with anammox reaction which is based on isotopic evolution of associated nitrogen species. In conservative mixing, $\delta^{15}N$ will reflect the concentration-weighted contribution of NH_4^+ from each primary source. In the present case, if no reaction, $\delta^{15}N$ of nitrogen species would be weighted results of wastewater from chemical company, fertilizer company with dilution water from background water. Fractionation of ^{15}N during cation exchange is considered to be minor to negligible (Kendall 1998), and so retardation is not expected to affect the $\delta^{15}N$ of NH_4^+ in the municipal aquifer. By contrast, reactive loss of NH_4^+ by oxidation, whether through nitrification or anammox, will impart a clear enrichment trend independent of any mixing relationships. A plot of $\delta^{15}N_{NH_4}$ against NH_4^+ concentration shows a strong contrast between the two waste water source areas and background NH_4^+ in the municipal aquifer (Fig 4.). The values for $\delta^{15}N_{NH_4}$ for the high NH_4^+ concentration sites near the former fertilizer company water storage pond average 5.8‰, while those for the chemical company average -2.7‰, providing an 8.5‰ contrast between the two. The conservative mixing envelope, calculated from binary mixing between each of the three endmembers, is shown in figure 4. Nonconservative behaviour of samples from the fertilizer company source area is observed by their trend toward $\delta^{15}N$-enriched values at lower NH_4^+ concentrations. Similarly, samples from the chemical company plume show nonconservative enrichment in ^{15}N. This is consistent with the conservative mixing calculations, showing reactive loss of NH_4^+ along the flowpath. Because cation exchange has been shown to be essentially nonfractionating (Ceazan et al., 1989; Kendall, 1998; Buss et al., 2004), this reactive loss must be through oxidation.

The usual pathway for NH_4^+ oxidation is nitrification by O_2. This is an energetically favourable reaction in oxic water. It follows a two-step reaction through nitrite by a mixture of aerobic bacteria, including *Nitrosomonas*, *Nitrobacter nitrosospira*, and *Nitrobacter pseudomonas*. However, according to our measurement, redox conditions are unfavourable for aerobic bacteria, and so NH_4^+ loss by nitrification is unlikely in these ground water. Further evidence against nitrification is found by the positive correlation between NO_3^- and

NH_4^+ in this water. NH_4^+ loss by oxidation to NO_3^- would show an inverse correlation and NO_3^- would remain the dominant species in the municipal aquifer. A third line of evidence against NH_4^+ nitrification is found in the comparison of $\delta^{15}N$ values in NH_4^+ coexisting with NO_3^- in individual water samples. Essentially all samples, NO_3^- were enriched in ^{15}N over coexisting NH_4^+. These rules out NH_4^+ nitrification as a source for NO_3^-, which would produce NO_3^- with lower $\delta^{15}N$ than the NH_4^+ precursor (Kendall, 1998). Furthermore, the $\delta^{15}N_{NH_4}$ enrichment trends with decreasing NH_4^+ concentration against the possibility of NH_4^+ nitrification (Fig 5.). The positive correlation for NH_4^+ and NO_3^-, the enrichment in $^{15}N_{NH_4}$, and the greater enrichment for ^{15}N in NO_3^- over NH_4^+ suggest that the loss of NH_4^+ is due to anaerobic oxidation by anammox bacteria. Two Rayleigh distillation trend lines trace the enrichment in $\delta^{15}N_{NH_4}$ in the residual NH_4^+ from different initial concentrations. The enrichment factor $\epsilon^{15}N_{NH_4-N_2}$ = 4‰ used for these trend lines provided the best fit for the range of source area data points and thus provides a first-order estimate of ^{15}N fractionation during anammox reaction. Additional evidence for anammox reaction in the NH_4^+-NO_3^- ground water at fertilizer company source area is found in the overpressing of N_2 gas in these samples. Normalization of measured N_2 concentrations to atmospherically derived Argon gas (Fig 6.) showed that overpressing in N_2 in excess of three times of atmospheric saturation. The $\delta^{18}O$ composition of NO_3^- further supported reactive loss of NO_3^-, where enrichment of $\delta^{18}O$ and $\delta^{15}N$ was seen for most samples (Data not shown).
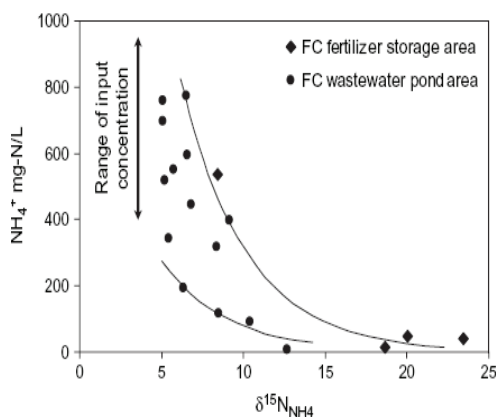

Fig 5. Evolution of $\delta^{15}N_{NH_4}$ during anammox reaction for the high NH_4^+-NO_3^- fertilizer company ground water. Trend lines calculated from a Rayleigh distillation with a reaction enrichment factor of 4‰.
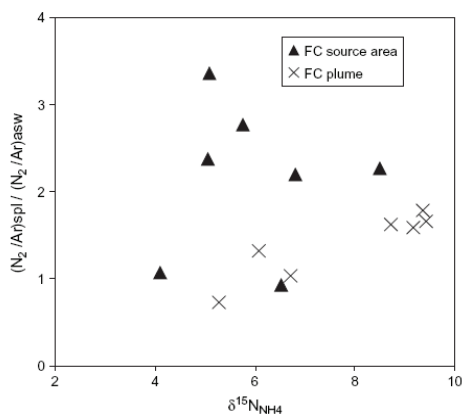
Fig. 6. Excess N_2 in fertilizer company ground water from reactive loss of NO_3^- and/ or NH_4^-, normalized to dissolved argon gas.

4.1.3 Summary

Anaerobic oxidation of the ammonium by anammox bacteria is concluded as the reason of the strong attenuation of NH_4^+ and NO_3^- observed between the source areas and the municipal ground water treatment wells. Several lines of evidence suggest the conclusion:

1. $\delta^{15}N$ measurements of NH_4^+ show progressive enrichment with decreasing concentration, demonstrating reactive loss by ammonium oxidation. Volatilization

along the flowpath is unlikely because it requires unsaturated conditions and because of the neutral pH of the water (negligible un-ionized NH_3).

2. NO_3^- concentrations decline along the flowpath and into the municipal aquifer. This precludes nitrification for the observed loss of NH_4^+ for which an increase in NO_3^- concentrations should be observed. The measured redox conditions are too low to support aerobic nitrification of NH_4^+.

3. $\delta^{15}N_{NO_3}$ is consistently 5‰ to 10‰ enriched over that of $\delta^{15}N_{NH_4}$ for water carrying both species, demonstrating that NH_4^+ loss is not by nitrification. Oxidation of NH_4^+ to NO_3^- would produce NO_3^- with depleted $\delta^{15}N$ values.

4. Strong correlations between $\delta^{15}N_{NH_4}$ and $\delta^{15}N_{NO_3}$ demonstrate reactive loss of both species, consistent with anammox reaction. Enrichment of $\delta^{15}N_{NO_3}$ correlates with enrichments in $\delta^{15}N_{NH_4}$, further supporting reactive loss of NO_3^- .

5. N_2 overpressuring above atmospheric equilibrium is observed to increase with increasing $\delta^{15}N_{NH_4}$ values along the flowpath from the FC source area. Increased N_2 in conjunction with enrichment in $\delta^{15}N_{NH_4}$ can occur only through anaerobic oxidation of NH_4^+ to N_2 by the anammox reaction.

4.2 Tracer experiments

Tracer experiments with ^{15}N-labeled nitrogen species are commonly used for elucidating nitrogen fate in both sediments and groundwater environments. Consumption of $^{15}NH_4^+$ and concomitant production of ^{15}N-labeled N_2 provided the first clear experimental evidence for anammox activity in a fluidized bed reactor (van de Graaf et al., 1995). So far, few labelling experiments have provided evidence of anammox in anoxic basin and in the suboxic zone of sea and lakes (Dalsgaard et al., 2003; Kuypers et al., 2003; Schubert et al., 2006; Hamersley et al., 2009), but there is no analogue application in groundwater systems yet. ^{15}N-labelling also provides a very sensitive technique for the determination of anammox rates. And a simultaneous determination of anammox and denitrification, gives in sights to the relative importance of the two N removal pathways (Thamdrup & Dalsgaard, 2002; Risgaard- Peterson et al., 2003). In addition, potential isotopic fractionation associated with anammox bacteria activity also indicates the presence of anammox reaction. From the simultaneous attenuation of NH_4^+ and NO_3^-, and a progress enrichment of $\delta^{15}N$-NH_4^+ and $\delta^{15}N$-NO_3^-, Clark et al., (2008) suggested that anammox may play a role in ground water. As a follow-up study, a series of ^{15}N labelling incubation experiments have been established to investigate anammox activity and reaction rates at several ground water sites.

4.2.1 ^{15}N labelling experiments

For ^{15}N-labelling experiments, the method was slightly modified from the previous publication (Dalsgaard et al., 2003). Ground water or sediment and groundwater in an industrial contaminated site Elmira and a turkey manure polluted site Zorra were collected directly to 12-mL exetainers (Labco, UK). In terms of the mixture of sediment and ground water incubation, around 4.5mL sediment and 7.5mL of groundwater were collected. In order to minimize oxygenation, exetainer was submerged into a big container completely filled with ground water and neither headspace nor bubbles in the vial. From each site, triplicates were sampled for ^{15}N labelling experiments. ^{15}N labelling experiments were conducted immediately after return to the laboratory (less than 2 hours). In brief, 3mL of water was withdrawn by a syringe to make a headspace for helium (He) flushing. Each

exetainer was flushed with He for at least 15min to remove background N_2 and dissolved O_2 and N_2. ^{15}N enriched compounds were added with syringe to a final concentration of 100µmol in 10ml of sample as $^{15}NH_4Cl$ and $Na^{15}NO_3$ (all >99% ^{15}N, Sigma-Aldrich). Even though the final concentration of enriched ^{15}N was variable in previous studies, ranging from 40 µmol to 10mmol L^{-1} (Dalsgaard et al, 2003; Thamdrup et al., 2006), the present addition was in higher range because that the concentration of ^{14}N species in study samples were very high and sometime can reach to 20mmol L^{-1}. An additional trial was carried out without any tracer addition as control to confirm that the whole incubation system functions well. ^{15}N-labelling experiments were incubated in a dark incubation chamber at 15°C, which is very close to the in situ temperature. $^{14}N^{15}N:^{14}N^{14}N$ and $^{15}N^{15}N:^{14}N^{14}N$ were determined by gas chromatography-isotope ratio mass spectrometry and expressed as $\delta^{14}N^{15}N$ values ($\delta^{14}N^{15}N = [\frac{(^{14}N^{15}N:^{14}N^{14}N)\text{sample}}{(^{14}N^{15}N:^{14}N^{14}N)\text{standard}} - 1] \times 1000$; air was used as the standard) (GG Hatch isotope laboratory, University of Ottawa). In terms of anammox contribution to total N_2 production, assuming that the $^{15}NH_4^+$ pool turns over at the same rate as the ambient $^{14}NH_4^+$ pool, the total anammox N_2 production can be calculated from the production of $^{29}N_2$ and the proportionate ^{15}N labelling in the whole NH_4^+ pool (Thamdrup & Dalsgaard, 2002; Thamdrup et al., 2006). The rates of anammox were extrapolated from linear regression of $^{14}N^{15}N$ as a function of time in the incubation with $^{15}NH_4^+$ and the rates of denitrification were determined from the slope of linear regression of $^{15}N^{15}N$ over time in the incubation with $^{15}NO_3^-$.

4.2.2 Results and discussion

At both of sampling sites except a pristine background well (Pu86 having not been impacted by NH_4^+ from the compost plume), the formation of $^{14}N^{15}N$ was observed in the incubation trials with $^{15}NH_4^+$ (Fig 7 a and c). However, the formation of $^{14}N^{15}N$ was very slow, and the concentration was lower than the detection limit after 72 hours incubation and the enrichment signal $\delta^{15}N/^{14}N$ was only 22.1 ± 4.2‰. The incubation experiments were extended to 3 months. The highest $\delta^{15}N/^{14}N$ increased to 14,278.03‰ at the end of incubation. At Elmira site, $^{14}N^{15}N$ accumulated linearly and stably with time without a lag phase, which indicates that anammox was the active process and no intermediates were involved in the reaction (Galán et al., 2009). Furthermore, the production of only $^{14}N^{15}N$ rather $^{15}N^{15}N$ was a clear evidence for the stoichiometry of N_2 production through anammox (van de Graaf et al., 1995; Jetten et al., 2001). At Zorra site, the formation of $^{14}N^{15}N$ reached the maximum at 1500hours incubation and started to decline. This is maybe due to the lack of another N donor NO_3^- which concentration was low at Zorra site. In control incubations without added tracer there was no production of ^{15}N-enriched N_2, indicating the eligibility of the incubation system. At Elmira sites, the average $^{14}N^{15}N$ formation rate was 0.014±0.003µmol L^{-1} h^{-1}, and the rate at Zorra site was 0.02±0.0021 µmol L^{-1} h^{-1}. The rate of $^{14}N^{15}N$ production essentially corresponded to the anammox rate (van de Graaf et al., 1995; Thamdrup & Dalsgaard 2002; Dalsgaard et al., 2003). So, according to the equation from Thamdrup & Dalsgaard (2002), the calculated anammox reaction was 0.04±0.008 µmol L^{-1} h^{-1} at Elmira and 0.021±0.0022 µmol L^{-1} h^{-1} at Zorra. Compared to Dalsgaard et al., (2003) reported reaction rates 42 to 61mmol N m^{-2} d^{-1} in anoxic water column of Golfo Dulce, the reaction rate in ground water was much lower. However, many lower rates have been found in the oxygen-deficient water such as in eastern South Pacific (≤0.7nmol L^{-1} h^{-1};

Thamdrup et al., 2006) and in the Black Sea (~0.007μmol d^{-1}; Kuypers et al., 2003). Our results were very close the reported reaction rates in freshwater lakes, ranging from 6 to 504 nmol N$_2$ L^{-1} d^{-1} (Hamersley et al., 2009).

The pronounced accumulation of ^{15}N^{15}N in the incubation of ^{15}NO$_3^-$ indicated that active and strong denitrification process (Fig 7b and d). The production of ^{15}N^{15}N was the major product at Zorra sites with an order magnitude higher than the mass of ^{14}N^{15}N. In the incubation of ^{15}NH$_4^+$, using the calculated anammox produced N$_2$ as a numerator and the total produced N$_2$ (^{14}N^{14}N+^{14}N^{15}N+ insignificant ^{15}N^{15}N) as a denominator, at Elmira sites 32.7% of N$_2$ gas was attributed to anammox; 21.4% for Zorra sites. ^{15}NO$_3^-$ tracer labelling experiment showed that anammox accounted for 44.79% of N$_2$ production at Elmira sites and 29.03% at Zorra sites. The two techniques demonstrated a fair agreement at both of study sites. To date, the reported relative contribution of anammox to N$_2$ production was variable with a wild range from below detection to 67% (Thamdrup & Dalsgaard 2002; Dalsgaard et al., 2005). The contribution of anammox activity to N cycle was fairly corresponding to the percentage of anammox bacteria biomass (bacteria biomass data will be shown following). In conclusion, ^{15}N labelling experiments directly and clearly proved that the presence and activity of anammox in ground water.

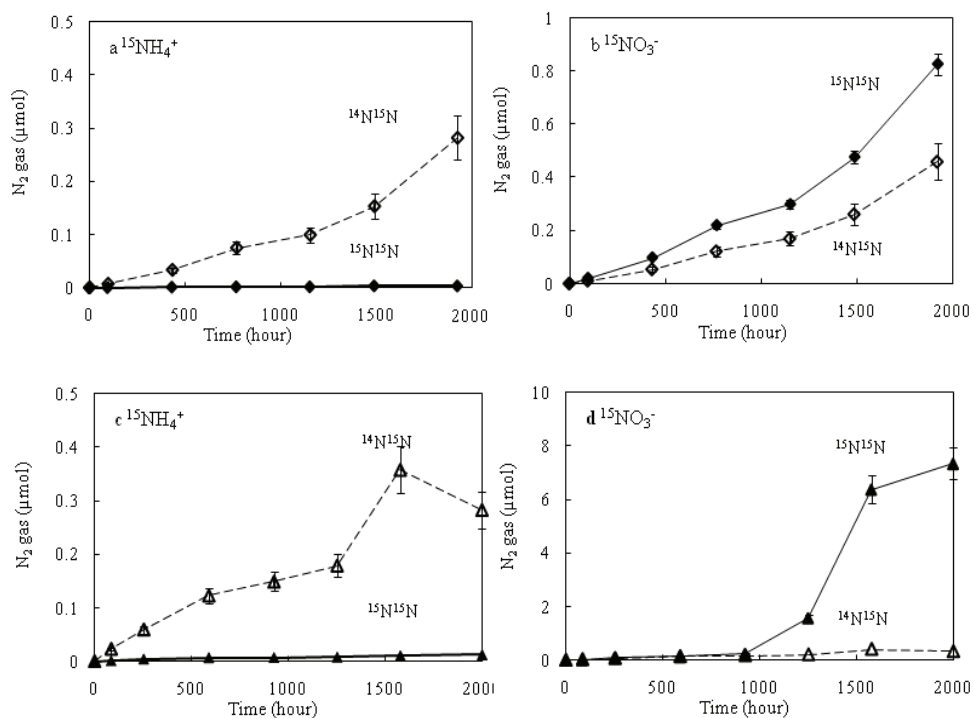

Fig. 7. Formation of ^{14}N^{15}N (open square) and ^{15}N^{15}N (solid square) in 3mL of headspace of incubation vials with samples from Elmira site(a and b) and Zorra site(c and d) after addition of ^{15}NH$_4^+$ and ^{15}NO$_3^-$.

4.3 Microbiological analyses

Molecular methods have been extensively utilized to identify the presence of anammox bacteria in environmental and wastewater samples. Fluorescence in situ hybridization (FISH) targeting the 16S rRNA gene has been used extensively, and described in detail by Schmid et al. (2005). Anammox bacteria have also been identified using PCR, using a variety of primers, often based on FISH probes, targeting the group as a whole or specific members (Schmid et al. 2005; Penton & Tiedje, 2006). Quantitative PCR (q-PCR) has been used for direct quantification of all known anammox-like bacteria in water columns (Hamersley et al. 2009), in wastewater enrichment cultures (Tsushima et al., 2007) and in terrestrial ecosystems (Humbert et al., 2010).

4.3.1 Microbiological methods

For the present study, between 240 mL and 1 L of groundwater was collected and filtered via piezometer for DNA extraction; filtrate was collected on a 0.22µm filter surface (Millipore). Filters were stored at –70∘C until DNA extraction. Nucleic acids were extracted from the filter surface using a phenol chloroform extraction technique, described previously by Neufeld et al., (2007). General bacterial 16S rRNA gene primers for denaturing gradient gel electrophoresis (DGGE; GC-341f and 518r; Muyzer et al., 1993) and anammox-specific 16S rRNA gene primers (An7f and An1388r; Penton et al., 2006) were used for PCR along with a series of reaction conditions (Moore et al, submitted). PCR products were cloned using a TOPO-TA cloning kit (Invitrogen) according to the manufacturer's instructions. DNA sequencing was performed at the Biochemistry DNA sequencing facility at the University of Washington (ABI 3700 sequencer), at The Center for Applied Genomics in Toronto (ABI 3730XL sequencer), and at the sequencing facility at the University of Waterloo (Applied Biosystems 3130xl Genetic Analyzer). DNA chromatograms were manually edited for base mis-calls and were visually inspected and trimmed to ensure only quality reads were included. Redundant sequences were removed using Jalview. Alignment and building phylogenetic trees were done with MEGA4.0 (Tamura et al., 2007). Sequences were aligned with known anammox reference sequences obtained from Genbank (DQ459989, AM285341, AF375994, DQ317601, DQ301513, AF375995, AF254882, AY257181, and AY254883) and a Planctomycete outgroup (EU703486). Phylogenetic trees were built using the neighbor joining method and the maximum composite likelihood model. Total bacterial community pie charts were constructed using phylum assignments provided by the Ribosomal Database Project and NCBI Blast. Anammox specific qPCR used An7f and An1388r (Penton et al., 2006) and general bacterial qPCR used 341f and 518r (Muyzer et al., 1993).

Fluorescently labelled oligonucleotide probes: EUB 338 (specific for all bacteria cells), Amx368 (specific for all anammox species) and Kst- 0157-a-A-18 (specific for an anammox species "*Kuenenia* Stuttgartiensis") all labelled with different fluorescent color were used to ground water and sediment samples in order to determine the abundance of the specific anammox bacteria cells in samples. Several protocols have been used and a suitable protocol for this type of environmental samples was modified. In order to give a quantitative point view of total cell versus anammox, cell counting was established. Total cell counting was carried by DAPI (4',6-diamidino-2-phenylindole) staining, which is a special fluorescent stain that binds strongly to the DNA's of only all bacterial cells (Tekin, in preparation).

4.3.2 Results and discussion

Planctomycete abundance in the total bacterial community increased with depth at Zorra according to clone library data, and planctomycetes reached 5.2 and 20.8% of the total

bacterial community at depths greater than 5 m below ground surface. Large Illumina libraries (~100 000) sequences indicated that anammox organisms made up ~10% of the bacterial community at Zorra. Quantitative PCR using anammox specific primers (An7f An1388r; Penton et al. 2006) confirmed that the abundance of anammox organisms increased with the observed increase in planctomycete abundance at Zorra site. The number of anammox 16S rRNA gene copies at Elmira was lower on average than that of Zorra. A pristine background well (having not been impacted by NH_4^+ from the compost plume) showed two orders of magnitude fewer anammox gene copies per nanogram of genomic DNA than at impacted area. Clone libraries targeting the 16S rRNA genes of anammox bacteria were used to examine the communities of anammox performing organisms at field sites. All Anammox organisms were present at the two contaminated groundwater sites however the community compositions differ (Fig 8). At Zorra site, *Can.* Brocadia dominated anammox community, where the vast majority of anammox sequence also grouped with known *Can.* Brocadia reference sequence, and a few clones grouped with known *Can.* Scalinadua. FISH images also showed the presence of anammox bacteria in both of two ground water sites (Data not shown).
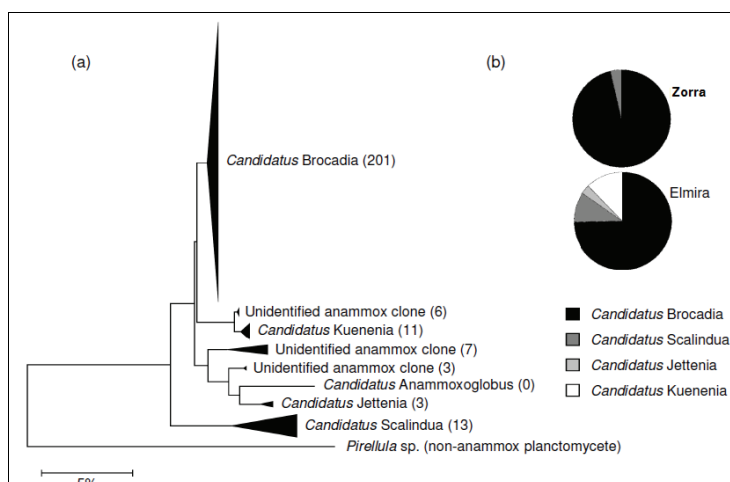

Fig. 8. (a) Phylogenetic tree of environmental anammox sequences aligned with known anammox reference sequences. Numbers in brackets represent the number of clones identifying with each cluster. (b) Distribution of anammox related 16S rRNA gene sequences found at each field site, by genus. (Modified from Moore et al., in preparation).

Anammox organisms are very hard to culture due to extremely slow growth rates, so there is a high reliance on molecular techniques for finding and identifying these organisms in mixed communities. PCR of environmental DNA extracts with general bacterial primers to generate clone libraries has been shown to underestimate the proportion of anammox organisms in the environment due to mismatches with "universal" primers (Jetten et al., 2009; Penton et al., 2006; Schmid et al., 2007). Anammox organism abundance may be greater than estimated by molecular methods due to known mismatches of anammox organisms with several "anammox," "planctomycete" or "universal bacterial" primer sets. Anammox organisms have at least 10 mismatches with 27f and 2 mismatches with 1492r,

primers used to create general bacterial 16S rRNA gene libraries for Zorra where the abundance of planctomycetes was estimated to be between 5.2 and 20.8% of the total bacterial population at 7.5 m. In summary, the results of microbiological investigation provided further evidence for anammox presence in ground water and additional insight of anammox bacteria community in ground water environments.

5. Anammox and denitrification in waste water

From a geochemical perspective, anammox and denitrification have the same implication, i.e., they both lead to a loss of fixed nitrogen, albeit with a somewhat different stoichiometry. The biogeochemical relationship between anammox bacteria and denitrifies appears quite complex. They always coexist in the same environment where they can be competitor to each other and also can play as a booster too.

In some environments with low NH_4^+, anammox depends on ammonification, which may connect with denitrifies' function on N-containing organics. In addition, the electron acceptor of anammox NO_2^- also highly relies on the production of denitrification. Therefore, the combination of anammox and denitrification is introduced in most of application in waste water treatment as above stated. Under the assumption that NO_2^- consumption by anammox can be described by Michaelis-Menten kinetics (Dalsgaard et al., 2003), the apparent half-saturation concentrations, Km for NO_2^- during anammox in natural environments has been constrained to <3 μM (Trimmer et al., 2003). Since maximum NO_2^- concentrations in natural environments are only few μmol per liter, tighter competition for NO_2^- may affect the balance between anammox and denitrification (Kuyper et al., 2006). The competition ability relies on the availability of organic matter and the physiology of bacteria. Anammox bacteria is regarded as autotrophic, so the activity of anammox bacteria may not be directly associated with organic matter. In contrast, organic matter provides both of energy and substrates to denitrification which sometime limits denitrification activity, especially in waste water treatment (Ruscalleda et al., 2008), but denitrifies grow faster than anammox bacteria which make the organisms easily outgrown in the competition. Similarly, NH_4^+ sometime derives from ammonification as mentioned above which more complicate the relationship of the two processes.

With more studies, more and more scientists argue that it is possible that anammox account for a substantial 30-50% of N_2 production in the ocean or oxygen minimum zone. Theoretically, 29% of N_2 production during the complete mineralization of Redfieldian organic matter through denitrification and anammox, is produced through anammox (Dalsgaard et al., 2003; Devol, 2003). Kuyper et al., (2006) supposed the number can exceed 48%. However, Gruber (2008) think this conclusion can not be easily extrapolated, since the dependence of anammox on denitrification, but he also pointed out that there is ample room for surprises since how little we know about the process and the associated organisms.

6. Conclusions and outlook

Over 40 years have passed since the anaerobic oxidation of ammonium with nitrite reduction was first proposed. However, our understanding of anammox is till far from complete. Anammox research is still in a very early state. All over the world, research groups are working on diverse aspects of the molecular biology, biochemistry, ultrastructure, physiology and metabolism and ecology of anammox process. As well as

assessing the impact of the activity on the environment and their application in waste water treatment. A lot of interesting facts have been revealed and certainly more will come in future. Identifying the genomes of anammox bacteria will help to cultivate these bacteria in pure cultures what wasn't achieved until now. Pure cultures could optimize the application of anammox in wastewater treatment plants and facilitate the research on the anammox bacteria. Several important questions remain to be answered are: how important the anammox process is in freshwater ecosystems, especially contaminated aquifer? How do anammox organisms interact with other nitrogen involved bacteria? From an isotope hydrological perspective, the relevant fractionation factors have yet to be established. Also, the limited applications on waste water treatment indicate that a further understanding of anammox is needed.

7. Acknowledgements

8. References

Abma, W.R.; Driessen, W. Haarhuis, R. & van Loosdrecht, M.C.M. (2010). Upgrading of swage treatment plant by sustainable and cost-effective separate treatment of industrial wastewater. Water Sci. Technol. 61., 1715-1722.

Aravena, R. & Robertson, W.D. (1998). Use of multiple isotope tracers to evaluate denitrification in ground water: Study of nitrate from a large-flux septic system plume. Ground Water. 36., 975-982.

Arrigo, K.R. (2005). Marine microorganisms and global nutrient cycles. *Nature*, 437., 15., 349-355.

Barcelona, M.J. & Naymik, T.G. (1984). Dynamics of a fertilizer contaminant plume in groundwater. *Environ. Sci. Technol*. 18., 4.,257-261.

Böttcher, J.; Strebel, O. Voerkelius, S. & Schmidt, H.-L. (1990). Using isotope fractionation of nitrate nitrogen and nitrate oxygen for evaluation of denitrification in a sandy aquifer. *Journal of Hydrology*. 114, 413–424.

Broda, E. (1977). Two kinds of lithotrophs missing in nature. *Z. Allg. Mikrobiogie*. 17., 491-493.

Buss, S.R.; Herbert A.W., Morgan, P. Thornton, S.F. & Smith, J.W.N. (2004). A review of ammonium attenuation in soil and groundwater. Quarterly Journal of Engineering Geology and Hydrogeology 37, 347–359.

Byrne, N.; Strous, M. Crépeau, V. Kartal, B. Birrien, J.L. Schmid, M. Lesongeur, F. Schouten, S. Jaeschke, A. Jetten, M.S.M. Prieur, D. & Godfroy, A. (2008). Presence and activity of anaerobic ammonium- oxidizing bacteria at deep-sea hydrothermal vents. *ISME Journal*. 3., 117-123.

Casciotti, K.L.; Sigman, D.M. Galanter Hastings, M. Böhlke, J.K. & Hilkert, A. (2002). Measurement of the oxygen isotopic composition of nitrate in marine and fresh waters using the denitrifier method. *Analytical Chemistry*. 74, 4905–4912.

Ceazan, M. L.; Thurman, E.M. & Smith, R. L. (1989). Retardation of ammonium and potassium transport through a contaminated sand and gravel aquifer. The role of cation exchange. *Environmental Science & Technology*. 23., 1402-1408.

Clark, I. ; Timlin, R. Bourbonnais, A. Jones, K. Lafleur, D. & Wickens, K. (2008). Origin and fate of industrial ammonium in anoxic ground water ^{15}N evidence for anaerobic oxidation (anammox). *Ground Water Monit. Remediat*. 28., 3., 73-82.

Dalsgaard, T.; Canfield D, E. Petersen, J. Thamdrup, B. & Acuña-González, J. (2003). Anammox is a significant pathway of N_2 production by the anammox reaction in the anoxic water column of Golfo Dulce, Costa Rica. *Nature*. 422., 606-08.

Dalsgaard, T.; Thamdrup, B. & Canfield, D.E. (2005) Anaerobic ammonium oxidation (anammox) in the marine environment. *Res Microbiol*. 156: 457–464.

Delwiche, C.C. & Steyn, P.L. (1970). Nitrogen isotope fractionation in soils and microbial reactions. *Environmental Science & Technology*. 4., 45–67.

Devol, A. H. (2003). Solution to a marine mystery. *Nature*, 422., 575-576.

Engström, P.; Dalsgaard, T. Hulth, S. & Aller, R.C. (2005). Anaerobic ammonium oxidation by nitrite (anammox): Implications for N2 production in coastal marine sediments. *Geochim Cosmochim Acta*. 69., 2057 – 2065.

Erksine, A.D. (2000). Transport of ammonium in aquifers: retardation and degradation. *Quart. J.Engin. Geol.Hydrogeol*. 33., 161-170.

Galán, A.; Molina, V. Thamdrup, B. Woebken, D. Lavik, G. Kuypers, M.M.M. & Ulloa, O. (2009). Anammox bacteria and the anaerobic oxidation of ammonium in the oxygen minimum zone off northern Chile. *Deep-Sea Research (II)*. 56., 1021-1031.

Gruber, N. (2008). The marine nitrogen cycle: overview and challenges. In: *Nitrogen in the marine environment, 2nd edition*. Capone, D.G. (Ed.). Elsevier Publisher, London, UK.

Hamersley, M. R.; Moebken, D. Boeherer, B. Schultze, M. Lavik, G. & Kuypers, M. M.M. (2009). Water column anammox and denitrification in a temperate permanently stratified lake (Lake Rassnitzer, Germany). *Systematic and Applied Microbiology*. 32., 571-582.

Hippen, A.; Rosenwinkel, K.-H. Baumgarten, G. & Seyfried, C.F. (1997). Aerobic de-ammonification: a new experience in the treatment of wastewaters. *Water Sci. Technol*. 35., 111–120.

Humbert, S.; Tarnawski, S. Fromin, N. Mallet, M-P. Aragno, M. & Zopfi, J. (2010). Molecular detection of anammox bacteria in terrestrial ecosystems: distribution and diversity. *The ISME Journal* 4, 450–454.

Hübner, H. (1986). Isotope effects of nitrogen in the soil and biosphere. In: *Handbook of Environmental Isotope Geochemistry*, *Vol. 2, The Terrestrial Environment*. B, Fritz, P. & Ch- Fontes, J.(Ed.), 361–425. Elsevier, Amsterdam, Netherlands.

Jetten, M.S.M.; Cirpus, I. Kartal, B. van Niftrik, L. van de Pas-Schoonen, K.T. Sliekers, O. Haaijer, S. van der Star, W. Schmid, M. van de Vossenberg, J. Schmidt, I. Harhangi, H. van Loosdrecht, M. Kuenen, J.G. Op den Camp, H.& Strous, M. (2005). 1994-2004: 10 years of research on anaerobic oxidation of ammonium. *Biochemical Society Transaction*. 33., 1., 119-123.

Jetten, M.S.M.; Horn, S.J. & van Loosdrecht, M.C.M. (1997) Towards a more sustainable municipal wastewater treatment system. *Water Sci. Technol*. 35., 171-180.

Jetten, M.; Wagner, M. Fuerst, J. van Loosdrecht, M. Kuenen, J.G. & Strous, M. (2001). Microbiology and application of the anaerobic ammonium oxidation (anammox) process. *Current Opinion in Biotechnology*. 12., 283–288.

Jetten, M.S.M.; van Niftrik, L. Strous, M. Kartal, B. Keltjens, J.T. & Op den Camp, H.J.M. (2009). Biochemistry and molecular biology of anammox bacteria. Crit. Rev. Biochem. *Mol. Biol*. 44(2-3)., 65-84.

Kartal, B.; Kuenen, J.G. & van Loosdrecht, M.C.M. (2010). Sewage treatment with anammox. *Science*. 328., 702-703.

Kartal, B.; Kuypers, M.M.M. Lavik, G. Schalk, J. Op den Camp, H.J.M. Jetten, M.S.M. & Strous, M. (2007). Anammox bacteria disguised as denitrifiers: nitrate reduction to dinitrogen gas via nitrite and ammonium. *Environ Microbiol*. 9., 635 – 642.

Kayuzhnyi, S.; Gladchenko, M. Mulder, A. & Versprille, B. (2006). DEAMOX-New biological nitrogen removal process based on anaerobic ammonia oxidation coupled to sulphide-driven conversion of nitrate into nitrite. *Wat. Res*. 40., 3637-3645.

Kendall, C. (1998). Tracing nitrogen sources and cycling in catchments, In*: Isotope Tracers in Catchment Hydrology*, Kendall C. & McDonnell, J.J. (Ed.), 526–531. Elsevier, Amsterdam, Netherlands.

Kuai, L.P. & Verstraete, W. (1998). Ammonium removal by the oxygen-limited antotrophic nitrification-denitrification system. *Appl. Environ. Microbiol*. 64., 4500-4506.

Kuenen, J. G. (2008). Anammox bacteria: from discovery to application. *Nature*. 6., 320-326.

Kuypers, M.M.M.; Sliekers, A.O. Lavik, G. Schmid, M. Jørgensen, B.B. Kuenen, J.G. Sinninghe Damsté, J.S. Strous, M. & Jetten, M.S.M. (2003). Anaerobic ammonium oxidation by anammox bacteria in the Black Sea, *Nature.* 422., 608-11.

Kuypers, M.M.M.; Lavik, G. Woebken, D. Schmid, M. Fuchs, B.M. Amann, R. Barker Jøregensen, B. & Jetten, M.S.M. (2005). Massive nitrogen loss from the Benguela upwelling system through anaerobic ammonium oxidation. *Proc. Natl Acad. Sci. USA*.102., 6478–6483.

Kuyper, M.M.M.; Lavik, G. & Thamdrup, B. (2006). Anaerobic ammonium oxidation in marine environment, In: *Past and present water column anoxia*. Neretin, L.N. (Ed.), NATO Science series. Springer. Dordrecth, The Netherlands.

Ladiges, G.; Thierbach, Beier R.D., & Focken, M. (2006). Versuche zur zweistufigen Deammonifikation im Hamburger Kla¨rwerksverbund. [Attempts to two-stage deammonification in the wastewatertreatment union of Hamburg]. 6. Aachener Tagung mit Informationsforum: Stickstoffru¨ ckbelastung -Stand der Technik 2006-, Aachen (Ger), ATEMIS GmbH.p. Fachbeitrag 13 (13p).

Lieu, P.K.; Hatozaki, R. Homan, H. & Furukawa, K. (2005). Singlestage nitrogen removal using Anammox and partial nitritation (SNAP) for treatment of synthetic landfill leachate. Jpn. J. *Water Treat. Biol*. 41 (2)., 103.

Meyer, R.L.; Risgaard-Petersen, N. & Allen, D.E. (2005). Correlation between anammox activity and microscale distribution of nitrite in a subtropical mangrove sediment. *Appl. Environ. Microbiol*. 71., 10., 6142-6149.

Moore, T.; Xing, Y.P. Tekin, E. Lazenby, B. Schiff, S. Robertson, W. Timlin, R. Lanza, S. M. Ryan, C. Aravena, R. Fortin, D. Clark, I. & Neufeld, J.D. Characterization of groundwater-associated communities of anaerobic ammonium-oxidizing bacteria. (Submittedd to Applied and Environmental Microbiology).

Mulder, A. (1992). Anoxic ammonia oxidation. Patent number: 5078884. USA.

Mulder, A.; van de Graff, A. A. Robertson, L.A. & Kuenen, J. G. (1995). Anaerobic ammonium oxidation discovered in a denitrifying fluidized bed reactor. *FEMS Microbiol. Ecol*. 16., 177-184.

Muyzer, G.; Dewaal, E.C. & Uitterlinden, A.G. (1993). Profiling of complex microbial-populations by denaturing gradient gel-electrophoresis analysis of polymerase chain reaction-amplified genes-coding for 16s ribosomal-RNA. Appl. Environ. Microbiol. 59(3): 695-700.

Neufeld, J.D.; Schafer, H. Cox, M.J. Boden, R. McDonald, I.R. & Murrell, J.C. (2007). Stable-isotope probing implicates *Methylophaga* spp and novel Gammaproteobacteria in marine methanol and methylamine metabolism. *ISME Journal*. 1., 480-491.

Op den Camp, H.J.M.; Kartal, B. Guvent, D. van Niftrik, L.A.M.P. Haaijer, S.C.M. van der Star, W.R.L. van de Pas-Schoonen, K.T. Cabezas, A. Ying, Z. Schmid, M.C. Kuypers, M.M.M. van de Vossenberg, J. Harhangi, H.R. Picioreanu, C. van Loosdrecht, M.C.M. Kuenen, J.G. Strous, M. & Jetten, M.S.M. (2006). Global impact and application of the anaerobic ammonium-oxidation (anammox) bacteria. *Biochemical Society Transactions*. 34., 174-178.

Penton, C.R.; Devol, A.H. & Tiedje, J.M. (2006). Molecular evidence for the broad distribution of anaerobic ammonium-oxidizing bacteria in freshwater and marine sediments. *Appl. Environ. Microbiol*. 72., 6829-6832.

Richard, F.A. (1965). Anoxic basins and fjords. In: *Chemical oceanography*, vol 1. Riley, J.P.& Skirrow, G. (Ed.), Academic Press, London, 611-645.

Risgaard-Petersen, N.; Meyer, R.L. Schmid, M. Jetten, M.S.M. Enrich-Prast, A. Rysgaard, S. & Revsbech, N.P. (2004). Anaerobic ammonium oxidation in an estuarine sediment. *Aquat Microb Ecol*. 36., 293 – 304.

Risgaard-Peterson, N.; Nielsen, P. L. Rysgaard, S. Dalsgaard, T. & Meyer, R. L. (2003). Application of the isotopic paring technique in sediments where anammox and denitrification coexist. *Limnology and Oceanography: method*. 1., 63-73.

Ritter, W.F.& Chirnside, A.E.M. (1995). Impact of dead bird disposal pits on groundwater quality on the delmarva peninsula. *Bioresour. Technol*. 53., 105-111.

Ruscalleda, M.; López, H. Ganiqué, R. Puig, S. Balaguer, M.D. & Colprim, J. (2008). Heterotrophic denitrification on granular anammox SBR treating urban landfill leachate. *Water Sci. technol.* 58., 1749-1755.

Rysgaard, S. & Glud, R.N. (2004). Anaerobic N_2 production in Arctic sea ice. *Limnol. Oceanogr*. 49., 1., 86-94.

Schmid, M.C.; Maas, B. Dapena, A. van de Pas-Schoonen, K. van de Vossenberg, J. Kartal, B. van Niftrik, L. Schmidt, I. Cirpus, I. Kuenen, J.G. Wagner, M. Sinninghe Damsté, J. S. Kuypers, M.M.M. Revsbech, N.P. Mendez, R. Jetten, M.S.M. & Strous, M. (2005). Biomarkers for the in situ detection of anaerobic ammonium oxidizing (anammox) bacteria. *Appl. Environ. Microbiol*. 71., 1677 – 1684.

Schmid, M.C.; Risgaard-Petersen, N. van de Vossenberg, J. Kuypers, M.M.M. Lavik, G. Petersen, J. Hulth, S. Thamdrup, B. Canfield, D. Dalsgaard, T. Rysgaard, S. Sejr, M.K. Strous, M. den Camp, H.J.M.O. & Jetten, M.S.M.(2007). Anaerobic ammonium-oxidizing bacteria in marine environments: widespread occurrence but low diversity. *Environ. Microbiol*. 9., 1476-1484.

Schubert, C. J.; Durish-Kaiser, E. Wehrli, B. Thamdrup, B. Lam, P.& Kuypers, M.M.M. (2006). Anaerobic ammonium oxidation in a tropical freshwater system (Lake Tanganyika). *Environmental Microbiology*. 8., 1857-1863.

Sigman, D.M.; Casciotti, K.L. Andreani, M. Barford, C. Galanter, M. & Böhlke, J.K. (2001). A bacterial method for the nitrogen isotopic analysis of nitrate in marine and fresh waters. *Analytical Chemistry*. 73., 4145–4153.

Sinninghe Damsté, J.S.; Rijpstra, W.I.C. Schouten, S. Fuerst, J.A. Jetten, M.S.M. & Strous, M. (2004). The occurrence of hopanoids in planctomycetes: Implications for the sedimentary biomarker record. *Org Geochem*. 35., 561 – 566.

Strous, M.; Fuerst, J. A. Kramer, E.H.M. Logemann, S. Muyzer, G. van de Pas-Schoonen, K. T. Webb, R. Kuenen, J.G. & Jetten, M.S.M. (1999). Missing lithotroph identified as new planctomycete. *Nature*. 400., 446-449.

Strous, M.; Heijnen, J.J. Kuenen, J.G. & Jetten, M.S.M. (1998). The sequencing batch reactor as a powerful tool for the study of slowly growing anaerobic ammonium-oxidizing microorganisms. *Appl. Microbiol. Biotechnol*. 50., 589-596.

Strous, M.; Pelletier, E. Mangenot, S. Rattei, T. Lehner, A. Taylor, M.W. Horn, M. Daims, H. Bartol-Mavel, D. Wincker, P. Barbe, V. Fonknechten, N. Vallenet, D. Segurens, B. Schenowitz -Truong, C. Médigue, C. Collingro, A. Snel, B. Dutilh, B.E. et al., (2006). Deciphering the evolution and metabolism of an anammox bacterium from a community genome. *Nature*. 440., 790 – 794.

Strous, M.; van Gerven, E. Kuenen, J.G. & Jetten, M.S.M. (1997a). Effects of aerobic and microaerobic conditions on anaerobic ammonium-oxidizing (anammox) sludge. *Appl. Environ. Microbiol*. 63., 2446-2448.

Strous, M.; van Gerven, E. Ping, Z. Kuenen, J.G. & Jetten, M.S.M. (1997b). Ammonium removal from concentrated waste streams with the Anaerobic Ammonium Oxidation (Anammox) process in different reactor configurations. *Water Res*. 31., 1955-1962.

Tekin, E. (2010) Anammox in contaminated ground water. Thesis (in preparation). University of Ottawa.

Tamura, K., Dudley, J., Nei, M., and Kumar, S. (2007). MEGA4: Molecular evolutionary genetics analysis (MEGA) software version 4.0. *Mol. Biol. Evol.* 24., 1596-1599.

Thamdrup, B. & Dalsgaard, T. (2002). Production of N_2 through anaerobic ammonium oxidation coupled to nitrate reduction in marine sediments. *Applied and Environmental microbiology*. 68., 1312-1318.

Thamdrup, B.; Dalsgaard, T. Jensen, M.M. Ulloa, O. Farías, L. & Escribano, R. (2006). Anaerobic ammonium oxidation in the oxygen-deficient water off northern Chile. Limnol. Oceanogr. 51., 2145-2156.

Third, K. A.; Slickers, A.O. Kuenen, J.G. & Jetten, M.S.M. (2001). The CANON system (completely autotrophic nitrogen-removal over nitrite) under ammonium limitation interaction and competition between three groups of bacteria. *System. Appl. Microbe*. 24., 588-596.

Trimmer, M.; Nicholls, J.C. & Deflandre, B. (2003). Anaerobic ammonium oxidation measured in sediments along the Thames estuary, United Kingdom. *Appl. Environ. Microb*.69., 6447-6454.

Tsushima, I,; Kindaichi, T. & Okabe, S. (2007). Quantification of anaerobic ammonium-oxidizing bacteria in enrichment cultures by real-time PCR. *Water Res*. 41.,785 – 794

Umezawa, Y.; Hosono, T.; Onodera, S. Siringan, F. Buapeng, S. Delinom, R. Yoshimizu, C. Tayasu, I. Nagata, T. & Taniguchi, M. (2008). Sources of nitrate and ammonium contamination in groundwater under developing Asian megacities. *Sci. Total Environ*. 404., 361-376.

van de Graaf, A. A.; de Bruijn, P. Robertson, L.A. & Kuenen, J.G. (1997). Metabolic pathway of anaerobic ammonium oxidation on the basis of N-15 studies in a fluidized bed reactor. *Microbology-UK*. 143., 2415-2421.

van de Graaf, A. A.; Mulder, A. de Bruijn, P. Jetten, M.S.M. Robertson, L.A. & Kuenen, J.G. (1995). Anaerobic oxidation of ammonium is a biologically mediated process. *Appl. Environ. Microbial*. 61., 1246-1451.

Van der Star, W.R.I.; Abma, W.R. Blommers, D., Mulder, J.W. Tokutomi, T. Strous, M. Picioreanu, C. & van Loosdrecht, M.C.M. (2007). Startup of reaction for anoxic ammonium oxidation: Experiences from the first full-scale Anammox reactor in Rotterdam. *Wat. Res*. 41., 4149-4163.

Van Loosdrecht, M.C.M. (2008). Innovative nitrogen removal. In: *Biological Wastewater Treatment Principles, Modelling and Design*. Henze, M. et al., (Eds.). IWA Publishing, London, UK.

Van Dongen, U.; Jetten, M.S.M. & van Loosdrecht, M.C.M. (2001). The SHARON-Anammox process for treatment of ammonium rich wastewater. *Water Sci.Technol.* 44., 1.,153-160.

Wada, E.; Kadonaga, T. & Matsuo, S. (1975). [15]N abundance in nitrogen of naturally occurring substances and global assessment of denitrification from isotopic view point. *Geochemical Journal*. 9., 139–148.

Wett, B. (2006). Solved upscaling problems for implementing deammonification of rejection water. *Water Sci. Technol*. 53., 12., 121–128.

Wyffels, S.; Boeckx, P. Pynaert, K. Zhang, D. van Cleemput, O. Chen, G. & Verstraete, W. (2004). Nitrogen removal from sludge reject water by a two-stage oxygen-limited autotrophic nitrification denitrification process. *Water Sci. Technol*. 49., (5–6)., 57–64.

Measurement Techniques for Wastewater Filtration Systems

Robert H. Morris[1] and Paul Knowles[2]

[1]Nottingham Trent University,
[2]Aston University
UK

1. Introduction

Filter-based microbiological wastewater treatment systems (such as subsurface flow constructed wetlands, trickling filters and recirculating sand filters) require a thorough understanding of system hydraulics for their correct design and efficient operation. As part of the treatment process, the filter media will gradually become clogged through a combination of solids filtration and retention, biomass production and chemical precipitation. Eventually the media may become so clogged that hydraulic malfunctions ensue, such as untreated wastewater bypassing the system. To achieve good asset lifetime a balance must be struck between these essential treatment mechanisms and the hydraulic deterioration that they cause. For many wastewater filtration systems the exact mechanism of clogging is not obvious, and few specialised techniques have been developed which allow the cause and extent of clogging to be measured in typical systems. The resultant lack of understanding regarding clogging hinders the ability of operators to maintain good hydraulic performance. In this chapter, for the first time, we compare three different families of standard hydraulic measurement techniques and discuss the information that they can provide: hydraulic conductivity measurements; clog matter characterisation and hydrodynamic visualisation. Each method is assessed on its applicability to typical wastewater filtration systems using horizontal subsurface flow constructed wetlands as a case study.

Furthermore, several new techniques will be considered which have been specifically developed to allow *in situ* determination of hydraulic health for subsurface flow constructed wetland wastewater filtration systems. These include *in situ* constant and falling head permeameter techniques and embeddable magnetic resonance probes.

Discussion is given to the ways in which different methods can be combined to gather detailed information about the hydraulics of wastewater filtration systems before exploring methods for condensing heterogeneous hydraulic conductivity survey results (that vary by several orders of magnitude) into a single representative value to describe the overall hydraulic health of the system.

2. Mechanisms of clogging

A typical subsurface flow wetland comprises a layered structure as seen in figure 1. Such a system usually comprises a gravel matrix in which Phragmites australis (the common reed)

is grown. These systems are used as an environmentally friendly method for wastewater sanitisation before eventual discharge into a watercourse. The wastewater flows under gravity through the gravel (below the surface), where it encounters optimum conditions for purification: solids are removed by the gravel substrate and the root network of the reeds, which also provide a surface on which to trap particulates and promote biofilms. Removal of organic material, pathogens and nutrients is predominantly due to biofilms. Many chemical compounds are absorbed or precipitated depending on the physicochemical conditions of the wastewater constructed wetland (Brix, 1994). Over time this causes the pore spaces between gravel grains to become occluded. A small amount of clogging will occur due to biofilm growth which helps to improve the overall efficiency and functionality of the system, although over time, excessive biofilm growth and retention of solids may lead to bypass flow of untreated influent. The balance between these two dominant clogging mechanisms often requires a multi-modal assessment methodology to elucidate the complete nature and severity of the clogging.
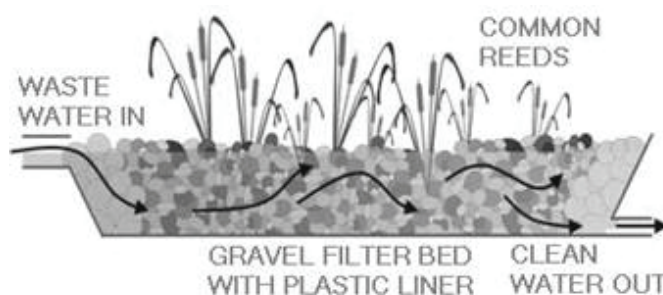

Fig. 1. Cross sectional view of a typical subsurface flow constructed wetland.

3. Traditional measurement strategies

There are a variety of measurement techniques available to determine the hydraulic conditions within the filter *in situ* (Knowles et al., 2009a; Lin et al, 2003), whilst determination of the composition and quantity of clog matter usually requires samples of the gravel matrix to be extracted prior to laboratory analysis. Each of these measurement techniques is discussed in this section along with the weaknesses and strengths of each strategy, which are summarised in Table 1. Whilst no individual technique is suitable for gaining a full insight into the true extent of clogging, they may be useful to understand individual contributions of system clogging or be used in combination for an understanding of the interplay between different factors.

3.1 Hydraulic conductivity measurements

Traditional measurements of hydraulic conductivity share two common elements. The first is that a test well or sample core must be made either *in situ* or remotely in a laboratory. The second is that the hydraulics of the system must be tested in some repeatable or measurable way to determine the hydraulic properties of the sample under test. In this section seven common hydraulic conductivity measurement techniques will be briefly discussed.

Test Family	Test	Description
Hydraulic Conductivity	Slug Test	A piezometer tube (devoid of media) is inserted into the media. The water level is rapidly changed by addition of water or a metal slug. The evolution of the water level back to equilibrium is used to calculate the permeability.
	Pumping Test	Water is pumped at a constant rate into or out of a well, and the resulting cone of depression in the filtration medium is monitored over time.
	Steady State Test	Flow through the filter medium results in a hydraulic gradient. Differences in the height of the water table are observed in different wells.
	Unlined Auger Hole	A borehole is made into the media and water is either added or removed. The recharge rate or flow rate into the media is measured.
	Infiltration Tests	A ring is impressed into the surface of the filtration medium and water is added to measure the infiltration rate through the surface.
	Laboratory Permeameter	A sample of the media is placed into a laboratory permeameter cell. A constant or variable head of water is then applied across the media. Manometer take off points allow the variation in resistivity across the sample to be determined.
	Modified Cube Method	A cubic sample of the filtration media is sealed in wax before removing single sets of opposing faces and passing flow through the media, the hydraulic conductivity in different planes can be determined.
Clog Matter Characterisation	Direct Porosity Measurements	Either saturated or drainable porosity of an extracted sample is measured in the laboratory. This approximates the ratios of free to interstitial water.
	Time Domain Reflectometry	A family of methods which rely on the dielectric constant of a medium being proportional to water saturation. Each method uses a different approach to measure this property. TDR and CP are inserted at various points and give readings in the immediate locality whilst the GPR is swept over the surface providing a subsurface image.
	Capacitance Probe	
	Ground Penetrating Radar	
	Solids Assays	Total and volatile solids of the interstitial clog matter are determined by drying the samples. Suspended fractions in interstitial water may also be measured.
Hydrodynamic Visualisation	Breakthrough Curve	The breakthrough of a pulse of tracer added to the system inlet is monitored at the outlet of the system
	Internal Tracing	The dynamics of an inlet injected tracer are monitored at different points in the system.

Table 1. Summary of available hydraulic measurement techniques separated into families.

3.1.1 Slug test

To perform a slug test, a hollow tube perforated at the lower end or a piezometer is inserted into the gravel substrate. A rapid and temporary change in water level, followed by return to the equilibrium state is used to determine the hydraulic conductivity of the substrate near the tube. This is achievable in one of two ways: the first (and the origin of its name) is shown in figure 2 and requires the introduction of a metal slug into the water which infiltrates the tube thus displacing some of it. The second is to add a known amount of water to the well. Measurements of the water level (or air pressure above the water) will show a sudden increase corresponding to the volume of the slug followed by an exponential decay back to the natural level of the water table. The hydraulic conductivity of the surrounding gravel can then be determined.
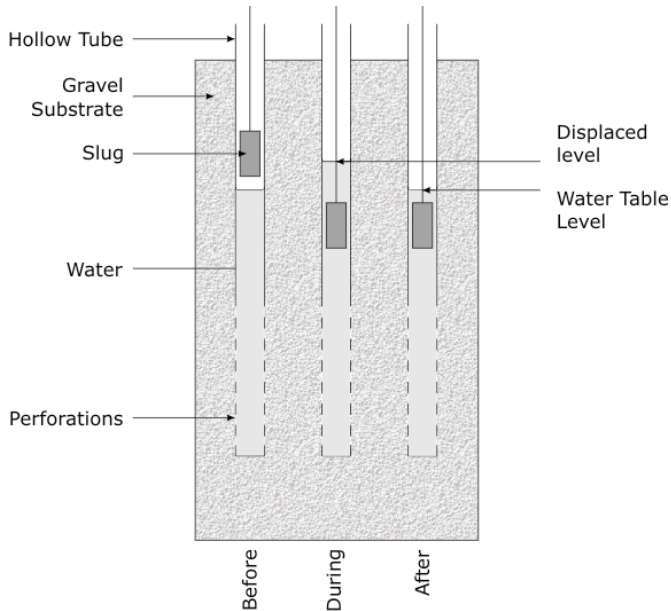
Fig. 2. Schematic representation of the measurement phases in the slug test used in a gravel substrate.

The analysis of the relaxation curve from the slug test relies on two assumptions. The first is that the water and gravel in the area around the tube is incompressible, which is typically a reasonable assumption in an established water saturated wetland. The second is that the surrounding medium is completely homogeneous which unfortunately is rarely the case. The method for determining the hydraulic conductivity is based on a modified Thiem equation (equation 1)

$$K = \frac{R_W^2 \ln(h_0/h_t)}{Ft},\tag{1}$$

where K is the hydraulic conductivity of the gravel substrate, R_W is the radius of the well, h_0 and h_t are the height of the water relative to the equilibrium level at the start and end of

the experiment lasting time t and F is a shape factor determined by the dimensions of the well using one of several methods. The shape factor presented in equation 2 is valid only for a well which has a perforated section with a length, L_P, shorter than sixteen times its radius. The reader is referred to the work of Hvorslev (1951) for more unusual well geometries.

$$F = \frac{2\pi L_P}{\sqrt{L_P/(2R_W + 0.25)}}.$$

(2)

For gravel substrates which contain fractions of different gravel sizes, the hydraulic conductivity determined using the slug test is often not representative and an alternative technique is required.

3.1.2 Pumping test

The pumping test is typically performed on aquifers but is equally applicable (with careful consideration of error) to water saturated gravel substrates. The pumping test can be performed either by pumping water into or out of the gravel substrate. In a clogged system this can be quite disruptive if the flow rates are too high and in shallower systems, it may not be possible to withdraw a sufficiency of water to yield valid results in the case where the water is pumped out. The test is set up as in figure 3 with at least one test well, although the results are more reliable with several.

As water is withdrawn (or added) to the substrate, a cone of depression develops (for water withdrawal), the geometry of which corresponds to the flow rate out of (into) the well and hydraulic resistance to flow offered by the substrate. By measuring the height of the water table at several places along the radius of the cone it is possible to determine the hydraulic conductivity of the gravel substrate. Most often this test is performed with a constant pumping flow rate and the changing geometry of the cone of depression is plotted against time. It is also possible however to repeat this test several times in succession with increasing pump rates to improve the quality of the analysis. The hydraulic conductivity is again determined from the measurements using a steady state solution to the Thiem equation (eq. 3)

$$K = \frac{Q}{2\pi d(h - h_0)} \ln\left(\frac{r}{R}\right),$$

(3)

where Q is the flow rate of the pump, d is the depth of the substrate, h-h_0 is the drawdown (i.e. the difference between the depth of the water before and after the pump is started) measured at a distance r from the pumping well. R is the distance from the pumping well at which the water level is unaffected. In a small wastewater treatment system, where the cone of depression may quickly extend to the inlet, R can be assumed as the distance to the inlet of the system with a usually small experimental error.

The results from this test are only truly representative of the actual hydraulics of the system when it has undergone little clogging and is relatively deep in comparison to the depth of the wells and the depth of the cone of depression.
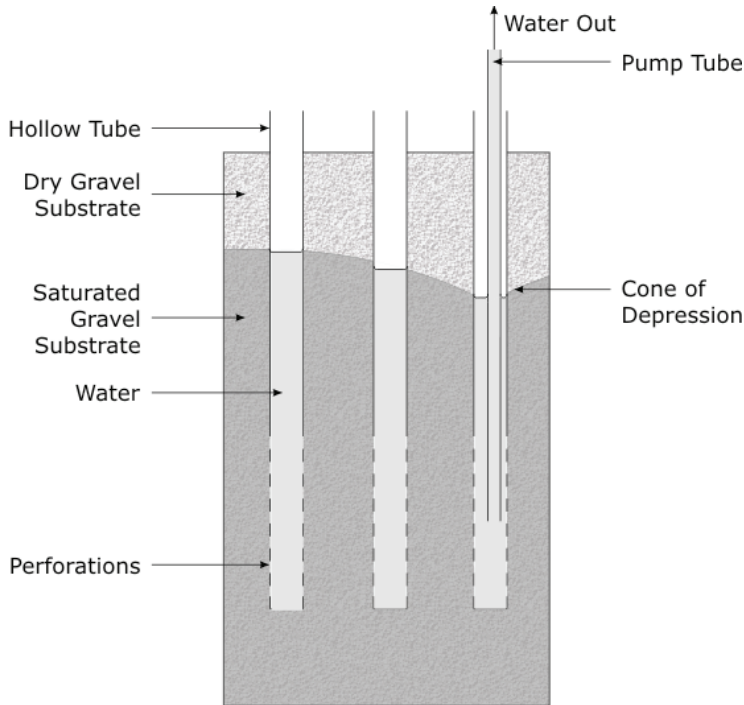
Fig. 3. Schematic of pump test set up. The right hand side is the pumping well whilst the left and centre are two test wells.

3.1.3 Steady state test

The steady state test is one of the least disruptive hydraulic conductivity tests. It requires only the insertion of several test wells (pipes with part perforation as used previously) at various lengths along the bed. The flow of water from one side of the bed to the other will result in a hydraulic gradient along its length, causing a variation in the height of the water table which can be measured in each test well. The determination of the hydraulic conductivity is then relatively simple using Darcy's law as in equation 4.

$$K = \frac{Qr}{Ah},$$ (4)

where h is the difference in height between the water table in each well separated by distance r, and A is the cross sectional area through which the flow has taken place. This analysis relies on a homogeneous flow path between the wells and assumes that the flow uses the whole of the cross sectional area. Although the impact of these assumptions can be minimised by keeping the test wells relatively close together, the extra number of wells that are required may cause too great a disturbance to the substrate to be fully representative. This test is best performed in a system which has not undergone long term clogging to ensure that the results are as reliable as possible.

3.1.4 Unlined auger hole

The unlined auger test is a means of measuring the hydraulic conductivity in a constructed wetland which has undergone a sufficient degree of clogging that the gravel matrix has become stabilised by clog matter. This allows an unlined bore hole to be made without too great a risk of the walls collapsing into it. The three tests discussed so far can all be performed in an unlined auger hole with the benefit of complete confidence that the whole surface of the bore hole is participating in the method thus ensuring complete assessment of the local environment. The drawback of this method is however ensuring that the walls do not become weakened to the point of collapse and to avoid the build up of silt and sediment in the base of the well. This is particularly critical for the pumping test in which the large flow rates increase the likelihood of this occurring.

3.1.5 Infiltration test

The testing strategies discussed in the previous sections are primarily affected by horizontal hydraulic conductivity only. As this is the typical direction of fluid flow in a typical horizontal constructed wetland this is acceptable. In many situations, particularly clogged gravel beds, overland flow occurs which results in a dual flow regime with vertical and horizontal components. Additionally, vertical flow constructed wetlands are also becoming more popular thanks to their smaller footprint and thus methods for measuring the vertical hydraulic conductivity are required. In the infiltration test, the vertical infiltration rate of flow across the surface of the system is measured. This is normally performed by burying two concentric metal rings partially in the surface of the gravel (the rings are typically 60cm and 30cm in diameter and about 25cm in height buried 15cm into the gravel) as in figure 4. Both the central ring and the space between the two rings are filled with water. The drop in water level is monitored every few minutes. The water level is kept relatively constant and
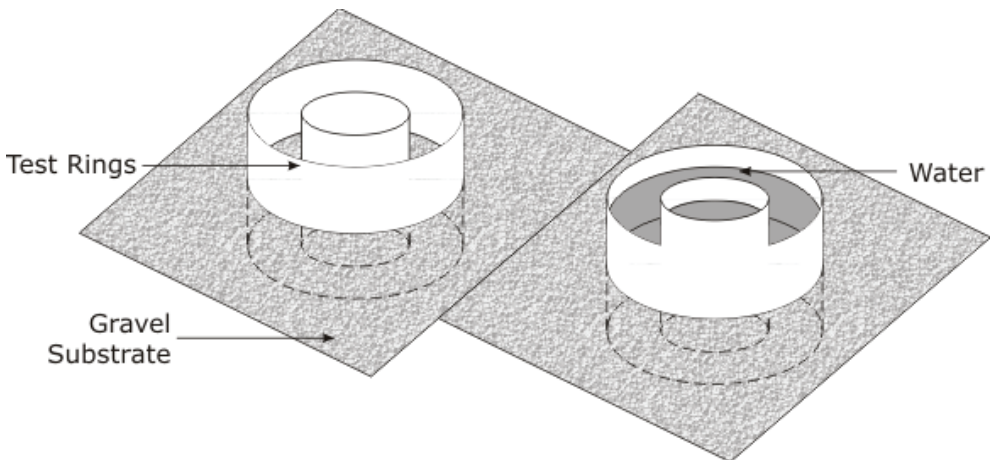

Fig. 4. Schematic representation of equipment used for infiltration testing before and after filling with water (left and right).

measurements are made frequently. Once the water is seen to be falling at a constant rate the value is noted as the basic infiltration rate. The time that this takes is also of some relevance, particularly on dry samples as it allows the tester to determine the wetability.

This test only indicates the infiltration rate through the surface of the substrate and does not indicate the hydraulic conductivity of the bulk substrate. It is worth noting that the test is only valid so long as the water between the two rings is at a similar level as that inside the inner ring, as it is used to prevent horizontal motion of the water from the centre.

3.1.6 Laboratory permeameter

The laboratory permeameter is often considered the most accurate means of assessing gravel permeability. However, to use a traditional permeameter, a sample of the gravel substrate must be extracted, in tact with the surrounding clog matter and transported to a laboratory. The sample is then loaded into the permeameter system and, using one of two techniques, the permeability is assessed. The standard setup for a laboratory permeameter is as shown in figure 5. A constant head of water is produced by using a top reservoir with a connection to the permeameter and a much larger overflow drain. Water is fed into the device at a rate that the overflow drain is utilised to a small degree, such that a constant flow rate into the permeameter is maintained. A bottom reservoir is used to create a water-lock and ensure that the sample remains saturated. The height difference between the water level in the top and bottom reservoir forces flow through the sample, with a flow-rate that corresponds to the hydraulic conductivity of the media. By measuring the outlet flow-rate, Darcy's law can be used to determine the hydraulic conductivity of the sample as in equation 5.

$$K = \frac{QL}{A\Delta h},$$ (5)

where Δh is the distance between the bottom of the reservoir overflow and the bottom of the sample overflow and L is the vertical length of the sample with cross sectional area A. In this experiment Q is calculated using the volume of water collected per unit time.

The accuracy of this method can be somewhat improved by varying the value of Δh and measuring Q. If Q is then plotted against $(A\Delta h)/L$, a linear relationship with gradient K is found.

An alternative set up which allows a similar measurement accuracy in a shorter time is known as a falling head permeameter. The equipment is the same as in the static head permeameter only instead of keeping the level of the cup constant, it is allowed to drop with time from a height h_0 to a height of h_t at time t. Typically the cup is narrower than the sample in this experiment to allow the height of the liquid to be measured easily. The experimental protocol is to monitor the height of the liquid in the reservoir over time. A rearrangement of Darcy's law can then be used to determine the value of the hydraulic conductivity. If $ln(h_0/h_t)$ is plotted against t, the slope will be KA/aL, where a is the cross sectional area of the cup.

The main drawback of this technique is that the samples must be extracted from the wetland. Careful measurements do however give reliable assessment of the hydraulic conductivity using both protocols which are often used as benchmarks for alternative testing strategies.
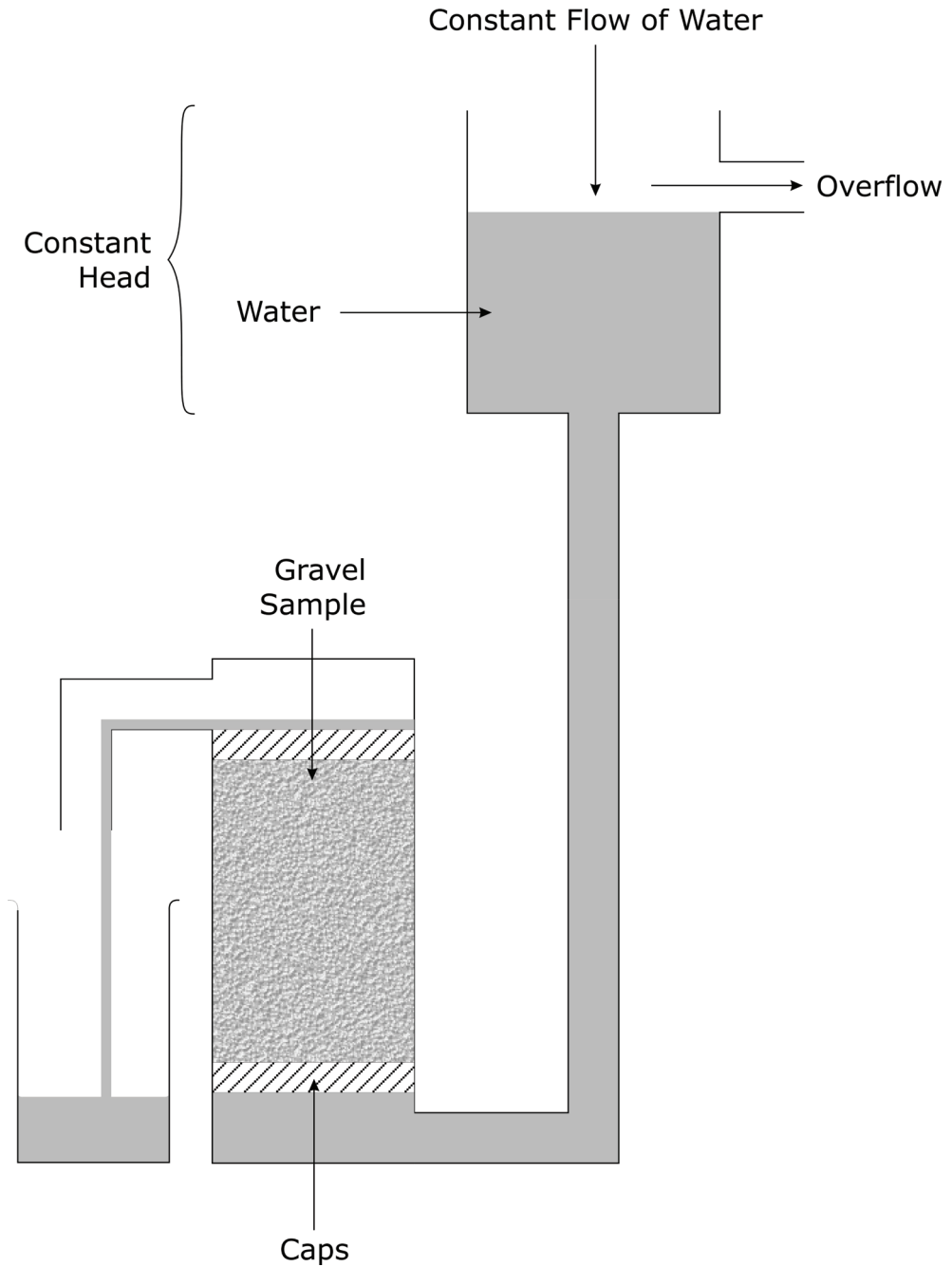
Constant Flow of Water

Overflow

Constant
Head

Water

Gravel
Sample

Caps

Fig. 5. Schematic representation of laboratory permeameter setup.

3.1.7 Measurements of anisotropic hydraulic conductivity

Hydraulic conductivity is a tensor with three nodes that represent hydraulic conductivity in different directions of flow. In an anisotropic medium, hydraulic conductivity at a point may vary depending on the flow direction. A simple example of this is whereby particle size stratification has created horizontal layers that encourage horizontal flow channelling, and do not encourage vertical flow across the layers. The previously discussed methods are axial tests which only allow measurement of hydraulic conductivity in one direction. Recent laboratory methods have been developed to allow anisotropic hydraulic conductivity to be evaluated in extracted soil samples (Renard et al., 2001). One such method called the Modified Cube Method has been applied to measure anisotropy in natural wetland peat samples (Beckwith et al.; 2003, Kruse et al.; 2008, Rosa and Larocque, 2008). The test involves cutting a cube of material from an extracted core and coating it in paraffin wax. One set of opposing sides of the wax case are removed and the sample subjected to an axial hydraulic conductivity test, such as the constant head laboratory permeameter test. After measurement the wax case is restored and a different set of opposing sides is removed, and the test repeated across this flow direction. This is performed for all three flow directions such that the hydraulic conductivity tensor can be ascertained.

3.2 Clog matter characterisation

The techniques described in the previous section are used to assess the hydraulic properties of the clogged porous media flow system. However, these tests cannot reveal information about the cause of clogging and the nature of the clog matter, which is often key in determining the health of a system. In this section we will consider the range of common tools available to determine the properties of the clog matter fraction in the system.

3.2.1 Direct porosity measurements

There are numerous methods for measuring the porosity of a sample directly. In this section we will discuss the two most commonly used for samples collected from constructed wetlands. This is a highly invasive technique and requires the extraction of sample cores from the gravel substrate. Once these cores are extracted, they are analysed in the laboratory using two tests to determine the amount of water which is free and the amount that is associated, that is to say the amount that is associated with the surface of the grains in biofilms for example. The first test is relatively straightforward and relies on taking a known volume of the core sample which is allowed to drain of water for a few minutes, possibly during gentle agitation, whilst preventing the loss of any clog matter. The sample is placed in a container and the amount of water needed to fill the sample (again with or without agitation) divided by the total apparent volume of the sample is the free water porosity. This measure is reliable in samples with well connected pores so that all of the free water is able to drain unhindered from the sample. The water is then drained again from the sample in preparation for the second test. Collection and determination of the volume of this second drain of water is advisable as a means to check the reliability of the first measurement.

Determination of the remaining, and hence associated, water in the sample can be achieved using one of two methods. The longer of the two methods allows the remaining water to drain slowly from the sample in a sealed vessel (as evaporation will result in much of the loss) until it is completely dry, the volume of the collected water then represents the pore space occupied by interstitial water in the sample. This is a lengthy process and requires a careful set up to avoid disrupting the sample. The alternative technique, which is often

combined with a solids assay as described in section 3.2.5 is to weigh the sample before and after gentle heating to evaporate the interstitial water fraction. The mass change is then used to determine the volume of water lost. This method may give unpredictable results in a sample which contains volatile solids which will contribute to the mass of the sample. Although these techniques both offer useful results, the need to collect a core of the gravel substrate often makes them less attractive than their *in situ* counterparts.

3.2.2 Time domain reflectometry

Time domain reflectometry is a technique which relies on the relationship between the dielectric properties of different materials and their water content. The principal for measuring clogging using Time Domain Reflectometry and the next two techniques to be reviewed; Capacitance Probes and Ground Penetrating Radar; is that they all measure properties that will vary depending on the amount of interstitial water in a sample. Therefore, it would be possible to detect where accumulation of clog matter has reduced the interstitial water volume compared to a calibrated clean sample. This, in itself, is an inherent limitation of these techniques as clog matter is typically well hydrated (often above 95% water by volume) and as such very small variations in water volume must be measured. The complexity of the system used to perform the measurements is such that a detailed description is beyond the scope of this chapter. Instead, the basic operating principles of the technology will be provided along with the relationship between the results and the physical properties of the sample. The technique is particularly difficult to use in a gravel substrate as the grains disrupt its underlying mechanism. Its use in heavily clogged media is however still valuable as a method for assessing water content.

The underlying principle of time domain reflectometry is similar to that of radar. An electromagnetic wave pulse is produced and transmitted into the gravel substrate, often using metal electrodes. The wave will propagate through the medium at a speed which is determined by the dielectric constant of the medium which is dependent on the water content. The wave will be reflected and picked up by the same electrodes as were used to deliver it into the medium. The time between the emission and absorption of this pulse is used to determine the speed with which it travelled through the medium. This is then converted to water content using a calibration produced from samples with known water content. Whilst the technique may offer very accurate results, it is heavily influenced by spurious reflections caused by local heterogeneities, may be affected by changes in electrical conductivity (such as those caused by salinity) and relies on calibration in similar samples to those under test to be representative. An alternative technique which relies on the same underlying principle is known as time domain transmissometry. In this technique, instead of using the same electrodes to generate and measure the pulse, separate electrodes are used. In this way it is possible to somewhat reduce the influence of local inhomogeneity on the results although this is often of little benefit in a filtration system containing gravel which is still highly reflective to the wave.

3.2.3 Capacitance probe

The operation of the capacitance sensor is similar in some respects to time domain reflectometry in that electrodes are used to determine the dielectric properties of the gravel substrate. In this technique however, the two electrodes are commonly metallic plates wrapped around a cylinder (see Figure 6). In combination with the surrounding gravel substrate, clog matter and water, a capacitor is formed. The capacitance of this arrangement is dependent on the size and spacing of the plates and the dielectric permittivity of the

surrounding medium. The dielectric permittivity is in turn dependent predominantly on the water content and salinity. Several of these probes are often included on a single plastic cylinder to maximise the measurements that can be made for a single insertion.
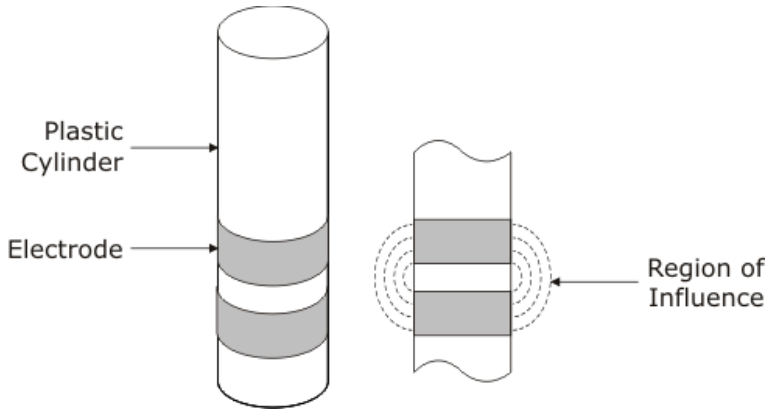

Fig. 6. Schematic of capacitance sensor. Right hand figure is front view of left hand figure showing the area in which measurements are made.

The measurement of the capacitance is typically made by including the capacitance probe as an element of a resonant circuit. The frequency at which the circuit resonates is determined by the value of the capacitor and thus may be used to determine the dielectric permittivity in the region of influence (see figure 6). The size of, and spacing between the plates may be adjusted to optimise the penetration distance from the cylinder into the medium based on the intended usage. For example, the plates would ideally be separated by a greater distance for measurements in gravel where the particle size is large in comparison to a measurement in a sand filter. As with time domain reflectometry, the capacitance probe must be calibrated. Owing to its considerably lower cost however, it is quite practical to have several probes along the bed including one in the influent, thus compensating for the effect of salinity.

3.2.4 Ground penetrating radar
Ground penetrating radar is a technique which uses pulses of microwaves to determine the properties of a sample non-destructively. The instruments are relatively expensive and complex but offer an unprecedented measure of the dielectric properties of a sample without requiring its extraction. In a typical setup, a unit is moved along the surface of a bed whilst the measurement is made. Microwave pulses are transmitted by a coil in contact with the surface of the ground. At changes in dielectric constant (such as different media or different water content) the microwaves are reflected back and picked up by the instrument. The use of ground penetrating radar in a typical constructed wetland is very challenging given the reed growth above ground making it difficult to place the equipment on the surface and the propensity for gravel to cause a great number of reflections before any measurements have been made. For this reason it is not usually practical for the majority of situations.

3.2.5 Solids assays
In order to assess the quantity of clog matter in an extracted sample from a wetland, solids assays may be used. The typical procedure is to extract a known volume or mass of sample

from a wetland and collect the water which drains from it. This sample is then dried and the remaining solids are weighed to determine the free particulates in the sample. In the case of a gravel substrate, the sample is washed to allow the clean gravel to be sieved out and removed. The accumulated solids fraction is then dried (often in an oven at a low temperature) and the remaining solid fraction weighed to determine the quantity of the clog matter. Whilst this method offers a good measure of the total quantity of solids in the sample, as a single measurement it may not offer much insight into the actual clogging process. This is because a large contribution of the clogging comes from biofilms which may contain up to 80% water by volume. When this water is removed, the volume occupied by the biofilm will be greatly reduced thus giving a misleading result in terms of the extent of the clogging. This test is best performed with the direct porosity measurements detailed in section 3.2.1 to provide a fuller understanding. If desired, ignition tests above 550°C can then be used to calculate the volatile fraction of the sample (BS-EN-872, 2005).

3.3 Hydrodynamic visualisation

All of the techniques presented thus far in this chapter have been localised measurements which rely on studying the material directly around a probe or the extraction of samples for laboratory analysis. In systems in which the flow path is in some way defined (as it is in constructed wetlands) hydrodynamic visualisation techniques are useful for determining how flow responds to clogging. Two strategies are discussed in this section both of which rely on injecting a tracer (for example rhodamine dye) near the inlet and then monitoring for its presence at one or more locations in the bed.

3.3.1 Breakthrough curve

The basic measurement using a tracer method is the breakthrough curve. In this technique, a tracer such as rhodamine dye is injected at the inlet of the bed. A specific sensor for the dye to be used (an optical fluorescence detector in the case of rhodamine dye) is installed at a location in the bed (typically the outlet in the case of breakthrough) and is monitored from the time of injection, through detection of the dye, when it passes through the sensor, until the detection level returns to that at the start of the test. A plot of the detected dye from injection to end is known as the breakthrough curve and will typically have a single peak of given amplitude and breadth. The integral of this curve should equal the amount of dye injected. Should this not be the case, it is likely that there are features of the flow path that result in stagnant water. Occasionally distinct peaks will be picked up other than the main peak which indicates flow short-circuiting along multiple preferential flow-paths and resulting in multiple peaks. The treatment performance of the system is directly linked to the hydraulic performance. Ideally, the system behaves as a Plug Flow Reactor which means that all of the fluid remains in the system for the same duration, the design retention time; which would correspond to a sharp pulse of tracer being detected at the outlet. The broader the breakthrough curve, the greater the extent of mixing and short-circuiting within the system, and the more likely that some flow will prematurely discharge before sufficient time for treatment has elapsed (Figure 7). It is always wise to repeat the measurement with the sensor at several outlet locations on several different occasions as there are many factors which affect the flow path including temperature, humidity and precipitation. The reader is

referred to Appendix B in Kadlec and Wallace (2009) for more information on such an analysis in constructed wetlands.
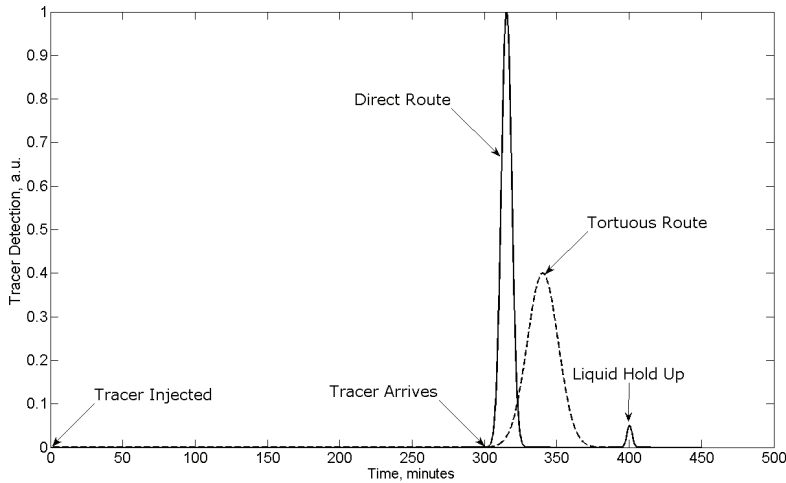

Fig. 7. Breakthrough curves from a direct (solid line) and tortuous (dashed line) system.

3.3.2 Internal tracing

If repeatedly monitored over the lifetime of the bed, the breakthrough curve method can be a good indicator of bed health. For a single or short term measurement, it can be beneficial to use a setup with several sensors to gain a better understanding of the local variations in the flow path. Such a setup is known as internal tracing. The same equipment is used as in the breakthrough curve system with a single injection of dye which is monitored over a grid or line of sensors. Typically at least three will be used in a line or nine in a grid. The analysis is very similar to that used for the breakthrough curve method only this time the dye front can be followed along the bed. As can be seen in the example in figure 8, it is common for the dye to arrive first at the detector nearest the injection with a sharp peak, as there has been little diffusion on the flow path. With high short circuiting a broader peak may then picked up on the next in line before the other two on the same row (detector 5 before 1 and 3 on figure 8) as the dye is carried primarily along the bed rather than across it. Ideally, the flow will be detected simultaneously across the width of the bed (detectors 1, 2 and 3) before advancing to the next row, which indicates good volumetric efficiency. In older, more clogged systems, this test often reveals areas of subsurface stagnation, bypass flows and blockages which core sampling using other techniques would not have found. The equipment is however quite costly and the analysis of many probes to achieve an in depth understanding is often challenging.

4. New Techniques for *in situ* measurements

Measurements made using more than one traditional method are often poorly correlated. This has lead scientists to conclude that it is the form and not the quantity of the clogging that is of primary importance (Caselles-Osorio et al., 2007). To improve the reliability of the

measurements made and ensure that the information collected is as useful as possible, two new techniques have been developed. The first of these is the *in situ* permeameter which allows localised measurements of hydraulic conductivity to be performed at several bed locations. The second uses embeddable magnetic resonance probes to determine localised relative ratios of biofilm and particulate clogging. Combination of these two techniques shows good promise as a method for fully determining the clog state of a constructed wetland and indeed any other large scale waste water filtration system.

4.1 *In situ* Permeameter tests

By using an adaptation of the Hvorslev Test, as proposed in the Naval Facilities Soil Mechanics Design Manual (NAVFAC, 1986), it has been possible to directly determine gravel conductivity in Horizontal Subsurface Flow Constructed Wetlands (Caselles-Osorio and García, 2007, Caselles-Osorio et al., 2007, Pedescoll et al., 2009). Here an open ended tube is used such that the piezometer encases the sample to be tested. In this way, the ability to easily delineate variations in vertical conductivity is sacrificed as the test measures the vertical conductivity of the entire gravel core. Regardless, these authors consider the method introduced by Caselles-Osorio and García (2007) to be highly preferable to laboratory based hydraulic conductivity studies, as direct measurements of substrate conductivity are made, thus removing the discussed uncertainties associated with sample extraction and transportation.

Recently, a novel method has been devised to allow the three dimensional hydraulic conductivity of HSSF TWs to be determined in situ. The method recreates the laboratory constant head permeameter test in situ by using a submersible permeameter cell that encapsulates a test specimen of media, and a Mariotte Siphon actuated recharge reservoir to maintain constant head conditions in the cell (figure 9). The apparatus is designed for use by one person in remote locations, weighing approximately 10 kg and utilising 10 L of water for one test, and is sized to be appropriate for the range of media hydraulic conductivities typically encountered in mature subsurface flow wetlands (from 0 to 10,000 m/d, Pedescoll et al., 2009). Manometer take off tubes are immersed to different depths within the permeameter cell so that the vertical variation of hydraulic conductivity can be found. By repeating the test at different locations over the surface of the bed and interpolating between results it is possible to generate a three-dimensional hydraulic conductivity profile for the wetland. The apparatus design and methodology are elaborated upon in Knowles and Davies (2009b).

4.2 Magnetic resonance probes

Magnetic resonance is a technique which is most often found in a medical setting. It is however also useful as a tool for making measurements in any aqueous environment. Its use for the study of porous media is well published in the literature although this usually involves the extraction of a sample core (typically under 10cm diameter and 70cm long) from the system of interest and measurement in a laboratory. An alternative system is used when prospecting for oil which involves an inside out magnetic resonance device that interrogates the physical properties of the rocks surrounding a trial bore hole. More recently a device has been produced (Morris, et al. 2009) which allows *in situ* determination of the relative ratios of particulate anvd biological clogging in porous filtration systems. The principles of operation and its benefits are discussed in this section.
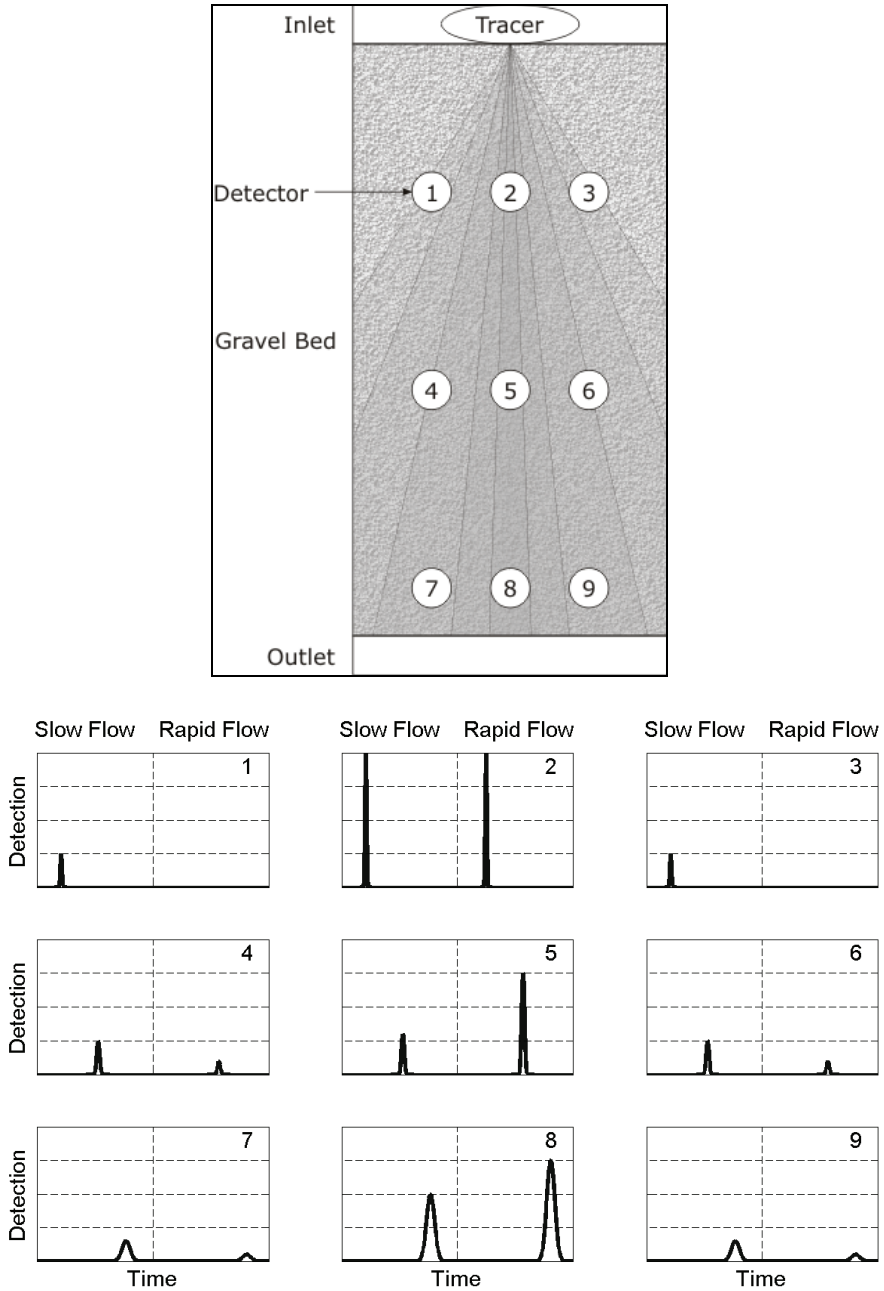
Fig. 8. Top: nine probe internal tracing setup. The grey shaded areas are flow paths, the darker the shade, the faster the flow it represents. Bottom: simulated results for each probe.

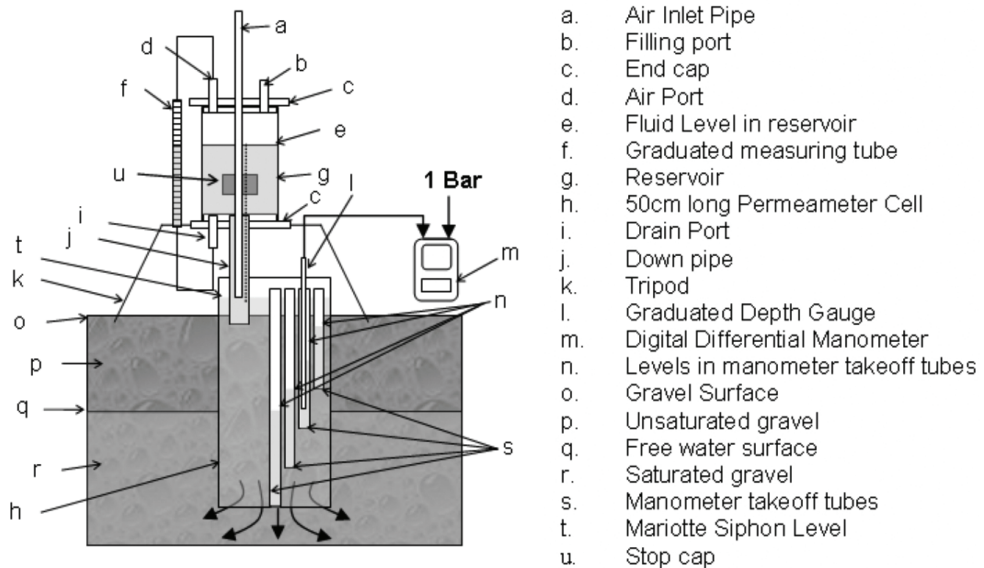|	
a.	Air Inlet Pipe
b.	Filling port
c.	End cap
d.	Air Port
e.	Fluid Level in reservoir
f.	Graduated measuring tube
g.	Reservoir
h.	50cm long Permeameter Cell
i.	Drain Port
j.	Down pipe
k.	Tripod
l.	Graduated Depth Gauge
m.	Digital Differential Manometer
n.	Levels in manometer takeoff tubes
o.	Gravel Surface
p.	Unsaturated gravel
q.	Free water surface
r.	Saturated gravel
s.	Manometer takeoff tubes
t.	Mariotte Siphon Level
u.	Stop cap

Fig. 9. Experimental set-up for the in situ determination of the vertical hydraulic conductivity profile of high porous media (not to scale). Reproduced from Knowles and Davies (2009b).

4.2.1 Theory

Magnetic resonance is a measurement technique which relies on the intrinsic properties of water molecules [9]. When in a magnetic field, the nuclei of hydrogen molecules align with the field in a process known as diamagnetism. This alignment can be perturbed by applying a time varying magnetic field. By applying such a field at an appropriate frequency, the nuclei can be made to rotate. Once the nuclei have been rotated away from the static magnetic field, they will attempt to realign. As this occurs, a process known as precession takes place in which the nuclei rotate about the axis of the static field much like a spinning top. Because each of the nuclei behaves like a tiny magnet, a very small current can be induced in a conducting coil placed around the sample. In combination, these effects can provide information about the properties of the molecules in the sample. The magnetic resonance probe developed for determining the ratios of biological and particulate clogging uses a series of applied time varying magnetic fields known as a spin echo sequence. This allows averaging of the signal before the system has returned to equilibrium. If the delay between repeating this sequence is not longer than the time it takes for the system to return to equilibrium, there will be a loss in signal. This characteristic is used to measure the 'spin lattice relaxation time' or T_1. By systematic variation of this delay (a process known as saturation recovery) an exponential relationship is found with time constant T_1 [11]. This time constant is dependent on the molecular environment and hence can be used to determine the local association of water. In the presence of several different water associations, the resulting data will be multi-exponential allowing the ratios of each environment to be determined.

4.2.2 Practical implementation

The magnetic resonance probes are produced with permanent magnets to generate the static magnetic field. This allows the probes to be sufficiently small that they can be embedded in the filtration system. Within these magnets is an insulated copper coil which is used to apply the time varying magnetic field to the sample and is also used to collect the resulting signal. This probe is attached to an electronic system which generates the required time varying fields, averages the resulting signals and processes the results to determine the ratios of the clogging components. The clog state of the medium under interrogation is then provided to the user. Probes have been produced which can be used to make individual localised measurements or to make several measurements at different heights (Figure 9) thus limiting the disturbance to the filter medium.

4.2.3 Data collection

For a typical subsurface flow constructed wetland, at least six of these probes would be placed at various locations across the bed (see figure 10). The relative ratios of biological and particulate clogging are determined at each of these locations over time from the saturation recovery curves. The ratios (R_{BP}) are determined from the curves automatically using the relationship in equations 5 and 6.

$$R_{BP} = \frac{M_{0B}}{M_{0P}},$$ (5)

$$S = M_0 \left[1 - \exp\left(\frac{1}{T_1} \right) \right],$$ (6)

where M_0 is proportional to the number of protons contributing to the signal, S, from that environment, T_1 is the spin lattice relaxation time and subscripts B and P represent the contributions from biological and particulate clogging respectively. Curves representative of the situations of dominant particulate clogging, dominant biological clogging and an equal ratio of the two are shown in figure 11. Although in established systems these are almost never seen as there are often as many as four water environments in the pore spaces of the gravel, the simple curves are presented here to give the reader a fundamental understanding of the process.

Fig. 9. Magnetic resonance probe used to determine the ratios of particulate and biological clogging. This version has three sensors spaced along its length.
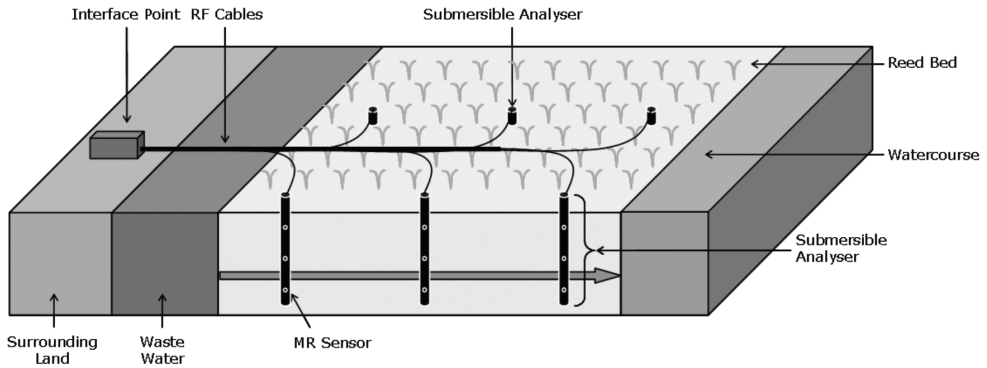
Fig. 10. Cross sectional view of subsurface flow wetland showing six submersible analysers each with three probes at different heights.

The time evolution of the clogging ratios and individual values should be monitored to provide an indication of the bed health. Typically the inlet plots will show a more rapid increase in biological clogging than those near the outlet of the system. A typical monitoring plot which would be obtained from a six probe system is shown in figure 12.

4.2.4 Limitations

The technique is intrinsically limited to dealing with filtration of aqueous systems which are free from magnetic compounds. Although this is not a concern in municipal waste water treatment, it may be an issue for the treatment of industrial run off, particularly ochre rich mine water. As the probes are embedded into the actual filter medium which is typically outdoors, temperature correction is a key issue which must be compensated for regularly. The current system relies on experiencing temperature changes less than 5K about the average for the system into which it is installed. A second generation probe system which automatically corrects for changes in temperature up to 20K about the average is currently under development.

5. Dealing with heterogeneous survey results

One of the challenges when performing measurements on several porous media filtration systems is the comparison of filters with different construction. It is often the case, particularly with industrial waste water treatment, that there will be several stages of filtration utilising different filter media, to remove a range of undesirable content to meet preset consents.

Recently a method has been introduced which allows several factors of a given filtration system to be considered and, in combination with measured parameters permits the determination of a clog factor. This numerical value provides a means of comparing the clog state of several diverse treatment stages thus allowing hydraulic health to be monitored over time. This information can then be fed back into the design of a new system which will last longer or operate more effectively. In this section we consider how the clog factor can be applied to wetlands for the measurement techniques discussed in the previous sections.

5.1 Clog factor

Due to the vide variation in hydraulic conductivity which occurs in clogged filters, the arithmetic mean of measurements may not provide a very representative indication of the hydraulic health of the system. A common practice in hydrology is to use the geometrical mean of the dataset as a more representative improvement on either the arithmetic or harmonic means (Binley et al., 1989). Representative homogeneous values for hydraulic conductivity are however generally misleading, as in actuality hydraulic conductivity spans several orders of magnitude. A single value model cannot capture the influence of varying hydraulic conductivity on the subsurface water table profile: a function that is imperative for determining wetted volume and hence predicting treatment performance (Persson et al., 1999). In response, the Clog Factor (CF) has recently been developed.

The CF is a novel metric that converts hydraulic conductivity, an intensive physical property, into an extensive bulk property that can be representatively averaged for subsequent analysis. It can be used to describe the state of clogging in any porous media flow system but has been derived intentionally to explore clogging dynamics in subsurface flow wetlands. The CF is based on the Kozeny-Carman equation (equation 7) which describes the theoretical hydraulic conductivity of porous media, based on the assumption of ideal spherical media of homogeneous diameter d and porosity θ. The fluid density ρ, dynamic viscosity μ and gravity g are also included in the Kozeny Carman equation. Applying this formulation in reverse, experimentally measured values of hydraulic conductivity and the median particle diameter of the sampled gravel are used to calculate corresponding theoretical clogged porosities θ_E.

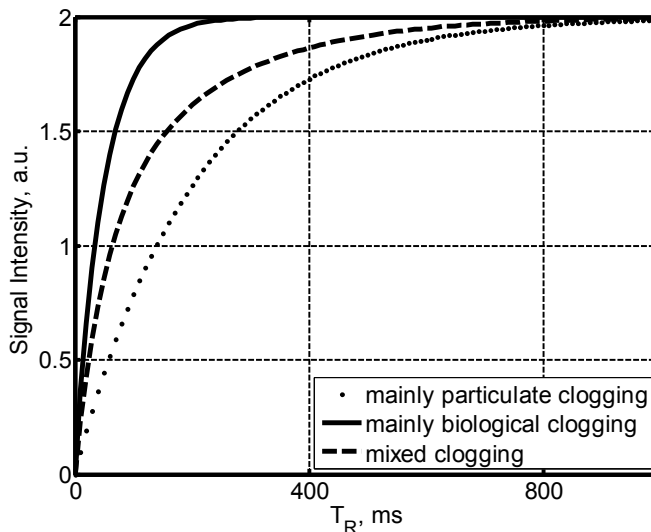$$k = \frac{\rho g d^2 \theta^3}{150 \mu (1-\theta)^2} \quad (7)$$

Fig. 11. Typical saturation recovery curves for three different clogging cases.
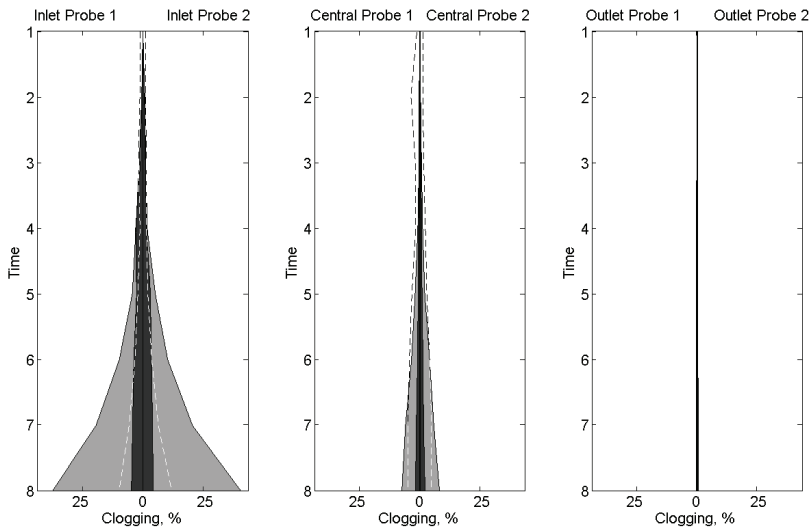
Fig. 12. Simulated results of typical monitored output for six probe system. Grey is biological clogging whilst black represents particulate clogging. The dashed line is 10 times the ratio between them.

The ratio of clogged to experimental clean porosity allows the CF to be calculated (equation 8), whereby a value of 0 indicates zero clogging and a value of 1 indicates complete clogging. It is important to emphasise that the CF may not represent the practical clogged porosity, as it has been shown that reductions in hydraulic conductivity often do not correspond to reductions in porosity, and rather it is the form and nature of clogging that are important (Caselles-Osorio et al., 2007; Platzer and Mauch, 1997; Tanner et al., 1998). In this way the CF actually represents the effective or relative reactor volume that has been lost to clogging.

$$CF = 1 - \frac{\theta_E}{\theta_I} \qquad (8)$$

The advantages of the Clog Factor are:
- It is an extensive bulk property so it can be applied to any scale porous media flow system
- Removes dimensions from the data so that comparisons can be performed between systems with different physical and media sizes
- Highlights deviations from theoretical clean conductivity due to both clogging and media non-ideality
- Allows reasonable statistical comparisons where orders of magnitude changes in hydraulic conductivity would skew a data set
- Allows single-parameter values to be published to indicate health of bed at a point in time

The Clog Factor provides a useful tool with which the inter- and intra-system variations of filter system hydraulic health can be objectively compared.

6. Conclusion

In this chapter we have detailed the various methods currently available to determine the extent to which a large scale porous media based filtration system has become clogged. By considering the traditional methods available to measure the clogging it has been shown that any single technique cannot provide a sufficiently detailed picture of the state of the system. We have presented two recent developments for *in situ* measurements of the clogging and have shown that they both provide more relevant information than their laboratory based counterparts. By combining these two techniques, the full nature of the clogging can be elucidated and used to inform remedial action leading to a life extension.

7. References

Binley, A., Beven, K. & Elgy, J. (1989). Physically Based Model of Heterogeneous Hillslopes: 2. Effective Hydraulic Conductivities. *Water Resources Research,* 25 (6), 1227-1233.

Brix, H. (1994) Functions of Macrophytes in Constructed Wetlands. *Water Science and Technology.* 29, 71.

Caselles-Osorio, A., Puigagut, J., Segu, E., Vaello, N., Granés, F., García, D. & García, J. (2007). Solids accumulation in six full-scale subsurface flow constructed wetlands. *Water Research,* 41 (6), 1388-1398.

Cooper, D., Griffin, P. & Cooper, P. (2005). Factors affecting the longevity of sub-surface horizontal flow systems operating as tertiary treatment for sewage effluent. *Water Science and Technology,* 51 (9), 127-135.

Cooper, P. F., Job, G. D. & Green, M. B. (1996). *Reed beds and constructed wetlands for wastewater treatment*. Water Research Centre.

EC/EWPCA (1990). *European Design and Operations Guidelines for Reed Bed Treatment Systems*. Swindon, UK: WRc.

García, J., Ojeda, E., Sales, E., Chico, F., Píriz, T., Aguirre, P. & Mujeriego, R. (2003). Spatial variations of temperature, redox potential, and contaminants in horizontal flow reed beds. *Ecological Engineering,* 21 (2-3), 129-142.

Green, M. B. & Upton, J. (1995). Constructed reed beds: Appropriate technology for small communities. *Water Science and Technology,* 32 (3), 339-348.

Griffin, P., Wilson, L. & Cooper, D. (2008). Changes in the use, operation and design of sub-surface flow constructed wetlands in a major UK water utility. *11th International Conference on Wetland Systems for Water Pollution Control,* Indore, India, 419-426.

Hvorslev, M.J. (1951). Time Lag and Soil Permeability in Ground-Water Observations, Bulletin Number 36, Waterways Experimental Station Corps of Engineers.

Kadlec, R. H. & Watson, J. T. (1993). Hydraulics and Solids Accumulation in a Gravel Bed Treatment Wetland. In: MOSHIRI, G. A. E. (ed.). *Constructed wetlands for water quality improvement : Conference : Selected papers.* Boca Raton: Lewis Pub, pp 227-235.

Knowles, P. R. (2010). Clogging and Hydraulics in Horizontal Subsurface Flow Constructed Wetlands. Doctorate in Mechanical Engineering and Design Thesis, Aston University.

Knowles, P. R., Griffin, P. & Davies, P.A. (2009a). Complementary methods to investigate the development of clogging within a horizontal sub-surface flow tertiary treatment wetland. *Water Research*. 44, 320.

Knowles, P. R. & Davies, P. A. (2009b). A method for the in-situ determination of the hydraulic conductivity of gravels as used in constructed wetlands for wastewater treatment. *Desalination and Water Treatment,* 1 (5), 257–266.

Knowles, P. R. & Davies, P. A. (2010). A Finite Element Approach to Modelling the Hydrological Regime in Horizontal Subsurface Flow Constructed Wetlands for Wastewater Treatment In: VYMAZAL, J. (ed.). *Water and Nutrient Management in Natural and Constructed Wetlands.* Dordrecht: Springer Science+Business Media B.V.

Knowles, P. R., Dotro, G. C., Nivala, J. & García, J. (2010a). Clogging in subsurface-flow treatment wetlands: Occurrence, contributing factors, and management strategies. *Ecololgical Engineering,* Submitted.

Knowles, P. R., Griffin, P. & Davies, P. A. (2010b). Complementary methods to investigate the development of clogging within a horizontal sub-surface flow tertiary treatment wetland. *Water Research,* 44 (1), 320-330.

Lin, A., Debroux, J., Cunningham, J. & Reinhard, M. (2003). Comparison of rhodamine WT and bromide in the determination of hydraulic characteristics of constructed wetlands. *Ecological Engineering*

Madigan, M. T., Martinko, J. M. & Brock, T. D. B. O. M. (2006). *Brock biology of microorganisms*. 11th ed. ed. Upper Saddle River, NJ: Pearson Prentice Hall.

Morris, R.H., Newton, M.I., Bencsik, M., Knowles, P.R., Davies, P.A. & Griffin, P. (2009). Long term monitoring of constructed wetlands using an NMR sensor. *IEEE Sensors.* 1733-1737.

Murphy, C. & Cooper, D. (2010). The Evolution of Horizontal Sub-Surface Flow Reed Bed Design for Tertiary Treatment of Sewage Effluents in the UK. In: VYMAZAL, J. (ed.). *Water and Nutrient Management in Natural and Constructed Wetlands.* Dordrecht: Springer.

Pedescoll, A., Uggetti, E., Llorens, E., Granés, F., García, D. & García, J. (2009). Practical method based on saturated hydraulic conductivity used to assess clogging in subsurface flow constructed wetlands. *Ecological Engineering,* 35 (8), 1216-1224.

Persson, J., Somes, N. L. G. & Wong, T. H. F. (1999). Hydraulic efficiency of constructed wetlands and ponds. *Water Science and Technology,* 40 (3), 291-300.

Platzer, C. & Mauch, K. (1997). Soil clogging in vertical flow reed beds - Mechanisms, parameters, consequences and.....solutions? *Water Science and Technology,* 35 (5), 175-181.

Speer, S., Champagne, P., Crolla, A. & Kinsley, C. (2004). Hydrodynamic Pathways in a Maturing Constructed Wetland. *8th International Conference on Wetland Systems for Water Pollution Control,* Avignon, France.

Suliman, F., Futsaether, C., Oxaal, U., Haugen, L. E. & Jenssen, P. (2006). Effect of the inlet-outlet positions on the hydraulic performance of horizontal subsurface-flow wetlands constructed with heterogeneous porous media. *Journal of Contaminant Hydrology,* 87 (1-2), 22-36.

Tanner, C. C., Sukias, J. P. S. & Upsdell, M. P. (1998). Organic matter accumulation during maturation of gravel-bed constructed wetlands treating farm dairy wastewaters. *Water Research,* 32 (10), 3046-3054.

USEPA (2000). Constructed wetlands treatment of municipal wastewaters. U.S. EPA Office of Research and Development: Washington, D.C., United States.

Excess Sludge Reduction in Waste Water Treatment Plants

Mahmudul Kabir, Masafumi Suzuki and Noboru Yoshimura
Akita University
Japan

1. Introduction

Household waste water is taken under WWT (Waste Water Treatment) process and treated water is removed to the nature. Biological analysis method using activated sludge is well known and used method for the treatment of waste water as the running cost is cheap. But, a large amount of excess sludge is produced in the Waste Water Treatment Plants (WWTPs) which is a great burden in both economical and environmental aspects. Fig.1 is an example of annual industrial waste of Japan (Ministry of the Environment, Government of Japan, 2010). Sludge related garbage occupied 44.2% of the total industrial waste. In which about 86,860,000 ton of sludge related to WWTPs was produced in 2007. The excess sludge contains a lot of moisture and which is not easy to treat. There are several works done by many scientists to treat the excess sludge (Ide, 1990; Eckenfelder & Grau, 1998; Miyoshi, 2006; Sawada et al., 2005; Wei et al., 2003). These byproducts of WWTPs are dewatered, dried and finally burnt into ashes. Some are used in farm lands as compost fertilizer. The less dump places for ashes and the high cost to treat the excess sludge are huge burdens to our society. In Japan, an average of Yen 20,000/t is needed to treat of excess sludge. Again, burning of excess sludge evacuates the CO_2 in air, which is a cause of global warming. So, the reduction of excess sludge is a growing demand to the modern society. It is not only a headache of Japan, but also to the rest of the world.

2. Excess sludge reduction

There are some reports informing the success in order to reduce the excess sludge by adding fallen leaves in the aeration tank where activated sludge is kept (Yoshida, 2000). But, the mechanism is no yet clearly understood. Some efforts were carried out to increase the self decay of activated sludge prolonging the aeration period (Yoshida, 2000). However, these attempts are dependant on biological properties of activated sludge and difficult to achieve good results at every time. Again, prolonging of the aeration period brings the excess economical burdens. However, recently, a new approach has been started to minimize the excess sludge of WWTPs. A part of activated sludge is treated under cell lysis. The treated sludge or a part of the treated sludge can be decomposed by non-treated sludge when they are sent to the aeration tank and thus the excess sludge can be minimized. Several reports regarding to cell lysis in order to reduce excess sludge were published including ozonation, milling process with beads, revolving disks methods etc. (Ide, 1990; Eckenfelder & Grau, 1998;

Miyoshi, 2006; Wei et al., 2003; Yoshida, 2000; Sano et al., 2005; Yasui & Shibata, 1994). But, however, the methods are still on the process and a new and effective technology is still a demand in this branch. We have developed a new process to minimize the production of excess sludge with the ferrite particles (Kabir et al., 2007). We will introduce some innovative methods for reduction of excess sludge by using ferrite particles and permanent magnets.
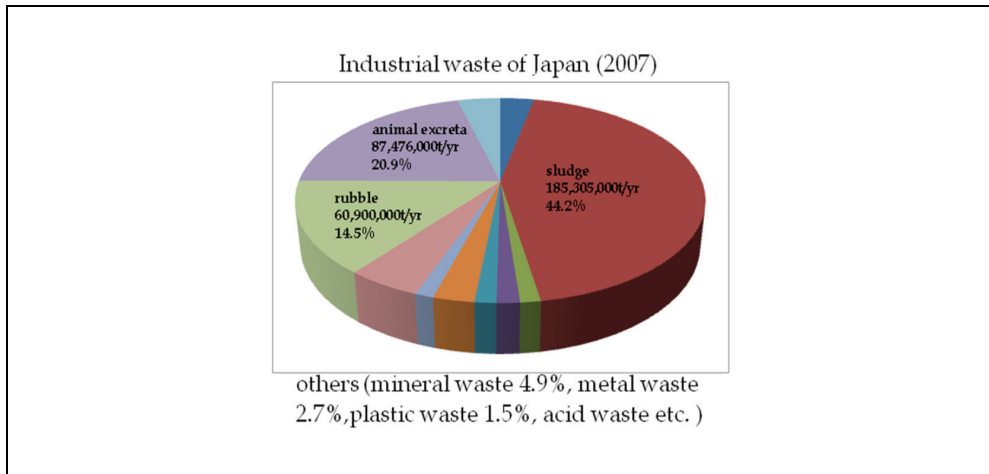

Fig. 1. Annual industrial waste in Japan

2.1 Excess sludge production process

Biological analysis method is the most widely used method for the household waste water treatment. This method uses biological groups of living organisms which possess good settling characteristics. In general, they are called activated sludge. The living organisms decompose the biological nutrients from the waste water and thus purify the waste water from biological waste. The diagram of the WWT using activated sludge can be seen in Fig.2 (Ide, 1990; Eckenfelder & Grau, 1998; Miyoshi, 2006). It shows a WWTP model diagram. In order to separate big wastes from waste water, it is run under some primary processes and then waste water is finally put to the aeration tank where activated sludge is kept. Air is supplied to decompose the biological waste in the aeration tank. From the aeration tank, the treated water is supplied to the settling tank where water is separated from activated sludge by settling the sludge naturally. The treated water is taken out as effluent and the activated sludge is returned to the aeration tank. The excess activated sludge is discarded from settling tank when it is necessary. The amount of excess sludge (ΔX)can be expressed by the following equation (Ide, 1990; Eckenfelder & Grau, 1998; Miyoshi, 2006);

$$\Delta X = aS_r - bX \qquad (1)$$

Here,
a = gross yield coefficient of sludge
S_r = BOD removal; $Q_I \times C_I \times (C_I - C_O) / C_I$ [kg/d]

b = Specific biomass decay due to self oxidization [1/d]
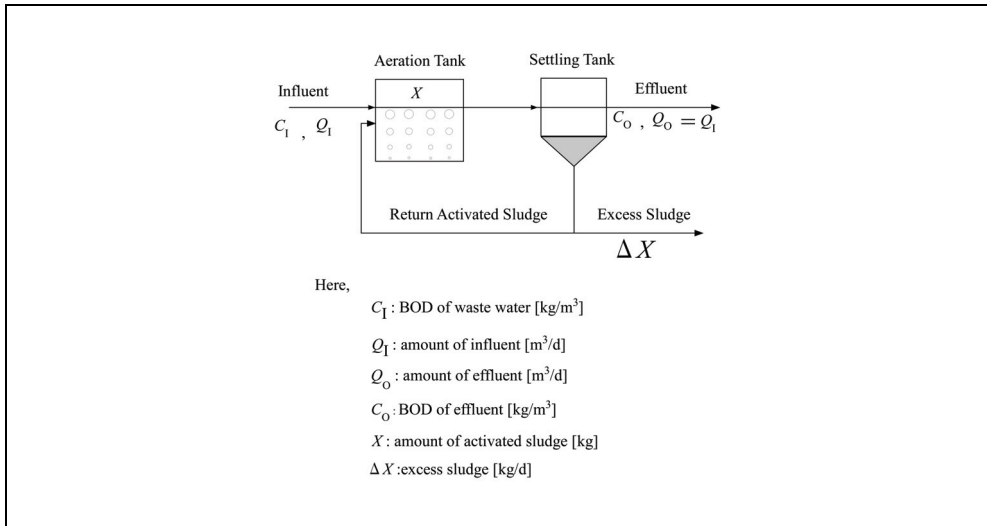X = amount of activated sludge [kg]

Fig. 2. Model diagram of a WWTP

It can be understood from the above equation that the zero emission is possible for a WWTP when aS_r is less or equal to bX. The parameters 'a' and 'S_r' are totally dependant on the biological characteristics of activated sludge and it is not easy to handle them. Again, increasing of self decay by oxidization needs extra electric power causing economical and environmental burden. If we consider an amount of return sludge (i.e. W) with cell lysis treatment and send them to the aeration tank for decomposing by non-treated sludge, the excess sludge production can be minimized theoritically. For 'h' is to be the diverting rate of treated sludge to activated sludge then the amount of 'W' can be calculated from the following equation (Yoshida, 2000),

$$W = \Delta X \ / \ (1\text{-}h) \tag{2}$$

2.2 Magneto-Ferrite treatment

This is a treatment method of excess sludge in which the collisions of ferrite particles with activated sludge can trigger to the sterilization and cell lysis of activated sludge. The treated sludge is sent to the aeration tank and decomposed by activated sludge. The motion of ferrite particles are controlled by magnetic flux. Sterilization of microorganisms was reported with magneto-ferrite treatments by Yoshimura group (Ito et al., 1992; Murayama et al., 1993; Yoshimura & Suzuki, 1991; Yoshimura et al. 1994). We used this treatment process to disrupt the cell wall of microbes of activated sludge. Ferrite particles are magnetic materials and can easily be separated from the activated sludge by a magnet. They are non toxic and in soluble in water. This idea is quite similar to the milling process but it is better than to use ceramic beads, as ferrite particles can be as small as ~μm order.

So, instead of beads, the collisions produced by the ferrite particles can hopefully break down the microbes of the activated sludge.

Ferrite particles are kept with activated sludge in a test tube and the test tube is exposed in the magnetic flux. The ferrite particles are gathered together in the magnetic flux and they are scattered when they are out of the magnetic flux. The ferrite particles of diameter D, make a gap with a diameter of $D\sqrt{(3/2)}-D$, as shown in Fig.3 (Murayama et al., 1993; Yoshimura et al. 1994). This gap changes its position with time as the ferrite particles are scattered and collected together in the test tube periodically. While the ferrite particles change their positions inside the test tube, activated sludge is captured in the gap produced by the ferrite particles. Thus, collisions occur in between the ferrite particles and the floc of activated sludge. The collisions can possibly crush the cell wall of microbes of the activated sludge which leads to sterilization of the microbes. Collisions occurred with ferrite particles and sludge which may lead to the cell lysis. The two miniature WWTPs were run for a fixed period of time with Conventional Activated Sludge (CAS) and Extended Aeration (EA) process (Kabir et al., 2007, 2009). Magneto-ferrite effect was applied for about 4 weeks in the case of CAS and found about 42% of excess sludge reduction with magneto-ferrite treatment of sludge comparing to the non-treated sludge. For EA process, we achieved the zero emission at lab. scale using this magneto ferrite treatment. For larger amount of sludge reduction, a rotary treatment plant was propsed and tested by miniature WWTPs and found 72% of sludge reduction (Kabir et al., 2010). Again, electromagnets were used to control the movements of ferrite particles (Kabir et al., 2012). Electro magnets can be controlled easily with an AC supply. Sterilization and cell lysis were found for activated sludge with the input voltage of 100Vp-p of square wave. Thus, these methods will pave the way of excess sludge reduction in WWTPs.

2.2.1 Test tube plant (Kabir et al., 2007, 2009)

The test tube plant diagram model can be seen in Fig.4. Two permanent magnets were placed in on a plate. The plate was connected to a shaft of a motor by a joint. The circular rotation of the motor is changed into linear motion with the shaft of the joints. Two test tubes were fixed on the way of the magnetic flux. The capacity of the test tubes is 100ml. Adequate ferrite particles were kept in the test tubes. The activated sludge from the settling tank was let to come to the test tube, treated and then sent back to the aeration tank. The amount of the activated sludge for treatment was controlled in a way so that the activated sludge can be kept in the magnetic flux for about 3 h. Thus the activated sludge was happened to get the magneto-ferrite effect for 3 h and the microbes of the sludge get disrupted.

The sterilization of the microbes was investigated by counting the viable cells of microbes in the activated sludge using Easicult T.T.C. (Orion Diagnostica) model chart. Easicult is a test tube with a slide of agar to culture the microbes. After culturing the microbes of the activated sludge for 24-48h at 28°C in a constant temperature and humidity chamber, the viable cell number in 1ml solution can be known by comparing with the model chart. After counting the viable cells of the treated activated sludge, the Viable Cell Coefficient (VCC) is calculated in the following way,

$$VCC = \frac{\text{viable cell number of treated activated sludge}}{\text{viable cell number of initial stage of the activated sludge}} \times 100 \qquad (2)$$
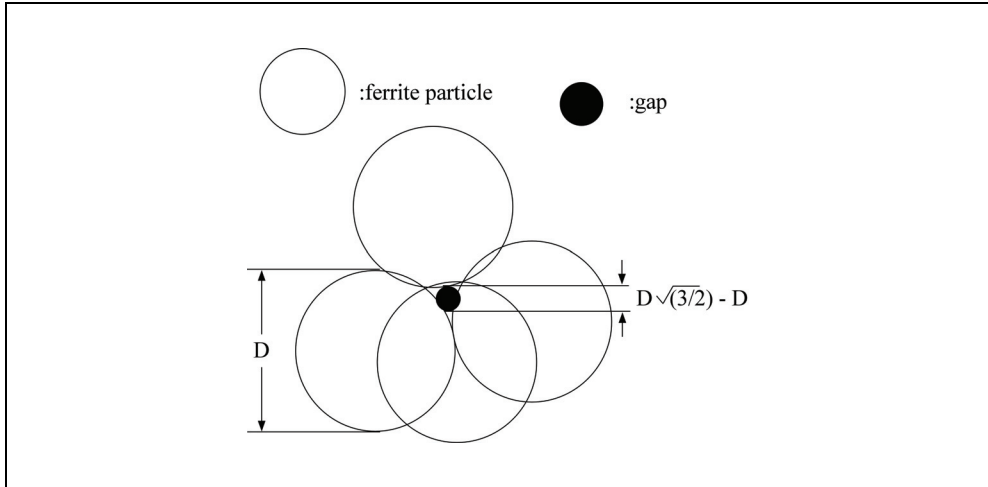
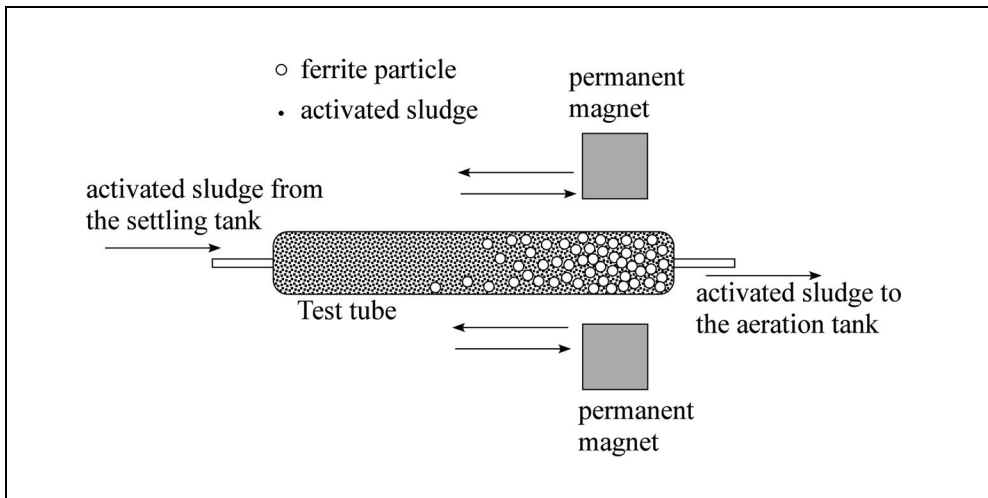Fig. 3. Estimated gap made by ferrite particles

Fig. 4. Model diagram of test tube treatment plant

The decrease of VCC means the proceeding of sterilization and cell lysis. The process and the idea are very simple and effective. The excess sludge is taken in a glass made test tube with ferrite particles and which is kept still. The test tube is located in between the changing magnetic flux produced by a pair of moving magnets. These magnets move periodically as shown in Fig.4. The ferrite particles are collected together when they are exposed in the magnetic flux. Oppositely, they are scattered in the test tube when they are out of the magnetic flux. This movement continues periodically and thus results to the local frequent changes of water pressure and collisions occurred between the ferrite particles and the activated sludge. To determine the parameters of the magneto-ferrite system, several

experiments were performed under several circumstances. These five types of experiments were performed to select the parameters,

a.   The shape of the ferrite particles,
b.   The size of the ferrite particles,
c.   The amount of the ferrite particles,
d.   The speed of the moving magnets and
e.   The density of magnetic flux.

Each experiment was followed by the written processes,

1.   Essential amount of activated sludge were taken to a beaker for the measurement of the initial amount of microbes.
2.   In a glass test tube, 90ml of activated sludge was taken.
3.   Necessary amount of a certain size of ferrite particles were added in the test tube.
4.   Magneto-ferrite treatment was applied to the activated sludge of the test tube for 2, 4 and 6 h.
5.   Viable cell was counted for treated activated sludge after each experiment. The living cell number was compared with that of the initial stage of activated sludge to justify the degree of sterilization.

Thus several experiments were performed to determine these parameters. The experiments showed that for a 100ml of test tube, the better sterilization of the microbes can be achieved with the 30g (333.3g/L) of ferrite particles. The necessary shape of the ferrite is round and the grain size is less than 53μm. 90ml of activated sludge can be treated at a time and the necessary magnetic flux and the speed of the magnets are 165 mT and 1.5~1.8 cycles/s, respectively. These parameters were used to evaluate sludge reduction experiment for miniature WWTPs.

Two miniature WWTPs (Fig.5) were run with CAS and EA method. The biological parameters used in this experiment were shown in Table 1 (Miyoshi, 2006). We measured the Mixed Liquor Suspended Solid (MLSS) for aeration tanks of both WWTPs. We cast out the excess sludge when the value of MLSS had crossed the level described in Table 1. The amount of the removed sludge was measured after the processes of dewatering and drying of sludge. Their values evaluated the effect of magneto-ferrite treatment. One thing is to be noted that the measurement of BOD takes about 5 days, so we preferred to measure Chemical Oxygen Demand (COD) instead of measuring BOD for relevant measurements. In this experiment, we used a COD meter (Quick COD; Central Kagaku Co.) to measure the COD of effluent. The COD removal efficiency was calculated for both treatment and non-treatment of magneto-ferrite effect. Here is the equation to calculate the value of COD removal efficiency (Miyoshi, 2006),

$$\text{COD removal effficiency} = \frac{\text{CODinfluent} - \text{CODeffluent}}{\text{CODinfluent}} \times 100 \qquad (3)$$

The methods to carry out the experiments will be described below;

1.   Certain amount of artificial waste water was put in the reservoir.
2.   The waste water was sent to the aeration tank by a pump (Cassette Tube Pump SMP-23, Tokyo Rikakikai Co.). The amount of the waste water is controlled by this pump according to the two methods described in Table 1.

3. The activated sludge which had gathered in the settling tank was sent back to the aeration tank by a pump (Roller Pump; Furue Science Co.) for a fixed period of time. It is to be noted that magneto-ferrite effect is applied on system 2 whether another system was kept without any of the treatment.

4. In order to verify the effect of the magneto-ferrite treatment, the MLSS was measured periodically for the each of the aeration tanks. The excess sludge was removed if necessary, then dried and measured the amount of the sludge.

5. The COD of the effluent was measured periodically by a COD meter and COD removal efficiency was calculated.

The experiments were performed to make clear the effect of the magneto-ferrite treatment; so the major conditions were kept same for both WWTPs (system 1) and system 2. However, the values of MLSS of the two aeration tanks were little different at the initial stage which was not so big in amount and was acceptable. The ingredients of the artificial influent were as follows;

1. Peptone (Becton, Dickinson and Co.) 0.5g/L
2. Glucose (Kanto Chemical Co.) 0.5g/L
3. Yeast (Becton, Dickinson and Co.) 0.25g/L
4. Ammonium Dihydrogenphosphate ($NH_4H_2PO_4$) (Kanto Chemical Co.) 7mg/L
5. 25% Ammonia water (Wako Pure Chemical Industries Ltd.) 1mL/L
6. The pH values (6-8.5) were measured regularly of the activated sludge and controlled the value with NaOH (Nacalai Tesque) dropping if needed.
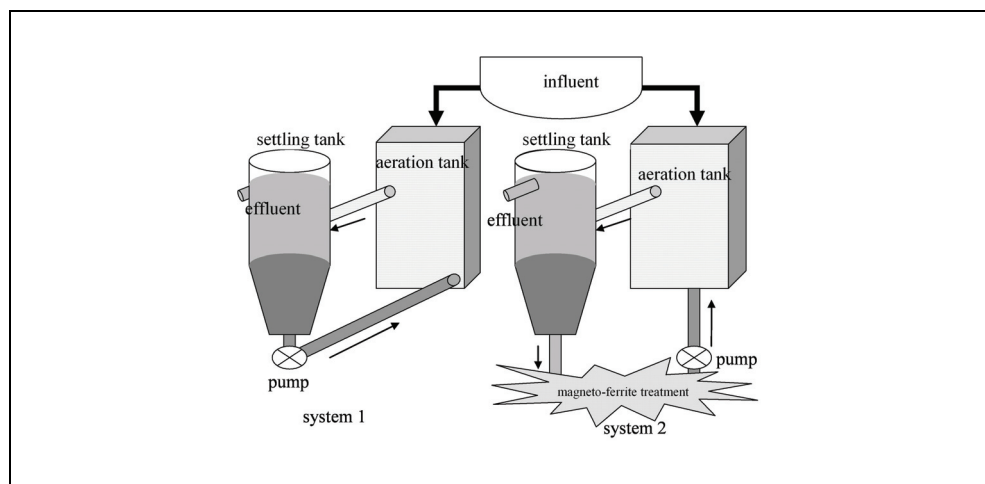

Fig. 5. Model diagram of two laboratory WWTPs

	CAS	EA
BOD-Sludge Loading	0.40	0.15
BOD-Volume Loading	0.20	0.05
MLSS [mg/L]	2000	3000
COD of Influent [mg/L]	300	150
Amount of Influent [L/d]	4.48	3.36
Aeration rate [L/min]	3.00	3.00

Table 1. The factors for the reduction of excess sludge

The COD of the influent was controlled at 300mg/L for both systems for CAS method. It was 150mg/L for EA method. The magneto-ferrite treatment device was run for 12h/d. The ability of the return pump was fixed at 30mL/min of activated sludge. The return pump was operated for 1min in every 30min (1min×2 times (in 1h)).

The experiments were continued for about 4 weeks for CAS method while it was run about 10 weeks for EA method. The MLSS of both two aeration tanks were measured periodically and controlled accordingly to the factors of the experiments. So, we drew up the excess sludge from the both aeration tanks and compared the amounts of the dried sludge. The results for CAS method will be described first. The amount of the excess sludge removed from the two systems can be seen in Fig. 6. It can be seen that for the first 2 weeks, the amount of excess sludge was about half comparing to the non treated sludge. However, later the difference in the amount of the excess sludge was getting closer to the non-treatment aeration tank's sludge. The BOD of the system 2 was not only from the waste
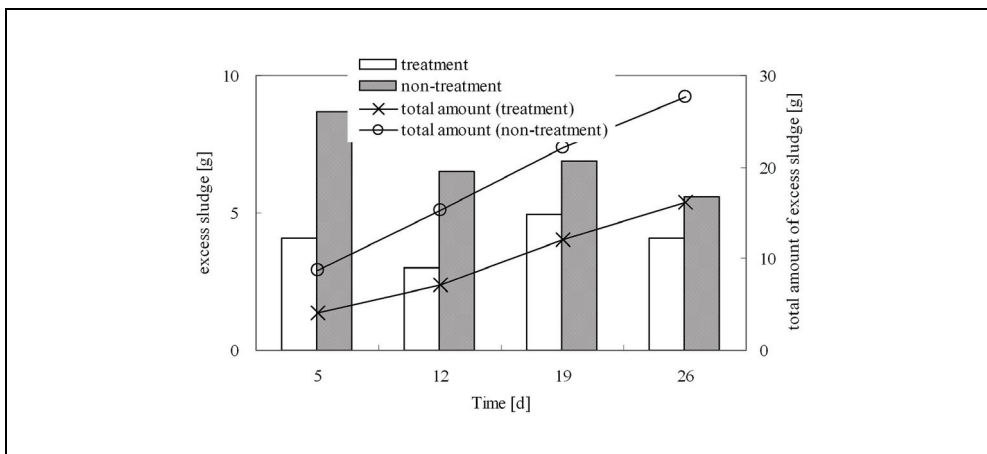

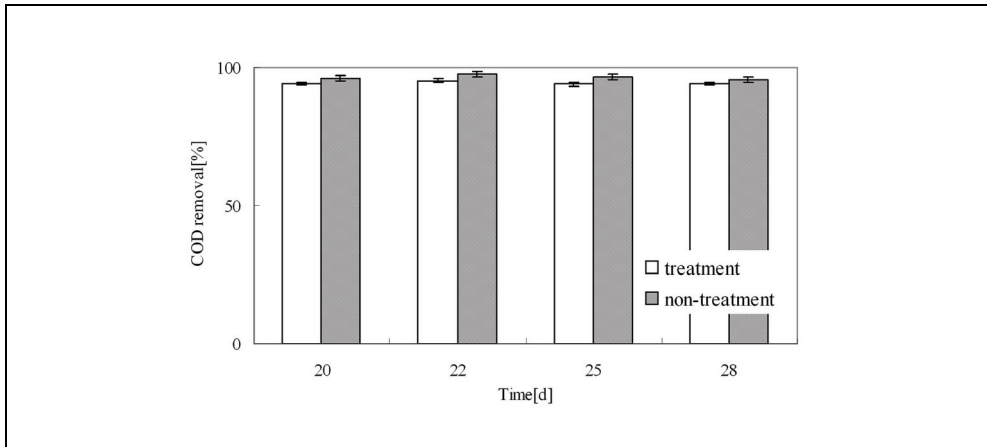Fig. 6. Amount of discarded sludge during test tube treatment plant (CAS)

Fig. 7. COD removal efficiency during test tube treatment plant (CAS)

water, but it can be understood that the treated activated sludge was also contributed in the increasing of BOD of the relevant aeration tank. Thus the input BOD was greater than the non treated aeration tank (system 1) comparing to the system 2. This reason may influence the increase of excess sludge in system 2. So, a less amount of BOD is preferable to check the validity of the magneto-ferrite treatment on activated sludge in laboratory environment. The COD removal efficiency for CAS method was calculated and plotted in Fig. 7. It can be seen that the removal efficiency of COD of the activated sludge had been more than 90% in average. The error bar shows the standard deviation of the efficiency of COD removal of sludge for both the systems 1 and 2.

Again, the same WWTPs were run with EA process on which one was exposed to the magneto-ferrite treatment while the other one was run without any treatment. The values of the amount of the discarded sludge can be found in Fig. 8. It is clear that no excess sludge was found in system 2 which had been exposed to magneto-ferrite treatment for 10 weeks. As the whole conditions but the magneto-ferrite effect were same for the two aeration tanks, it is clear that the excess sludge was disrupted by magneto-ferrite treatment system. The values of initial stage of two systems were 2744 mg/L (system 1) and 3084 (system 2), respectively. The average of the MLSS for both aeration tanks were 3303 (system 1) and 2843 (system 2). The standard deviation values for both aeration tanks' MLSS were 351 for magneto-ferrite treatment and 546 mg/L for non-treatment system. These figures also proved the effectiveness of magneto-ferrite treatment on the excess sludge. The COD removal efficiency for EA method was calculated and plotted in Fig.9. It can be seen that for EA method, the removal efficiency of COD of the sludge were quite similar. The error bar shows the standard deviation of the efficiency of COD removal of sludge for both the systems 1 and 2. At the same time, the values of COD of the effluent for both systems as they were less than 20mg/L in our observation period.

We checked the ferrite particles after 10 weeks after applying the magneto-ferrite treatment. The ferrite particles were collected, dried and observed by a photo microscope. The particles were found in the same size and shape of the initial stage of the experiment.
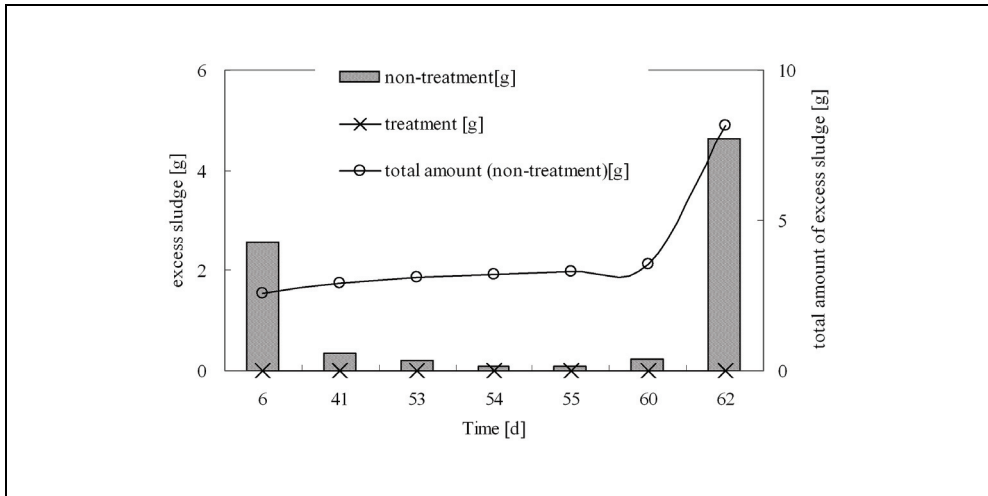
Fig. 8. Amount of discarded sludge during test tube treatment plant (EA)
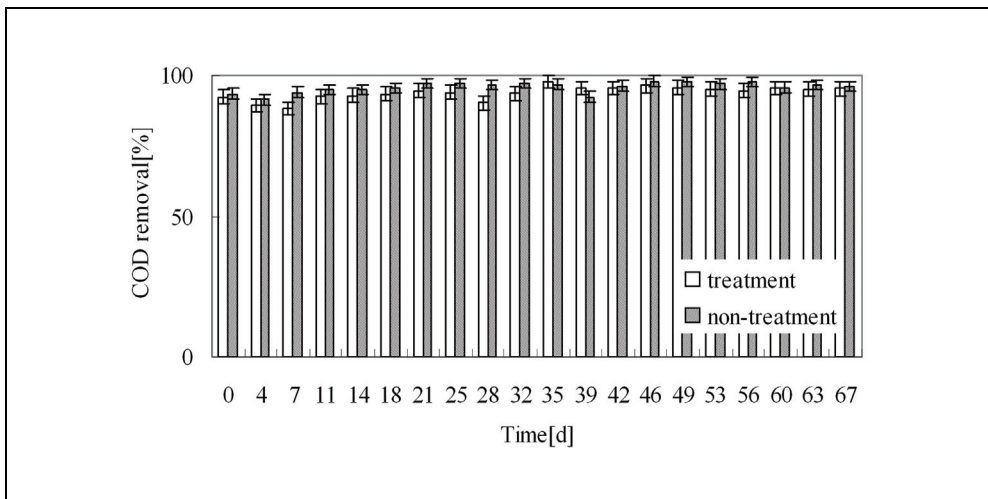
Fig. 9. COD removal efficiency during test tube treatment plant (EA)

Again, the magneto-ferrite treatment was applied for only 12h/d, which showed a good result. These results proved that our new method is quite effective to reduce excess activated sludge in miniature WWTPs.

2.2.2 Rotary Plant (Kabir et al., 2010)

We succeded in sludge reduction with test tube plant in lab. scale. The general use of this method can only be possible if we can build up a treatment plant which can treat large amount of sludge at a time. However, it is not wise to make a larger test tube for large

amount of sludge treatment. It can be understood that a larger plant should possess the following characteristics;

a.   It can be applicable easily,
b.   The setup cost is low and sound in economic,
c.   It can be usable with the WWTPs easily

A rotary treatment plant can fulfill these demands. So, we proposed a rotary treatment plant which can be easily applicable with WWTPs (Fig.5). By the two miniature WWTPs, the validity of this method can be evaluated at the same room temperature and humid conditions. A brief explanation of the magneto-ferrite devices will be introduced here.

The rotary magneto-ferrite treatment plant can be seen in Fig.10. Two permanent magnets are set up on a rotor which is coupled with the shaft of a motor (M590-501K, Oriental Motor co.). The size and shape of the rotor is shown in Fig.11(a). The strength of a permanent magnet is 220mT. An acryl plate is fixed above the rotor. This acryl plate is movable. A round shaped container is fixed on it. The magnetic flux in the container can be changed with the position of acryl plate. The size of the container is 17cm×5cm and it can contain 870ml of liquid. The material of the container is PVC. It is connected to the return sludge line of the miniature WWTP (system 2). A fixed amount of ferrite particles with activated sludge is kept in the container. A stirrer made of free plastic is placed in the container. Free plastic can be shaped in any size easily as it liquefies at 60°C. The stirrer has a metal plate installed in it. There are two cuts in the corner side of the stirrer. When the stirrer moves the activated sludge can easily get under the stirrer. The top and front view of the stirrer can be seen in Fig.11(b).

The rotor circles when the shaft of the motor starts to move. At the same time, the stirrer and the ferrite particles of the container start to move with the magnets (Fig.10). The distance between the stirrer and ferrite particles is a very important factor in this method. This distance can be controlled by the magnetic flux. Though we could not measure this distance in this system, we chose a suitable magnetic flux working on the stirrer as well as ferrite particles by changing the position of the acryl plate in vertical direction. The stirrer with a metal plate in it is attracted to the bottom of the treatment container. The activated sludge is oppressed and stirred in the container. The collision is occurred with ferrite particles that cause the breakdown of the cell wall of microorganisms. Thus the sterilization is performed and the organic compounds are to be hydrolyzed in the solution. It will plug into the reduction of activated sludge.

To determine the parameters of the rotary magneto-ferrite system, several experiments were performed under several circumstances. For a certain amount of activated sludge, there should be a certain amount of ferrite particles. The speed of the motor that is connected to the speed of the rotor is an essential parameter. It can be understood that a faster rotor as well as moving magnets can make more collisions of ferrite particles and sludge. The treatment time is also important as it is related with running costs of the system.

So, we have performed three types of experiments to determine the parameters. They are as follows,

a.   The density of magnetic flux,
b.   The speed of the moving magnets (speed of motor) and
c.   The amount of the ferrite particles.

Each experiment was followed by the written processes,

1.   Initial amount of microbes were measured. Essential amount of activated sludge was taken to a beaker for it and it was kept at the room temperature.

2. 300ml of activated sludge was taken to the container of rotary magneto-ferrite system. This activated sludge was cultured in laboratory's aeration tank.
3. Necessary amount of ferrite particles were added in the container.
4. The motor moved for a fixed time with a certain speed. Thus, the magneto-ferrite treatment was applied.
5. Viable cell was counted for treated activated sludge after each experiment. The living cell number was compared with that of the initial stage of activated sludge to justify the degree of sterilization. Sterilization linked to cell lysis.
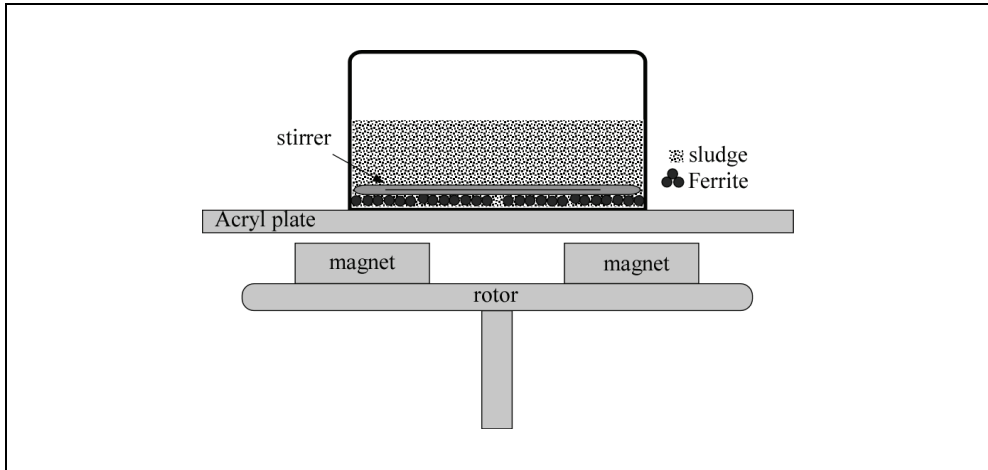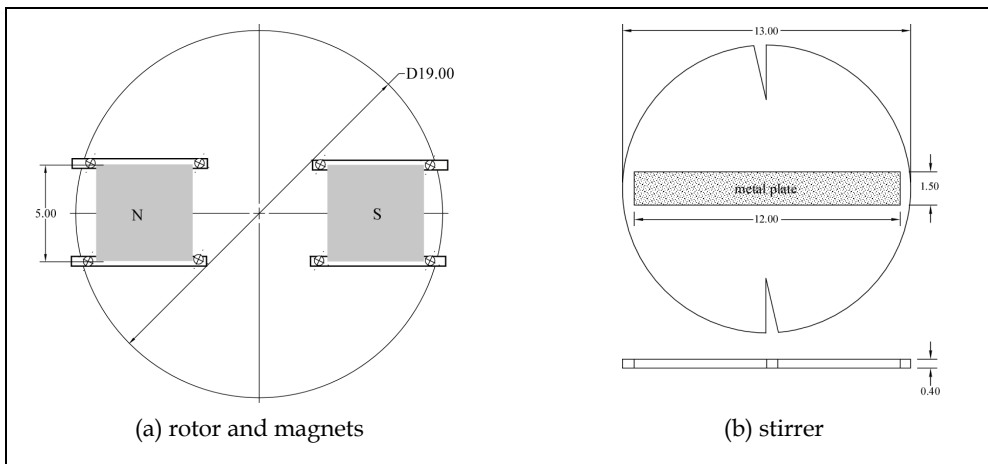

Fig. 10. Model diagram for rotary treatment plant

Fig. 11. Diagrams of the rotor and stirrer

The sterilization of the microbes was evaluated by calculating the VCC of the samples.

First, we considered the movements of stirrer in the treatment container. If the magnets are too closer to the container, the stirrer as well as ferrite particles cannot move with the magnets for the stronger magnetic flux. The stirrer itself gets stick on the bottom of the container. So, we chose a suitable distance for magnets where the ferrite particles and stirrer can move smoothly. We could not measure the distance between the bottom of the container and the stirrer. From the Fig.10, it can be understood that this distance was very short. The magnetic flux in the container was about 30-50mT in average with the suitable position of acryl plate.

100g of ferrite particles were taken with activated sludge in the treatment container. It was sealed well so that the sludge could not overflow from the container. The motor of the rotary plant could rotate up to 1400rpm. The speed of motor was 40rpm and treatment time was 1h. The viable cells of non-treated sludge and treated sludge were count before and after the experiments. Then VCC was calculated which had been 1-10%. Other experiments were performed with 50g of ferrite particles and speed of the motor. The conditions of the experiments and their results can be seen in Table 2. From, Table 2 it is clear that at least 1h of treatment is necessary for this system. On the basis of VCC, it can be said that the sterilization was performed for 2 types of conditions (e.g. 100g ferrite + 40rpm speed of motor & 50g ferrite + 90rpm speed of motor). Both these conditions showed good sterilization performances but the stirrer had extra frictions with 100g of ferrite particles which turned into the instability of the stirrer. So, we chose 50g of ferrite particles for rotary treatment system.

Two miniature WWTPs were used to evaluate the effect of rotary treatment plant. The experiments were carried out in CAS method. The shape and the volume of the treatment container were 17cm × 5cm and 870ml respectively. It can treat about 300ml of activated sludge at a time. The container was sealed tightly so that only the Roller pump could control the flow of the sludge in between settling tank and treatment container. The amount of influent and COD of influent were 3.36L/d and 400mg/L respectively. The treatment time was 1h. Again, as this system can treat a large amount of sludge at a time comparing to test tube plant, the running time of this plant was only 4h/d. In 6h, an hour of treatment was applied to the sludge. The Roller pump was used to send sludge from settling tank to treatment container.

The initial conditions for system 1 and system 2 were same. However, the initial values of MLSS of the two aeration tanks were little different. The experiment period was for about two weeks. MLSS of the two aeration tanks (system 1 and 2) were measured to evaluate the treatment effect. The measured data of MLSS and calculation data of COD removal efficiency are shown in Fig.12.

Amount of ferrite [g]	Speed of motor [rpm]	Treatment time [h]	VCC [%]
100	40	1	1-10
50	40	1	10
50	90	1	1-10
50	90	0.5	10-100

Table 2. Determination of parameters for the rotary plant

From the MLSS values, it can be seen that the activated sludge had been increasing with time in system 1 but it was well controlled in system 2. The initial values of MLSS for system 1 and 2 were 1960mg/L and 2482mg/L respectively. After 2 weeks, it became 3954mg/L for system 1 and 3056mg/L for system 2. A simple calculation of activated sludge from the MLSS values showed that in system 2 (with magneto-ferrite treatment) only 3.8g of sludge had increased while the non-treated aeration tank it had increased by 13.4g. So, it can be said that with this rotary plant, a total of 72% reduction had been possible in this experiment.

The calculation results of COD removal efficiency of the two WWTPs. There was not any significant difference between the removal efficiency of two miniature WWTPs due to the magneto-ferrite treatment. The magneto-ferrite treatment was applied for only 4h/d, which showed a good result. These results proved that our new method is quite effective to reduce excess activated sludge in miniature WWTPs.
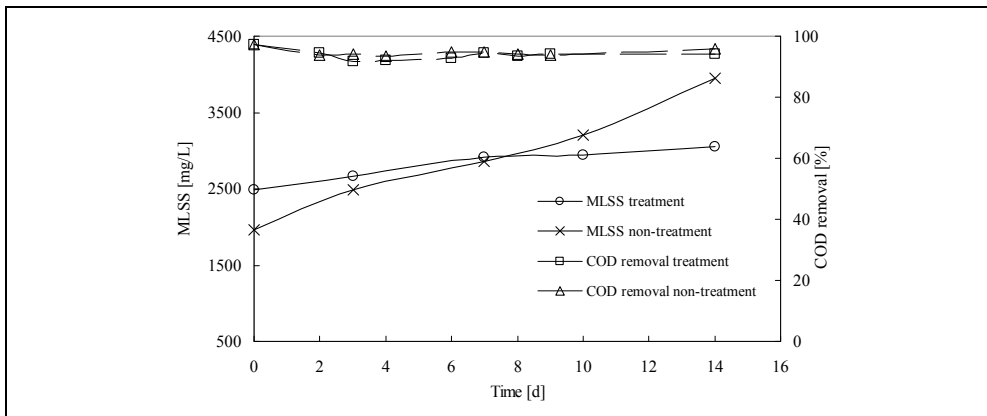

Fig. 12. Sludge reduction rotary treatment plant

2.2.3 Magneto-ferrite treatment with electromagnets (Kabir et al., 2012)

The motion of ferrite particles can be controlled by an electromagnet easily. Electromagnets can be operated with an AC supply. So, electromagnets may be helpful to use magneto-ferrite treatment. If ferrite particles taken with activated sludge, can be steered up at a height and let it be down with a certain velocity then it can produce a lot of collisions with activated sludge to switch on to sterilization as well as reduction of sludge. The results have showed that electromagnets with AC supply can easily control the motion of ferrite particles. By controlling the movements of ferrite particles with activated sludge, sterilization and cell lysis of sludge have been achieved. It will pave the way of excess sludge reduction in WWTPs.

Two coils (1.51H each) were set up in vertical direction with a certain gap in between them. These coils were connected with an AC voltage source (BP4610, NF). The coils were connected with 2 diodes (GSF05A40, VRRM=400V, IFAV=5A) which were installed in opposite direction to each other. The experimental setup model can be seen in Fig.13. The diodes were set up with the coil in a way that when the coils were connected with AC power supply, the electric current was provided alternative directions to the coils.
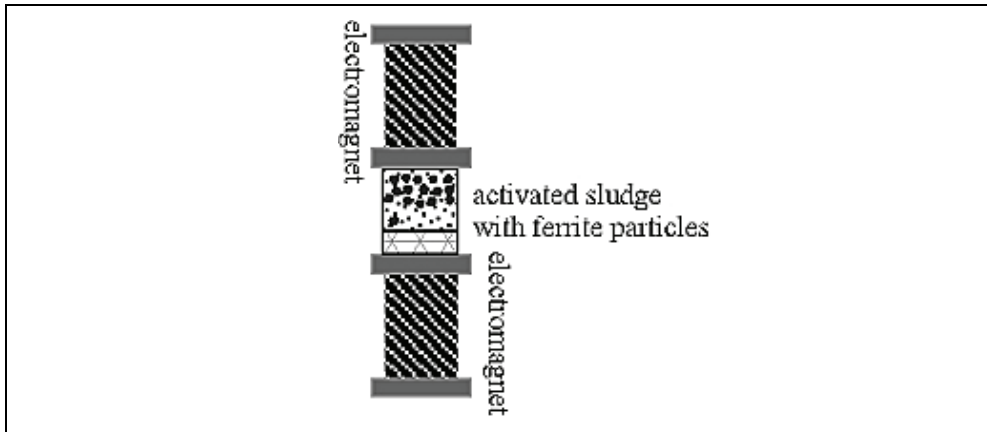
Fig. 13. Setup model diagram using electromagnets

Thus, the coils become electromagnets alternatively with the AC voltage source. A certain amount of ferrite particles and activated sludge were taken to the treatment container. Ferrite particles are magnetic substance and they move with the magnetic flux. While they moved in the container, collisions occured with the activated sludge. For a certain AC power supply with frequency, these collisions may break down the cell wall or cell membrane of bioorganisms of activated sludge. It may switch to sterilization and cell lysis of the activated sludge. If these treated sludge is taken to the aeration tank where they can be decomposed by the non-treated sludge, then the sludge reduction can be achieved.

At first, we measured the *I-V* relationship with 2 types of wave. Sine wave and square wave were applied to the coils and we measured the electric current in it. Due to the limit of the voltage source, the voltage applied in the range of 0-120Vp-p. The electromagnetical charateristics of the coils were measured by a Gauss meter (GM04, HIRST MAGNETIC Instrument). Thus after learning the electrical properties and magnetical properties, we utilized them for several measurements regarding on sterilization and cell lysis of activated sludge.

The material of the treatment container was soft polyethelen and the shape was cylindrical (ϕ 41mm×32mm). The capacity of the container was 40ml. Considering the previous results of magneto-ferrite treatment, 9g of ferrite particles were taken into the container with 20ml of activated sludge (Kabir et al., 2007, 2009). The treatment was applied for 1-3h.The ferrite particles and sludge were taken in this container and kept between the coils. A short description will be provided for the sterilization experiment. Activated sludge was taken from the aeration tank. An MLSS meter (SS-5F, KRK) was used to measure the MLSS of the sludge and the values were adjusted if needed. 20ml of sludge was taken in the container with 9g of ferrite particles. Then sterilization process was investigated.

The *I-V* relationship of the coils and voltage source was determined. The r.m.s. value was calculated for both voltage and current for the coils. The electrical characteristics were measured for the coils for square wave. The frequency was fixed at 1.0Hz. Fig.14 shows the measured data of current and magnetic flux produced by a coil. The current increased almost linearly in the coils with voltage. Magnetic flux also increased with current. As the maximum range of input voltage (120Vp-p) the maximum value of current was found at 4.8A in a coil and 594mT of magnetic flux was achieved. This magnetic flux was sufficient

enough to move ups and downs of ferrite particles in the treatment container in our experiment.

The treatment was performed with the determined parameters. The treatment container with 20ml of sludge and 9g of ferrite particles was set up on the lower coil. We made a room of 1-2mm between the lower coil and treatment container. The frequency was chosen 1.0Hz and the wave was 90Vp-p of square wave. The seed activated sludge was taken from the Yabase Sewage Treatment Plant of Akita city, Japan. The seed activated sludge was cultured in miniature WWTPs run at Suzuki Lab. of Akita University. The MLSS was 3000-4000mg/l of the sludge and their COD removal efficiency was about 94%.
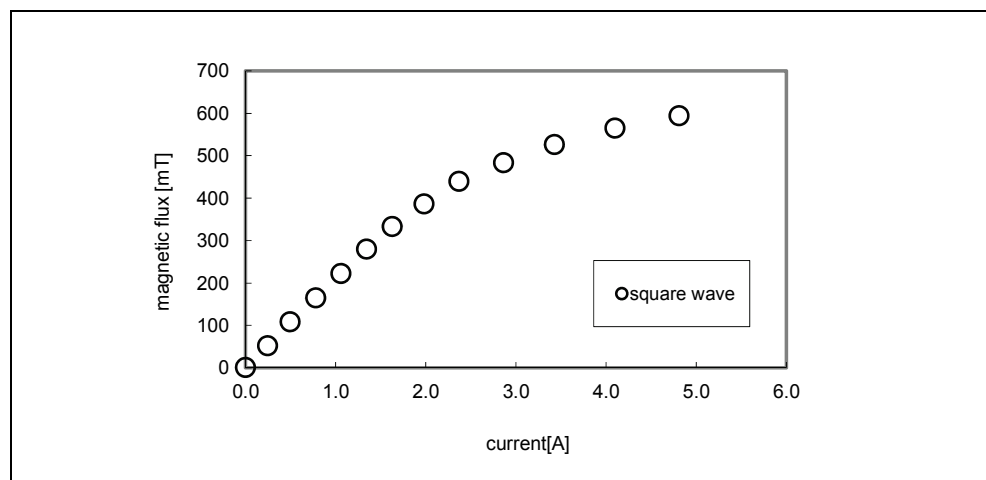

Fig. 14. *B-I* relationship of a coil

The sterilization of the activated sludge was investigated for 1-3h of treatment. When the treatment was carried on, 20ml of fresh activated sludge was kept at room temperature without any treatment. The viable cell was measured for each sample by Easycult T.T.C. The VCC was calculated after each experiment. The values of VCC for non-treated sludge was found 100% all the time during the experiments. The sterilization was confirmed with the treatment after 2-3h of treatment to the sludge. The VCC decreased to 10% after 2-3h of treatment to the activated sludge. The ferrite particles were moved ups and downs in the treatment container with magnetic flux. A larger magnetic flux can be helpful to produce more collisions of ferrite particles with the microorganism of activated sludge and thus sterilization is performed. Cell lysis can also be achieved at the same time of the sterilization with the electromagnets which can lead to the reduction of excess activated sludge.

3. Conclusion

Excess sludge is a problem which cannot be steered around in waste water treatment by biological analysis method. It is a growing demand to control the production of excess sludge for the sustainable WWT methods as well as the better society. We developed an innovative method with controlling ferrite particles' motion which resulted in the sterilization and cell lysis of sludge.

It also points towards the new possibilities of this magneto-ferrite treatment. The method can be applied in the sterilization of the water of swimming pool, ballast tank not only in the reduction of activated sludge but it can be used of a cargo boat etc. As this process is a non-thermal sterilization method, many other uses can be expected. Again, this process can be used as a hydrolyzed method of activated sludge. Activated sludge is well known byproduct for its water retention ability. So, dewatering is very important process for the treatment of excess sludge. Our method can be helpful in it. One thing is to be noted that if we can be successful in reducing even 1% of total excess sludge produced in Japan every year, it can save about billions of Yen (Japanese currency; Yen) in a year. Thus, our methods have pointed out several possibilities in the view of both economical and environmental aspects.

4. References

Eckenfelder, W.W. & Grau, P. (Eds.) (1998). *Activated Sludge Process Design and Control: Theory and Practice* (2nd ed.), Vol.1, Technomic Publishing Co., Lancaster

Ide, T. (1990). *Water Treatment Engineering* (2nd ed.), Gihodo Shuppan, ISBN 4-7655-3122-8, Tokyo [in Japanese]

Ito, T., Murayama, Y., Suzuki, M., Yoshimura, N., Iwano, K. & Kudo, K. (1992). Evidence for sterilization of Saccharomyces Cerevisiae K7 by an external magnetic flux. *Japanese Journal of Applied Physics*, Vol.31, No.6A, pp. L 676-L678

Ghyoot, W. & Verstraete, W. (1999). Reduced sludge production in a two-stage membrane-assisted bioreactor. *Water Resource*, Vol.34, No.1, pp.205-215

Kabir, M. Suzuki, M. & Yoshimura, N. (2007). Reduction of Excess Sludge by Ferrite Particles. *Japanese Journal of Water Treament Biology*, Vol.43, No.4, pp.189-197

Kabir, M. Suzuki, M. & Yoshimura, N. (2009). Reduction of Excess Sludge by Magneto-Ferrite Treatment: Observation on Lab Scale WWTPs. *IEEJ Transactions on Electrical and Electronic Engineering*, Vol.4, No.4, pp.584-586

Kabir, M. Suzuki, M. & Yoshimura, N. (2010). Reduction of Excess Activated Sludge by Ferrite Particles: Methods for Practical Use. *International Journal of the Society of Materials Engineering for Resources*, Vol.17, No.2, pp.120-125

Kabir, M. Suzuki, M. & Yoshimura, N. (2012). Excess Activated Sludge Reduction by Using Electromagnets and Ferrite Particles. *IEEJ Transactions on Electrical and Electronic Engineering*, Vol.7, No.2 (accepted)

Miyoshi, Y. (2006) *Ideas and Techniques of Sewage and Wastewater Treatment*, Ohmsha, ISBN 4-274-02480-6, pp.55-169, Tokyo [in Japanese]

Murayama, Y., Itoh, T., Suzuki, M. & Yoshimura, N. (1993). Effect of magnetic field and ferrite treatment on various organism. *Transaction IEE of Japan*, Vol.113-A, No.8, pp.594-595 [in Japanese]

Press release of Ministry of the Environment, Government of Japan (January 2010). Available from http://www.env.go.jp/recycle/waste/sangyo/sangyo_h19a.pdf [in Japanese]

Sano, A., Bando, Y., Yasuda, K., Nakamura, M., Senga, A. & Kiyokawa, E. (2005). Enhancement in biodegradability of excess sludge by using centrifugal vibration mill. *Journal of Chemical Engineering Japan*, Vol.38, No.6, pp.446-449

Sawada, Y., Nagashima, S., Uchida, T., Kawashima, N., Takeuchi, S., Akita, M. & Nagaoka, H. (2005). Basic study on sludge concentration and dehydration with ultrasonic exposure. *Japanese Journal of Applied Physics*, Vol.44, No.6B, pp.4678-4681

Yasui, H. & Shibata, M. (1994). An innovative approach to reduce excess sludge production in the activated sludge process. *Water Science Technology*, Vol.30, No.9, pp.11-20

Yoshida, T.(Publ.) (2000). *Technologies for Minimization of Sludge and Reduction of Sludge Growth*, NTS, Tokyo [in Japanese].

Yoshimura, N. & Suzuki, H. (1991). Sterilizing effect on Yeast cells by ferrite powders. *Transactions IEE of Japan*, Vol.111-D, No.11, pp.988-989 [in Japanese]

Yoshimura, N., Suzuki, M. & Sato, T. (1994). Microbic Handling by Means of Electricity and Magnetism. *Journal of the Institute of Electrostatics Japan*, Vol.18, No.1, pp.11-17 [in Japanese]

Microbial Fuel Cells for Wastewater Treatment

Liliana Alzate-Gaviria

Yucatan Centre for Scientific Research (CICY),
Mexico

1. Introduction

A typical domestic wastewater treatment plant consists of a series of unit processes, each of which is designed with specific functions. Process trains will be more variable for industrial wastewater and for nutrient control.
Conventional sewage treatment may involve these stages:

1.1 Screening
The influent is strained to remove all large objects carried in the sewage stream. This is most commonly performed with an automated mechanically-raked bar screen in modern plants serving large populations, whilst in smaller or less modern plants a manually-cleaned screen may be used. The raking action of a mechanical bar screen is typically paced according to the accumulation on the bar screens and/or flow rate. The solids are collected and later disposed of in landfill or incinerated. Bar screens or mesh screens of varying sizes may be used to optimise solids removal, so as to trap and remove the floating matter, such as pieces of cloth, paper, wood, kitchen refuse, etc. These floating materials will choke pipes or adversely affect the working of the pumps if not removed. They should be placed before the grit chambers. However, if the quality of grit is not of much importance, as in the case of landfilling etc., screens may even be placed after the grit chambers. They may sometimes be accommodated in the body of the grit chambers themselves.

1.2 Primary treatment
In the primary sedimentation stage, tanks commonly called "primary clarifiers" or "primary sedimentation tanks" are used to settle sludge while grease and oils rise to the surface and are skimmed off. Primary settling tanks are usually equipped with mechanically driven scrapers which continually drive the collected sludge towards a hopper in the base of the tank where it is pumped to sludge treatment facilities. Grease and oil from the floating material can sometimes be recovered for saponification. The dimensions of the tank should be designed to effect removal of a high percentage of the floatables and sludge. A typical sedimentation tank may remove from 60% to 65% of suspended solids, and from 30% to 35% of biochemical oxygen demand (BOD) from the sewage.

1.3 Secondary treatment
This is designed to substantially degrade the biological content of the sewage which is derived from human waste, food waste, soaps and detergent. The majority of municipal

plants treat the settled sewage liquor using aerobic biological processes. To be effective, the biota require both oxygen and food to live. The bacteria and protozoa consume biodegradable soluble organic contaminants (e.g. sugars, fats, organic short-chain carbon molecules, etc.) and bind much of the less soluble fractions into floc. Secondary treatment systems are classified as fixed-film or suspended-growth.

It has been estimated that the activated sludge process in publically owned treatment works in the U.S. requires 0.349 kWh of electricity per cubic metre of wastewater, accounting for about 21 billion kWh of electricity consumption per year (Goldstein and Smith, 2002). Pumping and aeration are the predominant energy consuming processes (21% and 30–55% of the total treatment energy demand, respectively) (EPA, 2008). Similarly in the UK, 3–5% of national electricity consumption goes towards wastewater treatments. If activated sludge processes were adopted by engineers in the rapidly developing world to serve, say 19 million people, this would produce an energy bill equivalent to 6.8% of the entire U.S. electricity consumption (UNICEF, 2000; Water, 2006). We suggest that this is unsustainable, both on economical and environmental grounds (Oh et al., 2010). The cost of energy will undoubtedly rise as carbon-based resources become depleted and renewable sources struggle to make up the shortfall. Operating costs of treating wastewater are therefore likely to become prohibitively expensive.

Anaerobic digestion of wastewater, particularly industrial wastewater, is usually a cheaper, if more fickle, option than aerobic technologies. However, the effluent often requires further treatment to remove residual organics.

1.4 Tertiary treatment

Finally, the purpose of tertiary treatment is to provide a final treatment stage to raise effluent quality before it is discharged to the receiving environment (sea, river, lake, ground, etc.). More than one tertiary treatment process may be used at any treatment plant. If disinfection is performed, it is always the final process. It is also called "effluent polishing".

The organic matter concentration in wastewater is usually evaluated in terms of either its biochemical oxygen demand (BOD) in a five day test (BOD_5) or its chemical oxygen demand (COD) in a rapid chemical oxidation test. Total BOD or COD can be viewed as consisting of two fractions: soluble BOD (sBOD) and particulate BOD (pBOD). Most pBOD is removed in the primary clarifier sludge and sBOD is converted to bacterial biomass (Logan, 2008).

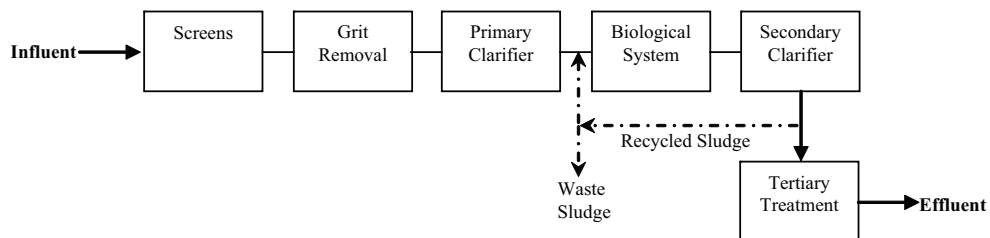Fig. 1. Process flow for a typical wastewater treatment plant. (Metcalf and Eddy, 2003)

Based on this summary of a wastewater treatment process train, we can see that a microbial fuel cell (MFC) would replace the secondary treatment system and tertiary treatment (removal of nutrients, ammoniacal nitrogen, phosphorus and organics components) (Yokoyama et al., 2006). These organics are often volatile fatty acids, which are metabolic

products of anaerobic digestion, whose accumulation has been reported to hinder the process (Hawkes et al., 2007; Logan and Regan, 2006b; Oh and Martin, 2009). However, these acids, such as acetate and butyrate, are effectively consumed in MFCs, even at low concentrations (Kim et al., 2010, Lee et al., 2008; Liu et al., 2005). The sensitivity of MFCs to low levels of organic contaminants is well documented and has led to their application as biosensors (Chang et al., 2004; Kim et al., 1999). In addition, multi-stage treatment combining anaerobic digestion and/or hydrogen fermentation and MFC technologies may result in reduced accumulation of inhibitory by-products and allow effluent polishing to more stringent discharge standards (Kim et al., 2010, Logan and Regan, 2006b; Pham et al., 2006). Combining an MFC with AD and Bio-hydrogen would therefore maximise total energy recovery and consequently increase the sustainability of wastewater treatment. The additional heating system to maintain temperature may not be necessary for energy recovery or wastewater treatment using MFC technology.

2. Exoelectrogens

The idea of using microorganisms as catalysts in an MFC has been explored since the 70s and 80s (Suzuki, 1976; Roller et al., 1984). MFCs used to treat domestic wastewater were introduced by Habermann and Pommer (1991). However, these devices have recently become attractive again for electricity generation, providing opportunities for practical applications (Schröder et al., 2003; Liu and Logan, 2004; Liu et al., 2004a).

Most microorganisms use respiration to convert biochemical energy into ATP. This process involves a cascade of reactions through a system of electron-carrier proteins in which electrons are ultimately transferred to the terminal electron acceptor. Most forms of respiration involve a soluble compound (e.g. oxygen, nitrate, and sulphate) as an electron acceptor. However, some microorganisms are able to respire solid electron acceptors (metal oxides, carbon, and metal electrodes) in order to obtain energy. Several mechanisms explain how microorganisms respire using a solid electron acceptor (Hernandez and Newman, 2001; Weber et al., 2006; Rittmann, 2008). Some of these mechanisms involve the use of chelators or siderophores which effectively solubilise the solid electron acceptor and introduce them into the cell (Gralnick and Newman, 2007). Other mechanisms involve extracellular electron transfer (EET), in which microorganisms externalise their electron transport to the surface of the solid electron acceptor. Researchers have proposed three distinct EET mechanisms, which are depicted in Figure 2. The first mechanism proposes direct electron transfer between electron carriers in the bacteria and the solid electron acceptor. This mechanism is supported by the presence of outer-membrane cytochromes which can interact directly with the solid surface to carry out respiration (Beliaev et al., 2002; Magnuson et al., 2001). Bacteria using this mechanism require direct contact with the solid electron acceptor and therefore cannot form a biofilm. The second mechanism proposes the presence of a soluble electron shuttle: a compound which carries electrons from the bacteria by diffusive transport to the surface of the metal oxide (or electrode) and is able to react with it, discharging its electrons. This compound in its oxidised state then diffuses back to the cells, which should be able to use the same compound repeatedly (hence the name 'shuttle'). Bacteria are known to produce compounds which act as electron shuttles, including melanin, phenazines, flavins, and quinones (Newman and Kolter, 2000; von Canstein et al., 2008). The third mechanism proposes a solid component which is part of the extracellular biofilm matrix and is conductive for electron transfer from the bacteria to the solid surface. This mechanism is
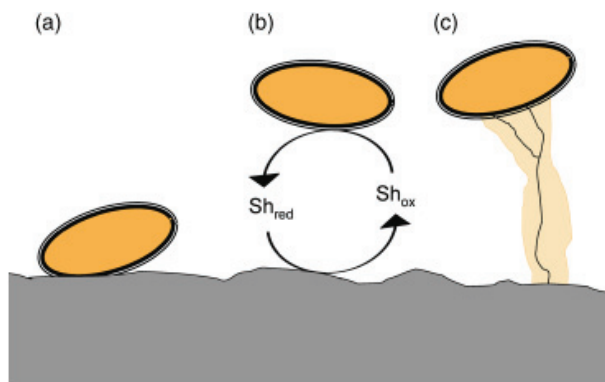
Fig. 2. Schematic of three EET mechanisms used by ARB: (a) direct electron transfer, (b) an electron shuttle, and (c) a solid conductive matrix. (Torres *et al*., 2010)

supported by the recent discovery of the possible role of cellular pili as nanowires (Reguera et al., 2005; Gorby et al., 2006), which are being characterised for their capability to conduct electrons. Other components may also be conductive and contribute in EET, such as extracellular cytochromes or bound electron mediators (Marsili et al., 2008; Rittmann, 2008).

Currently, researchers have not reached a consensus regarding the conditions under which these EET mechanisms are dominant in natural and engineered systems. Evidence can be found to support more than one EET mechanism in some cases. For example, recent discoveries have shown that Shewanella oneidensis is capable of producing shuttles (Marsili et al., 2008; von Canstein et al., 2008) and nanowires (Gorby et al., 2006). It is not obvious under which conditions an EET mechanism would be used and whether more than one mechanism is concurrently utilised by S. oneidensis and other bacteria.

The use of EET is of special importance in microbial fuel cells and electrolysis cells (collectively referred to as MXCs). In MXCs, anode-respiring bacteria (ARB) carry out a respiration process in which a solid electrode (the anode) is their electron acceptor. Because most MXC electrodes are solid conductors which can neither be solubilised nor reduced (they only act as a conductor), ARB can only externalise electrons through EET in order to respire using the anode. To date, ARB include members from diverse phyla, such as Alpha-, Beta-, Gamma-, and Deltaproteobacteria, Firmicutes, Acidobacteria, and a yeast (Logan, 2009, Alzate et al., 2010). Most of these members are known to utilise solid Fe (III) as an electron acceptor, and they are anaerobic, gram-negative oligotrophs. Substrate-utilisation capabilities of most of these bacteria are limited to simple fermentation products, such as acetate and H_2. However, some members can utilise a wider range of substrates, such as propionate, butyrate, lactate, and glucose (Debabov, 2008).

A few studies have shown that the maximum current densities produced by ARB are limited by proton transport inside the biofilm (Torres et al., 2008b; Franks et al., 2009). If protons produced as a result of substrate oxidation accumulate inside the biofilm, they decrease the pH and inhibit the ARB. The maximum current density obtained therefore appears to depend on proton transport rather than factors associated with EET. The highest current densities reported so far are consistent with relatively high buffer concentrations (4100mM buffer) (Fan et al., 2007; Logan et al., 2007; Torres et al., 2008; Xing et al., 2008). It is therefore possible that higher current densities are achievable in ARB biofilms if better proton transport is achieved (Torres et al., 2010).

3. MFC

MFCs convert a biodegradable substrate directly into electricity and are new types of bioreactors which use exoelectrogenic biofilms for electrochemical energy production (Logan, 2008; Logan and Regan, 2006b; Rabaey et al., 2005). (Figure 3).
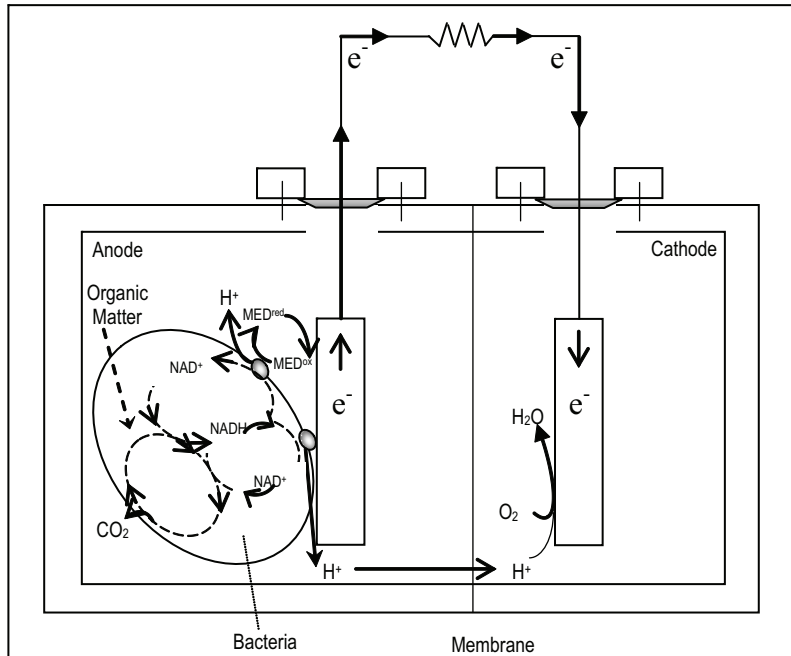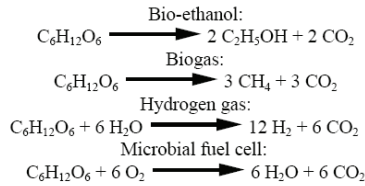
Fig. 3. Schematic of the basic components of a MFC. Bacteria grow on the anode, oxidising organic matter and releasing electrons. The cathode is sparged with air to provide dissolved oxygen for the reaction of electrons, protons and oxygen at the cathode, completing the circuit and producing power. (Logan, 2008)

MFCs have advantages over other technologies used for generating energy from organic matter. First, the direct conversion of substrate into electricity permits high conversion efficiencies. Second, they operate efficiently at ambient temperature, including low temperatures. Third, they do not require the treatment of biogas generated in the cell. Fourth, they do not require additional energy to aerate the cathode, given that it can be aerated passively. Fifth, they have the potential for application in remote areas without electrical infrastructure, making them an additional renewable energy option to meet global energy requirements. Finally, MFCs involve an anaerobic process, and bacterial biomass production will therefore be reduced compared to that of an aerobic system. Estimated cell yield from a MFC process is in the order of $Yx/s=0.16$ g-COD-cell/g-COD. This is about 40% of the value produced by an aerobic process of $Yx/s=0.4$ g-COD-cell/g-COD (Logan, 2008)

A variety of biofuels and by-products can be obtained from organic biomass present in solid and liquid waste, with glucose forming the main source of carbon (Logan, 2004; Alzate et al., 2007; He and Angenent, 2006). The main stoichiometric reactions in fermentative microbiological metabolism include:

$$\text{Bio-ethanol:}$$
$$C_6H_{12}O_6 \longrightarrow 2\,C_2H_5OH + 2\,CO_2$$
$$\text{Biogas:}$$
$$C_6H_{12}O_6 \longrightarrow 3\,CH_4 + 3\,CO_2$$
$$\text{Hydrogen gas:}$$
$$C_6H_{12}O_6 + 6\,H_2O \longrightarrow 12\,H_2 + 6\,CO_2$$
$$\text{Microbial fuel cell:}$$
$$C_6H_{12}O_6 + 6\,O_2 \longrightarrow 6\,H_2O + 6\,CO_2$$

There are three typical configurations amongst MFCs with a proton exchange membrane (PEM) (Figure 4): A. Bioreactor separate from the MFC: the microorganisms generate hydrogen, which is then used as fuel in a fuel cell. B. Bioreactor integrated into the MFC: the microorganisms generate hydrogen which is converted into electricity in a single cell. C. MFC with direct electron transfer: microbiological electricity generation and direct transfer to the anode (Rabaey et al., 2005).
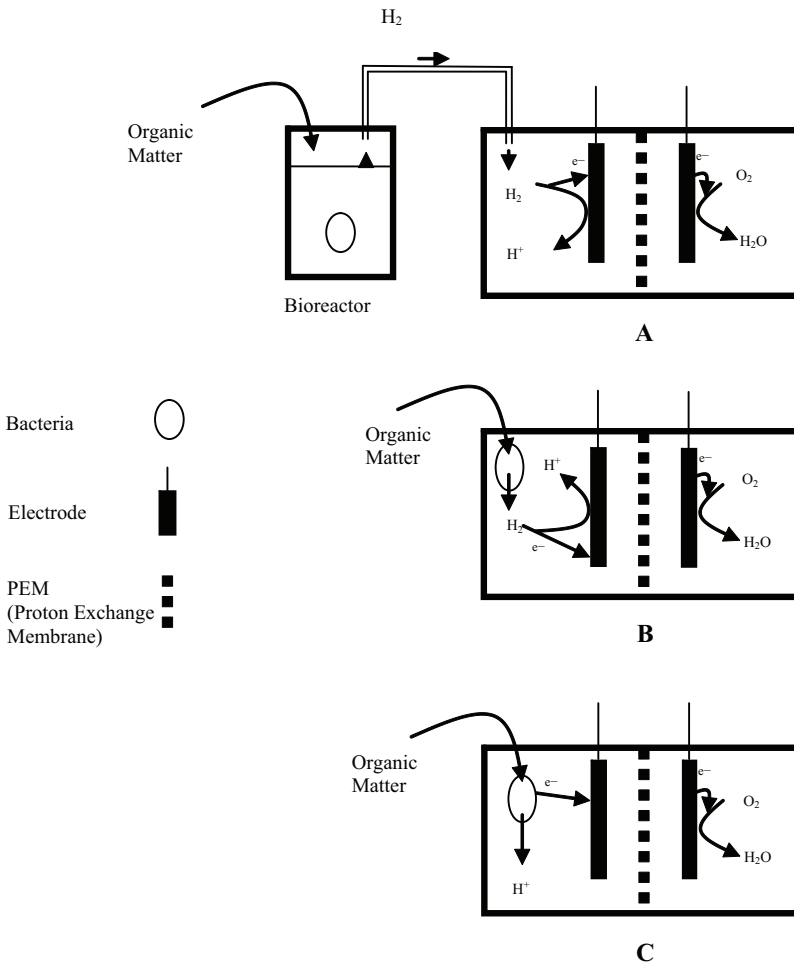

Fig. 4. Different MFC configurations with PEM. (Rabaey et al., 2005)

MFCs can be monitored via electrochemical parameters, such as power density, generated electrical current and voltage. Equally, a very important biological parameter is the organic load of the substrate to be used, expressed in Kg m^{-3} d^{-1} (Rabaey et al., 2003).

Recently, much attention has been focused on the tubular type of MFCs (Clauwaert et al., 2007; Kim et al., 2010; Rabaey et al., 2005a) which increase sludge retention time and reduce hydraulic retention time, which would reduce the long term operating cost. Power densities from industrial and domestic wastewater using MFCs range from 4 to 15 W/m^3 (Cheng et al., 2006; Feng et al., 2008; Liu and Logan, 2004). The anode has, for example, been made of graphite granules (diameters between 1.5 and 5 mm, surface areas between 1000 and 3000 m^2/m^3), which microorganisms can easily attach to. Rabaey et al. (2005) observed a maximum power density of 90 W/m^3 with acetate feeding at 1.1 kg COD/m^3/day. Clauwaert et al. (2007) used a similar configuration but with a biocathode exposed to air which produced a maximum power density of 65 W/m^3 at 1.5 kg COD/m^3/day (Oh et al., 2010).

Finally according to Oh et al. (2010), innovation in the design of new MFC reactors has been driven by the desire to increase power output and decrease capital costs. Therefore, materials which minimise internal electrical resistance, designs which maximise the surface area which electrogenic bacteria can attach to and the removal of expensive materials such as noble metal catalysts on the cathode have been the focus of much of the research activity. This iteration towards optimal design has paid dividends. Reported power outputs in laboratory-scale MFCs have increased from 0.001 to 6.9 W/m^2 (Fan et al., 2008) in less than a decade. Material costs have deceased, but need to decrease further to make MFCs attractive alternatives to other forms of wastewater treatment and pilot plants are emerging (Cha et al., 2009, Rabaey and Keller, 2008). Electricity produced by MFCs may never be a cost effective source of energy in its own right. Rather their contribution will be one of reducing the energy used in wastewater treatment. Switching wastewater treatment from an aerobic to anaerobic process would dramatically cut energy consumption by obviating the need to aerate the sludge. However, conventional anaerobic treatment technologies are often thought of as being slow, need concentrated waste and high temperatures to operate reliably, the effluent often requires further treatment before it can be discharged and sludge disposal is still required. Microbial fuel cells appear to operate at lower temperatures and yield less biomass. In addition, the fact that the bacteria donate electrons to an external circuit with a controllable resistance may ultimately make the whole treatment process amenable to real-time control. The electrical current is a continuous index of the efficiency of the process. This is a neglected area of research for microbial fuel cells which will assume greater importance when MFCs are scaled up for use in real wastewater treatment plants. Least is known about the ecology of microbial communities which metabolise the waste or catalyse the reactions on biocathodes. Microbial communities have been used in conventional wastewater treatment technologies without necessarily having a deep knowledge of the dynamics of the populations, so perhaps our lack of knowledge is not a barrier to the adoption of MFCs. However, when microbial communities behave in unexpected ways and treatment technologies go wrong it can be baffling. A good understanding of the acclimatisation of the communities in MFCs and their response to environmental perturbations would reduce the perceived risks and accelerate the adoption of MFCs. New sequencing technologies combined with proteomics and metabolomics could provide us with a much clearer picture of the changes in community composition and

metabolic pathways which occur in response to different operating conditions. However, even if this deep understanding of the biology at work in an MFC takes many years to achieve it seems clear that, even in the short term, MFCs will have a role to play in sustainable wastewater treatment.

We go on to present how a MFC can generate electricity with electron transfer from the anode to the cathode using a mixed microbial consortium previously adapted as biocatalysts. We examined three factors which could affect MFC operation: external resistance, pH and the effect of temperature.

4. Methodology

4.1 Microorganisms and substrate source

The biocatalysts used for electricity generation were obtained from a previously stabilised MFC (Alzate et al., 2010). The source of the substrate was Synthetic Wastewater (SW) (Poggi et al., 2005), with Sigma® brand reagent grade glucose as the carbon source. The SW had a pH of between 5 and 6 and the following composition per litre: 4g glucose; 310mg NH_4Cl; 130mg KCl; 4.97g NaH_2PO_4; and 2.75g $Na_2HPO_4.H_2O$ (Lovley and Philips, 1998).

4.2 Microbial fuel cell

A large range of materials and designs have been used in MFCs. In this study a MFC was built from glass with a working volume of 350 ml for both the anolyte and catholyte. The anode chamber was bubbled with N_2 to displace the O_2 present before the anode was closed. Untreated carbon paper distributed by Fuelcell (Toray carbon paper®) was used for the electrode.

The PEM cell consisted of 2 chambers, one for the anode and one for the cathode, joined by a proton exchange membrane called Nafion® 117, with a film thickness of 183μm reinforced with a PTFE copolymer (teflon/perfluorosulphonic acid). Its molecular structure permits the absorption of water and once moist, it selectively conducts positively charged ions, blocking those with a negative charge. This characteristic is combined with the established chemical inertness, mechanical resistance and stability of Teflon® resins (Fuelcell Internacional, USA). The membrane was activated before use with 1N H_2SO_4 at 45°C for 24h (Kim et al., 2005).

In the cathode chamber an aqueous catholyte with air bubbling for O_2 use was used with untreated carbon paper with Pt (0.5 mg Pt 10% per cm²) for the electrode, whilst the previously selected and stabilised flocculent-type mixed inoculum was used at the anode. No catalyst was applied to the latter electrode, given that this function is performed by the microorganisms present in the inoculum.

The carbon paper electrodes used in each chamber were 1.7 cm x 1.6 cm, with a total area of 5.44 cm².

MFC start-up consisted of colonising the electrode with the microbial consortium contained in the inoculum in order to form a biofilm; or a complex community of microorganisms which adhere to the electrode and produce a cellular polymer coating which helps them to retain nutrients and protect themselves from toxic agents, and finally produce electricity.

During this process three sequential inoculum transfers were performed until a constant electrochemical response with a constant voltage was obtained. In addition, the voltage pattern was reproduced on the third addition of mixed inoculum to the anode. It is worth noting that strict anaerobic conditions were not maintained for the change of inoculum. The

experiments were performed at mesophilic temperatures by placing the cell in a thermostatic bath.

Two external resistances were used for the PEM cell circuit, one of 1000Ω over a period of 102 days and a second of 600Ω during the remaining days. Based on previous experiments (Liu et al., 2004a; Logan, 2004), the MFC was operated for a period of no greater than 155 days, not including start-up. The changes which occurred in the microbial community during this time were monitored via electrochemical monitoring.

4.3 Electrochemical monitoring

This was performed by measurements of power density produced by the MFC, using a Fluke® multimeter. A resistance was set for the circuit to obtain current data. The current (I) in amps was obtained as: I=VxR-1=Qxt-1, where V is the voltage (volts), Q is the charge (coulombs) and t is the time (seconds). Power (P; watts) was measured as P=IxV and energy production was measured in joules using the equation E=Pxt.

Efficiencies are expressed based on the experimental coulombic efficiency compared to the theoretical one, which varies in accordance with the type of substrate used in the MFC (Rabaey et al., 2004).

4.4 Analysis

The electrode was monitored by taking measurements of volatile fatty acids by titration, hydrogen potential (pH), temperature and soluble chemical oxygen demand (COD) in the liquid current. These parameters were determined in accordance with APHA procedures (2005). Finally, current and voltage measurements were performed with a multimeter and coulombic efficiency was calculated as $CE = \dfrac{Cp}{Cti} \times 100\%$, where CP is total coulombs calculated as the integral of current with respect to time and Cti is the theoretical amount of coulombs calculated from the following equation $C_{ti} = \left[\dfrac{F \times b \times S \times v}{M} \right]$, where F: Faraday's constant, b: is the number of moles of electrons produced per mole of substrate, S: substrate concentration, V: liquid volume and M: molecular weight of the substrate used in the MFC.

5. Results and discussion

5.1 MFC Start-up

When the MFC was inoculated with biocatalysts from a previously stabilised MFC there was a 30h lag phase followed by a rapid increase in voltage over the following 40h, reaching a maximum voltage of 0.4V (Figure 5). The voltage subsequently decreased gradually as the organic matter contained in the inoculum was consumed. On adding the third transfer of inoculum to the MFC the behaviour was similar, producing a stability range of 0.37 ± 0.03V, comprising the last stage in the pattern of bacterial growth. Growth ceased and cell death occurred once the substrate was consumed, and voltage generation was affected.

After 120h in operation, part of the inoculum was replaced with SW and just 10% of the inoculum was conserved. Electricity was immediately seen to be generated in the previously inoculated MFC (Figure 6), reaching a maximum voltage of 1.05V and maintaining a range of 0.90 ± 0.1V over the following 55h.
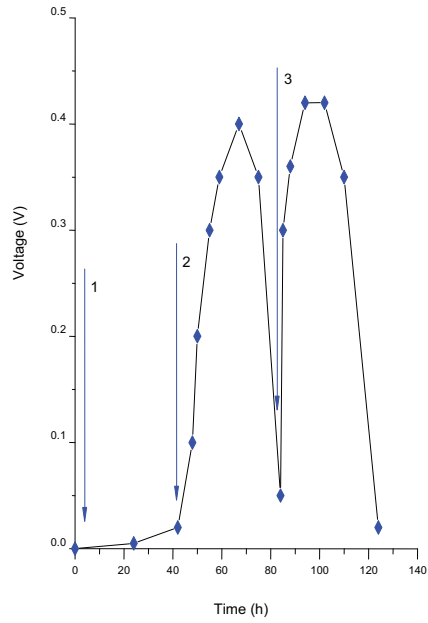
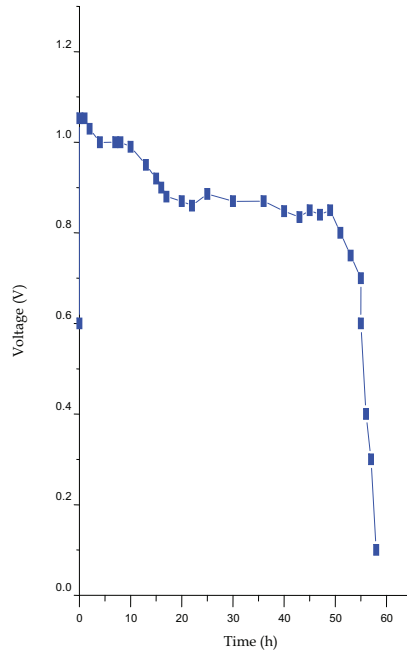Fig. 5. Voltage generation by MFC during start-up. Arrows indicate replacement.

Fig. 6. Voltage generation from glucose as substrate.

5.2 Effect of substrate concentration

Voltage production in the MFC (Figure 7) followed a saturation kinetic, or in other words, the use of substrate in biological systems according to concentration and transport speed (Liu and Logan, 2004). As can be seen in the figure, voltage increased as glucose concentration increased, and remained constant at 1.15 ± 0.05V from a concentration of 1000 mg·L-1. The maximum rate of substrate use therefore occurs in high concentrations of the same (Metcalf and Eddy, 2003).
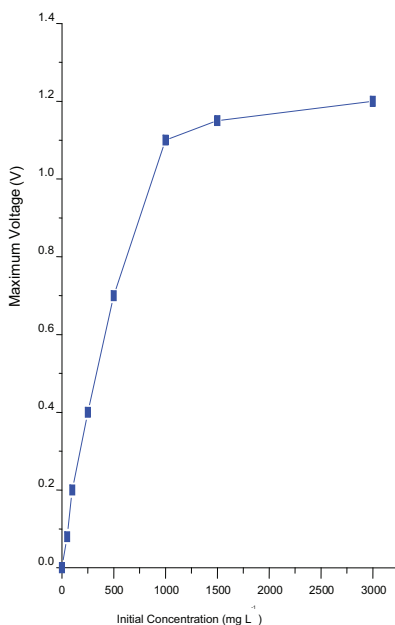
Fig. 7. Maximum voltage generation as a function of glucose concentration.

5.3 Continuous measurement of electricity generation

In this stage electricity generation was monitored over a period of 130 days. With a resistance of 1000Ω the voltage remained at 0.88 ± 0.17V during the first 102 days. After 102 days, a resistance of 600Ω was used, giving values of 0.91 ± 0.08V. With greater fuel oxidation by the microorganisms we expect greater oxidation rates of the electron transporters in the culture at low resistances. In addition, a MFC can be started at low resistances to remove pollutants with high organic indices (Jang et al., 2004).

5.4 Power generation in the MFC

The power density generated by the MFC was measured in W·m-3 based on liquid volume, and the power equation was used for calculations. Using a resistance of 1000Ω, the maximum power density generated was 4.41 W·m^{-3} with a voltage of 1.05V. When a resistance of 600Ω was used, a maximum power density of 6.53 W·m^{-3} was obtained with 0.99V and organic matter removal expressed in COD was 65% and 82%, with 1000 and 600Ω respectively. Table 1, shows the comparison of selected performance parameters of MFCs

with a proton exchange membrane, and we can see that there is a wide range of power values related to the electrode and MFC architecture, the substrate, the inoculum and the redox mediator. Our results are found in the mid-to-low range given that we used a basic architecture, without an external redox mediator.

Substrate	Mixed Culture	Electrode Type	Redox Mediator	CE (%)	P (W/m³)	References
Glucose	Mixed consortium	Plain graphite	Ferricyanide solution cathode	89	216	Rabaey, 2003
Acetate	Sewage sludge	Plain graphite	Ferricyanide solution cathode and Mn(4+) graphite anode and Fe (3+) graphite cathode	-	32	Park, 2003
Wastewater	Bacteria present in wastewater	Plain graphite	None	12	1.6	Liu, 2004
Wastewater	Activated sludge	Plain graphite	None	-	1.7	Kim, 2004
Glucose	Bacteria present in wastewater	Woven graphite	None	40	13	Liu, 2005
Synthetic wastewater	Anaerobic and aerobic sludge	Granular graphite	Hexacyanoferrate cathode	-	258	Aelterman, 2006
Acetate	Microbial fuel cell	Granular graphite	None Biocathode exposed to air	90	65	Clauwaert, 2007
Wastewater	Bacteria present in wastewater	Graphite brush anodes	None	23	2.3	Logan, 2007
Sucrose	Anaerobic sludge collected from septic tank	Stainless steel	None	7.29	36.72	Behera, 2009
Sodium acetate	Anaerobic digested sludge	Carbon cloth	None	39.6	16.7	Cha, 2010
Synthetic wastewater	Non-anaerobic	Carbon paper	None	59	4.41-6.53	Alzate, 2008

Table 1. Comparison of selected performance parameters of MFC with proton exchange membrane

The results show that operating with lower external resistances increases power density production and leads to increased organic matter removal (Jang et al., 2004). This system

uses an aqueous catholyte to provide the electrode with dissolved O_2, without using external mediators. Microbial consortiums generate greater power density than pure cultures (Pham et al., 2006; Rittmann, 2006).

One of the highest power densities reported in the literature is 386 $W \cdot m^{-3}$ (Aelterman et al., 2008), where sodium acetate was used as a substrate and potassium hexacyanoferrate was used to optimise cathode performance. Ferricyanide is very popular as an electron acceptor in MFC experiments and reaches greater voltages than using O_2. The great advantage of ferricyanide is the low overpotential using flat carbon cathodes. However, power generation with ferricyanide is not sustainable as a result of insufficient reoxidation via O_2, which requires regular replacement of the catholyte. Furthermore, long periods of system operation can be affected by ferricyanide diffusion to the anode chamber (Logan and Reagen, 2006b).

5.5 Influence of pH

Another important parameter in MFC performance is the pH of the anode chamber. The experimental results clearly showed the dependence of MFC performance on the influent pH. During the experiment the pH of the anolyte was maintained at 6.7. The highest power densities occurred at pH values near neutral, with results ranging from 3.68 to 4.41 $W \cdot m^{-3}$ in the case of 1000Ω. Recorded power density decreased slightly when the pH was < 7.0, remaining at 3.55 $W \cdot m^{-3}$. In the measurements taken when using a resistance of 600Ω, a maximum power density of 6.53 $W \cdot m^{-3}$ was obtained at a pH of between 6.8 and 7.0. This result agrees with the results reported by Gil et al. (2003) and He et al. (2008). Both studies observed that low pH (pH 5 and 6) resulted in lower electricity generation. The lower pH in the MFC might have inhibited the activity of electrogenic bacteria. Other researchers have also reported that an acidic pH in the anode chamber reduces power production. Ren et al. (2007) reported a significant decrease in power production when the pH in the anode compartment dropped to 5.2 due to the acidic products of fermentation, and power production was rapidly resumed when the pH of the anolyte was increased to 7.

5.6 Effect of temperature on MFC performance

Anaerobic digestion requires 30–50°C for optimal operation but MFCs are known to operate well at ambient temperature (Ahn and Logan, 2010; Jadhav and Ghangrekar, 2009; Min et al., 2008). Organic removal increased but the electricity production decreased, which might be due to increased activity of methanogens. The additional heating system to maintain temperature may not be necessary for energy recovery or wastewater treatment using MFC technology. The MFC operated at a mesophilic temperature of 35 ± 5°C during the first 102 days. During this period the maximum power density reached was (4.41 $W \cdot m^{-3}$) using 1000Ω at 37°C. A constant temperature of 40°C was maintained for the following days, obtaining a maximum power density of (6.53 $W \cdot m^{-3}$) with 600Ω. Under this last scheme the temperature was increased by 5°C, obtaining 6.54 $W \cdot m^{-3}$. We should note that the temperature increase to 45°C did not lead to significant increases in power density, given that the result obtained is very similar to the one reached at an operational temperature of 40°C. These results reflect the strong influence of the external resistance used, together with an optimum operational temperature (Rozendal et al., 2006).

A significant advantage of MFCs is that they can produce electricity from organic matter whilst operating at moderate temperatures, for example 20-40°C (Min and Logan, 2004; Niessen et al., 2004; Oh et al., 2004; Kim et al., 2005; Liu et al., 2005; Aelterman et al., 2006; Cheng et al., 2006; Zhao et al., 2006; Logan et al., 2007; Oh and Logan, 2007).

5.7 Efficiency obtained in the MFC

Current efficiency is determined based on Coulombic Efficiency (CE), which is defined as the quantity of organic matter recovered as electricity.

$$CE = \frac{Cp}{Cti} \times 100\%$$

The graph of current against MFC operation time was used to determine Cp. The total charge (q) in coulombs is obtained by integrating the area under the curve (from t = 0 to 130 days), which was Cp=12367.23 (Figure 8). Glucose was used as the substrate. The previously described equation (Liu et al., 2005) for Cti is used to calculate the theoretical quantity of coulombs which can be produced by glucose:

$$C_{ti} = \left[\frac{F \times b \times S \times v}{M} \right]$$

where F: is Faraday's constant (98485 C·mol-1 of electrons), b: number of moles of electrons produced per mole of substrate (glucose substrate b=24), S: substrate concentration (g·L-1), v: liquid volume and M: molecular weight of the substrate (glucose, M=180). We therefore obtain Cti=20681.85 and in turn, the coulombic efficiency of the MFC is:

$$CE = \left[\frac{12367.23}{20681.85} \right] \times 100 = 59.79\%$$

The CEs calculated for microbial fuel cells present in the literature vary, but they generally increase with power density because there is less time for substrate to be lost during competing physical and biological processes (Logan and Regan, 2006a).
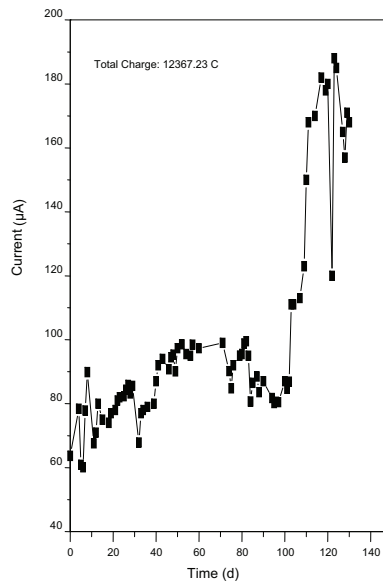

Fig. 8. Total charge calculated from the integration of current over time for substrate consumption.

In this study a CE of 59.79% was obtained. Table 1, presents efficiencies reported in other studies and we can see that the efficiencies produced vary in terms of the type of substrate or electrode used. For example, efficiencies of 23% (Logan et al., 2007) were obtained with bottle (B-MFC) air-cathode MFCs inoculated with wastewater which produced up to 2.3 $W \cdot m^{-3}$ and a CE = 23% with brush electrodes, versus 0.97 $W \cdot m^{-3}$ with a plain carbon paper electrode. These findings show that brush anodes which have high surface areas and a porous structure can produce high power densities, and therefore have qualities which make them ideal for scaling up MFC systems.

Efficiencies of 65% (Min and Logan, 2004) and 63-78% (Oh et al., 2004) were obtained with acetate. With glucose CEs were 89% using potassium hexacyanoferrate at the cathode (Rabaey et al., 2003), whilst Liu and Logan obtained 40-55% using a PEM and 9-12% without a membrane, but using an air cathode, and noting that the main disadvantage of this system was the loss of substrate due to aerobic oxidation at the anode. In other words, there is greater O_2 diffusion in the anode chamber in the absence of a PEM. With wastewater CEs were 3-12% (Liu et al., 2004), with protein efficiency was 6% (Heilman and Logan, 2006) and finally, using lactate and potassium ferricyanide efficiency was 2.4% (Ringeisen et al., 2006).

6. Conclusions

- A PEM microbial fuel cell can generate electricity and simultaneously purify wastewater, which makes it attractive for in situ treatments or for the modification of current conventional treatment plants.
- Switching from aerobic to anaerobic wastewater treatment would cut energy consumption by obviating the need to aerate the sludge. However, conventional anaerobic treatments are often thought of as being slow, need concentrated waste and high temperatures to operate reliably, the effluent often requires further treatment before it can be discharged and sludge disposal is still required. Microbial fuel cells appear to operate at lower temperatures and yield less biomass.
- An aspect to be improved in future studies is to increase the area of the anode to compensate for losses due to death and space occupied by other non-electricity generating bacteria in the biofilm.
- It was shown that as is the case with an external electron acceptor, the presence of conductivity is imminent in the anolyte of the MFC.

7. References

Aelterman P, Rabaey K, Pham T, Boon N, Verstraete W. (2006). Continuous electricity generation at high voltages and currents using stacked microbial fuel cells. *Env. Sci. Technol*. 40: 3388-3394.

Aelterman P, Versichele M, Marzorati M, Boon N, Verstraete W. (2008) Loading rate and external resistance control the electricity generation of microbial fuel cells with different three-dimensional anodes. *Biores. Tech*. 99: 8895–8902.

Ahn Y, Logan B. (2010). Effectiveness of domestic wastewater treatment using microbial fuel cells at ambient and mesophilic temperatures. *Bioresour Technol*. 101: 469–475.

Alzate-Gaviria L, Sebastian P, Pérez-Hernández A. (2007). Comparison of two anaerobic systems for hydrogen production from the organic fraction of municipal solid waste and synthetic wastewater. *Int. J. Hydrogen Energy* 32: 3141-3146.

Alzate-Gaviria L, Fuentes-Albarran C, Alvarez-Gallegos A and Sebastian PJ. (2008). Electricity generation from a pem microbial fuel cell. *Interscience* 33: 510-517.

Alzate –Gaviria L , González K, Peraza I, García O, Domínguez-Maldonado J, Vázquez J, Tzec–Simá M and Canto–Canché B. (2010). Performance evaluation and identification of exoelectrogens in two types of microbial fuel cells with different anode configuration. *Interscience* 35: 19-25.

Angenent L, Karim K, AL-Dahhan M, Wrenn B, Domingues-Espinosa R. (2004). Production of bioenergy and biochemicals from industrial and agricultural wastewater. *Trends Biotechnol*. 22: 477-485.

APHA (2005). Standard Methods for the Examination of Water and Wastewater (2005). 21st ed. APHA, AWWA, WEF. Washington, DC, EEUU. 1170 pp.

Beliaev A, Thompson D, Fields M, Wu L, Lies D, Nealson K and Zhou J (2001) Microarray Transcription Profiling of a Shewanella oneidensis etrA Mutant. *J Bacteriol*. 184: 4612-4616.

Cha J, Choi S, Yu H, Kim H, Kim C (2009) Directly applicable microbial fuel cells in aeration tank fro wastewater treatment. *Bioelectrochemistry* 78: 72–79.

Chang I, Jang J, Gil G, Kim M, Kim H, Cho B. (2004). Continuous determination of biochemical oxygen demand using microbial fuel cell type biosensor. *Biosens Bioelectron* 19: 607–613.

Cheng S, Liu H, Logan B. (2006). Increased Power generation in a continuous flow MFC with advective flow through the porous anode and reduced electrode spacing. *Env. Sci. Technol*. 40: 2426-2432.

Clauwaert P, van der Ha D, Boon N, Verbeken K, Verhaege M, Rabaey K. (2007). Open air biocathode enables effective electricity generation with microbial fuel cells. *Environ. Sci. Technol*. 41:7564–7569.

Debabov V. (2008). Electricity from microorganisms. *Microbiology* 77: 123-131.

EPA. (2008). Water and Energy: Leveraging Voluntary Programs to Save Both Water and Energy. *Environmental Protection Agency*.

Fan Y, Hu H and Liu H. (2007). Sustainable Power Generation in Microbial Fuel Cells Using Bicarbonate Buffer and Proton Transfer Mechanisms. *Environ. Sci. Technol*. 41: 8154–8158.

Fan Y, Sharbrough E, Liu H. (2008). Quantification of the internal resistance distribution of microbial fuel cells. *Environ. Sci. Technol.* 42:8101–8107.

Feng Y, Wang X, Logan B, Lee H. (2008). Brewery wastewater treatment using air-cathode microbial fuel cells. *Appl Microbiol Biotechnol*. 78: 873–880.

Franks A, Nevin K, Jia H, Izallalen M, Woodarda T and Lovley D. (2009). Novel strategy for three-dimensional real-time imaging of microbial fuel cell communities: monitoring the inhibitory effects of proton accumulation within the anode biofilm. *Energy Environ. Sci*. 2: 113-119.

Gil G, Chang I, Kim B, Kim M, Jang J, Park H, Kim H. (2003). Operational parameters affecting the performance of a mediator-less microbial fuel cell. *Biosensors & Bioelectronics* 18: 327–334.

Goldstein R, Smith W. (2002). Water & Sustainability (Volume 4): U.S. Electricity Consumption for Water Supply & Treatment—The Next Half Century. Electric Power Research Institute, Inc. (EPRI).

Gorby Y, Yanina S, McLean J, Rosso K, Moyles D, Dohnalkova A, Beveridge T, Chang I, Kim B, Kim K, Culley D, Reed S, Romine M, Saffarini D, Hill E, Shi L, Elias D, Kennedy D, Pinchuk G, Watanabe K, Ishii S, Logan B, Nealson K and Fredrickson J. (2006). Electrically conductive bacterial nanowires produced by Shewanella oneidensis strain MR-1 and other microorganisms. *PNAS* 103: 11358-11363.

Gralnick J, Newman D. (2007). Extracellular respiration. Molecular Microbiology 65: 1–11.

Haberman W, Pommer E. (1991). Biological fuel cells with sulphide storage capacity. *Appl. Microbiol. Biotechnol.* 35: 128-133.

Hawkes F, Hussy I, Kyazze G, Dinsdale R, Hawkes DL. (2007). Continuous dark fermentative hydrogen production by mesophilic microflora: principles and progress. *Int. J. Hydrogen Energy* 32: 172–184.

He Z, Angenent L. (2006). Application of bacterial biocathodes in microbial fuel cells. *Electroanalysis* 18: 2009-2015.

He Z, Huang Y, Manohar A, Mansfeld F. (2008). Effect of electrolyte pH on the rate of the anodic and cathodic reactions in an air-cathode microbial fuel cell. *Bioelectrochemistry* 74: 78–82.

Heilmann J, Logan B. (2006). Production of electricity from proteins using a single chamber microbial fuel cell. *Water Env. Res.* 78: 531-537.

Hernandez M and Newman D. (2001). Review Extracellular electron transfer. CMLS, Cell. *Mol. Life Sci.* 58: 1562–1571.

Jadhav G, Ghangrekar M. (2009). Performance of microbial fuel cell subjected to variation in pH, temperature, external load and substrate concentration. *Biosource Technol.* 100: 717–723.

Jang J, Pham T, Chang I, Khan K, Moon H, Cho K, Kim B. (2004). Construction and operation of a novel mediator- and membrane –less microbial fuel cell. *Proc. Biochem.* 39: 1007-1012.

Kim H, Hyun M, Chang I, Kim B. (1999). A microbial fuel cell type lactate biosensor using a metal-reducing bacterium, Shewanella putrefaciens. *J. Microbiol. Biotechnol.* 9: 365–367.

Kim J, Min B, Logan B. (2005). Evaluation of procedures to acclimate a microbial fuel cell for electricity production. *Appl. Microbiol. Biotechnol.* 68: 23-30.

Kim J, Premier G, Hawkes F, Rodríguez J, Dinsdale R, Guwy A. (2010). Modular tubular microbial fuel cells for energy recovery during sucrose wastewater treatment at low organic loading rate. *Bioresour Technol.* 101: 1190–1198.

Lee H, Parameswaran P, Kato-Marcus A, Torres C, Rittmann B. (2008). Evaluation of energy-conversion efficiencies in microbial fuel cells (MFCs) utilizing fermentable and non-fermentable substrates. *Water Res.* 42: 1501–1510.

Liu H, Logan B. (2004). Electricity generation using an air-cathode single chamber microbial fuel cell in the presence and absence of a proton exchange membrane. *Env. Sci. Technol.* 38: 4040-4046.

Liu H, Ramnarayanan R, Logan B (2004a) Production of electricity during wastewater treatment using a single chamber microbial fuel cell. *Env. Sci. Technol.* 38: 2281-2285.

Liu H, Cheng S, Logan B. (2005). Production of electricity from acetate or butyrate in a single chamber microbial fuel cell. *Env. Sci. Technol.* 39: 658-662.

Logan B. (2004). Extracting hydrogen and electricity from renewable resources. *Env. Sci. Technol.* 38: 160A-167A.

Logan B, Regan J. (2006a). Electricity-producing bacterial communities in microbial fuel cells. *Trends Microbiol.* 14: 512-518.

Logan B, Regan J. (2006b). Microbial fuel cells - challenges and applications. *Env. Sci. Technol.* 40: 5172-5180.

Logan B, Cheng S, Watson V, Estadt G. (2007). Graphite fiber brush anodes for increased power production in air- cathode microbial fuel cells. *Env. Sci. Technol.* 41: 3341-3346.

Logan B (2008). *Microbial Fuel Cells.* Wiley. Hoboken, NJ, EEUU. 200 pp.

Logan B (2009). Exoelectrogenic bacteria that power microbial fuel cells. *Nature Rev. Microb.* 7: 375-381.

Lovley D, Phillips E. (1998). Novel of microbial energy metabolism: Organism carbon oxidation coupled to dissimilatory reduction of iron and manganese. *Appl. Env. Microbiol.* 54: 1472-1480.

Magnuson T, Isoyama N, Hodges-Myerson A, Davidson G, Maroney M, Geesey G and Lovley D. (2001). Isolation, characterization and gene sequence analysis of a membraneassociated 89 kDa Fe(III) reducing cytochrome c from Geobacter sulfurreducens. *Biochem. J.* 359: 147–152.

Marsili E, Flickinger M, Bond D. (2008). Shewanella secretes flavins that mediate extracellular electron transfer. *PNAS* 105: 3968-3973

Metcalf and Eddy (2003). *Wastewater Engineering Treatment and Reuse.* 4a ed. Mc Graw-Hill. Madrid, España. 1485 pp.

Min B, Logan B (2004). Continuous electricity generation from domestic wastewater and organic substrates in a flat plate microbial fuel cell. *Env. Sci. Technol.* 38: 5809-5814.

Min B, Cheng S, Logan B (2005). Electricity generation using membrane and salt bridge microbial fuel cells. *Water Res.* 39: 1675- 1686.

Min B, Roman O, Angelidaki I. (2008). Importance of temperature and anodic medium composition on microbial fuel cell (MFC) performance. *Biotechnol. Lett.* 30: 1213–1218.

Newman D, Kolter R. (2000). A role for excreted quinones in extracellular electron transfer. *Nature* 405: 94-97.

Niessen J, Schröder U, Scholz F. (2004). Exploiting complex carbohydrates for microbial electricity generation – a bacterial fuel cell operating on starch. *Electrochem. Comm.* 6: 955-958.

Oh S, Min B, Logan B. (2004). Cathode Performance as a factor in electricity generation in microbial fuel cells. *Env. Sci. Technol.* 38: 4900-4904.

Oh S, Logan B. (2007). Voltage reversal during microbial fuel cell stack operation. *Power Sources* 167: 11-17.

Oh S, Martin A. (2009). Long chain fatty acids degradation in anaerobic digester: thermodynamic equilibrium consideration. *Process Biochem.* 45: 335–345.

Oh S, Kim J, Premier G, Lee T, Changwon K, Sloan W. (2010). Sustainable wastewater treatment: How might microbial fuel cells contribute. *Biotechnology Adv.* 28: 871-881.

Park D, Zeikus J. (2003). Improved fuel cell and electrode designs for producing electricity from microbial degradation. *Biotechnol. Bioeng.* 81: 348-355.

Pham T, Rabaey K, Aelterman P, Clauwaert P, Schamphelaire L, Boon N and Verstraete W. (2006). Microbial fuel cells in relation to conventional anaerobic digestion technology. *Eng. Life Sci.* 6: 285-292.

Poggi-Varaldo HM, Alzate-Gaviria LM, Nevárez- Morillón VG, Rinderknecht-Seijas N. (2005). A side by side comparison of two systems of sequencing coupled reactors for anaerobic digestion of the organic fraction of municipal solid waste. *Waste Manag. Res*. 23: 270-280.

Rabaey K, Lissens G, Siliciano S, Verstraete W. (2003). A microbial fuel cell capable of converting glucose to electricity at high rate and efficiency. *Biotechnol. Lett.* 25: 1531-1535.

Rabaey K, Boon N, Siciliano S, Verhaege M and Verstraete W. (2004). Biofuel cells select for microbial consortia that self-mediate electron transfer. *Appl. Env. Microbiol*. 70: 5373-5382.

Rabaey K, Boon N, Hofte M, Verstraete W. (2005). Microbial phenazine production enhances electron transfer in biofuel Cells. *Env. Sci. Technol*. 39: 3401-3408.

Rabaey K, Clauwaert P, Aelterman P, Verstraete W. (2005a). Tubular microbial fuel cells for efficient electricity generation. *Env. Sci. Technol*. 39: 8077–82.

Rabaey K, Keller J. (2008). Microbial fuel cell cathodes: from bottleneck to prime opportunity. *Water Sci. Technol*. 57: 655–659.

Reguera G, McCarthy K, Mehta T, Nicoll J, Tuominen M and Lovley D. (2005). Extracellular electron transfer via microbial nanowires. *Nature* 435: 1098-1101.

Ringeisen B, Henderson E, Wu P, Pietron J, Little B, Biffinger J, Jones-Meehan J. (2006). High power density from a miniature microbial fuel cell using Shewanella oneidensis DSP10. *Env. Sci. Technol.* 40: 2629-2634.

Rittmann B (2006). Microbial ecology to manage processes in environmental biotechnology. *Trends Biotechnol.* 24: 261-268.

Rittmann B (2008). Opportunities for renewable bioenergy using microorganisms. *Biotechnol. Bioeng*.100: 203–212.

Roller S, Bennetto H, Delaney G, Mason J, Stirling J, Thurston C. (1984). Electrontransfer coupling in microbial fuel cells. Comparison of redox-mediator reduction rates and respiratory rates of bacteria. *J. Chem. Technol. Biotechnol*. 34: 3-12.

Rozendal R, Hamelers H, Buisman C. (2006). Effects of Membrane Cation Transport on pH and Microbial Fuel Cell performance. *Env. Sci. Technol*. 40: 5206-5211.

Schröder U (2003). Anodic electron transfer mechanisms in microbial fuel cells and their energy efficiency. *Phys. Chem*. 9: 2619-2629.

Suzuki S (1976). Fuel cells with hydrogen forming bacteria. Hosp. Hyg. Gesundheitswes. *Desinfekt.* 68: 159.

Torres C, Marcus A, Rittmann B. (2008). Proton transport inside the biofilm limits electrical current generation by anode-respiring bacteria. *Biotech. Bioeng.* 100: 872–881.

Torres C, Marcus A, Lee H, Parameswaran P, Krajmalnik-Brown R, Rittmann B. (2009). A kinetic perspective on extracellular electron transfer by anode-respiring bacteria. *FEMS Microbiol. Reviews* 34: 3-17.

UNICEF. (2000). Global Water Supply and Sanitation Assessment 2000 Report. In: UNICEF, editor.: UN.

von Canstein H, Ogawa J, Shimizu S and Lloyd J. (2008). Secretion of Flavins by Shewanella Species and Their Role in Extracellular Electron Transfer. *Appl. Environ. Microb.* 74: 615-623.

Water UN. (2006). Gender, Water and Sanitation: A policy Brief. In: Water U, editor.: UN.

Weber K, Achenbach L and Coates J. (2006). Microorganisms pumping iron: anaerobic microbial iron oxidation and reduction. *Nature Reviews Microbiology* 4: 752-764.

Xing D, Zuo Y, Cheng S, Regan J and Logan B. (2008). Electricity Generation by Rhodopseudomonas palustris DX-1. *Env. Sci. Technol*. 42: 4146–4151.

Yokoyama H, Ohmori H, Ishida M, Waki M and Tanaka Y. (2006). Treatment of cow-waste slurry by a microbial fuel cell and the properties of the treated slurry as a liquid manure. *Animal Sci*. J. 77: 634-638.

Zhao F, Harnisch F, Schröder U, Scholz F, Bogdanoff P and Herrmann I. (2006). Challenges and constraints of using oxygen cathodes in microbial fuel cells. *Env. Sci. Technol*. 40: 5193-5199.

Perchlorate: Status and Overview of New Remedial Technologies

Katarzyna H. Kucharzyk, Terence Soule,
Andrzej, J.Paszczynski and Thomas F. Hess
University of Idaho
USA

1. Introduction

The reason for an increasing interest in perchlorate pollution includes recent advances in both analytical chemistry and better understanding of perchlorate's health impacts. The advances and developments of chemical methods have allowed detection of concentrations at low part-per-billion (microgram per liter [µg/L] (Urbansky, 2000), and the toxicological research has suggested that such concentrations may be a potential risk for developing fetuses and infants (USEPA, 2002; Kucharzyk et al., 2010). Perchlorate inhibits iodide uptake by the thyroid causing disruption in normal thyroid function, which can lead to a number of serious health problems, especially pertaining to early neurological development (Blount et al., 2006).

There have been several high-profile cases of perchlorate contamination of surface waters and drinking water supplies in major metropolitan areas (Gullick et al., 2001) and the parties such as U.S. Department of Defense (DoD) responsible for the events had to quickly respond to the regulatory and public demand to prevent further exposures and clean up contaminated sites (Stroo et al., 2009). In January 2009, the EPA issued a heath advisory to assist state and local officials in addressing local contamination of perchlorate in drinking water. The interim health advisory level of 15 micrograms per liter (mg/L), or ppb, is based on the reference dose recommended by the National Research Council (NRC) of the National Academy of Sciences (NAS) (Kucharzyk et al., 2009).

The most recent technologies for remediation of perchlorate in groundwater are in the group of phytobioremediation, *in situ* bioremediation with the application of the Genetic Algorithms (GAs). More detailed descriptions of the technologies listed, along with the discussion of their scientific basis, current status and specific advantages and limitations are provided in this chapter.

2. Perchlorate background

2.1 Properties and health effects

Perchlorate is widely known to be a poor complexing agent and is used extensively as a counter anion in studies of metal cation chemistry, especially in non-aqueous solution (Urbansky, 2000). Its low association with cations is responsible for the extremely high

solubilities of perchlorate salts in aqueous and non aqueous media. The predominant route of perchlorate exposure of humans (and animals) is via drinking of contaminated water and ingestion of contaminated foods like milk (Kirk et al., 2005) and vegetables (Jackson et al., 2005). Perchlorate is known to disrupt the uptake of iodine in the thyroid, potentially affecting thyroid function. A key concern is that, if sufficiently severe, impaired thyroid function in pregnant women can impair brain development in fetuses and infants (Urbansky, 2000). Because of the complex anatomy of the thyroid follicle, all of the locations where perchlorate inhibition is exerted remain to be established. One site of this inhibition is the sodium–iodide symporter, a membrane protein located on the basolateral side of the follicular cell, adjacent to the capillaries supplying blood to the thyroid (Urbansky, 2002; National Research Council, 2005). The competitive inhibition of iodide uptake is the only direct perchlorate effect on the thyroid, leading to a reversible chemical induced iodine deficiency. Alteration of hormones (T4, T3, and TSH) is considered to be the first observed effect of perchlorate exposure. Since perchlorate competitively inhibits iodine uptake in the thyroid it alters the levels of thyroid hormone, and during pregnancy even minute disruptions of thyroid hormone levels can have serious effects on a developing fetus. These effects can lead to a loss of hearing, deficiency in speech and motor skills, lowered IQ, and even mental retardation in infants and young children (EWG, 2007).

2.2 Uses

Perchlorate came into prominence as a pollutant in the late 1990s, and it has remained as an important issue for debate during the last decade. Along with the controversy, perchlorate contamination has also attracted an enormous amount of public interest (USEPA, 2002). In the early 1800s perchlorate became an alternative to the potassium nitrate containing black powder that had been used in fireworks until then. In the 1940s perchlorates became increasingly important as a component in propellants and explosives and still the main applications of perchlorate are in the explosives and chemical industries (Sellers et al., 2007). An important advantage of the oxidizer ammonium perchlorate over nitroglycerin as an additive to explosive is that is easy to use and can be handled relatively safely (Cunniff, 2006). Specific uses of the various perchlorate salts include: as a solid rocket fuel oxidizer, in flares and pyrotechnics, in explosives, and in chemical processes as a precursor to potassium and ammonium perchlorate (USEPA, 2002). Perchlorate salts are also used on a large scale as a component of air bag inflators and in small-scale laboratory applications as ionic strength adjustors or non-complexing counterions. In cotton production sodium chlorate is used as a defoliant and as a non-contact herbicide in other crops like sunflowers, rice, safflower, and sorghum (Kegley et al., 2008).

2.3 Sources of perchlorate

In nature, perchlorate may originate from two natural sources: soils and arid climates derived from ancient marine seabeds, and potentially, conditions during lightning storms. The main and largest known perchlorate source lies in Chile in Atacama Desert, where perchlorate is extracted from deposits of nitrate ores or brines. Other deposits are located in Death Valley, the high plains in Texas and New Mexico (Rajagopalan et al., 2006) , and the Bolivian playas (Orris et al., 2003) , i.e. perchlorate deposits generally occur in very arid regions (Rao et al., 2007). Recently, high levels of perchlorate were reported on Mars (Hecht et al., 2009). This founding is rather exciting since perchlorate could be used as a support for life on Mars as a potential electron acceptor. The mechanism of how naturally occurring

perchlorate is generated is not known or well investigated. Researchers suppose that perchlorate can be generated photochemically in the atmosphere or on chloride-coated mineral surfaces by ozone oxidation of chloride and by electrical discharge. The isotopic signature of perchlorate in arid regions points to a stratospheric origin of the compound (Jackson et al., 2006).

Anthropogenic sources of perchlorate are mainly associated with the manufactures of perchlorate or its use in defense-related operations such as rocket manufacture or munitions use or demolition (Cox, 2009). Perchlorate is principally a synthetic compound and its salts have a broad range of different industrial applications ranging from pyrotechnics to lubricating oils (Motzer, 2001). Its presence in the environment predominantly results from historical discharge of unregulated manufacturing waste streams, leaching from disposal ponds, and from the periodic servicing of military inventories (Urbansky, 2000; Urbansky, 20002). Specific uses of the various perchlorate salts include: as a solid rocket fuel oxidizer, in flares and pyrotechnics, in explosives, and in chemical processes as a precursor to potassium and ammonium perchlorate (USEPA, 2002). Perchlorate salts are also used on a large scale as a component of air bag inflators and in small-scale laboratory applications as ionic strength adjustors or non-complexing counterions. Sodium chlorate is produced predominantly electrochemically by electrolysis and can contain significant amounts of perchlorate as a contaminant, thus they significantly contribute to the total perchlorate load in the environments (Aziz & Hatzinger, 2009).

2.4 Biodegradation

It has been known that microorganisms can reduce oxyanions of chlorine such as chlorate (ClO_3^-) and perchlorate (ClO_4^-) [(per)chlorate] under anaerobic conditions. The high reduction potential of (per)chlorate (ClO_4^-/Cl^- E_o = 1.287 V; ClO_3^-/Cl^- E_o = 1.03 V) makes them ideal electron acceptors for microbial metabolism (Coates et al., 2000). Early studies indicated that unknown soil microorganisms rapidly reduced chlorate that was applied as herbicide for thistle control and the application of this reductive metabolism was later proposed for the measurement of sewage and wastewater biological oxygen demand (Bryan, 1966). Initially it was thought that chlorate reduction was mediated by nitrate-respiring microorganisms in the environment with chlorate uptake and reduction simply being a competitive reaction for the nitrate reductase system of these bacteria (de Groot & Stouthamer, 1969). This was supported by the fact that many nitrate-reducing microorganisms in pure culture were also capable of reducing (per)chlorate (Roland et al, 1994). Furthermore, early studies demonstrated that membrane-bound respiratory nitrate reductases and assimilatory nitrate reductases could alternatively reduce chlorate (Steward, 1988) and presumably perchlorate.

In the past decade understanding of the biological perchlorate reduction progressed dramatically due to the development of the genetic analysis that offer tools for detecting and monitoring dissimilatory perchlorate-reducing bacteria for bioremediative purposes (Achenbach et al., 2006). The perchlorate reduction pathway consists of two central enzymes: perchlorate reductase and chlorite dismutase. The first enzymatic step of the pathway, the reduction of perchlorate and chlorate to chlorite, is performed by (per)chlorate reductase (Fig.1).The chlorite formed from this reduction is cytotoxic and requires immediate detoxification which is catalyzed by chlorite dismutase converting chlorite to chloride and oxygen (Wolternik, 2005).The generation of oxygen makes anaerobic (per)chlorate reduction unique when compared to other anaerobic respiratory processes.

This aspect of (per) chlorate reduction has been of special interest because of its potential to introduce oxygen to anoxic sites to aide subsequent bioremediation strategies (Achenbach et al., 2006).

$$ClO_4^- \xrightarrow{\text{Perchlorate reductase (pcrA)}} ClO_3^- \xrightarrow{\text{pcrA}} ClO_2^- \xrightarrow{\text{Chlorite Dismutase (cld)}} Cl^- + O_2$$
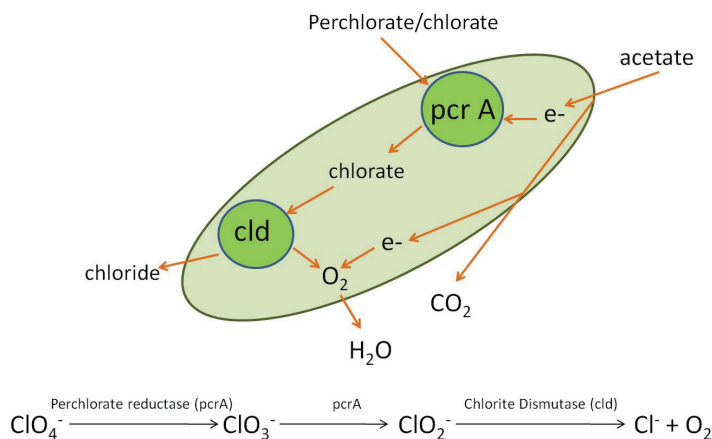
Fig. 1. Perchlorate reduction pathway. The reactions are catalyzed by perchlorate reductase (pcrA) that reduces perchlorate to chlorite and chlorite dismutase (cld) that converts toxic chlorite to chloride and oxygen (Adapted from Ederer et al., 2011).

3. Emerging technologies

3.1 *In situ* perchlorate bioremediation with the application of evolutionary computation.

3.1.1 Genetic Algorithm outline

Artificial intelligence (AI), such as Genetic Algorithms (GA), covers a wide range of techniques and tools that facilitate decision making and have often been found to be as powerful and effective as gradient search methods in many engineering applications (Schugerl, 2001). Genetic algorithms (GAs) (Holland, 1975) are search and optimization methods based upon the biological principal of evolution through natural selection and mimics biological evolution as a problem-solving strategy. GA tends to thrive in an environment in which there is a very large set of candidate solutions. Inspired by the Darwinian principle of evolution through natural selection, GA borrows part of the vocabulary from biology. Potential solutions to a problem (optimization trials) are conceptually considered to be individuals containing a chromosome encoding the details of the proposed solutions (Reeves, 1993). Such a chromosome consists of genes representing the system variables that are alleles of those genes. GA simultaneously operates on a collection of such solutions, called a population. Each candidate is evaluated accordingly to the fitness function that is quantitatively estimated (Goldberg, 1989).

Initially, the first generation of potential solutions is typically created at random. A new generation of solutions is created by selecting solutions from the old generation with a probability that is proportional to their fitness value (Vandecastelle, 2006). The selected individuals are called parents. After crossover and mutation are applied, these parents result in children that will make up the next generation of solutions (Fig.2). Crossover is a

process that typically occurs with a high probability and in which pieces of chromosome are exchanged between pairs of parents.
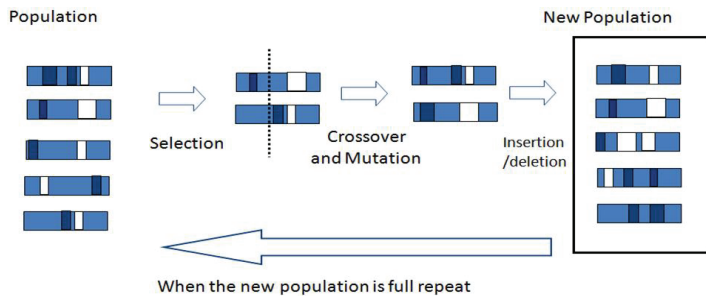

Fig. 2. Schematic outline of the operation of a Genetic Algorithm. (T. Soule, University of Idaho, personal communication)

During the process of mutation, each gene has a typically low probability of changing in allele value. The fitness value for the created generation is then evaluated, after which the process of selection, crossover, and mutation is repeated. The whole cycle is repeated until an acceptable solution is obtained or until experimental resources run out (Vandecastelle, 2006). This is best summarized with pseudocode, as shown below:

begin

> **create** initial population
> **evaluate** initial population
> gen = 0
> max _ gen = N
> while (gen < max_gen) do
>> gen+ = 1
>> **select** sub-population from initial population
>> **recombine** 'genes' of selected sub-population
>> **mutate** recombined offspring
>> evaluate offspring
>> **reinsert** best offspring replacing worst parents
> end while

Genetic algorithms can cope with multiple interacting variables, operate under considerable levels of noise, and do not require an intricate understanding of the internal dynamics of a system that is to be optimized.

3.1.2 Ecosystem manipulation

Stochastical approaches, using GAs, have proven to be extremely suitable for optimization problems regarding many variables, such as fermentation media development (Weuster-Botz & Wandrey, 1995; Weuster-Botz et al., 1995) or in the progress of growth optimization considering the process parameters (Muffler & Ulber, 2004). GAs have been successfully employed to search for the best subset from a large set of microbial isolates that can perform a variety of processes (Vandecasteele et al., 2004). The processes optimized include biomass production, biomass minimization, and xenobiotic compound degradation. The most recent studies are experimental multi-objective medium optimizations using a GA supported by

hybrid Genetic Algorithm Artificial Neural Network (GA-ANN) (Franco Lara et al., 2006), optimization of exo-polysaccharide production by hybrid methodology comprising Plackett-Burman design, ANN and GA (Desai et al., 2006), optimization of δ-endotoxin production by Response Surface Methodology (RSM) and ANN (Moreira et al., 2007), modeling and optimization of fermentation factors for alkaline protease production using a feed-forward neural network and GA (Rao et al., 2007), optimization of fermentation media using neural network and genetic algorithm (Nagata and Chu, 2003), optimization of biodegradation of naphthalene by an isolated microorganism by response surface methodology (Martin & Sivagurunathan, 2003), and tryptophan-5-halogenase activity assay formulation for enzyme activity optimization (Muffler et al., 2007).

A GA can be used to manipulate microbial ecosystem factors to obtain a desirable functional behavior. There are two ways being used to date. In the first approach, efficient mixed cultures can be designed by determining which isolated strains to combine for optimal functional performance (Jarvis & Goodacre, 2005; Vandecasteele, 2004). Here, when designed and constructed appropriately, artificial microbial ecosystems exhibit complex behaviors that are observed in a variety of large-scale ecological systems (Kambam et al., 2008), and perform functions that are difficult or even impossible for individual strains or species (Brenner et al., 2008). These attractive traits rely on two organizing features: communicating with one another and the division of labor. By trading metabolites or by exchanging dedicated molecular signals, each population or individual responds to the presence of others in the consortium (Keller and Surette, 2006). This improves the overall output of the consortium that relies on a combination of tasks performed by a constituent individual or sub-populations (Brenner et al., 2008). If the components of an artificial microbial ecosystem are manipulated, the consequence of altering system complexity can be further explored.

It is possible to use a genetic algorithm to manipulate environmental conditions and drive an already existing ecosystem in a desired direction, e.g. maximized degradation rate (Kucharzyk et al., 2010). Certain environmental conditions can influence and cause shifts in ecosystem dynamics (Vandecastelle et al., 2004). Most applications using microbial consortia are in the field of industrial fermentation, where medium compositions are manipulated to maximize production of various chemicals (Bapat & Wangikar, 2004; Etschmann et al., 2004; Fang et al., 2003; Patil et al., 2002; Weuster-Botz et al., 1995; Weuster-Botz et al., 1996). Similar attempts have been made to optimize medium conditions for oil degradation by a pure culture (Li et al., 2004) and for the growth of insect cells (Martin & Sivagurunathan, 2003). An approach based on changing environmental conditions would start with identifying a set of conditions that influence ecosystem dynamics and that can be manipulated experimentally. Such conditions taken under consideration may include chemical and physical factors such as temperature, pH, salinity, light treatment, and mixing. They could also include concentrations of electron donors, electron acceptors, and other chemicals (Vandecastelle et al., 2004).

3.1.3 Genetic algorithm application to optimization of *in situ* perchlorate biodegradation

Today, a wide variety of *in situ* biological treatment approaches are available to remediate perchlorate from ground and surface waters and soil, and remediation tools and techniques are available from a collection of technology vendors and environmental consultants (Ooi & Tan, 2003). Biological *ex situ* treatment systems for perchlorate, as well as the isolation and

characterization of numerous pure cultures of perchlorate-degrading bacteria from natural environments, has prompted significant research concerning the potential for *in situ* perchlorate treatment through electron donor amendment to soils and groundwater (Aziz & Hatzinger, 2009). Because of its unique chemical stability under environmental conditions and its high solubility (Urbansky, 2002), microbial reduction of perchlorate was identified as the most feasible method of remediation of contaminated environments. The presented technology avoids the production of hazardous waste streams that require further treatment or disposal and addresses the need to develop *in situ* approaches for the remediation of perchlorate contamination of groundwater.

The overall goal of the *in situ* perchlorate bioremediation with the GA application is to engineer natural subsurface microbial communities (aquifer biofilms), to give them the ability to degrade (reduce) perchlorate, even in the presence of oxygen and without the addition of genetically engineered microorganisms (GMOs) to the environment. This approach is called "*engineered intrinsic bioremediation*." In the search for efficiently degrading mixed microbial cultures two approaches can be implemented. The first approach uses a GA to manipulate environmental conditions and drives an existing ecosystem in a desired direction, and the second approach uses a different GA to design efficient mixed microbial consortia by determining which isolated strains to combine for optimal functional performance. For that purpose several members of the (per)chlorate strain collection identified and selected as the most efficient in the perchlorate degradation process can be candidates for optimization (Table 1).

NAME	ATTCC / DSMZ	CR/PR*
Pseudomonas chloritidismutans	ATCC # BAA-775	CR
Ideonella dechloratans	ATCC # 51718	CR
Dechlorosoma sp. KJ	ATCC # BAA-592	PR
Dechloromonas agitata	ATCC # 700666	PR
Dechlorosoma suillum	ATCC # BAA-33 / DSMZ 13638	PR
Azosypyra oryzae	DSMZ 1199	PR
Dechloromonas hortensis	MA-1 DSM 15637	PR
Dechloromonas sp. Miss R	Courtesy of J. Coates lab	PR
Dechloromonas denitrificans	ATCC BAA-841, CIP 109443	CR,PR
Rhodobacter capsulatus	DSMZ 155	CR,PR

Table 1. Examples of known perchlorate- and chlorate-degrading bacteria, used in the GA optimization experiment. *Perchlorate reducers are indicated as PR, chlorate as CR.

In the first part of the project a GA was used as an alternative method for directing and artificially defining a set of environmental conditions for naturally occurring microbial consortia and pure cultures to achieve maximum rates of perchlorate degradation. Samples collected from several areas contaminated with perchlorate were used along with pure cultures of perchlorate reducing microorganisms. The initial population (the algorithm's equivalent of a chromosome) was generated at random; a subunit of the bit string (the algorithm's equivalent of gene) gives the value of one parameter. Each experiment was performed in four replicates and a complete chromosome was composed of 36 bits, consisting of 9 medium components of 4 bit each (Table 2).

	GA configuration
Variables	9
Population size	11 (single strains); 12 (consortia)
Generation gap	1
Selection probability	0.5
Mutation probability	0.5
Total bits in chromosome	36

Table 2. Parameter settings for the genetic algorithm.

The GA used here followed the generational model and had a population size of 11 (single strains) or 12 (consortia). Each solution was represented as a string of 9 values, encoding values for variables of environmental conditions. In this way, each solution encoded for a specific set of environmental conditions selected in the experiment (Table 3).

INITIAL RANGES OF VARIABLES	
pH	6.8 - 8.0 every 0.1 unit
NH_4Cl	0.125 - 0.375 (g/L) every 0.02 g
NaH_2PO_4	0.3 – 0.9 (g/L) every 0.1 g
$NaHCO_3$	1.25 – 3.75 (g/L) every 0.2 g
KCl	0.05 – 0.015 (g/L) every 0.05 g
Acetate	1 - 10 mM every 1 mM
Perchlorate	60 - 400 every 10 ppm
Trace minerals	0-10 (ml/L) every 1ml/L
Vitamins	0-10 (ml/L) every 1ml/L

Table 3. Ranges of environmental conditions used for the optimization with the GA.

The initial population was generated at random. Fitness values were linearly rescaled, with $\mu' = \mu$ and $f_{max'} = 0$. Roulette Wheel selection was used and no elitism was applied. Single crossover was performed on each pair of selected individuals with probability of 0.5 per bit. Over the course of eleven generations of optimization using a GA, a statistically significant 78.9-fold increase in average perchlorate degradation rate by *Dechloromonas spp.* KJ and *Dechloromonas* Miss R was observed, when optimization of consortia (Pl6 and Cw3) resulted in 109 and 143-fold increase in average perchlorate degradation rate (Kucharzyk et al., 2011) (Fig.3). The data obtained in this part of GA optimization provided a composition of an optimal medium for maintaining mixed cultures in further analysis and entailed the use of the GA to artificially construct a consortium from 10 isolates such that the consortium is optimized for the reduction of perchlorate (in progress).

In the next experiment, the GA used followed the generational model and has a population size of 10. A higher population size would most likely increase the efficiency of the optimization; however, we consider 12 experiments in fourfold the maximum number that is logistically feasible. Each solution was represented as a string of 10 bits, encoding the presence or absence of the corresponding microorganism. In this way, each solution was encoded for a specific microbial consortium. The initial population was generated at random. Fitness values were linearly rescaled with $\mu'=\mu$ and $f_{max'}=2\mu$ (where μ and μ' are the

average fitness of the parent population before and after rescaling, respectively, and f_{max}' is the maximum fitness of the parent population after rescaling). If this yields negative values, the fitnesses is rescaled so that $\mu'=\mu$ and $f_{min}=0$ (where f_{min} is the minimum fitness of the parent population after rescaling). Roulette wheel selection is used, and elitism is applied. Single crossover is performed on each pair of selected individuals with a probability of 0.90. Mutation is performed by flipping bit values with a probability of 0.01 per bit (Goldberg, 1989). To evaluate the fitness (perchlorate reduction rate/extent) of each individual in a generation, a method for assaying perchlorate concentrations using a fluorescent dye (Kucharzyk et al., 2010) is used.
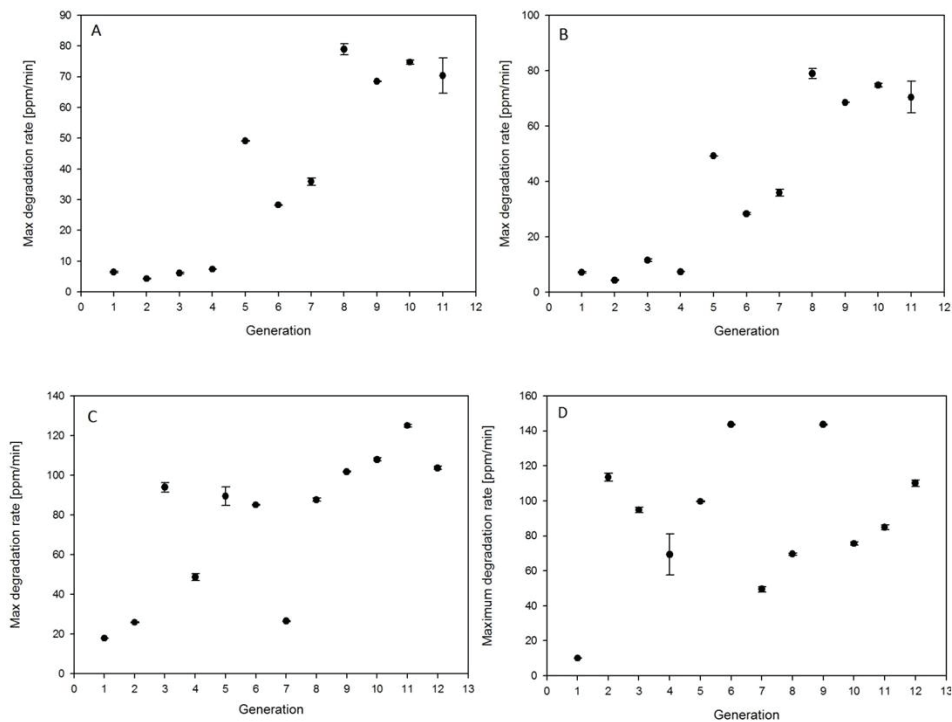

Fig. 3. Average degradation rates values of (A) Dechlorosoma sp. KJ, (B) Dechloromonas Miss R, (C) Cw3 consortium, (D) Pl6 consortium.

We expect that the analysis of the various fitness levels associated with particular strain combination show that the effect of single strains on the dynamics of mixed cultures will depend on what other strains the organism was combined with. The same strain can have positive, neutral or negative effect on between-generation variability.Similarly to results in several of Vandecasteele (2004) experiments, we expect the GA to be able to optimize efficient mixed microbial cultures in each of the experimental scenarios.

As Vandecasteele et al (2004) proposed, we believe that an ecological mechanism can be proposed to explain formation of highly effective microbial community. It appears as if early on in the optimization, the GA quickly eliminates certain strains from consortia. These could be strains that have a dominating overall negative influence on the productivity of the

consortia. On the other hand, some strains quickly seemed to be positively selected. These could be strains that have a high biomass production and an overall positive influence on the consortia they are a member of. We also propose that the algorithm is seeking out clusters of highly productive organisms i.e. building blocks (Holland (1975) that function well together and is then recombining these clusters into larger scale consortia. Such groups of organisms could have a high biomass production because they have a positive influence on each other's growth or because they target different ranges of nutrient sources within the growth medium.

3.1.4 Advantages and limitations of GA application

The use of stochastic search procedures based on genetic algorithms (GAs) in the experimental optimization of media formulation has been lately applied in an efficacious manner compared to other methods, like statistical design of experiments (Park et al., 1998). The success of this approach is specially associated with the recent advances in the application of miniaturisation and parallelization techniques to bioreactors allowing the implementation of a large number of simple batch experiments which can be carried out simultaneously (Zafar et al., 2010). The careful manipulation of environmental conditions can result in precise shifts in the make-up of a microbial ecosystem, which can in turn translate to desirable changes in overall functionality. The successful execution of the manipulation of microbial systems in either of these two manners will often be a challenging experimental task (Vandecasteele, 2006). While statistical methods give better interpretation of an optimized response in term of variance, GA gives better point of prediction. GA is capable of exploring large variable spaces with the additional advantage of an evolutionary adaptation through selection, information exchange (crossing over), and mutation. The strategy of "survival of the fittest" is applied according to the optimization objectives (Zafar et al., 2010). GA has been successfully utilized for kinetic parameters estimation in biotechnological processes (Park et al., 1997; Sa'iz et al., 2003) such as alcoholic fermentation.

In the field of bioinformatics there have been a number of reports showing the capability of GA to effect data reduction in order to improve the performance of predictive models. For example, for classification problems using gene expression data (Li et al., 2001; Ooi & Tan, 2003), improved classification accuracy was obtained following GA variable reduction. In a similar study, Chuzhanova et al. (1998) used GA with the Gamma (near-neighbour) test for feature selection of genetic sequence data, which again leads to improved classification results. GA optimization has also been applied to other bioinformatics-related problems such as sequence alignment (Notredame et al., 1998) and phylogenetic tree construction (Lewis, 1998). However, in work related to evolutionary algorithm optimization of laboratory processes, we observe that most research into noisy fitness functions make use of oversampling to improve the precision of the fitness estimate (Meekof & Soule, 2010). This noise is inherent in both the sensors and in the variability of the processes themselves, particularly in applications to biological processes. GAs cannot effectively solve problems in which the only fitness measure is a single right/wrong measure (like decision problems), as there is no way to converge on the solution. In these cases, a random search may find a solution as quickly as a GA. However, if the situation allows the success/failure trial to be repeated giving (possibly) different results, then the ratio of successes to failures provides a suitable fitness measure.

3.2 Perchlorate phytoremediation
3.2.1 Background and theory
Phytoremediation describes various *in situ* mechanisms by which vegetation is used to treat hazardous wastes. It is a demonstrated low-cost technology that has effectively treated a wide range of contaminants, involving perchlorate. The U.S. phytoremediation market now comprises $100–150 million per year, or 0.5% of the total remediation market (Glass, 1999). In comparison, bioremediation comprises about 2% of the total remediation market (Pilon-Smiths, 2005). Commercial phytoremediation involves about 80% organic and 20% inorganic pollutants. The U.S. phytoremediation market has grown two to threefold in the past 5 years, from $30–49 million in 1999 (Glass, 1999). The fact that phytoremediation is usually carried out *in situ* contributes to its cost-effectiveness and may reduce exposure of the polluted substrate to humans, wildlife, and the environment. Phytoremediation became popular among the general public as a "green clean" alternative (Pilon-Smiths, 2005).

Phytoremediation techniques	Mechanism	Media
Rhizodegradation	Contaminant uptake by plant roots	Surface water and water pumped through roots
Phytotransformation	Uptake and degradation of contaminants	Surface and groundwater
Plant-assisted bioremediation (microbial)	Degradation of contaminants in the rhizosphere using microbial enzymes	Groundwater , water within the rhizosphere and soil
Phytoextraction	Direct uptake of the contaminant by the plant tissue with the removal from the plant	Soil
Phytostabilization	Uptake of contaminants by the rhizosphere and movement of the contaminant to the aboveground parts of the plant	Groundwater, soil, mining tailings
Phytovolatilization	Uptake and transpiration of contaminants, primarily organic compounds, by plants	Soil, groundwater
Removal of aerial contaminants	Uptake of various volatile organics by leaves	Air

Table 4. Mechanisms for the removal of toxic contaminants from the environment and the techniques used in phytoremediation (Adapted from Singh et al., 2002).

Phytoremediation is a technique that takes advantage of plants' natural abilities to take up, accumulate and/or degrade constituents of their soil and water environment. It contains a variety of remediation techniques (Table 4) that include many treatment strategies.
Some forms of phytoremediation result in the destruction of the contaminant while others in the uptake of the contaminant into the plant roots, stems, and /or leaves (Van Nevel et al., 2007) (Fig.4).

Phytoaccumulation
Take up of perchlorate, water and nutrients through plant's roots; the contaminant mass is not destroyed but ends up in the plant shoots and leaves and can be harvested for disposal. Phytoaccumulation of a fraction of the perchlorate taken up by plants has been confirmed by the detection of perchlorate in food crops, dairy milk, and human breast milk.

Phytodegradation
Biodegradation of toxic contaminants by the enzymes present in plant tissues. Perchlorate taken up into plants is phytodegraded slowly by perchlorate reductase enzyme to chloride via intermediate products, chlorate ($ClO3^-$) and chlorite ($ClO2^-$). The slow phytodegradation results in accumulation of perchlorate in plant tissues, which potentially is recycled in some cases into the environment via leaching from decaying senesced leaves.

Rhizodegradation
Occurs in the soil surrounding plant roots. Natural substances released by plant roots serve as substrates for the microorganisms present in the rhizosphere and speed up contaminant degradation. Perchlorate-reducing bacteria can grow on a variety of substrates (*e.g.*, *organic* acids, ethanol, simple sugars, amino acids, and possibly hydrogen)
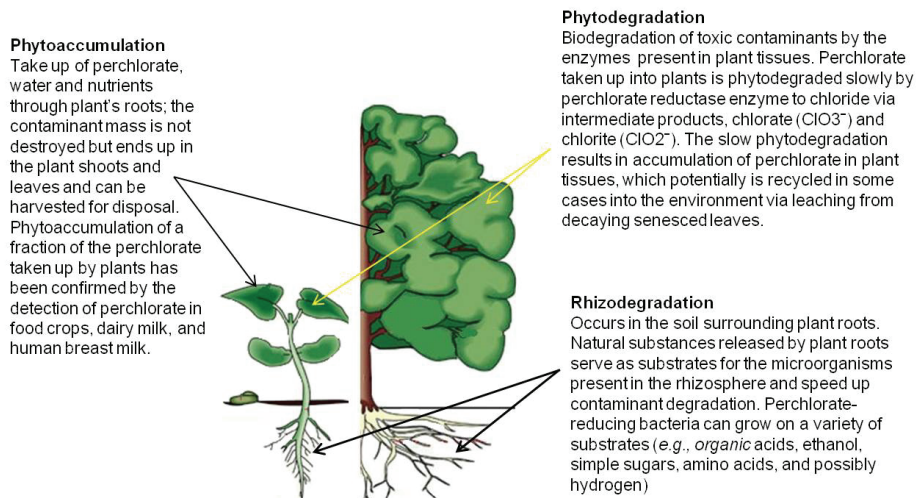
Fig. 4. Predominant processes occurring during perchlorate phytoremediation. Uptake and phytoaccumulation may pose risk to the environment because the slow phytodegradation result in accumulation of a fraction of the extracted perchlorate, primarily in the leaf tissue.

Phytoremediation avoids the need for soil excavation and transport, is relatively cheap, and causes less disruption to ecosystems than physical, chemical, or microbial remediation (Arthur et al., 2005). Plants can also stabilize contaminated soil and provide conditions favorable for microbial colonization of the rhizosphere for symbiotic degradation and detoxification of pollutants (Cherian & Oliveira, 2005).

However, using plants for environmental clean-up often takes longer than other remediation techniques and is most suited to sites where contaminants are present at shallow levels within the reach of plant roots (Doty, 2008). The ability of certain plants to tolerate, detoxify, and store high concentrations of heavy metals in their tissues is of great importance for the development of phytoremediation and phytomining applications (Doran, 2009). However, the metal accumulating species are generally too small and slow-growing for direct practical use. Any attempt to genetically modify high-biomass plants such as tobacco to equip them with metal accumulator traits depends on our understanding of the key biochemical and physiological mechanisms involved. At the present time, although substantial progress has been made in these areas in recent years, much further work is required to elucidate the interactions between plant cells and toxic chemicals in the environment (Doran, 2009).

3.2.2 Perchlorate phytoremediation status
Nowadays, several plant-based experimental systems are available and these include cell extracts, dedifferentiated plant cell cultures such as callus and cell suspensions, differentiated organ cultures such as roots and shoots, explants such as leaf disks and excised roots, whole plants in hydroponic culture, whole plants in potted soil under

greenhouse cultivation, and whole plants in the field (Chaudhry et al., 2005). Terrestrial plants that are able to remove perchlorate from groundwater and soil include species such as black willows (*Salix nigra, Salix caroliniana*), eucalyptus (*Eucalyptus*), and loblolly pine (*Pinus taeda*). Aquatic plants that have been successfully tested for perchlorate removal were water weed (*Elodea cadadensis*), parrot-feather (*Myriophyllum aquaticum*), duckweed (*Spirodela polyrhiza*) and cattails (*Typha spp*) (Nzegung & McCutcheon, 2003). Perchlorate has also been detected in tobacco (*Nicotiana tabacum* L.) (Ellington et al., 2001), food crops such as cucumber (*Cucumis sativus*) and soybean (*Glycine max)* (Yu et al., 2004). Up to 300 mg kg/L fresh water (on the basis of fresh wet weight) perchlorate uptake was found in salt cedar (*Tamarix ramosissima*) in Las Vegas Wash (Urbansky et al., 2000). Research up to date demonstrates that perchlorate is mainly accumulated in leaves rather than in roots. Laboratory studies also imply that phytodegradation in plant tissues occurs fairly slow (Nzegung & McCutcheon, 2003).

Two major mechanisms for the phytodegradation of perchlorate have been identified: the uptake and phytodegradation, and rhizodegradation (Nzegung et al., 2004) (Fig.4). The mechanisms of perchlorate transport in plants are not fully understood. Perchlorate is a nonvolatile and highly mobile anion, which is not readily adsorbed by the negatively charged surface of most soils. Perchlorate transport in plants might be linked with passive transport of water across the plasma membranes of root cells (i.e., simple diffusion or facilitated diffusion) (Tan et al., 2004). Perchlorate uptake may be also dependent on water mass flow or transportation. As long as it is not leached or precipitated as a salt, perchlorate in the rhizosphere has two main fates: it is either taken up by a plant or degraded in the rhizosphere. Under anaerobic condition, rhizodegradation dominates and is facilitated by low availability of electron donors (Nzengugn & McCutcheon, 2003) and high availability of electron donors. Certain anaerobic bacteria (perchlorate reducers) are necessary for this process, and they are capable of reducing perchlorate to chloride via chlorate and chlorite intermediates through a stepwise reaction (Urbansky, 2000):

$$ClO_4^- \rightarrow ClO_3^- \rightarrow ClO_2^- \rightarrow Cl \tag{1}$$

In anaerobic microcosms, direct evidence for this stepwise reduction has been demonstrated by the appearance of chlorate and chloride and disappearance of perchlorate in the rhizosphere; chlorite was nor detected and is believed to be a short-lived intermediate (Nzengung et al., 2004). Plant uptake of perchlorate dominates under the aerobic conditions and the compound is taken up by roots and stored in tissues where it may be phytodegraded (Nzengung et al., 2004). Phytodegradation appears to be an enzymatically driven process that takes place on the order of hours, whereas rhizodegradation takes place on the order of days. There are very limited data on the presence of chlorate and chlorite intermediates within plant tissues after perchlorate uptake. To date Aken and Schnoor (2002) have provided the most unequivocal evidence for perchlorate phytodegradation by using radiolabeled perchlorate ($^{36}ClO_4^-$) in a 4-week uptake experiment using hybrid poplar trees (*Pinus deltoids x nigra*). Radioactive chlorate, chlorite and chloride were detected in the solution after 30 days. These data provide evidence that perchlorate is metabolized within poplar plant tissues through chlorate and chlorite intermediates to chloride, which is then exuded from the plant roots to the surrounding soil. It remains unknown whether other plant species are capable of perchlorate phytodegradation or if phytodegradation differs in plant organs or as a function of tissue age (Aken & Schnoor, 2002).

3.2.3 Advantages and limitations

Phytoremediation is recognized as a fast-growing and cost-effective technology to remediate hazardous toxic metals from contaminated sites. However, delivering a remediation system that is applicable to specific contaminated soils is a relatively recent focus. It has the advantages of low cost, high public acceptance and low amounts of secondary waste products (Singh et al., 2003). Phytoremediation can treat other co-contaminants such as chlorinated solvents and explosives including (N-nitrosodimethylamine) (Yifru & Nzegung, 2006). Table 5, summarizes the advantages and limitations and reveals that many of them are a direct result of the biological aspect of this type of treatment system.

Advantages	Limitations
Cost effective	Depth of soil and climate restrictions
Remediation of large areas of soil	Slower than conventional methods
Environmentally friendly	Seasonally effective
Phytoremediation sites are low maintenance	Effective only for moderate hydrophobic contaminants
Involves no noisy equipment In situ	No direct regulations are known yet
Soils remain in place, are usable following treatment	Contaminants may enter food chain by animal consumption
Transfer is more rapid than natural attenuation	Accumulation of toxic contaminants may be toxic to plants
Fewer secondary wastes	Limited mass transfer associated with biotreatments
Fewer air and water emissions	Climatic changes may diversify the phytodegradation

Table 5. Advantages and limitations of phytoremediation of perchlorate and its co-contaminants.

The limitations of perchlorate phytoremediation include depth and climate restrictions as well as the potential for transfer for contaminants from soil and groundwater into the food chain (Nzgengung et al., 2009). Phytoremediation of perchlorate is also relatively slow comparing to its microbial reduction and it is subject to the seasonal climate variations. Perchlorate also may have a toxic effect on certain plant species and hyperaccumulating in the tissues could be toxic to the plant biodegrading it itself. Basic research is still needed by plant biologists for a deeper understanding of plant decontamination processes. The concept of genetically modified transgenic plants and their innovative genes that regulate toxic metal uptake is today's cutting-edge research (Rajagopalan et al., 2006).

4. Microbial ClO_4^- reduction with Fe(0) and inorganic electron donors

4.1 Background and theory

Inorganic electron donors can overcome the disadvantages of organic substrates such as acetate or lactate, and thus are currently the focus of the study for biological reduction of perchlorate. Batch and continuous flow bioreactors have been evaluated utilizing H_2 to support autotrophic perchlorate reduction (Nerenberg & Ritmann, 2004). Hydrogen gas (5%), along with carbon dioxide, was provided to achieve 30–39% perchlorate reduction in

an autotrophic bioreactor. Although H_2 is a good energy substrate, its handling and storage may be a safety issue. Fe(0) is a strong reducing agent (E^0 = -0.44V), and has been used in recent years to treat oxidized pollutants such as nitroaromatics, nitramines, and azo dyes through reductive transformation (Perey et al., 2002). It is also successfully applied in permeable reactive barriers for the remediation of chlorinated volatile organic compounds (Lai et al., 2006). Thermodynamically, perchlorate is readily reducible by Fe(0) ($\Delta G^{0'}$) -596.27 kcal mol^{-1}), however the energy barrier to the reduction is large (Moore et al., 2003) and the chemical reduction is too slow for the zero-valent iron to be used *in situ* for remediation. Under anaerobic conditions, iron corrosion produces hydrogen gas through the reduction of protons (Eq. 2) and in the presence of hydrogenotrophic organisms the cathodic hydrogen may be utilized to degrade perchlorate (Son et al., 2006), nitrate, chlorinated solvents and sulfate (Weathers et al., 1997).

$$Fe^0 + 2H_2O \rightarrow Fe_2^+ + 2OH^- + H_2 \text{ (gas)} \qquad (2)$$
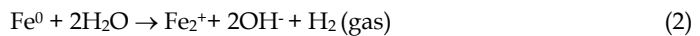
Fe^+ and S_2^- are examples of other inorganic electron donors used by ClO_4^- reducing bacteria (Achenbach et al., 2006). Granular S_0 in packed bed bioreactors has been used successfully as electron-donating substrate in autotrophic denitrification processes for drinking water (Koeing & Liu, 2001; Xu et al., 2003). Granular S_0 is insoluble and thus provides a slow release supply of electrons on demand, offering advantages of low maintenance and low cost. Therefore it's potential as an electron-substrate for ClO_4^- reduction is being explored. The expected stoichiometry of the reaction is as follows:

$$3ClO_4^- + 4S_0 + 4H_2O \rightarrow 4SO_4^{2-} + 8H^+ + 3Cl^- \qquad (3)$$

For the first time Ju et al. (2008) evaluated various inocula sources for their ability to utilize inorganic compounds such as H_2, Fe^0 and reduced sulfur compounds (i.e., S_0, S_2^- and $S_2O_3^{3-}$) as electron-donating substrates for the chemolithotrophic reduction of perchlorate. The coupling of perchlorate reduction to chloride with elemental sulfur oxidation to sulfate is an exergonic reaction with standard Gibb's free energy ($\Delta G^{0'}$) of -1146.9 kJ mol^{-1} ClO_4^- (37.6 mol ATP mol^{-1} ClO_4^-). This chemolithotrophic reaction is bioenergetically comparable to chemoorganotrophic perchlorate reduction, for example the ($\Delta G^{0'}$) of perchlorate reduction linked to acetate oxidation is -1210.9 kJ mol^{-1} ClO_4^- (39.7 mol ATP mol^{-1} ClO_4^-).

4.2 Technology development status
The most recent studies on microbial perchlorate reduction were conducted by Shrout et al. (2005). They ran the experiments in the presence of zero-valent iron using a mixed culture obtained from an anaerobic digester, however, they reported that the addition of Fe (0) to the anaerobic culture resulted in slower rate of perchlorate reduction. The inhibitory effect of zero-valent iron on perchlorate was attributed to the increase in pH and encapsulation of bacteria by iron precipitates. High concentrations of bicarbonate (1260 mg/L) and phosphate (430 mg/L) in the culture media resulted in the formation of vivianite, $Fe_3(PO_4)_2$, and siderite, $FeCO_3$, the major iron precipitates identified on Shrout et al. (2005) research, but Yu et al. (2006) claim they are not likely to occur in typical groundwater conditions.
In contrast, Yu et al. (2006) showed that zero-valent iron was capable of serving as electron donor for perchlorate reduction by providing hydrogen to a hydrogen utilizing autotroph (*Dechloromonas sp*. HZ). Initially, the activity of *Dechloromonas sp*. HZ pure culture was

strongly dependent on solution pH; however, once perchlorate reduction was established, the microbial reduction process was sustained even at pH 9 (Son et al., 2006). While Yu et al. demonstrated the feasibility of microbial perchlorate reduction supported by zero-valent iron, their experimental conditions were not typical of environment conditions commonly found in natural and engineered systems. As the logical extension to the proof-of-concept studies employing batch pure cultures studies, flow-through column studies with environmentally relevant mixed cultures were needed to further promote and enhance the potential of the integrated Fe(0)-cell system for perchlorate remediation.

The study of Son et al. (2006) investigated the feasibility of integrated iron-biological perchlorate reduction through both batch and column reactor experiments. The study proved the complete disappearance of perchlorate only in the presence of Fe(0) (Fig.5A), H_2 and acetate. Perchlorate (65 mg/L) in the reactors containing both Fe(0) and cells was completely removed to below the detection limit of 0.02 mg/L in 8 days. In contrast, only 15% of the initial perchlorate was removed in the Fe(0)- only reactors (no cells) over 10 days, indicating iron alone was not effective in removing perchlorate. A chloride balance performed in the batch experiments using high-purity iron (Alfa Aesar, Ward Hill, MA) indicated that perchlorate was reductively transformed to chloride (Cl^-) (Fig5B). In this integrated iron–biological system, iron could serve as a precursor of hydrogen gas, which could be used as electron donor for mixed cultures to reduce perchlorate.
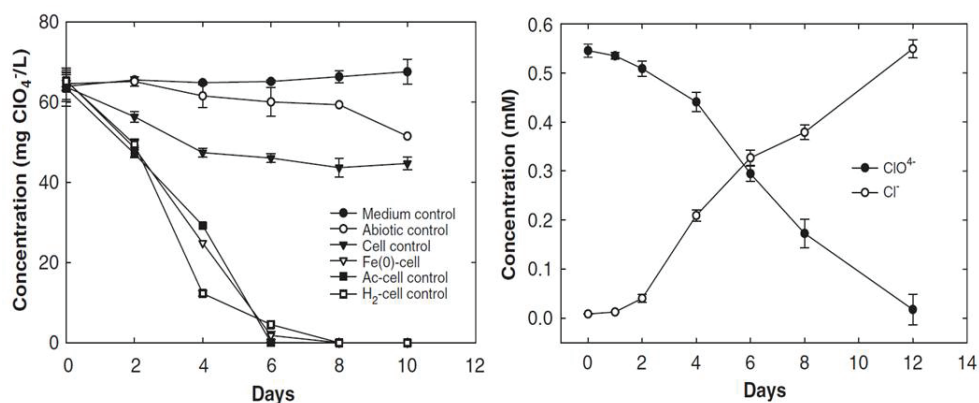

Fig. 5. A. Perchlorate removals in the iron-mediated microbial culture. Fe(0)-cell batch reactor contained 2 g of Master Builder's cast iron. B. Chloride balance in microbial perchlorate reduction by pure iron granules. Initial concentration of perchlorate was 55mg/L. Batch reactor contained 2 g of Alfa Aesar high purity iron granules. (Adopted from Son et al., 2006).

Bardiya and Bae (2005) studied ClO_4^- reduction with S^0 and $S_2O_2^{3-}$ as electron donors with various inocula sources such as digester sludge and primary settled sludge, but their results showed no perchlorate removal after 25-d incubation. Ju et al. (2008) experimental data showed that these inocula sources could utilize the reduced sulfur compounds to support ClO_4^- reduction, albeit at lower rates compared with H_2. However, when the S^0-oxidizing enrichment culture was used as the inoculum, the rates of ClO_4^- reduction were significantly

improved (Ju et al., 2008). Testing the enrichment culture utilizing S^0 sulfur as an electron donor revealed that S^0 was the best electron donor with more than 95% ClO_4^- removed after seven days of incubation (Fig.6a) and $S_2O_3^{2-}$ was the second best electron donor for perchlorate reduction. The patterns observed in perchlorate reduction were reflected in the Cl^- and SO_4^{2-} production.

S^0 has been discovered as a novel electron donor for microbial perchlorate reduction. Because it is insoluble in water, S^0 granules would be particularly suitable as a slow release electron donor for packed-bed bioreactors intended for perchlorate reduction. A comparable processes known as sulfur limestone autotrophic denitrification has been used for NO_3^--removal in wastewater and drinking water (Flere & Zhang, 1999; Koeing & Liu, 2001).
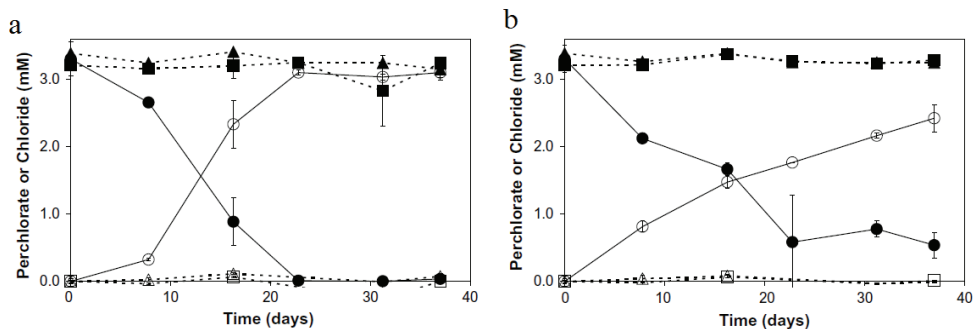
Fig. 6. Perchlorate reduction by various electron donors inoculated with activated sludge (5% v/v). (a) S^0 (0.64 g l-1) as electron donor. (b) Fe^0 (3.4 g l-1) as electron donor. Legend: (filled circles) ClO_4^- with live inoculum; (filled triangles) ClO_4^- in heat-killed inoculum control; (filled squares) ClO_4^- in medium only control; (empty circles) Cl^- with live inoculum; (empty triangles) Cl^- in heat-killed inoculum control; (empty squares) Cl^- in medium only control. (Adapted from Ju et al., 2008).

5. Conclusions

A variety of perchlorate remediation technologies are currently commercially available. One of them - biological degradation involves perchlorate-reducing bacteria (PRBs), which are widespread in the environment. PRBs have the ability to grow in either the presence or absence of air, provided proper nutrients are available in the environment. Both in situ and ex situ biological treatment systems have already been applied at full scale to treat perchlorate.

Implementation of novel techniques such as optimization and creation of microbial consortia using a Genetic Algorithm have a great a chance to improve the existing technology. Here, genetic algorithms could become a tool in environmental microbiology for an efficient control of the functioning of natural and undefined microbial ecosystems. Phytoremediation, a fairly new technology, is anticipated to be most applicable to vadose zone source areas in soil, groundwater, or surface runoff. Field-scale application of phytoremediation would require adequate space to establish the plants, and they may need special handling afterwards, if rhizodegradation is not enhanced and perchlorate salts

accumulate in the plant tissues. Complete removal of perchlorate by iron-supported anaerobic cultures could be achieved in bench-scale iron columns where zero-valent iron has a potential as a source of electrons in collaboration with biological perchlorate degradation. Use of zero-valent iron may eliminate the need to continually supply electron donors such as organic substrates or explosive hydrogen gas.

6. References

Achenbach, L.A., Bender, K.S., Sun,Y., & Coates,J.D. (2006). The Biochemistry and Genetics of Microbial Perchlorate Reduction. In *Perchlorate. Environmental Occurrance, Interactions and Treatment*. Springer Science and Business Media, Inc., pp. 297-310

Aken, B. & Schnoor, J.L. (2002). Evidence of perchlorate removal in plant tissues (Poplar trees) using radio-labeled 36ClO$_4^-$. *Env Sci and Technol,* 36, 2783-2788.

Arthur, E.L., Rice, P.J., Anderson, T.A., Baladi, S.M., Henderson, K.L.D. & Coats, J.R. (2005). Phytoremediation—An overview. *Crit Rev Plant Sci,* 24:109–122 Aziz, C. & Hatzinger, P.B. (2009). Perchlorate sources, source identification and analytical methods, *In Situ Bioremediation of Perchlorate in Groundwater*. Stroo,H.F. and Ward, C.H. (eds). Springer Science and Business Medi

Aziz, C. & Hatzinger, P.B. (2009). Perchlorate sources, source identification and analytical methods, *In Situ Bioremediation of Perchlorate in Groundwater*. Stroo,H.F. and Ward, C.H. (eds). Springer Science and Business Medi

Bapat, P. M. & Wangikar, P. P. (2004). Optimization of rifamycin B fermentation in shake flasks via a machine-learning-based approach *Biotechnol. Bioeng.*, 86, 201-208

Bardiya, N. & Bae, J. (2005). Bioremediation potential of a perchlorate-enriched sewage 556 sludge consortium. *Chemosphere*. 58:83–90

Blount, B.C., Pirkle, J.L., Osterloh, J.D., Valentin-Blasini, L. & Caldwell, K.L. (2006). Urinary perchlorate and thyroid hormone levels in adolescent and adult men and women living in the United States. *Env Health Perspectives* 114 : 1865–1871

Brenner, K., You, L. & Arnold, F.H. (2008). Engineering microbial consortia: a new frontier in synthetic biology. *Trends in Biotchnol*, Vol. 26 No.9

Bryan, E. H. (1966). Application of the chlorate BOD procedure to routine measurement of wastewater strength. *Journal of Water Pollution Control Federation* 38:1350-1362.

Chaudhry, Q., Blom-Zandstra, M., Gupta, S. & Joner, E.J. (2005). Utilising the synergy between plants and rhizosphere microorganisms to enhance breakdown of organic pollutants in the environment. *Environ Sci Pollut Res,* 12:34–48.

Cherian, S. & Oliveira, M.M. (2005). Transgenic plants in phytoremediation:Recent advances and new possibilities. *Environ Sci Technol*, 39:9377–9390.

Chuzhanova, N.A., Jones, A.J. &Margetts, S. (1998). Feature selection for genetic sequence classification. *Bioinformatics*, 14: 139–143.

Cunniff, S. (2006). Perchlorate: Challenges and lessons. In *Perchlorate: Environmental occurrance , Interactions and treatment*. Gu,B. and Coates,J.D. (eds). New   York, NY: Springer Science and Business Media Inc., pp. 1-15.

Coates, J.D., Michaelidou,U., O'Connor, S.M., Bruce, R.A. & Achenbach, L.A. (2000). The diverse microbiology of (per)chlorate reduction., p. 257-270. In E.D. Urbansky (ed.), Perchlorate in the Environment. Kluwer Academic/Plenum, New York.

de Groot, G. N. & Stouthamer, A.H. (1969). Regulation of reductase formation in *Proteus mirabilis*. I. Formation of reductases and enzymes of the formic hydrogenlyase complex in the wild type and in chlorate resistant mutants. *Archives of Microbiology,* 66:220-233.

Desai, K. M., Akolkar, S. K., Badhe, Y. P., Tambe, S. S. & Lele, S. S. (2006). Optimization of fermentation media for exopolysaccharide production from *Lactobacillus plantarum* using artificial intelligence based techniques. *Process Biochemistry,* 41:1842-1848

Doty, S.L. (2008). Enhancing phytoremediation through the use of transgenics and endophytes. *New Phytol,* 179:318–333.

Doran, P.M. (2009). Application of Plant Tissue Cultures in Phytoremediation Research: Incentives and Limitations. *Biotechnol and Bioengineering*, 103

Ederer, M., Kucharzyk, K.K., Crawford, R.L. & Hess, T.F. (2011). Microbial reduction of chlorate and perchlorate: phylogenetic analysis of the genes encoding the degradation pathways. Perchlorates Production, Uses and Health Effects. Nova Science Publishers, Inc (in print)

Ellington, J.J., Wolfe, N.L., Garrison, A.W., Evans, J.J & Teng, Q. (2001). Determination of Perchlorate in Tobacco Plants and Tobacco Products; *Environ. Sci. Technol,* 35:3113-3218

Etschmann, M.M.W., Sell, D. & Schrader, J. (2004). Medium optimization for the production of the aroma compound 2-phenylethanol using a genetic algorithm. *J Mol Catal B Enzym* 29:187–193

EWG (2007). Rocket fuel in Drinking water: perchlorate pollution spreading nationwide. Copyright 2007-2009, Environmental Working Group. All Rights Reserved. 2007

Fang, B. S., Chen, H.W., Xie, X.L., Wan, N. & Hu, Z.D. (2003). Using genetic algorithms coupling neural networks in a study of xylitol production: medium optimization. *Process Biochem*, 38:979-985

Flere, J.M. & Zhang, T.C. (1999). Nitrate removal with sulfur-limestone autotrophic denitrification processes. *J. Environ. Eng.–ASCE* 125, 721–729

Franco-Lara, E., Link, H. & Weuster-Botz, D. (2006). Evaluation of artificial neural network for modeling and optimization of medium composition with a genetic   algorithm. *Process Biochemistry*, 41: 2200-2206

Glass, D.J. (1999). U.S. and International Markets for phytoremediation, 1999-2000, Needham, MA: D, Glass Assoc.

Gullick, R.W., LeChevallier, M. & Barhorst, T. (2001). Occurrence of perchlorate in drinking water sources. *J Am Water Works Assoc*, 93:66-77

Goldberg, D. E. (1989). Genetic algorithms in search, optimization & machine learning. Reading, MA: Addison-Wesley

Hecht, M.H., Kounaves, S.P., Quinn, R.C., West, S.J., Young, S.M. & Ming, D.W.(2009) Detection of perchlorate and the soluble chemistry of martian soil at the Phoenix lander site. *Science,* 325: 64-67

Holland, J. H. (1975). Adaptation in natural and artificial systems: an introductory analysis with applications to biology control and artificial intelligence. Ann Arbor, MI: University of Michigan Press.

Jackson, P.E., Joseph, P., Patil, L., Tan, K., Smith, P.N., Yu, L., & Anderson,T.A. (2005). Perchlorate accumulationin forage and edible vegetation. *J of Ag Food Chemi,* 53: 369-373

Jackson, W.A., Anderon, T., Harvey, G.J., Orris, G.J., Rajagopalan, S., & Kang,N. (2006). Occurrence and formation of Non-Anthropogenic perchlorate. In *Perchlorate: Environmental Occurrance, Interaction and Treatment.* Gu,B. and Coates,J.D. (eds). pp. 49-69

Jarvis, R.M. & Goodcare, R. (2005). Genetic algorithm optimization for pre-processing and variable selection of spectroscopic data. *Bioinformatics,* 21 (7): 860–868

Ju, X., Sierra-Alvarez, R., Field, J.A., Byrnes, D.J., Bentley, H. & Bentley, R. (2008). Microbial perchlorate reduction with elemental sulphur and other inorganic electron donors. *Chemosphere* 71: 114-121

Kambam, P.K., Eriksen, D.T., Lajoie, J., Sayut,D.J. & Sun, L.. (2008). Design and mathematical modeling of a synthetic symbiotic ecosystem. *IET Syst. Biol*, 2:33–38

Kegley, S.E., Hill, B.R., Orme, S. & Choi,A.H. (2008). Sodium Chlorate - Identification, toxicity, use, water pollution potential, ecological toxicity and regulatory information. PAN pesticide Dababase, Pesticide Action Network, North America . San Francisco, CA.

Keller, L. & Surette, M.G. (2006). Communication in bacteria: an ecological and evolutionary perspective. *Nat. Rev.Microbiol*, 4:249–258

Kirk, A.B., Martinelango, P.K., Tian,K., Aniruddha,D., Smith E.E. & DasGupta,P.K. (2005). Perchlorate and iodide in dairy and breast milk. *Env Sci and Technol* 39: 2011-201

Koenig, A. & Liu, L.H. (2001). Kinetic model of autotrophic denitrification in sulphur packed-bed reactors. *Water Res*. 35, 1969–1978

Kucharzyk, K.H., Crawford, R.L., Cosens, B. & Hess, T.F. (2009). Development of drinking water standards for perchlorate in the United States. *J Environ Manage*, 91(2), 303 10.

Kucharzyk, K.H, R. L. Crawford, A.J. Paszczynski & Hess, T.F. (2010). A Method for Assaying Perchlorate Concentration in Microbial Cultures Using the Fluorescent Dye Resazurin *J. Microbiol. Methods*, 81(1):26-32

Kucharzyk, K.H., Crawford, R.L., Paszczynski, A.J., Soule, T. & Hess, T.F. (2011). Maximizing microbial perchlorate degradation using a genetic algorithm: media optimization. *Appl Environ Microbiol,* (in progress).

Lewis, P. (1998).Agenetic algorithm for maximum-likelihood phylogeny inference using nucleotide sequence data. *Mol. Biol. Evol*, 15:277–283.

Li, L.,Weinberg, C.R., Darden,T.A. & Pederson,L.G. (2001). Gene selection for sample classification based on gene expression data: study of sensitivity to choice of parameters of the GA/KNN method. *Bioinformatics*, 17, 1131–1142

Li, S. X, D. Xing, H. M. Qin, X. B. Yang, and S.C. Tan. (2004). Experimental study on genetic algorithms of medium optimization for oil-degradation. *Chinese J. Analyt. Chem,* 32:481-484.

Martin, A. & Sivagurunathan, M. (2003). Optimization of the biodegradation of naphthalene by a microorganism isolated from petroleum contamination soil. Communication in *Ag and Appl Biol Sci*, v. 68 (2Pt A), 175-180.

Meekhof,T. & Soule, T. (2010). Noise pressure: systematic overestimation of population fitness in genetic algorithms with noisy fitness functions. GECCO 2010: 833-834

Moore, A.M., De Leon, C.H. & Young, M. (2003). Rate and extent of aqueous perchlorate removal by iron surfaces. *Environ. Sci.Technol.* 37, 3189–3198

Moreira, G. A., Michelouf, G. A., Beccaria, A. J. & Goicoechea, H. C.(2007) Optimization of the Bacillus thuringiensis var. kurstaki HD-1δ-endotoxins production by using experimental mixture design and artificial neural networks. *Biochem Engineering Journal*, v. 35:48-55

Motzer, W. E. (2001). Perchlorate: problems, detection, and solutions. *Environmental Forensics,* 2 (4):301-311.

Muffler, K., Retzlaff, M., van Pee, K-H. & Ulber, R. (2004). Optimization of halogenase enzyme activity by application of a genetic algorithm. *J Biotechnol* 127: 425-433

Muffler, K.,Retzlaff, M., P'ee, K-H., Ulber, R. (2007). Optimisation of halogenase enzyme activity by application of a genetic algorithm. *J Biotechnol,* 127:425–433

Nagata, Y. & Chu, H. (2003). Optimization of a fermentation medium using neural networks and genetic algorithms. *Biotechnol Letters* 25: 1837-1842

National Research Council (2005). Health Implications of Perchlorate Ingestion Committee to Assess the Health Implications of Perchlorate Ingestion. National Academy of Sciences, p. 9.

Nerenberg, R., Rittmann, B.E. & Najm, I. (2002). Perchlorate reduction in a hydrogen-based membrane-biofilm reactor. *J. Am. Water Works Assoc.* 94, 103–114

Notredame,C., Holm,L. and Higgins,D. (1998). Coffee: an objective function for multiple sequence alignments. *Bioinformatics*, 14, 407–422.

Nzengung,V.A. & McCutcheon,S.C. (2003). Phytoremediation of perchlorate. In McCutcheon, S.C. & Schnoor, J.L., eds Phytoremediation: transformation and control of contaminants. Wiley-Interscience Publichers, Hoboken, NJ, USA, pp 863-885

Nzegung, V.A, Penning, H. & O'Niell, W. (2004). Mechanistic changes during phytoremediation of perchlorate under different root zone conditions. *Int J Phytoremediation*, 6:63-83

Nzengung, V.A., Lieberman, M.T., Stroo, H.F. & Evans, P.J. (2009) Emerging technologies for perchlorate remediation. In Ward, C.H & Stroo, H.F. eds In situ bioremediation of perchlorate in groundwater. Springer Science Business Media, LLC, New York, NY, USA

Orris, G.J., Harvey, G.J., Tsui, D.T., & Eldrige,J.E. (2003). Preliminary analyses for perchlorate in selected ntural materials and their derivative products. US Geological Survey, Open field Report 03-314.

Ooi, C.H. & Tan, P. (2003). Genetic algorithms applied to multi-class prediction for the analysis of gene expression data. *Bioinformatics*, 19:37–44.

Park, T.Y. & Fromet, G.F. (1998). A hybrid genetic algorithm for the estimation of parameters in detailed kinetic models. *Comp Chem Eng,* 22:103–10.

Patil, S. V., Jayaraman, V.K. & Kulkarni, B.D. (2002). Optimization of media by evolutionary algorithms for production of polyols. *Appl. Biochem. Biotechnol,* 102-103:119-128.

Perey, J.R., Chiu, P.C., Huang, C.P. & Cha, D.K. (2002). Zero-valent iron pretreatment for enhancing the biodegradability of azo dyes. *Water Environ. Res*. 74, 221–225

Pilon-Smiths, E. (2005). Phytoremediation. *Annu Rev Plant Biol,* 56: 15-39

Rao, S.C., Sathish, T., Mahalaxmi, M., Laxmi, G.S., Rao, S.R. & Prakasham, R.S. (2007). Modelling and Optimization of fermentation factors for enhancement of alkaline protease production by isolated Bacillus circulans using feed-forward neural network and genetic algorithm. *J Appl Microbiol*, 104 : 889-898

Rajagopalan, S., Anderson,T.A., Fahlquist,L., Rainwater,K.A., Ridley,M., and Jackson,W.A. (2006). Widespread Presence of Naturally Occurring Perchlorate in High Plains of Texas and New Mexico. *Environmental Science & Technology,* 40: 3156-3162

Reeves, C. R. (1993).Using genetic algorithms with small populations. In Proceeding of the Fifth International Conference on Genetic Algorihms, pp. 92-99. Edited by S. Forrest. San Mateo, CA.

Roldan, M. D., F. Reyes, C. Moreno-Vivian, and F. Castillo. (1994). Chlorate and nitrate reduction in phototrophic bacteria *Rhodobacter capsulatus* and *Rhodobacter sphaeroides*. *Curr. Microbiol*, 29:241-245.

Stewart, V. (1988). Nitrate respiration in relation to facultative metabolism in enterobacteria. *Microbiol. Rev*, 52:190-232.

Sa´iz, J.M.G., Pizarro, C., Vidal, D.G. (2003). Evaluation of kinetic models for industrial acetic fermentation: proposal of a new model optimized by genetic algorithm. *Biotechnol Prog*, 19:599–611.

Schugerl, K. (2001) (2001). Progress in monitoring, modeling and control of bioprocess during the last 20 years. *J Biotechnol,* 85:149–73.

Sellers,K., Alsop,W., Clough,S., Hoyt,M., Pugh,B., Robb,J. & Weeks,K. (2007) *Perchlorate. Environmental Problems and Solutions*. New York, NY: CRC Taylor and Francis Group.

Shrout, J.D., Williams, A.G.B., Scherer, M.M. & Parkin, G.F., (2005). Inhibition of bacterial perchlorate reduction by zero-valent iron. *Biodegrad* 16, 23–32

Singh,O.V., Labana,S., Pandey,G., Budhiraja,R. & Jain, R.K. (2003). Phytoremediation: an overview of metallic ion decontamination from soil. *Appl Microbiol Biotechnol,* 61:405–412

Son, A., Lee, J., Chiu, P.C., Kim, B.J., Cha, D.K. (2006). Microbial reduction of perchlorate with zero-valent iron. *Water Research* 40: 2027-2032

Stroo, H.F., Loehr, R.C. & Ward, H. (2009). In situ bioremediation of perchlorate in groundwater: an overview. In: In situ bioremediation of perchlorate in groundwater. Ward, C.H., 1-13, Springer Science+Business Media, LCC, New York, USA

Tan,K., Anderson,T.A., Jones,M.W., Smith, P.N. & Jackson, J.A.W.(2004). Accumulation of Perchlorate in Aquatic and Terrestrial Plants at a Field Scale. *Environ.Qual,* 33:1638 1646

Urbansky,E.T. (2000) Quantitation of perchlorate ion: practices and advances applied to the analysis of common matrices. Critical Review of Analytical Chemistry.

Urbansky, E.T. (2002). Perchlorate environmental contamination: Toxicological review and risk characterization. Perchlorate in the Environment. Kluwer Academic/ Plenum, New York USEPA. NCEA-1-0503, External Review Draft. National Center for Environmental Assessment, Office of Research Development, USEPA, Washington, DC, USA.

USEPA (2002). Report on the Peer Review of the U.S. Environmental Protection Agency's Draft External Review Document ''Perchlorate Environmental Contamination: Toxicological Review and Risk Characterization''.

Vandecasteele, F.P.J., T.F. Hess & Crawford, R.L. (2004). Constructing microbial consortia with minimal growth using a genetic algorithm, pp. 123-129. In G. R. Raidl, et al. (eds.), EvoBIO Workshops 2004, LNCS 3005. Springer-Verlag, Berlin Heidelberg.

Vandecasteele, F.P.J (2006). Genetic algorithms to optimize functions of microbial ecosystems. PhD dissertation. University of Idaho

Van Nevel, L., Mertens, J., Oorts, K. & Verheyen, K. (2007). Phytoextraction of metals from soils: How far from practice? *Environ Pollut,* 150:34–40.

Weathers, L.J., Parkin, G.F. & Alvarez, P.J. (1997). Utilization of cathodic hydrogen as electron donor for chloroform cometabolism by a mixed, methanogenic culture. *Environ. Sci.Technol*. 31, 880–885

Weuster-Botz, D. & Wandrey,C. (1995). Medium optimization by genetic algorithm for continuous production of formate dehydrogenase, Process. Biochem, 30: 563–571.

Weuster-Botz, D., Pramatarova, V., Spassov,G., & Wandrey, C. (1995). Use of a genetic algorithm in the development of a synthetic growth medium for *Arthrobacter simplex* with high hydrocortisone Δ1-dehydrogenase activity. *J. Chem. Technol. Biotechnol,* 64:386-392

Wolterink, A., Kim, S., Muusse, M., Kim, I.S., Roholl, P.J.M. & van Ginkel,C.G. (2005). Dechloromonas hortensis sp. nov. and strain ASK-1, two novel (per)chlorate-reducing bacteria, and taxonomic description of strain GR-1. *Int J Syst Evol Microbiol,* 55: 2063-2068

Xu, J., Song, Y., Min, B., Steinberg, L. & Logan, B.E. (2003). Microbial degradation of perchlorate: principles and applications. *Environ Eng. Sci*. 20, 405–422

Yifru, D.D. & Nzengung, V. A. (2006). Uptake of Perchlorate by Vegetation Growing at Field Sites in Arid and Subhumid Climates. *Remediation,* Autumn 2007. p. 53-68.

Yu,L., Ca~nas,J.E, Cobb,G.P., W.A. Jackson, W.A. & Anderson, T.A. (2004). Uptake of perchlorate in terrestrial plants. *Ecotoxicol. Envi-Qual,* 29:866–870

Yu, X., Amrhein, C., Deshusses, M.A. & Matsumoto, M.R. (2006). Perchlorate reduction by autotrophic bacteria in the presence of zero-valent iron. *Environ. Sci. Technol*. 40, 1328–1334

Zafar, M., Kumar, S. & Kumas, S. (2010). Optimization of napthalene biodegradation by a genetic algorithm based response surface methodology. *Braz J Chem Engin,* 27(01) 89-99

Application of *Luffa Cylindrica* in Natural form as Biosorbent to Removal of Divalent Metals from Aqueous Solutions - Kinetic and Equilibrium Study

Innocent O. Oboh, Emmanuel O. Aluyor and Thomas O. K. Audu

University of Benin,
Nigeria

1. Introduction

Environmental pollution due to the discharge of heavy metals from various industries, including metal plating, mining, painting and agricultural sources such as fertilizers and fungicidal sprays are causing significant concern because of their toxicity and threat to human life, especially when tolerance levels are exceeded (Gupta et al., 2009).

The species with the most toxicological relevance found in the industrial effluents are the heavy metals. These species are bio-accumulative and not biodegradable over time (Abdel-Ghani et al., 2009).

Activated carbon is the most employed adsorbent for heavy metal removal from aqueous solution (Mohan et al., 2005). However, the extensive use of activated carbon for metal removal from industrial effluents is expensive (Babel and Kurniawan, 2003), limiting its large application for wastewater treatment. Therefore, there is a growing interest in finding new alternative low-cost adsorbents for metal removal from aqueous solution, such as: microorganisms (Martins et al., 2006; Klen et al., 2007), and residuals of agricultural products (Basil et al., 2006; Lima et al., 2007).

The greatest demand for metal sequestration today comes from the need to immobilize the metals released to the environment (or mobilized) by and partially lost through human technological activities. It has been established that dissolved metals (particularly heavy metals) escaping into the environment pose a serious health hazard (Kuyucak and Volesky, 1990). They accumulate in living tissues throughout the food chain, which has humans at its top, multiplying the danger. Thus, it is necessary to control emissions of heavy metals into the environment.

Urban and industrial wastewaters with toxic metal ions are a serious environmental problem (Santhy and Selvapathy, 2004). Metals have a high degree of toxicity, which can be deleterious for both the human beings and the environment. Inorganic micro pollutants are of considerable concern because they are non-biodegradable, highly toxic and have a carcinogenic effect (Cimino, et al., 2000).

"Heavy metals" are chemical elements with a specific gravity that is at least 5 times the specific gravity of water. Some well-known toxic metallic elements with a specific gravity that is 5 or more times that of water are arsenic, 5.7; cadmium, 8.65; iron, 7.9; lead, 11.34; and mercury, 13.546 (Graeme and Pollack, 1998). There are 35 metals that concern us because of

occupational or residential exposure; 23 of these are the heavy elements or "heavy metals": antimony, arsenic, bismuth, cadmium, cerium, chromium, cobalt, copper, gallium, gold, iron, lead, manganese, mercury, nickel, platinum, silver, tellurium, thallium, tin, uranium, vanadium, and zinc (Life Extension, 2009).

Generally, heavy metals inflict toxicity by forming highly stable ligands as giant molecular complexes with the organic compounds in the body. The bioaccumulated heavy metal bounded with the organic compound modifies the biological organic molecule which in many occasions losses their ability to function properly, consequently, resulting in malfunction, change major constituents of the affected cells, and in some instances, the cell dies. At the death of the cell, the normal functions of the body systems are interfered and common symptoms are manifested depending on the organ affected (David and Norman, 1986).

In the present study, the following heavy metals namely: lead, copper, zinc and nickel were investigated.

a. Lead can contaminate the environment through natural geochemical and anthropogenic processes. The anthropogenic sources of lead to the environment include coal combustion, sewage wastewaters, automobile emissions, battery industry, mining activities and the utilization of fossil fuels (King et al., 2007). Various plant materials viz. rice husk, maize cobs, coconut and seed hull, saw dust, maize leaf and olive pomace have been studied for Pb removal from water bodies. An investigation dealt with the abatement of Pb (II) ions from aqueous system using *Saraca indica* leaf powder (SILP). The manuscripts also reported the applicability of leaf biomass for Pb (II) metal ion recovery and regenerate the exhausted biosorbent thereby making the process more economical, beneficial and cost effective (Goyal et al., 2008).

b. Copper metal contamination exists in aqueous waste streams from many industries such as electronic and electrical, metal plating, mining, manufacture of computer heat sinks, Copper plumbing, as well as biostatic surface, as a component in ceramic glazing and glass colouring (Tumin et al., 2008). Copper is regularly used in agricultural chemicals for mildew prevention, and as algicides in water treatment of industrial waters. It is also used as a preservative for wood, leather, and fabrics. Workers in, or those living near mines, smelters, metal fabrication and manufacturing plants, wood treatment plants, phosphate fertilizer plants, and waste water plants may also experience excessive copper exposure (Jolley et al., 2003). Probably the most likely route of excessive copper intake for most people will be through drinking water. Although high copper concentrations are rare in most water sources, all water is aggressive toward copper, brass and bronze plumbing fixtures to some extent. In some cases the water will dissolve some of the copper, especially when it sits for long in pipes. Soft water is more aggressive than hard water, because hard water will often lay down a protective scale layer that keeps the water from direct contact with the pipe (Jolley et al., 2003).

c. Nickel metal contamination exists in natural deposits; industrial processes that use nickel catalysts, such as coal gasification, petroleum refining, and hydrogenation of fats and oils. They have also been identified in residual fuel oil and in atmospheric emissions from nickel refineries. Nickel is toxic and relatively widespread in the environment. It is used in a wide variety of industries such as plating and cadmium–nickel battery, phosphate fertilizers, mining, pigments, stabilizers and alloys, and find its way to the aquatic environment through wastewater discharge. Therefore, a systematic study on the removal of nickel from wastewater is of considerable significance from an environmental point of view (Singh, 2008).

d. Although zinc occurs naturally, most zinc find its way into the environment because of human activities. Mining, smelting metals (like zinc, lead and cadmium) and steel

production, as well as burning coal and certain wastes can release zinc into the environment. High level of zinc in soil may result from the improper disposal of zinc-containing wastes from metal manufacturing industries and electric utilities. Drinking water that flows through metal pipes coated with zinc also are sources of zinc exposure. Zinc is often found in effluents discharged from industries involved in acid mine drainage, galvanizing plants, natural ores and municipal waste water treatment plants and is not biodegradable and travels through the food chain via bioaccumulation. Therefore, there is significant interest regarding zinc removal from waste waters since its toxicity for humans is 100-500 mg/day. World health organization (WHO) recommended the maximum acceptable concentration of zinc in drinking water as 5.0 mg/l (Rakesh et al., 2010).

Loofa sponge is a lignocellulosic material composed mainly of cellulose, hemicelluloses and lignin (Rowell et al., 2002). The fibers are composed of 60% cellulose, 30% hemicelluloses and 10% lignin (Mazali and Alves, 2005). The fruits of *L. cylindrica* are smooth and cylindrical shaped (Mazali and Alves, 2005). *L. cylindrica* is a sub-tropical plant, which requires warm summer temperatures and long frost-free growing season when grown in temperate regions. It is an annual climbing which produces fruit containing fibrous vascular system. It is a summer season vegetable. It is difficult to assign with accuracy the indigenous areas of *Luffa* species.

They have a long history of cultivation in the tropical countries of Asia and Africa. Indo-Burma is reported to be the center of diversity for sponge gourd. The main commercial production countries are China, Korea, India, Japan and Central America (Bal et al., 2004).

The structure of *Luffa cylindrica* for example, is cellulose based (Rowell et al., 2002; Mazali and Alves, 2005), and the surface of cellulose in contact with water is negatively charged. Metal compounds used in this study will dissolve to give the cationic metal and this will undergo attraction on approaching the anionic *Luffa cylindrica* structure (Ho et al., 2002). On this basis, it is expected that a metal cation will have a strong sorption affinity for *Luffa cylindrica*.

The study investigated time dependence and concentration dependence studies on the sorption of some selected divalent metal ions on the seeds and sponge mixture of *Luffa cylindrica*. The data obtained from the batch concentration studies were fit into Langmuir, Sips, Redlich-Peterson and Freundlich adsorption isotherms to establish mechanism for the biosorption process. The kinetics of the biosorption process was established by fitting the data from the time dependency study into pseudo-first order, Avrami (Fractional order), Intra-particle diffusion and pseudo-second order kinetic models.

2. Materials and methodology

2.1 Preparation of *Luffa cylindrica*
The plant materials (sponge and seeds) were dried at room temperature for a period of three days. The biosorbent was screened to obtain a geometrical size of 0.25 - 0.5mm. The ground seed and sponge were mixed at a ratio of 1:1.

2.2 Preparation of aqueous solutions
Stock solutions of Nickel, Lead, Copper, and Zinc were prepared with distilled water and Nickel (II) tetraoxosulphate (VI), Lead (II) trioxonitrate (V), Copper (II) tetraoxosulphate (VI) and Zinc chloride respectively. All working solutions were obtained by diluting the stock solutions with distilled water. The pH of the effluent was adjusted to 5. The concentration of metal ions in effluent was analyzed by Atomic Absorption Spectrophotometer. A duplicate was analyzed for every sample to track experimental error and show capability of reproducing results (Marshall and Champagne, 1995).

2.3 Scanning electron microscope and elemental analysis

The microstructures, composition, and morphology of *Luffa cylindrica* the biosorbent material was analysed by means of scanning electron microscopy (SEM). A Philips scanning electron microscope (ESEM XL30) equipped with energy dispersive X-ray spectrometer (EDX) was used to analyse the various elemental composition found in the powders.

2.4 Fourier transform infra red analysis

Fourier transform infrared spectroscopy (FTIR) of the adsorbent was done by using an FTIR spectrometer (Model FTIR 2000, Shimadzu, Kyoto, Japan). About 150 mg KBr disks containing approximately 2% of *Luffa cylindrica* sample was prepared shortly before recording the FTIR spectra in the range of 400 – 4000.0 cm^{-1} and with a resolution of 4 cm^{-1}. The resulting spectra were average of 30 scans.

2.5 Surface area

The surface area of the *Luffa cylindrica* sample was determined using Flowsorb 2300 manufactured by Micrometrics Instrument Corporation, USA. Krypton gas was used in conducting single-point surface area measurements. Liquid nitrogen was used in setting the adsorption of nitrogen gas by the samples. The *Luffa cylindrica* was degassed at 100°C for 30 minutes and were then cooled to liquid nitrogen temperature. The surface area of the sample under measurement was then read from the display-meter. The value of the surface area recorded was then converted to specific surface area (m^2/g) by dividing the reading on the display by the weight of the *Luffa cylindrica* sample.

2.6 Biosorption experiment

The experiments were carried out in the batch mode for the measurement of adsorption capabilities. The bottles with 500ml capacity were filled with 50ml of the synthetic wastewater, and 1g of dried plant materials (ground). The bottles were shaken for a predetermined period of 2h at room temperature in a reciprocating shaker 300 rpm. The separation of the adsorbents and solutions was carried out by filtration with Whatman filter paper No. 42 and the filtrate stored in sample cans in a refrigerator prior to analysis. The residual metallic ion concentrations were also determined using an Atomic Absorption Spectrophotometer (AAS).

The amount of the metal ion sorbed and percentage of removal of metal ion by the biosorbent were calculated by applying the Equations (1) and (2), respectively:

$$q = \frac{\left(C_0 - C_f\right)}{m} . V \tag{1}$$

$$\% \text{ Removal} = \frac{\left(C_0 - C_f\right)}{C_0} . 100 \tag{2}$$

where q is the amount of metal ion sorbed by the biosorbent (mg/g); C_0 is the initial ion concentration put in contact with the biosorbent (mg/L), C_f is the final concentration (mg/L) after the batch biosorption procedure, V is the volume of aqueous solution (L) put in contact with the biosorbent and m is the mass (g) of biosorbent.

2.7 Kinetic and equilibrium studies

The kinetic equations, which are, Avrami (Lopes et al., 2003), pseudo first-order (Largegren, S., 1898), pseudo-second order (Ho, Y.S., Mckay, G.M., 1999), Elovich (Ayoob et al., 2008) and intra-particle diffusion model (Weber Jr. and Morris, 1963) are given in Table 1.

Kinetic model	Equation
Pseudo-first-order (Largegren, S., 1898)	$q_t = q_e \cdot [1 - \exp(-k_p.t)]$
Pseudo-second-order (Ho, Y.S., Mckay, G.M., 1999)	$\dfrac{t}{q_t} = \dfrac{1}{kq_e^2} + \dfrac{1}{q_e}t$
Elovich (Ayoob et al., 2008)	$q_t = \dfrac{1}{\beta}\ln(\alpha\beta) + \dfrac{1}{\beta}\ln t$
Avrami (Lopes et al., 2003)	$q_t = q_e \cdot (1 - \exp[-(k_{AV}.t)]$
Intra-particle diffusion (Weber Jr.and Morris, 1963)	$q_t = k_{id}\sqrt{t} + C$

Table 1. Kinetic adsorption models

The isotherm equations which are, Langmuir (Langmuir, 1918), Freundlich (Freundlich, 1906). Sips (Sips, 1948) and Redlich–Peterson (Redlich and Peterson, 1959) are given in Table 2.

Isotherm	Equation
Langmuir (Langmuir,1918)	$Q_e = \dfrac{x}{m} = \dfrac{K_L C_e}{1 + aC_e}$
Freundlich (Freundlich, 1906)	$Q_e = K_F C_e^{1/n}$
The Redlich-Peterson (Redlich and Peterson, 1959)	$Q_e = \dfrac{K_j C_e}{1 + \alpha_L C_e^{\beta}}$
Sips (Sips,1948)	$Q_e = \dfrac{abC_e^n}{1 + aC_e^n}$

Table 2. Equilibrium isotherm models

2.8 Evaluation of the kinetic and isotherm parameters

In this work, the kinetic and equilibrium models were fitted employing the non-linear fitting method, using the non-linear fitting facilities of the software NLREG version 6.5.

3. Results and discussion

3.1 Results

Specific surface area - BET (m²/g)	0.28
Total Surface area (m²/g)	1.1895
Pore Diameter Range (μm)	1051.309204 to 0.003577

Table 3. Physical properties of the *Luffa cylindrica* biosorbent

Elements	Weight%	Atomic%
C	79.33	86.91
O	12.25	10.07
P	00.95	00.40
S	00.75	00.31
Cl	01.58	00.59
K	03.86	01.30
Ca	01.29	00.42

Table 4. Elemental composition of the *Luffa cylindrica* biosorbent

(a) Subfigure A

(b) Subfigure B

(c) Subfigure C

(d) Subfigure D

(e) Subfigure E

(f) Subfigure F

(g) Subfigure G

(h) Subfigure H
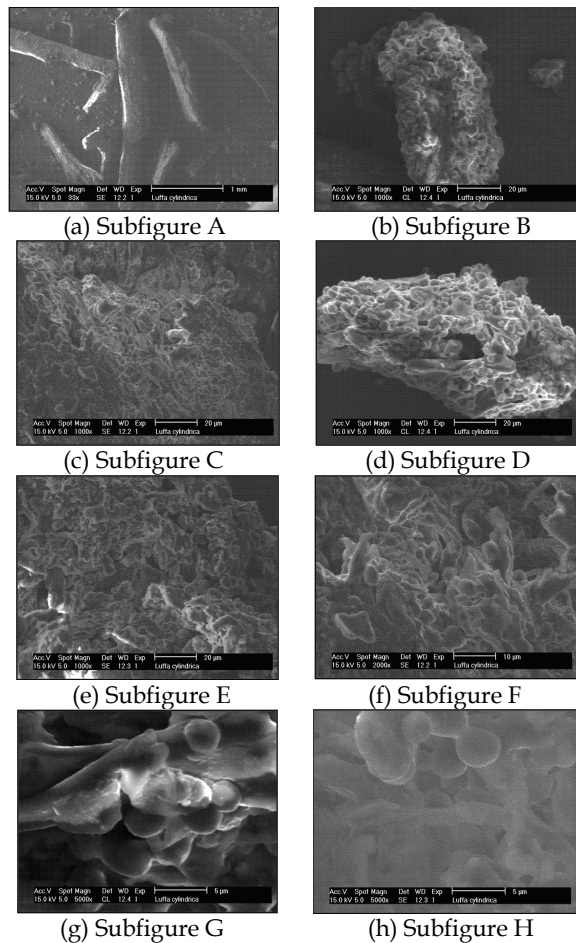
Fig. 1. Scanning electron microscopy of *Luffa cylindrica* seeds and sponge mixture biosorbent: (A) transversal view of the mixture of seed and sponge 33×; (B, C, D, E) transversal view of the mixture of seed and sponge 1000×; (G, H) transversal view of the mixture of seed and sponge 5000×.
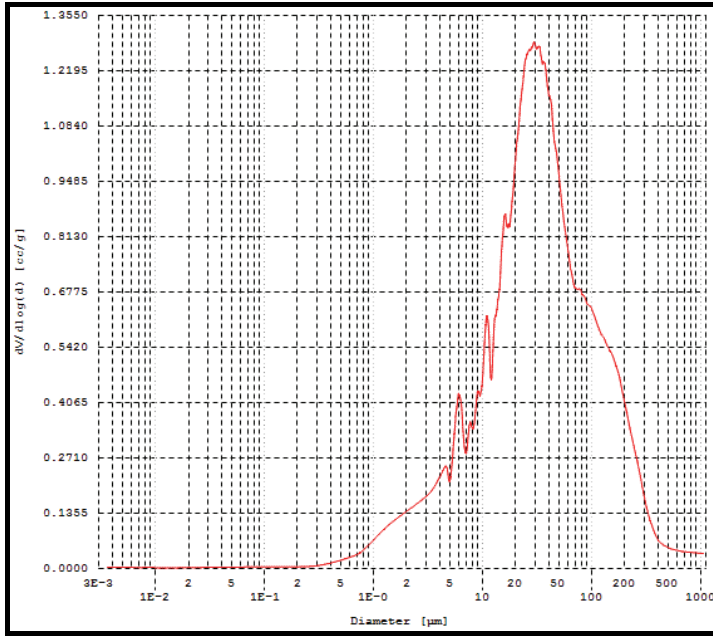
Fig. 2. A plot showing the pore size distribution of the biosorbent - *L. cylindrica*
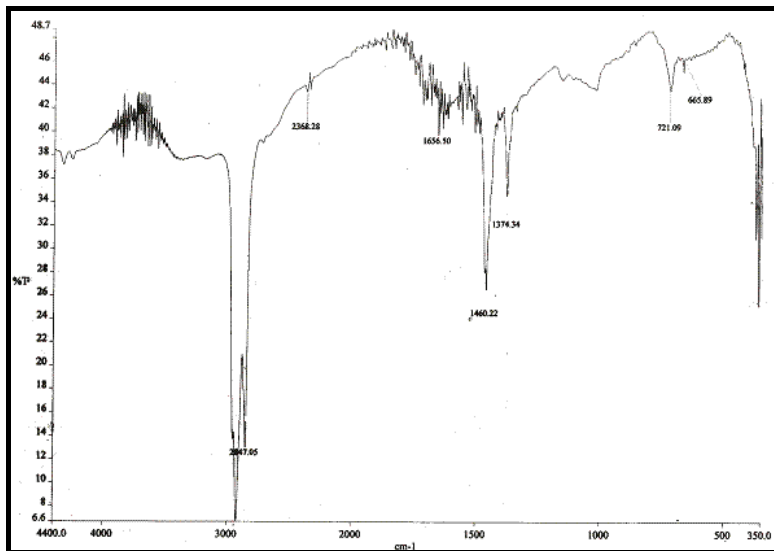
Fig. 3a. FTIR spectrum of the mixture of seed and sponge of *L. cylindrica* biosorbent before biosorption.
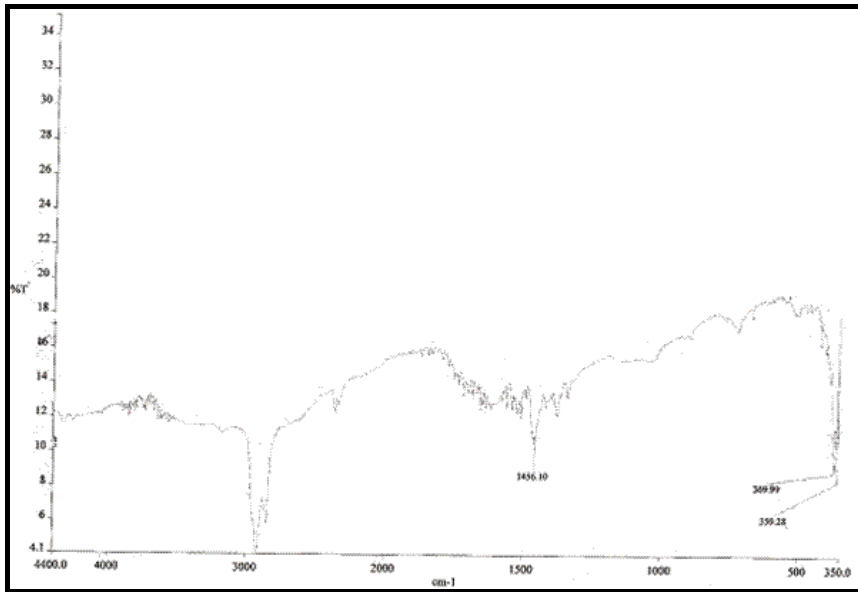
Fig. 3b. FTIR spectrum of the mixture of seed and sponge of *L. cylindrica* biosorbent after biosorption of Ni^{2+}ions .
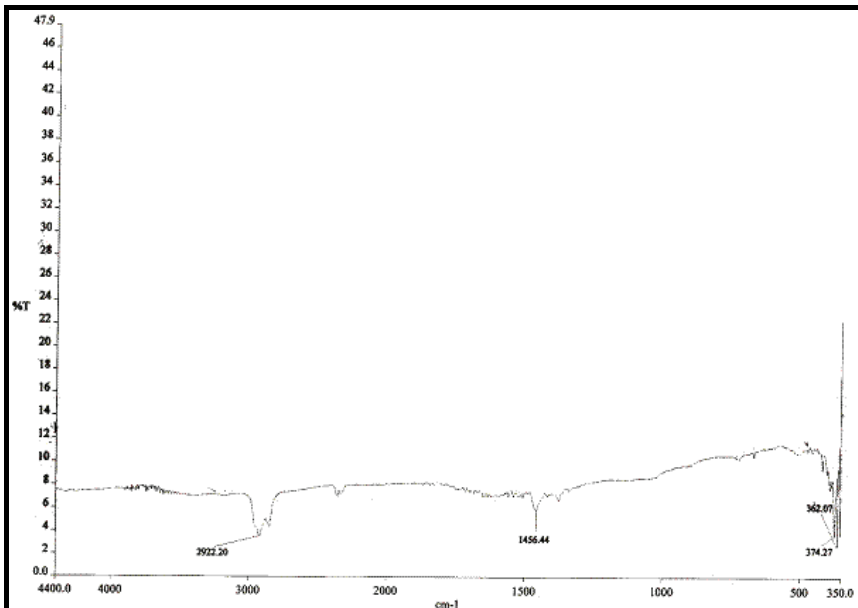
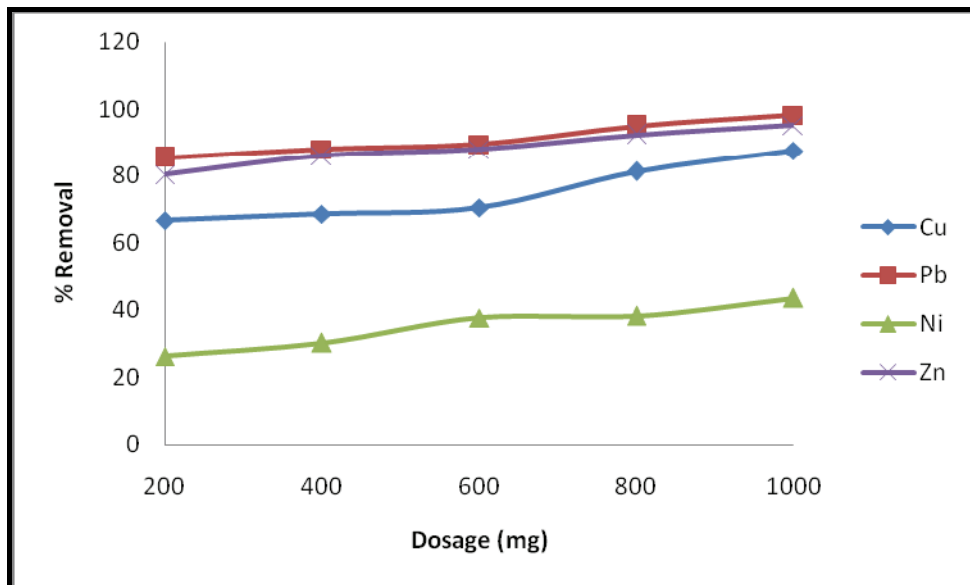Fig. 3c. FTIR spectrum of the mixture of seed and sponge of *L. cylindrica* biosorbent after biosorption of Cu^{2+}ions.
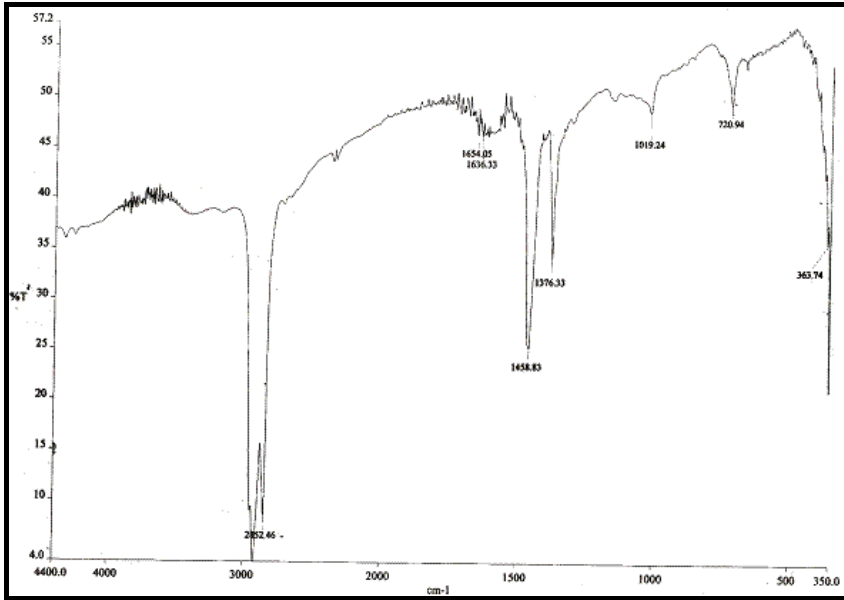
Fig. 3d. FTIR spectrum of the mixture of seed and sponge of *L. cylindrica* biosorbent after biosorption of Pb^{2+} ions.
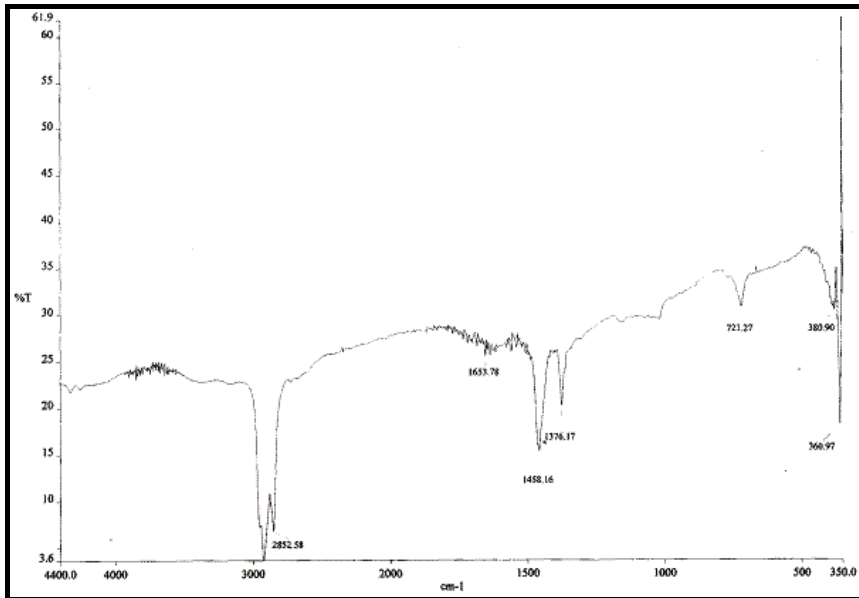
Fig. 3e. FTIR spectrum of the mixture of seed and sponge of *L. cylindrica* biosorbent after biosorption of Zn^{2+} ions.

Fig. 4. % Removal of heavy metal ions from aqueous solutions (50 ml, pH 5.0) with increasing dosage of the heavy metals using *L. cylindrica* (1.0 g) as biosorbent for 2h.
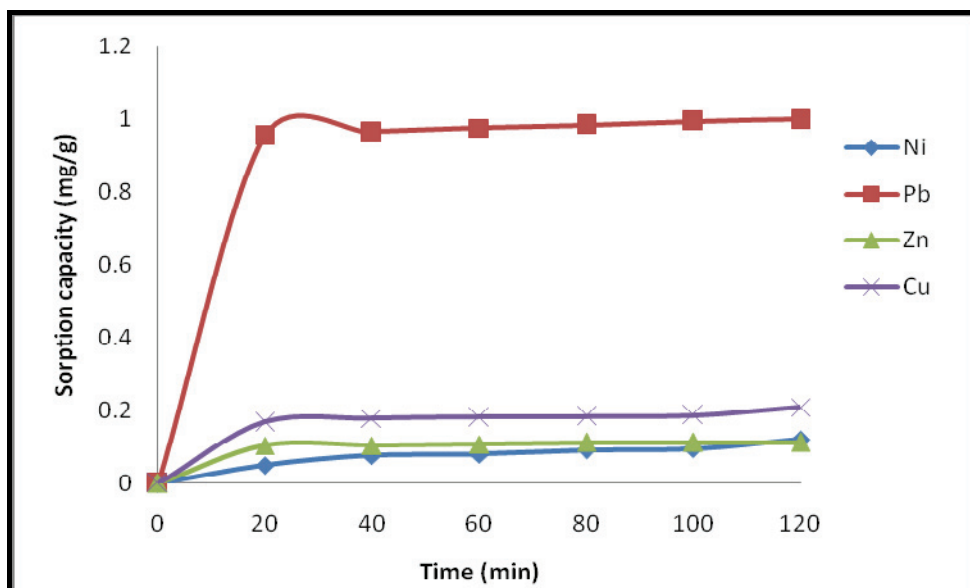
Fig. 5. Time dependent study of the sorption of lead, copper, zinc and nickel on *L. cylindrica* seeds and sponge mixture using 1.0 g biosorbent dose. Initial lead, Nickel, Copper and Zinc concentrations were 20.0, 4.0, 5.0 and 2.5 mg/L respectively with pH 5.0.

Kinetic model	Parameters	Metal ions (M^{2+})			
		Cu	Pb	Zn	Ni
Pseudo-First order	q_e (mg/g)	0.1886	0.9843	0.1100	0.1141
	k_{e1} (g/mg min)	0.1044	0.1720	0.1364	0.0240
	r^2	0.9819	0.9991	0.9947	0.9556
Pseudo-Second order	q_e (mg/g)	0.2002	1.0004	0.1138	0.1490
	k_{e2} (g/mg min)	1.1300	0.9183	3.7011	0.1522
	r^2	0.9883	0.9997	0.9977	0.9666
Intra-particle diffusion	k(mg/g min$^{0.5}$)	0.0168	0.0824	0.0094	0.0102
	C (mg/g)	0.0419	0.2691	0.0278	0.0026
	r^2	0.7933	0.6989	0.7401	0.9752
Elovich	α (mg/g min)	10.2050	1.292E+13	7649.602	0.0070
	β (g/mg)	56.7641	38.7968	167.0520	29.3910
	r^2	0.7375	0.9704	0.8709	0.9054
Avrami	K_{av}(min^{-1})	0.3228	0.5434	0.3374	-0.1163
	n_{av}	0.3235	0.5434	0.4042	-0.2064
	q_e(mg/g)	0.1886	0.9794	0.1099	0.1141
	r^2	0.9819	0.9983	0.9947	0.9556

Table 5. Kinetic model rate parameters obtained using the nonlinear methods.

Isotherm	Parameters	Metal ions (M^{2+})			
		Cu	Ni	Pb	Zn
Langmuir	Q_{max}	2.26E+04	8.20E+03	1.36E+05	2.89E+04
	K_L	1.4580	7.01E-06	8.32E-06	3.00E-05
	r^2	0.4922	0.3518	0.6571	0.8576
Freudlich	K_F	0.2519	0.0015	0.2544	1.3655
	n	0.5897	0.2121	0.3846	0.6801
	r^2	0.5381	0.9231	0.7189	0.9212
Sips	Q_{max}	1.19E+04	1.59E+03	7.90E+04	1.14E+04
	K_s	0.5897	9.51E-07	3.22E-06	1.20E-04
	n	2.11E-05	0.2120	0.3845	0.6801
	r^2	0.5381	0.9231	0.7189	0.9212
Redlich-Peterson	A_{rp}	-0.5421	-0.2936	-0.2525	-1.0178
	K_{rp}	0.0458	0.0117	0.3875	0.5072
	g	1.0000	1.0000	1.0000	1.0000
	r^2	0.7449	0.9632	0.8218	0.9539

Table 6. Equilibrium isotherm parameters obtained using the nonlinear methods.

3.2 Discussion

Table 3 show the surface area and pore diameter range for the biosorbent used for this study. The Specific surface area using the BET method was 0.28m²/g and the Pore diameter range was between 1051.309204 to 0.003577µm. As observed, the surface area for the seed and sponge mixture of *L. cylindrica* is relatively low, with pore diameter values in agreement with those found for typical mesoporous materials (Hamoudi and Kaliaguine, 2003).

Table 4 shows the elemental composition of *Luffa cylindrica* that was analysed by means of scanning electron microscopy (SEM). The *Luffa cylindrica* sample showed a very high percentage of carbon.

Scanning electron microscopy (SEM) of the *Luffa cylindrica* biosorbent was taken in order to verify the presence of macropores in the structure of the fiber. In the micrographs presented Figure 1 (A - J) is observed the fibrous structure of *Luffa cylindrica*, with some fissures and holes, which indicated the presence of the macroporous structure. These, should contribute a little bit to the diffusion of the Ni (II), Pb (II), Cu (II) and Zn (II) to the *Luffa cylindrica* biosorbent surface. The small number of macroporous structure is confirmed by the low specific surface area of the biosorbent (see Table 3). As the biosorbent material presents few numbers of macroporous structure, it adsorbed low amount of nitrogen, which led to a low BET surface area (Passos et al., 2006; Vaghetti et al, 2003; Arenas et al., 2004; Passos et al., 2008). Therefore the major contribution of the Ni (II), Pb (II), Cu (II) and Zn (II) uptake can be attributed to micro- and mesoporous structures (see Figure 1 (A-J)).

The pore size distribution of the *Luffa cylindrica* sample was obtained by Mercury intrusion method, and it is shown in Figure 2. The distribution of average pore diameter curve presents a maximum with an average pore diameter of about 30 µm. The amount of pores seen in the *Luffa cylindrica* biosorbent decreases for average pore diameters ranging from 30 to 1000 µm. On the other hand, the amount of average pores ranging from 3.0E-03 to 30 µm is predominant. Therefore, this biosorbent can be considered mixtures of micro- and mesoporous materials (Passos et al., 2006; Vaghetti et al, 2003; Arenas et al., 2004; Passos et al., 2008).

Figure 4 show the percent removal of Ni^{2+}, Pb^{2+}, Cu^{2+} and Zn^{2+} ions from the aqueous solution using *Luffa cylindrica* seeds and sponge mixture. The highest percent removal for the dosage of 1000 mg of the biosorbent was 98.2 for Pb^{2+} and was followed by 95.2, 87.6 and 43.5 for Zn^{2+}, Cu^{2+} and Ni^{2+} ions respectively.

Figures 3 a - e show the FTIR spectral. The functional groups on the binding sites were identified by FTIR spectral comparison of the free biomass with a view to understanding the surface binding mechanisms. The significant bands obtained are shown in Figure 3 a - e. Functional groups found in the structure include carboxylic, alkynes or nitriles and amine groups (Pavia et al., 1996).

The stretching vibrations of C-H stretch of -CHO group shifted from 2847.05 to 2922.20, 2852.58, 2852.46 and 2852.43 cm^{-1} after Cu^{2+}, Zn^{2+}, Pb^{2+} and Ni^{2+} ions biosorption. The assigned bands of the carboxylic, amine groups and alkynes or nitriles vibrations also shifted on biosorption. The shift in the frequency showed that there was biosorption of Cu^{2+}, Zn^{2+}, Pb^{2+} and Ni^{2+} ions on the *L. cylindrica* biosorbent and the carboxylic and amine groups were involved in the sorption of the Cu^{2+}, Zn^{2+}, Pb^{2+} and Ni^{2+} ions.

Adsorption kinetic study is important in treatment of aqueous effluents as it provides valuable information on the reaction pathways and in the mechanism of adsorption reactions.

In this study nonlinear kinetic equations were preferred to the linear equations, since there are always errors associated with linearization (Mohan et al., 2005; Kumar, 2007; Kumar, 2007). Therefore large errors in kinetic and equilibrium parameters could be obtained, if a not suitable linear equation is utilized (Mohan et al., 2005; Kumar, 2007; Kumar, 2007). In addition, the nonlinear kinetic equations have successfully been employed to obtain these adsorption parameters with excellent accuracy for different adsorbates and adsorbents (Kumar, 2007; Kumar, 2007; Arenas et al., 2007; Jacques, et al., 2007; Jacques, et al., 2007; Lima et al., 2007; Lima et al., 2008).

The kinetic study carried out showed that the sorption was best described by all the models used. The experimental data for all the metal ions studied fitted very well to the Pseudo-second order model then followed by Pseudo-first order, Avrami, Elovich and Intra-particle diffusion models. This was shown in Table 5. It was observed that Pb^{2+}, Zn^{2+}, Cu^{2+} and Ni^{2+}ions had regression values (r^2) for Pseudo-second-order as 0.9997, 0.9977, 0.9883 and 0.9666 respectively. Both Pseudo first order, Pseudo-second order and Avrami models had values higher than that of Elovich and Intra-particle diffusion models which had a values of 0.7401, 0.7933, 0.6989 and 0.9752 for Zn^{2+}, Cu^{2+} , Pb^{2+} and Ni^{2+}ions respectively. Thus it can be concluded that sorption kinetics using *Luffa cylindrica* seed and sponge mixture as biosorbent followed the Pseud-first-order, Pseudo-second-order and Avrami kinetic models. Hence, the pseudo-second-order model is better in explaining the observed rate. This suggests that sorption of the metal ions involve two species, in this case, the metal ion and the biomass (Herrero et al., 2008). These results are in accordance with similar researches carried out (Ho et al., 2004; Kumar et al., 2006; Lodi et al., 1998) with several natural sorbents.

The time profile for the various metal ions studied on *L. cylindrica* is presented in Figure 5. The rate of Zn^{2+}, Cu^{2+}, Pb^{2+} and Ni^{2+}ions removal was rapid in the first 20 minutes and it decreased progressively afterwards. It was observed that the biosorption process reached equilibrium after 120 minutes.

The observed fast biosorption kinetics was consistent with the biosorption of metal involving non-energy mediated reactions, where metal removal from solutions is due purely to physico-chemical interactions between biomass and metal solution. This fast metal uptake from solution indicates that binding might have resulted from interaction with functional groups on the cell wall of the biosorbent rather than diffusion through the cell wall of the biomass this is in agreement with results that have been reported in many studies using different biosorbents on the uptake of different heavy metals (Kumar et al., 2006; Pan et al., 2006; Bueno et al., 2008).

The fitting of data to Redlich-Peterson, Sips, Langmuir and Freundlich isotherms suggest that biosorption of Pb (II) ions onto the biosorbent could be explained by Redlich-Peterson isotherm with correlation coefficient of 0.8218 as outlined in Table 6. The biosorption of Zn (II) ions onto the biosorbent could be explained by all the isotherms studied with correlation coefficients of 0.8576, 0.9212, 0.9212 and 0.9539 for Langmuir, Freundlich, Sips and Redlich-Peterson isotherms respectively. The biosorption of Ni (II) ions onto the biosorbent could be explained by Freudlich, Sips and Redlich-Peterson isotherms with correlation coefficients of

0.9231, 0.9231 and 0.9632 respectively. The biosorption of Cu (II) ions could be explained by Redlich-Peterson isotherm with the correlation coefficient of 0.7449. Because experimental q_e values were lower than that of Q_{max}, considering the reported approaches in the literature (Hall et al., 1996; Ozer and Ozer, 2003), it may be suggested that biosorption takes place as monolayer phenomena and that *L. cylindrica* biomass was not fully covered by the metal ions.

4. Conclusion

The removal of metal ions from aqueous solution is of importance both environmentally and for water re-use. The *Luffa cylindrica* seeds and sponge mixture has been presented here as a good alternative biosorbent for Ni^{2+}, Pb^{2+}, Cu^{2+} and Zn^{2+} ions removal from aqueous solution. This biosorbent has the ability to sorb the Ni^{2+}, Pb^{2+}, Cu^{2+} and Zn^{2+} ions at the solid/liquid interface, when the sample were suspended in water at a pH of 5.0 and a contacting time of 2h to saturate the available sites located on the biosorbent surface. Out of the five kinetic models used to adjust the sorption, the best fit was the Pseudo-second order model and for the isotherm the best fit was Redlich-Peterson isotherm for Ni (II) ion biosorption onto *L. cylindrica* seeds and sponge mixture biosorbent.

5. References

Abdel-Ghani, N. T., Ahmad K. H., El-Chaghaby, G. A. and Lima, E. C. (2009). Factorial experimental design for biosorption of iron and zinc using Typha domingensis phytomass. Desalination 249: 343–347.

Arenas, L. T., Lima, E. C., dos Santos Jr., A. A., Vaghetti, J. C. P., Costa, T. M. H., Benvenutti, E.V. (2007). Use of statistical design of experiments to evaluate the sorption capacity of 1,4-diazoniabicycle[2. 2. 2] Octane/silica chloride for Cr (VI) adsorption, Colloid Surf. A. 297, pp. 240–248.

Arenas, L. T., Vaghetti, J. C. P. Moro, C. C. Lima, E. C. Benvenutti, E. V. Costa, T. M. H. (2004). Dabco/silica sol–gel hybrid material. The influence of the morphology on the CdCl2 adsorption capacity, Mater. Lett. 58, pp. 895–898.

Ayoob, S. Gupta, A. K. Bhakat, P. B. Bhat, V. T. (2008). Investigations on the kinetics and mechanisms of sorptive removal of fluoride from water using alumina cement granules, Chem. Eng. J. 140, 6–14.

Babel, S., Kurniawan, T. A. (2003). Low-cost adsorbents for heavy metals uptake from contaminated water: a review, J. Hazard. Mater. 97, 219–243.

Bal K. J., Hari B. K. C., Radha K., Ghale G. M., Bhuwon R.S., Madhusudan P.U.(2004) Descriptors for Sponge Gourd [*Luffa cylindrica* (L.) Roem.], NARC, LIBIRD & IPGRI.

Basil JL, Ev RR, Milcharek CD, Martins LC, Pavan FA, dos Santos, Jr. AA, Dias SLP, Dupont J, Noreña CPZ, Lima EC (2006). Statistical Design of Experiments as a tool for optimizing the batch conditions to Cr (VI) biosorption on *Araucaria angustifolia* wastes. J Hazard Mater; 133: 143-153.

Bueno, B. Y. M., Torem, M. L., Molina, F., de Mesquita, L. M. S. (2008).Biosorption of lead(II), Chromium(III) and copper(II) by R. opacus: Eqilibrium and kinetic studies. Miner.Eng. 21, 65-75.

Cimino, G., Passerini, A. and Toscano, G., (2000). Removal of toxic cations and Cr (VI) from aqueous solution by hazelnut shell. Water Res., 34 (11), 2955-2962.

David, W. O. and Norman, H. N. (1986). Principles of Modern Chemistry. Saunders Golden Sunburts Series Printed by the Dryden Press. 383 Madison Avenue, New York. N. Y.10017. USA.

Freundlich, H. M. F. (1906). Über die adsorption in lösungen, Zeitschrift für Physikalische Chemie (Leipzig) 57A, 385–470.

Goyal, P., Sharma, P., Srivastava, S, Srivastava, M. M. (2008). *Saraca indica* leaf powder for decontamination of Pb: removal, recovery, adsorbent characterization and equilibrium modeling, International Journal of Enviornmental Science and Technology, Vol. 5, No. 1, pp. 27-34.

Gupta, N., Prasad, M., Singhal, N. and Kumar, V. (2009). Modeling the Adsorption Kinetics of Divalent Metal Ions onto Pyrophyllite Using the Integral Method. Ind. Eng. Chem. Res., 48 (4), 2125-2128.

Graeme, K. and Pollack C., Jr (1998). Heavy metal toxicity, Part I: Lead and metal fume fever. Journal of Emergency Medicine, Volume 16, Issue 2, Pages 171-177.

Hall, K. R. Egleton, L. C. Acrivos, A., Vemeulen, T. (1966). Pore and solid diffusion kinetics in fixed bed adsorption under constant pattern conditions. Ind. Eng. Chem. Fund. 5, 212-223.

Hamoudi, S., Kaliaguine, S.(2003). Sulfonic acid-functionalized periodic mesoporous organosilica. Micropor. Mesopor. Mater. 59, p. 195-204.

Herrero, R. Lodeiro, P. Rojo, R. Ciorba, A. Rodriguez, P. Sastre deVicente, M.E.(2008). The efficiency of the red alga Mastocarpus stellanua for remediation of cadmium pollution. Bioresour. Technol. 99, 4138-4146.

Ho, Y. S., Chui, W. T., Hsu, C. Huang, C. (2004). Sorption of lead ions from aqueous solution using tree fern as a sorbent. Hydrometallurgy. 73, 55-61.

Ho Y. S., Huang C. T. Huang H.W. (2002).Equilibrium sorption isotherm for metal ions on tree fern.Process Biochemistry 37, 1421-1430.

Ho, Y. S., Mckay, G. M. (1999). Pseudo-second order model for sorption process, Proc. Biochem. 34,451–465.

Jacques, R. A., Bernardi, R., Caovila, M., Lima, E. C., Pavan, F. A., Vaghetti, J. C. P., Airoldi, C. (2007). Removal of Cu(II) Fe(III) and Cr(III) from aqueous solution by aniline grafted silica gel, Sep. Sci. Technol. 42, pp. 591–609.

Jacques, R. A., Lima, E.C., Dias, S.L.P., Mazzocato, A.C., Pavan, F.A. (2007).Yellow passion fruit shell as biosorbent to remove Cr(III) and Pb(II) from aqueous solution, Sep. Purif. Technol. 57, pp. 193–198.

Jolley, O. D., O'Brien, G. and Morrison, J. (2003).Evolution of Chemical Contaminant and Toxicology Studies, Part 1 - An Overview, South Pacific Journal of Natural Science, Vol 21, 1-5.

King, P., Rakesh, N., Beenalahari,Y., Kumar, Y.P., Prasad, V.S.R.K. (2007). Removal of lead from aqueous solution using *Syzygium cumini L.*: Equilibrium and Kinetic studies. J. Harzad. Mater. 142: 340 – 347.

Klen, M. R. F., Ferri, P., Martins, T. D., Tavares, C. R. G. and Silva, E. A. (2007) Equilibrium study of the binary mixture of cadmium–zinc ions biosorption by the *Sargassum filipendula* species using adsorption isothermsmodels and neural network, Biochem. Eng. J. 34,136–146.

Kumar, K. V. (2007). Optimum sorption isotherm by linear and non-linear methods for malachite green onto lemon peel, Dyes Pigment 74, pp. 595–597.

Kumar, K. V. (2007). Pseudo-second order models for the adsorption of safranin onto activated carbon: comparison of linear and non-linear regression methods, J. Hazard. Mater. 142, pp. 564–567.

Kumar, Y. P, King, P. Prasad, V.S. (2006). Equilibrium and kinetic studies for the biosorption system of copper(II) ion from aqueous solution using *Tectona grandis* L. f. leaves powder, J. Hazard. Mater. 137, 1211-1217.

Kuyucak, N.; Volesky, B. In Biosorption of Heavy Metals; Volesky, B., ed.; CRC Press: Boca Raton, FL, 1990, pp. 173-198.

Langmuir, I. (1918). The adsorption of gases on plane surfaces of glass, mica and platinum, J. Am. Chem. Soc. 40, 1361–1403.

Largegren, S, (1898). About the theory of so-called adsorption of soluble substances, Kungliga Suensk Vetenskapsakademiens Handlingar 241,1–39.

Life Extension. Heavy metal toxicity.
http://www.lef.org/protocols/prtcls-txt/t-prtcl-156.html.
Assessed on the 7th of November, 2009.

Lima, E. C., Royer, B., Vaghetti, J. C. P., Brasil, J. L., Simon, N. M., dos Santos Jr., A. A., Pavan, F. A., Dias, S. L. P., Benvenutti, E. V. and da Silva, E. A. (2007). Adsorption of Cu (II) on *Araucaria angustifolia*wastes: determination of the optimal conditions by statistic designof experiments, J. Hazard. Mater. 140, 211–220.

Lima, E. C., Royer, B., Vaghetti, J. C. P., Simon, N. M., da Cunha, B. M., Pavan, F. A., Benvenutti, E. V., Veses, R. C., Airoldi, C. (2008). Application of Brazilian-pine fruit coat as a biosorbent to removal of reactive red 194 textile dye from aqueous solution. Kinetics and equilibrium study, J. Hazard. Mater. 155, pp. 536 – 550.

Lodi, A., Solisio, C., Converti, A. Borghi, M. (1998). Cadmium, zinc, copper, silver and chromium (III) removal from wastewaters by *Sphaerotilus natans*. Bioprocess Biosyst. Eng. 19, 197-203.

Lopes, E. C. N. dos Anjos, F. S. C. Vieira, E. F. S. Cestari, A. R. (2003). An alternative Avrami equation to evaluate kinetic parameters of the interaction of Hg (II) with thin chitosan membranes, J. Colloid Interface Sci. 263 , 542–547.

Marshall, W. E. and Champagne, T. E. (1995). Agricultural Byproducts as Adsorbents for Metal ions in Laboratory Prepared Solutions and in Manufacturing Wastewater, Journal of Environmental Science and Health, Part A: Environmental Science and Engineering. Vol. 30, No. 2, 241 – 261.

Martins, B. L., Cruz, C. C. V., Luna, A. S. and Henriques, C. A. (2006). Sorption and desorption of Pb^{2+} ions by dead *Sargassum* sp. biomass, Biochem. Eng. J. 27, 310 - 314.

Mazali I. O. Alves O. L. (2005). Morphosynthesis: high fidelity inorganic replica of the fibrous network of loofa sponge (*Luffa cylindrica*). Anais da Academia Brasileira de Ciências, Vol. 77, No. 1, p. 25-31.

Mohan, D., Singh, K. P., Singh, V. K. (2005). Removal of hexavalent chromium from aqueous solution using low-cost activated carbons derived from agricultural waste materials and activated carbon fabric cloth, Ind. Eng. Chem. Res. 44, 1027–1042.

Ozer, A., Ozer, D. (2003).Comparative study of the biosorption of Pb(II), Ni(II) and Cr(VI) ions onto *S. cerevisiae*: determination of biosorption heats. J. Harzad. Mater. 100: 219-229.

Pan, J., Ge, X., Liu, R., Tang, G.H. (2006). Characteristic features of Bacillus cereus cell surfaces with biosorption of Pb (II) ions by AFM and FT-IR. Colloids Surf., B. 52, 89-95.

Passos, C. G. Lima, E. C. Arenas, L. T. Simon, N. M. da Cunha, B. M. Brasil, J. L. Costa, T. M. H. Benvenutti, E. V. (2008). Use of 7-amine-4-azahepthylsilica and 10-amine- 4-azadecylsilica xerogels as adsorbent for Pb (II). Kinetic and equilibrium study, Colloids Surf. A .316, pp. 297–306.

Passos, C. G. Ribaski, F., Simon, N. M., dos Santos Jr., A. A., Vaghetti, J. C. P., Benvenutti, E. V. , Lima, E. C. (2006). Use of statistical design of experiments to evaluate the sorption capacity of 7-amine-4-azahepthylsilica and 10-amine- 4-azadecylsilica for Cu (II) Pb (II) and Fe (III) adsorption, J. Colloid Interface Sci. 302, pp. 396–407.

Pavia, D. L., Lampman, G. M., Kriz, G. S. (1996). Introduction to Spectroscopy, 2nd edn., Saunders Golden Sunburst Series, New York.

Rakesh N., Kalpana P., Naidu T. V. R and Venkateswara Rao M. (2010). Removal of Zinc Ions from Aqueous Solution by Ficus Benghalensis L.: Equilibrium and Kinetic Studies. International Journal of Engineering Studies. Volume 2, Number 1, pp. 15–28.

Redlich, O., Peterson, D.L. (1959). A useful adsorption isotherm, J. Phys. Chem. 63, 1024–1027.

Rowell R. M., James S. H., Jeffrey S. R. (2002). Characterization and factors effecting fibre properties, In Frollini E, Leao, AL, Mattoso LHC, (ed.), Natural polymers and agrofibres based composites. Embrapa Instrumentacao Agropecuaria, San Carlos, Brazil pp.115-134.

Santhy, K. and Selvapathy, P., (2004). Removal of heavy metals from wastewater by adsorption of coir pith activated carbon. Sep. Sci. Technol., 39 (14), 3331- 3351.

Sherrod, P. NLREG version 6.5 (Demonstration) copyright © 1992-2008.

Singh, S., Verma, L. S., Sambi, S. S., Sharma, S. K.. Adsorption Behaviour of Ni (II) from Water onto Zeolite X: Kinetics and Equilibrium Studies. Proceedings of the World Congress on Engineering and Computer Science 2008(WCECS 2008), October 22 - 24, 2008, San Francisco, USA.

Sips, R. (1948). On the structure of a catalyst surface, J. Chem. Phys. 16, 490–495.

Tumin, N. D., Chuah, A. L., Zawani, Z., Abdul Rashid, S. (2008). Adsorption of Copper from
        aqueous solution by *Elais guineensis* kernel activated carbon. Journal of Engineering
        Science and Technology Vol. 3, No. 2, 180 – 189.
Vaghetti, J. C. P. Zat, M., Bentes, K. R. S., Ferreira, L. S., Benvenutti, E. V., Lima, E. C. (2003).
        4-Phenylenediaminepropylsilica xerogel as a sorbent for copper determination in
        waters by slurry-sampling ETAAS, J. Anal. Atom. Spectrom. 18, pp. 376–380.
Weber Jr. W. J., Morris, J. C. (1963). Kinetics of adsorption on carbon from solution, J. Sanit.
        Eng. Div. Am. Soc. Civil Eng. 89, 31–59.

Part 2

Physicochemical Methods for Waste Water Treatment

Degradation of Nitroaromatic Compounds by Homogeneous AOPs

Fernando S. García Einschlag, Luciano Carlos and Daniela Nichela
Instituto de Investigaciones Fisicoquímicas Teóricas y Aplicadas
(UNLP, CCT CONICET), La Plata
Argentina

1. Introduction

Nitroaromatic compounds are environmental contaminants associated with anthropogenic activities such as production and use of dyes, explosives, pesticides and pharmaceuticals. Many of these substances, such as nitrobenzene and nitrophenols, usually found in wastewaters of these industries are considered potentially toxic. Because nitro-substituted aromatic compounds have strong electron withdrawing groups, they are poorly biodegradable by aerobic treatments. The detoxification of wastewaters containing these hazardous substances is very difficult since, due to their high stability, they are usually refractory to conventional biological treatments.

Research on alternative or additional methods of wastewater treatment is of current interest. Wastewater treatment by means of advanced oxidation processes (AOPs) has become one of the issues of major interest in modern environmental chemistry. Various AOPs are nowadays available and applicable at laboratory, pilot or even technical levels for achieving oxidative degradation of organic pollutants in aqueous media. These processes are based on the production of highly reactive species. Among them, the hydroxyl radicals ($HO^\bullet$) are the main oxidizing species. Hydroxyl radicals are able to oxidize most organic compounds due to their high reactivity and low selectivity. The reaction of $HO^\bullet$ with organic compounds (by addition to double bonds and/or by hydrogen abstraction) generates C-centered radicals that are subsequently trapped by dissolved oxygen to yield peroxides and peroxyl radicals. These intermediates initiate thermal chain autooxidation reactions and the overall processes may, if necessary, lead to complete mineralization. A clear understanding of the effect of reagent concentrations on the evolution of reaction byproducts is critical for producing proper engineering designs. Therefore, the optimization of AOP-methods for waste water treatment requires a comprehensive understanding of the chemical events that govern the transformation rates of the pollutants.

The main objective of this chapter is to provide a comprehensive description of physicochemical phenomena that govern both the transformation rates of nitroaromatic pollutants and the overall degradation efficiencies during waste water treatments by different advanced oxidation processes in homogeneous phase. The chapter summarizes the results obtained in studies related with the degradation of nitroaromatic compounds of environmental relevance by different homogeneous AOPs. Simple tools for describing the

main kinetic features of each system are presented. In addition, the influence of reaction conditions in the transformation pathways of nitrobenzene is discussed.

2. Methods

2.1 Substrate characterization
Physicochemical properties of the organic pollutants (i.e., absorption coefficients, rate constants, and acid-base behavior, among others) should be known to develop reaction models capable of predicting oxidation efficiencies. Speciation of the model pollutants may influence the kinetic trends observed in AOP systems since both the spectral behavior and the reactivity towards $HO^{\bullet}$ radicals depend on speciation. Speciation studies presented include the analysis of acid base and, for Fenton systems, complexation equilibria. In addition, spectral characterization of reaction mixtures is required for evaluating inner filter effects in photoenhanced technologies. Another relevant parameter to be considered is the substrate reactivity towards hydroxyl radicals since it governs the fraction of $HO^{\bullet}$ that effectively attack the model pollutant in a given reaction mixture. Therefore, rate constant values are usually required to evaluate $HO^{\bullet}$ scavenging effects. A brief summary of the basic tools used to characterize important physicochemical properties of the benzoic acid derivatives studied in subsections 3.6.3 and 3.7.2 is given below.

2.1.1 Acid base properties
The absorption spectra of the model substrates were recorded from pH 1.5 to pH 5.5. The values of the first deprotonation constants (pK_{a1}) were estimated by nonlinear fitting of the absorbance versus pH profiles obtained at selected wavelengths (Nichela et al., 2010)

$$f = \alpha_0 \times \left(Abs_P - Abs_D\right) + Abs_D \tag{1}$$

where α_0 are given by $10^{-pH} / (10^{-pKa} + 10^{-pH})$, Abs_P are the absorptions of the protonated forms and Abs_D are the absorptions of the deprotonated forms.

2.1.2 Substrate speciation and formation of ferric complexes
In order to characterize the substrate speciation conditional formation constants (K) at pH 3.0 for the 1:1 ferric complexes were estimated by nonlinear fitting of the absorbance versus [Fe(III)] profiles at the maximum wavelengths corresponding to each ferric complex. The following expression was used to obtain K values (Nichela et al., 2010)

$$f = a_o + \Delta\varepsilon \times b \times \frac{\left(K \times \left(M_0 + L_0\right) + 1\right) - \sqrt{\left(K \times \left(M_0 + L_0\right) + 1\right)^2 - 4 \times K^2 \times M_0 \times L_0}}{2K} \tag{2}$$

where a_0 is the absorbance of the initial solution containing the free ligand; M_0 and L_0 are the initial metal and ligand concentrations, respectively; b is the optical path length and $\Delta\varepsilon$ is the difference of absorption coefficients between the complex and the ligand.

2.1.3 Evaluation of rate constants by competition kinetics
The analysis of the consumption profiles of different compounds within the same environment in a competition experiment is a means to evaluate their relative reactivity (Pignatello et al., 1999). Assuming that the substituted benzoic acids (S_i) and a reference

compound (S_{Ref}) are solely decomposed by hydroxyl radicals, the following reactions show the competition for the oxidizing species:

$$\text{HO}^\bullet + \text{S}_i \rightarrow \textbf{Products} \qquad \text{k}_i \tag{3}$$

$$\text{HO}^\bullet + \text{S}_{ref} \rightarrow \textbf{Products} \qquad \text{k}_{ref} \tag{4}$$

Thus, the respective consumption rates can be expressed as

$$\frac{-d[S_i]}{dt} = k_i[HO^\bullet][S_i] \quad \Rightarrow \quad \frac{d\ln[S_i]}{dt} = -k_i[HO^\bullet] \tag{5}$$

$$\frac{-d[S_{ref}]}{dt} = k_{ref}[HO^\bullet][S_{ref}] \quad \Rightarrow \quad \frac{d\ln[S_{ref}]}{dt} = -k_{ref}[HO^\bullet] \tag{6}$$

If no assumption for the time dependence of the concentration profile for hydroxyl radicals is made, integration of eqns (5) and (6) yields

$$-\ln\frac{[S_i]_t}{[S_i]_0} = k_i\int_0^t[HO^\bullet]\,dt \tag{7}$$

$$-\ln\frac{[S_{ref}]_t}{[S_{ref}]_0} = k_{ref}\int_0^t[HO^\bullet]\,dt \tag{8}$$

From the kinetic profiles, measured for the substrate and the reference in a competition experiment, the relative reactivity ($\beta=k_i/k_{ref}$) can be obtained by plotting $\ln[S_i]$ against $\ln[S_{ref}]$ as described elsewhere (García Einschlag et al., 2003). Hence, if k_{ref} is known the absolute rate constant for the different substrates S_i can be calculated as $k_i = \beta \cdot k_{ref}$.

2.2 Monitoring the substrate transformation

Different analytical techniques are used to follow substrate consumption and product formation, among them UV/vis, HPLC-UV/vis, HPLC-MS, GC-MS, selective electrodes (i.e., Cl- and pH), IC and TOC. The reaction rates calculated from the concentration profiles allow obtaining kinetic information, whereas the analysis of reaction intermediates distributions are used for drawing mechanistic conclusions. Finally, the characterization of the initial toxicity and its evolution by means of toxicity tests is recommended.

2.3 Analysis of product distributions

For a detailed study of the contribution of different reaction channels of substrate degradation it should be taken into account that the initial attack of HO$^\bullet$ to nitroaromatic substrates produces hydroxynitrocyclohexadienyl-like radicals (HNCHD·). These radicals subsequently form different primary products through parallel reaction pathways. The yield of the i-th primary product (η_i) is defined as the degraded substrate fraction that converts into the corresponding product (X_i) as a result of the aforementioned reaction steps. As primary products also suffer the attack of HO$^\bullet$ radicals, the calculation of η values should be carried out by considering the following expressions describing the kinetic profiles of nitrobenzene (NBE) and its products (Carlos et al., 2008)

$$r_{NBE} = -\frac{d[NBE]}{dt} = -k_{NBE}[HO^\bullet][NBE] \tag{9}$$

$$r_i = \frac{d[Xi]}{dt} = \eta_i k_{NBE}[HO^\bullet][NBE] - k_i[HO^\bullet][X_i] \tag{10}$$

According to eqn (9), $[HO^\bullet]$ values can be obtained from measured r_{NBE} values as

$$[HO^\bullet] = \frac{r_{NBE}}{k_{NBE}[NBE]} \tag{11}$$

Hence, combining eqns (10) and (11) it is possible to deduce a general expression for η_i

$$\eta_i = \frac{r_i}{r_{NBE}} + \frac{k_i[X_i]}{k_{NBE}[NBE]} \tag{12}$$

If only initial reaction stages are considered, product concentrations are negligible and the second term of eqn (12) can be disregarded. Under these conditions, η_i values can be estimated as $\eta_i^{INI} = r_i^{INI}/r_{NBE}^{INI}$ which is strictly valid in the limit of zero conversion degree. In addition, normalized yields (η^N) may be used to compare the formation pathways of the phenolic products, the normalization factor being the sum of their yields

$$\eta^N{}_i = \frac{\eta_i}{\sum \eta_i} \tag{13}$$

Normalized yields permit a more direct comparison of relative contributions of the pathways that lead to the formation of phenols since their sum is independent from the nitrobenzene fraction transformed into other products.

2.4 Kinetic modeling

In order to obtain quantitative expressions describing simplified reaction models, the application of the steady state approximation for $HO^\bullet$ radicals is a very useful strategy. Thus, equations governing the production and fate of $HO^\bullet$ radicals (i.e., $r_{Prod}^{HO^\bullet}$ & $r_{Cons}^{HO^\bullet}$ = $k_{app}^{HO^\bullet}$ x $[HO^\bullet]$) should be taken into account. The evaluation of $r_{Prod}^{HO^\bullet}$ is presented for both dark and irradiated systems; whereas the $HO^\bullet$ scavenging factor, that governs the $HO^\bullet$ lifetimes, is calculated by taking into account the main decay pathways.

3. Reaction rates and simplified reaction schemes for homogeneous AOPs

This section presents simplified reaction schemes that allowed to obtain quantitative expressions for the experimental trends in different homogeneous AOP systems.

3.1 UV photolysis

In UV photolysis systems ultraviolet irradiation is directly absorbed by a chemical substrate (S), this process is followed by the decomposition of the excited species transforming the parent compound into one or more products. This transformation may involve homolytic or heterolytic breaking of the chemical bonds. These reactions can be represented as follows

$$\mathbf{S + h\nu \rightarrow S^* \rightarrow Prod \qquad P_a^S \Phi^S} \tag{14}$$
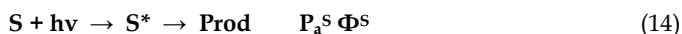
where P_a^S is the rate of photons absorbed by S and Φ^S is the quantum yield of substrate photolysis given by eqn (15) (Braun et al., 1986)

$$\Phi^S = \frac{r^S}{P_a^S} = \frac{-d[S]/dt}{P_0(1-10^{-A^S})} \qquad (15)$$

where r^S is the rate of substrate transformation (mol L^{-1} s^{-1}), P_a^S is the rate of photons absorbed by the substrate S (einstein L^{-1} s^{-1}), P_0 is the incident photonic rate (einstein L^{-1} s^{-1}) obtained by actinometry and $A^S = \varepsilon^S.l.[S]$ is the absorbance of S at the wavelength of irradiation. Given that many waste water plants use polychromatic irradiation, polychromatic quantum efficiencies (η_S) are a better parameter for practical purposes. The polychromatic quantum efficiency in these processes may be calculated using eqn (16)

$$\eta^S = \frac{-d[S]/dt}{P_0 \sum_i p_i(1-10^{-A^s_i})} \qquad (16)$$

where $d[S]/dt$ is the substrate degradation rate obtained from the slope of [S] vs. irradiation time, A_i is the absorbance at the ith irradiation wavelength, P_0, is the total incident photon rate, defined as the number of photons entering the solution per unit time and unit volume, p_i is the probability mass function of the photonic lamp emission and the factor $(1-10^{-A_i})$ accounts for the fraction of photons absorbed by the substrate within the reactor.

In order to test the efficiency of UV photolysis for the treatment of nitroaromatic substrates, aqueous solutions of 1-chloro-2,4-dinitrobenzene (CDNB); 2,4-dinitrophenol (DNP); nitrobenzene (NBE); 3-nitrophenol (MNP) and 4-nitrophenol (PNP) were irradiated at pH 2.5 using an HPK125 medium-pressure mercury arc lamp (García Einschlag et al., 2002b). In all cases, the conversion degrees of the different substrates were less than 4% after continuous irradiation for 2-3 h. Polychromatic quantum efficiencies were in the range 1.3×10^{-4}-7.8×10^{-4}. These results are in agreement with reported quantum yields of photolysis of various aromatic compounds that have been determined to be in the range 10^{-3} - 10^{-4} (Lipczynska-Kochany and Bolton, 1991; Lopez et al., 2000). Given the low values obtained for η_S, it is clear that UV photolysis is a rather inefficient method for treating nitroaromatic compounds in waste water.

3.2 VUV photolysis
Water strongly absorbs at irradiation wavelengths shorter than 190 nm, the absorption cross section increasing as the wavelength decreases between 190 and 160 nm (Heit et al., 1998). The VUV photolysis of water may be described by the following processes

$$H_2O + h\nu \rightarrow H^{\bullet} + HO^{\bullet} \qquad P_a^{H2O} \, \Phi^{H^{\bullet}} \qquad (17)$$

$$H_2O + h\nu \rightarrow H^+ + HO^{\bullet} + e^-_{aq} \qquad P_a^{H2O} \, \Phi^{e-} \qquad (18)$$
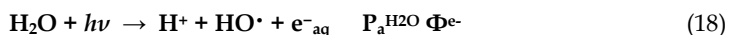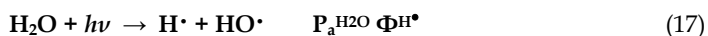
where P_a^{H2O}, $\Phi^{H^{\bullet}}$ and Φ^{e-} are the rate of photons absorbed by water, the quantum yield of H$^{\bullet}$ formation and the quantum yield of e- formation, respectively. It is important to recall that, given the high cross section of water molecules within the irradiation wavelength range, $P_a^{H2O} = P_0$. The quantum yield for the production of solvated electrons is low (0.05) and almost wavelength independent. In contrast, values of 0.42 and 0.33 at 172 and 185 nm, respectively, have been reported (Heit et al., 1998) for the quantum yield of HO$^{\bullet}$ production

($\Phi^{HO\bullet}$). In aerated solutions, H atoms and hydrated electrons are efficiently trapped by dissolved oxygen, yielding hydroperoxyl radicals ($HO_2^\bullet$) and its conjugated base, the superoxide anion ($O_2^{\bullet-}$). Since the latter species are much less reactive than hydroxyl radicals, the main pathway leading to the substrate decomposition is given by rxn (19)

$$\textbf{S} + \textbf{HO}^\bullet \ \rightarrow \ \textbf{Prod} \qquad \textbf{k}_\textbf{S} \tag{19}$$

The degradation of the substrate 4-chloro-3,5-dinitrobenzoic acid (CDNBA) by VUV process was studied (Lopez et al., 2000) with two VUV irradiation sources, a low pressure mercury arc with Suprasil envelope allowing irradiation at 185 nm and a xenon-excimer lamp emitting at 172 nm.
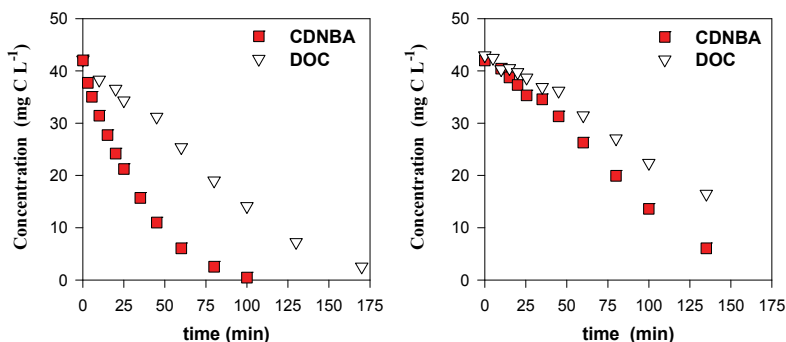
Fig. 1. Degradation of CDNBA by VUV photolysis of water. Left: 172 nm. Right: 185 nm.

Fig. 1a shows that irradiation of aerated aqueous solutions of CDNBA using the Xe-excimer lamp resulted in a relatively fast CDNBA degradation and an efficient mineralization within the first three hours. The disappearance of CDNBA and the DOC depletion were slightly slower under VUV irradiation at 185 nm than at 172 nm (Fig. 1b). The initial rates of CDNBA disappearance (r^S) were used to obtain the apparent quantum yields of substrate disappearance at each wavelength

$$\Phi_{app}^{S} = \frac{r^S}{P_0} \tag{20}$$

the initial Φ_{app}^{S} values being 1.1×10^{-2} and 0.90×10^{-2} at 172 and 185 nm, respectively. This slightly lower value of Φ_{CDNBA} may result from the lower $\Phi_{HO\bullet}$ at 185 nm than at 172 nm. The efficiency of $HO^\bullet$ radicals trapping by CDNBA was obtained from ratio of Φ_{CDNBA} and $\Phi_{HO\bullet}$ values. The low value obtained at both wavelengths (approx. 0.025) is related to the limited penetration of the VUV radiation in water. Relative high concentrations of short lived $HO^\bullet$ radicals are formed in a narrow layer around the lamp shaft, thus diffusion is not fast enough to avoid depletion of the substrate and molecular oxygen in this layer.

3.3 UV/H$_2$O$_2$ systems

In the UV/H$_2$O$_2$ process, the photolysis of H$_2$O$_2$ results in the homolysis of the oxygen-oxygen bond and the production of hydroxyl radicals (HO$^\bullet$).

$$\mathbf{H_2O_2 + h\nu \rightarrow 2\ HO^{\bullet}} \qquad \mathbf{P_a^{H2O2}\ \Phi^{H2O2}} \tag{21}$$
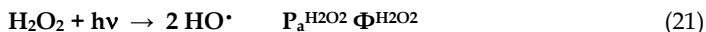
where P_a^{H2O2} is the rate of photons absorbed by H_2O_2 and Φ^{H2O2} is the quantum yield of H_2O_2 photolysis. Techniques based on the use of H_2O_2 are advantageous (Stefan et al., 1996) since H_2O_2 can be readily mixed with water in all proportions and costs associated to production and handling of H_2O_2 are not high. This process leads, in most cases, to the mineralization of the organic substrate, i.e. production of CO_2, H_2O, and mineral acids.

We studied the degradation of the substrates CDNBA, CDNB, DNP, MNP, NBE and PNP by the UV/H_2O_2 process (García Einschlag et al., 2002a; García Einschlag et al., 2002b). Dramatic changes in the absorption spectra were observed indicating that nitroaromatic substrates are rapidly consumed under these conditions. The degradation rates were strongly dependent on substrate and H_2O_2 concentrations. The initial rates of substrate disappearance (r=-d[S]/dt) under different conditions show that when increasing the concentration of H_2O_2, a maximum rate (r_{max}) could be observed. When increasing the initial substrate load $[S]_0$, the optimal H_2O_2 concentration ($[H_2O_2]_{OPT}$, defined as the initial H_2O_2 concentration for which r_{max} was reached) increased proportionally. Fig. 2 shows the behavior of the r/r_{max} represented as a function of the parameter R (defined as $[H_2O_2]_0/[S]_0$).
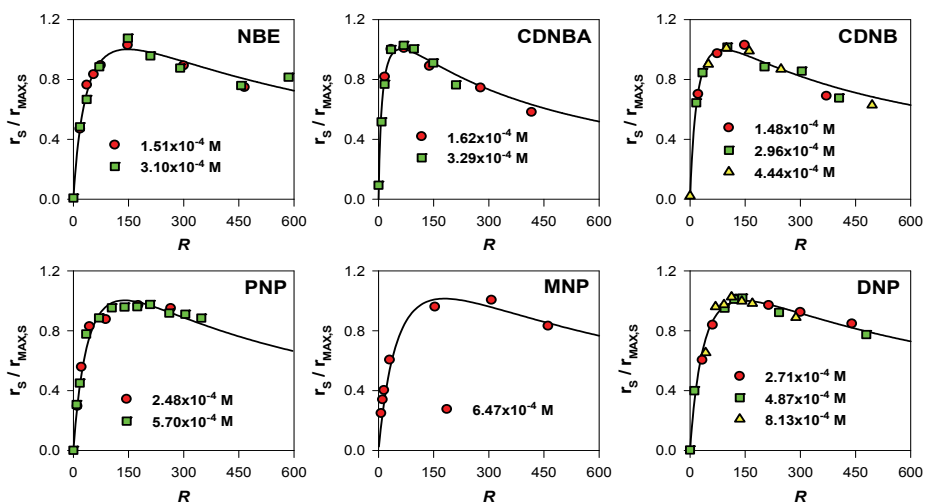
Fig. 2. Normalized initial consumption rates for the different substrates in UV/H_2O_2 processes.

Interestingly, optimal concentration ratios R_{OPT} (=$[H_2O_2]_{OPT}/[S]_0$) were independent of $[S]_0$. As $[H_2O_2]_0$ increased for a given $[S]_0$, a remarkable change in the initial rate was observed, but when $R > R_{OPT}$, this rate showed a smooth decrease. This behavior is of great importance from both a practical and an economical point of view, since there is a wide range of R values corresponding to oxidation rates of at least 90% of the optimal rate.

The degradation of pollutants by the UV/H_2O_2 technique involves a complex set of reactions. Although a detailed analysis of all the reactions involved in the oxidative degradation manifold of each compound is a very difficult task (Glaze et al., 1995; Stefan and Bolton, 1998; Crittenden et al., 1999; Stefan et al., 2000), the general trends observed are

very similar (Fig. 2). Hence, we proposed a simple kinetic model for describing the observed behavior (García Einschlag et al., 2002b). During the initial oxidation stages, only S and H_2O_2 are present in substantial amounts. Accordingly, the $HO^\bullet$ radicals generated by H_2O_2 photolysis rxn (21) may be trapped either by the substrates rxn (19) or by H_2O_2 rxn (22)

$$H_2O_2 + HO^\bullet \rightarrow HO_2^\bullet + H_2O \qquad k_{H2O2} \tag{22}$$
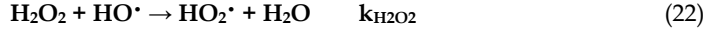
Reactions implying $HO_2^\bullet$ or $O_2^{\bullet-}$ have not been considered, as their reactivity is much lower than that of $HO^\bullet$ (Simic, 1975; Nadezhdin and Dunford, 1979; Getoff, 1997). A similar remark applies to the reactions associated with the intermediate products, whose concentrations during the first irradiation stages may be neglected. UV photolysis of the substrates was also disregarded (see section 3.1).

3.3.1 Initial degradation rates under monochromatic irradiation

According to the reduced set of reactions proposed, the substrate consumption rate (r) is governed by

$$r = \frac{-d[S]}{dt} = k_S\,[S][HO^\bullet] \tag{23}$$

Assuming that the steady-state hypothesis holds for $HO^\bullet$, their concentration is given by

$$[HO^\bullet] = \frac{r_{HO^\bullet}}{k_{H_2O_2}\,[H_2O_2] + k_S\,[S]} \tag{24}$$

where r_{HO} stands for the rate of $HO^\bullet$ production. Under monochromatic irradiation, r_{HO} may be expressed as

$$r_{HO^\bullet} = \frac{2\,P_0\,\Phi^{H_2O_2}\,(1 - 10^{-A})\,\varepsilon^{H_2O_2}\,[H_2O_2]}{\varepsilon^{H_2O_2}\,[H_2O_2] + \varepsilon^S\,[S]} \tag{25}$$

where $(1-10^{-A})[(\varepsilon_{H2O2}[H_2O_2])/(\varepsilon_{H2O2}[H_2O_2] + \varepsilon_S c_S)]$ is the fraction of photons absorbed by H_2O_2. Combining eqns (23), (24) and (25) and assuming absorbance values greater than 2, the oxidation rate of the substrate (r) may be expressed as (García Einschlag et al., 2002b)

$$r = \frac{2\,P_0\Phi^{H_2O_2}\varepsilon\,R}{(\varepsilon\,R + 1)(k\,R + 1)} \tag{26}$$

where $R=[H_2O_2]_0/[S]_0$, $\varepsilon=\varepsilon_{H2O2}/\varepsilon_S$ and $k=k_{H2O2}/k_S$. The optimal ratio R_{OPT} leading to the highest initial rate can be obtained by differentiation of eqn (26) (i.e. $R=R_{OPT}$ for $dr/dR=0$)

$$R_{OPT} = \sqrt{\frac{1}{k\,\varepsilon}} = \sqrt{\frac{k_S\,\varepsilon^S}{k_{H_2O_2}\,\varepsilon^{H_2O_2}}} \tag{27}$$

This simple expression of R_{OPT} ($=[H_2O_2]_{OPT}/[S]_0$) might be used, either to evaluate $[H_2O_2]_{OPT}$ if k_S and ε_S are known or to estimate k_S if $[H_2O_2]_{OPT}$ is determined experimentally. The validity of eqns (26) and (27) was tested by comparing experimental and simulated trends of the oxidation rates. Solid lines in Fig. 2 were calculated using eqn (26).

3.3.2 Initial degradation rates under polychromatic irradiation

The previous ideas can be extended to processes induced by polychromatic irradiation sources. A typical HPK125 lamp exhibits a continuous background and various emission lines. Therefore, the rate of photon absorption by hydrogen peroxide, P_a^{H2O2}, is described by

$$P_a^{H_2O_2} = P_0 \int_\lambda \frac{(1 - 10^{-A_\lambda}) \, \varepsilon_\lambda^{H_2O_2} \, [H_2O_2]}{\varepsilon_\lambda^{H_2O_2} \, [H_2O_2] + \varepsilon_\lambda^{S} \, [S]} \, p_\lambda \, d\lambda \tag{28}$$

where the quantity A_λ represents the total absorbance of the solution, $\varepsilon_\lambda^{H2O2}$ and ε_λ^{S} are the molar absorption coefficients of substrate and H_2O_2 at a given wavelength, and p_λ is the probability density function of the photonic emission. Although this integral cannot be solved in a simple way, the calculation of P_{H2O2} can be carried out as a discrete sum. Eqn (28) was solved for the wavelength range between 200 and 500 nm

$$P_{H_2O_2} = P_0 \sum_i p_i (1 - 10^{-A_i}) \frac{\varepsilon_i^{H_2O_2} \, [H_2O_2]}{\varepsilon_i^{H_2O_2} [H_2O_2] + \varepsilon_i^{S} \, [S]} \tag{29}$$

where subscript i refers to a very small finite wavelength interval (i.e., 1 nm) and p_i is the probability mass function of the photonic emission of the lamp. Thus, the expression equivalent to eqn (26) under polychromatic irradiation turns out to be

$$r_S = \frac{2 \, P_0}{(k \, R + 1)} \sum_i \frac{p_i \, \Phi_i^{H_2O_2} \, \varepsilon_i \, R}{(\varepsilon_i \, R + 1)} \tag{30}$$

where $\varepsilon_i = \varepsilon_i^{H2O2} / \varepsilon_i^{S}$. As already indicated r_S exhibits a maximum at R_{OPT}. After setting $dr_S/dR = 0$ the following expression can be obtained (García Einschlag et al., 2002a)

$$\sum_i \frac{p_i \, \Phi_i^{H_2O_2} \, \varepsilon_i}{(\varepsilon_i \, R_{OPT} + 1)^2} = k \sum_i \frac{p_i \, \Phi_i^{H_2O_2} \, \varepsilon_i^2 \, R_{OPT}^2}{(\varepsilon_i \, R_{OPT} + 1)^2} \tag{31}$$

It is clear that the latter equation cannot be rearranged to obtain R_{OPT} since it is an implicit equation (in R_{OPT}). In order to obtain an expression for R_{OPT} we defined the quantity $f(i)$ as

$$f(i) = \frac{p_i \, \Phi_i^{H_2O_2} \, \varepsilon_i}{(\varepsilon_i \, R_{OPT} + 1)^2} \tag{32}$$

which is a function of the spectral and kinetic properties of the system. Eqn (31) may be rearranged to give (García Einschlag et al., 2002a)
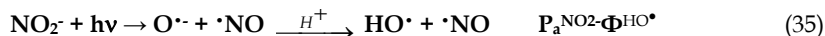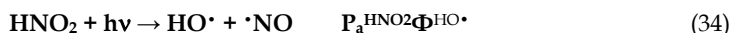
$$R_{OPT} = \sqrt{\frac{k_s}{k_{H_2O_2}} \left\langle \frac{\varepsilon^{H_2O_2}}{\varepsilon^{S}} \right\rangle^{-1}} \tag{33}$$

where $\langle \varepsilon^{H2O2} / \varepsilon^{S} \rangle$ is the statistical expectance of the ratio $\varepsilon_i^{H2O2} / \varepsilon_i^{S}$, the quantity $f(i)$ being the probability distribution function. Although eqn (33) does not allow the calculation of R_{OPT}, it is interesting to note its similarity with eqn (27) derived for monochromatic irradiation.
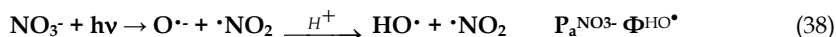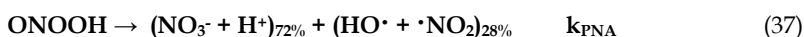
3.4 UV/NO$_3^-$ and UV/NO$_2^-$ systems

The photolysis mechanisms of nitrous acid, nitrite and nitrate involve photolytic pathways that result in the formation of HO$^•$ and nitrogen species such as $^•$NO, $^•$NO$_2$ and ONOO$^-$, as primary photoproducts (Mark et al., 1996; Mack and Bolton, 1999; Goldstein and Rabani, 2007). The primary photoprocesses and the main subsequent reactions leading to the production of HO$^•$ in acidic media are

Nitrous acid/nitrite systems

$$\mathbf{HNO_2 + h\nu \rightarrow HO^• + {}^•NO} \qquad \mathbf{P_a^{HNO2}\Phi^{HO•}} \qquad (34)$$

$$\mathbf{NO_2^- + h\nu \rightarrow O^{•-} + {}^•NO} \xrightarrow{H^+} \mathbf{HO^• + {}^•NO} \qquad \mathbf{P_a^{NO2-}\Phi^{HO^•}} \qquad (35)$$

Nitrate systems:

$$\mathbf{NO_3^- + h\nu \rightarrow ONOO^-} \xrightarrow{H^+} \mathbf{ONOOH} \qquad \mathbf{P_a^{NO3-}\Phi^{PNA}} \qquad (36)$$

$$\mathbf{ONOOH \rightarrow (NO_3^- + H^+)_{72\%} + (HO^• + {}^•NO_2)_{28\%}} \qquad \mathbf{k_{PNA}} \qquad (37)$$

$$\mathbf{NO_3^- + h\nu \rightarrow O^{•-} + {}^•NO_2} \xrightarrow{H^+} \mathbf{HO^• + {}^•NO_2} \qquad \mathbf{P_a^{NO3-}\Phi^{HO^•}} \qquad (38)$$

Among the photogenerated species, HO$^•$ is much more reactive and less selective than other primary photoproducts and peroxynitrite is unstable in acid media (Goldstein et al., 2005). Consequently, the kinetic behavior of many UV/HNO$_2$/NO$_2^-$ and UV/NO$_3^-$ systems is expected to be dominated by the production and fate of hydroxyl radicals.

We have studied the degradation of the substrates NBE and PNP by using UV irradiation in the presence of HNO$_2$/NO$_2^-$ or NO$_3^-$ as sources of HO$^•$ radicals at pH 3.0 (García Einschlag et al., 2009). It was found that both methods are capable of destroying the substrates within a few hours. The concentration profiles obtained by HPLC analyses follow pseudo-first-order kinetics for both substrates during several minutes of irradiation.
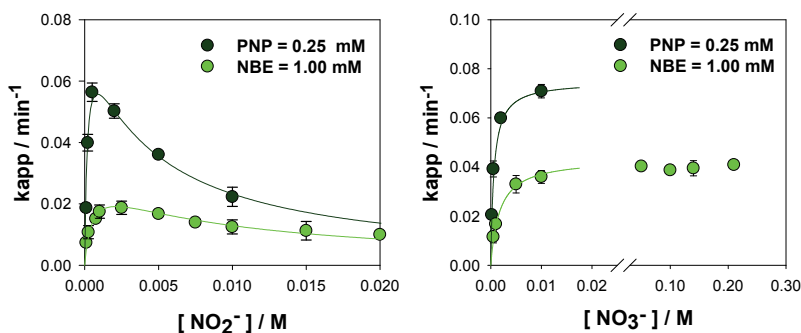
Fig. 3. Dependence of k$_{app}$ values for PNP and NBE degradation on additive concentrations.

The initial apparent rate constants (k$_{app}$) were found to depend on both the substrate and additive (I= HNO$_2$/NO$_2^-$ or NO$_3^-$) concentrations. In all cases, k$_{app}$ decreased with increasing initial substrate concentration. The dependencies of k$_{app}$ for PNP and NBE on the initial additive concentration for both UV/HNO$_2$/NO$_2^-$ and UV/NO$_3^-$ systems are shown in Fig. 3.
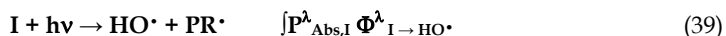
3.4.1 UV/HNO$_2$/NO$_2^-$ systems

Similarly to the behavior observed for UV/H$_2$O$_2$ systems, the apparent rate constants of NBE and PNP degradation induced by HNO$_2$/NO$_2^-$ photolysis show a maximum value and then decrease with increasing additive concentration (Fig. 3a). As in UV/H$_2$O$_2$ systems, this decrease in the apparent rate constant of substrate degradation is due to a scavenging effect of HO$^\bullet$ by the additive (similar scavenging effects have already been reported (Vione et al., 2004))**.** For the same additive concentration, higher values of k$_{app}$ are observed for PNP, the substrate present in lower concentration. In addition, the highest PNP and NBE degradation rates are observed for HNO$_2$/NO$_2^-$ concentrations of 0.9 mM and 2.1 mM, respectively. This result correlates well with the increase of the optimal additive concentration with substrate loading observed for UV/H$_2$O$_2$ systems**.** By contrast, rather low optimal ratios (R$_{OPT}$ = [I]$_{OPT}$/[S]) were observed (*i.e.* 3 for PNP and 2 for NBE) in comparison with those reported for UV/H$_2$O$_2$ systems (*i.e.* 160 for PNP and 150 for NBE) (García Einschlag et al., 2002b).

3.4.2 UV/NO$_3^-$ systems

The study of the effect of NO$_3^-$ concentration on k$_{app}$ yielded plots (Fig. 3b) with shapes that diverge from the trends observed in UV/HNO$_2$/NO$_2^-$ and UV/H$_2$O$_2$ systems, since no decrease of k$_{app}$ values was observed even at very high NO$_3^-$ concentrations. This result reveals that the effectiveness of NO$_3^-$ as HO$^\bullet$ scavenger is negligible due to the small value of the related rate constant (Mack and Bolton, 1999).

3.4.3 Simplified reaction model

The model proposed for UV/H$_2$O$_2$ systems can be easily extended to the UV/HNO$_2$/NO$_2^-$ and UV/NO$_3^-$ systems. The most important reactions involving the additives (I) may be represented as (García Einschlag et al., 2009)

$$\mathbf{I + h\nu \rightarrow HO^\bullet + PR^\bullet} \qquad \int \mathbf{P^\lambda_{Abs,I} \, \Phi^\lambda_{I \rightarrow HO^\bullet}} \tag{39}$$

$$\mathbf{I + HO^\bullet \rightarrow SR^\bullet} \qquad \mathbf{k_I} \tag{40}$$

where I represents the photoactive species (*i.e.* HNO$_2$/NO$_2^-$, NO$_3^-$ or H$_2$O$_2$) capable of generating HO$^\bullet$ radicals, PR$^\bullet$ denotes primary radicals accompanying HO$^\bullet$ generation (*i.e.* $^\bullet$NO, $^\bullet$NO$_2$ or HO$^\bullet$) and SR$^\bullet$ are radicals produced by HO$^\bullet$ attack towards the photoactive species (*i.e.* $^\bullet$NO$_2$, $^\bullet$NO$_3$ or HO$_2^\bullet$). In addition, P$^\lambda_{Abs,I}$ is the rate of photons absorbed by the additive I at a given wavelength of irradiation, $\Phi^\lambda_{I \rightarrow HO^\bullet}$ is the wavelength dependent quantum yield of HO$^\bullet$ photoproduction and k$_I$ is the bimolecular rate constant for the reaction of hydroxyl radicals with the photoactive species. As in the case of UV/H$_2$O$_2$ systems, reactions of the primary (PR$^\bullet$) and secondary (SR$^\bullet$) radicals as well as the reactions associated with the intermediate products may be neglected. Assuming steady-state conditions for HO$^\bullet$ radicals, an expression similar to eqn (24) can be obtained. In order to evaluate the rate of HO$^\bullet$ production in UV/I systems, the following expression can be used

$$r_{Prod,HO^\bullet} = P_0 \sum_\lambda \Phi^{I \rightarrow HO^\bullet}_\lambda \times (1 - 10^{-A_\lambda}) \times \frac{\varepsilon^I_\lambda [I]}{\varepsilon^I_\lambda [I] + \varepsilon^S_\lambda [S]} \times p_\lambda \tag{41}$$

Hence, the initial apparent rate constant of substrate consumption is given by

$$k_{app} = \frac{P_0}{\frac{k_I}{k_S}[I]+[S]} \sum_{\lambda} \frac{\Phi_{\lambda}^{I \rightarrow HO^{\bullet}}(1-10^{-A_{\lambda}})[I]}{[I]+\frac{\varepsilon_{\lambda}^{S}}{\varepsilon_{\lambda}^{I}}[S]} p_{\lambda} \qquad (42)$$

Replacing the summation with a factor of the form $[I]/([I] + c[S])$ and using R in place of $[I]/[S]$, the latter equation may be approximated by

$$k_{app} \cong \frac{a \times R}{[S] \times (bR+1) \times (R+c)} \qquad (43)$$

where the parameter "a" depends on both the incident photon rates and the polychromatic quantum efficiencies.

Equation (43) is a rough approximation of k_{app} that may be used to account for the trends observed. Nonlinear fitting was used to obtain the parameters "b" and "c" for the substrates NBE and PNP in the $UV/HNO_2/NO_2^-$, UV/NO_3^- and UV/H_2O_2 systems (García Einschlag et al., 2009). Although the constants obtained have no straightforward physical interpretation, the parameter "b" is mainly related to the ratio of rate constants k_I/k_S, whereas the parameter "c" may be considered as an effective value for the relative absorption coefficient. The solid lines in Fig. 3 show that the model is capable of describing the observed trends. The analysis of "b" values obtained with eqn (43) are in reasonable agreement with reported bimolecular rate constants (Buxton et al., 1988). On the other hand, the values obtained for parameter "c" reflect the fact that average inner filter effects are much more noticeable for UV/H_2O_2 systems than for $UV/HNO_2/NO_2^-$ and UV/NO_3^- systems. Thus, the trends experimentally observed for k_{app} against the concentration of $HO^{\bullet}$ photoproducers may be rationalized by considering two opposite effects. The increase of additive concentrations increases the amount of photons absorbed by the photoactive species whereas high additive concentrations may either result in significant decreases of the degradation rates or not, depending on the additive's ability to trap hydroxyl radicals.

3.5 Fenton systems

It is generally accepted that, in Fenton systems, the most important reactive species are hydroxyl radicals, produced by interaction of H_2O_2 with ferrous ions in acid media (Pignatello et al., 2006)

$$Fe^{2+} + H_2O_2 \rightarrow Fe^{3+} + HO^{\bullet} + HO^{-} \qquad k_{Fe+2} \qquad (44)$$
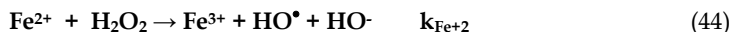
The removal of organic compounds in reaction mixtures starting with Fe^{2+} and having H_2O_2 in large stoichiometric excess (10 to 100 peroxide-to-iron molar ratio) generally exhibits an initial fast degradation phase due to the high amount of $HO^{\bullet}$ produced by rxn (44). Subsequently, a much slower phase is usually observed (where the reduction of Fe^{+3} is rate-limiting (De Laat and Gallard, 1999)). The extent of each phase usually depends on the iron/organic compound molar ratio (Chan and Chu, 2003). We studied the degradation of NBE using the Fenton reagent in different experimental conditions (Carlos et al., 2008). Fig. 4 shows the concentration profiles obtained in a representative experiment for NBE and the primary phenolic derivatives.

3.6 Fenton-like systems

Fenton-like processes involve a series of thermal reactions catalyzed by transition metal salts (ferric and cupric salts, among others) that lead to H_2O_2 decomposition. In addition to the
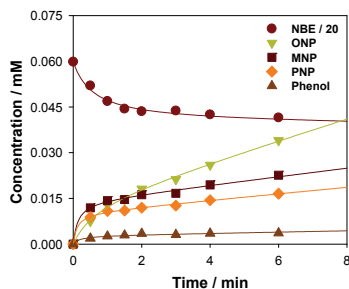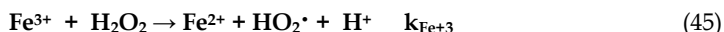
Fig. 4. Kinetic profiles of NBE and its primary phenolic products obtained in Fenton treatment.

oxidation of Fe^{+2} by H_2O_2 rxn (44), ferric ions can also react with H_2O_2 through rxn (45) thereby regenerating Fe^{2+} and supporting the Fenton process (Walling, 1975)

$$Fe^{3+} + H_2O_2 \rightarrow Fe^{2+} + HO_2^\bullet + H^+ \quad k_{Fe+3} \tag{45}$$

In the absence of organic matter, the latter reaction is rate limiting for H_2O_2 decomposition since the rate constant for rxn (44) is about 4 orders of magnitude higher than that of rxn (45). However, it has been established that organic compounds can remarkably affect the kinetics of H_2O_2 decomposition, because they can significantly increase the rates of chain propagation steps. It has been reported (Chen and Pignatello, 1997) that catalytic amounts of quinone-like intermediates (QLH_2 and $QLH^\bullet$) enhance organic matter oxidation since they can readily accelerate the reduction of ferric species to ferrous species.

$$Fe^{3+} + QLH_2 \rightarrow Fe^{2+} + QLH^\bullet + H^+ \tag{46}$$

$$Fe^{3+} + QLH^\bullet \rightarrow Fe^{2+} + QL + H^+ \tag{47}$$
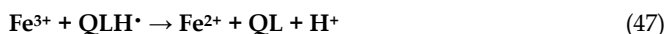
Given the complexity of Fe^{3+}/H_2O_2 systems, many variables may significantly influence the efficiency and the economic competitiveness of these techniques.

3.6.1 Autocatalytic concentration profiles

We have studied NBE oxidation kinetics in excess of H_2O_2 and catalytic concentrations of Fe^{3+} (Nichela et al., 2008). We found that NBE kinetic profiles display an autocatalytic behavior with an initial ''slow phase'', where [NBE] slightly decreases at a practically constant rate for conversion degrees lower than 10%, followed by a ''fast phase'' where the process is substantially accelerated obeying pseudo first-order kinetics. A typical concentration profile is presented in Fig. 5. The complex consumption profiles were analyzed by calculating the rates during the slow phase (r^{NBE}_{slow}), the average rates of the fast phase (r^{NBE}_{fast}), the apparent pseudo first-order rate constants for the fast phase (k^{NBE}_{fast}), and the transition times from the slow to the fast phase (t_{tr}^{NBE}). The slopes fitted for NBE consumption throughout each phase and the transition time, obtained by the intersection of the straight lines linked to each phase, are depicted in Fig. 5.

Although Fenton-like processes may involve very complex reaction mechanisms (Pignatello et al., 2006) a reduced set of reactions allow explaining the experimental trends observed (Nichela et al., 2008). The organic matter oxidation is induced by hydroxyl radicals produced through rxn (44). According to the value of k_{Fe+2} and the typical [H_2O_2] used in
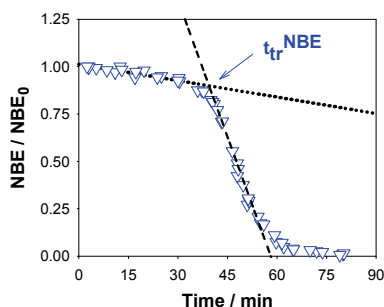
Fig. 5. Normalized autocatalytic profiles obtained for NBE in Fenton-like systems.

Fenton-like systems, the overall reaction rates are mainly controlled by the reduction of Fe^{3+} to Fe^{2+}. The autocatalytic profiles can be explained considering that during the first reaction stages the rate limiting step is Fe^{2+} production via rxn (45). This is supported by the dependence of r^{NBE}_{slow} on $[Fe^{3+}]_0$ and $[H_2O_2]_0$. As the reaction advances, quinone-like species such as hydroquinone, semiquinone radical and structurally related nitro-derivatives are generated. Some of these aromatic intermediates can provide alternative pathways for Fe^{3+} reduction such as rxns (46) and (47), thereby promoting the global acceleration of the process (Chen and Pignatello, 1997).

During the initial phase only a 10% of NBE is consumed, however this phase covers more than 50% of the time required for complete NBE oxidation. Thus, from a technical viewpoint it is wise to perform a detailed analysis of the reaction rates for the slow phase. In order to describe several kinetic features, the parameter z^{NBE}_{slow} was used (Nichela et al., 2008)

$$z_{Slow}^{NBE} \equiv \frac{r_{Slow}^{NBE}}{[NBE]_0} \tag{48}$$

Hence, z^{NBE}_{slow} corresponds to NBE oxidation rate during the slow phase relative to $[NBE]_0$. It was experimentally observed that z^{NBE}_{slow} increases with $[H_2O_2]_0$ and $[Fe^{3+}]_0$ but decreases with $[NBE]_0$, within the analyzed concentration range. In addition, as z^{NBE}_{slow} increases, the transition time towards the fast phase diminishes. Figure 6 shows linear dependencies among functions of z^{NBE}_{slow} and $[NBE]$, $[Fe^{3+}]$, $[H_2O_2]$ and t_{tr}^{NBE} values.

3.6.2 Simplified model for the slow phase

The increase of r^{NBE}_{slow} with $[H_2O_2]_0$ and $[Fe^{3+}]_0$ may be ascribed to an enhanced $HO^\bullet$ production by reactions (44) and (45). On the other hand, an increase of NBE concentration diminishes the steady-state concentration of hydroxyl radicals by scavenging effect through rxn (19), resulting in lower z^{NBE}_{slow} values. Neglecting the effect of organic byproducts during early reaction stages, reactions (19), (22), (44) and (45) can be considered as the key steps of the slow phase. As a result, simple equations for r_{Slow}^{NBE} and r_{Slow}^{H2O2} can be deduced assuming steady-state for Fe^{2+} and $HO^\bullet$

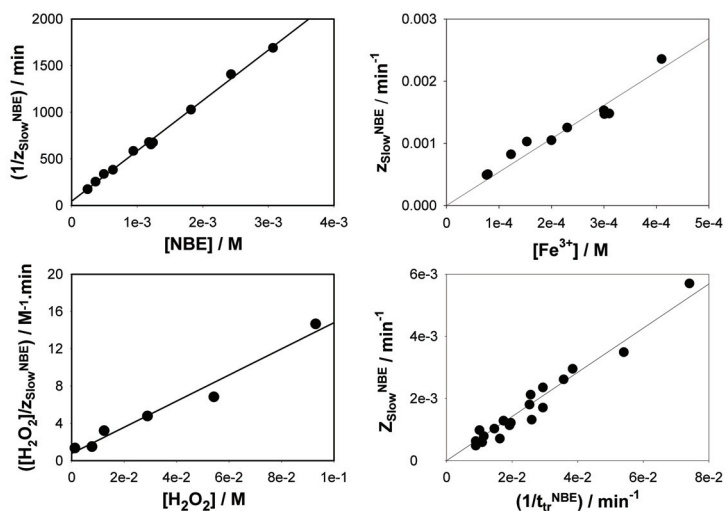$$[Fe^{2+}]_{Slow} \cong \frac{k_{Fe^{+3}}}{k_{Fe^{+2}}} \cdot [Fe^{3+}] \cong \frac{k_{Fe^{+3}}}{k_{Fe^{+2}}} \cdot [Fe^{3+}]_0 \tag{49}$$

Fig. 6. Linear relationships among functions of z^{NBE}_{slow} and different parameters

$$[HO^{\bullet}]_{Slow} \cong \frac{k_{Fe^{+2}} . [Fe^{2+}]_{ss} . [H_2O_2]}{k_{NBE} . [NBE] + k_{H_2O_2} . [H_2O_2]} \qquad (50)$$

Given that $k_{Fe+3} << k_{Fe+2}$, during the slow phase the Fe^{2+} concentration is negligible and $[Fe^{3+}]_{slow} \approx [Fe^{3+}]_0$. By combining the rate equations for NBE and H_2O_2 with eqns (49) and (50), the following expressions for the slow phase can be obtained (Nichela et al., 2008)

$$r^{NBE}_{Slow} = k_1 . [Fe^{3+}] . [H_2O_2] \left\{ \frac{k_{NBE} . [NBE]}{k_{NBE}[NBE] + k_{HP}[H_2O_2]} \right\} \qquad (51)$$

$$r^{HP}_{Slow} = k_1 . [Fe^{3+}] . [H_2O_2] . \left\{ 2 + \frac{k_{HP} . [H_2O_2]}{k_{NBE}[NBE] + k_{HP}[H_2O_2]} \right\} \qquad (52)$$

It is worth to mention that eqns (51) and (52) are in excellent agreement with the experimental trends, as it is observed in Fig. 6.

3.6.3 Semi quantitative analysis of the autocatalytic profiles

We also used Fenton-like process for the oxidation of a series of structurally related substrates, in order to test the autocatalytic nature of these systems (Nichela et al., 2010). The model compounds were 2-hydroxybenzoic (2HBA), 2,4-dihydroxybenzoic (24DHBA), 2-hydroxy-5-nitrobenzoic (2H5NBA), 4- hydroxy-3-nitrobenzoic (4H3NBA) and 2- hydroxy-4-nitrobenzoic (2H4NBA) acids. The normalized profiles of [S] and [H$_2$O$_2$] are shown in Fig. 7. The kinetic behavior is strongly dependent on the nature of the substrate and, excepting 4H3NBA, the substrates clearly display autocatalytic decays, the profiles being like inverted S-shaped curves. The quantitative description of this kinetic traces is rather complicated and, to the best of our knowledge, no simple equation has been proposed to model
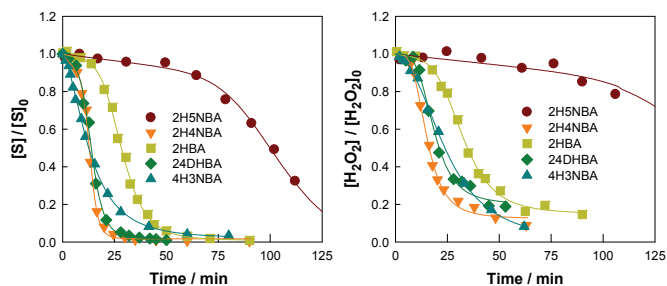
Fig. 7. Normalized concentration profiles of model substrates obtained in dark Fenton-like process.

concentration profiles of this kind that are frequently found in degradation studies of environmental relevance. For the quantitative comparison of the kinetic curves we proposed an empirical equation for fitting the normalized decay profiles (Nichela et al., 2010)

$$f = \frac{(1 - a \times t - d)}{1 + (t/b)^{c}} + d \tag{53}$$

In this equation, the parameters a, b, c and d may be employed to characterize the average oxidation rate during the slow phase (the normalized initial rate), the time required to reach half of the initial concentration (the apparent half-life), the average slope during the fast phase and the final residual value, respectively. The solid lines in Fig. 7 show that eqn (53) allows a precise estimation of the temporal dependence of concentration profiles. Although the chemical structures of the substrates are closely related, the degradation timescales are remarkably different. During early reaction stages, the depletion rates follow the trend 4H3N-BA > 2H4N-BA ≈ 24DH-BA > 2H-BA >> 2H5NBA. It should be noted that, despite lacking a precise kinetic meaning, eqn (53) has a key advantage from a practical point of view: it requires only a few experimental points to draw S-shaped curves that closely describe the complex autocatalytic profiles frequently observed in Fenton-like systems.

3.7 Photo-Fenton systems

The strategy most frequently used in Fenton systems to increase the reaction rates and improve the mineralization efficiencies is the use of UV and/or visible irradiation. The enhancement is mostly due to the photolysis of Fe^{3+} complexes which dissociate in the excited state to yield Fe^{2+} and an oxidized ligand (Sima and Makanova, 1997)

$$[Fe^{3+}(OH)]^{2+} + h\nu \rightarrow Fe^{2+} + HO^{\bullet} \tag{54}$$

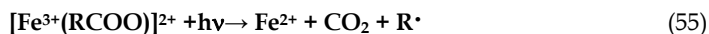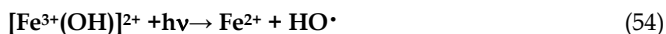$$[Fe^{3+}(RCOO)]^{2+} + h\nu \rightarrow Fe^{2+} + CO_2 + R^{\bullet} \tag{55}$$

Photo-Fenton techniques are useful since even at low $[Fe^{3+}]$ high reaction rates are obtained. Besides, mineralization may be achieved through the photolysis of stable ferric complexes.

3.7.1 Influence of reaction conditions

The photo-Fenton degradation of NBE was studied under different conditions using simulated solar irradiation (Carlos et al., 2009). The induction period preceding the catalytic

phase is significantly shortened since the rates of the initial slow phase are enhanced by irradiation, although the effect of simulated solar light on the rates of the fast phase is negligible. The enhancement of the slow phase may be explained taking into account the contribution of photoinduced processes, such as the photoreduction of Fe^{3+} in the predominant Fe^{3+}–aquo complex at pH 3 by inner-sphere ligand-to-metal charge transfer (LMCT) (Lopes et al., 2002). At early stages, rxn (54) provides an alternative Fe^{3+} reduction pathway that is faster than rxn (45), thus substantially increasing Fe^{2+} and $HO^{\bullet}$ production rates. By contrast, the rates associated to the fast phase are independent of irradiation since they are mainly governed by thermal reactions (46) and (47). The effect of the initial concentrations on NBE and H_2O_2 profiles are shown in Fig. 8.
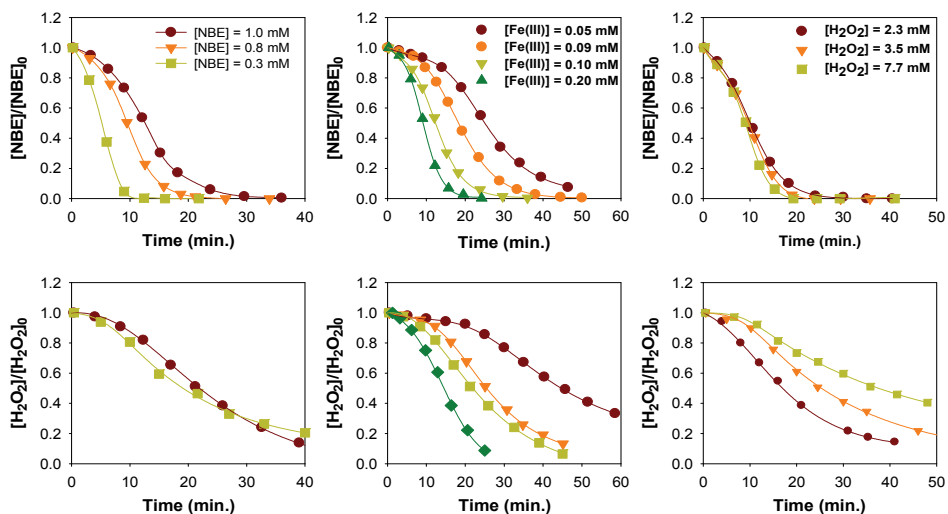
Fig. 8. Effect of initial conditions on the concentration profiles obtained during NBE photo-Fenton treatment.

In line with the results shown in section 3.6.1, the rates of the slow phase increase with $[Fe^{+3}]$ and $[H_2O_2]$, whereas z^{NBE}_{slow} values decreases with organic matter loading.

3.7.2 Influence of substrate structure

Degradation of the substrates of section 3.6.3 was studied under identical conditions but using UV irradiation (Fig. 9) (Nichela et al., 2010). As in the case of NBE, the slow initial phase is shortened in irradiated systems. The comparison between the different substrates reveals the same reactivity order as observed for Fenton-like systems. The solid lines in Fig. 9 confirm the utility of eqn (53) for describing autocatalytic profiles.

3.7.3 Photoenhancement factor

With the purpose of making a rough estimation of the relative contribution of photo stimulated pathways in photo-Fenton systems, we proposed (Nichela et al., 2010) the parameter photo enhancement factor (PEF) defined by
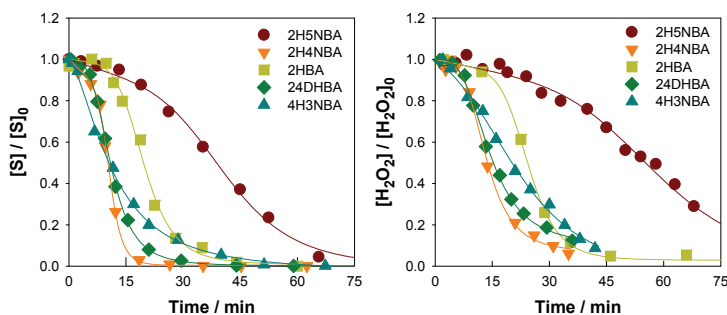
Fig. 9. Normalized concentration profiles of model substrates obtained in the photo-Fenton process.

$$PEF = \frac{k_{App}^{Phot} - k_{App}^{Dark}}{k_{App}^{Phot}} \qquad (56)$$

where k_{App}^{Dark} and k_{App}^{Phot} are the rate constants linked to the dark and photo enhanced reactions, respectively. The PEF is a useful index that allows evaluating the contribution of photo induced processes in photo-Fenton systems. In addition, the "apparent half-lives" can be used to define an "overall photo enhancement factor" (PEF_O) by the following relation

$$PEF_O = 1 - \frac{t_{1/2}^{Phot}}{t_{1/2}^{Dark}} \qquad (57)$$

The analysis of PEF_O values corresponding to the normalized profiles showed that higher photo enhancements are found for conditions where the dark reaction is slower. This behavior may be interpreted assuming that the rates of the photo induced reactions mostly depend on the photon flux and do not significantly depend on the nature of the substrate or the reaction conditions. Therefore, for a relatively constant photochemical contribution, the slower the dark reaction is, the greater the effect of photoinduced pathways results.

4. Product yields and mechanism of nitrobenzene transformation

Nitrobenzene thermal degradation was investigated using Fenton´s reagent in several experimental conditions. This section deals with the analysis of the distributions of intermediate reaction products and the mechanisms of nitrobenzene decomposition.

4.1 Initial steps of NBE transformation

From the analysis of reaction products distributions as a function of NBE conversion degree, a mechanism was proposed for NBE degradation in AOP systems (Carlos et al., 2008). The first steps involve two main pathways: hydroxylation pathways which yield phenolic derivatives and the nitration pathway which yields 1,3-dinitrobenzene (scheme 1).

Hydroxyl radicals usually react with benzene derivatives by electrophilic addition to form hydroxycyclohexadienyl-like radicals (Walling, 1975; Oturan and Pinson, 1995) that can undergo different processes according to the reaction conditions (i.e. [Fe^{2+}], [H_2O_2], [Fe^{3+}],
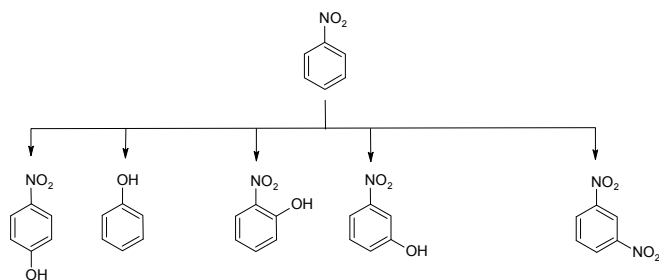
Scheme 1. Nitrobenzene primary hydroxylation and nitration pathways

[O_2], etc.) (Pignatello et al., 2006). Since $HO^\bullet$ reacts with both the target substrate and its reaction products, the concentration profiles of reaction intermediates during AOP treatments result from a balance between their formation and degradation rates. As the composition of the reaction mixture changes with time, both the formation yields and degradation rates of intermediate products can vary during the course of reaction. Therefore, an important feature to be considered is the dependence of the mechanism with reagent concentrations since these parameters may influence the kinetics as well as the distribution of products thereby affecting the global efficiency of the detoxification process.

4.2 Analysis of primary product yields
The equations derived in section 2.3 were used to analyze the influence of reaction conditions on the primary reaction yields. The results are given below.

4.3 Hydroxylation Pathways
Normalized yields obtained in Fenton systems reveal significant differences in the product distributions associated to each reaction stage (Carlos et al., 2008). The η^N_{ONP} values observed during the initial fast phase are at least 30% lower than those determined in the slow one. On the contrary, η^N_{phenol} values are higher in the fast phase than in the slow one. In addition, increasing $[Fe^{2+}]_0$ markedly decreases η^N_{ONP} while significantly increases η^N_{phenol} values.

The observed differences in the normalized yields may be explained taking into account that the first oxidation step is the $HO^\bullet$ radical addition on the aromatic ring to form hydroxycyclohexadienyl-type radicals.

$$\tag{58}$$
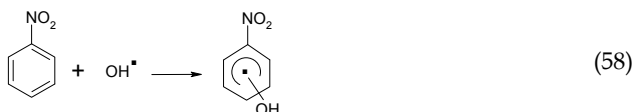
This type of radicals can undergo different reactions such as dimerization, disproportionation, oxygen addition to give corresponding peroxy-radical or can participate in electron transfer reactions with transition metals depending on the substituents in the aromatic ring and on the medium nature (Chen and Pignatello, 1997). The addition of $HO^\bullet$ radical in ortho, meta and para positions of the nitrobenzene ring can yield 2-nitrophenol (ONP), 3-nitrophenol (MNP) and 4-nitrophenol (PNP) by oxidation or disproportionation of the corresponding $HNCHD^\bullet$ radicals (Bathia, 1975)

$$(59)$$

o, m, p - isomers

$$(60)$$

o, m, p - isomers
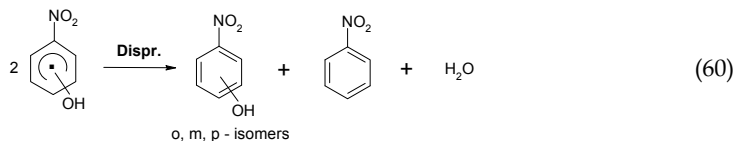
Usually, the distribution of isomers in HO$^\bullet$ mediated hydroxylation does not obey the foreseen orientation according to deactivating characteristics of the nitro group but it depends significantly on reaction conditions.

4.3.1 Effect of O_2

In the presence of oxygen the second-order reactions have a secondary contribution to the primary phenolic yields, since HNCHD$^\bullet$ radicals rapidly decay following a pseudo first order kinetics by addition of O_2. The oxidation of HNCHD$^\bullet$ radicals by O_2 is a very complex process and several pathways leading to different reaction products can compete (Pan et al., 1993). Among the reaction routes involving the peroxyl radicals formed by O_2 addition to HNCHD$^\bullet$, the elimination of HO$_2^\bullet$ yields the corresponding nitrophenols. Hence, $[O_2]$ plays an important role in NBE degradation pathways. In the absence of O_2, bimolecular processes become significant. Our results suggest that in crossed disproportionation reactions, meta-HNCHD$^\bullet$ radicals may act as oxidizers with respect to para-HNCHD$^\bullet$ or ortho-HNCHD$^\bullet$ radicals, yielding PNP or ONP and NBE (rxn (60)).

4.3.2 Effect of Fe^{2+}

The low ONP yields obtained with high $[Fe^{2+}]$ can be explained by considering two consecutive processes, i.e. the selective reduction of ortho-HNCHD$^\bullet$ radicals by Fe^{2+} to give Fe^{3+} and the corresponding organic anion followed by the regeneration of the starting nitrobenzene

$$\mathbf{Fe^{2+} + {^\bullet}OHC_6H_5NO_2 \rightarrow C_6H_5NO_2 + Fe^{3+} + OH^-} \qquad (61)$$
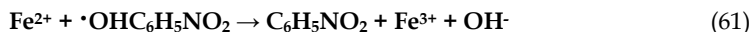
4.3.3 Effect of Fe^{3+}

The tests carried out in air saturated solutions show an increase of η^N_{ONP} with the $[Fe^{3+}]$. Since it is well known that Fe^{+3} is not a strong oxidant in aromatic hydroxylation (Fang et al., 1996), the increase of ONP yield with $[Fe^{3+}]_0$ can be explained if it is assumed that ortho-HNCHD$^\bullet$ radicals are stabilized by means of Fe^{3+} complexation through one of the oxygen atoms belonging to the nitro group and the oxygen of the HO group. Within this context, the relatively high stability of ortho-NHCHD$^\bullet$ radicals complexed with Fe^{3+} ions would allow explaining the observed results.
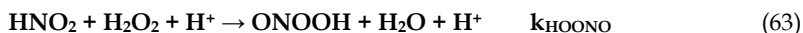
4.3.4 Phenol production

The presence of traces of phenol and NO_2^- among the initial reaction products shows that a small fraction of HO$^\bullet$ radicals attacks the nitrobenzene ipso position and induces the

cleavage of the nitro group. The experimental results showed that the increase of [Fe^{2+}] is accompanied by an increase of phenol yiled. Therefore, phenol may be formed from nitrobenzene through rxn (62)

$$(62)$$
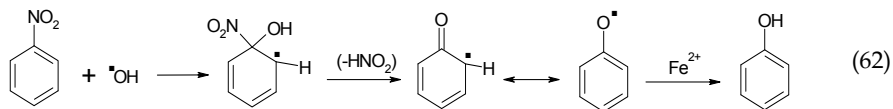
4.4 Nitration Pathways

As NBE degradation proceeds in AOP systems, the organic nitrogen is mainly released as nitrite ions (García Einschlag et al., 2002b; Carlos et al., 2008; Carlos et al., 2009). In the darkness and at pH 3, the released HNO_2/NO_2^- (pKa = 3.3) can lead to the formation of different nitrating agents such as peroxynitrous acid (ONOOH) and the $\cdot NO_2$ radical through the following reactions (Fischer and Warneck, 1996; Merenyi et al., 2003):

$$HNO_2 + H_2O_2 + H^+ \rightarrow ONOOH + H_2O + H^+ \qquad k_{HOONO} \qquad (63)$$

$$HNO_2/NO_2^- + \cdot OH \rightarrow \cdot NO_2 + H_2O/HO^\cdot \qquad k_{NO2-} \qquad (64)$$

The ONOOH decomposes in acid media yielding NO_3^-/H^+ and $\cdot NO_2/ HO^\cdot$. Therefore, $\cdot NO_2$ radicals can be in situ formed by NO_2^- oxidation trough either thermal or photochemical reactions. On the other hand, in UV/I systems both HNO_2/NO_2^- and NO_3^- photolysis may also contribute to the production of reactive nitrogen species through the photolytic reactions (34), (35), (36) and (38) (Mack and Bolton, 1999; Goldstein and Rabani, 2007). $\cdot NO_2$ and ONOOH are nitrating agents capable of participating in the formation of 1,3-DNB under the reaction conditions used in the different AOPs.

In this section we analyze the conditions that favor the formation of 1,3-DNB during NBE treatment using different AOPs (Carlos et al., 2010). Fig. 10 plots the amount of 1,3-DNB formed (expressed as [1,3-DNB]/[NBE]$_0$) against the conversion degree of nitrobenzene (defined by 1-[NB]/[NBE]$_0$). In all cases, the production of 1,3-DNB is practically negligible for NBE degradation percentages lower than 20%. Subsequently, the formation of 1,3-DNB increases until reaching a maximum for conversion degrees of about 0.9. Finally, as NBE is completely consumed, a steady decrease in 1,3-DNB concentration is observed. The latter trend is consistent with the hypothesis that 1,3-DNB is a primary product of NBE degradation (Carlos et al., 2008). It is important to note that, although curves in Fig. 10 show similar trends of 1,3-DNB formation, UV/H_2O_2 process yielded much lower 1,3-DNB levels than Fenton systems, thus suggesting an important contribution of iron species in NBE nitration pathways.

4.4.1 Influence of HNO_2/NO_2^- and NO_3^- in dark processes

NBE degradation experiments using Fenton's reagent in the dark and with different initial concentrations of NO_2^- or NO_3^- show that the presence of NO_3^- does not affect the consumption of NBE nor the production of 1,3-DNB while the presence of NO_2^- decreases NBE consumption and significantly increases the fraction of NBE transformed to 1,3-DNB. The latter trends can be explained by considering the enhancement, through rxn (64) of both HO$\cdot$ radical scavenging and $\cdot NO_2$ production as [NO_2^-]$_0$ is increased. Taking into account
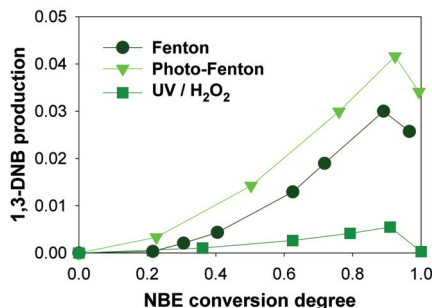
Fig. 10. Relative production of 1,3-dinitrobenzene against the conversion degree of nitrobenzene.

these results, the feasibility of a direct reaction between NBE and $\cdot NO_2$ was tested by incubating NBE in solutions of HNO_2 at acid pH. In the latter conditions HNO_2 decomposes yielding $\cdot NO_2$, $\cdot NO$ and H_2O (Vione et al., 2005). Since [NBE] remained constant and no formation of 1,3-DNB was observed the direct reactions of either $\cdot NO_2$ or $\cdot NO$ with NBE were neglected.

4.4.2 Influence of HNO_2/NO_2^- and NO_3^- in photochemical processes

NBE degradation experiments were conducted at pH 3 in both $UV/HNO_2/NO_2^-$ and UV/NO_3^- systems using different additive concentrations (García Einschlag et al., 2009). In $UV/HNO_2/NO_2^-$ systems DNB yield ($\eta^0_{1,3-DNB}$) was negligible below 1mM of $[NO_2^-]_0$, then increased up to a value of 0.06 and remained constant above 8mM of $[NO_2^-]_0$. On the other hand, in UV/NO_3^- systems significant amounts of 1,3-DNB were observed even for very low $[NO_3^-]$ and $\eta^0_{1,3-DNB}$ increased with $[NO_3^-]$, 1,3-DNB being the most important by-product at high NO_3^- concentrations.

4.4.3 Influence of Fe^{3+} and O_2 in $UV/HNO_2/NO_2^-$ and UV/NO_3^- systems

An enhancement of 1,3-DNB formation upon Fe^{3+} addition was observed in $UV/HNO_2/NO_2^-$ systems. The increase of 1,3- DNB production with increasing $[Fe^{3+}]_0$ in $UV/HNO_2/NO_2^-$ systems was explained by considering the production of $\cdot NO_2$ through the sequence of reactions (54) and (64). In contrast, the presence of Fe^{3+} in UV/NO_3^- systems significantly increased NBE consumption rate while strongly decreased $\eta^0_{1,3-DNB}$. The latter result may be explained by taking into account: (i) an enhanced contribution of NBE oxidation pathways since higher production rates of nitrophenol isomers were observed, and (ii) the decrease of the relative importance of reactions (36) and (38) due to the lower fraction of photons absorbed by NO_3^-. In addition, UV/NO_3^- systems in the absence of O_2 showed $\eta^0_{1,3-DNB}$ values higher than those obtained under oxygenated conditions.

4.4.4 Nitration mechanism of NBE under mild AOP conditions

The set of results presented in section 4.4 is consistent with a nitration pathway involving a $HO\cdot$ + $\cdot NO_2$ mechanism. In the experimental domain tested, the prevailing NBE nitration pathway is most probably the reaction between the $\cdot OH$-NB adduct and $\cdot NO_2$ radicals (rxn 65A).

$$(65)$$
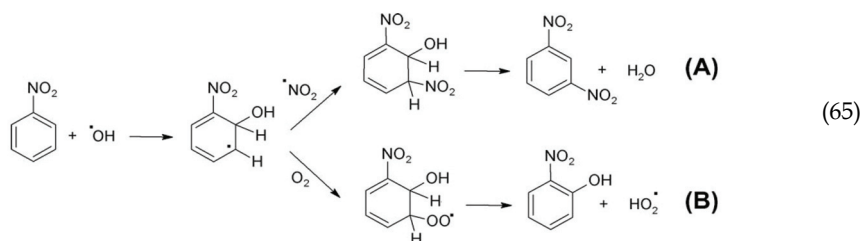
5. Conclusions

It is well known that rather complex reaction manifolds with many reaction steps are involved in the degradation of aromatic pollutants. However, results obtained in degradation experiments of nitroaromatic compounds using different homogeneous AOPs can be analyzed by using simplified models that take into account only a reduced number of kinetically key steps. These models are capable of correctly describing the main kinetic features of the studied systems by using only a few parameters as predictive tools. This kind of approach has important implications from a practical-technological viewpoint since it may be used for the rational design of efficient processes.

6. Acknowledgements

7. References

Bathia, K., 1975. Hydroxyl radical induced oxidation of nitrobenzene. Journal of Physical Chemistry 79, 1032-1038.

Braun, A.M., Maurette, M.T., Oliveros, E., 1986. Photochemical Technologies. J. Willey & Sons., New York.

Buxton, G.V., Greenstock, C.L., Helman, W.P., Ross, A.B., 1988. Critical review of rate constants for reactions of hydrated electrons, hydrogen atoms and hydroxyl radicals in aqueous solution. J. Phys. Chem. Ref. Data 17, 513-886.

Carlos, L., Fabbri, D., Capparelli, A.L., Bianco Prevot, A., Pramauro, E., García Einschlag, F., 2009. Effect of simulated solar light on the autocatalytic degradation of nitrobenzene using Fe3+ and hydrogen peroxide. Journal of Photochemistry and Photobiology A: Chemistry 201, 32-38.

Carlos, L., Fabbri, D., Capparelli, A.L., Prevot, A.B., Pramauro, E., Einschlag, F.S.G., 2008. Intermediate distributions and primary yields of phenolic products in nitrobenzene degradation by Fenton's reagent. Chemosphere 72, 952-958.

Carlos, L., Nichela, D., Triszcz, J.M., Felice, J.I., García Einschlag, F.S., 2010. Nitration of nitrobenzene in Fenton's processes. Chemosphere 80, 340-345.

Crittenden, J.C., Hu, S., Hand, D.W., Green, S.A., 1999. A kinetic model for H2O2/UV process in a completely mixed batch reactor. Water Research 33, 2315-2328.

Chan, K.H., Chu, W., 2003. Modeling the reaction kinetics of Fenton's process on the removal of atrazine. Chemosphere 51, 305-311.

Chen, R., Pignatello, J.J., 1997. Role of quinone intermediates as electron shuttles in fenton and photoassisted fenton oxidations of aromatic compounds. Environmental Science and Technology 31, 2399-2406.

De Laat, J., Gallard, H., 1999. Catalytic decomposition of hydrogen peroxide by Fe(III) in homogeneous aqueous solution: Mechanism and kinetic modeling. Environmental Science and Technology 33, 2726–2732.

Fang, X., Mark, G., Sonntag, C.v., 1996. OH· radical formation by ultrasound in aqueous solutions Part I: The chemistry underlined the terephtalate dosimeter Ultrason. Sonochem. 3, 57-63.

Fischer, M., Warneck, P., 1996. Photodecomposition of nitrite and undissociated nitrous acid in aqueous solution. Journal of Physical Chemistry 100, 18749-18756.

García Einschlag, F.S., Carlos, L., Capparelli, A.L., 2003. Competition kinetics using the UV/H2O2 process: A structure reactivity correlation for the rate constants of hydroxyl radicals toward nitroaromatic compounds. Chemosphere 53, 1-7.

García Einschlag, F.S., Carlos, L., Capparelli, A.L., Braun, A.M., Oliveros, E., 2002a. Degradation of nitroaromatic compounds by the UV-H2O2 process using polychromatic radiation sources. Photochemical and Photobiological Sciences 1, 520-525.

García Einschlag, F.S., Felice, J.I., Triszcz, J.M., 2009. Kinetics of nitrobenzene and 4-nitrophenol degradation by UV irradiation in the presence of nitrate and nitrite ions. Photochemical and Photobiological Sciences 8, 953-960.

García Einschlag, F.S., Lopez, J., Carlos, L., Capparelli, A.L., Braun, A.M., Oliveros, E., 2002b. Evaluation of the efficiency of photodegradation of nitroaromatics applying the UV/H2O2 technique. Environmental Science and Technology 36, 3936-3944.

Getoff, N., 1997. Peroxyl radicals in the treatment of waste solutions. Peroxyl Radicals, 483-506.

Glaze, W.H., Lay, Y., Kang, J.W., 1995. Advanced oxidation processes. A kinetic model for the oxidation of 1,2-dibromo-3-chloropropane in water by the combination of hydrogen peroxide and UV radiation. Industrial and Engineering Chemistry Research 34, 2314-2323.

Goldstein, S., Lind, J., Merenyi, G., 2005. Chemistry of peroxynitrites as compared to peroxynitrates. Chemical Reviews 105, 2457-2470.

Goldstein, S., Rabani, J., 2007. Mechanism of nitrite formation by nitrate photolysis in aqueous solutions: The role of peroxynitrite, nitrogen dioxide, and hydroxyl radical. Journal of the American Chemical Society 129, 10597-10601.

Heit, G., Neuner, A., Saugy, P.-Y., Braun, A.M., 1998. Vacuum-UV (172 nm) Actinometry. The Quantum Yield of the Photolysis of Water. Journal of Photochemistry and Photobiology A: Chemistry 102, 5551-5561.

Lipczynska-Kochany, E., Bolton, J.R., 1991. Flash photolysis/HPLC method for studying the sequence of photochemical reactions: applications to 4-chlorophenol in aerated aqueous solution. Journal of Photochemistry and Photobiology, A: Chemistry 58, 315-322.

Lopes, L., De Laat, J., Legube, B., 2002. Charge transfer of iron(III) monomeric and oligomeric aqua hydroxo complexes: Semiempirical investigation into photoactivity. Inorganic Chemistry 41, 2505-2517.

Lopez, J.L., García Einschlag, F.S., González, M.C., Capparelli, A.L., Oliveros, E., Hashem, T.M., Braun, A.M., 2000. Hydroxyl radical initiated photodegradation of 4-chloro-3,5-dinitrobenzoic acid in aqueous solution. Journal of Photochemistry and Photobiology A: Chemistry 137, 177-184.

Mack, J., Bolton, J.R., 1999. Photochemistry of nitrite and nitrate in aqueous solution: A review. Journal of Photochemistry and Photobiology A: Chemistry 128, 1-13.

Mark, G., Korth, H.G., Schuchmann, H.P., Von Sonntag, C., 1996. The photochemistry of aqueous nitrate ion revisited. Journal of Photochemistry and Photobiology A: Chemistry 101, 89-103.

Merenyi, G., Lind, J., Czapski, G., Goldstein, S., 2003. Direct determination of the Gibbs' energy of formation of peroxynitrous acid. Inorganic Chemistry 42, 3796-3800.

Nadezhdin, A., Dunford, H.B., 1979. Oxidation of nicotinamide adenine dinucleotide by hydroperoxyl radical. A flash photolysis study. Journal of Physical Chemistry 83, 1957-1961.

Nichela, D., Carlos, L., Einschlag, F.G., 2008. Autocatalytic oxidation of nitrobenzene using hydrogen peroxide and Fe(III). Applied Catalysis B: Environmental 82, 11-18.

Nichela, D., Haddou, M., Benoit-Marquiè, F., Maurette, M.T., Oliveros, E., García Einschlag, F.S., 2010. Degradation kinetics of hydroxy and hydroxynitro derivatives of benzoic acid by fenton-like and photo-fenton techniques: A comparative study. Applied Catalysis B: Environmental 98, 171-179.

Oturan, M.A., Pinson, J., 1995. Hydroxylation by electrochemically generated OH· radicals. Mono- and polyhydroxylation of benzoic acid: Products and isomers' distribution. Journal of Physical Chemistry 99, 13948-13954.

Pan, X., Schuchmann, M.N., von Sonntag, C., 1993. Oxidation of benzene by the OH radical. A product and pulse radiolysis study in oxygenated aqueous solution. Journal of the Chemical Society, Perkin Transactions 2 3, 289-297.

Pignatello, J.J., Liu, D., Huston, P., 1999. Evidence for an additional oxidant in the photoassisted Fenton reaction. Environmental Science and Technology 33, 1832-1839.

Pignatello, J.J., Oliveros, E., MacKay, A., 2006. Advanced oxidation processes for organic contaminant destruction based on the fenton reaction and related chemistry. Critical Reviews in Environmental Science and Technology 36, 1-84.

Sima, J., Makanova, J., 1997. Photochemistry of iron (III) complexes. Coordination Chemistry Reviews 160, 161-189.

Simic, M., 1975. The chemistry of peroxy radicals and its implication to radiation biology. Fast Processes in Radiation Chemistry and Biology, 162-179.

Stefan, M.I., Bolton, J.R., 1998. Mechanism of the degradation of 1,4-dioxane in dilute aqueous solution using the UV/hydrogen peroxide process. Environmental Science and Technology 32, 1588-1595.

Stefan, M.I., Hoy, A.R., Bolton, J.R., 1996. Kinetics and mechanism of the degradation and mineralization of acetone in dilute aqueous solution sensitized by the UV photolysis of hydrogen peroxide. Environmental Science and Technology 30, 2382-2390.

Stefan, M.I., Mack, J., Bolton, J.R., 2000. Degradation pathways during the treatment of methyl tert-butyl ether by the UV/H2O2 process. Environmental Science and Technology 34, 650-658.

Vione, D., Maurino, V., Minero, C., Lucchiari, M., Pelizzetti, E., 2004. Nitration and hydroxylation of benzene in the presence of nitrite/nitrous acid in aqueous solution. Chemosphere 56, 1049-1059.

Vione, D., Maurino, V., Minero, C., Pelizzetti, E., 2005. Nitration and photonitration of naphthalene in aqueous systems. Environmental Science and Technology 39, 1101-1110.

Walling, C., 1975. Fenton's reagent revisited. Accounts of Chemical Research 8, 125-131.

Ferrate(VI) in the Treatment of Wastewaters: A New Generation Green Chemical

Diwakar Tiwari[1] and Seung-Mok Lee[2]
[1]Department of Chemistry, School of Physical Sciences, Mizoram University,
[2]Department of Environmental Engineering, Kwandong University,
[1]India
[2]Korea

1. Introduction

Fresh water resources are under tremendous stress throughout the globe. Many areas all along the developing or even developed nations indicated, the fresh waters are greatly contaminated by the discharge of untreated sewage/industrial effluents and even variety of toxins entering naturally. Environmental regulations and public health concerns stated that wastewaters collected from municipalities and communities supposed to be treated as to meet the standards given prior its discharge/disposal into the aquatic environment. An advanced primary treatments aiming to enhanced the removal of colloidal particles and organic constituents from wastewaters, known to be an essential primary step and a starting point leading to fewer remaining particles and organic/inorganic contaminants, which in turn favorable for subsequent biological or physico-chemical treatment process. It is observed that the coagulation and oxidation/disinfection are two important unit processes for water treatments. Coagulation destabilizes colloidal impurities and transferred small particles into large aggregates and facilitates the several dissolved contaminants to adsorb onto the surface of these aggregates, which can then be removed by sedimentation and filtration. Disinfection is design to introduce the chemical dose enabled to kill the harmful organisms' *viz.*, bacteria, pathogens and viruses etc. from the wastewaters. Additionally, the usual method of sewage/municipal or even several industrial waste effluents treatment processes contained with large amount of sludge having various organic and inorganic compounds occurred, pose serious safely and quality aspects related to environmental concerns. Further, the final dewatered sludge (often called biosolids), which is to be land applied, endocrine disruptors and odors of the solids as well as pathogens have been brought under the serious attention towards its impact of the biosphere. However, such biosolids once treated carefully, may serve as an economic values as a soil conditioners and fertilizers etc. Further, the usual sludge handling processes *viz.*, thickening, drying, digestion and lime stabilization contribute to the on-site odors, became a severe environmental burden. Different types of organic sulfides and amines are produced in wastewater treatment facilities to give unpleasant odors. These processes are not effective in destroying toxic components of sludge *viz.*, endocrine disruptors and potential pathogens.

Complaints of illness related to the land application of biosolids are found to be increased at several places.

Similarly, the increased level of pharmaceuticals caused for enhanced level of its occurrence into the aquatic environment. Studies implied that the pharmaceuticals in surface waters and their existence in the environment may result in ecotoxicological effects. Ozonation and filtration with granular activated carbon or even advanced oxidation process (AOP) are commonly known technological implications for its removal or oxidation. In a line the heavy burden of surfactants are not directly toxic, but they inhibit both settling of floating particles and dissolution of atmospheric oxygen into natural waters. The biodegradation of several surfactants are seemingly slow in the wastewaters treatment plants.

The wastewaters treatment processes included in general the screening/skimming, followed by the biological/chemical treatment. Further, the advanced treatment methods composed with disinfections. Hence, the treatment process possessed with several steps comprising of variety of potentially needed chemicals. It is noteworthy to mention that sometimes the chemicals used, caused for release/discharge of harmful/toxic chemicals, and ultimately made additional burden to the environment. The applications of these chemicals restricted or even banned for its use in the environmental remediation particularly in the treatment of waste waters. Therefore, the use of conventional treatment methods required to be modified with adequate selectivity/suitability possessed with optimum efficiency but composed with more environments friendly. In a line the role of ferrate(VI) seems to be one of possible alternatives to be used for such treatment methods. The interesting chemistry of ferrates intended it to various possible applications in diverse area of research. However, its application in wastewaters treatment is known to be promising way of treatment showed several interesting observations. Recently, Sharma [1] has reviewed the extrinsic properties of ferrate in solution along with mechanistic and kinetic evaluation of the use of ferrate towards several inorganic pollutants.

1.1 Ferrate(VI)

Iron is one of very common element present in nature mainly as elemental iron Fe(0) along with the ferrous (Fe(II)) and ferric (Fe(III)) ions. The minerals of ferrous and ferric oxides further include the wuestite, hematite, magnetite, goethite, akagameite etc. (Table 1). Further, the iron and iron oxide based materials showed immense applications in different area. Some of the possible applications are magnetic pigments in recording, catalysis and magnetic fluids etc. Amorphous iron oxides potentially applied in industrial and water purification technologies. The photocatalytic processes includes the amorphous iron-oxide as an electrode, transforms water into hydrogen peroxide which further available for effective degradation of degradable impurities. Recent years, iron/iron oxides in the form of nano-particles showed unique properties for many advanced technological applications. Nano-particles of iron and iron-oxides in combination of oxygen and hydrogen peroxides are capable of oxidizing recalcitrant compounds. Salts of hypoferrite and ferrite as reported in Table 1 synthesized because of their use as magnetic materials in the modern electronic industry *viz.,* microwave devices, memory cores of compounds, radar and satellite communications and usage as permanent magnets.

In addition to three stable oxidation states of iron i.e., 0, +2 and +3, the strong oxidizing environment caused for the occurrence of higher oxidation states of iron *viz.,*+4, +5, +6, +8 etc. These higher oxidation states of iron are commonly known as ferrates. Among these

ferrates the +6 state is relatively stable and easy to synthesize hence, during last couple of decades greater interest and several research studies conducted using the +6 state of iron. Additionally, some *in situ* studies conducted with +4 and +5 oxidation state of iron. The reactivity of +5 and +4 oxidation state of iron is relatively high comparing to the +6 state.

Ferrate(VI) which was first observed by Stahl in 1902 when he conducted an experiment detonating a mixture of saltpeter and iron filings, and dissolved the molten residue in water. This colored solution was subsequently identified as potassium ferrate(VI) (K_2FeO_4). Eckenber and Becquerel in 1834 detected the same color when they heated red mixtures of potash (potassium hydroxide) and iron ores. Similarly, in 1840, Fremy hypothesized this colour to be an iron species with high valence, but its formula was suggested FeO_3 [2]. Moreover, because of its stability and cumbersome of its synthesis, it was not used and studied further. However, some 100 years before systematic studies on ferrates started and explored the various applications of these compounds.

Compound	Name	Mineral/Salt
FeO	Ferrous oxide	Wuestite
Fe_2O_3	Ferric Oxide	Hematite
Fe_3O_4	Ferrosoferric oxide	Magnetite
$Fe_2O_3.H_2O$	Ferric oxide monohydrate	Goethite
FeOOH	Ferric oxyhydroxide	Akaganeite
FeO_2^{2-}	Hypoferrite	Na_2FeO_2
FeO^{2-}	Ferrite	$NaFeO_2, KFeO_2$
FeO_3^{2-}	Ferrate(IV)	Na_2FeO_3
FeO_4^{4-}	Ferrate(IV)	Na_4FeO_4
FeO_4^{3-}	Ferrate(V)	K_3FeO_4
FeO_4^{2-}	Ferrate(VI)	Na_2FeO_4, K_2FeO_4
FeO_5^{2-}	Ferrate(VIII)	Na_2FeO_5

Table 1. Iron oxide compounds at different oxidation sates of iron

1.2 Preparation of Ferrate(VI)

Three different preparation methods are known for Fe(VI) preparation in laboratory. These are:
   i.   Dry oxidation of iron at high temperature
   ii.   An electro-chemical method
   iii.   Wet oxidation of iron(III) using chemical oxidizing agents
Briefly these methods are described here:

i. Dry oxidation of iron at high temperature

Initially the ferrate(VI) was obtained by heating the iron filings with nitrates or the mixture of iron oxides with alkali and nitrates at temperatures of red heat. The final mixtures includes the ferrate(VI) salts, by-products and remaining reactants. Later, very systematically several metal salts of Fe(VI) obtained which are described briefly:

Sodium ferrate(VI) was obtained by taking Fe_2O_3-NaOH-Na_2O_2-O_2 at different temperatures. Moreover, the fusion of Na_2O_2 with Fe_2O_3 at a molar ratio under dry oxygen conditions at high temperature, yields sodium ferrate(VI). Ferrate(VI) yield which depends on the initial reagent molar ratio and temperature conditions. The entire process to be

conducted in a dry glove box and in presence of diphosphorouspentaoxide (P_2O_5) and using high purity iron oxide (99.9 mol %). This was heated prior to use in dry oxygen at 150-200 ^{0}C as to remove sorbed water. This dried iron oxide was mixed with alkali metal peroxides and placed in a silver crucible for further thermal treatment. The 100% yield of the ferrate(VI) as in the form of Na_4FeO_5 was obtained at the molar ratio of Na:Fe = 4:1 at the exposition temperature of 370 ^{0}C for more than 12 hours.

Similarly, Fe(VI) was prepared using the galvanizing wastes as the wastes were mixed with ferric oxide in a muffle furnace at 800 ^{0}C for a while and the sample was cooled and stirred with solid sodiumperioxide and heated gradually for few minutes. The mixtures were melted and then cooled resulting with the formation of sodium ferrate(VI):

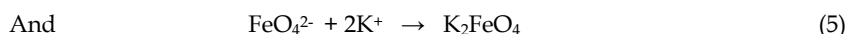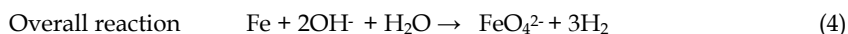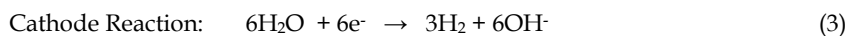$$Fe_2O_3 + 3Na_2O_2 \ \rightarrow \ 2\,Na_2FeO_4 + Na_2O \tag{1}$$
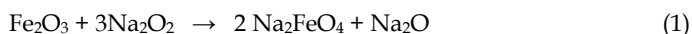
On the other hand potassium and cesium ferrate(VI) was prepared reacting with the superoxides of potassium and cesium with iron oxide powder at elevated temperatures of about 200 ^{0}C and the exposition time of *Ca* 10 hours.

It can also be prepared at room temperature by mixing iron(II) or iron(III) salt with an oxidizing chlorine-containing agent in a strong base such as potash or soda. The ferrate(VI) thus obtained show the formula $M(Fe,X)O_4$, where M denotes to two atoms of Na or K or one atom of Ca or Ba, and X corresponds to atoms whose cation has the electronic structures of a rare gas.

ii. An electro-chemical method

Ferrate was first prepared electrochemically in 1841 by anodic oxidation of iron electrode in strongly alkaline solution [3]. The basic principle of ferrate production by electrochemical method is the dissolution of iron anode in the electrolysis process having a strongly alkaline electrolyte solution. Hence, the preparation of ferrate consists of a sacrificial iron anode in an electrolysis cell containing a strongly alkaline solution of NaOH or KOH having electric current serving to oxidize the dissolved iron to Fe(VI) (Fig. 1). The possible anodic and cathodic reactions involved are;

Anode Reaction:	$Fe + 8OH^- \ \rightarrow \ FeO_4^{2-} + 4H_2O \ + \ 6e^-$	(2)
Cathode Reaction:	$6H_2O \ + 6e^- \ \rightarrow \ 3H_2 + 6OH^-$	(3)
Overall reaction	$Fe + 2OH^- + H_2O \rightarrow \ FeO_4^{2-} + 3H_2$	(4)
And	$FeO_4^{2-} + 2K^+ \ \rightarrow \ K_2FeO_4$	(5)

Different mechanism are proposed for the formation of ferrate(VI). Christian [5] assumed that the reduction proceeds stepwise first to Fe(III), then to Fe(II) and finally to Fe(0). However, the three steps mechanism based on intermediate formation are proposed as [6]:

a) The formation of intermediate species
b) The formation of ferrate and the passivation of the electrode
c) The formation of passivating layer that prevents further ferrate generation

The electrochemical production of Ferrate(VI) gives high purity of the product and the anodic polarizarion of iron electrode in the molten hydroxides is more adequate as compared to the classical electrolysis in water since water decomposes ferrate(VI) and passivation greatly reduced in this environment. The current yield during electrochemical

production increased with the carbon content in the iron anode material used; current yields were 15% for raw iron, 27% for steel and 50% for cast iron at a current density of 10 Am^{-2} with the NaOH concentration of 16.5 mol/L. Moreover, a current efficiency greater than 70% was achieved in preparing the ferrate when silver steel with carbon content of 0.09% was used. However, with the same conditions, the current efficiency was reduced to 12% when an alloy with a carbon content of 0.08% was used [7,8].
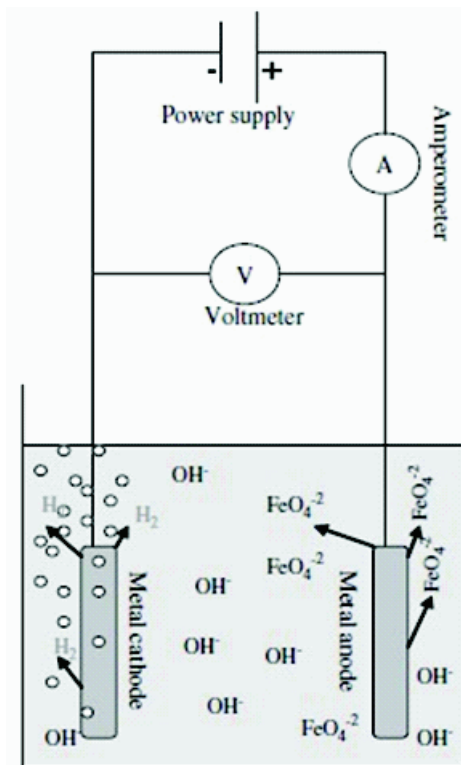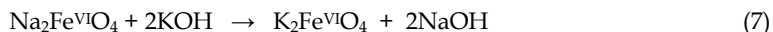

Fig. 1. Eletrochemical cell used for Ferrate synthesis [4].

Bouzek optimized the optimum conditions for ferrate production particularly the anodic iron behavior in respect to the anode composition and the influence of the anode material used in highly concentrated NaOH solutions [9]. Previously, the sinusoidal alternating current was used to synthesize the ferrate electrochemically [10-12]. The electrodes used were 99.95 % pure of iron with 14 mol/L NaOH solution as electrolytes and the temperature was kept between 30 and 60 ^{0}C. These results revealed that the maximum current efficiency for generating the ferrate was 43% at the conditions adopted (a.c. amplitude 88 mA/cm², a.c. frequency 50 Hz and temperature 40 ^{0}C).

iii.   Wet oxidation of iron(III) using chemical oxidizing agents

Wet chemical method includes the oxidation of ferric ion by sodium hypochlorite solution (preferably with higher concentration i.e., more than 12%) in presence of sodium hydroxide which may yield the sodium ferrate(VI) followed by the recrystallization with potassium

hydroxide yields potassium ferrate(VI). Reactions involved in the preparation process are given as:

$$2Fe(OH)_3 + 3NaOCl + 4NaOH \rightarrow 2Na_2Fe^{VI}O_4 + 3NaCl + 5H_2O \qquad (6)$$

$$Na_2Fe^{VI}O_4 + 2KOH \rightarrow K_2Fe^{VI}O_4 + 2NaOH \qquad (7)$$
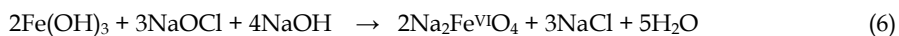
This procedure produces 10-15% yield of potassium ferrate(VI) and many separation steps with several recrystallization steps including washing with dry methanol are required to obtain more than 90% purity of the product. Li et al. [13] and Tiwari et al. [14] modified slightly the same basic procedure as to obtain the purity of ferrate(VI) more than 99%.

Rubidium and cesium ferrate(VI) are also prepared using similar procedure. The alkaline earth metals (Strontium and Barium) ferrates(VI) are prepared by the reaction of metal chloride solution with a basic solution of potassium ferrate(VI) at 0 ^{0}C. In this process the CO_2 free water and inert atmosphere need to be prevailed. Rapid filtration gave the pure form of barium and strontium ferrate.

1.3 Characterization and estimation of Ferrate(VI)

The possible application of ferrate(VI) is greatly depends upon the characterization of the synthesized product and its purity. There are several analytical tools which enabled to characterize the ferrate(VI) efficiently. The analytical techniques used are FTIR, Mössbauer spectroscopy, UV/Vis spectroscopy, ICP titrimetric, electroanalytical methods and XRD analyses. The oxidation state of iron can be obtained with the help of Mössbauer spectroscopy, both for Fe(VI) and other iron species.

Mössbauer Spectroscopic Analysis

Sharma et al. [15] described the Mössbauer chemistry of different oxidation state of iron which can be given as:

Mössbauer spectroscopy, which is based on the recoilless nuclear resonance absorption/emission of gamma radiations, because of its low line width of gamma rays, makes it possible to hyperfine interaction of the nucleus with surrounding electrons. The electrons in surrounding will be measured precisely, which could provide the information on the structure of valance shell of the particular Mössbauer atom. This method is successfully applied when the conditions of recoilless nuclear resonance absorption/emission are met (Mössbauer effect), and, from this point of view, iron-57 is the best nuclide ever found. This is the reason Mössbauer Spectroscopy could become an important method in material science and especially unique for iron containing compounds. The oxidation state of iron can be learned from the Mössbauer isomer shift (δ) which is directly (and mostly) related to the s electron density within the nucleus. Absolute electron densities may not be measured, thus the isomer shift is a relative quantity. In ^{57}Fe Mössbauer Spectroscopy the most common reference material is metallic iron (α-Fe). Due to the fact that the ^{57}Fe nucleus in its excited state (with nuclear spin I=3/2) has a smaller radius than in its ground state (I=1/2), an increasing electron density in the nucleus results in decreasing isomer shift. However, the valance shell of iron normally involves 3d-electrons which virtually screen the effect of the 3s electrons (the former being closer to the nucleus), and thus if the 3d electron density increases in the valance shell of iron (e.g., when Fe^{3+} is reduced to Fe^{2+}) the 3s density will decrease in the nucleus, and one may observe an increasing isomer shift. Such considerations are of basic importance for the assignment of Mössbauer pattern to a particular oxidation state.

Similarly, the quadrupole splitting (Δ) is characteristic of the symmetry of electron density distribution around the nucleus, and it is mostly related to the 3d shell configuration of the Fe atom/ion. Completely filled or half filled 3d levels or 3d sublevels (i.e., t_{2g} and e_g) result in zero quadrupole splitting if nothing else perturbs the electron density distribution. The magnetic splitting caused by the magnetic field (B) is additional information from the Mössbauer spectrum, which can be crucial to identify a particular iron-containing phase.

Figure 2 shows the 3d valance shell configuration of iron in its four most important oxidation states, using ligand field theory, together with the most common values of the Mössbauer parameters. The ligand field splitting corresponds to the most abundant cases i.e., octahedral for Fe^{II}, Fe^{III} and Fe^{IV}, and tetrahedral for Fe^{VI}. Only high-spin cases (small ligand field splitting) are discussed.
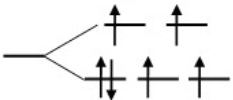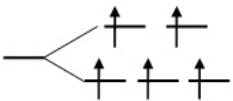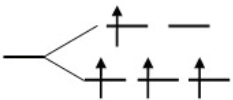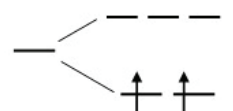

Fig. 2. Schematic representation of the 3d shell configuration of iron in selected oxidation states with characteristic Mössbauer parameters. Isomer shifts are given at room temperature relative to α-Fe, note that, the ligand field splitting corresponding to the most common octahedral coordination for Fe^{II} to Fe^{IV} while it is tetrahedral for Fe^{VI} [15].

Among regular iron compounds, Fe^{II} has the highest isomer shift, and the $3d^6$ configuration of the valence shell represents one more t_{2g} electron compared to $3d^5$ of spherical symmetry, thus the quadrupole splitting is also large.

Fe^{III} has only five 3d electrons, and therefore the isomer shift becomes smaller. Since the illustrated 3d splitting is only an idealized non-distorted case, the observed quadrupole splitting is very rarely zero, it is mostly below 1 mm/s and may even be larger. The distortion of the octahedron can be caused by the Jahn-Teller effect, lattice symmetry, neighboring charges, defects, etc.

Fe^{IV} has only four 3d electrons, which is manifested in a further decrease of the isomer shift. The asymmetry of the 3d density distribution is somewhat similar to the case of Fe^{III} but the quadrupole splitting are surprisingly small or zero. It can be explained if one takes it into account that with increasing oxidation number, originally ionic states have a tendency to become covalent and the extra electron which would cause the asymmetry gets delocalized on the two e_g sublevels. Zero quadrupole splitting means that the perfect octahedral ligand environment is preserved.

Fe^{VI} cannot exist as a Fe^{6+} ion, it should form an oxoanion, FeO_4^{2-}. Although ligand field approximation may not work in this case and MO theory would be more appropriate, the observed Mössbauer parameters fit in the tendency qualitatively very well, and very low isomer shift and zero quadrupole splitting found. Distortion of the rather stable tetrahedral FeO_4^{2-} anion is very rarely observed.

The characteristics of alkali and alkaline earth metal ferrate(VI) are shown in Table 2 [16] which obviously demonstrate that ferrate(VI) basic Mössbauer parameters *viz.*, isomer shift (δ), reflecting chemical state of iron(VI) changes in narrow limits i.e., 0.87 to 0.91 mm s^{-1} (with respect to standard α-Fe). This indicates a weak influence of the outer ion on iron bonding in oxygen tetrahedron, which is main structural unit of all ferrates(VI).

Property	$K_3Na(Fe^{VI}O_4)_2$	$K_2Fe^{VI}O_4$	$Rb_2Fe^{VI}O_4$	$Cs_2Fe^{VI}O_4$	$K_2Sr(Fe^{VI}O_4)_2$	$BaFe^{VI}O_4$
Δ mm s^{-1}	-0.89	-0.90 -0.88	-0.89	-0.87	-0.91	-0.90
Δ mm s^{-1}	0.21	0.0	0.0	0.0	0.14	0.16
H (T,K)	No magnetic ordering down to 4.2K	14.2±2.0 (2.8K) 14.7 (0.15K)	14.9±2.0 (2.8K)	15.1±2.0 (2.8K)	8.7 (2.0K) unresolved sexlet	11.8±2.0 (2.8K)
T_N (K)		3.6-4.2	2.8-4.2	4.2-6.0	~3	7.0-8.0

Table 2. Characteristics of ferrate(VI) [16]

IR spectra of potassium ferrate(VI) showed very characteristic peaks at the wave numbers 324 and 800 cm^{-1} (*cf* Figure 3).
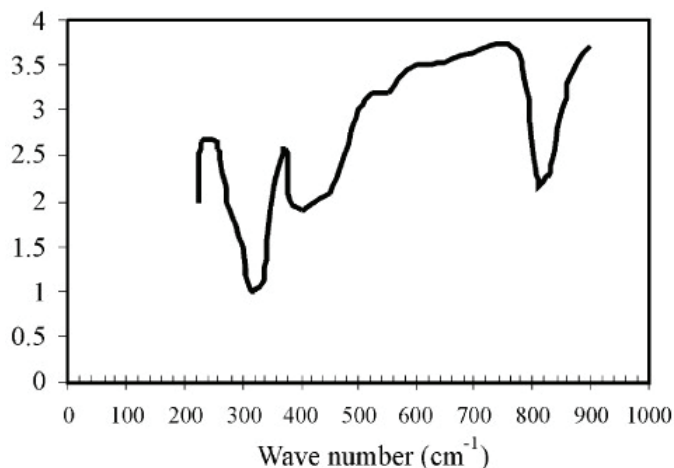

Fig. 3. IR spectrum of potassium ferrate [17].

Single crystal X-ray structural determination of K_2FeO_4 was performed and suggested four equivalent oxygen atoms are covalently bonded to central iron atom in +6 oxidation state [18]. The tetrahedral structure was also confirmed by isotopic exchange study as performed in aqueous solutions [19]. The reliable simulated powder XRD patterns (ICSD file 2876 and 32756, [20]) and an experimental one (PDF file No. 25-652, [18]) as reference for the pure substance is available. Moreover, it was also proposed that Fe(VI) ions can have three resonance hybrid structures in aqueous solution as shown in figure (4) [21]. Of these three resonance structures in figure 4, the structures of '1' and '2' were suggested as main contributors to the resonance structures of Fe(VI) based on theoretical studies of metal oxide structures.
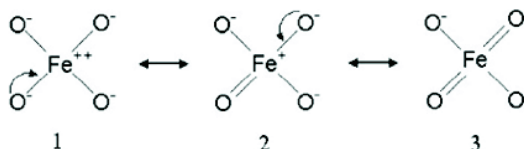

Fig. 4. Three resonance hybrid structures of Fe(VI) ion in an aqueous solution [21].

Quantitative estimation of Ferrate(VI):

Potassium ferrate $K_2Fe^{VI}O_4$, is most common and relatively easily synthesized ferrate salt. Moreover, the stability of this compound is fairly good under certain specified conditions. It is black-purple in color and remains stable in moisture excluded air exposure for longer period. In aqueous solution the ion $Fe^{VI}O_4{}^{2-}$ is monomeric with a high degree of four 'covalent character' equivalent oxygen atoms [19,22]. Potassium ferrate is insoluble in commonly used organic solvents and can be suspended in benzene, ether, chloroform etc. without having rapid decomposition of compound [23]. Alcohols containing more than 20% water rapidly decomposed ferrate(VI) and resulted in the formation of aldehydes or ketones [23].

Ferrate(VI) can be easily analyzed quantitatively by the two different methods:

i. *Volumetric titration method, and (ii) UV-Visible Spectroscopic method*

The brief description of these methods is given below.

i. *Volumetric titration method*

This method is based on the strong oxidative power of the Fe(VI). In this method, the Fe(VI) was intended to oxidize the chromite salt (equation 8) and the oxidized chromate was titrated with the standard ferrous salt solution in an acidic medium, and sodium diphenylamine sulphonate was used as an indicator [24]. This method is useful to analyze the solutions containing low concentration of Ferrate(VI) ion in aqueous solutions.

$$Cr(OH)_4{}^- + FeO_4{}^{2-} + 3H_2O \ \rightarrow \ Fe(OH)_3(H_2O)_3 + CrO_4{}^{2-} + OH^- \qquad (8)$$
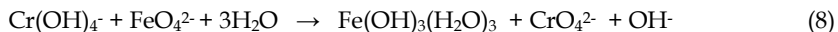
Another method which is developed based on the oxidation of alkaline arsenite to arsenate using the ferrate(VI) in aqueous solution [25]. The chemical reactions took place given in equation (9). In this analytical method a known amount of ferrate(VI) was added to a standard alkaline solution, in which, the amount of arsenite was greater than that required for the reduction of ferrate(VI) ions. The excess arsenite was back titrated with standard bromate solution (equation (10)) or cerate solution equation (11). The equivalent of consumed bromate or cerate is then calculated and subsequently, the equivalent of ferrate was estimated.

$$2\,FeO_4{}^{2-} + 3AsO_3{}^{3-} + 11H_2O + \;\rightarrow\; 2Fe(OH)_3(H_2O)_3 + 3AsO_4{}^{3-} + 4OH^- \qquad (9)$$

$$2BrO_3{}^- + 5AsO_3{}^{3-} + 2H^+ \;\rightarrow\; Br_2 + 5AsO_4{}^{3-} + H_2O \qquad (10)$$

$$2Ce^{3+} + 3AsO_3{}^{3-} + 6OH^- \;\rightarrow\; 2Ce + 3AsO_4{}^{3-} + 3H_2O \qquad (11)$$
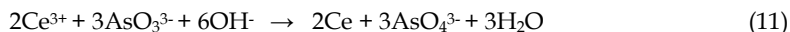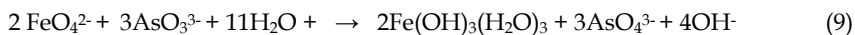
It was further reported that although, the arsenite-bromate and arsenite-cerate methods shown equally satisfactory results but the back-titration with cerate is to be preferred comparing to the bromate titration, since the bromate titration is carried out while the solution is still hot and the acidity of the hydrochloric acid must be carefully controlled. However, arsenite-cerate method is not recommended for analyzing highly decomposed ferrate solutions (that contains large amounts of ferric hydroxide), as the o-phenanthroline end point is observed by the color of the excess ferric ions [2].

Further, it is to be noted that although the volumetric titration method is useful for quantitative determination of ferrate(VI), however, the decomposition of ferrate(VI) is rapid hence, a buffer solution of phosphate is required to maintain pH of the ferrate(VI) sample at 8, at which the self decomposition of ferrate(VI) is significantly suppressed and the results obtained are more reliable. Moreover, the samples wastes need to be stored and treated specifically owing to the existence of residual chromite in the wastes if the chromite-ferrous titration method was employed, or the presence of arsenite if arsenite-bromate/arsenite-cerate methods were used.

ii. UV-Visible Spectroscopic

This is the most useful and robust method of ferrate(VI) quantification. In this method the aqueous solution of ferrate, which is red-violet in color and gives a characteristic absorption maxima at around 500 and 800 nm (*cf* Figure 5), can be used for its qualitative as well as quantitative estimation. Moreover, the aqueous solution of ferrate(VI) prepared in phosphate buffer between pH 9.0 and 10.5 are stable for hours makes it easy to obtain the spectral measurements at this pH.
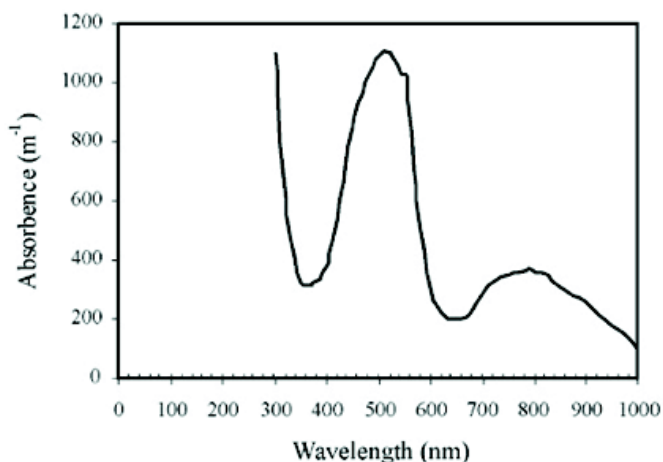

Fig. 5. UV-Vis spectrum of potassium ferrate(VI) [25].

The spectral measurements of FeO_4^{2-} were obtained in 0.0075M phosphate solution at different pH at 25 ^{0}C and it showed that the absorption spectra has a peak at ~510nm. Further, the accepted value of molar extinction coefficient for FeO_4^{2-} at pH 9.0 is 1150 $M^{-1}cm^1$ [26-27,41].

An indirect method of ferrate(VI) determination was proposed using the spectrophotometric determination [28]. ABTS (2,2'-azino-bis(3-ethylbenzo-thiazoline-6-sulfonate) interacts with Fe(VI) and gives a green radical cation of ABTS ($ABTS^{•+}$) which showed a characteristic absorption maxima at 415 nm. This was observed that the increase in absorbance at 415 nm for the radical $ABTS^{•+}$ is linear with the increase in Fe(VI) concentration (0.03 to 35 µM) in the acetate/phosphate buffer solution at pH 4.3. The molar extinction coefficient was calculated and found to be $3.40 \pm 0.05 \times 10^4$ M^{-1} cm^{-1}.
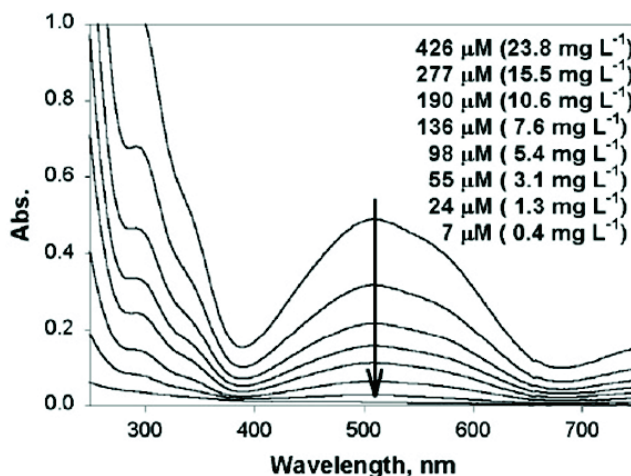
Fig. 6. UV-Vis absorption spectrum of Fe(VI) in aqueous solution as a function of its concentration, pH = 9.2, 25 mM phosphate buffer [27].

In addition to above said two methods, reports included the chemical precipitation method of its estimation [29]. In a small glass-stopped bottle, 10 mL of potassium ferrate(VI) solution was mixed with 20 mL of 0.1 M silver nitrate solution (equation (12)) and the resulting precipitate was filtered, which contained the silver ferrate and its color was black with a pink reflection, indicating the presence of potassium ferrate(VI) in the solution. After heating, the precipitate dissociated into silver oxide, ferric oxide and oxygen (equation (13)).

$$K_2FeO_4 + 2AgNO_3 \quad \rightarrow \quad 2KNO_3 + Ag_2FeO_4 \tag{12}$$

$$4Ag_2FeO_4 \quad \rightarrow \quad 4Ag_2O + 2Fe_2O_3 + 3O_2 \tag{13}$$
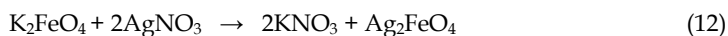
1.4 Stability and speciation of Ferrate(VI)

The stability of ferrate(VI) of its aqueous solutions depends on several factors *viz.*, ferrate(VI) concentration, temperature of the solution, co-existing ions, pH etc. [30]. The dilute solutions of Fe(VI) seems to be more stable than concentrated [31]. The solution of 0.025M Fe(VI) will remain 89% even after the 60 min but if the initial concentration of Fe(VI) was increased to 0.03 M, almost all the ferrate ions will get decomposed within the same period of time i.e., 60 min. Other reports also demonstrated that a 0.01M potassium ferrate

solution decomposed to 79.5% over a period of 2.5 h, while a 0.0019M potassium ferrate solution decreased to only 37.4% after 3 h and 50 min at 25 ^{0}C [32].

The stability of K_2FeO_4 in 10 M KOH is increased from hours to week if no Ni^{2+} and Co^{2+} impurities are present (< 1µM) [33]. However, nitrate salts of Cu^{2+}, Fe^{3+}, Zn^{2+} Pb^{2+}, Ba^{2+}, Sr^{2+}, Ca^{2+}, Mg^{2+} and other salts including $K_2Zn(OH)_4$, KIO_4, $K_2B_4O_9$, K_3PO_4, $Na_2P_2O_7$, Na_2SiF_6, Na_2SiO_3, Na_2MoO_4 and Na_2WO_4 have no affect on the stability of K_2FeO_4 [33]. A 0.5 M K_2FeO_4 solution, containing KCl, KNO_3, NaCl and FeOOH was studied to observe the ferrate(VI) stability in presence of these salts. It was found that the ferrate(VI) decomposed rapidly in the initial stage and appeared relatively stable at low ferrate concentrations when KCl and KNO_3 were present [31]. Phosphate was shown to retard the ferrate(VI) decomposition.

The spontaneous decomposition of ferrate(VI) in aqueous solutions was reported to be increased significantly with decreasing the solution pH. Figure 7 obtained with using the 1 mM solution of K_2FeO_4 in aqueous solution showed that at pH ~5, just after 7 min, the Fe(VI) was decomposed completely, however, at pH ~9 and ~10, it was fairly stable even after elapsed time of 20 min [34]. Other studies, conducted with 2h test period, the concentration of potassium ferrate slightly decreased when it was in 6M KOH, but decreased rapidly when it was in 3M KOH. The ferrate solution prepared with buffer solution at pH 8 was more stable than that prepared at pH 7 [31]; 49% of the original potassium ferrate remained after 8 h when the pH was 7, and 71.4% of that remained after 10 h when the pH was 8.
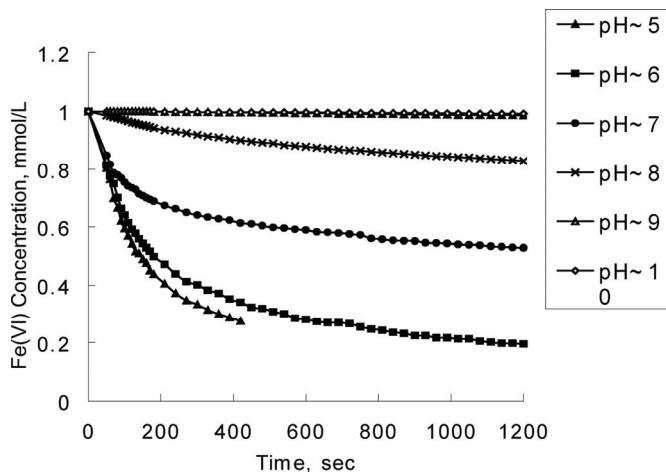
Fig. 7. The change of the Fe(VI) concentration as a function of time at various pH values [Initial concentration of Fe(VI): 1 mM] [34].

Temperature dependence data showed that ferrate(VI) solutions are relatively stable at low temperature conditions (0.5 ^{0}C) [32]. The 0.01 M solution of Fe(VI) was reduced by 10% at a constant temperature of 25 ^{0}C and almost unchanged at 0.5 ^{0}C for a period of 2 h.

Speciation and Decomposition of Fe(VI)

The presence of at least two unstable protonated form of Fe(VI) i.e., H_2FeO_4 and $HFeO_4^-$ was reported in 0.2 M phosphate buffer solutions at 25 ^{0}C [35]. However, a similar study in 0.025 M phosphate/acetate buffers at 23 ^{0}C showed three protonated forms of Fe(VI)

(equations (14-16)) [36]. The pk_a for $HFeO_4^-/FeO_4^{2-}$ (equation (16)) were also found different in the two different studies. The discrepancy in pk_a^3 was attributed to the difference in the buffer concentrations used.

$$H_3FeO_4^+ \leftrightarrow H^+ + H_2FeO_4 \,(pk_a^1 = 1.6 \pm 0.2 \,[36]) \tag{14}$$

$$H_2FeO_4 \leftrightarrow H^+ + HFeO_4^- \,(pk_a^2 = 3.5 \,[35, 36]) \tag{15}$$

$$HFeO_4^- \leftrightarrow H^+ + FeO_4^{2-} \,(pk_a^3 = 7.3 \pm 0.1 \,[36]; 7.8 \,[35]) \tag{16}$$
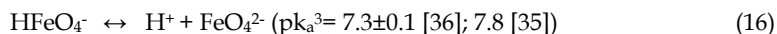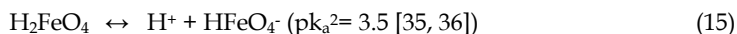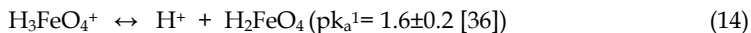
These pKa values indicated that the presence of four different ferrate(VI) species in the entire pH range (Figure 8). Figure 8 clearly indicated that $HFeO_4^-$ and FeO_4^{2-} species are predominant species in neutral and alkaline solutions, at which the Fe(VI) was known to be relatively stable towards its spontaneous dissociation [37].
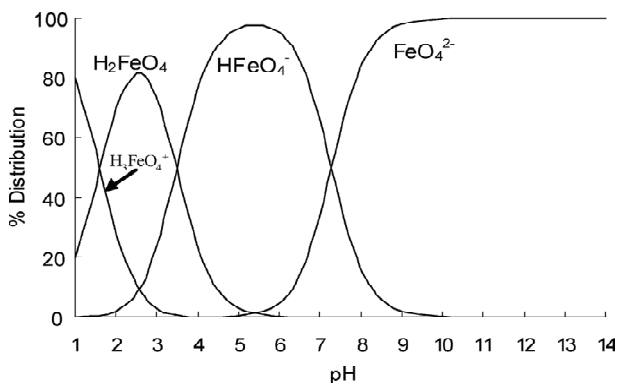
Fig. 8. Speciation of ferrate(VI) in aqueous solutions [Concentration of Fe(VI): 1mM] [34].

The ferrate salts when dissolved in water, oxygen is evolved and ferric hydroxide is precipitated (equation (14)).

$$4K_2FeO_4 + 10H_2O \rightarrow 4Fe(OH)_3 + 8KOH + 3O_2 \tag{14}$$
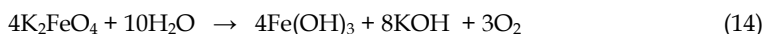
The rate of decomposition of ferrate(VI) has already seen that it is strongly pH dependent. The lowest rate of decomposition was occurred at pH higher than ~9-10, while it increased significantly at lower pH values [35,38]. The reaction kinetics followed second-order below pH 9.0, while first order above pH 10.0 [37]. The decomposition of ferrate(VI) hence, described by the following equilibrium and kinetic models [36]:

$$2H_3FeO_4^+ \leftrightarrow [H_4Fe_2O_7]^{2+} + H_2O \quad k_{15} = 3.5 \times 10^5 \,M^{-1}\,s^{-1} \tag{15}$$

$$[H_4Fe_2O_7]^{2+} + 2H^+ + 6H_2O \rightarrow Fe_2(OH)_2(H_2O)_8^{4+} + 3/2\,O_2 \qquad \text{Fast step} \tag{16}$$

$$H_3FeO_4^+ + H_2FeO_4 \leftrightarrow [\text{diferrate}] \quad k_{17} \approx 3.5 \times 10^5 \,M^{-1}\,s^{-1} \tag{17}$$

$$2H_2FeO_4 \leftrightarrow [\text{diferrate}] \quad k_{18} = 1.5 \times 10^4 \,M^{-1}\,s^{-1} \tag{18}$$

$$H_2FeO_4 + HFeO_4^- \leftrightarrow [\text{diferrate}] \quad k_{19} \approx 1.5 \times 10^4 \,M^{-1}\,s^{-1} \tag{19}$$

$$2HFeO_4^- \leftrightarrow [Fe_2O_7]^{2-} + H_2O \qquad k_{20} = 2.5 \times 10^2 \text{ M}^{-1} \text{ s}^{-1} \qquad (20)$$
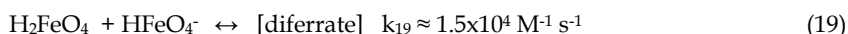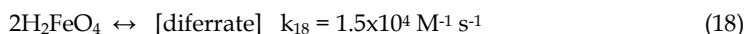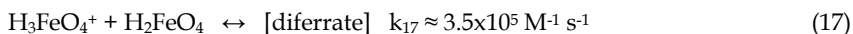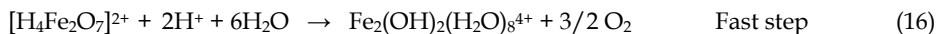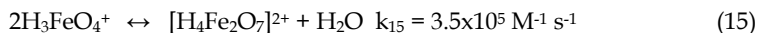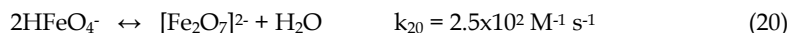
Reactions clearly showed that the forward reactions (15) to (20) (except reaction (16)) are relatively slow steps hence, could be the rate determining steps. The rate constants were then calculated for the self decomposition of Fe(VI), which is to be second order reactions. The second order rate constants for the decomposition of Ferrate(VI) to iron(II) in 5 mM phosphate/acetate buffers are obtained and shown in figure 9 [36].
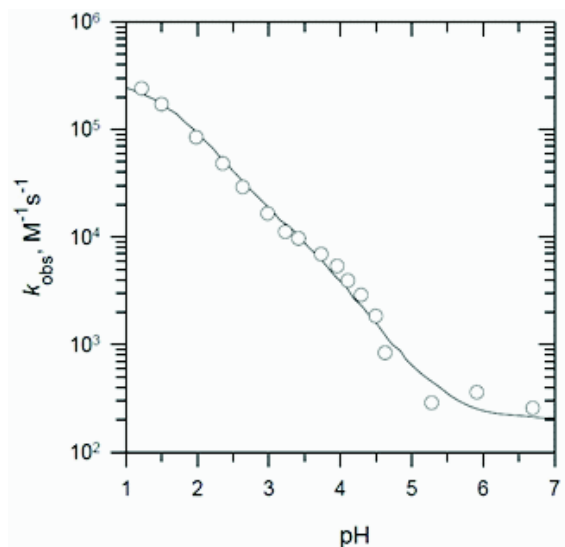
Fig. 9. The second-order rate constants for the decay of ferrate(VI) to iron(II) in 5 mM (phosphate/acetate) buffers [36].

1.5 Basic principle of Fe(VI) treatment in the wastewater

Ferrate(VI) applications in general lies in different area of research *viz.*, environmental remediation (i.e., oxidant, coagulant, disinfectant, antifouling oxidant etc.), cathode material for batteries (i.e., Super iron battery); Green synthesis oxidant (i.e., selective organic synthesis); and source of hypervalent iron (i.e., several biochemical research as to use more powerful oxidant) etc. Most of these applications are based on the reactivity or the oxidizing capacity of the ferrate(VI). The oxidizing power in general increases from chromium to manganese to iron (table 3). The closure observation showed that the reduction potential of Cr(VI)/Cr(III) and Mn(VII)/Mn(IV) were significantly lower than that of Fe(VI)/Fe(III). Even the commonly used oxidant *viz.*, ozone, hydrogen peroxide, hypochlorite, chlorine, perchlorate etc. are also possessed comparably less reduction potential [Table 3]. Moreover, the oxidation process usually occurred with Fe(VI), completed in shorter periods than oxidations carried out by permanganate or chromate. Therefore, these properties makes ferrate(VI) a potential chemical for the various applications, in particular to its oxidative properties.

In other words, taking Fe(VI) in aqueous medium it decomposes to Fe(III) and produces nascent oxygen (reaction (14)) which makes it highly reactive hence, could be applied for the treatment of wastewaters. This is the basic principle lies with ferrate(VI) application particularly for the treatment of wastewaters since, it degraded the degradable organic or

even inorganic impurities. Similarly, it could be potentially applied towards the disinfection of the water bodies as it may serve as one of the promising chemical to destroy/kill various pathogens/bacteria/viruses. Moreover, the reaction (14) also indicated that, it produces Fe(III) after its reduction which termed to be remarkably a good coagulant/flocculants hence, in the later stage it can serve as a coagulant/flocculants which may be able to remove the non-degradable impurities. Keeping in view with such basic properties of Ferrate(VI), it was first used by the Murmann and Robinson as a multi-purpose water treatment chemical for the oxidation, coagulation and disinfection of water [39]. Presently, it has already been assessed and successfully employed for the treatment of variety of wastewaters contaminated with several organic and inorganic pollutants along with as a potential disinfectant. Applications of ferrate(VI) in the waste waters treatment was intended with fast effective and less sludge producing method hence, in recent past it attracted an enhanced attention for its wider application in such treatment techniques.

Oxidant	Reaction	E^0, V
Chlorine	$Cl_2(g) + 2e^- \leftrightarrow 2Cl^-$	1.358
	$ClO^- + H_2O + 2e^- \leftrightarrow Cl^- + 2OH^-$	0.841
Hypochlorite	$HClO + H^+ + 2e^- \leftrightarrow Cl^- + H_2O$	1.482
Chlorine dioxide	$ClO_2(aq) + e^- \leftrightarrow ClO_2^-$	0.954
Perchlorate	$ClO_4^- + 8H^+ + 8e^- \leftrightarrow Cl^- + 4H_2O$	1.389
Ozone	$O_3 + 2H^+ + 2e^- \leftrightarrow O_2 + 2H_2O$	2.076
Hydrogen peroxide	$H_2O_2 + 2H^+ + 2e^- \leftrightarrow 2H_2O$	1.776
Dissolved oxygen	$O_2 + 4H^+ + 4e^- \leftrightarrow 2H_2O$	1.229
Permanganate	$MnO_4^- + 4H^+ + 3e^- \leftrightarrow MnO_2 + 2H_2O$	1.679
	$MnO_4^- + 8H^+ + 5e^- \leftrightarrow Mn^{2+} + 4H_2O$	1.507
Chromate	$Cr_2O_7^{2-} + 14H^+ + 6e^- \leftrightarrow 2Cr^{3+} + 7H_2O$	1.33
Ferrate(VI)	$FeO_4^{2-} + 8H^+ + 3e^- \leftrightarrow Fe^{3+} + 4H_2O$	2.20
	$FeO_4^{2-} + 8H_2O + 3e^- \leftrightarrow Fe(OH)_3 + 8H_2O$	0.70

Table 3. Redox potential for the different oxidants used in water and wastewater treatment

1.6 Fe(VI): a green chemical

The application of ferrate(VI) in various applications of applied sciences is associated with a non-toxic by-products which exaggerates its applications in different purposes. In particular, the ferrate(VI) treatment technology for the treatment of wastewaters as described earlier (equation (14)) associated with the Fe(III) by-product which is rendered as non-toxic chemical hence, the ferrate(VI) treatment is absolutely free from the toxic by-products. Therefore, the entire treatment is known as the 'Green-Treatment' and ferrate(VI) is termed as a 'Green-Chemical'. Based on its unique multifunctional properties as well possessed with green nature it may be one of the chemical of next generation and could be used widely in future for the remediation of the aquatic environment. Moreover, Ferrate(VI) is an emerging water-treatment disinfectant and coagulant, which can address the stringent water standards maintained by the agencies. The concerns of disinfectant by-products (DBPs) associated with currently used chemicals such as free chlorine, chloramines, and ozone can be addressed using Fe(VI). Additionally, like ozone, Fe(VI) does not react with bromide ion; so carcinogenic bromate ion is not produced in the treatment of bromide containing water [40].

2. Fe(VI) treatment in the degradation of degradable pollutants

Because of its strong oxidizing capacity, ferrate(VI) employed as potential chemical to degrade the variety of inorganic and organic impurities in aqueous solutions. The important aspects of such degradation is the reactivity of the Ferrate(VI), the mechanism involved in the degradation process and the kinetics with possible stoichiometry are the point of discussion. These parameters are useful inputs for the technology development and further implication of this technique. These are well discussed in the following sections and summarized in the proceeding tables and figures. The reaction of Fe(VI) was categorized into two pathways, (i) its self decomposition (i.e., k_S[Fe(VI)][Fe(VI)], reactions (15-20), except (16)), and (ii) reaction with other compounds (i.e., k_P[Fe(VI)][P]), which can be well conceptualized by the following reaction of rate expression:

$$-d[Fe(VI)]/dt \quad = \quad k_S\,[Fe(VI)]\,[Fe(VI)] \quad + \quad k_P\,[Fe(VI)]\,[P] \qquad (21)$$

$$\text{Self decomposition} \qquad \text{Reaction with compounds}$$

The rate of reaction because of its self-decomposition can be minimized under the certain conditions *viz*., at higher pH values, using phosphate buffers or even while studying the kinetic studies of unknown compounds, this may be subtracted as a blank run. The second rate determining step is an important factor which determines the rate of decomposition of compounds. This is of second order reaction and the rate constants for such second order reactions are evaluated and discussed. Moreover, in excess of Fe(VI) concentration, and with ignoring the self-decomposition of ferrate(VI) the above reaction may be treated as pseudo first-order rate equation and the rate constants may be evaluated.

2.1 Application of Fe(VI) for organic pollutants

Ferrate(VI) showed significantly reactive towards a variety of aliphatic and aromatic organic compounds. The application of Fe(VI) was studied including the alcohols, carboxylic compounds, amino acids, phenol, 1,2-Diols, organic nitrogen and sulphur containing compounds, aliphatic sulphur, nitrosamines, hydrazine etc. The degradation of these compounds with Fe(VI) was reported to be relatively fast and the increase of Fe(VI) dose favored the decomposition of these compounds. The reaction mechanism proposed with Fe(VI) was one-electron and two-electron transfer reactions to be associated with the degradation process for these organics. Bielski and Thomas [41] first proposed the one electron reduction of Fe(VI) to Fe(V) by its reaction with hydrated electron (e_{aq}^-), (reaction (22)). Further, studies showed that Fe(VI) could be reduced to Fe(V) through one electron transfer by its reaction to organic radical compounds, which was well-known one-electron reductants (reaction (23)) and reaffirmed with their pulse radiolysis and fast spectroscopic results [42-44].

$$FeO_4^{2-} + e_{aq}^- \quad \rightarrow \quad FeO_4^{3-} \qquad (22)$$

$$FeO_4^{2-} + R\dot{C}OH \quad \rightarrow \quad HFeO_4^{2-} + RCO \qquad (23)$$

Similarly, the reaction of phenol with Fe(VI) was demonstrated with the phenoxy radical formation through hydrogen abstraction pathway (one-electron transfer), based on their reaction products analysis [45]. It was further, supported by the EPR studies, showed that

Organic Compound	pH	Rate constant k_P ($M^{-1}s^1$)	$t_{1/2}$	Reference
Aniline	9.0	1.3×10^4	0.15s	[50]
Acetaldehyde	8.0	4.0×10^{-1}	1.39h	[35]
Benzenesulfinate	9.0	1.4×10^2	14.3s	[51]
Chloral	8.0	6.0×10^0	5.55min	[35]
Cysteine	12.4	7.6×10^2	2.6s	[52]
Cystine	12.4	1.2×10^2	16.7s	[52]
Diethylamine	8.0	7.0×10^{-1}	47.6min	[35]
Diethylsulfide	8.0	1.0×10^2	20.0s	[35]
Dimethylamine	8.0	2.0×10^2	10.0s	[35]
Dimethylsulphoxide	8.0	1.0×10^0	33.3min	[35]
Dimethylglycine	8.0	2.5×10^0	13.3min	[35]
Ethylene glycol	8.0	4.0×10^{-2}	13.9h	[35]
Ethyl alcohol	8.0	8.0×10^{-2}	6.94h	[35]
Formic acid	8.0	4.0×10^{-1}	1.39h	[35]
Formaldehyde	8.0	5.0×10^{-1}	1.11h	[35]
Glycine	8.0	1.0×10^2	20.0s	[35]
Glycoladehyde	8.0	3.0×10^0	11.1 min	[35]
Glycolic acid	8.0	4.0×10^{-1}	1.39h	[35]
Glyoxal	8.0	3.0×10^2	6.7s	[35]
Glyoxalic acid	8.0	7.0×10^2	2.9s	[35]
p-Hydroquinone	9.0	2.0×10^5	10.0ms	[42]
Iminodiacetic acid	8.0	1.0×10^2	20.0s	[35]
Isopropyl alcohol	8.0	6.0×10^{-2}	9.26h	[35]
2-Mercaptobenzoic acid	10.0	2.5×10^4	89.0ms	[53]
2-Mercaptoethanesulfonic acid	9.0	3.0×10^4	66.7ms	[53]
Mercaptopropionic acid	9.0	1.3×10^4	0.15s	[54]
Methylhydrazine	9.0	9.8×10^3	0.20s	[47]
Methionine	9.0	1.3×10^2	15.4s	[52]
Methylamine	8.0	4.0×10^1	50.0s	[35]
Methyl alcohol	8.0	3.0×10^{-2}	18.5h	[35]
N-methyliminodiacetic acid	8.0	2.0×10^0	16.7min	[35]
Nitriloacetic acid	8.0	2.0×10^0	16.7min	[35]
Neopentyl alcohol	8.0	1.0×10^{-1}	5.55h	[35]
Oxalic acid	8.0	1.0×10^{-1}	5.55h	[35]
Phenol	9.0	8.0×10^1	25.0s	[35]
p-Hydroquinone	9.0	2.0×10^5	10.0s	[42]
p-Toluidine	9.0	1.3×10^3	1.5s	[50]
p-Aminobenzoic acid	9.0	4.3×10^1	46.9s	[50]
p-Nitroaniline	9.0	3.0×10^1	1.10min	[50]
Sarcosine	8.0	1.2×10^2	16.7s	[35]
Thiodietanol	8.0	1.0×10^2	20.0s	[35]
Thioxane	9.0	5.8×10^1	34.5s	[55]
Trimethylaldehyde	8.0	2.0×10^0	16.7min	[35]

Table 4. Fe(VI) oxidation of various organic compounds

the oxidation of phenol by Fe(VI) proceeded through an intermediate radical species which was presumed as phenoxy radical (reaction (24)) [46].
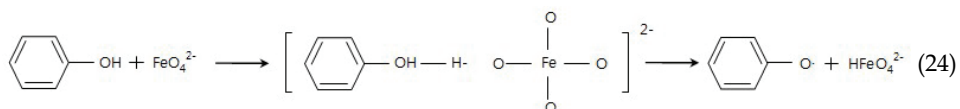
Further, the two-electron transfer mechanism of Fe(VI) was proposed for the degradation of several nitrogen containing compounds [47-49]. The oxidation of hydroxylamine was suggested to occur by concerted two hydrogen abstraction mechanism via the adduct formation between Fe and N atom of both reactants (reaction (25)) [49]. This argument was based on their several experimental results, including the stoichiometric, kinetic and products analysis of the reaction. The results of one-electron *viz.*, ascorbates, amino acids, esters, phenol, thiourea, thioacetamide etc. or two electron *viz.,* hydrazine, methylhydrazine, thiosulfate, benzenesulfinate, methionine, alcohols, thiol compounds, 1,4-thioxane, hydroxylamines, aniline etc. processes are compiled elsewhere [27].
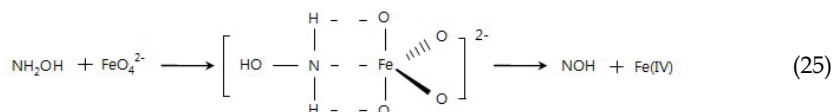
The second order reaction rate constants i.e., k_P (equation (21)) for the degradation of several organic pollutants in aqueous solutions are obtained and compiled in Table 4. Since, reaction rate is dependent to the solution pH hence, the pH was also specified. This table also includes the half-life period of reaction. These results inferred that most of the studies conducted at relatively higher pH condition where the Fe(VI) is stable. Moreover, the dominant species of the Fe(VI) are the FeO_4^{2-} and $HFeO_4^-$ (figure 8). The reaction rate constants are high enough, whereas the half life period is relatively low (except few cases) suggesting fast and effective degradation reaction occurred with ferrate(VI).

2.2 Application of Fe(VI) for inorganic pollutants

The oxidation of inorganic pollutants present in the aquatic environment is a major concern for several environmental remediation strategies. The possible impurities are free or metal complexed species including the heavy metal toxic ions, cyanide, dissolved ammonia, hydroxylamines, hydrogen sulphide, thiourea, thioacetamide etc. These potential contaminants are treated with Fe(VI). The mechanism of oxidation of inorganic compounds with ferrate(VI) was suggested to be one and two-electron process. Compounds like iodides, cyanides, sulfite etc. demonstrated to be one electron process whereas, the oxy compounds of arsenic, selenium, nitrogen and sulphur are possessed with the two-electron mechanism while these are reacted/degraded with Fe(VI).

The reactions of ferrate(VI) with a series of inorganic compounds such as iodide, cyanide, superoxide, sulfide, hydrazine, ammonia, azide and oxy-compounds of nitrogen, sulphur, selenium and arsenite possessed with seconds-order kinetics [38,47,49,51,57-65]. In general, similar to the organic compounds the reaction with inorganic compounds (P) may be demonstrated as equation (26):

$$-d[Fe(VI)]/dt = k_P\,[Fe(VI)][P] \qquad (26)$$

where k_P is the second-order rate constant for the reaction. It was found that the reactions of ferrate(VI) with cadmium(II)cyanide $(Cd(CN)_4^{2-})$, zinc(II)cyanide $(Zn(CN)_4^{2-})$, and selenite (SeO_3^{2-}) showed the following rate equations (27 and 28) [56,66-67]. The order of ½ was found with respect to the concentrations of Cd(II) and Zn(II) cyanides (equation (27)). This is different from the second-order rate law observed for the reaction of Fe(VI) with other cyanides $(CN^-, SCN^-, Cu(CN)_4^{3-}$ and $Ni(CN)_3^-)$ [61,64,67-68]

$$-d[Fe(VI)]/dt = k_P[Fe(VI)][M(CN)_4^{2-}]^{0.5} \text{ where M= Cd(II), Zn(II)} \qquad (27)$$

The reaction of ferrate(VI) and selenite possessed with first and second-order selenite concentrations dependence terms in the rate law (equation (28)) [56].

$$-d[Fe(VI)]/dt = k_P[Fe(VI)][SeO_3^{2-}] + k_2 [Fe(VI)][SeO_3^{2-}]^2 \qquad (28)$$

where k_2 is the third order rate constant.

Recently, the rate constants estimated for various inorganic compounds are tabulated in the Table 5 [69]. Moreover, the stoichiometry and the products obtained by oxidation of Fe(VI) are compiled and returned in Table 6 [69,59].

Compound (P)	Rate constant k_P $(M^{-1}s^{-1})$	
	$HFeO_4^- + P$	$FeO_4^{2-} + P$
Iodide (I^-)	$1.06\pm0.07x10^4$	-
Cyanide (HCN+CN^-)	$1.76\pm0.07x10^2$	$4.45\pm0.08x10^{2a}$
Thiocyanate, SCN^-	$3.25\pm0.20x103$	-
Iron(II)tetracyanide, $Fe(CN)_4^{2-}$	$3.00x10^3$	-
Copper(I)tetracyanide, $Cu(CN)_4^{3-}$	$5.33\pm0.71x10^7$	$2.51\pm1.42x10^4$
Nickel(II)tetracyanide, $Ni(CN)_4^{2-}$	$1.19\pm0.12x10^3$	$1.50\pm0.15x10^0$
Cadmium(II)tetracyanide, $Cd(CN)_4^{2-}$	$6.71\pm0.17x10^2$	$2.26\pm1.47x10^{-1b}$
Zinc(II) tetracyanide, $Zn(CN)_4^{2-}$	$4.05\pm0.20x10^2$	$2.39\pm0.14x10^{-1b}$
Hydrogen sulfide, H_2S	$2.37\pm0.70x10^7$	$1.52\pm0.52x10^3$
Bisulfite, SO_3^{2-}	$1.31\pm0.04x10^5$	-
Thiosulfate, $S_2O_3^{2-}$	$4.14\pm0.19x10^4$	-
Dithionite, $S_2O_4^{2-}$	$5.59\pm0.53x10^7$	$2.84\pm0.25x10^4$
Trithionate, $S_3O_6^{2-}$	$3.31\pm0.60x10^1$	$4.41\pm1.23x10^{-1}$
Pentathionate, $S_5O_6^{2-}$	$1.10\pm0.10x10^2$	-
Hydroxylamine, NH_2OH	$6.47\pm1.49x10^5$	-
Hydrazine, N_2H_4	$1.76\pm0.02x10^6$	$6.76\pm0.05x10^1$
Azide, N_3^-	$8.54\pm0.20x10^{6c}$	-
Nitrite, NO_2^-	$7.56\pm0.11x10^3$	-
Selenite, SeO_3^{2-}	$3.98\pm0.20x10^2$	-
Arsenite, $As(OH)^3$	$2.56x10^3$	-

[a]HCN ; [b]$M^{0.5}s^{-1}$; [c]N_3H^+

Table 5. Rate constants for the oxidation of inorganic compounds by Fe(VI) [1,69]

Similarly, the degradation of thiourea and thioacetamide was studied [70-71] and it was proposed that thiourea and thioacetamide are to be converted into sulphate at pH 9.0 using the ferrate(VI). The stoichiometric ratios of Fe(VI) and thiourea and thioacetamide was found to be 1:0.38±0.02 (*cf* Figures 10 and 11). Moreover, the proposed reaction was suggested as equations (29) and (30).

$$8HFeO_4^- + 3NH_2CSNH_2 + 9H_2O \rightarrow 8Fe(OH)_3 + 3NH_2CONH_2 + 3SO_4^{2-} + 2OH^- \quad (29)$$

$$8HFeO_4^- + 3CH_3CSNH_2 + 9H_2O \rightarrow 8Fe(OH)_3 + 3CH_3CONH_2 + 3SO_4^{2-} + 2OH^- \quad (30)$$
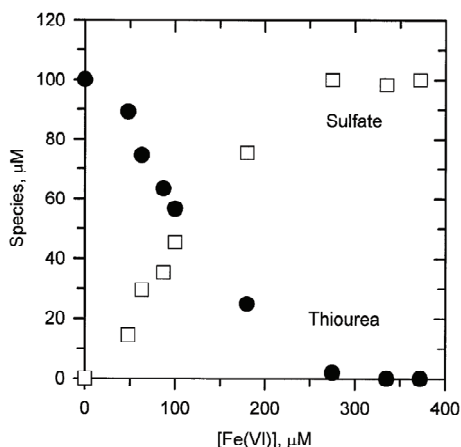

Fig. 10. A plot of thiourea consumption and sulfate formation versus [Fe(VI)] at pH 9.0 (Initial Thiourea: 100×10^{-6} M; [Fe(VI)] = 50-375 µM) [70].
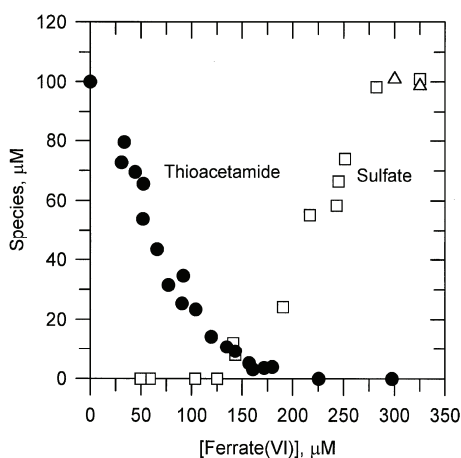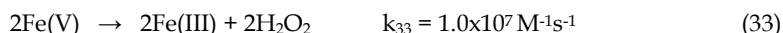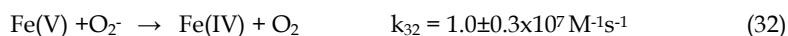

Fig. 11. A plot of thioacetamide consumption and sulfate formation versus [Fe(VI)] at pH 9.0 (Δ-acetamide) (Initial Thioacetamide: 100×10^{-6} M; [Fe(VI)] = 50-375 µM) [71].

Pollutant (P)	pH	Stoichiometric equation
Cyanide ($HCN+CN^-$)	9.0	$2HeFeO_4^- + 3CN^- + OH^- \rightarrow 2Fe(OH)_3 + 3NCO^-$ [61]
Thiocyanate, SCN^-	9.0	$4HFeO_4^- + SCN^- + 5H_2O \rightarrow 4Fe(OH)_3 + NC^{O-} + SO_4^{2-} + O_2 + 2OH^-$ [64]
Iron(II)tetracyanide, $Fe(CN)_4^{2-}$	9.0	$HFeO_4^- + 3Fe(CN)_6^{2-} + 3H_2O \rightarrow Fe(OH)_3 + 3Fe(CN)_6^{3-} + 4OH^-$ [58]
Copper(I)tetracyanide, $Cu(CN)_4^{3-}$	9.0	$HFeO_4^- + Cu(CN)_4^{3-} + 8H_2O \rightarrow 5Fe(OH)_3 + 4NCO^- + Cu^{2+} + 6OH^- + 3/2\,O_2$ [63]
Nickel(II)tetracyanide, $Ni(CN)_4^{2-}$	9.0	$4HFeO_4^- + Ni(CN)_4^{2-} + 6H_2O \rightarrow 4Fe(OH)_3 + 4NCO^- + Ni^{2+} + 4OH^- + O_2$ [66]
Cadmium(II)tetracyanide, $Cd(CN)_4^{2-}$	9.0	$4HFeO_4^- + Cd(CN)_4^{2-} + 6H_2O \rightarrow 4Fe(OH)_3 + 4NCO^- + Cd^{2+} + 4OH^- + O_2$ [66]
Zinc(II)cyanide, $Zn(CN)_4^{2-}$	9.0	$4FeO_4^- + Zn(CN)_4^{2-} + 6H_2O \rightarrow 4Fe(OH)_3 + 4NCO^- + Zn^{2+} + 4OH^- + O_2$ [67]
Hydroxylamine, NH_2OH	Alkaline	$HFeO_4^- + 2NH_2OH \rightarrow Fe(OH)_2 + N_2O + OH^- + 2H_2O$ [49]
Hydrazine, N_2H_4	Alkaline	$HFeO_4^- + N_2H_4 \rightarrow Fe(OH)_2 + N_2 + OH^- + H_2O$ [47]
Azide, N_3^-	Alkaline	$HFeO_4^- + N_3^- + 2H_2O \rightarrow Fe(OH)_3 + N_2 + N_2O + 2OH^-$
Nitrite, NO_2^-	Alkaline	$HFeO_4^- + 3NO_2^- + 3H_2O \rightarrow 2Fe(OH)_3 + 3NO_3^- + 2OH^-$ [61]
Hydrogen Sulphide, H_2S	7.0 9.0-11.3	$3HFeO_4^- + 4H_2S + 7H^+ \rightarrow 2Fe^{2+} + S_2O_3^{2-} + 2S(s) + 9H_2O$ $8HFeO_4^- + 3H_2S + 6H_2O \rightarrow 8Fe(OH)_3 + 3SO_4^{2-} + 2OH^-$ [60]
Bisulfite, SO_3^{2-}	Alkaline	$2HFeO_4^- + 3SO_3^{2-} + 3H_2O \rightarrow 2Fe(OH)_3 + 3SO_4^{2-} + 2OH^-$
Thiosulfate, $S_2O_3^{2-}$	7.5-11.0	$2HFeO_4^- + S_2O_3^{2-} + 2OH^- + 3H_2O \rightarrow 4Fe(OH)_3 + 6SO_3^{2-}$ [51]
Dithionite, $S_2O_4^{2-}$	Alkaline	$2HFeO_4^- + 3S_2O_4^{2-} + 4OH^- \rightarrow 2Fe(OH)_3 = 6SO_3^{2-}$
Trithionate, $S_3O_6^{2-}$	Alkaline	$10HFeO_4^- + 6S_3O_6^{2-} + 12H_2O \rightarrow 10Fe(OH)_3 + 9S_2O_6^{2-} + 4OH^-$
Pentathionate, $S_5O_6^{2-}$	Alkaline	$10HFeO_4^- + 2S_5O_6^{2-} + 12H_2O \rightarrow 10Fe(OH)_3 + 5S_2O_6^{2-} + 4OH^-$
Selenite, SeO_3^{2-}	Alkaline	$2HFeO_4^- + 3SeO_2^{2-} + 3H_2O \rightarrow 2Fe(OH)_3 + 3SeO_4^{2-} + 2OH^-$ [56]
Arsenite, $As(OH)_3$	9.0	$2HFeO_4^- + 3As(OH)_3 + 7OH^- \rightarrow 2Fe(OH)_3\ 3AsO_4^{3-} + 6H_2O$ [65]

Table 6. Stoichiometry and product of oxidation of inorganic compounds by ferrate(VI) [1,59]

Fe(VI) Reaction with Superoxide and Hydrogen Peroxide

Superoxides interacted with Fe(VI) and the second order rate equation demonstrated the reaction mechanism [72]. Further, the stoichiometry of the reactions ($[Fe(VI)]/[O_2^-]$) were found to be 1:2 and 1: 1 at pH 10.0 and 8.2, respectively. Reactions (31 – 33) are suggested for the observed stoichiometry:

$$Fe(VI) + O_2^- \rightarrow Fe(V) + O_2 \qquad k_{31} = 1.2x10^6 \text{ M}^{-1}\text{s}^{-1} \qquad (31)$$

$$Fe(V) + O_2^- \rightarrow Fe(IV) + O_2 \qquad k_{32} = 1.0\pm0.3x10^7 \text{ M}^{-1}\text{s}^{-1} \qquad (32)$$

$$2Fe(V) \rightarrow 2Fe(III) + 2H_2O_2 \qquad k_{33} = 1.0x10^7 \text{ M}^{-1}\text{s}^{-1} \qquad (33)$$
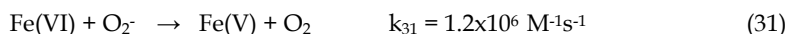
The stoichiometries of the reactions between ferrate(VI) with hydrogen peroxide at pH 9.0 was presented (reaction (34)) [19].

$$FeO_4^{2-} + 2H_2O_2 + 2H_2O \rightarrow Fe(OH)_3 + O_2 + 2OH^- \qquad (34)$$
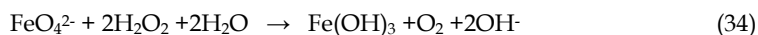
The oxygen produced in this reaction showed the same isotopic composition as in the H_2O_2, which suggested that the O-O bond was retained in the oxidation of H_2O_2 by ferrate(VI) [19].

2.3 Endocrine disrupting compounds degradation using Fe(VI)

Endocrine disrupting compounds (EDCs) are chemicals with the potential to elicit negative effects on the endocrine systems of humans and wildlife. Various synthetic and natural compounds are known to induce estrogen-like responses; including pharmaceuticals, pesticides, industrial chemicals and heavy metals [73]. The US environmental protection agency (USEPA) defines an EDC as: "An exogenous agent that interferes with the synthesis, secretion, transport, binding, action or elimination of natural hormones in the body that are responsible for the maintenance of homeostasis, reproduction, development, and/or behaviour" [74].

The broad class of EDCs chemicals includes natural estrogens such as estrone (E1), 17β-estradiol (E2), and estriol (E3); natural androgens such as testosterone (T), dihydrotestosterone (DHT), and androsterone (A); artificial synthetic estrogens or androgens such as 17α-ethynylestradiol (EE2), Norgestrel (N), and Trenbolone (Tr); phytoestrogens including isoflavonoides and coumestrol as well as other industrial compounds such as bisphenol A, nonylphenol etc. These chemicals are found in the aquatic environment. Moreover, the wastewater plants are known to be the major source of these EDCs. Natural and synthetic EDCs are released into the environment by humans, animals and industry; mainly through the sewage treatment plants before reaching the receiving bodies (soil, surface water, sediment and ground water), EDCs' main distribution in the environment is shown in Figure 12 [75]. EDCs are one of major concern towards the environmentalist and it has to be dealt adequately/properly. The possible option is the complete removal of EDCs from the environment. Since, sewage plants are the major source of EDCs, hence, it has to be removed completely from the sewage at sewage plants prior to final release to the environment. Moreover, several methodologies are adopted for its removal/degradation using the physical and chemical methods however, in the last couple of decades the chemical treatment based on the ferrate(VI) technology received an enhanced attention because of the reasons underlying:

(i) relatively higher oxidation potential of Fe(VI), (ii) the non-toxic by-products generated in the degradation process, and (iii) fast and effective treatment.
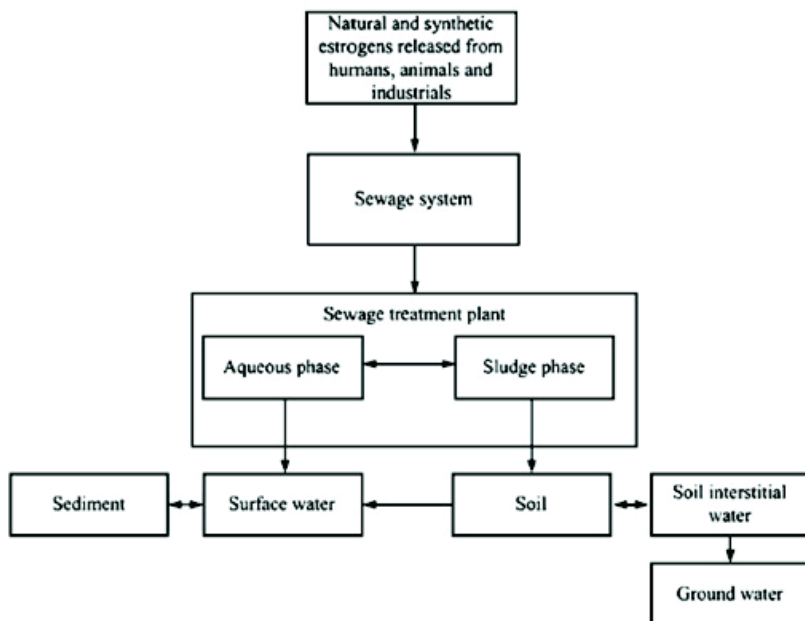
Fig. 12. EDCs distribution in the environment [75].

The reactivity of commonly used oxidants as mentioned previously (Table 3) is FeO_4^{2-} >O_3>$S_2O_4^{2-}$>H_2O_2>Cl_2>ClO_2. Keeping in view the several studies showed the effectiveness of ferrate(VI) for such studies. The degradation of estrone (E1), 17β-estradiol (E2) and 17α–ethynylestradiol (EE2) was conducted with varied ferrate(VI) doses and solution pH. It was demonstrated that at pH 9.0 the maximum degradation of these compounds took place and complete degradation was reported for *Ca* three times of Fe(VI) dose (*cf* Figure 13) [76]. Similarly, ferrate(VI) was found to be superior oxidant than usual electrochemical reduction of bisphenol-A, E2 and 4-tert-octylphenol (*cf* Figure 14) [77].
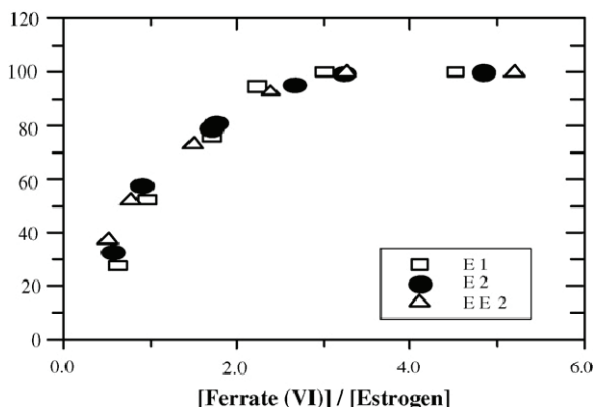
Fig. 13. Degradation of estrogens at pH 9, ferrate dose vs. removal percentage [76].
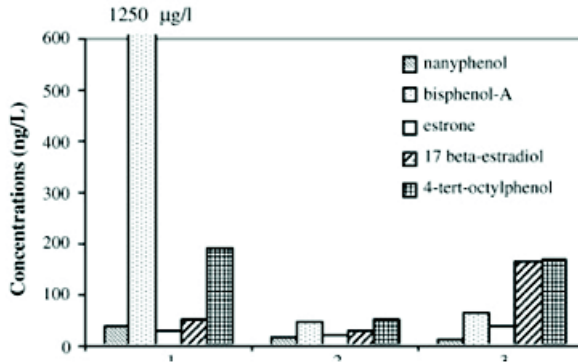
Fig. 14. Comparative EDCs residual concentrations. (1) Wastewater sample taken from the post-sedimentation; (2) treated sample with ferrate oxidation; (3) treated sample with electrochemical oxidation [77].

The kinetic model and path of degradation process for five different EDCs *viz.*, BPA (Bisphenol A), EE2 (17α-ethynylestradiol), E1 (Estrone), E2 (β-estradiol) and E3 (Estriol) are studied using the LC/MS and GC/MS spectroscopic methods [78]. The proposed model is useful to discuss here. The dissociated (EDC-) and un-dissociated (EDC') form of EDCs were considered using the known pk_a values along with the species of ferrate (VI) i.e., FeO_4^{2-} and $HFeO_4^-$ in the studied pH region using the pk_a^3 for ferrate(VI). The oxidation reactions may be summarized as:

$$\left(\frac{d[EDC]}{dt}\right)_1 = -[FeO_4^{2-}](k_1[EDC'] + k_1'[EDC^-]), \tag{35}$$

$$\left(\frac{d[EDC]}{dt}\right)_2 = -[HFeO_4^-](k_2[EDC'] + k_2'[EDC^-]). \tag{36}$$

The overall rate of EDC compound degradation was assumed to be sum of these two rates and can be expressed as:

$$\frac{d[EDC]}{dt} = (\frac{d[EDC]}{dt})_1 + (\frac{d[EDC]}{dt})_2. \tag{37}$$

The corresponding rates of oxidant (FeO_4^{2-} and $HFeO_4^-$) reduction during the reaction were expressed by equation (38) and (39), respectively:

$$\frac{d[FeO_4^{2-}]}{dt} = -[FeO_4^{2-}](k_{11}[EDC'] + k_{11}'[EDC^-]), \tag{38}$$

$$\frac{d[HFeO_4^-]}{dt} = -[HFeO_4^-](k_{21}[EDC'] + k_{21}'[EDC^-]). \tag{39}$$

In the case of the ferrate(VI) reduction, the overall rate of ferrate(VI) reduction was assumed to be the sum of the two rates, plus the thermodynamic decomposition of ferrate in water; this can be expressed as:

$$\frac{d[Fe(VI)]}{dt} = \frac{d[FeO_4^{2-}]}{dt} + \frac{d[HFeO_4^-]}{dt} - k_d[Fe(VI)], \tag{40}$$

where k_d is the decomposition constant of ferrate(VI) in the solution. Since, at higher pH range (i.e., 8~10), the self decomposition of ferrate(VI) is almost negligible hence, may be ignored. Therefore, the rate expression may be simplified to:

$$\frac{d[Fe(VI)]}{dt} = \frac{d[FeO_4^{2-}]}{dt} + \frac{d[HFeO_4^-]}{dt} \tag{41}$$

According to the equilibrium of the two ferrate species at different pH, the concentrations of $HFeO_4^-$ and FeO_4^{2-} should have specific ratio at a given pH. The species concentration may be given as:

$$[HFeO_4^-] = \propto_{HFeO_4^-} [Fe(VI)] = \frac{[HFeO_4^-]}{[Fe(VI)]}[Fe(VI)], \tag{42}$$

$$[FeO_4^{2-}] = \propto_{FeO_4^{2-}} [Fe(VI)] = \frac{[FeO_4^{2-}]}{[Fe(VI)]}[Fe(VI)], \tag{43}$$

Moreover, the relationship between the concentrations of un-dissociated and dissociated EDCs and pH can be described by the following expressions:

$$[EDC^-] = \frac{k_{aEDC}}{[H^+]+ k_{aEDC}}[EDC], \tag{44}$$

$$[EDC'] = \frac{H^+}{[H^+]+ k_{aEDC}}[EDC], \tag{45}$$

$$\frac{d[EDC]}{dt} = -\left(k_1 \propto_{FeO_4^{2-}} \frac{H^+}{[H^+]+ k_{aEDC}} + k_1' \propto_{FeO_4^{2-}} \frac{k_{aEDC}}{[H^+]+ k_{aEDC}} + k_2 \propto_{HFeO_4^-} \frac{H^+}{[H^+]+ k_{aEDC}} + \right.$$
$$\left. k_2' \propto_{HFeO_4^-} \frac{k_{aEDC}}{[H^+]+ k_{aEDC}}\right) \times [Fe(VI)] = k_e[EDC][Fe(VI)], \tag{46}$$

$$\frac{d[Fe(VI)]}{dt} = -\left(k_{11} \propto_{FeO_4^{2-}} \frac{H^+}{[H^+]+ k_{aEDC}} + k_{11}' \propto_{FeO_4^{2-}} \frac{k_{aEDC}}{[H^+]+ k_{aEDC}} + k_{21} \propto_{HFeO_4^-} \frac{H^+}{[H^+]+ k_{aED^-}} + \right.$$
$$\left. k_{21}' \propto_{HFeO_4^-} \frac{k_{aEDC}}{[H^+]+ k_{aEDC}}\right) \times [EDC][Fe(VI)] = k_f[EDC][Fe(VI)]. \tag{47}$$

Dividing equation (46) by (47) and integrating d[EDC] = (k_e/k_f) d[Fe(VI)] with the initial conditions (when t=0, [EDC]=[EDC]$_0$ and [Fe(VI)] = [Fe(VI)]$_0$, a pair of second-order equations for EDC degradation and Fe(VI) reduction versus reaction time were expressed by the following equations (48) and (49), respectively:

$$[EDC] = \frac{k_e [EDC]_0[Fe(VI)]_0 - k_f[EDC]_0^2}{k_e[Fe(VI)]_0 e^{(k_e[Fe(VI)]_0 - k_f[EDC]_0)t} - k_f[EDC]_0}, \tag{48}$$

$$[Fe(VI)] = \frac{k_f [EDC]_0[Fe(VI)]_0 - k_e[Fe(VI)]_0^2}{k_f[EDC]_0 e^{(k_f[EDC]_0 - k_e[Fe(VI)]_0)t} - k_e[Fe(VI)]_0}, \tag{49}$$

where

$$k_e = \frac{k_1 k_{aFE}[H^+] + k_1' k_{aFE} k_{aEDC} + k_2 [H^+]^2 + k_2'[H^+] k_{aEDC}}{[H^+]^2 + [H^+] k_{aEDC} + [H^+] k_{aFE} + k_{aFE} k_{aEDC}}$$

$$k_f = \frac{k_{11} k_{aFE}[H^+] + k_{11}' k_{aFE} k_{aEDC} + k_{21} [H^+]^2 + k_{21}'[H^+] k_{aEDC}}{[H^+]^2 + [H^+] k_{aEDC} + [H^+] k_{aFE} + k_{aFE} k_{aEDC}}$$

The rate constants k_1, $k_1`$, $k_2$, $k_2`$, k_{11}, $k_{11}`$, $k_{21}$ and $k_{21}`$ were obtained by the least-square fitting method. Results obtained were given in Table 7. Similarly, the fitted results and experimentally observed data at pH 9.2 with $[EE2]_0 = [E1]_0 = [E2]_0 = [E3]_0 = 0.01$ mM, $[EPA]_0 = 0.1$ mM and $[Fe(VI)]_0 = 0.05$ or 0.1 mM were shown in Figure 15. These results, again suggested that protonated species of ferrate(VI) i.e., $HFeO_4^-$ is more reactive than non-protonated species FeO_4^{2-} towards all these EDCs studied. However, the dissociated (ionized) EDCs are more reactive towards the protonated ferrate(VI).

Compound	k_1 (M^{-1}s^{-1})[a]	$k_1`$ (M^{-1}s^{-1})[b]	k_2 (M^{-1}s^{-1})[c]	$k_2`$ (M^{-1}s^{-1})[d]
BPA	2.80×10^2	5.16×10^2	8.20×10^2	7.76×10^4
EE2	3.05×10^2	8.52×10^2	9.10×10^2	5.11×10^5
E1	7.10×10^2	8.97×10^2	9.80×10^2	5.31×10^5
E2	7.32×10^2	9.41×10^2	1.08×10^3	5.40×10^5
E3	9.28×10^2	1.003×10^3	1.12×10^3	5.44×10^5

[a] FeO_4^{2-}; undissociated EDC; [b] FeO_4^{2-} dissociated EDC; [c] $HFeO_4^-$ un-dissociated EDC; [d] $HFeO_4^-$ dissociated EDC

Table 7. Rate constants of EDC degradation with Ferrate(VI) [reproduced from [78]]
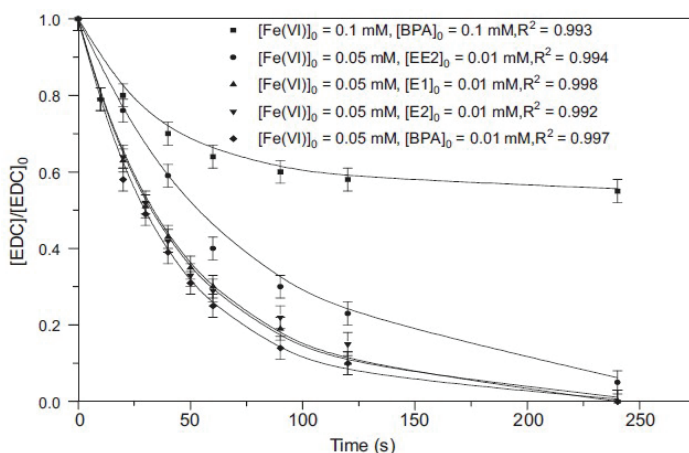
Fig. 15. Composition between experimental data and kinetic model for the degradation of EDCs by ferrate(VI) [78].

3. Fe(VI) in the removal of non-degradable pollutants

The non-degradable impurities particularly the heavy metal toxic ions or radionuclides is received a greater importance in the treatment of waste waters. These metallic impurities are present in the aquatic environment either in its free form or to its complexed form. Ferrate(VI) as discussed (reaction (14)) reduced to Fe(III), which possessed with fairly good coagulation/flocculation properties hence, able to coagulate these impurities and with sedimentation/filtration can be removed. Moreover, the Fe(III) as iron(III) hydroxides are known to be a potential adsorbent, possibly can remove the free metallic impurities even by adsorption process.

3.1 Removal of metal cations/anions

The arsenic (III) oxidation to As(V) and hence, the removal of As(V) by reduced Fe(III) via coagulation process was effectively achieved [65]. The two moles of Fe(VI) required to oxidize three moles of As(III) (reaction 50). The oxidation of As(III) followed second order rate law at pH 8.4 to 9.0. It was noted that the complete oxidation took place within a second.

$$2Fe(VI) + 3As(III) \rightarrow 2Fe(III) + 3As(V) \tag{50}$$
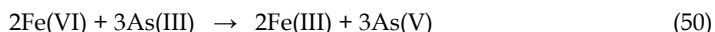
Further, it was demonstrated that with even smaller dose of Fe(VI) along with the supplementary dose of Fe(III) may achieve the efficiency to remove the arsenic from the arsenic contaminated river water (Nakdong River, Korea).

Potassium ferrate(VI) is an potential chemical to remove several metal cations/anions including Mn^{2+}, Cu^{2+}, Pb^{2+}, Cd^{2+}, Cr^{3+} and Hg^{2+} from aqueous solutions via oxidation/coagulation/adsorption process using lower dose of Fe(VI) 10-100 mg/L [79].

Similarly, the metal complexed species were studied and discussed previously particularly the metal(II) cyanide complexes [58,63,66-67]. An interesting study using Cu(II)and Ni(II) cyanide complexed were used and showed that complete degradation of cyanide along with the complete removal of free copper and partial removal of nickel (*cf* Figure16) [80]. Further the study was extended to employ it for the treatment of real electroplating wastes containing the copper and nickel complexed cyanides [34]. Recently, the removal of As(III) by Fe(VI), ferrate(VI)/Fe(III) and ferrate(VI)/Al(III) salts was studied as a function of pH (8.0 to 6.0) and anion concentration [81]. Removal of As(III) was increased with decrease in pH from 8 to 6. The effects of different anions on the removal of As(III) in the ferrate(VI)/Al(III) system at pH 6.5 (*cf* Figure 17). It was suggested that phosphate and silicate formed inner-sphere complexes and compete strongly with arsenic for Fe or Al oxy/hydroxide surfaces and such competition exist only at higher concentrations of phosphate and silicate, causing an apparent decrease in removal efficiency of the system. Bicarbonate also influenced the removal of As(III), but much higher levels were needed than that of phosphate and silicate [81]
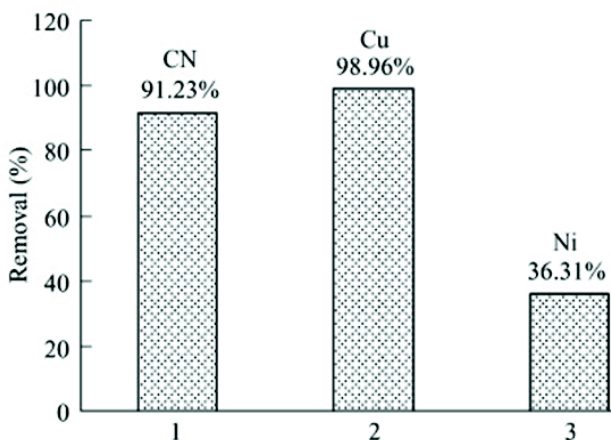
Fig. 16. Fe(VI) treatment for CN oxidation and simultaneous removal of Cu and Ni in CN-Cu-Ni system. CN: 1.00 mmol/L, Cu: 0.100 mmol/L, Ni: 0.170 mmol/L, Fe(VI) dose: 2 mmol/L [80].
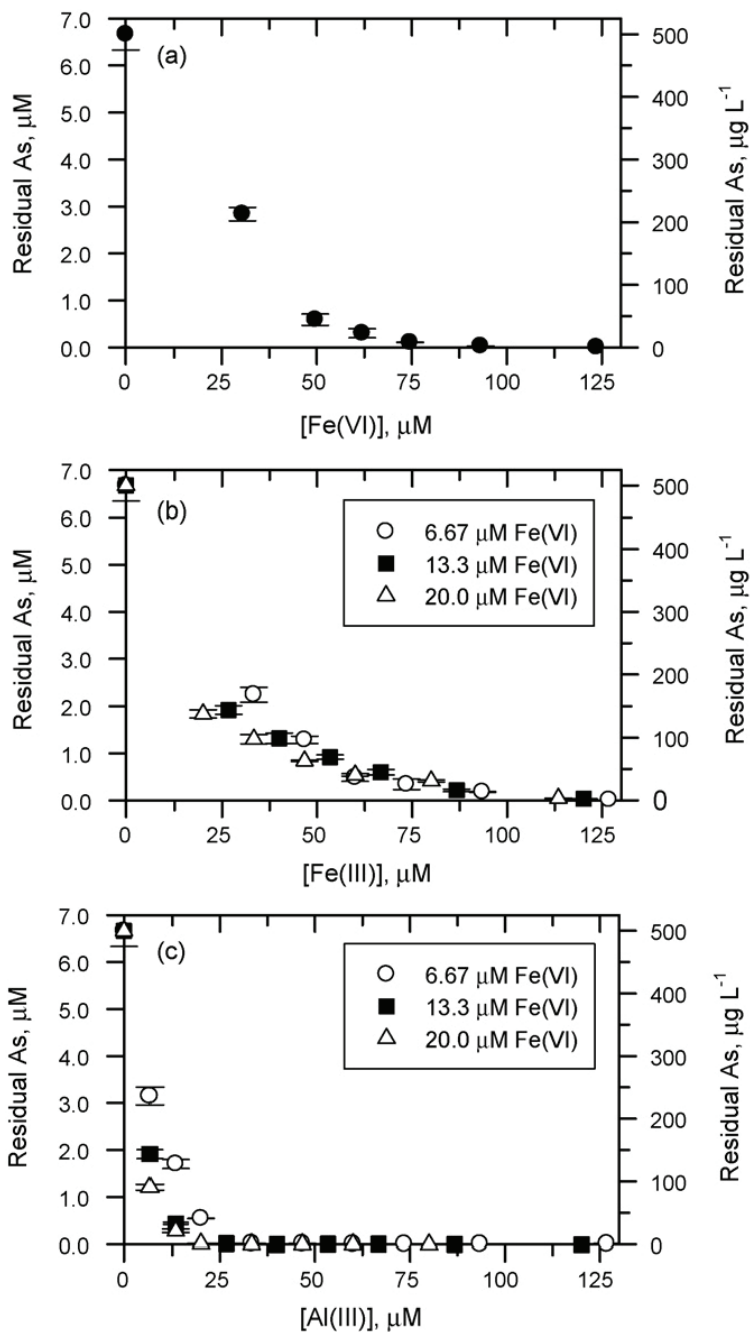
Fig. 17. Removal of arsenite by Fe(VI) (a), Fe(VI)/Fe(III) salts (b), and Fe(VI)/Al(III) salts (c) at pH 6.5. Initial concentration = 500 μg As(III)/L [81].

The decomplexation of Zn(II)-NTA with Fe(VI) showed second order rate kinetics and the rate constant value was found to be 8.80×10^{-1} $M^{-1}s^{-1}$. Further, the reaction was almost unaffected in presence of 1000 times $NaNO_3$, $NaCl$ and $NaClO_4$. However, it was greatly suppressed in presence of Na_2SO_3 and $NaNO_2$ elctrolyte. This suggests that Fe(VI) prefer the oxidation of SO_3^{2-} and NO_2^- rather the Zn(II)-NTA complex [82].

Interestingly, the americium and plutonium radionuclides were treated with ferrate(VI) at pH 11.5-12.0 and results showed that the treated water samples contain significantly less radioactivity [83]. This was assumed that these radionuclides are coagulated with reduced Fe(III). Similarly, other radinuclides are treated with Fe(VI) showed, Fe(VI) could play a wider possible role in radioactive waste management studies [84-85].

4. Other possible applications of Fe(VI) in the remediation of wastewater treatment

The possible role of Fe(VI) is in the treatment of real wastewaters and to study the parameters involved. The various physical/chemical parameters studied and showed the applicability of Fe(VI) in the remediation of the waste water treatment. In addition the important aspect of ferrate(VI) technology is the property of disinfection. In the proceeding section the disinfection of Fe(VI) is discussed and possible mechanistic aspects are discussed in detail.

4.1 Disinfection of wastewater

Coagulation and oxidation/disinfection are to be the important unit processes associated with the water or wastewater treatment. The role of ferrate(VI) towards the degradation of several degradable materials shown to be promising and it possessed remarkably good coagulating/adsorbing capacity via the reduced Fe(VI) into Fe(III). The disinfection was rather, studied scarcely but several reports encourages the potential use of ferrate(VI) towards the disinfection reagent to be applied in the wastewater treatment plants.

The disinfection property of ferrate(VI) was first optimized to kill two pure laboratory cultures of bacteria (Non-recombinant *Pseudomonas* and Recombinant *Pseudomonas* [39]). At a dose of 0-50 ppm as FeO_4^{2-}, the bacteria were removed completely. The oxidation of *E. Coli* DNA *polymerase-I* by Fe(VI) resulted in loss of polymerization and *3-5 exonuclease* activity and thus the irreversible inactivation of the enzyme was reported [86]. Moreover, the reactivity of *deoxyribonucleosides* by Fe(VI) cuased DNA chain cleavage through a mechanism in which base loss is followed by β-elimination at the abasic site [87]. The results suggested irreversible inactivation of *E. Coli* by ferrate(VI).

The ferrate(VI) showed sufficient disinfection capability as to kill the *Escherichia coli* (*E. coli*). At pH 8.2 with a dose of 6 mg/L as Fe, the *E. coli* percentage kill was 99.9% but when the contact time was extended to 18 min even with the reduced dose of 2.4 mg/L as Fe facilitate the complete kill of *E. coli* [88]. The results also demonstrated that the disinfecting ability of FeO_4^{2-} increased markedly if water pH was below 8.0. Similarly, the secondary effluent disinfection study showed 99.9% of total *coliforms* and 97% of the total viable bacteria were removed at a dose of 8 mg/L of ferrate(VI) (*cf* Figure 18) [89].

The real sewage wastewater and a model water *E. coli* (concentration 3.2×10^8 /100mL) were used to assess the Fe(VI) capability as coagulant behavior (compared to ferric and aluminum

sulfate) for real wastewater and disinfection for the model *E.coli* water (compared with sodium hypochlorite) [90]. The Fe(VI) showed significantly better performance over ferric and aluminum sulphate. Moreover, the disinfection towards *E. coli* was also comparatively better than hypochlorite. In a line the comparative performance of ferrate(VI) with ferric sulfate and aluminum sulfate are carried and reported that ferrate possessed better treatment chemical (*cf* Table 8) [91].
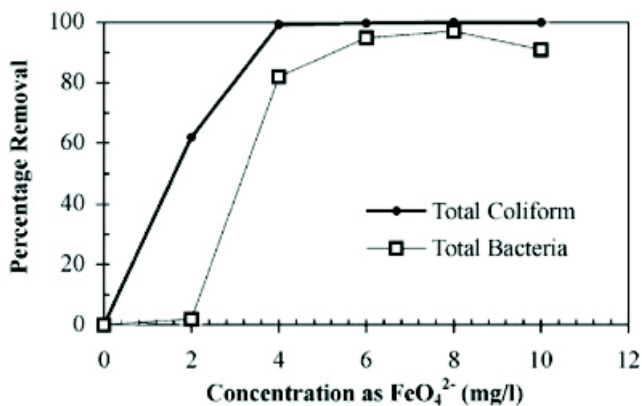
Fig. 18. Total *coliform* organisms and total bacteria removal with Fe(VI) [89].

	AS	FS	Fe(VI)
pH	6.75-7.48	6.75-7.48	7
Optimum dose as Al(III)) or Fe(III) (mmol/L)	0.37	0.36	0.36
Turbidity removal (%)	80	86	94
Colour (Vis400-abs) removal (%)	50	50	92
Total COD removal (%)	6	16	32
Dissolved COD removal (%)	4	7	14
Bacteria inactivation (in $\log_{10}$ terms)[a]	1	1.05	>4

[a] AS and FS achieved 1-$\log_{10}$ bacteria inactivation at doses >0. 50 mmol/L as either Al or Fe, whilst FR achieved >4-$\log_{10}$ bacteria inactivation at doses <0.27 mmol/L as Fe.

Table 8. Comparative performance of coagulants at optimum dose [91]

The disinfection kinetic model was proposed by Chick-Watson relation (equation (51)) as to derive the rate constants:

$$N/N_0 = e^{-kt} \tag{51}$$

Where, N and N_0 are the number concentrations of the organisms remaining and originally, respectively, t is disinfectant-organism contact time, and k is the rate constant (time^{-1}); and k

can be written as $k = k'C^b$ to relate the rate constant of inactivation to the disinfectant concentration C. b is termed as dilution coefficient and can be obtained by the slope of a log-log plot of t *vs* C. Previously, the k was evaluated for *E. coli* using the equation (51) at different pH for the disinfection of *E. coli* [90].

The modified Delayed Chick-Watson law with time averaged Fe(VI) concentration (equation (52)) was used in order to discuss the kinetics of the inactivation [27,92].

$$Log(N|N_0) = -k\overline{[Fe(VI)]}\,T = -k\bar{C}\,T \tag{52}$$

where N_0 is the initial number of viable *E.coli* (CFU mL^{-1}), N is the remaining number of viable *E. coli* (CFU mL^{-1}) at time T (min), $\overline{[Fe(VI)]} = \int_0^T [Fe(VI)]dt/T$ is the time averaged Fe(VI) concentration, which can be determined by integrating time-dependent Fe(VI) concentration profiles with time. This can be predicted by using self-decomposition rate constants of Fe(VI) or measured directly. This model is based on the assumption that the degree of *E.coli* inactivation (Log (N/N_0)) is proportional to the time-dependent amount of *E. coli* exposed to ($\overline{[Fe(VI)]}$T), which reflects a more realistic oxidative environment for *E. coli* inactivation. It was further, demonstrated the inactivation ability of different Fe(VI) species using the different pk$_a$ values of ferrate(VI) [92]. The different species of Fe(VI) would have variable reactivity towards the inactivation of *E. coli* hence would have different rate constants of inactivation:

$$H_2FeO_4 + E.\ coli \rightarrow \text{Inactivation (rate constant } k_{53}) \tag{53}$$

$$HFeO_4^- + E.\ coli \rightarrow \text{Inactivation (rate constant } k_{54}) \tag{54}$$

$$FeO_4^{2-} + E.\ coli \rightarrow \text{Inactivation (rate constant } k_{55}) \tag{55}$$
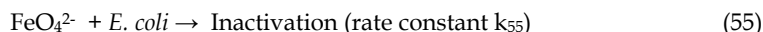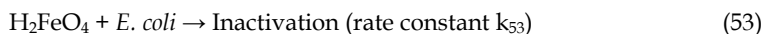
By assuming an additive inactivating efficiency for H_2FeO_4, $HFeO_4^-$ and FeO_4^{2-} toward *E. coli,* the log inactivation level of *E. coli* can be expressed in the form of equation (56):

$$Log\left(\frac{N}{N_0}\right) = -\{k_{53}\overline{[H_2FeO_4]} + k_{54}\overline{[HFeO_4^-]} + k_{55}\overline{[FeO_4^{2-}]}\}\,T$$

$$= -\int_0^T k_{53}\overline{[H_2FeO_4]} + k_{54}\overline{[HFeO_4^-]} + k_{55}\overline{[FeO_4^{2-}]}dt. \tag{56}$$

Accordingly, the k_{obs} can be expressed as equations (54), which can be deduced from the comparison of equation (56) with equation (52):

$$k_{obs} = \alpha_0 k_{53} + \alpha_1 k_{54} + \alpha_2 k_{55} \tag{57}$$

$$\propto_0 = \frac{[H_2FeO_4]}{[Fe(VI)_T]} = \frac{[H^+]^2}{T}, \tag{58}$$

$$\propto_1 = \frac{[HFeO_4^-]}{[Fe(VI)_T]} = \frac{k_a^3[H^+]}{T}, \tag{59}$$

$$\propto_2 = \frac{[FeO_4^{2-}]}{[Fe(VI)_T]} = \frac{k_a^3\,k_a^4}{T}, \tag{60}$$

$$\text{where } T = [H^+]^2 + k_a^3 [H^+] + k_a^3 k_a^4$$

Hence, the three inactivation constants (k_{53}, k_{54} and k_{55} can be estimated with measured pH dependence data. The data obtained with this study showed that $HFeO_4^-$ and H_2FeO_4 were found to be 3 and 265 times as effective as FeO_4^{2-} at least towards the inactivation of *E. coli* [92].

Moreover, it was reported that ferrate(VI) can rapidly inactivate the *f2 Coliphage* at low concentrations; 99% of *f2 Coliphage* was inactivated at 1 mg/L of ferrate(VI) in 5.7 min at pH 6.9 and only 0.77 min at pH 5.9. A higher dose (10 mg/L of ferrate(VI) was required in order to achieve 99.9% inactivation at pH 7.8 with a contact time to 30 min [93,94].

4.2 Degradation of pharmaceuticals present in aquatic environment

The enhanced level of pharmaceuticals present in the aquatic environment shown a greater concern for its degradation/removal from the aquatic environment. These chemicals includes with variety of antibiotics. Several reports demonstrated the use of advanced oxidation using O_3/H_2O_2, UV/H_2O_2, Fenton/Photon-Fenton or UV/TiO_2 processes or even simple biological or chemical degradation employed to degrade these micro pollutants from the wastewater. However, the use of ferrate(VI) attained greater interest in recent past because of green treatment and significant reactivity of the compound (vide Table 3). Several sulphur containing antibiotics including sulfamethoxazole, sulfametazine, sulfamethizole, sulfadimethoxine, sulfasoxazole etc. were treated with ferrate(VI) and rate expressions were obtained. It was reported that 1:1 stoichiometry occurred in the degradation of these drugs with Fe(VI) and rate law for each reactant is of pseudo first-order using excess of Fe(VI). Further, second order rate constants were evaluated and given in Table 9 [95-97].

Sulfonamide	k_{HFeO4} $(10^3 M^{-1}s^{-1})$		k_{FeO4} $(10^1 M^{-1}s^{-1})$	K_{app} $(10^3 M^{-1}s^{-1})$	$t_{1/2}$ (s)
	SH	S-	SH	pH 7.0	
Sulfamethoxazole	30.0	0.17	0.12	1.50	91
Sulfametazine	1.90	0.55	22.5	0.87	157
Sulfamethizole	22.3	0.22	-	0.64	214
Sulfadimethoxine	18.8	0.38	-	-	-
Sulfasoxazole	11.0	2.42	-	0.85	161

Half lives for the dose of 1 mg/L of K_2FeO_4 at pH 7.0 and 25 ^0C

Table 9. Second-order rate constants for reactions of sulfonamides at 25 ^0C [95]

5. Conclusions

The ferrate(VI) which possessed significantly high oxidation capability along with significantly high coagulation/flocculation and disinfection properties showed that it may be one of potential chemical towards the several aquatic environmental remediation strategies. Moreover, as the ferrate(VI) treatment is absolutely free from the occurrence of

toxic/harmful by-products hence, found to be more environmentally benign or termed as 'Green Chemical' and the ferrate(VI) technology may be known as "Green Technology'.

6. References

[1] Sharma, V.K., J. Environ. Manag. (2010). Article in Press doi: 10.1016 / j.jenvman. 2010.11.026.

[2] Jiang, J.Q. and Lloyd, B., Wat. Res. 36 (2002) 1397-1408.

[3] Poggendorf, J.C. Pogg. Ann. 54 (1841) 372.

[4] Alsheyab, M. and Jiang, J. Q., Stanford, C., J. Environ. Management 90 (2009) 1350-1356.

[5] Christian, G.D., Sensmeier, R.K. and Wagner, W. I., Monatshefte fuer Chemie 106 (1975) 813-822.

[6] Koninck, M.D., Brousse, T., Belanger, D., Electrochim. Acta 48 (2003) 1425-1433.

[7] Denvir, A. and Pletcher, D., J. Appl. Electrochem. 26 (1996) 815-821.

[8] Denvir, A. and Pletcher, D., J. Appl. Electrochem. 26 (1996) 823-827.

[9] Bouzek, K. and Macova, Z. Proc. of the International Symp. on Innovative Ferrate(VI) Technology in Water and Wastewater Treatment, Pub. ICT Press, Prague pp. 9-19 (2004).

[10] Bouzek, K. and Rousar, I., Electrochim. Acta 38 (1993) 1717-1720.

[11] Bouzek, K., Lipovska, M., Schmidt, m., Rousar, I. and Wragg, A.A., Electrochim. Acta 44 (1998) 547-557.

[12] Bouzek, K., Flower, L., Rousar, I. and Wragg, A.A., J. Appl. Electrochem. 29 (1999) 569-576.

[13] Li, C., Li, X.Z. and Graham, N., Chemosphere 61 (2005) 537-542.

[14] Tiwari, D., Kim, H.U., Choi, B.J., Lee, S. M., Kwon, O.H., Choi, K.M., Yang, J.K., J. Environ. Sci. Health A42 (2007) 803-810.

[15] Homonnay, Z., Perfiliev, Y.D., Sharma, V.K., Proc. of the International Symp. on Innovative Ferrate(VI) Technology in Water and Wastewater Treatment, Pub. ICT Press, Prague pp. 55-63 (2004).

[16] Dedushenko, S. K., Perfiliev, Y.D., Goldfield, M. G., and Tsapin, A.I., Hyperfine Interactions 136 (2001) 373-377.

[17] Neveux, N., Aubertin, N., Gerardin, R., Evrard, O., Stabilized ferrate(VI): Synthesis method and applications. In: Klute R., Hahn, H.H. Editors. Chemical water and wastewater treatment III. Berlin Heidelberg: Springer, 1994 pp. 95-103.

[18] Hopp, M.L., Schlemper, E.O. and Murmann, R.K., Acta Cryst. B38 (1982) 2237-2239.

[19] Goff, H. and Murmann, R.K., J. Am. Chem. Soc. 93 (1971) 6058-6065.

[20] Inorganic Crystal Structure Database, Version 1.3.1 December 2003, National Institute of Standards and Technology (NIST) and Fach Informationszentrum Karlsruhe (FIZ).

[21] Norcross, B.E., Lewis, W.C., Gai, H., Noureldin, N.A., and Lee, D.G., Can. J. Chem. 75 (1997) 129-139.

[22] Hoppe, M. L., Schlemper, E.O. and Murmann, R. K., Acta Cryst. B38 (1982) 2237-2239.

[23] Moeser, L., J. Prakt. Chem. 56 (1897) 425.

[24] Vicenteperez, S., Losada, J., Hernandez, P., Anales Quim B81 (1984)93-99.

[25] Carrington, A., Schonland, D. and Symons, M.C.R., J. Chem. Soc. (1957) 659-665.

[26] Sharma, V.K., Burnett, C.R. and Millero, F.J., Phys. Chem. Chem. Phys. 3 (2001) 2059-2062.
[27] Lee, Y., Cho, M., Kim, J.Y. and Yoon, J., J. Ind. Eng. Chem. 10 (2004) 161-171.
[28] Lee, Y., Yoon, Y. and Gunten, U. von, Wat. Res. 39 (2005) 1946-1953.
[29] Cici, M. and Cuci, Y., Waste Manage. 17 (1998) 407-410.
[30] Johnson, M.D. and Sharma, K.D., Inorg. Chim. Acta 293 (1999) 229-233.
[31] Schreyer, J.M. and Ockerman, L.T., Anal. Chem. 23 (1951) 1312-1314.
[32] Wagner, W.F., Gump, J.R. and Hart, E.N., Anal. Chem. 24 (1952) 1397.
[33] Stuart, L., Wang, B. and Ghosh, S., Science 285 (1999) 1039-1042.
[34] Tiwari, D., Kim, H.U., Choi, B.J., Lee, S.M., Kwon, O.H., Choi, K.M., Yang, J.K., J. Environ. Sci. Health A42 (2007) 803-810.
[35] Carr, J.D., Kelter, P.B.,Tabatabai, A., Splichal, D., Erickson, J. and McLaughlin, C.W., Properties of Ferrate(VI) in Aqueous Solutions: An Alternative Oxidant in Wastewater Treatment. In: Jolley, R.L. (Ed.) Proceedings of Conference on Water Chlorination Chem. Environment Impact Health Eff. Lewis Chelsew, pp 1285-1298 (1985).
[36] Rush, J.D., Zhao, Z. and Bielski, B.H.J., Free Rad. Res. 24 (1996) 187-198.
[37] Lee, D.G. and Gai, A.H., Can. J. Chem. 71 (1993) 1394-1400.
[38] Carr, J.D., ACS Symposium Series 985(Ferrates) (2008) 189-196.
[39] Murmann, R.K. and Robinson, P.R., Wat. Res. 8 (1974) 543-547.
[40] Zhou, W., Boyd, J.M., Qin, F., Hrudey, S.E. and Li, X., Environ. Sci. Technol. 43 (2009) 8443-8448.
[41] Bielski, B.H.J. and Thomas, M.J., J. Am. Chem. Soc. 109 (1987) 7761-7764.
[42] Bielski, B.H.J., Free Rad. Res. Comms. 12 (1991) 469-477.
[43] Bielski, B.H.J., Annl. Neurol., 32 (1992) 528-532.
[44] Rush, J.D. and Bielski, B.H.J., Am. Chem. Soc. 108 (1986) 523-525.
[45] Rush, J.D. and Bielski, B.H.J., Free Rad. Res. 22 (1995) 571-579.
[46] Huang, H., Sommerfield, D., Dunn, B., Eyring, E.M. and Lloyd, C.R., J.Phys. Chem. A195 (2001) 3536-3541.
[47] Johnson, M.D. and Hornstein, B.J., Inorg. Chim. Acta 225 (1994) 145-150.
[48] Johnson, M.D. and Hornstein, B.J., Chem. Commun. (1996) 965-966.
[49] Johnson, M.D. and Hornstein, B.J., Inorg. Chem. 42 (2003) 6923-6928.
[50] Sharma, V.K. and Hollyfield, S., Prep. Pap. Matl. Meet.- Am. Chem. Soc. Div. Environ. Chem. 35 (1995) 63-66.
[51] Jhonson, M.D. and Read, J.F., Inorg. Chem. 35 (1996) 6795-6799.
[52] Sharma, V.K. and Bielski, B.H.J., Inorg. Chem. 30 (1991) 4306-4310.
[53] Read, J.F., Adams, E.K., Gass, H.J., Shea, S.E. and Theriault, A., Inorg. Chim. Acta 281 (1998) 43-52.
[54] Read, J.F. and Wyand, E.H., Transition Met. Chem. 23 (1998) 755-762.
[55] Read, J., Boucher, K.D., Mehlman, S.A. and Watson, K.J., Inorg. Cheim. Acta 267 (1998) 159-163.
[56] Jhonson, M.D. and Bernard, J. Inorg. Chem. 31 (1992) 5140-5142.
[57] Jhonson, M.D., Hornstein, B.J. and Wischewsky, J., ACS Symposium Series 985 (Ferrates) (2008) 177-188.
[58] Jhonson, M.D. and Sharma, K.D., Inorg. Chim. Acta 293 (1999) 229-235.
[59] Sharma, V.K., J.Environ. Sci. Health A45 (2010) 645-667.
[60] Sharma, V. K., Smith, J. O. and Millero, F. J., Environ. Sci. Technol. 31 (1997) 2486-2491.

[61] Sharma, V.K., Rivera, W., Smith, J.O. and O'Brien, B., Environ. Sci. Technol. 32 (1998) 2608-2613.

[62] Sharma, V.K., Adv. Environ. Res. 6 (2002) 143-156.

[63] Shrama, V.K., Bumett, C.R.,Yngard, R. And Cabelli, D., Environ. Sci. Technol. 39 (2005) 3849-3854.

[64] Shrama, V.K., Bumett, C.R., O'Connor, D.B. and Cabelli, D., Environ. Sci. Technol. 36 (2002) 4182-4186.

[65] Lee, Y.H., Um, I.H. and Yoon, J., Environ. Sci. Technol. 37 (2003) 5740.

[66] Yngard, R.A., Sharma, V.K., Filip, J. And Zboril, R., Environ. Sci. Technol. 42 (2008) 3005-3010.

[67] Yngard, R.A., Damrongsiri, S. and Sharma, V.K., Chemosphere 69 (2007) 729-735.

[68] Sharma, V.K., Kazma, F., Jiangyong, H. and Ray, A.K., J.Wat.Health 3 (2005) 45-58.

[69] Sharma, V.K., Environ. Sci. Technol. 44 (2010) 5148-5152.

[70] Sharma, V.K., Rivera, W., Joshi, V.N., Millero, F.J and O'Connor, D., Environ. Sci. Technol. 33 (1999) 2645-2650.

[71] Sharma, V.K., Rendon, R.A., Millero, F.J. and Vazquez, F.G., Mar. Chem. 270 (2000) 235-242.

[72] Rush, J.D., Zhao, Z. and Bielski, B.H.J., Free Rad. Res. 24 (1996) 187-192.

[73] Giesy, J.P., Hilscherova, K, Jones, P.D., Kannan, K. and Machala, M., Mar. Pollut. Bull. 45 (2002) 3-16.

[74] United States Environmental Protection Agency (USEPA). Special Report on Environmental Endocrine Disruption: An Effects Assessment and Analysis. Washington, DC: Office of Research and Development (1997).

[75] Flemming, I. and Bent, H.S., Evaluation of Analytical Chemical Methods for Detection of Estrogens in the Environment. Denmark, Vol. 44 (2003) 1-69.

[76] Jiang, J.Q., Yin, Q., Zhou, J.L. Pearce P., Chemosphere 61 (2005) 544-550.

[77] Lee, Y., Yoon, J. and von Gunten, U., Environ. Sci. Technol. 39 (2005) 8978-8984.

[78] Li, C., Li, X.Z., Graham, N. and Gao, N.Y., Wat. Res. 42 (2008) 109-120.

[79] Bartzatt, R., Cano, M. and Jhonson, D., J.Toxicol.Environ. Health 35 (1992) 205-210.

[80] Lee, S. M. and Tiwari, D., Environ. Technol. 21 (2009) 1347-1352.

[81] Jain, A., Sharma, V.K. and Mbuya, M.S., J.Haz. Mater. 169 (2009) 339-344.

[82] Yang, J., Tiwari, D., Yu, M., Pachuau, L., Kim, W., Lee, S., Environ. Technol. 31 (2010) 791-798.

[83] Potts, M.E. and Churchwell, D.R., Wat. Environ. Res. 66 (1994) 107-109.

[84] Midkiff, W. S., Covey, J. R. and Johnson, M. D., Wat. Environ. Res. 67(1995) 1007-1008.

[85] Stupin, D.Y. and Ozernoi, M.I., Radiochem. 37 (1995) 329-332.

[86] Basu, A., Williams, K.R. and Modak, M.J., J. Biol.Chem. 262 (1987) 9601-9607.

[87] Stevenson, C. and Davies, J.H. Biochem. Soc. Trans. 23 (1995) 387S.

[88] Gilbert, M. B., Waite, T. D. and Hare, C., J. Am. Wat. Works Assoc. 68 (1976) 495-497.

[89] Waite, T.D., J. Environ. Eng.-ASCE 105 (1979) 1023-1034.

[90] Jiang, J.Q., Wang, S. and Panagoulopoulos, A., Desalination 210 (2007) 266-273.

[91] Jiang, J.Q., Panagoulopoulos, A., Bauer, M. And Pearce, P., J. Environ. Manag. 79 (2006) 215-220.

[92] Cho, M., Lee, Y., Choi, W., Chung, H. And Yoon, J., Wat. Res. 40 (2006) 3580-3586.

[93] Schink, T. and Waite, T.D., Wat. Res. 14 (1980) 1705-1717.

[94] Jiang, J.Q., J. Haz. Mater. 146 (2007) 617-623.

[95] Sharma, V. K., Mishra, S. K. and Nesnas, N., Environ. Sci. Technol. 40 (2006) 7222-7227.
[96] Sharma, V.K., Chemosphere 73 (2008) 1379-1386.
[97] Sharma, V.K., Mishra, S.K. and Ray, A.K., Chemosphere 62 (2006) 128-134.

Purification of Waste Water Using Alumina as Catalysts Support and as an Adsorbent

Akane Miyazaki[1] and Ioan Balint[2]
[1]Japan Women's University
[2]Institute of Physical Chemistry
[1]Japan
[2]Romania

1. Introduction

Alumina is one of the most widely used adsorbent for removal of dissolved pollutants from waste water. Various chemical species, especially ions, are known to be adsorbed onto alumina. On the other hand, alumina is a typical support for catalysts. Many kinds of metal supported catalysts are prepared using alumina as their support. These two roles of alumina, i.e., as adsorbent and support, are closely related to each other due to two reasons. Firstly, most supported catalysts are prepared by impregnation. Impregnation is the process in which solid alumina is contacted with liquids which contain various metal precursors. Thus, adsorption phenomena play a crucial role in this process. Since a new phase is formed on the surface of the support after the impregnation process, alumina has been reported to have an essential role in the formation of catalysts active sites. Secondly, alumina used as a catalysts support can adsorb reactants in the course of catalytic reaction. Such adsorption onto support must be taken into account when the conversion and selectivity of the catalyst are calculated.

In this chapter, the two roles of alumina and their relationship are discussed in the light of experimental result. Former part of this chapter, behavior of alumina in the process of impregnation is examined and its relationship with the formation of active sites is discussed. Alumina is one of a very active adsorbent for heavy metal ions. This feature is used both in purification of waste water containing heavy metal and preparation of metal supported catalysts. In order to prepare Cu/Al_2O_3 catalyst, alumina was suspended in aqueous solution of $CuSO_4$. This is a typical impregnation process and in the meantime alumina had been thought to be inactive. However, after long contacting time, alumina was found to dissolve even in the neutral pH range. Because alumina did not dissolve in the same experimental condition in the absence of Cu^{2+} ions, the dissolution was found to be induced by contacting with Cu^{2+} ions. Alumina dissolution was observed during impregnation with $PdCl_4^{2-}$ in acid pH range, too. These facts mean that the active site formed on alumina after impregnation can contain significant amount of aluminum, and thus the catalytic performance may different from pure metal particles supported on alumina. In order to examine this possibility, Ru/Al_2O_3 catalyst was prepared by both impregnation and colloidal Ru methods. In the colloidal method, it is possible to minimize support effect by preparing metal particles in the absence of the support, and then deposit them onto the support. Although the two catalysts prepared had same composition, their catalytic

behavior for ammonia synthesis was completely different, and this was attributed to the structure of active site, i.e., contaminated with aluminum or not. These results suggest the importance of adsorption behavior in the process of catalysis preparation, because alumina support is not completely inert in impregnation process.

In the latter part of this chapter, cases in which alumina used as a catalysts support but at the same time behaves as an adsorbent are introduced. Catalytic reduction of NO_3^- and NO_2^- ions are thought to be one of the most promising way to treat contaminated drinking water. This reaction is generally performed by using Pd or Pt-based catalysts supported on Al_2O_3. The conversion of NO_2^- is conventionally calculated from the decrease in NO_2^- concentration of the reacting solution. However, it was found that significant amounts of NO_2^- disappeared from the reacting solution not because of chemical conversion, but because of its adsorption onto alumina which is the support of the catalyst. Furthermore, the equilibrium amount of adsorbed NO_2^- was affected by the size of supported Pt. This result suggests that the adsorption of NO_2^- onto alumina should be considered when the performance of denitration catalysts is evaluated. In addition, utilizing the high adsorption capacity of alumina for NO_2^- may realize its potential as an adsorbent for the removal of NO_2^- ions in waste waters.

2. Adsorption of heavy metal ions onto alumina

Aluminum is a ubiquitous element comprising nearly 8% (w/w) of the earth's crust, and aluminum oxide is a common adsorbent in aqueous electrolyte solutions. The concentration of dissolved metal ions in aqueous systems are controlled to a large extent by the partitioning of solute to solid phases through adsorption and presipication. Therefore, solid-liquid interfacial reactions of heavy metal ions on the surface of alumina has drawn great interest in areas such as water quality and treatment, heavy metal transport, potential bioavailability of aqueous metal species, and biogeochemiscal cycling of metal ions (Trainor et al., 2000). The interfacial reactions on alumina also play an important role in heterogeneous catalyst preparation.

The adsorption phenomena of ions to oxides have been explained mainly by three models: surface complex formation model (ligand model), hydrolysis moderl (ion-solvent interaction model), and crystal field model. Currently, the surface complex formation model seems to be the most general and widely accepted model. Surface complex formation models are chemical models that use an equilibrium approach to describe the formation of complex at the oxide-solution interface (Goldberg, 1991). Unlike empirical models, such as the Langmuir and Freundlich adsorption isotherm equations, chemical models explicitly define surface species, chemical reactions, equilibrium constant expressions, and surface activity coefficient expressions. Additional advantages of the surface complex formation models are inclusion of mass and charge balance equations and consideration of the charge on both adsorbate and the adsorbent. According to the surface complex formation model, the extent of metal ion partitioning and stability of the resulting products is a function of the speciation of the sorbate metals. For example, weakly bound outer-sphere adsorption complex are more rapidly exchangeable than more strongly bound inner-sphere adsorption complexes. This explains so-called *specific adsorptpion*, which suggests alumina can adsorb heavy metal ions 1,000 to 10,000 times more readily than alkaline or alkaline earth metal ions (Wada & Abd-Elfattah, 1979).

2.1 Three-steps reaction on the surface of alumina
Surface complex formation between heavy metal ions and aluminol groups (Al-OH) on the surface of alumina has been observed by many researchers using potentiometry,

spectroscopic methods such as EXAFS, and so on. Adsorption experiments of Zn^{2+} onto alumina was performed using a method described by Miyazaki and Tsurumi (1995). Using this potentiometric method, where the ionic strength and pH value of the reacting suspension are kept strictly constant, while the concentration of heavy metal ions in the suspension was increased stepwise. By this method, it is possible to determine the amount of heavy metal ions retained by the solid, and the corresponding amount of H^+ ions released from the surface –OH groups.

Figure 1 shows the result of Zn^{2+} adsorption onto alumina, which was synthesized by hydrolysis of $Al_2(SO_4)_3$ and confirmed to be X-ray amorphous (Miyazaki et al., 2003). In the
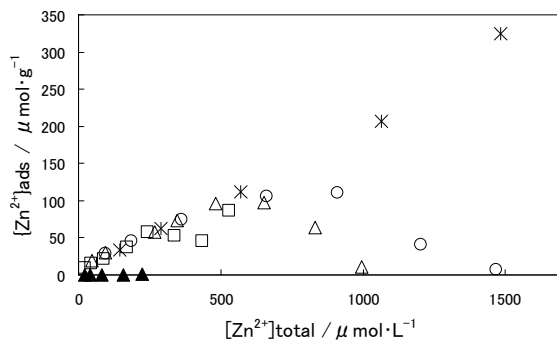
Fig. 1. Adsorption of Zn^{2+} ions onto Al_2O_3. Relationship between the total concentration of Zn^{2+} and amount of Zn adsorbed by 1g of Al_2O_3 is shown. The experiments were performed at constant pH of 6.50 for Zn^{2+} concentrations ranging up to 600 µmol/L(□), 1000 µmol/L(△), 1,500 µumol/L (○), and 3,000 µmol/L (✳). Blank experiment was carried out in the absence of solid (▲).

experiment, the concentration of alumina was kept 1g/L. The ionic strenght of the suspension was maintained at 0.1 by addding $NaNO_3$ and pH was 6.5. The concentration of Zn^{2+} in the suspension was increased from 0 to 600, 1000, 1500 or 3000 µmol/L, by using Zn^{2+} stock solution with different concentrations, and the results of each experiment are represented by different symbols. Each set of symbols represents the measurement at each stepwise increase in the concentration of Zn^{2+} ions in the suspension. From Fig. 1, it can be seen that the adsorption behavior of Zn^{2+} ions differed among the total concentration range of Zn^{2+}. In all cases of experiments shown in Fig. 1, the amount of Zn^{2+} ions adsorbed on the solid increased to a maximum corresponding to the concentration of Zn^{2+} stock solution. Further increase in total Zn^{2+} ions concentration caused a decrease in the propotion of adsorbed Zn^{2+} ions. This means some amount of Zn^{2+} ions adsorbed on the surface of the alumina desorbed.

In Fig. 1, every experiment showed the adsorption of Zn^{2+} ions, even if the total concentration was less than 250 µmol/L, which is below the concentration that can form $Zn(OH)_2$ in the bulk solution. Because this concentration range of Zn^{2+} ions was significantly lower than that of the solubility product of $Zn(OH)_2$ (3,000 µmol/L), it is reasonable to suggest that Zn^{2+} ions are retained on the surface of alumina, not by hetrogeneous nucleation on the solid surface, but by some adsorption mechanism. Figure 2(a) illustrates the relationship between the adsorption amount and the total concentration of Zn^{2+} ions (up to 800 µmol/L), as

(a)   (b)
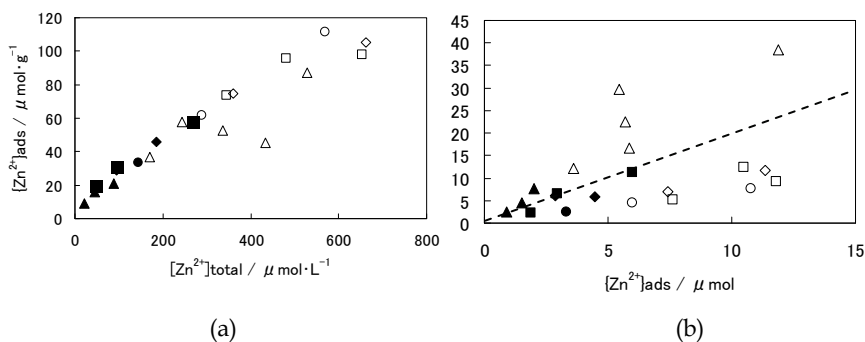
Fig. 2. Adsorption of Zn^{2+} ions onto alumina. (a) Relationship between total concentration of Zn^{2+} and adsorbed amount of Zn by 1g of Al_2O_3. The results obtained by using several concentration of Zn stock solutions are depicted with different symbols. The closed symbols are used for the results which seems to fit a line, while open symbols are used for the other. (b) Relationship between absolute amount of adsorbed Zn^{2+} and released H^+, which are calculated for the same experimental data shown in Fig. 2(a). The type of symbols is followed Fig. 2 (a). The line represents a slope 2.

shown previously in Fig. 1. The region in Fig. 2(a), in which the total concentration of Zn^{2+} ions is up to ~ 300 µmol/L, corresponds to the first adsorption region in Fig. 1. Since the results in this adsorption region exhibited good liniarity and reproducibility, it can be assumed that this region exists in an equilibrium state. Figure 2(b) shows the relationship between the absolute amount of adsorbed Zn and the released H^+ ions, corresponding to the same data that was presented in Fig. 2(a). Results in Fig. 2(b) that generally fit the overlaid line (with slope of 2) were designated with solid symbols, which were also assigned to the corresponding data in Fig. 2(a). Similarly, these solid symbols in Fig. 2(b) also showed good liniarity. Since this relationship can be explained as the equilibrium in the formation of a surface complex between two aluminol groups and one Zn^{2+} ion, the first stage of Zn adsorption onto alumina can be defined according to the reaction:

$$2\{Al\text{-}OH\} + Zn^{2+} = \{(Al\text{-}O)_2Zn\} + 2H^+ \tag{1}$$
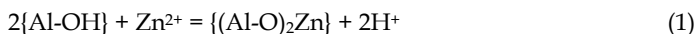
where { } indicates the chemical species on the surface of solid.
The equilibrium constantt of this reaction was calculated using the data obtained by the potentiometric studies. The equilibrium constant for equation (1) can be expressed as:

$$K = \frac{\{(Al\text{-}O)_2 Zn\}\left[H^+\right]^2}{\{Al\text{-}OH\}^2\left[Zn^{2+}\right]} \tag{2}$$

Where $\{(Al\text{-}O)_2Zn\}$ and $[Zn^{2+}]$ represent the concentrations of Zn^{2+} on the surface of solid (mol/g) and in the liquid phase (mol/L), respectively. This equilibrium constant represents the intrinsic microscopic formation constant for solutions of constant ionic strength. Herein, surface potential was defined as the potential difference between the aluminol site [(Al-O)$_2$Zn] and the bulk of solution, and for simplification, this value can be assumed as zero, and therefore, equation (2) does not contain an electrostatic term. Langumuir plots were

obtained using the experimental data, and using the slope of Langumuir plots, the concentration of aluminol sites on the surface of alumina was calculated to be 177 µmol/g. Equilibrium constant log K calculated by this value was log K = -5.67 (standard deviation was 0.0278). The reported equilibrium constant for the surface complexation between the silanol groups and Zn^{2+} ions was log β = -11.6   (Vlasova., 2001). Comparably, the equilibrium constant calculated for alumina was similar.

Figure 1 shows that the Zn^{2+} ions, which were adsorbed onto alumina by surface complexation, were desorbed at higher total concentration of Zn^{2+} ions. This desorption phenomenon did not follow a linear relationship between the total concentration of Zn^{2+} ions and the amount of Zn^{2+} ions adsorbed onto 1 g of solid. As shown in Fig. 2, the desorption behavior of Zn revealed a noticeable deviation from the equilibrium for surface complex formation. The timing for this deviation depended on the experimental conditions, in which the early desorption process seemed to be controlled by the total concentration of Zn^{2+} ions and by the reaction time, which took to increase the concentration of total Zn^{2+} ions. It remains unclear as to why desorption would occur for the Zn^{2+} ions, which initially adsorbed to form the surface complex with aluminol groups at lower total concentration of Zn^{2+} ions. However, as described in next sections, this dissolution phenomenon is not special for Zn^{2+} but general for heavy metal ions adsorbed onto alumina. Moreover, this process is accompanied with dissolution of alumina. The results shown in Fig. 2 suggest that the Zn^{2+} ions, which were desorbed from alumina, can be resorbed onto alumina. This process also included the sorption of Al^{3+} ions.

As it was observed in Fig. 1, the solid-liquid interfacial reaction of Zn^{2+} ions on alumina can be divided into three processes: adsorption, desorption, and re-adsorption. In the adsorption process, one Zn^{2+} ion and two aluminol groups formed a surface complex. This reaction was fast, and the equilibrium constant can be calculated for this surface complexation. The second process, the desorption of Zn, occurred when the surface density of Zn increased above a threshold value. Lastly, the re-sorption process happened as the third and the last process, which may be attributed to the hydroxide coprecipitation of Zn and Al.

2.2 Alumina dissolution induced by Zn^{2+} adsorption

In the process of adsorption of heavy metal ions onto alumina, it has been thought that adsorbed heavy metal ions would never be desorbed and alumina is inert in neutral pH range. However, adsorption experiment described in previous section revealed the Zn^{2+} ions adsorbed on the surface of alumina can be desorbed by increasing of reaction time or Zn^{2+} concentration in the experimental system. Moreover, the existence of Al^{3+} ions was observed at the same time (Miyazaki et al., 2003). This suggests that adsorbed Zn^{2+} ions are not desorbed alone but together with the support. This kind of rearrangement of adsorbed metal ions is reported by some researchers. Trainor et al. (2000) have studied the structure of Zn sorbed on the surface of high-surface-area alumina powders, and found that, at low sorption densities, Zn^{2+} predominantly formed inner-sphere bidentate surface complexes with AlO_6 polyhedra, whereas at high sorption densities, a mixed-metal Zn^{2+}-Al^{3+} hydroxide co-precipitate with a hydrotalcite-type local structure was formed. Based on the Zn^{2+}/Al^{3+} ratios in the precipitate, they have assumed the continuous dissolution of the alumina substrate (or secondary precipitated Al hydroxides), and the rapid re-precipitation of Al^{3+} together with Zn^{2+} for the formation of the mixed metal co-precipitate. Pauliac and Clause (1993) have reported on the formation of zinc-aluminum co-precipitates when 5 g of γ-alumina was in contact with 0.01 mol/L $Zn(NO_3)_2$ (200 mL) for 3 h at near-neutral pH (6.5 <

pH < 8.5). Jacquat et al. (2009) determined the local coordination of Zn in hydroxyl-interlayered smectite (HIS) as a function of Zn loading. They observed a progressive shift from Zn incorporation in the vacancies of gibbsitic Al-polymers to Zn adsorption to incomplete Al-polymers and finally uptake by cation exchange in the polymer-free interlayer space of HIS with increasing Zn loading.
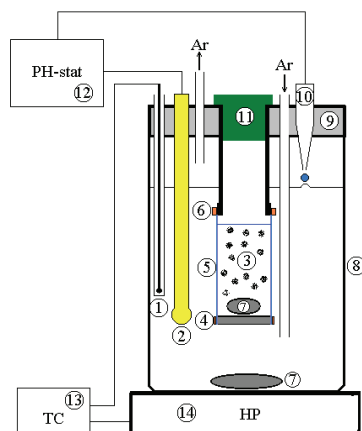
Fig. 3. The experimental system used for the investigation of alumina dissolution at constant pH. (1) glass-shielded   thermocouple,   (2) pH electrode, (3) alumina, (4, 6) Teflon rings, (5) dialysis bag,   (7) Teflon-coated   magnetic stirring rods, (8) glass beaker, (9) Teflon cap, (10)   buret, (11) Teflon cap with screw, (12) pH-stat, (13) temperature controller, (14)   hot plate and stirrer.

It has been difficult to monitor the evolution of heavy metal ions and alumina at the same time in the process of solid-liquid interfacial reactions, because of the most of the experimental arrangements utilized by now. Even if metal ions, which were once adsorbed on the surface of alumina, would be desorbed, they will be re-adsorbed immediately on the surface of alumina. Thus, it was difficult to distinguish the solid which was formed secondly by re-adsorption of dissolved aluminum ions and desorbed heavy metal ions, from original alumina and surface complex of heavy metal ions formed on its surface. In order to overcome these difficulties, experimental system using dialysis membrane proposed by Balint et al, (1999) has significant advantages. As shown in Fig. 3, the experimental system was composed of two parts that were separated from each other by a dialysis membrane (Wako/Wiscase Scales Corp., MWCO 12000-14000: pore diameter 25 Å). The tubular membrane was tightly closed with a Teflon cap and two Teflon rings. γ-Alumina (1 g, Aerosil) and 0.1 mol/L $NaNO_3$ aqueous solution (10 mL) were placed in a dialysis bag, then tightly sealed from the bulk solution using two Teflon rings. The γ-Al_2O_3 was produced by flame-hydrolysis of $AlCl_3$. The grains of the fine powder produced were approximately spherical in shape with an average diameter of 13 nm. The pH_{ZPC} of the alumina used in the experiment was determined to be 8.0 by a mass titration method (Subramanian, 1998). The beaker was filled with the solution (240 mL) containing 0.1 mol/L $NaNO_3$ and 1.8 mmol/L $Zn(NO_3)_2$. Before suspending the dialysis bag (containing alumina) in the beaker, the solution outside the bag was adjusted to pH 6.50 by the addition of 0.1 N NaOH. The pH value of the solution was monitored using a pH electrode; 0.1 N NaOH solution was added

using a pH-stat (TOA AUT-211) to maintain pH 6.50. These experimental conditions are corresponding to those adopted in adsorption experiment, whose results are shown in Figs. 1 and 2. Periodically, 2 mL aliquots from the impregnating solution outside the bag were subjected to ICP measurements to determine the concentrations of Al^{3+} and Zn^{2+} ions. The experiments were performed at constant temperature (25 °C), and the system was slowly purged (3.6 L/h) using Ar gas.
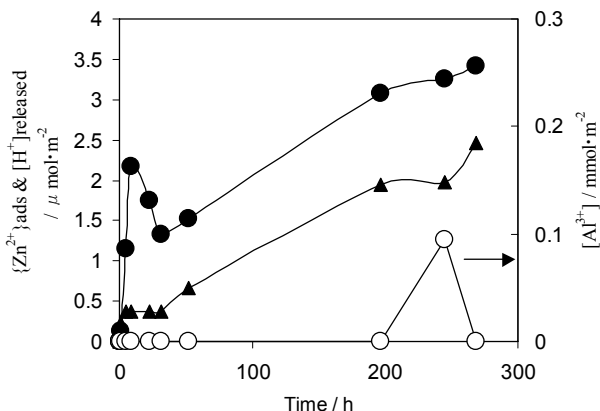
Fig. 4. Alumina dissolution promoted by adsorption of Zn^{2+} ions investigated with the experimental system presented in Fig. 3. The amounts of Zn^{2+} ions adsorbed onto the alumina (●) and the amount of H^+ released from the solid (▲) are shown together with the amount of Al^{3+} observed in the solution outside of the membrane bag   (○).

Measured concentration of Zn^{2+} and Al^{3+} ions in the solution outside the dialysis membrane bag, as a function of time, are shown in Fig. 4. Results showed that the amount of adsorbed Zn^{2+} ions increased in 0 to 8 h, which indicated that the Zn^{2+} ions added to the solution (in the beaker) passed through the membrane, and were adsorbed onto the alumina inside the bag. From 9 to 30 h, the adsorbed amount of Zn^{2+} ions decreased, which was attributable to the desorption of the adsorbed Zn^{2+} ions. After 30 h, slow uptake of Zn^{2+} ions was again observed. It is noteworthy that these three steps, as revealed by the membrane separation experiment, are in good agreement, qualitatively, with the result of the adsorption experiments, as shown in Fig 1. However, the time scale for the processes presented in Fig. 1 and Fig. 4 are significantly different. Since the alumina dissolution experiments (Fig. 4) were performed using a dialysis membrane, it is likely that the diffusion of Zn^{2+} ions was relatively restricted.
As for the initial adsorption process (0 to 9 h in Fig. 4), the ratio between the amounts of Zn^{2+} ions adsorbed and H^+ ions released was calculated as 1.8. This result confirmed that the initial adsorption process is the formation of the surface complex between two aluminol groups and one Zn^{2+} ion.
As shown in Fig. 4, the results clearly indicated the formation of Al^{3+} ions after 245 h of the reaction. Since these Al^{3+} ions originated from the alumina that was loaded inside the dialysis membrane, a measurable amount of alumina must have dissolved into the liquid phase during the adsorption of Zn^{2+} ions onto alumina at pH 6.5. A blank experiment without the addition of Zn^{2+} in the solution outside of the membrane confirmed that no Al^{3+} ions was released into the solution outside the bag. Thus, it is clear that the release of Al^{3+} ions was induced by Zn^{2+}.

To reveal the mechanism of this phenomena, $Zn(OH)_2$ was assumed to be the promoter of alumina dissolution. Fendorf et al. (1994) have reported that Cr^{3+} ions form a monodentate surface complex on silica when the surface coverage is below 20%; however, at higher surface coverage, a polynuclear chromium hydroxide surface phase is formed. It is highly possible that $Zn(OH)_2$ - like structure is formed on the surface of alumina, by increasing reaction time and concentration of metal ions on the surface of alumina.

The activity of $Zn(OH)_2$ for the dissolution of alumina was investigated, again by employing the membrane reactor (Fig. 3). In this experiment, $Zn(OH)_2$ was prepared by adding 0.1 mol/L NaOH solution to a $ZnNO_3$ solution, then mixed with alumina, in which the ratio between $Zn(OH)_2$ and Al_2O_3 was adjusted as equimolar (molar ratio = 1). The dialysis membrane bag, which contained the mixture, was suspended in the beaker filled with 0.1 mol/L $NaNO_3$ (pH 6.5).
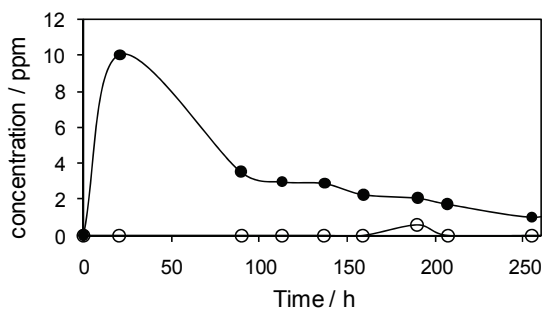
Fig. 5. Alumina dissolution promoted by $Zn(OH)_2$ investigated with the experimental system shown in Fig. 3. The time course of Zn^{2+} (●) and Al^{3+} (○) concentrations in the solution outside of the dialysis membrane.

Concentrations of the Zn^{2+} and Al^{3+} ions in the solution outside the dialysis membrane, as a function of time, are shown in Fig. 5. From 0 to 20 h, the concentration of Zn^{2+} ions in the solution increased dramatically, indicating that some $Zn(OH)_2$ dissolved and diffused into the solution outside the bag. From 20 to 255 h, the concentration of Zn^{2+} ions in the solution constantly decreased due to the re-adsorption of Zn^{2+} ions. Interestingly, after 190 h, the presence of Al^{3+} ions was observed in the solution outside the dialysis membrane bag. Comparatively, the time line for the formation of Al^{3+} ions is in good agreement with the results as described above (Fig. 4). In both cases, Al^{3+} ions were formed during the Zn^{2+} ion resorption process. The results presented in Figs. 4 and 5 proved that the formation of $Zn(OH)_2$ was mainly responsible for the dissolution of alumina. The $Zn(OH)_2$ phase, which is formed by increasing surface coverage, may possibly promote the dissolution of alumina.

2.3 Alumina dissolution induced by Cu^{2+} adsorption

Alumina dissolution induced by adsorption of heavy metal ions is deeply related to heavy metal behavior in environment and catalyst preparation. Support impregnation with metal(s) precursor(s) solution is a widespread method for catalysts preparation. The impregnation step has been reported to have an essential role for the formation of active sites (Foger, 1984). After the process of impregnation, a new phase is formed on the surface

of the support and it is likely to contain the precursor(s) of the active sites. Therefore, the impregnation process has been the focus of a large number of studies that attempted to reveal the relationship between the catalyst's preparation and its final activity (Zhang et al. 1992). The process of active site formation is not well-known, because the amount of the new phase formed is very small compared to the bulk, i.e., the support. However, it is important to acknowledge that not only the precursor but also the supports can contribute to active site formation. The alumina dissolution observed by Zn^{2+} adsorption strongly supports this possibility. In order to see if alumina dissolution is not a special phenomena observed by Zn^{2+} adsorption but general phenomena induced by other metal cations, solid-liquid interfacial reaction between alumina and Cu^{2+} was studied. Copper was selected because copper catalysts supported on alumina are of great interest for many important reactions, including methanol synthesis, steam reforming of methanol (Agaras et al, 1998), selective reduction of NO_x, and adsorption of SO_2 (Katheuser, et al, 1991). Such catalysts are generally prepared by impregnation of alumina with various precursors.

The processes associated with the impregnation of alumina with $CuSO_4$ at 50ºC and at pH values close to pH_{ZPC}, i.e., pHs 7 and 9, were studied. All the experiments were performed with the system shown in Fig. 3. A 1 of γ-Al_2O_3 (Aerosil) was loaded inside of the membrane bag with 12 mL of 0.1 mol/L K_2SO_4 solution. A 250 mL of 0.1 mol/L K_2SO_4 solution was poured into a glass beaker, and the membrane bag containing alumina was suspended in the beaker. The alumina was equilibrated overnight, with the pH kept constant at 7 or 9 by adding 0.1 mol/L KOH at 50ºC. A peristaltic pump was then used to gradually add 3 mL of a 1 mol/L $CuSO_4$ solution to the solution outside of the bag. At the end of the experiment, the precipitate formed outside of the bag was collected by filtration, washed several times with distilled water, and then dried at 100ºC. The alumina inside of the bag was treated in the same way.

Impregnation experiment at pH 9 lasted 240 h and formed 0.306 g of black precipitate, which contained 67.9 wt% of Cu and 0.355 wt% of Al. The XRD pattern of the precipitate formed outside of the bag suggested that the main components of the precipitate were CuO and $3Cu(OH)_2 \cdot CuSO_4$. The presence of a small amount of $Cu(OH)_2$ and Al_2O_3 in the precipitate was observed, too. A blank experiment without addition of $CuSO_4$ resulted neither the release of Al^{3+} ions nor the formation of the precipitate, even after 220 h.

On the other hand, impregnation experiment at pH 7, slightly lower than pH_{ZPC}, formed green precipitate after 336 h. The molar ratio between Cu and Al (Cu/Al) was 222, and this is smaller than the value observed at pH 9 (Cu/Al = 80.8). The total amount of alumina dissolved was 0.51 mg, and this corresponds to 23% of the amount of alumina dissolved at pH 9 (2.21 mg).

From the impregnation experiments conducted at pHs 7 and 9, it is clear that $CuSO_4$ promotes alumina dissolution at pH value near to pH_{ZPC}. To reveal the mechanism of this phenomena, $Cu(OH)_2$ and $3Cu(OH)_2 \cdot CuSO_4$ were assumed to be the main promoters of alumina dissolution. This assumption was based on the composition of the precipitates formed outside of the bag: CuO and $3Cu(OH)_2 \cdot CuSO_4$ at pH 9 and $3Cu(OH)_2 \cdot CuSO_4$ at pH 7. It is well-known that $Cu(OH)_2$ rapidly decomposes into oxide in the presence of excess hydroxyl ions, due to spontaneous dehydration (Massey, 1973). Heavy metal sulfates are known to stabilize $Cu(OH)_2$ as a basic sulfate. Thus, the interaction of copper hydroxide with the alumina was examined in order to assess its activity in alumina dissolution. The experiment was performed in the same way to alumina dissolution by $Zn(OH)_2$. A 1 g sample of γ-Al_2O_3 kept inside of the bag was equilibrated with 0.1 M K_2SO_4 solution at pH 9, 50ºC for 12 h. Then, 0.127 g (1 · 10^{-3} mol) of wet $Cu(OH)_2$ was added to the alumina inside of the bag. The $Cu(OH)_2$ was prepared

by adding KOH solution to $CuSO_4$ solution at room temperature with constant stirring. The light blue precipitate obtained was washed several times with distilled water and mixed with alumina quickly in order to avoid hydroxide decomposition.

Figure 6 shows that the concentration of aluminum released in to solution outside of the bag increased progressively over time. It can be seen that the aluminum concentration in the
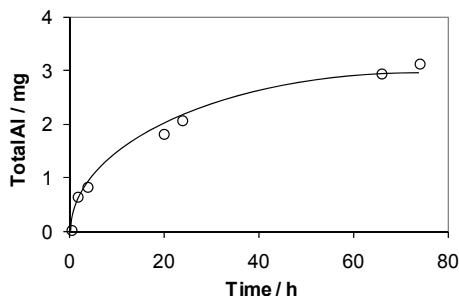
Fig. 6. Aluminum ion released in the solution outside the bag during $Cu(OH)_2$ interaction with alumina.

solution was 3.3 ppm at the end of the experiment. The total amount of alumina dissolved after 74 h of experiment was calculated to be 6.06 mg from the aluminum content of the solution. This amount of alumina dissolved is significantly higher than when alumina was impregnated with $CuSO_4$ at pH 9 for 240 h. The presence of copper was not detected in the solution outside of the bag. The color of $Cu(OH)_2$ inside of the bag did not change even after 74 h of experiment. Therefore, it can be said that $Cu(OH)_2$ did not decompose (at pH 9, 50°C) when it was mixed in a slurry with an appropriate amount of alumina. On the basis of the above observations, additional experiments were performed to determine the adsorption capacity of γ-Al_2O_3 for $Cu(OH)_2$.

A 0.1 g sample of alumina was added to the fresh $Cu(OH)_2$ precipitate (0.127 g) under stirring, and the pH was adjusted to 9 at temperature of 50°C. It was observed that the amount of alumina, 0.1 g was too small to stabilize the $Cu(OH)_2$ completely, because some of the $Cu(OH)_2$ had decomposed into CuO and the color of the slurry had turned black. The amount of added alumina was increased gradually in 0.05 g increments. Ultimately it was found that 0.6 g of the alumina was necessary to completely stabilize 0.127 g of $Cu(OH)_2$. The alumina adsorption capacity for copper was calculated to be ~$1.66 \cdot 10^{-5}$ mol $Cu \cdot m^{-2}$. This value is almost completely in agreement with the value reported by Dumas et al., (1989); $3.3 \cdot 10^{-6}$ mol $Cu \cdot m^{-2}$ in a basic medium and $0.7 \cdot 10^{-5}$ mol $Cu \cdot m^{-2}$ in an acidic medium.

On the other hand, activity of copper basic sulfate, $3Cu(OH)_2 \cdot CuSO_4$ was assessed. A 0.204 g ($2 \cdot 10^{-3}$ mol) of alumina (in the bag) was equilibrated at 50°C, pH 7, with 0.1 M K_2SO_4 solution. Then, $3Cu(OH)_2 \cdot CuSO_4$ was added into the bag. The experiment lasted for 371 h. $3Cu(OH)_2 \cdot CuSO_4$ was prepared from $Cu(OH)_2$ by adding $CuSO_4$ (0.1 mol/L). $3Cu(OH)_2 \cdot CuSO_4$ was obtained as green precipitate, then filtered and washed several times with distilled water.

At the end of the experiment, no precipitate had formed outside of the bag. Furthermore, neither aluminum nor copper was detected in the solution outside of the bag. This result suggests two possibilities: one is that it is not $3Cu(OH)_2 \cdot CuSO_4$ that promotes the alumina dissolution, and the other possibility is that aluminum ions resulting from alumina dissolution were trapped by the $3Cu(OH)_2 \cdot CuSO_4$ phase and could not diffuse outside the bag. The latter hypothesis was checked by another experiment, which is described briefly as follows.

A 5 g sample of copper basic sulfate was equilibrated with 250 mL of 0.1 mol/L $Al_2(SO_4)_3$ solution at 50°C for 44 h. During the experiment, the colorless solution outside of the bag turned blue as a result of $CuSO_4$ formation. At the end of the experiment, the new compound that had formed inside of the bag consisted of 9.13% of Al and 32.27 % of Cu. The molar ratio between Cu and Al was 1.5. This means that the $CuSO_4$ units were replaced completely by $Al_2(SO_4)_3$ units in the copper basic sulfate structure:

$$Al_2(SO_4)_3 + 3Cu(OH)_2 \cdot CuSO_4 \rightarrow 3Cu(OH)_2 \cdot Al_2(SO_4)_3 + CuSO_4 \qquad (3)$$
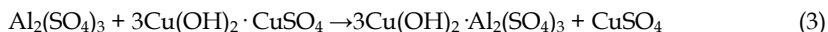
This result clearly shows that $Cu(OH)_2$ has a higher affinity to $Al_2(SO_4)_3$ than $CuSO_4$ in forming basic sulfate. This provides a convincing reason for the absence of aluminum in the solution outside of the bag when aluminum interacted with copper basic sulfate in the bag. The small amount of aluminum ions formed were trapped by $3Cu(OH)_2 \cdot CuSO_4$ to form $3Cu(OH)_2 \cdot Al_2(SO_4)_3$.

From the above experiments, the processes that occur during alumina impregnation with $CuSO_4$ may be explained as follows. First, copper ions outside of the bag diffuse into the bag and precipitate on the surface of the alumina as $Cu(OH)_2$ and/or $3Cu(OH)_2 \cdot CuSO_4$. Then, the $Cu(OH)_2$ precipitate strongly adsorbed on the surface of the alumina and promote alumina dissolution. The aluminum ions released from the alumina dissolution diffuse outside of the bag, and they are preferentially trapped in the $3Cu(OH)_2 \cdot CuSO_4$ phase by coprecipitation or ion exchange. Another parallel reaction which should be considered is the coprecipitation of aluminum ions and copper ions outside of the dialysis bag. The aluminum uptake by the copper precipitate is limited. At pH 9, the amount of aluminum ions formed was too high to be taken up completely by the precipitate. Therefore, the presence of aluminum was detected in the solution, too.

The experimental results demonstrate that the impregnation step in catalyst preparation can be thought of as a complex chemical solid-liquid interfacial reaction. The support should be considered as an active participant with a specific reactivity dependent upon the experimental conditions, in the formation process of the active phase during the impregnation step. The presence of the ions dissolved from the support may have an important effect on the formation of active site in catalysts. The presence of small (0.51 Å) and high charge-carrying aluminum ions in the catalyst active phase may induce strong local perturbation in the host lattice as a result of defects formation (Balint & Aika, 1997). Therefore, the aluminum presence in the copper active phase should be taken into consideration in explaining the active site formation and the catalytic activity of Cu/Al_2O_3.

2.4 Alumina dissolution in the presence of $PdCl_4^{2-}$

In the former sections, it was shown that adsorption of heavy metal cations, i.e., Zn^{2+} and Cu^{2+}, onto alumina can induce alumina dissolution. Hydroxides of heavy metals, which were formed on the surface of alumina after some amount of coverage was accomplished, are found to be responsible for alumina dissolution. Such alumina dissolution induced by heavy metal adsorption must be paid great attention because of various reasons. For example, aluminum is known to be toxic to a wide range of aquatic organisms under conditions of low pH and hardness (Dobbs, et al., 1989). Oxide of aluminum, i.e., alumina, is known to be one of the most effective adsorbent to remove heavy metal ions from aqueous phase (Bold & Van Riemsdijk, 1987). Thus, dissolved aluminum, produced in the process of heavy metal removal, may have great impact on aquatic environment. On the other hand,

alumina dissolution induced by heavy metal adsorption may have significant effect on active site formation on catalysts prepared by impregnation.

It was shown that alumina dissolution is induced by heavy metal cations. However, many heavy metals, especially platinum group metals used in catalysts, exist in aqueous solution forming anions. Therefore, it is of great importance to see whether alumina dissolution can be induced by adsorption of heavy metal anion, too. The possibility of alumina dissolution in the course of Pd/Al_2O_3 catalysts preparation was studied by using $PdCl_4^{2-}$ ion (Balint et al., 2001). $PdCl_4^{2-}$ was selected because palladium is one of the mostly used metals in heterogeneous catalysts and $PdCl_4^{2-}$ ions have good stability and solubility in the acid pH range. Pd/Al_2O_3 catalyst prepared using $PdCl_4^{2-}$ and activated properly has reported to have high activity for reactions such as, methane oxidation (Burch, 1990).

To find out the influence of $PdCl_4^{2-}$ on alumina dissolution in the acid pH range, the following procedure was applied. First, the proton-promoted dissolution of alumina was investigated, in the absence of any additional ligand, at pH 3.5, 4 and 5. Then, the dissolution of alumina in the presence of $PdCl_4^{2-}$ was studied in similar conditions. In this manner, the differences observed would be due to the presence of $PdCl_4^{2-}$. All the impregnation experiments were performed with the system shown in Fig. 3.

Alumina dissolution was observed at pH 3.5 and 4. At pH 3.5, the total amount of dissolved alumina during 74 h of experiment, calculated from the concentration of Al^{3+} in solution, was 1.07 % of the initial amount of alumina. The rate of Al^{3+} formation was 0.0603 µmol m^{-2} h^{-1}. It was evidenced that the dissolution rate for alumina was lower (0.0353 µmol m^{-2} h^{-1}) when $PdCl_4^{2-}$ was present in the system. The amount of dissolved alumina after 96 h of experiment was 1.47%. The amount of $PdCl_4^{2-}$ adsorbed on the alumina surface, calculated from the decrease in palladium concentration in the impregnating solution, increased rapidly to 0.32 µmol m^{-2} in the first 2 h of impregnation. Then, the rate of adsorption of $PdCl_4^{2-}$ decreased to reach finally (after 46 h of impregnation) an equilibrium value at ~ 0.68 µmol m^{-2}. After impregnation, alumina was dissolved in a mixture of HF : $HClO_4$: HNO_3 and then the composition was determined by ICP-AES. There was a fair agreement between the palladium coverage estimated from the impregnation experiment and from ICP-AES analysis. The adsorption densities of $PdCl_4^{2-}$ on alumina obtained were close to those obtained by classic impregnation methods. The densities of $PdCl_4^{2-}$ on alumina range depending upon the condition of impregnation, between 0.8 and 1.2 µmol m^{-2} (Caillerie et al., 1995, Santhanam et al., 1994, Contescu & Vass, 1987).

The proton consumption in time during the impregnation of alumina with $PdCl_4^{2-}$ and adsorption density of $PdCl_4^{2-}$ is shown in Fig. 7 (a) and (b), respectively. As it can be seen in Fig. 7 (a), the proton consumption at pH 3.5 decreased progressively. This is same as in the case of proton-promoted dissolution of alumina. From the result shown in Fig. 7 (a), the rate of proton consumption was calculated to be ~ 0.206 µmol m^{-2} h^{-1}. This value roughly corresponds to ~ 5.8 protons for each Al^{3+} released into solution. For a longer impregnation time (t > 32 h), the rate of proton consumption decreased to ~ 0.108 µmol m^{-2} h^{-1} (Fig. 7 (a)). A simple calculation shows that 3.05 protons were consumed for the formation of one Al^{3+}. The amount of $PdCl_4^{2-}$ adsorbed on the alumina surface calculated from the decrease in palladium concentration in the impregnation solution, increased rapidly to 0.32µmol m^{-2} in the first 2 h of impregnation (Fig. 7 (b)). Then, the rate of adsorption of $PdCl_4^{2-}$ decreased to reach finally (after 46 h of impregnation) an equilibrium value at ~ 0.68 µmol m^{-2}.

In the first 2 h of impregnation, the quick adsorption of $PdCl_4^{2-}$ takes place parallel to alumina dissolution. As the surface of alumina became saturated in $PdCl_4^{2-}$, the rate of

palladium adsorption decreased below that of alumina dissolution. The amount of $PdCl_4^{2-}$ on alumina is limited by the (i) strong electric forces of adsorbed species and (ii) dissolution of alumina. However, it is clear that some amount of the adsorbed $PdCl_4^{2-}$ is detached together with Al^{3+} during the dissolution process. Therefore, it can be assumed that one important consequence of alumina dissolution, in addition to the effect of ionic strength, is the retardation of $PdCl_4^{2-}$ adsorption.
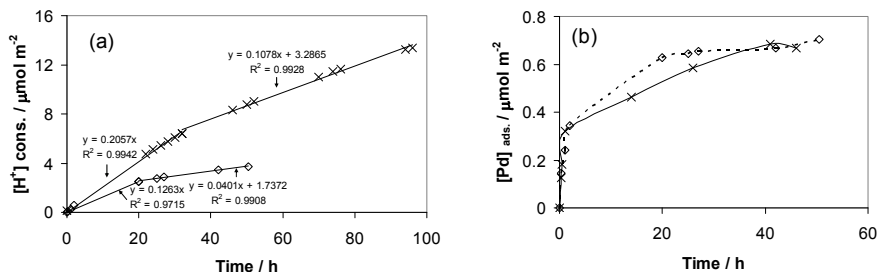
Fig. 7. Time course of (a) proton consumption and (b) adsorption density of $PdCl_4^{2-}$ on alumina, during the impregnation of γ-Al_2O_3 with $PdCl_4^{2-}$ at pH 3.5 (x) and pH 4 ($\diamond$).

To find out whether the proton consumption is affected by $PdCl_4^{2-}$ adsorption, the ratio between $[H^+]_{cons.}$ and $[Al^{3+}]_{sol.}$ is analyzed in Table 1. From Table 1, it is clear that $PdCl_4^{2-}$ does not promote alumina dissolution, because the rate between $[H^+]_{cons.}$ and $[Al^{3+}]_{sol.}$ remained practically constant (~ 4.2), regardless of whether $PdCl_4^{2-}$ was present or not in the solution. If $PdCl_4^{2-}$ would promote alumina dissolution, the proton consumption should decrease significantly in comparison to the amount of Al^{3+} formed. In practice, only the rate of alumina dissolution was affected by $PdCl_4^{2-}$. It is likely that one of the reasons for the retardation of $PdCl_4^{2-}$ adsorption is alumina dissolution.

$[H^+]_{cons.}/[Al^{3+}]_{sol.}$	experiment time/h	pH	system
3.99	72	3.5	$Al_2O_3 + H^+$
4.24	74	3.5	$Al_2O_3 + H^+ + PdCl_4^{2-}$
4.23	70	4.0	$Al_2O_3 + H^+$
4.19	50.5	4.0	$Al_2O_3 + H^+ + PdCl_4^{2-}$

Table 1. Influence of $PdCl_4^{2-}$ on $[H^+]_{cons.}/[Al^{3+}]_{sol.}$ ratio at pH 3.5 and 4

In the course of $PdCl_4^{2-}$ impregntion, three types of simultaneous process could be analyzed: (I) alumina dissolution, (II) proton consumption, and (III) adsorption density of $PdCl_4^{2-}$ on the surface of alumina. It was observed that some amount of support was mobilized in the liquid phase during impregnation. The amount of dissolved alumina depends on the pH of the solution as well as on the nature of the impregnating ion ($PdCl_4^{2-}$). It was demonstrated that the protons are consumed in two distinct processes, i.e., reversible adsorption of H^+ (Langmuir-type adsorption) and irreversible adsorption of H^+ (leading to dissolution of alumina). A clear distinction between the reversible and irreversible adsorbed proton has been made for the first time.

Alumina dissolution during impregnation may have significant consequences on the formation of the catalytic active phase. It is expected that aluminum ions, originating from

the support, will always be present in the catalytic phase (i.e., palladium phase), inducing the formation of lattice defects (Balint & Aika, 1997). Therefore, the aluminum presence in the palladium active phase should be taken into consideration in explaining the catalytic behavior in a chemical reaction.

3. Alumina as catalytic support

3.1 Effect of support on active site formation

Alumina is frequently used as a support for metal catalysts due to its high surface area and good thermal stability. However, as shown above, alumina can be dissolved during the process of impregnation. The dissolution of alumina is induced by adsorption of heavy metal ions. Then, dissolved aluminum species may be included in the newly formed phase on the surface of the support, which is the precursor of active site. It is highly possible that such contamination of active site by aluminum may have significant effect on catalyst performance. In order to assess the effect of possible aluminum inclusion in the active site, Ru/Al_2O_3 catalysts were prepared by two different methods; one is conventional impregnation and the other is metal colloid synthesis and supporting them onto alumina support (Miyazaki et al, 2001). Then, their performance in ammonia synthesis was compared (Balint & Miyazaki, 2007).

Ruthenium is known to have one of the highest catalytic activities for ammonia synthesis (Aika, 1994). Typically, the conventional Ru catalysts are prepared by impregnation of the
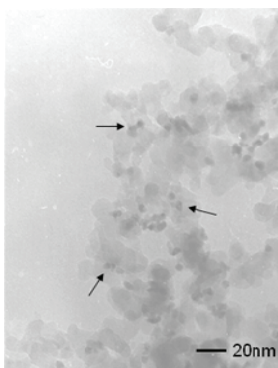
Fig. 8. TEM image of 6.3% Ru/Al_2O_3. Some typical Ru particles are indicated by arrows.

oxide support either with and aqueous solution of $RuCl_3 \cdot 3H_2O$ or with $Ru_3(CO)_{12}$ dissolved in tetrahydrofuran (Murata & Aika, 1992a, b). When catalysts are prepared by impregnation of alumina with $RuCl_3$, the metal particles, after drying, calcinations, and reduction, are not uniform in size and shape. It is well known that the catalytic activity of a supported metal is strongly related to the morphology of the particle, i.e., size and shape (Ahmadi, et al., 1996). However, the conventional preparation of catalysts, consisting of the impregnation of a support with an aqueous solution of a soluble metal precursor, makes it difficult to control the final size and shape of the supported metal particles. Additionally, it is highly possible that the support has a great influence on the catalytic activity of the metal when the catalyst is prepared by impregnation. An alternative method to obtain supported catalysts with well-defined metal particles is the preparation of supported catalysts from metal colloids.

The great advantage of the colloid method is that it provides relatively monodispersed metal particles. Moreover, it is shown that not only the particle size but also the crystal structure of the metal nanoparticles can be controlled to some extent by using appropriate structure-directing polymers for colloid preparation (Miyazaki, et al., 2000).

Ru colloid was prepared by reducing $RuCl_3 \cdot nH_2O$ in ethylene glycol. The average diameter of the particle measured by TEM was 5 nm. The colloid particles were supported on γ-Al_2O_3 (Aerosil) to realize the Ru loading of 6.3 wt%. Figure 8 shows the TEM image of Ru/Al_2O_3. EPMXA measurement proved that the black spots corresponded to ruthenium particles. It can be seen that the Ru particles was uniform in size and shape, and they were dispersed well on the surface of γ-Al_2O_3. The particle size of Ru obtained by TEM was 4.2 nm. This value agreed well with the values obtained by H_2 and CO chemisorption; 4.8 and 5.4 nm, respectively. It is noteworthy that by using colloid method, Ru particles can be supported without affecting the particle size and dispersion, even when the metal loading was increased up to 6.3%.
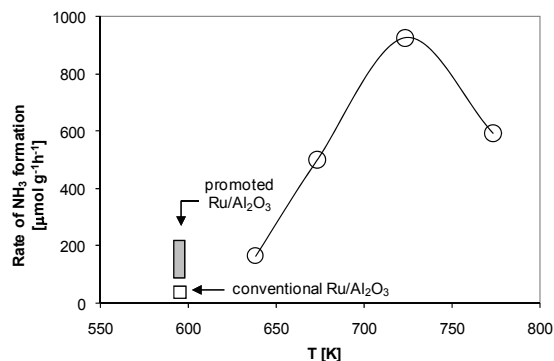
Fig. 9. Temperature dependence of the rate of ammonia synthesis over Ru/Al_2O_3 (6.3 wt%). The rates over conventional Ru/Al_2O_3 catalysts are also shown for comparison.

The catalytic activity of Ru/Al_2O_3 was measured for ammonia synthesis. The catalytic tests were performed at atmospheric pressure in a stainless steel reactor containing 0.4 g of 6.3 wt % Ru/Al_2O_3. Prior to the catalytic tests, the Ru/Al_2O_3 was pelletized, crushed, and then sieved. The fraction, from 335 to 1000 μm, was collected and loaded into the reactor. Before the test, the sample was reduced in H_2 flow at 550°C for 2 h. The catalytic activity tests were carried out at a flow rate of the reaction mixture 60 cm³/min STP (45 cm³/min H_2 and 15 cm³/min N_2). The rate of ammonia synthesis was measured in a 365 to 500°C temperature range. The produced ammonia was trapped by $1 \cdot 10^{-3}$ mol/L solution of sulfuric acid, and the rate of ammonia formation was determined from the decrease in the conductivity of the solution.

The catalyst which was prepared by supporting the Ru colloid on γ-Al_2O_3 showed a remarkably high activity for ammonia synthesis. The reaction rates expressed as micromoles per gram-hour as a function of temperature are shown in Fig. 9. Figure 9 shows that the rate of ammonia synthesis over 6.3 wt% of Ru/Al_2O_3 increased progressively with an increase in temperature, reaching a maximum at 723 K. Above this temperature, the reaction is thermodynamically limited and therefore the overall rate decreased. The highest reaction rate of 923 μmol g^{-1} h^{-1} was observed at 723 K. The reproducibility at each reaction temperature was within the range of experimental error (± 25 μmol g^{-1} h^{-1}). Apparent activation energy of 76.9 kJ/mol was estimated, and this value agreed well with the previously published data. For

example, the apparent activation energies determined for promoted and nonpromoted Ru/Al_2O_3 catalysts range between 44 and 101 kJ/mol (Murata & Aika, 1992a,b).

From the above results there are two points that are worthy of note. One is the temperature of highest activity for ammonia synthesis. The highest activity of the conventional Ru/Al_2O_3 catalysts was observed at 315°C (Murata & Aika, 1992), whereas the catalyst prepared from the Ru colloid had a maximum activity at a higher temperature, 450°C (723 K). From industrial point of view, it is preferable for ammonia synthesis to have a catalyst that is more active at a lower temperature. Thermodynamically, the increase in temperature is not favourable for ammonia synthesis reaction. Therefore, it is of great interest to obtain the higher equilibrium conversions at lower temperatures.

The other point is that Ru/Al_2O_3 catalysts prepared from the Ru colloid showed unusually high activity although it was not promoted. The conventional Ru/Al_2O_3 catalysts are known to exhibit quite low activities for ammonia synthesis, and this has been attributed to the acidity of alumina. The addition of alkaline or lanthanide promoters was reported to be an effective way of enhancing the catalytic activity (Murata & Aika, 1992a). The highest catalytic activities of the promoted and nonpromoted Ru/Al_2O_3 catalysts prepared by conventional methods using $RuCl_3$ or $Ru_3(CO)_{12}$ as precursors together with the activity of the catalyst prepared from the Ru colloid are shown in Fig. 9. The reported activity of the nonpromoted conventional Ru/Al_2O_3 catalysts is very small, ranging from 10 to 60 µmol g^{-1} h^{-1}. It was reported that the nonpromoted catalysts prepared from $RuCl_3$ exhibited significantly lower activities as compared to those obtained from $Ru_3(CO)_{12}$.

The acidity of alumina has been considered to be the main reason for the low activity of the conventional Ru/Al_2O_3 catalysts for ammonia synthesis. The addition of alkaline (Cs, Rb, K) or rare earth (La, Ce, Sm) elements to Ru/Al_2O_3 leads to a significant increase in the catalytic activity (Murata & Aika, 1992b, Moggi, et al., 1995). Typically, the activity of the promoted Ru/Al_2O_3 catalysts ranges from 130 to 250 µmol g^{-1} h^{-1} (Fig. 9). The Ru/Al_2O_3 catalyst prepared from the Ru colloid showed a significantly higher activity than that from promoted catalysts. A notable exception is the K^+-promoted Ru/Al_2O_3 catalyst, prepared from $Ru_3(CO)_{12}$, whose catalytic activity for ammonia synthesis was reported to be 2470 µmol g^{-1} h^{-1} under conditions comparable to those shown in Fig. 9 (0.4 g catalyst, 60 ml min^{-1}) (Moggi, et al., 1995). However, the activity of the conventionally prepared Ru catalysts strongly depend on the conditions of preparations. Slight changes of the preparation variables result in significant changes in catalytic activity.

The differences observed between the Ru/Al_2O_3 catalysts prepared by the conventional impregnation methods and the catalyst obtained via colloid deposition raise problems regarding the role that supports play in the formation of catalytically active phases. In the former part of this chapter, we reported that the support (alumina) plays an essential role in the formation of the active phase(s) when the catalysts were prepared by the impregnation method. The impregnation process can be regarded as complex sequences of chemical reactions taking place at the solid (the support)-liquid (solution of the metal salt) interface. During the impregnation process, the metal particles, i.e., the active site of the catalysts, are contaminated more or less by the supports. In this case, the acid or base character of the supports plays an important role in determining the final catalyst activity. In contrast to the impregnation method, metal colloid deposition onto a support gives metal particles that are uncontaminated by the support. Therefore, the influence of the support on the metallic active phase is minimized. The Ru/Al_2O_3 catalyst prepared by Ru colloid, is supposed to have Ru nanoparticles that do not interact significantly with the support, and this should be the reason for the remarkably high catalytic activity demonstrated for ammonia synthesis.

3.2 Support as adsorbent

Nitrate and nitrite ions are one of the world's major pollutants of drinking-water resources. In order to remove nitrate and nitrite ions in drinking water, physicochemical methods (e.g. ion exchange, reverse osmosis, and electrodialysis) and biological denitration methods have been studied (Fanning, 2000). However, these methods have disadvantages, in that they are consuming, complex, and sometimes require costly post-treatment of the effluent. The catalytic reduction of nitrate and nitrite in the liquid phase with hydrogen over a solid catalyst has recently been confirmed to be a promising method for the treatment of drinking water (Corma, et al., 2004). The most widely used catalyst is Pd-Cu/Al_2O_3. On the other hand, the catalytic performance of the Pt-Cu/Al_2O_3 catalyst is comparable to that of Pd-Cu/Al_2O_3 (Gauthard, 2003). Alumina is a typical support used in this reaction. The reduction of nitrate is known to proceed in two reaction steps, i.e., reduction of nitrate to nitrite and further reduction of nitrite to N_2 (desired product) and/or NH_4^+ (byproduct). Epron et al., (2001) found that two metal components of the catalyst are active for distinct reasons. Less noble metals, such as Cu, are catalytically active for the reduction of nitrate to nitrite, whereas the nitrite is reduced on the surface of noble metals, i.e., Pd or Pt. However, the two reactions do not seem to be completely independent of each other. Gao et al., (2003) reported that the bimetallic Pd-Cu catalyst (especially in the case of Pd:Cu = 2:1 molar ratio) exhibits much higher activity for nitrite reduction compared with the monometallic palladium catalyst.

In studies of the catalytic reductions of nitrate and nitrite, the catalytic activity is generally calculated from the decrease in the concentration of nitrate or nitrite ions in the reaction solution. In practice, the nitrate and nitrite ions that disappear from the reaction solution are presumed to be converted to N_2 and NH_4^+, without taking the possibility of adsorption onto the catalyst into account. In fact, there is very little information regarding to the nitrate and/or nitrite adsorption onto alumina; however, there have been recent reports regarding such adsorption (Handa et al., 2001, Kney et al., 2004, Ebbesen, et al., 2008). If significant amounts of nitrate or nitrite ions are adsorbed onto an alumina support, then such adsorption phenomena should be taken into consideration when the catalytic activity of denitration is calculated, especially for batch experiments. Measurement of the actual catalytic activity for liquid phase reduction of nitrate is an important issue, due to the potential application of this method. Conversion over denitration catalyst must be significantly high to overcome the regulation limits, and this is one of the critical point that would allow or prevent practical applications. Therefore, it is necessary to evaluate the amounts of nitrate and nitrite ions removed from the reaction solution, not only by reaction, but also by adsorption. Therefore, adsorption of nitrite onto alumina and Pt/Al_2O_3 was focused (Miyazaki et al., 2009). Nitrite was selected because it is the reaction intermediate of the nitrate reduction reaction, and because its toxicity is higher than nitrate.

NO_2^- catalytic reduction experiments were performed in a four-neck flask. The necks were used for the Ar (inert gas) inlet, H_2 (reduction gas) inlet, and gas outlet, and for sampling of the liquid phase, respectively. One hundred and fifty milliliters of the 2 mmol/L $NaNO_2$ solution was stirred in a flask with a magnetic stirrer and the solution was kept at 25°C using a water bath. γ-Al_2O_3 (Aerosil) or Pt/Al_2O_3 (0.3 g) was then added to the nitrite solution. Prior to the reduction, dissolved air in the suspension was removed by bubbling Ar gas for 20 min. H_2 gas was then bubbled into the solution with a flow rate of 10 min/min. Two milliliter aliquots of the reaction solution were sampled periodically and filtered immediately. The concentrations of NO_2^- and NH_4^+ ions in the solution were measured using a UV-vis spectrophotometer.

On the other hand, adsorption experiments were performed in the same manner as the reduction experiments, excepting H_2 flow. Ar gas was continuously bubbled in the suspension, so that no NO_2^- loss by reduction was presumed to occur, due to the absence of reductant H_2 gas.

A catalytic reduction experiment was performed using γ-Al_2O_3 without Pt in the presence and absence of H_2 flow. The concentration of NO_2^- decreased, even though there was no noble metal on the support (Fig. 10). In the catalytic reduction of nitrate, the reduction of nitrite by H_2 to N_2 and/or NH_4^+ is reported to take place on the surface of supported noble
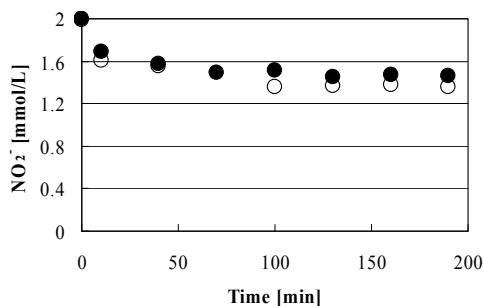
Fig. 10. Time course of nitrite concentration in the reacting solution. Experiment was performed with H_2 flow (●) and without H_2 flow (○).

metal particles. It is generally assumed that the catalytic activity can be ascribed only to the supported metal (i.e., Pd and Pt), and that the support (i.e., alumina, silica, carbon, etc.) is completely inert (Epron, 2002). Therefore, the decrease of NO_2^- in the presence of H_2 may not be due to catalytic conversion. To confirm this, the same experiment was performed without the reductant (H_2 gas). Interestingly, a decrease in NO_2^- concentration was also observed as shown in Fig. 10. In both cases, no formation of NH_4^+ (product) was observed. Thus, the decrease in NO_2^- concentration was not due to reduction, i.e., alumina was completely inert toward NO_2^- reduction. Therefore, the disappearance of NO_2^- is attributed to adsorption on alumina. The result showed that around 30% of the initial amount of NO_2^- was absorbed after 100 min of reaction time.
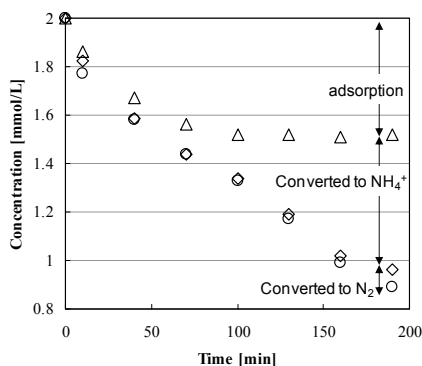
Fig. 11. 2 mmol/L $NaNO_2$ was reduced by H_2 gas on 0.1 wt% Pt/Al_2O_3 catalyst. The decrease of NO_2^- (○) was found to be caused by catalytic conversion to N_2 or NH_4^+, and by adsorption onto alumina (Δ).

Because a significant amount of NO_2^- was found to be adsorbed onto alumina, the adsorption experiment was performed using a 1 wt% Pt/Al_2O_3 catalyst, in order to determine whether the same adsorption phenomena occurred on Pt supported catalyst. Figure 11 shows the result of both the adsorption and reduction experiment on 1 wt% Pt/Al_2O_3 catalyst. The Pt/Al_2O_3 catalysts were prepared by impregnation using aqueous solution of K_2PtCl_4. The Pt/Al_2O_3 catalysts were pelletized, crushed, and then sieved. The fraction of powder with size from 335 to 1000 µm was collected. The adsorption experiment was carried out in the absence of H_2, whereas the catalytic reduction was performed under H_2 flow. The H_2 flow induces the reduction of NO_2^- over Pt; therefore, it is not possible to evaluate the amount of adsorbed NO_2^- under H_2 flow. In the absence of a H_2 flow, the concentration of NO_2^- was decreased with the 1wt% Pt/Al_2O_3 catalyst. The adsorption behaviour of NO_2^- onto 1wt% Pt/Al_2O_3 catalyst was similar to that on alumina without Pt. For both cases, the adsorption equilibrium was reached after 100 min of reaction time. As much as 24% of the NO_2^- was adsorbed on the 1wt% Pt/Al_2O_3 catalyst.

The calculation of NO_2^- conversion and selectivity to N_2 can be subjected to significant error if adsorption by the support is not taken into consideration. There are very few papers discussing the adsorption of NO_3^- or NO_2^- on the support, as well as possible influence of the supporting metal on the metal catalytic activity. If adsorption of NO_2^- onto the catalyst occurred during the reduction experiment, the actual amount of NO_2^- catalytically converted should be obtained as the difference between the amount of NO_2^- removed by catalytic reduction and by adsorption. According to this assumption, NO_2^- conversion with 1wt% Pt/Al_2O_3 was calculated to be 31.5% at 190 min, but 55.5% if adsorption is not considered. Adsorption of NO_2^- onto the catalyst has an even more dramatic effect on the selectivity to N_2 production. Generally, the catalytic reduction of NO_3^- and NO_2^- is monitored by analyzing the species in the liquid phase, i.e., by measuring the concentration of NO_3^-, NO_2^- and NH_4^+ ions in the reaction solution. In most cases, the gaseous products (i.e., N_2) are not quantitatively determined (Epron, 2001). If adsorption is not considered, then the selectivity to N_2 on 1wt% Pt/Al_2O_3 is calculated to be 49.5%, while the selectivity is only 11.1% if adsorption is taken into account. In the reduction experiment on 1wt% Pt/Al_2O_3, an attempt was made to detect gaseous N_2 by gas chromatography; however, the detectable amounts were negligible. The mass balance suggested that the decrease of NO_2^- in the reaction solution can be ascribed to either adsorption onto the catalyst or conversion to N_2 and NH_4^+. NO_2^- adsorption on Pt/Al_2O_3 is of great practical importance, because Pt/Al_2O_3 is one of the most common catalysts used to reduce NO_2^- and NO_3^- in waste waters by reduction with H_2. Thus, it is necessary to make a clear distinction between the NO_2^- ions removed from a reaction solution by catalytic reaction (reduction) and those removed by adsorption. One the other hand, alumina has a possible application as NO_2^- scavenger in the treatment of waste water, due to its relatively high adsorption capacity for NO_2^- ions.

4. Conclusion

Two aspects of alumina, i.e., heavy metal adsorbent and catalysts support, were discussed and it was shown that they are closely related each other. Alumina is one of the most frequently used adsorbent to remove heavy metal ions from waste water. The adsorption process of heavy metal cations onto alumina is not a simple phenomenon but a complex process composed by three main steps, i.e., adsorption, desorption and re-sorption. The first adsorption step can be explained as surface complexation between heavy metal cation and

surface aluminol groups. However, the adsorbed heavy metal cations can be desorbed by accomplishing some surface coverage. It was shown that the formation of hydroxide of the heavy metal is the reason for this process. In the desorption process, alumina was found to be dissolved, too. Then, in the third step, aluminium ions dissolved from alumina may coprecipitate with desorbed heavy metal cations. Alumina dissolution was proved to be induced not only heavy metal cations (Zn^{2+} and Cu^{2+}), but also anions, $PdCl_4^{2-}$ in acid pH range.

Alumina dissolution induced by heavy metal adsorption must have significant impact for heavy metal behaviour in natural aquatic systems and catalyst active site formation. Actually, Ru/Al_2O_3 catalysts prepared by impregnation and colloid showed quite different activity for ammonia synthesis. The difference must be caused by the composition of active site. In the case of colloid, ruthenium particles do not contain aluminium, but the active site of the catalyst prepared by impregnation must include aluminium, which was dissolved in the process of impregnation. On the other hand, alumina used as catalyst support can play a role of adsorbent, too. When NO_2^- was reduced on the surface of Pt/Al_2O_3 catalyst, significant amount of NO_2^- was found to be adsorbed on the support. Thus, in order to adequately evaluate conversion and selectivity of the catalyst, it is necessary to take into account the adsorption.

The two different aspect of alumina, i.e., adsorbent and support, are closely related to each other and both are quite important for waste water treatment. Therefore, in near future, it is very necessary to study the relation between these two roles of alumina and apply it to waste water treatment.

5. References

Aika, K. (1994). Synthetic process of ammonia. *Petrotech*, 17, 2, 127-132, 0386-2963

Agaras, H.; Cerella, G. & Laborde, M. A. (1988). Copper catalysts for the steam reforming of methanol: analysis of the preparation variables. *Appl. Catal.* 45, 1, 53-60, 0166-9834

Armadi, T. S.; Wang, Z. L.; Green, T. C.; Henglein, A. & El-Sayed. M. A. (1996). Shape-controlled synthesis of colloidal platinum nanoparticles. *Science*, 272, 1924-1926, 0036-8075

Baldwin, T. R. & Burch, R. (1990). Catalytic combustion of methane over supported palladium catalyst. I. Alumina supported catalysts. *Appl. Catal*. 66, 2, 337-358, 0166-9834

Balint, I. & Aika, K. (1997). Defect chemistry of lithium-doped magnesium oxide. *J. Chem. Soc. Faraday Trans*., 93, 9, 1797-1801, 0956-5000

Balint, I. & Miyazaki, A. (2007). Minimization of the metal-support interaction by using Ru nanoparticles for ammonia synthesis. *Trans. Mater. Res. Soc. Jpn*., 32, 2, 387-390, 1382-3469

Balint, I.; Miyazaki, A. & Aika, K. (1999). Alumina dissolution promoted by $CuSO_4$ precipitation. *Chem. Mater*., 11, 2, 378-383, 0897-4756

Balint, I.; Miyazaki, A. & Aika, K. (2001). Alumina dissolution during impregnation with $PdCl_4^{2-}$ in the acidic pH range. *Chem. Mater*., 13, 3, 932-938, 0897-4756

Bold, G. H. & Van Riemsdijk, W. H. (1987). Surface chemical processes in soil, In: *Aquatic Surface Chemistry*, Stumm, W. (Ed.), 127-164, Jhon Willy & Sons, 0-471-82995-1, New York

Caillerie, J. B. E.; Kermarec, M. & Clause, O. (1995). Impregnation of gamma-alumina with Ni(II) or Co(II) ions at neutral pH: hydrotalcite-type coprecipitate formation and characterization. *J. Am. Chem. Soc.*, 117, 11471-11481, 0002-7863

Contescu, C. & Vass, M. I. (1987). Effect of pH on the adsorption of palladium (II) complexes on alumina. *Appl. Catal*. 33, 2, 259-271, 0166-9834

Corma, A.; Palmares, A. E.; Rey, F. & Prato, J. G. (2004). Catalytic reduction of nitrates in natural water: is this realistic objective? *J. Catal*., 227, 561-562, 0021-9517

Dobbs, A. J.; French, P.; Gunn, A. M.; Hunt, D. T. E. & Winnard, D. A. (1989). Aluminum speciation and toxicity in upland waters, In: *Environmental Chemistry and Toxicology of Aluminum*, Lewis, T. E., (Ed.), 209-228, Lewis Publishers, Inc., 0-87371-194-7, Michigan

Dumas, J.; Geron, G.; Kribbi, A. & Barbier, J. (1989). Preparation of supported copper catalyst. II. Reduction of copper/alumina catalysts. *J. Appl. Catal*., 47, L9-L15, 0936-860X

Ebbesen, S. D. ; Mojet, B. L. & Lefferts, L. (2008). In situ attenuated total relfection infrared (ATR-IR) study of the adsorption of NO_2^-, NH_2OH, and NH_4^+ on Pd/Al_2O_3 and Pt/Al_2O_3. *Langmuir*, 24, 869-879, 0743-7463

Epron, F.; Gauthard, F.; Pineda, C. & Barbier, J. (2001). Catalytic reduction of nitrate and nitrite on $Pt-Cu/Al_2O_3$ catalysts in aqueous solution: role of the interaction between copper and platinum in the reaction. *J. Catal*., 198, 2, 309-318, 0021-9517

Epron, F.; Gauthard, F. & Barbier, J. (2002). Catalytic reduction of nitrate in water on a monometallic Pd/CeO_2 catalyst. *J. Catal*., 206, 2, 363-367, 0021-9517

Fanning, J. C. (2000). The chemical reduction of nitrate in aqueous solution, *Coord. Chem. Rev*., 199, 159-179, 0010-8545

Fendorf, S. E.; Lamble, G. M.; Stapleton, M. G.; Kelley M. J. & Parks, D. L. (1994). Mechanism of chromium (III) sorption on silica. 1. Cr(III) surface structure derived by extended x-ray absorption fine structure spectroscopy. *Env. Sci. Tech*., 28, 284-289, 0013936X

Foger, K. (1984). Dispersed metal catalysts, In: *Catalysis Science and Technology*, Andersen, J. R. & Boudart, M. (Eds.), 6, 227-335, Springer-Verlag, 3540128158, Berlin

Gao, W.; Jin, R. ; Chen, J.; Guan, X.; Zeng, H.; Zhang, F.; Liu, Z. & Guan, N. (2003). Titania-supported Pd-Cu bimetallic catalyst for the reduction of nitrite ions in drinking water. *Catal. Lett*., 91, 25-30, 1011-372X

Gauthard, F.; Epron, F. & Barbier, J. (2003). Palladium and platinum-based catalysts in the catalytic reduction of nitrate in water: effect of copper, silver, or gold addition. *J. Catal*., 220, 1, 182-191, 0021-9517

Goldberg, S. (1991). Sensitivity of surface complexation modeling to the surface site density parameter. *J. Colloid Interface Sci*., 145, 1, 1-9, 0021-9797

Handa, E.; Kotaki, H. & Kaneda, Y. (2001). Anion scavengers, selective and adsorption removal of nitrate and nitrite ions from wastewater, and recovery of generated slightly soluble anion-exchange products. *Jpn. Kokai Tokkyo Koho*, JP 2001252648

Jacquat, O.; Voegelin, A. & Kretzschmar, R. (2009). Local coordination of Zn in hydroxy-interlayered minerals and implications for Zn retention in soils. *Geochemica. Cosmochim. Acta,* 73, 348-363, 0016-7037

Katheuser, B.; Hodnett, B. K.; Riva, A.; Centi, A.; Matralis, H.; Ruwet, M.; Grange, P. & Passarini, N. (1991). Temperature-programmed reduction and x-ray photoelectron

spectroscopy of copper oxide on alumina following exposure to sulfur dioxide and oxygen. *Ind. Eng. Chem. Res.*, 30, 2105-2113, 0888-5885

Kney, A. D. & Zhao, D. (2004). A pilot study on phosphate and nitrate removal from secondary wastewater effluent using a selective ion exchange process. *Environ. Technol.*, 25, 5, 533-542, 0959-3330

Massey, A. G. (1973). Copper, In: *Comprehensive Inorganic Chemistry*, Bailer, J. C.; Emeleus, H. J.; Nyholm, R. & Trotman-Dickenson, A. F. (Eds.), 3, 1-78, Pergamon Press Ltd., 0-08-017275-X, Oxford

Miyazaki, A.; Asakawa, T. & Balint, I. (2009). NO_2^- adsorption onto denitration catalysts. *Appl. Catal. A. Gen.*, 363, 81-85, 0936-860X

Miyazaki, A.; Balint, I.; Aika, K. & Nakano, Y. (2001). Preparation of Ru nanoparticles supported on γ-Al_2O_3 and its novel catalytic acitivity for ammonia synthesis. *J. Catal.*, 204, 364-371, 0021-9517

Miyazaki, A.; Balint, I. & Nakano, Y. (2003). Solid-liquid interfacial reation of Zn^{2+} ions on the surface of amorphous aluminosilicates with various Al/Si ratios. *Geochemica. Cosmochim. Acta,* 67, 20, 3833-3844, 0016-7037

Miyazaki, A. & Nakano, Y. (2000). Morphology of platinum nanoparticles protected by poly(N-isopropylacrylamide). *Langmuir*, 16,18, 7109-7111, 0743-7463

Miyazaki, A. & Tsurumi, M. (1995). The H^+/Zn^{2+} exchange stoichiometry of surface complex formation on synthetic amorphous aluminosilicate. *J. Colloid Interface Sci.*, 172, 2, 331-334, 0021-9797

Moggi, P.; Albanesi, G.; Predieri. G. & Spato, G. (1995). Ruthenium cluster-derived catalysts for ammonia synthesis. *Appl. Catal. A. Gen.*, 123, 145-159, 0936-860X

Murata, S. & Aika, K. (1992a). Preparation and characterization of chlorine-free ruthenium catalysts and the promoter effect in ammonia synthesis: 1. An alumina-supported ruthenium catalyst. *J. Catal.*, 136, 110-117, 0021-9517

Murata, S. & Aika, K. (1992b). Preparation and characterization of chlorine-free ruthenium catalysts and the promoter effect in ammonia synthesis: 2. A lanthanide oxide-promoted Ru/Al_2O_3 catalyst. *J. Catal.*, 136, 118-125, 0021-9517

Pauliac, J. & Clause, O. (1993). Surface coprecipitation of cobalt(II), nickel(II), or zinc(II) with aluminium(III) ions during impregnation of gamma-alumina at neutral pH. *J. Am. Chem. Soc.*, 115, 11602-111603, 0002-7863

Santhanam, N.; Conforti, T. A.; Spieker W. & Regalbuto, J. R. (1994). Nature of metal catalyst precursors adsorbed onto oxide supports. *Catal. Today*, 21, 1, 141-156, 0920-5861

Subramanian, J.; Noh, S. & Schwarz, J. A. (1998). Determination of the point of zero charge of composite oxides. *J. Catal.*, 114, 433-439, 0021-9517

Trainor, T. P.; Brown, G. E. & Parks, G. A. (2000). Adsorption and precipitation of aqueous Zn(II) on alumina powders. *J. Colloid Interface Sci.*, 231, 359-372, 0021-9797

Vlasova, N. N. (2001). Effect of 2.2'-bipyridine on the adsorption of Zn^{2+} ions onto silica surface. *J. Colloid Interface Sci.*, 233, 227-233, 0021-9797

Wada, K. & Abd-Elfattah, A. (1979). Effects of cation-exchange material on zinc adsorption by soil. *J. Soil Sci.*, 30, 281-290, 0022-4588

Zhang, R.; Schwarz, J.; Datye, A. & Baltrust, J. P. (1992). The effect of second-phase oxides on the catalytic properties of dispersed metals: Palladium supported on 12% WO_3/Al_2O_3. 138, 55-39, 0021-9517

Absolute Solution for Waste Water: Dynamic Nano Channels Processes

Rémi Ernest Lebrun
Université du Québec à Trois-Rivières
Canada

1. Introduction

The new concept, which will be discussed in this chapter emerged from the observation that the wastewater contained, in fact, large quantities of elements with high added value, and primarily - water, H_2O. Then the problem to be solved is to sort these elements by using clean technologies that we draw from the whole set of the unit operations of Chemical Engineering. The possibilities offered by flourishing nanotechnologies are tremendous for the characterization of aqueous solutions and for the development of new processes as well.

In fact, there is a wide variety of problems. In the 60s, the idea that nature was capable, if helped a little, to treat all wastewater was widespread because it was considered that the amounts released were small in comparison to the flow of the rivers and the vastness of the seas and oceans. The brutal fact that the vastness is only relative, came from CO_2 emissions, reducing the oxygen available and the recent invasion of oil into the Gulf of Mexico that affects shores, the sea bottom and intermediate layers and this, in a large volume. In the past and more recently, the choice was made at large scale to collect and mix the wastewater for a global treatment, usually, municipal, which includes industrial, domestic and medical wastewater. In the context of sustainable development, attitudes change, the selective collection is allowable. But we must go further, much further, recognizing the presence of different resources in each type of waste water and therefore to extract them as much as possible at source, or reuse them on site or to market them after being given an economical value. Nanotechnology can perform these upgrades. Intensive processes allow to perform these small-scale operations at the site of production, reducing the mixing and transport.

In this chapter we will relate progress made over the last 50 years, whether scientific, technological, sociological, ecological, emphasizing nanoscience and miniaturization aspects as well as the integration of expertise in the process management. We will expose specific cases, chosen as the most demonstrative of those we treated, for example:

- treatment of contaminated soil after a burial or a discharge, deliberate or not, of pollutants;
- treatment of municipal wastewater resulting from the collection of releases that uses water as a transport vector,
- regeneration of glycols in airports depending on weather conditions and others;
- reuse of brines for dyeing textile fibers;
- the transfer of copper removed during the etching of printed circuits to the plating of new plates.

We will present the multidisciplinary theoretical reflections that converge and we will develop a mathematical model describing the phenomenological behavior of aqueous solutions at a nanometer scale that interact with materials constituting the geometric boundaries of the pores. We will describe the experimental methods we have adapted to each case and the tools used in the laboratory and at the pilot scale. We will explain the appropriateness of applying simultaneously exergy analysis and economic analysis as a tool for decision support in the short, medium and long term. The main results will be highlighted and will demonstrate a great potential, offering insight into creative and efficient solutions for the near future. In a context of population and consumption growth, natural resources can no longer be considered inexhaustible. The new resources are those made by humans then discarded after use. They are found largely in waste water and thus in close proximity to areas of consumption.

2. Fundamental aspects

2.1 Phenomenological aspects and modelling

In the late 50s, after the Second World War, in front of the Gibbs adsorption equation (Gibbs, 1928), exhibited in a corridor at UCLA (University of California at Los Angeles), S. Sourirajan had a luminous interpretation (Sourirajan & Matsuura, 1985) that led to the development of the first reverse osmosis asymmetric membranes made of cellulose acetate for the desalination of seawater on an industrial scale, but especially to the birth of a new science of flow separation in nanoscale spaces as a result of many interactions between the molecules involved.

$$\Gamma = -\left(\frac{1}{RT}\right)\left(\frac{\partial \gamma}{\partial \ln(a)}\right)_{T,A} \tag{1}$$

A : Surface area involved in adsorption (m^2)
a : Activity of solute (mol m^{-3})
R : Gaz constant (J K^{-1})
T : Temperature of the solution (K)
Γ : Gibbs surface excess of solute (mol m^{-2})
γ : Interfacial tension at the air-solution interface (N m^{-1})

It was not until the 2000s and the availability of fast and powerful computers for us to find that the work of Jungwirth (Vrbka et al., 2004) in molecular simulation in nanometer space was, unwittingly, in line with the Sourirajan's interpretation of the Gibbs adsorption equation. The following figure describes perfectly what is considered a crucial step in fluid dynamics in nano-spaces and called by some nanofluidic, which will create a vast field of investigation and discovery in the area of waste water which then become new resources.

Replace the air-salt water interface by pore-salt water interface having the same properties as the air-solution interface allows to rearrange the molecules with a very fast kinetics causing the separation of the solvent in a layer of nanometer range. Moreover, all these models predict an increase in surface acidity and an increase of basicity in the middle. However, during operations to pre-concentration of the sap in Quebec and across the north-eastern North America, tens of thousands of maple producers have all found that the reverse osmosis produced permeate was acid when water collected from maple trees was not (Allard, 1998) that we also confirmed in experimental studies on the subject. Recently,
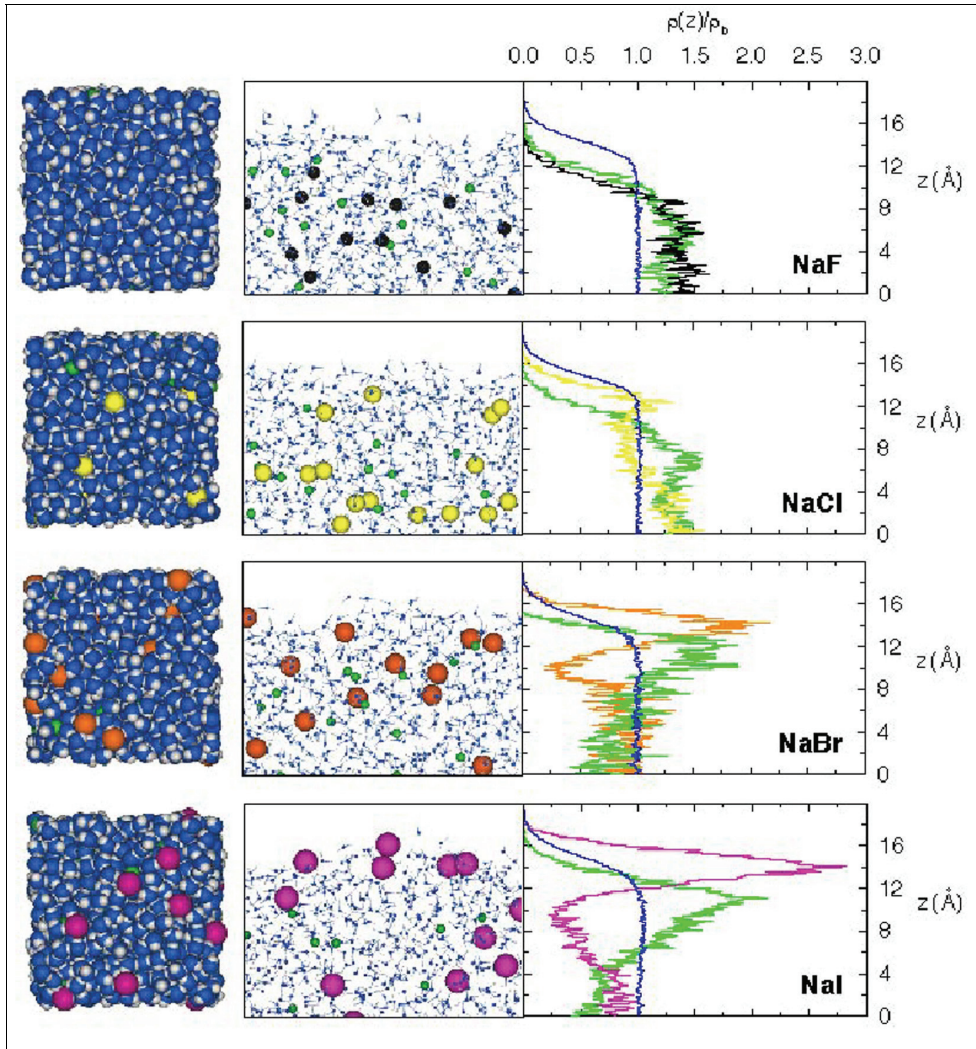
Fig. 1. Left and middle columns: top and side views of snapshots of solution/air interfaces from MD simulations of 1.2 M sodium halide solutions. Right: corresponding number density profiles. Coloring scheme: water oxygen, blue; water hydrogen, gray; sodium ions, green; chloride ions, yellow; bromide ions, orange; iodide ions, magenta. (Vrbka et al., 2004)

the Nobel Price has been given to Peter Agre and Roderick MacKinnon (Agre & MacKinnon, 2003) for their work on the aquaporin channel and the transport of water and ions through the bilipidic membrane cell. This discovery connected in relation with the models, shown before, represent a new approach at the nanoscale to open a great field of research.

On the other hand, always in the late 50s, at the University of Wisconsin, B. Bird clearly defines the concentrations, velocities and fluxes for solutions in motion (Bird et al., 2002). This approach, using the relative velocities of solute and solvent compared to the average

velocity of the solution, enables him to express the molar flux of solute compared to the molar average velocity of the solution according to the molar concentration gradient and thus, to give Fick's law its true meaning and render it all the necessary rigor. The differential equations of momentum, heat and mass are expressed in terms of a balance on a volume element.

In 1999, we have shown that all these approaches remained fully valid at the nanoscale and that was enough to express different fluid properties and pore geometry to obtain an excellent fit between the predictions of model obtained and the experimental data. We have advanced the concept of dynamic permeability and interpreted from experimental data at very low pressure drop. The water behaves like a Bingham fluid as it flows in nanoscale spaces, highlighting the interactions between molecules.
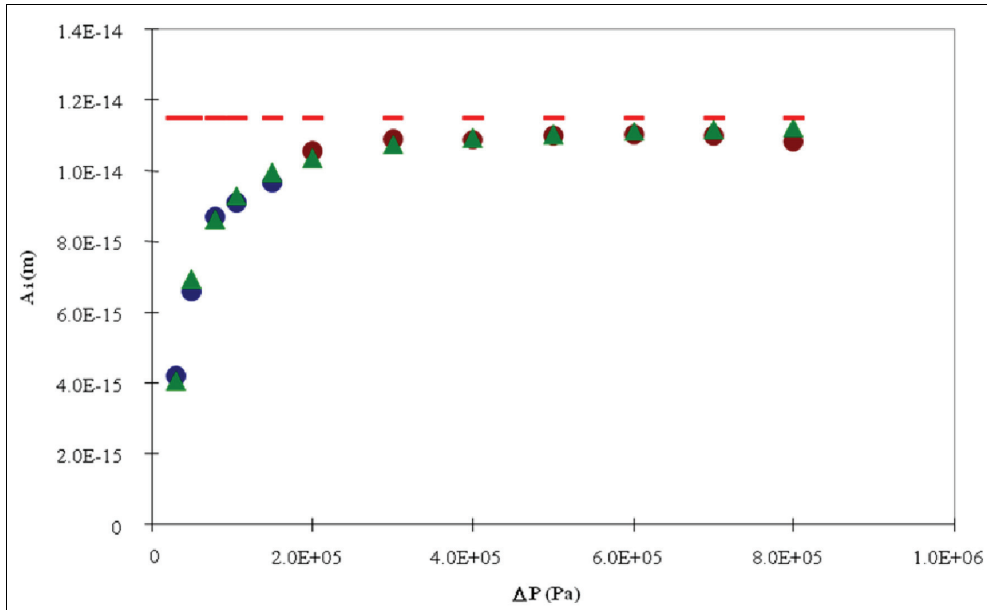
Fig. 2. Permeability of pure water at 25°C: comparison of Bingham and Poiseuille models with experimental data in hyperfiltration.

We have defined the dynamic permeability Aid, by analyzing the asymptotic limits of phenomenological equations of transport in a nano filtration module as

$$Q_p = \frac{A_{id}S_m}{\mu}\left[\Delta P_a - \left(\Pi\left(X_m\right) - \Pi\left(X\right)\right)\right]$$

(2)

$$\Delta P_a = \Delta P_m - \left(\Pi\left(X\right) - \Pi\left(X_p\right)\right)$$

(3)

$$Q_p = \frac{A_{id}S_m\Delta P_a}{\mu} \qquad when \quad X_m \to X$$

(4)

A_{id} : Dynamic permeability (m)

Q_p : Permeate flow rate (m³ s⁻¹)

S_m : Membrane surface (m²)

X : Molar fraction of the bulk solution in the membrane module (-)

X_m : Molar fraction in the boundary layer at the membrane surface (-)

X_p : Molar fraction in the permeate (-)

ΔP_a : Apparent differential pressure (Pa)

ΔP_{eff} : Effective differential pressure (Pa)

$\Pi(X)$: Osmotic pressure at the molar fraction X (Pa)

$\Pi(X_m)$: Osmotic pressure at the molar fraction X_m (Pa)

$\Pi(X_p)$: Osmotic pressure at the molar fraction X_p (Pa)

μ : Solution viscosity of the solution in the membrane pore (Pa s)

We also showed that the pore size consisting of material such as polyamide, could shrink depending on temperature and this, in a reversible manner. The geometry of the pores can also vary depending on the pH or the concentration in solute of flow solutions. Other similar effects, due to the presence of an electric field, have also been shown.

We modeled the coupling of mass transport in the boundary concentration layer and in the pores using the double distribution of pores (Sourirajan & Matsuura, 1985). Then, we described each of these phenomena according to the Fick's law of diffusion as expressed by Bird (Bird et al., 2002), to find different expressions in the boundary concentration layer.

$$J_A^* = -D_{AB}\nabla(cX_A) \tag{5}$$

c : Molar concentration of the solution (mol m⁻³)

D_{AB} : Diffusion coefficient (m² s⁻¹)

J_A^* : Solute molar flux relatively to average molar velocity of the solution (mol m⁻² s⁻¹)

In this case, the flow rate of fluid or backdiffusion flow rate is proportional to the concentration gradient (driving force). The coefficient of proportionality is the diffusion coefficient.

We expressed the flow separation in a pore by an entirely new model.

$$\nabla(cX_A) = +c\Re_{AB}^M J_A^* \tag{6}$$

$\Re_{AB}^M$: Diffusion coefficient in the membrane pore (m² s⁻¹)

By integrating this differential equation we have shown the existence of a minimum and maximum separation (and not asymptotic as in other models). This finding represents a situation with no interaction. If we insert into the model the affinities between solvent-solute-porous material, the obtained leverage will depend on the relative dimensions between the different components.

$$\frac{f_1^{'} - f^{'}}{f_1^{'} - f_0^{'}} = \exp\left(-\frac{r_p^2 \Delta P_M}{8\mu^M \Re_{AB}^M}\right) \tag{7}$$

$f^{'}$: Intrinsic separation factor define by $f^{'} = \left(\dfrac{X_m = X_p}{X_m}\right)$ (-)

$f_0^{'}$: Minimum intrinsic separation factor (-)

$f_1^{'}$: Maximum intrinsic separation factor (-)
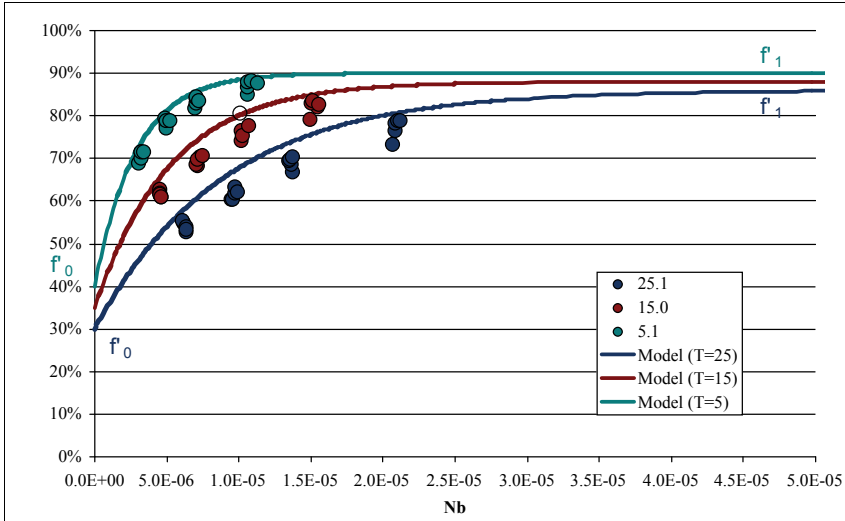
Fig. 3. Experimental data for nanofiltration of DEG in aqueous solution at different temperatures. Adequacy of the model of separation flow in a nanoscale pore.

Related to very important developments made by Sourirajan who expressed the interactions as changes of Gibbs free energy in a micro-canonical ensemble described by the following equations:

$$\ln\left(\frac{D_{AM}}{K\delta}\right) = \ln\left(C_{NaCl}^{*}\right) + \ln\left(\Delta^{*}\right) + \left(\frac{-\Delta\Delta G}{RT}\right) + \delta^{*}\sum E_s + \omega^{*}\sum s^{*} \tag{8}$$

$$\frac{-\Delta\Delta G}{RT} = \frac{-\left(\Delta G_I - \Delta G_B\right)}{RT} \tag{9}$$

$$\Delta G_I = \sum \gamma_I (\text{structural groups}) + \gamma_{I,0}$$

With:

$$\Delta G_B = \sum \gamma_B (\text{structural groups}) + \gamma_{B,0}$$

For this purpose these definitions are sufficient. To know more refer to Sourirajan (Sourirajan & Matsuura, 1985 p.131)

From these different groups, it is possible to define the properties of a material, the pore size to obtain the desired separation for a given solution.

This set of models allowed us to understand and express the geometric variations of nanoscale spaces between the polymer chains according to the presence of ionic species. The

figure below shows that the adequacy between model and experiments, clearly expresses the phenomenological behavior of molecules (solvent, solute, pore material) at the nanoscale.
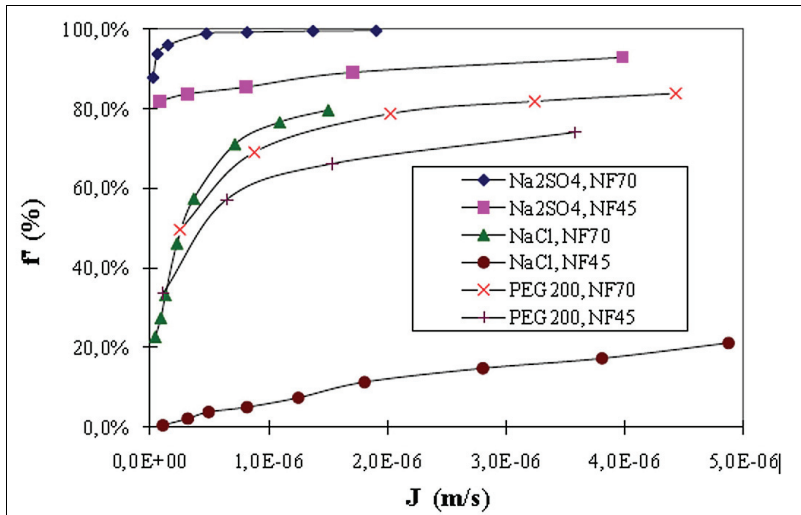
Fig. 4. Experimental data for nanofiltration (NF70 and NF45) for solutions of PEG, Na_2SO_4, NaCl: Modeling maximum and minimum separation factors based on permeation flux.

These new insights have enabled the development of new processes for treating wastewater. After defining the desired permeate and concentrate flows, from a wastewater properly characterized, the choice of polymer and pore size provides a synergistic effect. On this basis the process design is then possible and the optimization is based on industrial and economic constraints.

2.2 Analysis tools for the design optimization

Modeling and understanding of transport phenomena in nanoscale pores help design the processes required to sort the elements present in wastewater and choose to isolate them, group them or turn them into new elements. The objective function must be defined in terms of possible added value of the various flows that can be created by minimizing releases to the environment in relation to expressed needs. A scientific tool for analyzing the performance of the new process is the exergy analysis. This analysis, coupled with an economic analysis, allows to know the degree of valorization over the maximum possible in the context of wastewater available and immediate needs.

Here is an example of exergy analysis of a method for wastewater valorization: The simplest configuration is illustrated in the figure below (one-stage continuous process). Several parameters are defined as follows:

- Average operating pressure

$$P = \left(\frac{P_{me} + P_{ms}}{2} \right) \tag{10}$$
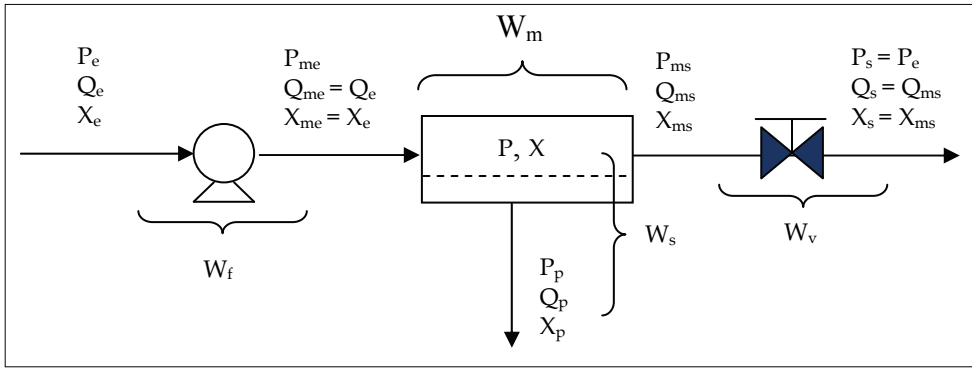
Fig. 5. Systemic diagram of a simple process.

- Average recirculation flow rate in the module

$$Q = \left(\frac{Q_{me} + Q_{ms}}{2} \right) \tag{11}$$

- Average molar fraction of the solute in the module

$$X = \frac{X_{ms} - X_{me}}{\ln\left(\frac{X_{ms}}{X_{me}} \right)} \tag{12}$$

- Osmotic pressure gradient

$$\Delta\pi = \pi(X) - \pi(X_p) \tag{13}$$

- Apparent transmembrane pressure

$$\Delta P_a = P - P_p \tag{14}$$

- Effective transmembrane pressure

$$\Delta P_{eff} = \Delta P_a - \Delta\pi \tag{15}$$

Ideal system: minimum work of separation
The separation of a homogeneous binary mixture of different compositions needs certain devices that consume energy in the form of work and/or heat. The minimum work to make a separation, whatever the method used, is calculated by considering a reversible and isothermal separation. This minimum work of separation depends only on the composition, temperature and pressure of the initial mixture and different final fractions. For a separation of a homogeneous mixture into pure products at constant temperature, the minimum work to provide can be calculated by the formula:

$$W_{\min} = -NRT \sum_j X_j \ln(\gamma_j X_j) \tag{16}$$

where W_{min} is the minimum work required for separating of the mixture flow (W);

N is the molar flow of the mixture flow (mol s^{-1});

R is the constant of ideal gases (J mol^{-1} K^{-1});

T is the temperature of the system and its environment that is kept constant (K);

X_j is the mole fraction of component j in the initial mixture;

γ_j is the activity coefficient of component j in the initial mixture.

Where products are not pure, the minimum energy consumption can be calculated by subtracting from the equation (16), the minimum work to transform impure products to pure products. In the case where the solute concentration is low, the activity coefficients are taken equal to 1, and that to simplify calculations. If we use the same symbols shown in Figure 5, we obtain the following equation to calculate the minimum work to separate a feed stream (N_e) in a permeate flow (N_p) and a concentrate stream (N_s) :

$$W_{min} = -RT\left\{ N_e\left[X_e \ln X_e + (1-X_e)\ln(1-X_e)\right] \right.$$
$$- N_p\left[X_p \ln X_p + (1-X_p)\ln(1-X_p)\right] \tag{17}$$
$$\left. - N_s\left[X_s \ln X_s + (1-X_s)\ln(1-X_s)\right] \right\}$$

where N_e is the molar flow of the input solution (mol s^{-1});

N_p is the molar flow rate of permeate (mol s^{-1});

N_s is the molar flow of concentrate (mol s^{-1}).

A method for doing the separation of a mixture where there are changes in temperature, pressure and concentration, the exergy of a fluid stream can be presented as the sum of the thermal exergy $E_x{}^T$, the mechanical exergy $E_x{}^P$ and chemical exergy $E_x{}^C$ [equation 18-21]:

$$E_X = E_X^T + E_X^P + E_X^C \tag{18}$$

where thermal exergy

$$E_X^T = Q\left[C_P(T-T_0) - c_p \ln\left(\frac{T}{T_0}\right)\right] \tag{19}$$

mechanical exergy

$$E_X^P = Q\left[(P-P_0)\right] \tag{20}$$

chemical exergy

$$E_X^C = -NRT_0 \sum\left[e_i - X_i \ln(\gamma_i X_i)\right] \tag{21}$$

E_x is the flow exergy (W)

c_p is the specific heat of the solution (J m^3 K^{-1})

e_i is the exergy of pure product i.

T_o, P_o are the temperature and pressure of the reference state.

For the process (fig. 5) the following hypothesis have been done:

1. T_0, the operating temperature is constant
2. The binary solution is homogenous and the activity coefficients are fixed to 1;
3. Pressures are $P_e = P_p = P_s = P_{atm}$;
4. The pump efficiency is equal to 100%.

The exergy balance on this process is defined as follow:

$$W_f = W_{min} + T_0 \Delta S \tag{22}$$

Where W_{min} et W_f are calculated by equations (17) et (22) and ΔS is the entropy generation. Equation (22) appears as:

$$Q_p(\frac{P_{me}+P_{ms}}{2}-P_p)+Q_{ms}(P_{me}-P_{ms})+Q_{ms}(P_{ms}-P_s) =$$
$$W_{min}+T_0\left(\Delta S_{e\text{-}p}+\Delta S_{e\text{-}ms}+\Delta S_{ms\text{-}s}\right) \tag{23}$$

Where $\Delta S_{e\text{-}p}$, $\Delta S_{e\text{-}ms}$ et $\Delta S_{ms\text{-}s}$ are the entropy generations between the referred points of the fig.(1). The exergetic efficiency of such a system can be defined by (Brodyansky et al,1995):

$$\eta_e = \frac{W_{min}}{W_f} \tag{24}$$

2.3 Examples of general application

The following example is generic to show how this tool can be applied: a concentrated solution which, after use, is diluted and contaminated by other elements.

Considered as waste before government standards, the wastewater was discharged into the environment. To continue production operations, the pure products (solid) were purchased and then mixed with pure water, purchased or produced from a local source, to obtain the desired concentrated solution.This solution was heated to the operating temperature to be used in the production process. However, exergy analysis shows that there is energy generation when mixing pure products and pure water: energy, which usually is not recovered. If we consider that contamination may be removed, we obtain a dilute solution of good quality. The temperature level is maintained at the lowest energy cost since the solution is recycled. From a viewpoint of exergy analysis, the best performance is to concentrate the resulting solution to obtain the desired solution. The same analysis can compare various processes to determine for each process the most efficient operating range. It also helps to optimize each process on the basis of thermodynamic irreversibility.

The wastewater can be classified according to the exergy analysis. Leachate contaminated soil or municipal wastewater, generated naturally or by simple collection, represent a category.

The primary interest is often to treat this wastewater for discharge into the receiving environment based on standards. There are still few places where we seek to enhance their content. However, domestic wastewater is treated and reused in the space station. Indeed, water is prohibitive, reuse water becomes clear. Whole buildings in Japan treat wastewater generated internally, based on the idea of Yamamoto (Choi et al., 2006), and a single booster is used, which allowed for significant space savings by reducing the pipes.

A large category includes wastewater at the exit of processes that have a greater level of exergy that water supply. This exergy is thermal exergy (hot water discharge), or mechanical exergy (high pressure discharge) or chemical exergy (water of high purity). Another category includes wastewater containing chemicals used in excess in the production process, which are rejected because in the presence of contaminants. Presumably another category contents washing cars or textiles with the use of detergents and high temperatures, cleaning with acids or bases that are found in pulp and paper industry in the plating. The solution in this case, was to neutralize the waste to meet environmental standards and to purchase acid and basic production needs. However, these products

represent costs, risks (storage and transport) and standards for salts are closing more and more. This situation prevents the neutralization that generates salts.

From another point of view, the human body can be perceived as a real chemical engineering plant. It is an excellent example of exergy efficiency. The introduction of drugs, often in excess, in the entire body is an example of exergy losses. Moreover, the presence of endocrine precursors (from these drugs) in wastewater is now recognized as a serious public health problem. Fortunately more and more controlled drugs diffusion and the possibility of detecting the target to be treated are promising solutions.

2.4 Characterization of nanoscale pores

We have seen that the pore size and surface forces of the material forming these pores are of crucial importance to minimize energy costs. An essential tool for characterizing the pore size is the analysis of structures by near-field scanning microscopy. The image analysis of generated images allow quantification of the size and size distribution of pores and their surface distribution. The great advantage of this method is that it is not destructive and it works in an ambient or controlled atmosphere as well as in liquid medium that can be modified depending of temperature, pressure, pH, salt concentrations, etc.

The following figures, we have realized in the laboratory, illustrate the topology of membranes at different scales. The depth of 3-D images is indicated. Areas of 2 µm each side up to areas of 10 nm each side are presented below. Different materials have been studied (ceramics, polymers). Figure 8 shows the cyclodextrins of 100 nm, retained by the ceramic membrane with pores of about 20 nm, during a permeation of an aqueous solution of 100 ppm of cyclodextrins. Figure 9 presents a surface modification of the ceramic membrane with an polyvinil oxide solution. Figure 10 shows a detail of the morphology of the new surface. These images show the beginning of a characterization of dynamic pores.
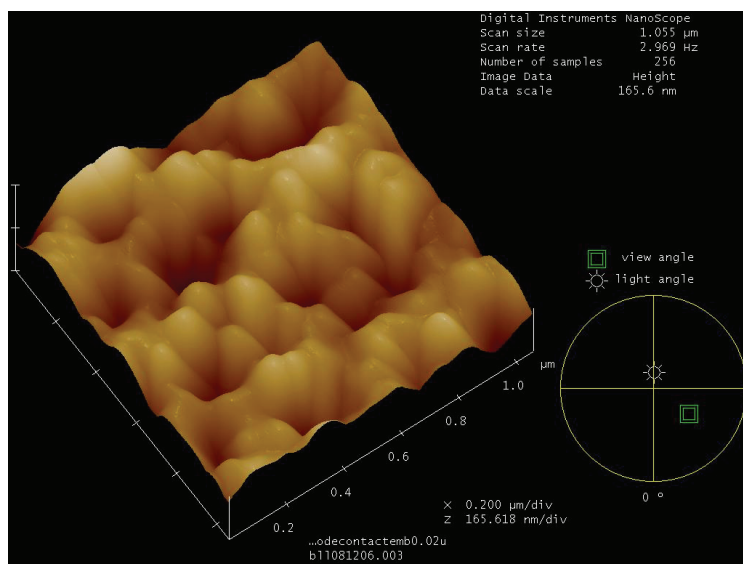
Fig. 6. Ceramic membrane D_P = 20 nm. Image Scanning Probe Microscope 1x1µm, contact mode, ambient air.
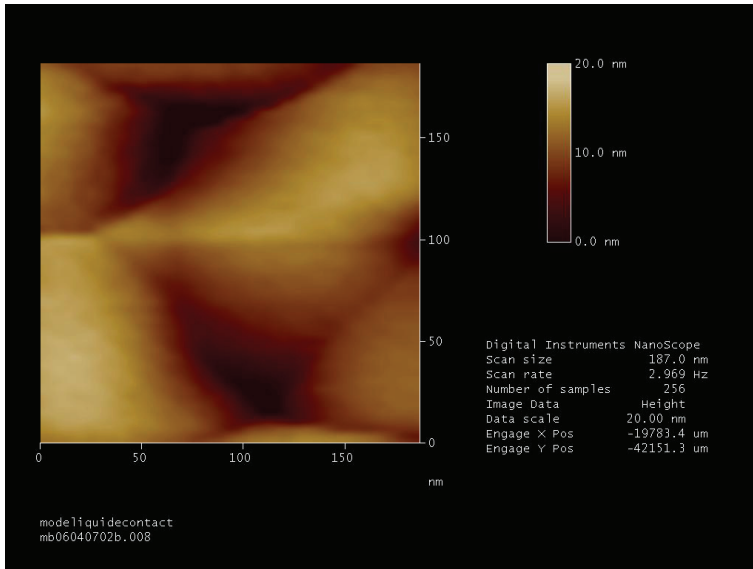
Fig. 7. Ceramic membrane D_P = 20 nm. Image Scanning Probe Microscope 200x200 nm, contact mode, ambient air.
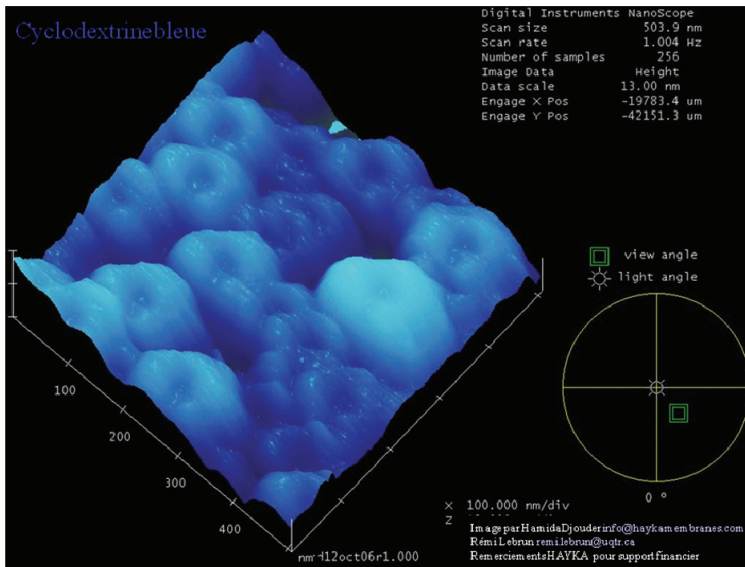
Fig. 8. Blue cyclodextrin on ceramic membrane D_P = 20 nm. Image Scanning Probe Microscope 500x500 nm, contact mode, aqueous medium, ambient temperature and pressure.
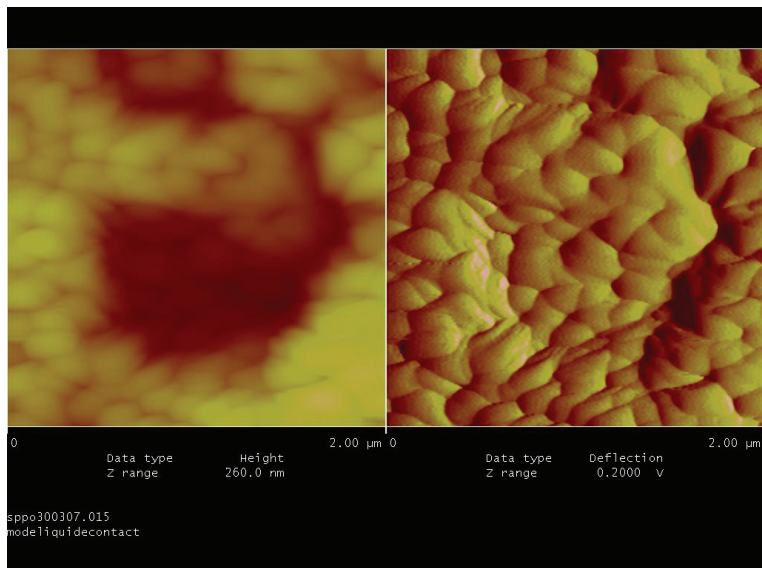
Fig. 9. Surface modification of ceramic membrane Dp = 20 nm with sulfonated oxide of polyphenyl. Image Scanning Probe Microscope 2x2 μm, contact mode, aqueous medium, ambient temperature and pressure.
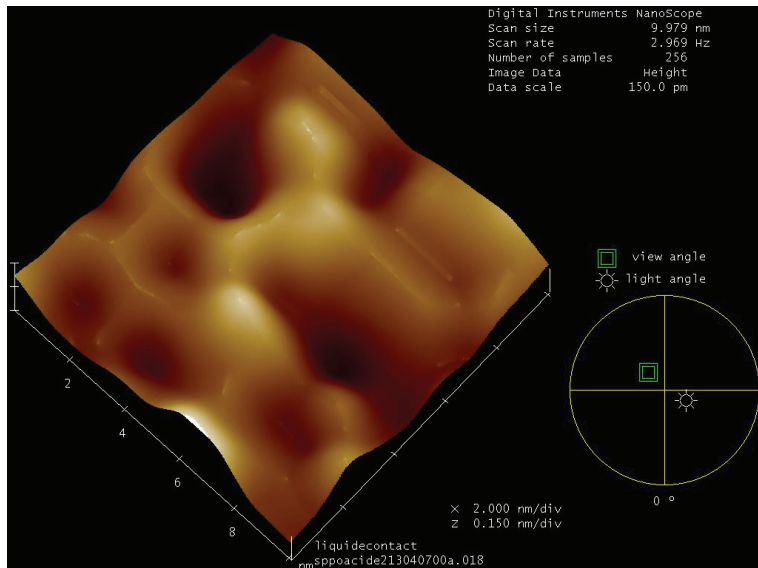
Fig. 10. Surface modification of ceramic membrane D_P = 20 nm with sulfonated oxide of polyphenyl. Image Scanning Probe Microscope 10x10 nm, contact mode, aqueous medium, ambient temperature and pressure.
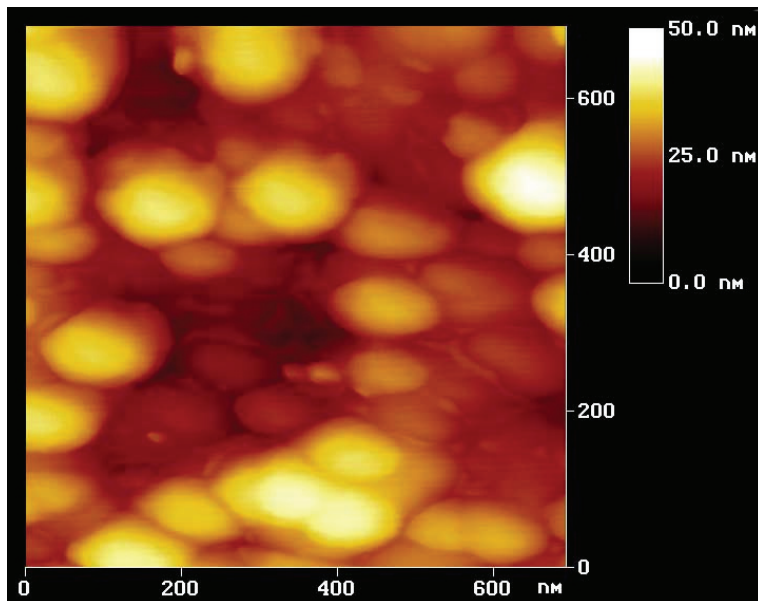
Fig. 11. Cellulose acetate membrane manufactured according to the recipe of the first membranes of Loeb and Sourirajan. Image Scanning Probe Microscope 600x600 nm, contact mode, aqueous medium, ambient temperature and pressure.

In the case of processes based on organized nanoscale pores, two avenues can be considered:

- Minimize losses due to irreversible phenomena

Maintaining the maximum separation of solute compared to the solvent, it is possible to minimize losses by reducing charge losses in a pore or by reducing its length or by providing flared shapes (Sourirajan & Matsuura, 1985). We can also increase the radius of the pore and maintain the separation. It may be noted that the number of pores increase the exergy efficiency by decreasing the operating pressure and therefore allows to approach the minimum work of separation, provided that it respects the maximum separation, and the minimum pressure corresponding to this maximum separation. By opposite when the separation varies with the pressure, which represents the irreversible thermodynamics, the margin for maneuver is limited. It is the same with the variable temperature, to a lesser extent.

- Make processes more intensive (maximum production with minimal bulk)

If the most important criterion is to have a process as compact as possible, then it is possible to organize the material to increase the number of pores per surface unit and increase the operating conditions (temperature and pressure). The energy cost of the operation of such a process will then increase and other risks may be associated with this avenue. Often the exergy of the concentrate current will be increased to an unnecessary value which may very often lead to energy loss during the operation.

Processes such as evaporation, vacuum evaporation, multiple effect evaporation, hyperfiltration, nanofiltration, electrodialysis, membrane distillation, etc. Each of these processes can be most efficient for a certain range of concentration and, therefore, a process

consisting of several of these unit operations may be the most efficient method for a given problem. For cons, the chosen solution may be slightly different because of the availability of equipment and according to economic analysis. Some of these unit operations have marked scale effects, othera as membrane processes are much less sensitive.

3. Strategy of the process design

3.1 Wastewater, its origin: a systemic analysis

The origin of the wastewater is very important in our conceptual framework. For a long time the grouping of wastewater has been a strategy to benefit from scale effects of treatment processes. Currently, whether municipal or industrial, the selective collection is increasingly applied. The analysis means of wastewater is becoming increasingly sophisticated for a wide variety of molecules and are more accurate but costs remain high.

Our strategy applies to a unit of industrial production (defined as a system situated in an environment with its inputs and outputs). Systemic analysis begins with mass balances and exergy balances (energy, temperature level, air pressure, chemical potential) on each of the currents on the global system and subsystems to explore opportunities to create loops of internal recycling process.

This methodology is based on different principles :

Know the production line, its inputs, its outputs, the present reactions, the necessary energy levels, the separations and mixtures used will help to reduce analysis costs by reducing their frequency and their level of accuracy. A program for analyzing the quality of raw materials and products to help maintain constant operating conditions.

- The mixture of two or more fluid currents or energy must be at the same level of exergy. If one of the currents is below this level its exergy must be increased and this expense should be accounted. This represents an extension of the pinch technology applied in energy saving.

These tools cannot give an objective analysis because they can optimize an existing situation (a process in place) or optimize a newly developed method which is subjected to the method. In no case they cannot directly provide an optimum process. Moreover, the constraints imposed upon the posing of the problem restrict the degrees of freedom of the designer.

An interesting example is the treatment of toxic groundwater resulting from leaching of contaminated soils. Indeed, the fact of using the word "toxic" leads the designer towards what might be considered as a red herring. It must reflect the standards and regulations and optimize a method based on those constraints that apply to the current that must return to the receiving environment and other currents that may be released into the environment. However, if we define the wastewater according to its composition, the elements responsible for the toxicity and ecotoxicity represent a very small amount of dissolved matter (in the order of 10^{-1} kg m^{-3} or 100 ppm). So we can consider that these waters contain a large amount of very pure water. The proposed method allowed to produce high quality water that could have multiple uses for treated water:

- Flow to the river
- Back to the site for irrigation as leaching water to accelerate soil washing.
- Use as process water for industry
- Use as drinking water

For other currents there are several possibilities:
- Use of a concentrate as fertilizer
- Use of a produced baking soda
- Using other solids in the manufacturing of concrete

The content of some currents, in very small percentages, is destroyed by an elementary chemical reaction. What is remarkable is that this reaction is not possible when the element is part of the mix. Its separation allowed the reaction without producing pollution.

Other separations were carried out to avoid adverse reactions. A peculiarity of this type of separation in nanoscale pores is that the composition of the concentrate side of the fluid current is always changing, which means that the exergy varies throughout the process. In principle, if separation does not depend on the composition of the fluid, operating conditions must change. Moreover, if the separation depends on the composition, then the pore size should change with changes in concentrations and composition. A simple criterion of optimization is to adjust the pore size and operating conditions to obtain a permeate composition and constant concentration.

3.2 Designing a sequence of unit operations

Considering the above principles, based on the analysis of wastewater, it is possible to characterize their content in different groups of particles or molecules. Consider a ground water containing suspended particles, bacteria, hydrocarbons and ions in solutions. For each category it is possible to optimize the pores to make the complete separation of the category. Systematically we can define the system by the following sequence:

Input Current	Unit 01	Concentrate current 01	particles
Permeate current 01	Unit 02	Concentrate current 02	bacteria
Permeate current 02	Unit 03	Concentrate current 03	hydrocarbon
Permeate current 03	Unit 04	Concentrate current 04	type I ions = solid
Permeate current 04	Unit 05	Concentrate current 05	type II ions = solid
Permeate current 05	Unit 06	Output current 06	water + ions = quality

Analysis of reuse and of the nature of the valorization of each of the currents.
Concentrate 01:
Most of the particles can be put back on the ground and be washed again by water produced in the current 06. This surface wash continue thoroughly to accelerate the leaching of this former landfill.
Concentrate 02:
Bacteria with specific properties extracted from groundwater are concentrated and can be a base for supplying a bioreactor.
Concentrate 03:
The hydrocarbons extracted have energy value.
Concentrate 04:
These divalent salts can be separated by selective precipitation and form dry product or be used as additives for different applications.
Concentrate 05:
Other types of monovalent salts can be recovered in the same manner as before.
Process 06:

This advanced oxidation process allows the destruction of toxic material (eg.: Ammonia nitrogen). This reaction is not possible in the feed water

Energy costs throughout the process are related only:

-    to losses in nanoscale pores,
-    to pressure levels that are depending on the osmotic pressure difference,
-    to pumps and motors performance,
-    but independent of temperature level (operating at room temperature).

The charge losses are the same whether the fluid flows through a pipe (macro level) or that flows into microscopic pores (hollow fiber or micropores) or nanoscopic (with few exceptions), provided that the number of pores are enough in comparison to the length of the pores.

$$\Delta P = \frac{64\mu(T)\ Q_p L_T}{D_T^4} = \frac{64\mu(T)\ Q_p L_P}{n_p D_P^4} \tag{25}$$

So there are no limitations due to having a flow in nanoscale pores. The only energy barrier is the exergy differential between currents. This can be translated in terms of osmotic pressure, level of chemical potential, etc. The temperature level can play a role but it is not a necessity. An example of application that illustrates these results is the treatment of wastewater that must be transported from point A to point B in a pipe using pumps. Then we can design a set of organized systems in nanoscale pores that can be installed in series-parallel in a tree form. If the pore size is smaller than the size of particles or molecules to be separated, then no additional energy is required to effect the separation, provided that one adjusts consequently the number of pores and that the flow is laminar (Equation 25).

Another example allows to choose between two methods depending on the concentration range of wastewater. If we consider a wastewater containing monovalent salts that must be addressed. If the salt concentration is low, then the hyperfiltration is a common solution. If the salt concentration is high, the electrodialysis is a popular choice. The fundamental difference between the two processes is the transport of molecules. In the first one it is the water that flows through the pores; in the other it is the salt ions that are the subject of transportation. When the concentration is low, the osmotic pressure is low and the operation pressure (which is the driving force for hyperfiltration) is common, on the other side to migrate the salt ions under a difference of electric potential (which is the force motive for the electrodialysis) power consumption is important. When the concentration increases it is the opposite. This leads us to design a sequential process consisting of hyperfiltration then electrodialysis. This configuration provides synergy and reduces the losses of exergy from a process that would do the same separation whatsoever hyperfiltration.

4. Case studies

Over the past 25 years we have had the opportunity to work on many cases of wastewater treatment in Canada. We will present them a summarily based on their category and not in chronological order. In most cases, the request was to treat the wastewater to allow its release into the environment. In all cases it was possible to provide sustainable solutions for all or part of the fluid streams. For this we have designed, fabricated and operated pilot units to demonstrate the feasibility of the proposed treatment. We have also, using a software, designed and simulated processes scaling. At the laboratory scale, were used to

test units used at UCLA (Sourirajan & Matsuura, 1985). We also designed and produced pioneering experimental assemblies to characterize both commercial membranes and those manufactured in the laboratory. We were able to transfer the methods of characterization, from laboratory to pilot scale, which also allowed us to transfer the methods enabling changes of structure and membranes surface available on the market. We could adjust the size of pores and surface affinities to the problem studied.

We will present summaries of these experiments using the categories presented in Chapter 2. The important progress made in the last 50 years, both in research and the industry have made available on the market the membrane modules with a variety of materials and structures (Drioli E. & Giorno, L, 2010). The surface/volume ratio was significantly reduced to allow achievement of intensive processes. Permeability and separation also increased resulting in improved process efficiency. Costs, usually compared with the standard $/m^2 of membrane, were greatly reduced from $100 to $25/m^2 of membrane. But because performance per m2 of membrane surface increased, costs per m^3 of treated wastewater decreased. In addition, improving the treatment strategy, as we have seen above, greatly reduced operating costs.

4.1 Groundwater from old municipal landfills

In this case, the wastewater becomes an obligation because the stormwater becomes charged with toxic elements while seeping in the soil then the toxic groundwater flows off-site to discharge into surrounding watercourses. This water cannot be recovered and mixed with municipal wastewater because it does not meet standards. Many characterization studies were conducted over the past 25 years, which provide familiarity with their composition and geographical distribution.

The first approach, based on our systematic approach has been to separate the collection of oily water, for which treatment method will be developed, from the groundwater. It is obvious that the mixture of these two waters is probably the worst operation to be performed. Then, analysis of groundwater revealed that few elements, in mass, contaminate groundwater. Suspended solids, mainly soil, small amounts of bacteria, some traces of hydrocarbons and dissolved salts whose main ecotoxicity source is known to be ammonia nitrogen.

Our strategy was to extract suspended particles and get rid of harmful elements still present before being used for landscaping of the site. The leachate will then be reprocessed by the main system. Bacteria in groundwater form a consortium developed at low temperature under anaerobic conditions. Extract and concentrate them is on one hand valorize them, and, secondly, sterilize water to be treated which for the sequence of unit operations downstream, allows to avoid the formation of biofilm representing a limiting factor for system operation. In these conditions it is easier to design a appropriate system to perform the right separation with minimized exergy loses as shown below.

Traces of hydrocarbons are also extracted and concentrated to, again, promote subsequent operations of separation of dissolved salts. Although physico-chemical analysis only reveals the presence of hydrocarbons as trace we must not forget that the objective is to treat completely or 100% of groundwater. In general, the disadvantage attributed to the separation systems is to produce a concentrate that you cannot treat. In most methods of treating wastewater, sludge is produced, its analysis is not always easy and its disposal by landfill is not well regulated. The mass balance of the process is rarely done strictly and allows to forget the quantities of material.

Our strategy allows to isolate the ammonia nitrogen to perform an advanced oxidation reaction converting, in ideal conditions of the stoichiometric ratio, the molecule into gaseous nitrogen and other harmless ions. This is an important advantage, because this reaction can be produced from the original wastewater because oxidants will first react with the other products present, before the ammonia nitrogen. Achieving a reaction in a stoichiometric ratio minimizes the exergy and therefore, the consumption of oxidants and the presence of by-products. The pilot tests have allowed, through a sequence of selective separations and optimized reactions to produce a nanopure water and completely destroy the ammonia nitrogen, responsible for the toxicity and ecotoxicity. The process does not generate sludge or concentrates. The produced water, of nanopure quality, can be used as process water for industry, rather than rejected in the river and then pumped out later by an industry and treated for use. We kept these waters under ambient conditions and light in transparent plastic bottles, closed from 2006 to 2010. New physico-chemical, toxicity and ecotoxicity acute and chronic analysis performed in specialized laboratories according to Canadian standards and procedures, demonstrated the high stability of the water quality.

Another category of wastewater includes leachate of contaminated soil from which we want to extract heavy metals responsible for the contamination. Generally, they are acidic waters put in contact with the soil, in situ or in a reactor, and will dissolve heavy metals and carry out from the soil. Often this water is collected and processed to meet the discharge standards in the receiving environment. Our approach, according to a material balance, evaluates the effectiveness of our method based on heavy metals extracted and valorized. Indeed, we do not think that to decontaminate the soil, because of its market value, allows to transfer the contamination to a lower value site, such as burial in the bottom of a mine, encased in concrete. So we conducted laboratory and pilot tests have demonstrated the feasibility of the process. From these tests we revealed the behavior of some polymer materials whose performance depends on pH. Another interesting aspect is the presence of salts such as NaCl, which increases the efficiency of leaching. The proposed method allows large separations of heavy metals (greater than 95%) and at the same time a small separation of monovalent salts like NaCl and good permeability to acids such as hydrochloric acid. These important properties and good resistance of new membranes to acidic conditions make this type of process very promising. In this case we can reuse the treated water to leach again, with the possibility to adjust the pH by concentrating. The fact that H+, Na+, Cl- can be transported with water in the pores, while heavy metals can not, is very important from the viewpoint of exergy balance because the motive force is much lower than if there were no salts or that the salts were separated by the process. Heavy metals contained in the other stream can be recovered by selective precipitation and/or electroplating. The net process balance uses no water, very little acid and salts which play the same role as a catalyst. The metals are recovered and recycled. No release is then issued and we have a clean process (clean technology) without discharge, consumption of chemical products and with low energy consumption.

Further tests were carried out successfully on various wastewater contaminated with hydrocarbons, heavy metals, trichlorethylene, etc.

4.2 Waste water containing glycols

Used in the industry as a coolant or antifreeze, or in airports, aqueous solutions of glycol are recovered and should be treated. Often, the bioreactors are used because of the good biodegradability of glycols, in other cases of authorization certificates are issued for

discharging it with municipal wastewater. The advantage to reuse these glycols appeared in the 90s and processes such as distillation have been developed and installed sometimes on an industrial scale. However, the investment costs are high and these methods consume a great amount of energy. As with other applications users want absolutely recycled glycols but pure. What is remarkable with the aqueous solutions of glycol is their maximum efficiency depending on temperature and concentration. Pure glycols do not have antifreeze properties, but, when mixed with water the properties become very interesting. From a point of view of exergy, it will depend on concentration. In an initial step, preparing solutions with nanopure water and suitable additives for use, the wastewater collected as soon as possible after use can be treated, adjust with new additives and reused in the process. We designed a process that first removes suspended solids, then sterilizes water and purifies both the water and glycol. What makes this operation possible, is a judicious combination of pore size and affinity of the polymer to water and glycol. Osmotic pressure, as well as the boiling point of a glycol solution varies greatly with the concentration of glycol in the solution. The purified solution is then concentrated to the desired value, and the required additives are adjusted.

4.3 Wastewater from the electronics industry

In the electronics industry, we had the opportunity to design, fabricate and test a pilot process to treat wastewater from baths where are engraved printed circuits. This wastewater comes from purges of the baths necessary to adjust the concentration of copper by compensating the purge volume by an aqueous solution of hydrochloric acid pH = 0 with H_2O_2. When this is done daily or weekly the bath cannot function at the optimum, but in a range around the optimum point. Therefore a continuous treatment maintaining optimum conditions of the engraving bath is wished for. This is the type of treatment we designed by recycling the treated solution. We determined the characteristics of the treated solution corresponding to those of the optimum bath. The copper extracted corresponds to the copper taken off printed circuit boards during their passage through the engraving bath. the Development by manufacturers of membrane module resistant to these conditions of pH and aggressiveness of the solution enabled us to design this process. Another aspect arising from the exergy analysis is that we could modify the pore size to allow the system to perform the required separation. For example, if the optimum concentration of Cu is 12%, as it increases to 15% for treatment, one must add the same flow rate for the solution at 10% of Cu to recover the optimal operating conditions followed by the extraction of copper.

The system must operate to meet these conditions (entry 15%, output 10%). Exergy analysis indicates that the motive force is depending on the concentration difference thus 15-10 = 5%. Indeed, if we wanted to perform a separation of 15% to 0%, the osmotic pressure would be too large and the current systems cannot perform this operation. The concentrate is then processed in a new process of electrofiltering that will allow, due to an electrical field as motive force, to transfer the excess copper in sulfuric acid solution which is the fluid of the plating process for the preparation of plates of printed circuits. Transferred copper is of excellent quality and there is no need for mineral extraction and processing. The resource is there and the quality is perfect.

Other cases were treated and in all these cases the exergy analysis guided the design. Adjusting of the pore size and the strengthening of affinities are the keys to the feasibility of these processes. An interesting and important case is the continuous growth of modern membrane engineering, whose basic aspects satisfy the requirements of process

intensification. Membrane operations—with the intrinsic characteristics of efficiency, high selectivity and permeability for the transport of specific components, compatibility between different membrane operations in integrated systems, low energetic requirements, good stability under operating conditions and environment compatibility, easy scale-up, and large operational flexibility—represent an interesting answer for the rationalization of chemical and industrial productions (Drioli & Giorno, 2010).

5. Conclusion

Today we can say that the theoretical means, models and technological tools are available to address the wastewater management in the context of sustainable development, starting by seeing it as a resource not to lose provided it is recovered in time.

Year 2010 recent environmental disasters are proof that we must reconsider how the industries that use water as process fluid or generate wastewater must proceed. A plant must be regarded as a system subjected to analysis of the exergy balance. For a long time in Canada and worldwide, the paper mills were established near rivers that carried the trunks of trees and supplied the mills, large consumers of water and energy. But a simple balance shows, and experience has shown it before, the timber itself contains more water than is needed for the process and unused parts have sufficient heating value to operate the plant and even provide energy to spare. Some plants have shown that circuit closure was possible and co-generation is commonplace, although there is still room for improvement.

The storage of hazardous materials shall be subject to security criteria and restricted to minimum volumes. In the past, and even now, the custom is to subtract of the costs of production the costs of wastewater treatment, considered to be prohibitive. Releases to the environment, moves to areas of lesser geopolitical regulations, hidden storage and number of irresponsible actions are part of the arsenal of industrial strategies. Sustainable development is increasingly entered into government policies. Indeed, it is extremely difficult, with a growing consumption (see the last sixty years), to turn the tide and act the opposite of traditional ways. Anthropic development has always been to make the most of resources with the least effort considering the nature as inexhaustible.

Those days are coming to an end: the deterioration of the ozone layer, the increase of CO_2 in the atmosphere and its corollary that is the decrease of oxygen O_2, oil resources, the reduction of forest areas, limiting cropland, dwindling water tables, melting glaciers are phenomena of global impact. It was not that long the earth was flat and the discovery of new worlds left to the imagination leisure to wander.

However, since the 70s, in some industrial countries, pollution of rivers, which had become veritable open sewers, has fallen sharply and even does not exist anymore. Two main reasons: the closure of many factories in the steel, textile, pulp and paper, primary processing; and the major effort to restore watercourses. Rising land prices, especially in urban areas, led to the rehabilitation of soils contaminated with hydrocarbons, buried waste or wastewater from old incinerators that produce toxic leachate continuously flowing into rivers or mingle to groundwater.

It has long been considered, even now, that wastewater is a necessary evil, it must be addressed without additional costs and if we can postpone their treatment may be that Mother Nature will do the job. Unfortunately it shows its limits today. The Gulf of Mexico, so large yesterday, appears today in 2010, as a large pool soiled with oil at the surface along the coast, in depth and even between two waters. Artificial lakes of wastewater from mines

and oil sands alarm more and more in Canada. Salt-laden discharges following the desalination of sea water are visible from the air and affect the ecosystem. Realize that all wastewater must be treated as a new resource allows, in context, analyze its potential for valorization. Understand that the theoretical tools, mathematical models, computer simulations exist, know the rapid development of nanotechnology applied to this area as a means to act, will open the way for sustainable development without creating a new burden for generations future but by allowing them to expand these new intensive processes to maintain and improve their lifestyle.

Over one billion people lack access to clean water is a famous phrase a thousand times repeated by everyone and attributed to a report by the WHO or the UN in 1999. Since the world population increased from 6 to 7 billion and the number of people without access to drinking water has exceeded the 1.5 billion. For a long time the lack of potable water was associated with to a water shortage, which is the case in desert regions. It was also considered that the only way to access water was to dig wells.

One wonders now if the Nile can supply all of its residents. In fact, in most cases, water is available, but it is wastewater. The technologies exist to extract from the wastewater the vital resource, drinking water.

Energy, water, food and oxygen are our main resources and are not ready to be virtual. They represent the inevitable challenges of growth of humanity.

6. References

Agre, P., MacKinnon, P., (2003). Membrane Proteins: Structure, Function, and Assembly. *Presented at the Nobel Symposium* 126, Friibergh's Herrgård, Örsundsbro, Sweden, (August 23, 2003),

Allard, G., (1998). Application de l'osmose inverse à l'eau d'érable : Évaluation de membranes dans un prototype québécois. Technical Report, *Ministère de l'Agriculture, des Pêcheries et de l'Alimentation du Québec*. p.25-30 (1998),

Bird, R.D., Stewart, W.E., Lightfoot, E.N., (2002). Transport Phenomena, *John Wiley*, (2003),

Brodyansky, V.M., Sorin M., LeGoff, P., (1995). The Efficiency of Industrial Processes, Exergy Analysis and Optimization, *Elsevier Science Publishers B.V.*, 487p, (1995),

Choi, J. H., Fukushi, K., Ng, H. Y., Yamamoto, K., (2006). Evaluation of a long-term operation of a submerged nanofiltration membrane bioreactor (NF MBR) for advanced wastewater treatment, Water Sci. & Technol., 53(6), 131-136, (2006),

Drioli, E., Giorno, L., (2010). Comprehensive Membrane Science and Engineering. *Elsevier Science Publishers* , 2000 p., (2010) ISBN: 9780444532046

Gibbs, J. W., (1928). The Collected Works of J. Willard Gibbs. *Longmans: New York*, (1928),

Sourirajan, S. and Matsuura, T., (1985). Reverse Osmosis/Ultrafiltration Process Principles. *National Research Council Canada*, 113 p., (1985),

Le-Clech, P., Chen, V., Fane, A.G., (2006). Fouling in membrane bioreactors used for wastewater treatment – A review. *Journal of Membrane Science*, 284, 17-53, (2006),

Vrbka, L., Mucha, M., Minofar, B., Jungwirth, P., Brown, E. C., Tobias, D. J., (2004). Propensity of Soft Ions for the Air/Water Interface. *Current Opinion in Interface and Colloid Science*, 9, 67, (2004).

Immobilization of Heavy Metal Ions on Coals and Carbons

Boleslav Taraba and Roman Maršálek
University of Ostrava
Czech Republic

1. Introduction

Adsorption of heavy metals from the aqueous phase is a very important and attractive separation techniques because of its ease and the ease in the recovery of the loaded adsorbent. For treatment of waste as well as drinking water, activated carbons are widely used (Machida et al., 2005; Guo et al., 2010). Due to an increasing demand on thorough purification of water, there is a great need to search for cheaper and more effective adsorbents. Thus, alternative resources for manufacturing affordable activated carbons are extensively examined (e.g. Guo et al., 2010; Qiu et al., 2008; Giraldo-Gutierrez & Moreno-Pirajan, 2008). Simultaneously, natural coals are investigated as economically accessible and efficient adsorbents to remove heavy metals (Kuhr et al., 1997; Zeledon-Toruno et al., 2005; Mohan & Chander, 2006).

Radovic et al. (2001) published a principal comprehensive review of the adsorption from aqueous solutions on carbons with incredible 777 references. Their analytical survey covers adsorption of both organic and inorganic compounds (including heavy metals) and, certainly, it remains a basic source of information on the topics.

This chapter is concerned with the immobilization of heavy metals on carbonaceous surfaces, and, it attempts to compare adsorption behaviour of activated carbons with that of natural coals. Here, references published in the last decade are mainly reported, the literature findings being immediately confronted with experimental data as obtained from laboratory examinations of two natural coals. First, a brief insight into adsorption kinetics is given, followed by a survey of models to describe adsorption at equilibrium. The issue of thermodynamics of heavy metals adsorption follows. Finally, the possible immobilization mechanisms of heavy metals on carbons/coals are carefully considered and discussed.

2. Sample basis and experimental approaches

A sample of bituminous coals from the Upper Silesian Coal Basin (denoted as OC) and a sample of low rank subbituminous coal (SB) from the North Bohemian Coal District were investigated. Sample OC represents a type of oxidative altered bituminous coal, the occurrence of which is connected with changes in the development of coal seams underground. These changes are due to oxidation and thermal alteration processes, and they took place in the post-sedimentary geological past (Klika & Krausova, 1993). Because of increased content of oxygen, the oxidative altered bituminous coal should be of increased

ability in cation exchange. Thus, their potential to remove heavy metals from aqueous solutions is expected to be comparable with that of subbituminous coal SB, the effectiveness of low rank coals for heavy metals adsorption having already been reported (Kuhr et al., 1997). Basic analyses and properties of the coal are summarised in table 1.

	Sample OC	Sample SC
Ash content (%, dry basis)	11.5	8.0
Elemental composition		
C (%, daf basis)	76.6	74.4
H (%, daf basis)	4.1	6.5
N (%, daf basis)	1.8	1.0
O_{dif} (%, daf basis)	15.1	16.8
S_{total} (%, dry basis)	2.4	1.2
Textural parameters		
Surface area, BET (m^2/g)	1.5	49
Volume of micropores (ml/g)	0.084	0.055
Carbon aromaticity, f_C	0.97	0.50
Iso-electric point, pH_{IEP}	1.6	2.4
Mineral composition in ash (%)		
CaO	22.7	4.0
SiO_2	8.8	51.2
Al_2O_3	7.4	27.5
Fe_2O_3	21.9	6.4
MnO	0.1	0.01
MgO	3.3	0.8
TiO_2	0.1	3.2
V_2O_5	0.03	0.15

Table 1. Analyses and properties of the studied coal samples; BET surface areas were determined from adsorption isotherm of nitrogen at -196°C; volumes of micropores were evaluated from carbon dioxide isotherm at 25°C using Dubinin-Radushkevich model; carbon aromaticities were determined from ^{13}C CP/MAS NMR measurements using Bruker Avance 500 WB/US spectrometer (Germany) at 125 MHz frequency; pH values of iso-electric point were ascertained from zeta-potential measurements by Coulter Delsa 440 SX analyser (Coulter Electronic, USA)

Basic adsorption investigations were performed using lead(II) ion as a representative of heavy metals. Preferential adsorption ability of coals for heavy metals was studied with Cd(II), Cu(II) and Pb(II) cations (nitrate salts). Both for equilibrium adsorption and kinetics examinations, 0.5 g of dried sample (grain size 0.06-0.25 mm) was added to 50 mL of adsorbate solutions of initial concentration to be given. The suspensions were continuously (kinetics measurements) or occasionally (equilibrium adsorption) shaken. The pH value of each suspension was measured using a combination single-junction pH electrode with Ag/AgCl reference cell. Adsorption equilibration usually took 5 days. Then, the coal sample was removed by filtering through a paper filter. Metal concentration of filtered solutions was determined by means of the ICP optical emission spectrometry (Perkin-Elmer Optima 3000 spectrometer). All adsorption measurements were at least duplicated. In addition to

the basic measurements, some other experiments were performed and they are briefly reported in the appropriate sites of this chapter.

3. Kinetics of adsorption of heavy metals on coals and carbons

The study of adsorption kinetics is significant as it provides valuable information (at least) on time required for equilibration of the adsorption system. Thus (e.g. for adsorption of Pb(II) on activated carbons or coal), one can see in literature equilibration time elapsing from one hour (Imamoglu & Tekir, 2008) to two hours (Lao et al., 2005) to 48 hours (Song et al., 2010) or even up to 7 days (Giraldo-Gutierrez & Moreno-Pirajan; 2008). In a more detailed view, the kinetics of adsorption process on porous solid is controlled by three consecutive steps (Baniamerian et al., 2009; Mohan & Chander, 2006; Mohan et al., 2001): (i) transport of the adsorbate from the bulk solution to the film surrounding the adsorbent, (ii) diffusion from the film to the proper surface of adsorbent, and (iii) diffusion from the surface to the internal sites followed by adsorption immobilization on the active sites. Some authors aimed at expressing the kinetics of the individual diffusion steps (e.g. Oubagaranadin & Murthy, 2009; Qadeer & Hanif, 1994). In most cases, however, adsorption kinetics is considered as a global process. To express the adsorption kinetics quantitatively, three kinetic models are mainly used:

i. A simple first-order reaction kinetics (El-Shafey et al., 2002; Kuhr et al., 1997), which can be expressed generally as:

$$\ln(c_t) = \ln(c_o) - k_a \cdot t \tag{1}$$

where c_t is the concentration of metal ions to be adsorbed (mmol/L) at time t (min), c_0 is the initial concentration of the ions (mmol/L) and k_a is the rate constant of adsorption at given temperature (1/min). Plotting the $\ln(c_t)$ versus t, it is then possible to obtain a straight line with the slope corresponding to the value of rate constant k_a.

ii. The pseudo-first order kinetic model given by Lagergren equation (Eq. (2)), e.g. Boudrahem et al., 2009; Shibi & Anirudhan, 2006; Erenturk & Malkoc, 2007:

$$\ln(a_e - a_t) = \ln(a_e) - k \cdot t \tag{2}$$

where a_e and a_t are the adsorbed amounts of ions (mmol/g) at equilibrium time and any time t (min), respectively, and k is the rate constant of adsorption (1/min). Again, the rate constant k can be obtained from the slope of $\ln(a_e - a_t)$ versus t plots.

iii. The pseudo-second order model assuming the driving force for adsorption to be proportional to the available fraction of active sites (Oubagaranadin & Murthy, 2009). In the linear form the pseudo-second order rate equation can be expressed as:

$$t/a_t = 1/(k_2 \cdot a_e^2) + t/a_e \tag{3}$$

where k_2 is the rate constant of pseudo-second-order adsorption (g/mmol.min). Its value can be determined experimentally (together with equilibrium adsorption capacity a_e) from the slope and intercept of plot t/a_t versus t (Li et al., 2009; Shibi & Anirudhan, 2006). As confirmed by the authors that applied several kinetic models to analyse experimental data, the pseudo-second order kinetics usually gives the tightest courses with the adsorption data to be measured (Erenturk & Malkoc, 2007; Li et al., 2009).

Our study of adsorption kinetics of lead(II) ions was performed on subbituminous and bituminous natural coals (SC and OC) at temperatures of 30 and 60°C. For the experiments, solutions with initial concentration of lead(II) ions = 5 mmol/L were used, sample grain size was 0.06 - 0.25 mm. Ratio between mass of the sample and volume of the lead(II) ions solution was 0.5 g/50 mL. Time elapsed during the measurements was 2.5 hours, each dependence being at least triplicated. For the initial stage of lead(II) adsorption, kinetics was found to satisfactorily follow a simple first-order reaction for both temperatures giving coefficients of determination R^2 better than 0.98, cf. fig 1.
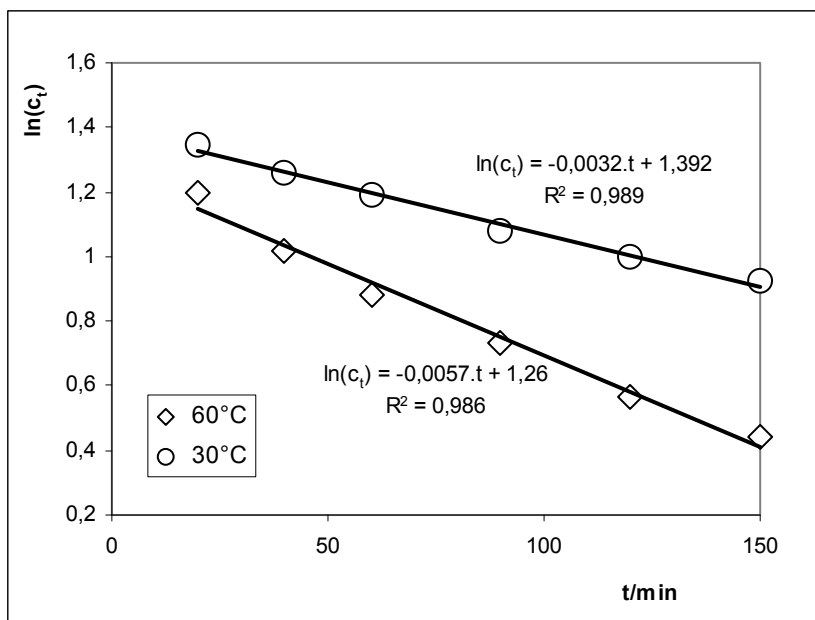
Fig. 1. Kinetic plots of lead(II) adsorption on bituminous coal OC, coal grain size 0.06-0.25 mm, initial concentration of lead(II) ions = 5 mmol/L

From the slopes of the linear plots $\ln(c_t)$ versus t, values of the adsorption rate constant k_a were calculated (see table 2).

Sample	Temperature	Rate konstant k_a (1/min)
SC	30°C	$(4.8 \pm 0.5) \cdot 10^{-4}$
	60°C	$(8.4 \pm 2.5) \cdot 10^{-4}$
OC	30°C	$(3.2 \pm 0.7) \cdot 10^{-3}$
	60°C	$(5.7 \pm 1.5) \cdot 10^{-3}$

Table 2. Rate constants as evaluated from kinetic measurements at 30 and 60°C

We are aware of difficulties in comparing such values of k_a with published data as they depend on experiment conditions, namely on the ratio between mass of adsorbent and the volume of metal solution. Nevertheless, using the Arrhenius equation, the knowledge of the adsorption rate constants at different temperatures enables us to estimate values of the

activation energy of lead(II) adsorption E. Thus, activation energies of 15.7 kJ/mol and 16.2 kJ/mol were found for sample of SC and OC, respectively. Such values of E correspond with the general view on energetics of the adsorption process (Adamson & Gast, 1997), and they are close to 17.1 kJ/mol obtained by Kuhr et al. (1997) for cobalt (II) adsorption on lignite. They are also quite comparable with activation energy 12.3 kJ/mol as was found by Li et al. (2009) for lead(II) adsorption on modified spent grain; however, their interpretation that "positive value of E suggests …the adsorption process is an endothermic in nature" is hardly acceptable.

4. Adsorption of heavy metals on coals/carbons at equilibrium

4.1 Adsorption isotherms

An overwhelming majority of authors correlate their data on metal ion sorption at equilibrium with the Langmuir adsorption model of monolayer coverage (e.g. Mohan & Chander, 2006; Oubagaranadin & Murthy, 2009). In a linear form, the Langmuir equation is given as:

$$c/a_e = c/a_m + 1/(a_m \cdot K) \tag{4}$$

where a_e is the equilibrated amount of the metal ion adsorbed at concentration c (mmol/L) of the ion in solution; K represents monolayer binding constant (L/mmol) and a_m is the monolayer adsorption capacity (mmol/g).

A similarly preferred model to analyse adsorption data, as that of Langmuir is the Freundlich isotherm (Li et al., 2005; Erenturk & Malkoc, 2007; Machida et al., 2005). It is also a two-parameter equation that can be, in the linearized form, presented as:

$$\ln(a_e) = (1/n) \cdot \ln(c) + \ln(K_F) \tag{5}$$

where n, K_F are the Freundlich constants. Constant K_F can be denoted as adsorption capacity (Erenturk & Malkoc, 2007; Machida et al., 2005), and its value corresponds to adsorbed amount in the solution with concentration c = 1 mmol/L.

In comparison with Langmuir and Freundlich models, further adsorption isotherms are used with considerably lower frequency. Thus, Sekar et al. (2004) or Erenturk & Malkoc (2007) correlated data on lead(II) adsorption using the Temkin isotherm:

$$a_e = B \cdot \ln(c) + B \cdot \ln(K_T) \tag{6}$$

where K_T is the Temkin constant and B is the parameter related with linear decrease in heat of the adsorption (Asnin et al., 2001). Similarly, also for adsorption of lead(II) ions, Oubagaranadin & Murthy (2009) or Li et al. (2009) used Dubinin-Radushkevich (D-R) isotherm:

$$\ln(a_e) = \ln(a_{mi}) - D \cdot \ln^2(1+(1/c)) \tag{7}$$

where a_{mi} is the D-R adsorption capacity (originally ascribed to adsorption in micropores, (Adamson & Gast, 1997)) and D is the constant related with free energy of adsorption.

In general, it should be stressed that all the above-mentioned adsorption isotherm equations (4) - (7) were originally developed for adsorption of gases (vapours) on solid surfaces (Adamson & Gast, 1997). Thus, their usage to analyse data on adsorption behaviour of metal ions on carbons/coals should be treated carefully, mainly as far as the physical meaning of

the obtained parameters is concerned. This can be demonstrated, for example, by evidently inconsistent values of adsorption heat of lead(II) ions on activated carbon as were published by Sekar et al. (2004). Namely, using parameter B from the Temkin equation (6), heats of adsorption between -125 and -302 J/mol were obtained. On the other hand, using thermodynamic analysis of the same adsorption system, they came to the value of adsorption heat +93 420 J/mol. The most valuable and widely used parameter from the above models is obviously adsorption capacity a_m derived from Langmuir isotherm (4) that enables to quantify adsorption potential of the carbons/coals to individual metal ions. However, also this parameter is certainly "valid for a very limited set of operating conditions (e.g., constant pH)" as pointed out by Radovic et al. (2000).

Based on our measurements of lead(II) equilibrium adsorption on bituminous coal OC at temperatures 30, 60 and 80°C, we have tried to compare consistency of the obtained data with the above-mentioned adsorption models (4) - (7). Experimental courses of the lead(II) adsorption isotherms are graphically presented in figure 2.
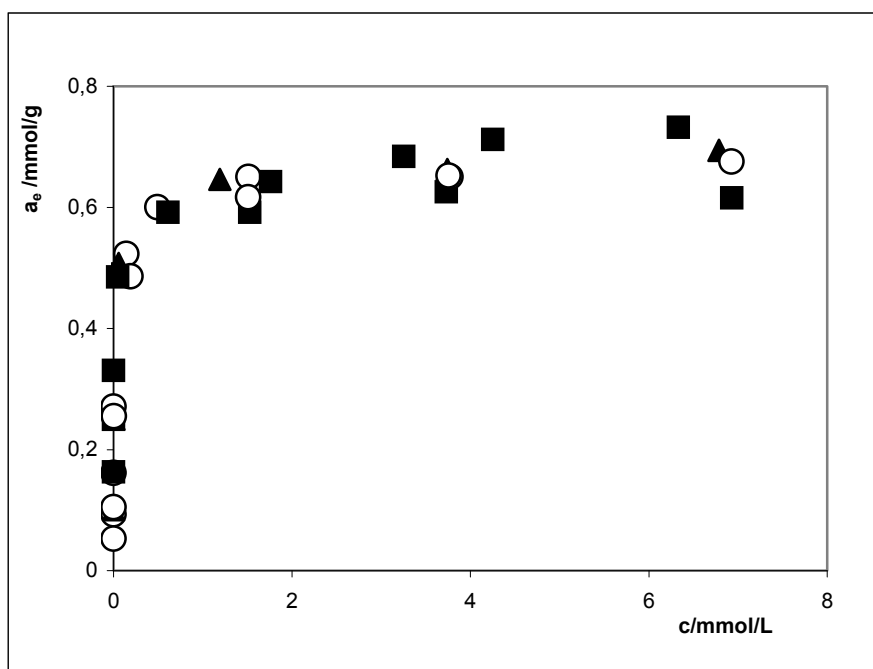
Fig. 2. Adsorption of lead(II) ions on bituminous coal OC at temperatures 30°C (■), 60°C (o) and 80°C (▲), coal grain size 0.06 – 0.25 mm, pH of solution at equilibrium 3.5, equilibration time 120 h.

Linearized forms of the isotherm equations (4) – (7) were applied to regression analysis of the adsorption data. Using the slopes and intercepts of the plots, the adsorption constants and model parameters were then evaluated. The values including coefficient of determination R^2 are given in table 3.

Isotherm type	Parameter	30°C	60°C	80°C
Langmuir	a_m (mmol/g)	0.69	0.67	0.69
	K (L/mmol)	14	27	25.5
	R^2	0.992	0.999	0.999
Freundlich	K_F (L/g)	0.60	0.59	0.58
	n	6.5	5.2	5.6
	R^2	0.872	0.880	0.850
Temkin	B	0.053	0.057	0.061
	K_T (L/g)	1.83	1.81	1.84
	R^2	0.970	0.975	0.962
Dubinin - Radushkevich	a_{mi} (mmol/g)	0.67	0.62	0.68
	D	0.0198	0.0199	0.032
	R^2	0.958	0.977	0.968

Table 3. Parameters of isotherm models, adsorption of lead(II) on coal OC (cf. Fig. 2)

As can be deduced from table 3, high values of the coefficient R^2 indicate practical applicability all of the above models. The equilibrium adsorption data are consistent mainly with the Langmuir model giving values of R^2 closest to 1. Conformity of the adsorption data with the Langmuir equation as the best fitting model is usually reported (Erenturk & Malkoc, 2007). However, we are aware that other sophisticated statistical approaches should be used to make the analysis more convincing (Boudrahem et al., 2009). With respect to the parameters resulting from the analysis, it is worth mentioning that the values of monolayer adsorption capacities a_m from Langmuir isotherm are consistent with adsorption capacities a_{mi} from the D-R equation. Simultaneously, they are quite comparable with values of adsorption capacities K_F of the Freundlich model indicating that the adsorption capacities are basically reached at equilibrium concentration c = 1 mmol/L, i.e. according to the shape, the isotherms can be denoted as those of the H-type (high affinity, Qadeer et al., 1993).

4.2 Preferential adsorption of metal ions

What type of metal ion is immobilized on carbon/coal surface more preferably than the other ones is a question of great practical importance. In this respect, the Irving-Williams series is often referred to, showing that the adsorption selectivity of ions follows the stability order of metal – ligand complex formation (Murakami et al., 2001; Kuhr et al. 1997). Guo et al. (2010) confirmed the adsorption of metal ions on carbons to proceed exclusively through surface complexation regarding the importance of acidic functional groups in the complexation reactions. However, published series of metal ions adsorption affinities differ for various types of carbon/coal. For example, for activated carbon from flax shive, El-Shafey et al. (2002) found the following sequence in adsorption capacities: Cu(II) > Pb(II) > Zn(II) > Cd(II). On the other hand, for poultry litter-based activated carbon, Guo et al. (2010) came to the series: Pb(II) > Cu(II) > Cd(II) ≈ Zn(II). Evidently, adsorption selectivity of the ions to carbons/coals should be perceived as a more complex problem reflecting both textural parameters of sorbents and ionic properties such as electronegativity, ionization potential and ionic radius (Lao et al., 2005).

Our experimental study was focused on adsorption selectivity of lead(II), cadmium(II) and copper(II) ions on bituminous coal OC. All the ions were supplied as nitrate salts. Single-ion solutions were applied for the adsorption equilibrium measurements. The obtained

isotherms were analysed using the Langmuir model (4). Adsorption potential for each ion was expressed using its adsorption capacity a_m. Data are summarised in table 4.

pH	Monolayer adsorption capacity, a_m (mmol/g)		
	Pb(II)	Cu(II)	Cd(II)
3	0.37	0.22	0.11
5	0.75	0.61	0.39

Table 4. Adsorption capacities a_m of metal ions on bituminous coal OC at temperature 22°C, coal grain size 0.06 – 0.25 mm.

From table 4, it is obvious that sorption capacities for the ions are in the order of Pb(II) > Cu(II) > Cd(II). The same order could be expected for competitive sorption of the ions from their mixture in solution (Rao et al., 2007). An identical sequence of the three metals was found by Guo et al. (2010) for litter-based activated carbon, and it also agrees with the order published by Rao et al. (2007) for carbon nanotubes.

To elucidate different adsorption behaviour of lead(II), cadmium(II) and copper(II) ions from the point of varieties present in the solutions, we have performed species analysis. Namely, based on the values of the proper stability constants, percentages of hydrolyzed [Me(OH)$^+$] and nitrate [Me(NO$_3$)$^+$, Me(NO$_3$)$_2$] species of the studied ions were evaluated. Thus, at a pH of 5, concentrations of hydrolyzed species of all ions were found to be insignificant, with Me(OH)$^+$ < 0.2 %. Similarly, only small amounts of dinitrate species (Me(NO$_3$)$_2$ < 0.8 %) were ascertained for the ions at maximum concentration of nitrate anions in the solutions to be investigated, i.e. at (NO$_3$)$^-$ = 0.02 mol/L. More significant contents were found only for mononitrate complexes Me(NO$_3$)$^+$, namely, Cu(NO$_3$)$^+$ ≅ Cd(NO$_3$)$^+$ ≅ 6 %, and Pb(NO$_3$)$^+$ ≅ 23 %. Thus, evidently, hydrated forms of "free" metallic ions predominate in the solutions with percentages of about 93% for Cu(II) and/or Cd(II) ions, and 76 % for Pb(II). According to the most probable hydration numbers of the ions (Marcus, 1997), the following hydrated species appear to be mainly present in the solutions: Cu(H$_2$O)$_{10}$, Cd(H$_2$O)$_{7-11}$ and Pb(H$_2$O)$_6$. From this point of view, the greatest adsorption capacity observed for lead could relate to its small hydration shell, the loss of which (during adsorption process) consumes the smallest enthalpic effect in comparison with the other hydrated cations (1572 kJ/mol instead of 1833 and 2123 kJ/mol for Cd(H$_2$0)$_{7-11}$ and Cu(H$_2$0)$_{10}$, respectively (Marcus, 1997)).

Finally, within the section, we have compared the adsorption potential of the different carbons/coals for heavy metals as were found in the literature. As a representative of the heavy metals, lead(II) ion was chosen because of its evident affinity to carbonaceous surface. Simultaneously, the adsorption behaviour of this very metal ion has been frequently reported in literature (e.g. Machida et al., 2005; Song et al., 2010; Li et al., 2009). Such a comparison is summarised in table 5, adsorption potential of the carbon/coal for lead(II) ion being expressed (again) by monolayer adsorption capacity a_m as evaluated from the Langmuir isotherm.

In general, lower adsorption capacities of activated carbons than those of natural coals can be deduced from the table 5. However, both coals referred to (Leonardite, sample OC) should be stressed to represent low rank coal types with an increased ability to immobilize metal ions. A closer look into the question will be given within section 6 of this chapter.

Sorbent	pH	d (mm)	t (°C)	a_m mmol/g)	Reference
AC from sal wood	4	-	30	0.04	Oubagaranadin, 2009
Modified spent grain	5.5	< 0.355	25	0.165	Li et al., 2009
Coal-based AC	5.5	0.125-0.25	25	0.15	Machida et al., 2005
Oak-based charcoal	5.5	0.125-0.25	25	0.096	Machida et al., 2005
Coconut-based AC	5.8	< 60 mesh	25	0.11	Song et al., 2010
AC from coffee res.	5.5	< 0.063	25	0.31	Boudraham et al., 2009
AC from hazelnut husk	5.7	0.5 - 2	18	0.063	Imamoglu et al., 2008
AC from sugar cane husk	5	0.2 – 0.3	Lab.	0.41	Giraldo-Gutierrez, 2008
Low rank coal -Leonardite	5-6	0.09 – 0.2	Lab.	1.21	Lao et al., 2005
Bituminous coal (OC)	5	0.06–0.25	22	0.75	This study (cf. table 3)

Table 5. Comparison of carbons/coals abilities to lead(II) adsorption as published in the literature, d – grain size diameter, t – temperature, a_m – monolayer adsorption capacity, AC – activated carbon

5. Thermodynamics of heavy metals adsorption

Thermodynamic analysis should provide information on the energetics of the adsorption process. As basic thermodynamic parameters, changes in Gibbs energy ΔG (J/mol), enthalpy ΔH (J/mol) and in entropy ΔS (J/(mol · K)) for the adsorption process are usually calculated. As a rule, such calculations arise from fundamental thermodynamic equation for Gibbs energy:

$$\Delta G = - R \cdot T \cdot \ln(K_a) \tag{8}$$

where R is the universal gas constant (8.314 J/(mol K), T is temperature (K) and K_a is the thermodynamic equilibrium constant.

Enthalpy change ΔH and change in entropy ΔS is possible to evaluate from the slope, respectively from the intercept of the linearized dependence of equilibrium constant K_a on temperature in coordinates $\ln(K)$ versus $1/T$:

$$\ln(K_a) = - \Delta H/(R \cdot T) + \Delta S/R \tag{9}$$

Formula (9) is known as van´t Hoff equation, and it was derived provided that ΔH as well as ΔS are invariables within the temperature interval to be studied.

Both of the above equations (8) and (9) deal with thermodynamic equilibrium constant K_a of the adsorption process. Thus, of course, the result of such thermodynamic analysis strongly depends on reliability of the K_a determination. In literature, several possibilities to evaluate the equilibrium constant of adsorption have been published; however, not one of them was generally accepted and recommended for such thermodynamic analyses.

As equilibrium constant K_a, most of the authors accept the value of the Langmuir constant K ascertained from the Langmuir model applied to equilibrium adsorption data (Kuo, 2009; Mohan et al., 2001; Shibi & Anirudhan, 2006; Kuhr et al., 1997; Mohan & Chander, 2006). Although the "proper" thermodynamic equilibrium constant K_a should be dimensionless, Klucakova & Pekar (2006) indicate the way how to consider the Langmuir constant (with usual dimension L/mmol, cf. eq. (4)) even for the thermodynamic analysis.

Another approach to estimate the value of equilibrium constant K_a arises from determination of the ratio (denoted also as distribution coefficient K_D) between adsorbed amount a_e and concentration c of the metal ion in equilibrium, $a_e/c = K_D$ (Li et al., 2009; Erenturk & Malkoc, 2007). However, a more sophisticated procedure to estimate equilibrium constant K_a using the coefficient K_D appears to be plot a_e/c versus a_e and extrapolate it to zero a_e. The approach was used by Li et al. (2005) and Sekar et al. (2004) for thermodynamic analysis of lead(II) adsorption.

As resulted from the literature studied, analyses of all adsorption systems confirmed negative values of changes in Gibbs energy giving thus thermodynamic evidence of feasibility and spontaneous nature of metal ions adsorption on carbons/coal. Concerning changes in enthalpy ΔH and entropy ΔS, however, the situation is not so clear. Practically only for immobilization of mercury(II) on activated carbon (Mohan et al., 2001), the adsorption was confirmed to be exothermic ($\Delta H = -23.6$ kJ/mol) and entropy decreasing ($\Delta S = -20.5$ kJ/mol·K [sic]) process. In principle, such changes in enthalpy and entropy are consistent with the "classical" view on the thermodynamics of the adsorption process. For all other cases, adsorption of metal ions was found to cause an increase in entropy with values of ΔS from $+26$ J/mol·K (adsorption of Pb(II) on carbon nanotubes, Li et al., 2005) to $+312$ J/mol·K (adsorption of Pb(II) on activated carbon, Sekar et al., 2004). As a rule, the positive value of ΔS is explained by increased randomness at the solid-solution interface during adsorption of the metal ion on a carbon/coal surface (Li et al., 2009; Erenturk & Malkoc, 2007; etc.). On the other hand, it is not so easy to explain endothermicity of the process, as was thermodynamically confirmed e.g. for adsorption of Cu(II) ions (Kuo, 2009), Fe(II) ions (Mohan & Chander, 2006), Cd(II) ions (Shibi & Anirudhan, 2006) or Pb(II) ions (Li et al., 2005; Sekar et al., 2004; etc.). Most of the authors give no comment to the finding. Erenturk & Malkoc (2007) as did Qadeer et al. (1993) see the reason of the endothermicity in the change of hydration shells in the environment of the adsorbed and non-adsorbed metal ions. However, as Radovic et al. (2001) indicate, the solution of the aspect appears to be more complicated.

Our study in the field consisted in thermodynamic analysis of the experimental data on Pb(II) ions adsorption on bituminous coal sample OC at temperatures 30, 60 and 80°C (cf. fig. 2). In addition, we have explored our experience with calorimetric techniques, and we have measured values of adsorption enthalpy ΔH to make their comparison with calculated ones possible.

The usage of Langmuir constants K as values of equilibrium constants for the thermodynamic analysis of the Pb(II) ions adsorption on OC sample unfortunately failed. The reason was an unconvincing (non-monotonous) trend in the Langmuir constants with increasing temperature, see table 3. Thus, as equilibrium constants at given temperatures, extrapolated values of a_e/c to zero a_e were evaluated, according to Sekar et al. (2004). For better reading, the dependences of a_e/c versus a_e were plotted in coordinates $\ln(a_e/c)$ versus a_e , see figure 3.

In addition to the a_e/c versus a_e dependences, we have adapted the alternative approach to calculate the distribution coefficient reported earlier by Qadeer & Hanif (1994). Namely, instead of a_e/c extrapolation to zero a_e, ratios $(c_0 - c)/c$ were evaluated and extrapolated to zero uptake (c_0 is the initial concentration of the ions). A certain advantage of such a procedure can be seen in the dimensionless character of the obtained value of equilibrium constant K. Results of the thermodynamic analysis applied to Pb(II) ions adsorption on OC
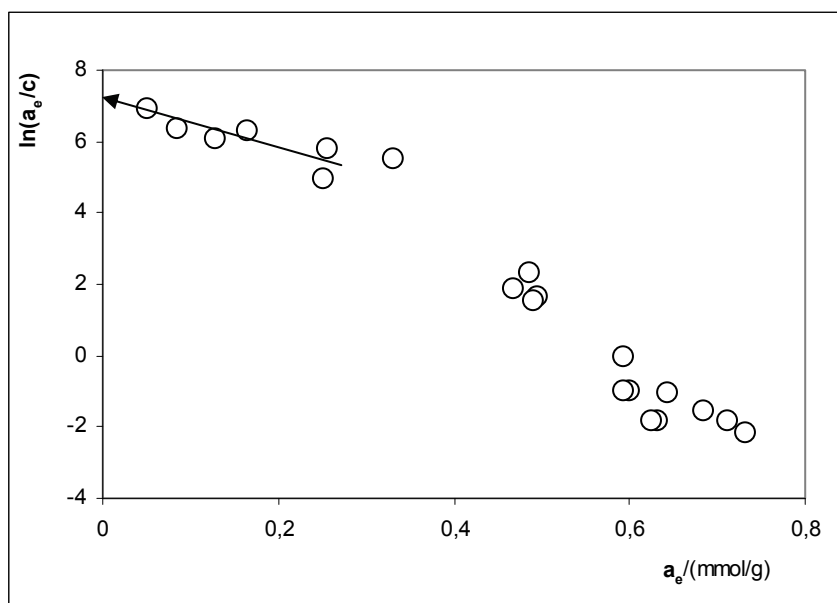
Fig. 3. Dependence of a_e/c versus a_e as obtained for lead(II) adsorption on sample OC at 30°C

sample using both the above-mentioned procedures are summarised in table 6. It is also worth mentioning that regression coefficients R^2 of the plots in coordinates $\ln(K)$ versus $1/T$ to evaluate enthalpy and entropy changes were 0.856 and 0.925, respectively.

temp. °C	a_e/c extrapolated to $a_e = 0$				$(c_o - c)/c$ extrapolated to $a_e = 0$			
	K L/g	ΔG kJ/mol	ΔH kJ/mol	ΔS J/mol·K	K	ΔG kJ/mol	ΔH kJ/mol	ΔS J/mol·K
30	1095	-17.5			11000	-23.5		
60	665	-18	- 28.5	-34.5	5500	-24	-30	- 20.5
80	200	-15.5			1900	-22		

Table 6. Thermodynamic analysis of Pb(II) ions adsorption on OC sample

Irrespective of the different values of "equilibrium constants" K, comparable values of changes both in enthalpy ΔH and (more or less) in entropy ΔS were obtained from the procedures. Quite opposite to the published data, however, values of both parameters were found to be evidently negative. In the context with literature that has been studied, it is the first time when adsorption of Pb(II) ions on carbonaceous surface proved to be exothermic.

In order to check the thermodynamic finding of exothermicity of Pb(II) ions adsorption, we have performed direct calorimetric determination of the adsorption enthalpy. For this purpose, a SETARAM C80 calorimeter equipped with percolation vessel was used. The flow calorimetric technique was adapted when the flow of water (percolating through sample) was changed for flow of Pb(II) ions solution. The corresponding heat effect (related to Pb(II) adsorption) was then determined. Subsequent changeover of Pb(II) ions solution flow back

for water flow then enabled to evaluate desorption heat of the Pb(II) ions from the sample. For the experiments, natural coal samples of OC and SC were used. In addition, a representative sample of activated carbons (denoted as HS3) was investigated. Typical shape of Pb(II) adsorption/desorption calorimetric curve as obtained for subbituminous coal SC is illustrated in figure 4.
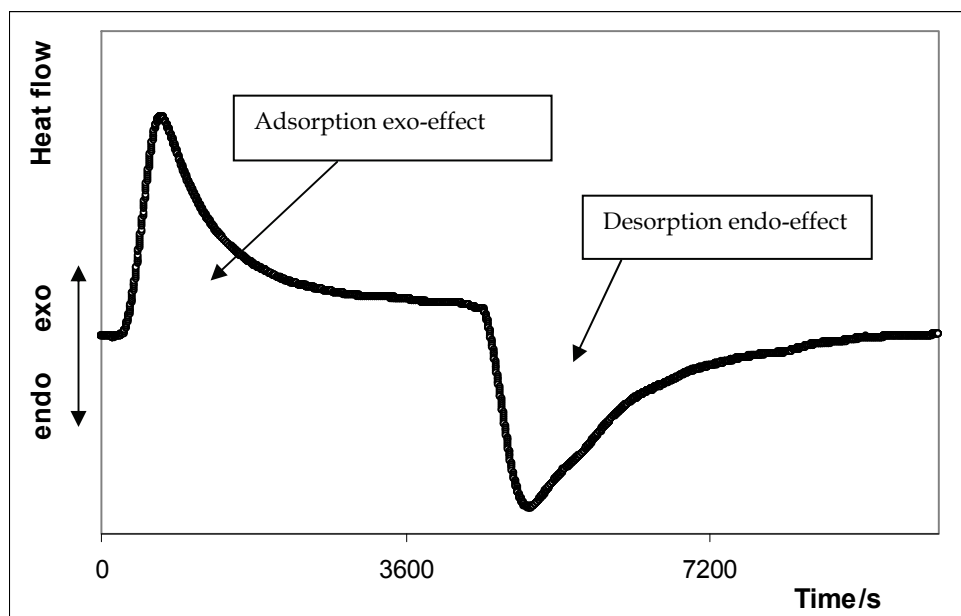
Fig. 4. Calorimetric curve of Pb(II) ions adsorption/desorption cycle ascertained for sample SC, grain size = 0.06 –0.25 mm, temperature = 30°C, Pb(II) ions concentration = 20 mmol/L, flow rate = 0.4 ml/min

No doubt, the performed calorimetric investigations clearly confirmed exothermicity of the Pb(II) ions adsorption (as well as endothermicity of the Pb(II) ions desorption process) for all investigated samples. Comparison of the calorimetric results with adsorbed amounts of the Pb(II) ions determined from adsorption isotherms then made it possible to estimate values of the molar enthalpy changes ΔH. The results are tabulated in table 7.

Sample	Adsorption heat J/g	Adsorbed amount mmol Pb(II)/g	Molar enthalpy ΔH kJ/mol
Coal sample OC	- 1.65	0.7	- 2.5
Coal sample SC	- 0.55	0.09	- 6
Activ. carbon HS3	- 6.3	0.21	- 30

Table 7. Values of molar enthalpy of Pb(II) ions adsorption as estimated from calorimetric and Pb(II) ions uptake measurements at 30°C.

Surprisingly low molar enthalpies for natural coals in comparison with ΔH of activated carbon are evident from the table 7, indicating quite different immobilization mechanisms of

the samples. For highly microporous activated carbon HS3 (volume of micropores = 0.48 mL/g, D-R isotherm of CO_2 adsorption), preferred adsorption in the micropores could be suggested. On the other hand, as will be discussed in more detail in the next section, interaction of the Pb(II) ions with natural coals OC and SC is expected to proceed mainly through oxygen functional groups. Irrespective of the evident disagreement between calorimetrically determined values of ΔH and these calculated from thermodynamic analysis (table 6), the experimentally obtained enthalpies for natural coals OA and SC are quite comparable with values of ΔH as resulted from metal ion versus oxygen group simulations using a semiempirical method of quantum chemistry "INDO", $\Delta H \approx -3$ kJ/mol (Klucakova et al., 2000).

6. Considerations on immobilization mechanism of heavy metals on coals

Radovic et al. (2001) in their analytical review summarize that immobilization of metal ions on carbons is largely governed by electrostatic adsorbate-adsorbent interactions. At values of pH exceeding the level of iso-electric point of carbon (pH_{IEP}), carbonaceous surface gains negative charge and its interactions with positively charged metals begin to be of an attraction character. Thus is reflected a significant role of pH on metal ions uptake, an evident rise in adsorption capacity of carbons to metals with increasing pH being generally known. For analysed coals OC and SC in this case, the influence of pH on lead(II) uptake is illustrated by fig. 5.

As a type of the electrostatic interactions, mainly cation exchange is mentioned, even for range of pH above the value of the iso-electric point (Radovic et al., 2001). A governing role of the ion exchange was confirmed both for activated carbons (Sekar et al., 2004; El-Shafey et al., 2002) and coals (Murakami et al., 2001; Burns et al., 2004). In addition to cation exchange, other possible mechanisms for metal ion immobilization such as surface precipitation or physical adsorption have been mentioned (Le Cloirec & Faur-Brasquet, 2008; Mohan & Chander, 2006). However, as the most probable alternative to cation exchange, surface complexation of metals is referred to (Guo et al., 2010; Zeledon-Toruno et al., 2005; Klucakova et al., 2000). The question thus arises as to the proportion between the cation exchange and the other mechanisms taking part in metal ions immobilization on carbon/coal.

The original way to understand the actual role of the cation exchange offers measurement of the change in pH in adsorbate solution during equilibration process (Burns et al., 2004; El-Shafey et al., 2002; Klucakova & Pekar, 2006). Namely, in the case of exclusive cation exchange between bivalent metals Me(II) and protons H^+, twice the amount of protons should be released from carbon into solution in comparison with the metal uptake. Indeed, a value of 2 was found for adsorption of cadmium(II) both on activated carbon (El-Shafey et al., 2002) and on low-rank Australian coals at pH 6 (Burns et al., 2004). Mohan & Chander (2006) then showed that during the sorption of Fe(II), Mn(II) or Fe(III) ions on lignite, calcium ions were mainly released to the solution. In this case, the ratio between released ions and the metal(s) bound to lignite was proved to even exceed the theoretical value (Mohan & Chander, 2006). On the other hand, quite a low amount of released H^+ ions was found when copper(II) was adsorbed on lignite-based humic acids at pH 2.8 (Klucakova & Pekar, 2006), proving thus only a minor role of cation exchange. For cation exchange as well as surface complexation of metals, it is reasonable to expect that surface acidic oxygen-containing groups such as carboxyl or hydroxyl play a decisive role (Klucakova et al., 2000). Experimental findings that metal uptakes on carbons are of very tight correlations neither
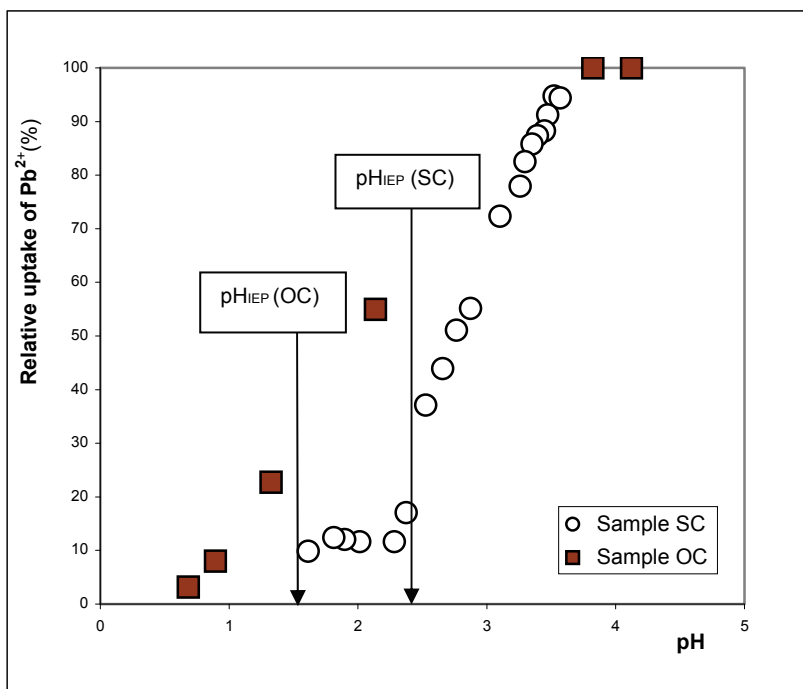
Fig. 5. Influence of pH on adsorption of lead(II) on coal samples SC and OC at 30°C; initial concentration of lead(II) nitrate was 1 mmol/L and 5 mmol/L, respectively; pH_{IEP} = value of iso-electric point

with specific surface area nor pore volume, but with the amount of the acidic oxygen functionalities thus support the leading role of these immobilization mechanisms (Song et al., 2010; Giraldo-Gutierrez & Moreno-Pirajan, 2008).

Our investigations of immobilization mechanisms focused on lead(II) adsorption on natural coals OC and SC. Namely, both the studied samples are of very similar elemental composition including oxygen content (see table 1). Infrared and ^{13}C CP/MAS NMR spectroscopies then confirmed hydroxyl and carboxyl groups as prevailing oxygen functionalities for both the sample. However, adsorption capacities a_m of the samples to lead(II) ions were found to be considerably different, giving values of 0.69 mmol/g for OC coal and 0.089 mmol/g for SC (at 30°C, pH 3.5). To elucidate the possible reason of the discrepancy, measurements of the pH changes in solutions during the lead(II) adsorption were performed first. With this respect, it is worth pointing out that before the adsorption measurements, the samples were repeatedly water leached in order to avoid release of other cations than H^+ during lead(II) adsorption. Experimentally obtained dependences of lead(II) uptake and H+ released from OC coal are demonstrated in figure 6.

Based on the measurements, average values of H^+/Pb(II) ratios were found to be 0.15 for the OC sample and 0.9 for SC coal, thus showing a more pronounced role of ion exchange for sample SC. Such a value for the SC sample indicates that a bit more than 50 % of lead(II) ions is immobilized by a way other than cation exchange. In this case, complexation fixation
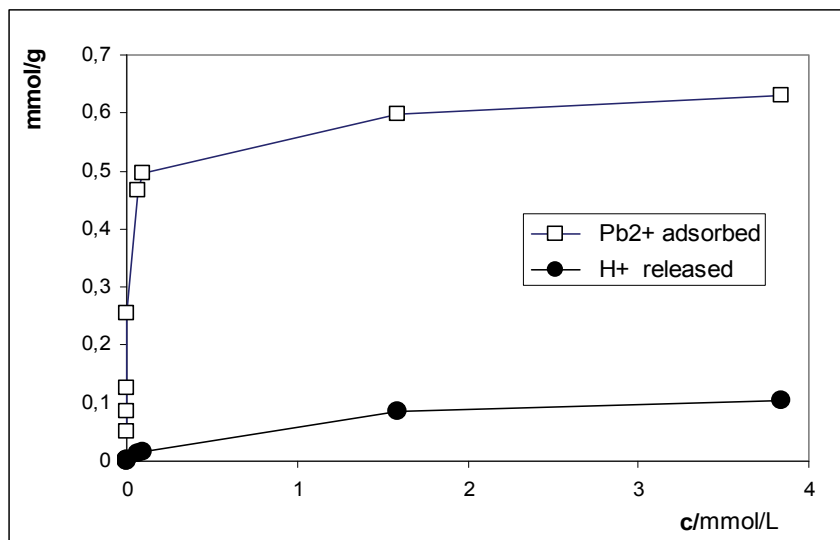
Fig. 6. Comparison between amounts of adsorbed lead(II) and H^+ released from OC coal, 30°C, initial pH = 4.2

of the ions appears to be the most probable alternative, simultaneous combination of both the immobilization mechanisms being already recognised (Klucakova et al., 2000). However, such an immobilization alternative can hardly explain about 90 % of cation non-exchanged lead(II) for sample OC. After some considerations on the possible influence of different aromaticity of the samples (see table 1), we have concluded that the reason of increased ability of OC sample to lead(II) probably lies in the composition of the inorganic parts of the sample. Namely, increased content of Mn and Mg oxides in ash of OC coal (see table 1) has been anticipated to be the main cause of the different adsorption behaviour of the coal, since these two very oxides were ascertained as effective solids for heavy metal adsorption (Machida et al., 2005). To recognize the role of ash in the lead(II) immobilization, adsorption measurements with ashes (0.15 g) prepared from both coal samples were performed at 30°C using the solutions of lead(II) at initial concentration 1.5 mmol/L (50 mL). Based on the investigations, markedly enlarged adsorption potential of OC ash for lead(II) was confirmed, more than one order exceeding that of SC ash. Namely, 0.58 mmol/g for OC ash instead of 0.032 mmol/g for SC ash was found to be adsorbed at equilibrium pH 4.

Thus, one can conclude that the differences in binding forces of the ashes toward Pb(II) were the main reason of the different adsorption behaviour of the coal samples.

7. Conclusion

Natural coals proved to have great potential in the immobilization of heavy metal ions with adsorption capacities usually exceeding the level of those referred for activated carbons. Especially for low rank coals of high ash, there is a possibility of synergy leading to a considerable increase in the adsorption affinity to heavy metals. The synergic effect results both from high concentration of oxygen functionalities on the coal surface and from the

propitious composition of the inorganic parts, namely the presence of metals such as Mg or Mn.

8. Acknowledgement

9. References

Adamson,A.W. & Gast,A.P. (1997). *Physical Chemistry of Surfaces*, John Wiley and Sons, Inc., ISBN 0-471-14873-3, New York

Asnin, L.D., Fedorov, A.A. & Chekryshkin, Y.S. (2001). Thermodynamic parameters of adsorption described by the logarithmic Temkin isotherm.. *Russian Chemical Bulletin,* Vol. 50, No. 2, 217-219, ISSN 1066-5285

Baniamerian, M.J., Moradi, S.E., Noori, A. & Salahi, H. (2009). The effect of surface modification on heavy metal ion removal from water by carbon nanoporous adsorbent. *Applied Surface Science,* Vol. 256, No. 5, 1347-1354, ISSN 0169-4332

Boudrahem, F., Aissani-Benissad, F. & Ait-Amar, H. (2009). Batch sorption dynamics and equilibrium for the removal of lead ions from aqueous phase using activated carbon developed from coffee residue activated with zinc chloride. *Journal of Environmental Management,* Vol. 90, No. 10, 3031-3039, ISSN 0301-4797

Burns, C.A., Boily, J.F., Crawford, R.J. & Harding, I.H. (2004). Cd(II) binding by particulate low-rank coals in aqueous media: sorption characteristics and NICA-Donnan models. *Journal of Colloid and Interface Science,* Vol. 278, No. 2, 291-298, ISSN 0021-9797

El-Shafey, E., Cox, M., Pichugin, A.A. & Appleton, Q. (2002). Application of a carbon sorbent for the removal of cadmium and other heavy metal ions from aqueous solution. *Journal of Chemical Technology and Biotechnology,* Vol. 77, No. 4, 429-436, ISSN 0268-2575

Erenturk, S. & Malkoc, E. (2007). Removal of lead(II) by adsorption onto Viscum album L.: Effect of temperature and equilibrium isotherm analyses. *Applied Surface Science,* Vol. 253, No.10, 4727-4733, ISSN 0169-4332

Giraldo-Gutierrez, L. & Moreno-Pirajan, J.C. (2008). Pb(II) and Cr(VI) adsorption from aqueous solution on activated carbons obtained from sugar cane husk and sawdust. *Journal of Analytical and Applied Pyrolysis,* Vol. 81, No. 2, 278-284, ISSN 0165-2370

Guo, M.X., Qiu, G.N. & Song, W.P. (2010). Poultry litter-based activated carbon for removing heavy metal ions in water. *Waste Management,* Vol. 30, No. 2, 308-315, ISSN 0956-053X

Imamoglu, M. & Tekir, O. (2008). Removal of copper (II) and lead (II) ions from aqueous solutions by adsorption on activated carbon from a new precursor hazelnut husks. *Desalination,* Vol. 228, No. 1-3, 108-113, ISSN 0011-9164

Klika, Z. & Kraussova, J. (1993). Properties of Altered Coals Associated with Carboniferous Red Beds in the Upper Silesian Coal Basin and Their Tentative Classification. *International Journal of Coal Geology*, Vol. 22, No. 3-4, 217-235, ISSN 0166-5162

Klucakova, M. & Pekar, M. (2006). New model for equilibrium sorption of metal ions on solid humic acids. *Colloids and Surfaces A-Physicochemical and Engineering Aspects,* Vol. 286, No. 1-3, 126-133, ISSN 0927-7757

Klucakova, M., Pelikan, P., Lapcik, L., Lapcikova, B., Kucerik, J. & Kalab, M. (2000). Structure and properties of humic and fulvic acids. I. Properties and reactivity of humic acids and fulvic acids. *Journal of Polymer Materials,* Vol. 17, No. 4, 337-356, ISSN 0973-8622

Kuhr, J.H., Robertson, J.D., Lafferty, C.J., Wong, A. S. & Stalnaker, N.D. (1997). Ion exchange properties of a Western Kentucky low-rank coal. *Energy & Fuels,* Vol. 11, No. 2, 323-326, ISSN 0887-0624

Kuo, C.Y. (2009). Water purification of removal aqueous copper (II) by as-grown and modified multi-walled carbon nanotubes. *Desalination,* Vol. 249, No. 2, 781-785, ISSN 0011-9164

Lao, C.X., Zeledon, Z., Gamisans, X. & Solé, M. (2005). Sorption of Cd(II) and Pb(II) from aqueous solutions by a low-rank coal (leonardite). *Separation and Purification Technology,* Vol. 45, No. 2, 79-85, ISSN 1383-5866

Le Cloirec,P. & Faur-Brasquet, C. (2008). Adsorption of Inorganic Species from Aqueous Solutions, In: *Adsorption by Carbons*, E.J.Bottani and J.M.D. Tascon (Ed.), 631-651, Elsevier, ISBN 978-0-08-044464-2, Amsterdam

Li, Q.Z., Chai, L.Y., Yang, Z.H. & Wang, Q. (2009). Kinetics and thermodynamics of Pb(II) adsorption onto modified spent grain from aqueous solutions. *Applied Surface Science,* Vol. 255, No. 7, 4298-4303, ISSN 0169-4332

Li, Y.H., Di, Z.C., Ding, J., Wu,D., Luan,Z. & Zhu,Y. (2005). Adsorption thermodynamic, kinetic and desorption studies of Pb2+ on carbon nanotubes. *Water Research,* Vol. 39, No. 4, 605-609, ISSN 0043-1354

Machida, M., Yamazaki, R., Aikawa, & Tatsumoto, H. (2005). Role of minerals in carbonaceous adsorbents for removal of Pb(II) ions from aqueous solution. *Separation and Purification Technology,* Vol. 46, No.1-2, 88-94, ISSN 1383-5866

Marcus, Y. (1997). *Ion properties*. New York, Marcel Dekker, ISBN 0-8247-0011-2

Mohan, D. & Chander, S. (2006). Single, binary, and multicomponent sorption of iron and manganese on lignite. *Journal of Colloid and Interface Science,* Vol. 299, No. 1, 76-87, ISSN 0021-9797

Mohan, D., Gupta, V.K., Srivastava, S.K. & Chander, S. (2001). Kinetics of mercury adsorption from wastewater using activated carbon derived from fertilizer waste. *Colloids and Surfaces A-Physicochemical and Engineering Aspects,* Vol. 177, No. 2-3, Special Issue, 169-181, ISSN 0927-7757

Murakami, K., Yamada, T., Fuda, K. & Matsunaga, T. (2001). Selectivity in cation exchange property of heat-treated brown coals. *Fuel,* Vol. 80, No. 4, 599-605, ISSN 0016-2361

Oubagaranadin, J.U.K. & Murthy, Z.V.P. (2009). Removal of Pb(II) from aqueous solutions by carbons prepared from Sal wood (Shorea robusta). *European Journal of Wood and Wood Products,* Vol. 67, No. 2, 197-206, ISSN 0018-3768

Qadeer, R., Hanif, J., Saleem, M. & Afzal, M. (1993). Surface characterization and thermodynamics of adsorption of Sr^{2+}, Ce^{3+}, Sm^{3+}, Gd^{3+}, Th^{4+}, UO_2^{2+} on activated charcoal from aqueous-solution. *Colloid and Polymer Science,* Vol. 271, No. 1, 83-90, ISSN 0303-402X

Qadeer, R. & Hanif, J. (1994). Kinetics of zirconium ions adsorption on activated-charcoal from aqueous-solutions. *Carbon,* Vol. 32, No. 8, 1433-1439, ISSN 0008-6223

Qiu, Y.P., Cheng, H.Y., Xu, C. & Sheng, G.D. (2008). Surface characteristics of crop-residue-derived black carbon and lead(II) adsorption. *Water Research,* Vol. 42, No. 3, 567-574, ISSN 0043-1354

Radovic, L.R., Moreno-Castilla, C. & Rivera-Utrilla, J. (2000). Carbon materials as adsorbents in aqueous solutions. *Chem. Phys. Carbon* (Ed. Ljubisa R. Radovic) 27:227-405.

Rao, G.P., Lu, C. & Su, F. (2007). Sorption of divalent metal ions from aqueous solution by carbon nanotubes: A review. *Separation and Purification Technology,* Vol. 58, No. 1, 224-231, ISSN 1383-5866

Sekar, M., Sakthi, V. & Rengaraj, S. (2004). Kinetics and equilibrium adsorption study of lead(II) onto activated carbon prepared from coconut shell. *Journal of Colloid and Interface Science,* Vol. 279, No. 2, 307-313, ISSN

Shibi, I.G. & Anirudhan, T.S. (2006). Polymer-grafted banana (Musa paradisiaca) stalk as an adsorbent for the removal of lead(II) and cadmium(II) ions from aqueous solutions: kinetic and equilibrium studies. *Journal of Chemical Technology and Biotechnology,* Vol. 81, No. 3, 433-444, ISSN 0268-2575

Song, X.L., Liu, H.Y., Cheng, L. & Qu, Y. (2010). Surface modification of coconut-based activated carbon by liquid-phase oxidation and its effects on lead ion adsorption. *Desalination,* Vol. 255, No. 1-3, 78-83, ISSN 0011-9164

Taraba, B. & Marsalek, R. (2007). Immobilization of heavy metals and phenol on altered bituminous coals. *Energy Sources Part A-Recovery Utilization and Environmental Effects,* Vol. 29, No. 10, 885-893, ISSN 1556-703

Zeledon-Toruno, Z., Lao-Luque, C. & Sole-Sardans, M. (2005). Nickel and copper removal from aqueous solution by an immature coal (leonardite): effect of pH, contact time and water hardness. *Journal of Chemical Technology and Biotechnology,* Vol. 80, No. 6, 649-656, ISSN 0268-2575

Part 3

Waste Water Reuse and Minimization

Low-Value Maize and Wheat By-Products as a Source of Ferulated Arabinoxylans

Claudia Berlanga-Reyes[1], Elizabeth Carvajal-Millan[1],
Guillermo Niño-Medina[4], Agustín Rascón-Chu[2],
Benjamín Ramírez-Wong[3] and Elisa Magaña-Barajas[3]
Centro de Investigación en Alimentación y Desarrollo,
A.C. Hermosillo, Sonora,
[1]Laboratorio de biopolímeros, CTAOA,
[2]Laboratorio de biotecnología. CTAOV,
[3]Departamento de Investigación y Posgrado en Alimentos, Universidad de Sonora,
[4]Facultad de Agronomía, Universidad Autónoma de Nuevo León,
[1,2,3,4]México

1. Introduction

The major polymers in the cell walls are cellulose (25-35%), hemicelluloses (40-50%) and lignin (7-10%). Both cellulose and hemicelluloses function as structural supporting materials in the cell walls; cellulose has a high tensile strength and gives rigidity to the walls, whereas hemicelluloses impart elasticity to the structure by cross-linking cellulose micro fibrils (Ishii, 1997). Xylans occur as the most common hemicelluloses, and after cellulose they are the second most abundant polysaccharides in the plant kingdom.

Arabinoxylans (AX) are hemicelluloses built up of pentose sugars, mostly arabinose and xylose residues, and are therefore often referred to as pentosans (Izydorczyk & Biliaderis, 1995). AX consist of backbone chains of β(1,4) linked-linked D-xylopyranosyl units to which α-L arabinofuranosyl substituents are attached through O-2 and/or O-3 (Fincher & Stone, 1974). Some of the arabinose residues are ester linked on (O)-5 to ferulic acid (FA) (3-methoxy, 4 hydroxy cinnamic acid) (Smith & Hartley, 1983). AX are mayor dietary fiber components of many cereals like wheat, rye, corn, barley, oat, rice and sorghum (Fincher & Stone, 1974). AX are classified into water-extractable (WEAX) and water-unextractable AX (WUAX). The WUAX present a combination of no covalent interactions and covalent bonds with other cell walls components, such as proteins, cellulose and lignin (Andrewartha *et al.*, 1979).

AX can be isolated by water and by alkali extraction (Cui *et al.*, 2001). The extractability of these polysaccharides is based on the conformational aggregation, the covalent ester bonds between ferulic acid and other components such as lignin, the degree, and substitution patter of arabinoses at side chain, and nature of physical entanglement. Once extracted AX form highly viscous solutions with gelling capacity by covalent cross-linking through dimerization of ferulic acid substituents under oxidative conditions (e.g., use of enzymatic free radical generating agents as laccase and peroxidase H_2O_2) (Geissman *et al.*, 1973; Figueroa Espinoza *et al.*, 1998). Diferulic acids (di-FA) and triferulic acid (tri-FA)

(Vansteenkiste *et al.,* 2004; Carvajal-Millan *et al.,* 2005a) have been identified as covalently cross-linked structures in AX gels.

AX gels present interesting properties like neutral taste and odor, high water absorption capacity and absence of pH or electrolyte susceptibility (Izydorczyk & Biliaderis, 1995). Interest on AX and AX gels has increased in the last years and new information on their sources and applications are being reported. Recuperation of AX from cereal by-products of the food industry has been reported (Niño-Medina (2009), b; Carvajal-Millan *et al.*, 2007) and would offer new advantages for future industrial applications of this biomolecule.

Maize and wheat are important sources of food in Mexico. They are used to obtain different food products such as cereal breakfasts, bread, tortilla, among others. During processing, maize and wheat generate high amounts of low-value by products. In the past, Mesoamerican Indians learned that wood ashes facilitated maize cooking, the removal of the hard outer covering, and improved the quality of the resulting material. We now know that this process also releases the bound niacin in the maize into a readily available form. Thus, the population did not suffer the ravages of what we now call pellagra. In Mexico, this alkali cooking, called 'nixtamalization' (from the Nahuatl nixtli=ashes and tamalli=dough) is widely used to improve the maize nutritional value.

Maize nixtamalization is important in Mexico as half of the total volume of consumed food is maize, which provides approximately 50 % of the energy intake, this proportion being even greater for lower income groups. Nixtamalization consists of cooking maize grains in a lime solution, soaking for 2-8 hours and washing them by hand to remove the pericarp. The product obtained is then ground to obtain nixtamal (dough or masa) used to prepare a variety of products, tortilla being the most popular one. The nixtamalization process degrades and solubilizes maize cell wall components and this facilitates pericarp removal. As a matter of fact, the 'nejayote' (maize nixtamalization waste water) contains, in general, more than 60% of non-starch polysaccharides. These alkali-soluble non-cellulosic cell wall polysaccharides present in maize pericarp (mainly arabinoxylan) show interesting functional properties as thickeners, stabilizers, emulsifiers and film and gel formers.

The nejayote obtained from nixtamalization is highly alkaline waste water, with high chemical and biological oxygen demands and is considered an environmental pollutant. A typical maize nixtamalization facility processing 50 kg of maize every day uses over 75 liters of water per day and generates nearly the equivalent amount of alkaline waste water in 24 hours. Thus, alternatives of nejayote residues utilization in Mexico are needed. Niño-Medina et al., (2009) recently reported that nejayote can be a novel source of AX. During the milling process of maize and wheat the starchy endosperm is isolated with the minimum contamination by peripheral layers of the grain (i.e. aleurone layer and bran).

Maize and wheat bran are by-products of the commercial flour industry in Mexico. Because of the high volume of maize and wheat bran produced in Mexico, these residues are becoming into potential sources of added-value biomolecules as AX for the food industry. Maize bran contains heteroxylans (approximately 50%), cellulose (approximately 20%) and phenolic acids (approximately 4%, mainly ferulic and diferulic acid) (Saulnier *et al.* 1995a). Starch (9-23%), proteins (10-13%), oil (2-3%) and ash (2%) are also present in maize bran (Hespell, 1998). The heteroxylans portion of maize bran can be extracted with alkaline (Whistler, 1993; Saulnier et al. 1995b; Carvajal-Millan *et al.*, 2007) or acid solutions (Saulnier *et al.*, 1995a) to produce water-soluble AX. Wheat bran contains approximately 19% of water-insoluble AX, which can be extracted with alkaline or acid solutions to produce water-soluble AX (Hashimoto *et al.*, 1987).

This chapter includes some of the most recent findings on physico-chemical and functional properties of water-soluble ferulated arabinoxylans from three cereal by-products: nejayote (nixtamalization waste water), maize bran and wheat bran.

2. Experimental

2.1 Materials and methods

Nejayote, maize bran and wheat bran were kindly provided by commercial milling industries in Northern Mexico. All chemical products were purchased from Sigma Chemical Co. (St Louis, MO, USA).

2.2 Arabinoxylans extraction

AX from nejayote (FAXN) and AX from maize bran (FAXMB) presented in this study were previously extracted and characterized (Carvajal-Millán *et al.* 2007; Niño-Medina (2009)).

AX from wheat bran (FAXWB) were extracted as follows. Wheat bran was ground to a 20-mesh particle size using a M20 Universal Mill (IKA®, Werke Staufen, Germany). Wheat bran (500 g) was treated with ethanol (2500 ml) for 12 h at 25 °C to remove lipophilic components.

The ethanol treated bran was then filtered and subjected to starch gelatinization and enzymes inactivation (boiling for 30 min in 3500 ml of water). After boiling, wheat bran was recovered by filtration and treated with 2500 ml of NaOH 0.5 N solution at 25 °C in darkness for 1 h under shake (100 rpm). Residual bran was then eliminated by filtration and the filtrate was centrifuged (12,096g, 20 °C, 15 min).

Supernatant was acidified to pH 4 with HCl 3N. Acidified liquid was centrifuged (12,096g, 20 °C, 15 min) and supernatant was then recuperated and precipitated in 65 % (v/v) ethanol for 4 h at 4°C. Precipitate was recovered and dried by solvent exchange (80 % (v/v) ethanol, absolute ethanol and acetone) to give FAXWB.

2.3 Chemical composition of FAXWB

Sugar composition was determined according to Carvajal-Millan et al. (2007) after FAXWB hydrolysis with 2 N trifluoroacetic acid at 120 °C for 2 h. The reaction was stopped on ice, the extract was evaporated under air at 40 °C and rinsed twice with 200 μL of water and resuspended in 500 μL of water.

All samples were filtered through 0.45 μm (Whatman) and analyzed by high performance liquid chromatography (HPLC) using a Supelcogel Pb column (300 × 7.8 mm; Supelco, Inc., Bellefont, PA) eluted with 5mM H_2SO_4 (filtered 0.2 μm, Whatman) at 0.6 mL/min and 50 °C. A refractive index detector Star 9040 (Varian, St. Helens, Australia) and a Star Chromatography Workstation system control version 5.50 were used. The internal standard was inositol.

Ferulic acid was quantified by high performance liquid chromatography (HPLC) after deesterification step as described by Vansteenksite et al., (2004). An Alltima C_{18} column (250 × 4.6 mm) (Alltech associates, Inc. Deerfield, IL) and a photodiode array detector Waters 996 (Millipore Co., Milford, MA) were used. Detection was by UV absorbance at 320 nm.

Ash content was determined according to the AACC methods (AACC, 1998). Protein was determined by using the Bradford method (Bradford, 1976).

2.4 Intrinsic viscosity of FAXWB

Specific viscosity, ηsp was measured by registering FAXWB solutions flow time in an Ubbelohde capillary viscometer at 25 ± 0.1 °C, immersed in a temperature controlled bath. FAXWB solutions were prepared at different concentrations, dissolving dried polysaccharide in water for 10 h with stirring at room temperature. FAXWB solutions and water were filtered using 0.45 μm membrane filters before viscosity measurements.

The intrinsic viscosity ([η]) was estimated from relative viscosity measurements, ηrel, of FAXWB solutions by extrapolation of Kraemer and Mead and Fouss curves to "zero" concentration.

2.5 Viscosimetric molecular weight of FAXWB

The viscosimetric molecular weight (Mv) was calculated from the Mark–Houwink relationship, Mv = ([η]/k)1/α.

2.6 FAXN, FAXMB and FAXMB gelation

FAXN, FAXMB and FAXWB solutions (4, 3.5 and 5.0 % w/v) were prepared in 0.05 M citrate phosphate buffer pH 5. Laccase (1.675 nkat per mg polysaccharide) was used as gelling agent. Gels were allowed to form at 25 °C.

2.7 Small deformation measurements

The formation of FAXN, FAXMB and FAXWB gels was followed using a strain-controlled rheometer (AR-1500ex, TA Instruments, U.S.A.) in oscillatory mode as follows. Cold (4 °C) solutions of FAXN, FAXMB and FAXWB at 4, 3.5 and 5.0%, respectively (w/v) were mixed with laccase (1.675 nkat per mg polysaccharide) and immediately placed in the cone and plate geometry (5.0 cm in diameter, 0.04 rad in cone angle) maintained at 4 °C.

Exposed edges of the sample were covered with silicone fluid to prevent evaporation during measurements. Gelation kinetic was started by a sudden increase in temperature from 4 °C to 25 °C and monitored at 25 °C over time by following the storage (G′) and loss (G′′) modulus.

All measurements were carried out at a frequency of 0.25 Hz and 5 % strain (linearity range of viscoelastic behavior). Frequency sweep (0.1 to 50 Hz) was carried out at the end of the network formation at 5 % strain and 25 °C.

2.8 Large deformation measurements

The hardness of FAXN, FAXMB and FAXWB gels was analyzed with a TA.XT2 Texture Analyzer (RHEO Stable Micro Systems, Haslemere, England) equipped with a XTRAD software version 3.7.

The gels were deformed by compression at a constant speed of 1.0 mm/s to a distance of 4 mm from the gel surface using a cylindrical plunger (diameter 25.4 mm). The peak height at 4 mm compression was called gel hardness (Carvajal-Millan et al., 2005a).

2.9 Gel swelling

After laccase addition, FAXN, FAXMB and FAXWB solutions were quickly transferred to a 5 ml tip-cut-off syringe (diameter 1.5 cm) and allowed to gelify for 2 h at 25°C. After gelation, the gels were removed from the syringes, placed in glass vials and weighted.

The gels were allowed to swell in 20 ml of 0.02% (w/v) sodium azide solution to prevent microbial contamination. During 20 h the samples were blotted and weighed. After weighing, a new aliquot of sodium azide solution was added to the gels. Gels were maintained at 25°C during the test.

The equilibrium swelling was reached when the weight of the samples changed by no more than 3% (0.06 g). The swelling ratio (q) was calculated as:

$$q = (Ws - Wd) / Wd$$

where Ws is the weight of swollen gels and Wd is the weight of polysaccharide in the gel.

2.10 Gel structure

From swelling measurements, the molecular weight between two cross-links (Mc), the cross-linking density (ρc) and the mesh size (ξ) values of the FAXN, FAXMB and FAXWB gels were obtained as reported by Carvajal-Millan *et al*. (2005b). Mc, ρc and ξ were calculated using the model of Flory and Rehner modified by Peppas and Merrill for gels where the cross-links are introduced in solution.
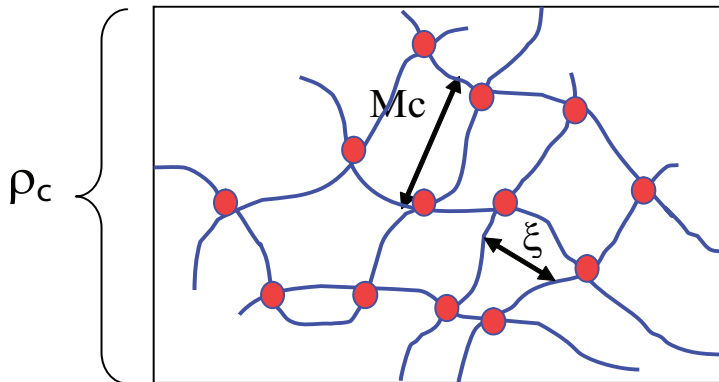
Fig. 1. Schematic representation of gel structural parameters. Mc=Molecular weight between two cross-links, ρc= cross-linking density and ε= mesh size.

3. Results and discussion

In a previous report, FAXN and FAXMB have been extracted and characterized Niño-Medina (2009). Yield of FAXN and FAXMB were 8 (w FAXN/v nejayote) and 29 % (w FAXMB/w maize bran), respectively.

In FAXN, pure arabinoxylans represented 81 % dry basis (db) of the recovered sample (Table 1). This value was estimated from the sum of xylose + arabinose. The ratio arabinose-to-xylose (A/X) was 0.65 indicating a moderately branched structure, similar to that reported by Singh *et al.* (2000) in maize bran arabinoxylans. Residues of glucose, galactose, mannose, proteins and ash were also detected in FAXN.

The ferulic acid content, [*η*] and Mw values were lower to those reported for ferulated arabinoxylans from other sources (Izydorczyk et al., 1990; Dervilly-Pinel *et al.*, 2001; Vansteenkiste *et al.,* 2004; Carvajal-Millan *et al.,* 2006).

Arabinose (%)	33.0 ± 0.70
Xylose (%)	39.0 ± 1.20
Glucose (%)	4.90 ± 0.15
Galactose (%)	3.90 ± 0.11
Mannose (%)	0.60 ± 0.04
Protein (%)	2.70 ± 0.20
Ash (%)	3.58 ± 0.14
Ferulic acid (%)	0.003 ± 0.05
A/X (mass ratio)	0.85 ± 0.20
[η] (mL/g)	208 ± 6.2

Table 1. Composition of ferulated arabinoxylans from nejayote (FAXN) (adapted from Niño-Medina (2009)).

As presented in Table 2 , FAXMB presented an arabinoxylan content of 72% (w/w), a ferulic acid content of 0.003 (% w/w), an A/X ratio of 0.85, an intrinsic viscosity [η] of 208 mL/g and a molecular weight (Mw) of 190 kDa.

Arabinose (%)	32.0 ± 0.80
Xylose (%)	49.0 ± 1.90
Glucose (%)	5.10 ± 0.40
Galactose (%)	3.70 ± 0.20
Mannose (%)	0.60 ± 0.04
Protein (%)	4.50 ± 0.20
Ash (%)	5.10 ± 0.21
Ferulic acid (%)	0.002 ± 0.01
A/X (mass ratio)	0.65 ± 0.10
[η] (mL/g)	183 ± 5.4
Mw (kDa)	60 ± 6.0

Table 2. Composition and physico-chemical characteristics of ferulated arabinoxylans from maize bran (FAXMB) (adapted from Niño-Medina (2009)).

The higher ferulic acid content and [η] and Mw values in FAXMB in comparison with FAXN could be attributed to the differences in the extractions conditions used. FAXN are recovered after maize nixtamalization which consists of cooking maize grains in a lime solution, after soaking for 2 to 8 hours while FAXMB are alkali-extracted under mild conditions (NaOH 0.5 N solution at 25 °C in darkness for 8 h).

In this chapter is presented for the first time the extraction and characterization of FAXWB. FAXWB yield was 17% (w FAXWB/w wheat bran), which is higher than the value previously reported for FAXN (8% w/v) but lower than that found for FAXMB (29% w/w).

Composition of FAXWB is presented in Table 3. Arabinoxylan (AX) represented 76 % dry basis (db) of the recovered FAXWB. This value was estimated from the sum of xylose + arabinose. This arabinoxylan content is in the range found for FAXN and FAXMB (86 and 72 %, respectively).

The ratio arabinose-to-xylose was high (A/X = 0.80) indicating a highly branched structure, similar to that reported by Schooneveld-Bergmans *et al.* (1999) in wheat bran arabinoxylans. A high A/X ratio was also found in FAXMB (0.85) in comparison to the moderate A/X value found in FAXN (0.65).

Arabinose (%)	33.00 ± 1.20
Xylose (%)	43.00 ± 1.30
Glucose (%)	3.10 ± 0.40
Galactose (%)	2.10 ± 0.30
Mannose (%)	0.30 ± 0.03
Protein (%)	2.70 ± 0.20
Ash (%)	2.30 ± 0.21
Ferulic acid (%)	0.0050 ± 0.05
A/X (mass ratio)	0.80 ± 0.40
[η] (mL/g)	198 ± 5.6
Mw (kDa)	60 ± 3.0

Table 3. Composition of ferulated arabinoxylans from wheat bran (FAXWB)

These differences in A/X ratio could explain the higher water solubility of FAXN as arabinose residues increase the molecule hydrophilic characteristic. As in FAXN and FAXMB, residues of glucose, galactose, mannose, proteins and ash were detected in FAXWB. The ferulic acid content (0.005%) was higher in FAXWB than in FAXN and FAXMB but lower than that obtained by Schooneveld-Bergmans *et al.* (1999) in wheat bran arabinoxylans recovered by using a different extraction method.

The intrinsic viscosity ([η]) and a molecular weight (Mw) values in FAXWB were 168 mL/g and 60 kDa, respectively, which are in the range found in FAXN and FAXMB. Due their different nature, the ferulated arabinoxylans extracted from each low-value maize and wheat by-product showed different yield, composition and physico-chemical characteristics. FAXN and FAXMB have been reported to form covalent gels in presence of a laccase. According to Niño-Medina (2009), treatment of FAXN with laccase as oxidizing agent formed a gel after 4-6 hours at 25°C.

The formation of 4% (w/v) FAXN gels over time was rheologically investigated by small amplitude oscillatory shear. These authors found that the storage (G′) and loss (G′′) modulus rose over the time to reach a plateau with a final G′ value of 2 Pa, which is lower than those reported for arabinoxylan gels from other sources (20-40 Pa) at lower polysaccharide concentrations (1-2% w/v) (Carvajal-Millán *et al.,* 2005a). On the other hand, a final G′ value of 20 Pa was found in 3.5% (w/v) FAXMB (Berlanga-Reyes *et al.*, 2009) after gelation by a laccase.

Concerning FAXWB, during laccase induced gelation G′ modulus rose to reach a plateau (Fig. 1). The final G′ value was 177 Pa in a 5% (w/v) FAXWB gel.

The mechanical spectrum of FAXWB gel is presented in Fig. 2. After 90 minutes gelation spectrum was typical of solid-like materials with a linear G′ independent of frequency and G′′ much smaller than G′ and dependent on frequency (Doublier & Cuvelier, 1996). This behavior is similar to that previously reported for other arabinoxylan gels cross-linked by laccase or peroxidase/H_2O_2 system (Izydorczyk *et al.*, 1990; Dervilly-Pinel *et al.*, 2001; Vansteenkiste *et al.*, 2004; Carvajal-Millan *et al.*, 2006).

The hardness of FAXN, FAXMB and FAXWB gels are presented in Fig. 3. In agree with small deformation rheological results (G′, G′′) discussed above, large deformation measurements (gel hardness) showed that FAXWB can form gels more elastic than those from FAXN and FAXMB.
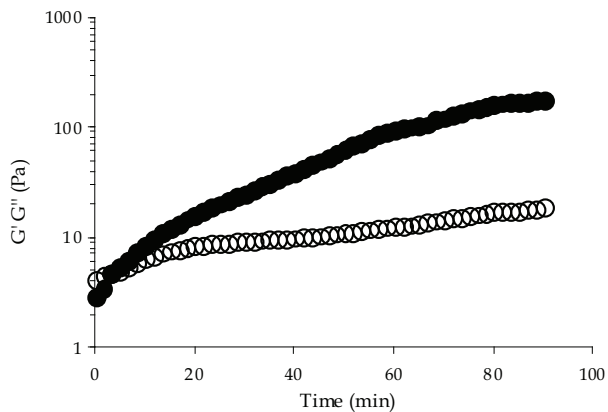
Fig. 1. Laccase induced gelation of FAXWB solutions at 5 % (w/v) (G´ ●, G´´o). Rheological measurements made at 25°C, 0.25 Hz and 5% strain.
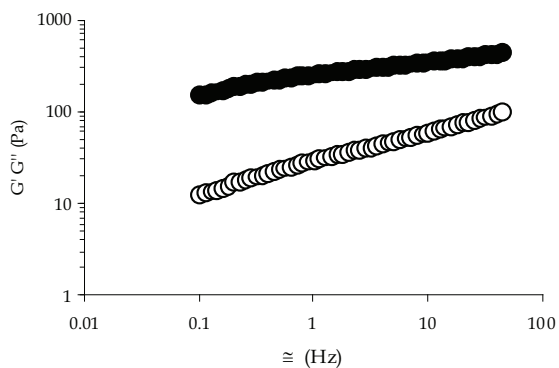

Fig. 2. Mechanical spectra of FAXWB gels at 5.0 % (w/v) (G´ ●, G´´o). Rheological measurements made at 25°C and 5% strain.
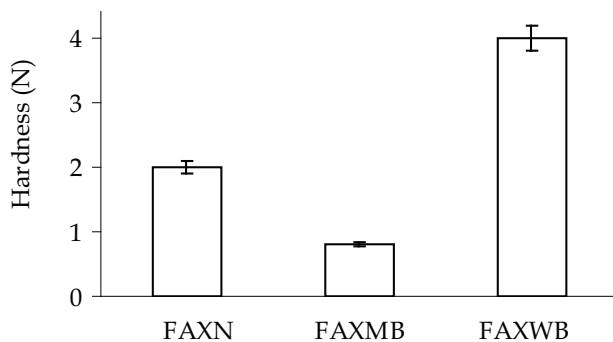
Fig. 3. Hardness of FAXN, FAXMB and FAXWB gels at 4, 3.5 and 5.0 % (w/v), respectively. Rheological measurements made at 25°C.

The rheological differences between FAXN, FAXMB and FAXWB gels might have its origin in the structural and/or conformational characteristics of these macromolecules. Clearly, further studies on the distribution of arabinose and feruloyl groups along the polymer chain backbone of these different arabinoxylans are needed to establish relationships between the molecular structure, gelling ability and gels properties.

The equilibrium swelling of FAXN, FAXMB and FAXWB gels was reached between 15-20 h. The swelling ratio (q, g water/g polysaccharide) in FAXN, FAXMB and FAXWB gels were 40, 22 and 20, respectively (Table 4).

AX Source	Swelling ratio (q, g water/g AX)	M_c [a] x10³ (g/mol)	ρ_c [b] x10⁻⁶ (mol/cm³)	ε [c] (nm)
FAXN	40 + 1.5	95 + 0.1	9.0 + 0.01	183 + 4
FAXMB	22 + 1.9	20 + 0.1	75 + 0.01	48 + 1
FAXWB	20+ 1.7	29 + 0.1	59 + 0.01	58 + 1

[a] Molecular weight between two cross-links

[b] Cross-linking density

[c] Mesh size

Table 4. Structural characteristics of FAXN, FAXMB and FAXWB gels.

The lower swelling ratio values obtained for FAXMB and FAXWB can be related to the more compact polymeric structure that limits the water absorption in comparison to the FAXN gels. The higher water uptake of gels made from FAXN can be explained in terms of a decrease in ferulic acid content and therefore the existence of longer un-cross-linked polysaccharide chains sections in the network. Uncross-linked polymer chains sections in the gel can expand easily conducting to higher amounts of water uptake.

The molecular weight between two cross-links (Mc), the cross-linking density (ρc) and the mesh size (ξ) values of the different gels are presented in Table 3. Higher Mc and ξ and lower ρc values have been reported in laccase induced water soluble arabinoxylan gels from wheat at similar AX concentrations (Carvajal-Millan et al., 2005b).

The latter could be related to a high molecular weight in arabinoxylans from wheat endosperm (400-600 kDa) in comparison to alkali-extracted arabinoxylans from maize and wheat bran (60-240 kDa) used in the present study. The involvement of physical interactions between polysaccharide chains could also be responsible of these differences. Different arabinoxylan gel structural characteristics were therefore obtained by modifying the polysaccharide source (FAXN, FAXMB, FAXWB).

The results discussed above indicate that by changing the arabinoxylan source gels with different rheological and structural properties can be obtained. To illustrate how the possible covalent cross-links content in the gel can affect network structure, we propose in Fig. 4 a model of the FAXN, FAXMB and FAXWB gels. As showed in Fig. 4 a decrease in the initial ferulic acid content could decrease the covalent bonds content. These differences in the network structure could induce changes in the functional properties of the gel.

FAXN gel
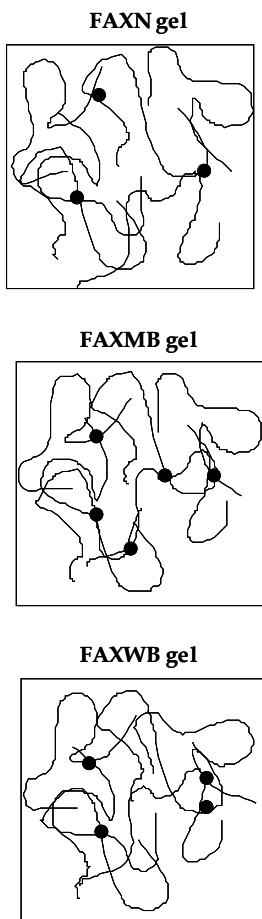
FAXMB gel

FAXWB gel

Fig. 4. Schematic representation of FAXN, FAXMB and FAXWB gels.

4. Conclusion

Nejayote (a maize processing waste water), maize bran and wheat generated from flour industries can be potential sources of ferulated arabinoxylans as added-value hydrocolloids for the food industry. Due their different nature, the arabinoxylans extracted from each showed different physico-chemical and gelling properties. Recuperation of these hydrocolloids from low-value maize and wheat by-products could represent a commercial advantage face to other polysaccharides commonly used in the food industry.

5. Future considerations

New sources of polysaccharides continue to be investigated and different functional properties are being discovered. Concerning ferulated arabinoxylans from low-value low-value maize and wheat by-products, several questions remained to be elucidated, especially

those concerning the relationships between the molecular structure, gelling ability and gels properties.

Additional studies will also be required on the application of these polysaccharides in food products. In this regard, technological and nutritional evaluation of these food products would be necessary. FAXN, FAXMB and FAXWB would have health benefits such as lowering of blood cholesterol and sugar as well as antioxidants properties but complementary studies are required.

6. Acknowledgements

7. References

AACC. (1998). In: Approved Methods of the American Association of Cereal Chemists, The Association. Minnesota, USA.

Andrewartha, K. A., Phillips, D. R. & Stone, B. A. (1979). Solution properties of wheat-flour arabinoxylans and enizmatically modified arabinaoxylans. *Carbohydrate Research*, 77, 191-204.

Berlanga-Reyes, C., Carvajal-Millán, E., Caire-Juvera, G., Rascón-Chu, AS. Marquez-Escalante, J.A. & Martínez-López, A.L. (2009). Laccase induced maize bran arabinoxylan gels: structural and rheological properties. *Journal of Food Science and Biotechnology*, 18, 1027-1029.

Bradford, M. (1976). A rapid and sensitive method for the quantification of microgram quantities of protein utilizing the principle of protein-dye binding. *Analytical Biochemistry*, 72, 248-254.

Carvajal-Millán, E., Landillon, V., Morel, M.H., Rouau, X., Doublier, J.L., Micard, V. (2005b). Arabinoxylan gels: impact of the feruloylation degree on their structure and properties. *Biomacromolecules*, 6, 309-317.

Carvajal-Millán, E., Guigliarelli, B., Belle, V., Rouau, X. & Micard, V. (2005a). Storage stability of arabinoxylan gels. *Carbohydrate Polymers*, 59, 181-188.

Carvajal-Millán, E., Guilbert, S., Doublier, J. L. & Micard, V. (2006). Arabinoxylan/protein gels: structural, rheological and controlled release properties. *Food Hydrocolloids*, 20, 53-61.

Carvajal-Millán, E., Rascón-Chu, A., Márquez-Escalante, J. Ponce de León, N., Micard, V. & Gardea, A. (2007). Maize bran gum: characterization and functional properties. *Carbohydrate Polymers*, 69, 280-285.

Cui S. W. 2001. Chapter 4. Cereal non-starch polysaccharides II: Pentosans/Arabinoxylans. Polysacharide gums from agricultural products. Processing, structures and functionality. Lancaster, Penn. Technomic Publishing Company. pp. 167-227.

Dervilly-Pinel, G., Rimsten, L., Saulnier, L., Andersson, R. & Áman, P. (2001). Water-extractable arabinoxylan from pearled flours of wheat, barley, rye and triticale. Evidence for the presence of ferulic acid dimmers and their involvement in gel formation. *Journal of Cereal Science*, 34, 207-214.

Doublier, J.L., Cuvelier, G. Gums and hydrocolloids: functional aspects. Vol. I, pp. 283-318. In: Carbohydrates in Food. Eliasson, A.C. (ed). Marcel Dekker, New York:, USA. (1996).

Figueroa-Espinoza, M. C. & Rouau, X. (1998). Oxidative cross-linking of pentosans by a fungal laccase and a horseradish peroxidase: mechanism of linkage between feruloylated arabinoxylans. *Cereal Chemistry*, 75, 259-265.

Fincher, G. B. & Stone, B. A. (1974). A water-soluble arabinogalactan-peptide from wheat endosperm. *Australian Journal of Biological Science*, 27, 117-132.

Geissman, T. & Neukom, H. (1973). On the composition of the water-soluble wheat flour pentosanes and their oxidative gelation. *Lebensmittel-Wissenchaft-und-Technologie*, 6, 59-62.

Hashimoto, S., Shogren, M.D. & Pomeranz, Y. (1987) Cereal pentosans: their estimation and significance. III. Pentosans in abraded grains and miling products of wheat and milled wheat products. *Cereal Chemistry*, 64, 39-41.

Hespell, R.B. (1998). Extraction and characterization of hemicellulose from the corn fiber produced by corn wet-milling processes. *Journal of Agriculture Food Chemistry*, 46, 2615-2619.

Ishii, T. 1991. Isolation and characterization of a diferuloyl arabinoxylan hexasaccharide from bamboo shoot cell walls. Carbohydrate Research. 219: 15-22.

Izydorczyk, M. S. & Biliaderis, C. G. (1995). Cereal arabinoxylans: advances in structure and physicochemical properties. *Carbohydrate Polymers*, 28, 33-48.

Izydorczyk, M. S., Biliaderis C. G. & Bushuk, W. (1990). Oxidative gelation studies of water-soluble pentosans from wheat. *Journal of Cereal Science*, 11, 153-169.

Lapierre, C., Pollet, B., Ralet, M. C. & Saulnier, L. (2001). The phenolic fraction of maize bran: evidence for lignin-heteroxylan association. *Phytochemistry*, 57, 765-772.

Niño-Medina, G., Carvajal-Millán, E., Rascón-Chu, A., Lizardi, J., Márquez-Escalante, J., Gardea, A., Martínez-López, A.L. & Guerrero, V. (2009b). Maize processing waste water arabinoxylans: gelling capability and cross-linking content. *Food Chemistry*, 115, 1286-1290.

Niño-Medina, G. (2009). Gelling capability of ferulated arabinoxylans from maize by-products. PhD Dissertation, Center for Food and Development, CIAD, A.C. Mexico.

Saulnier, L., Marot, C., Chanliaud, E., & Thibault, J.-F. (1995b). Cell wall polysaccharide interactions in maize bran. *Carbohydrate Polymer*, 26, 279-287.

Saulnier, L., Vigouroux, J., & Thibault, J.-F. (1995a). Isolation and partial characterization of feruloylated oligosaccharides from maize bran. *Carbohydrate Research*, 272, 241-253.

Schooneveld-Bergmans, M. E. F., Dignum, M. J. W., Grabber, J. H., Beldman, G. & Voragen, A. G. J. (1999). Studies on the oxidative cross-linking of feruloylated arabinoxylans from wheat flour and wheat bran. *Carbohydrate Polymers*, 38, 309-317.

Singh, V., Doner, L.W., Johnston, D.B., Hicks, K. B. & Eckhoff, S.R. (2000). Comparison of coarse and fine corn fiber for corn fiber gum yields and sugar profiles. *Cereal Chemistry*, 77, 560-561.

Smith, M. M. & Hartley, R. D. (1983). Occurrence and nature of ferulic acid substitution of cell-wall polysaccharides in graminaceous plants. *Carbohydrate Research*, 118, 65-80.

Vansteenkiste, E., Babot, C., Rouau, X. & Micard, V. (2004). Oxidative gelation of feruloylated arabinoxylan as affected by protein. Influence on protein enzymatic hydrolysis. *Food Hydrocolloids*, 18, 557-564.

Whistler, R. L. (1993). Hemicelluloses. In R. L. Whistler & J. N. BeMiller (Eds.), Industrial gums, polysaccharides and their derivatives (pp. 295–308). Orlando: Academic Press.

Possible Uses of Wastewater Sludge to Remediate Hydrocarbon-Contaminated Soil

Luc Dendooven
Cinvestav,
Mexico

1. Introduction

Mexico is one of the most important producers of petroleum in the world. According to the Economist (2009) it was ranked 6th in the world in 2006. Consequently, in areas surrounding drilling sites and during transport contamination occurs frequently. Although autochthonous microorganisms in any given ecosystem are well capable of degrading petroleum (Grant et al., 2007), different techniques, such as phytoremediation, bioaugmentation or biostimulation, have been applied to accelerate removal of hydrocarbons and reduce the residual concentration (Fernández-Luqueño et al., On line). Cultivation of plants in a petroleum contaminated soil or phytoremediation is known to accelerate removal of hydrocarbons from soil, but not always (Barea et al., 2005; Álvarez-Bernal et al., 2007). Bioaugmentation or the application of microorganisms to soil that are capable of degrading petroleum components should normally accelerate removal of hydrocarbons, but their low mobility and survival in soil often hamper dissipation of the contaminants (Bouchez et al., 1999; Teng et al., 2010). Biostimulation or the application of organic wastes to a contaminated soil is the easiest and most forward way to accelerate removal of hydrocarbons from soil (Scullion, 2006; de Lorenzo, 2008).

Urban wastewater was traditionally discarded in rivers contaminating the environment, although that apart from pathogens, the effect on the ecosytems was not excessive. With the onset of the industrial revolution, these practices become less and less sustainable as chemical contamination altered the river ecosystems. Treatment plants were used to treat the wastewater avoiding contamination of the surface water, but generating large amounts of wastewater sludge. This wastewater sludge was often used in agricultural practices, but its large heavy metal content and organic contaminants often limited its use. In Mexico, urban wastewater is generally low in chemical contaminants and heavy metal content, although exceptions do exist, e.g. wastewater generated in the tanneries of Leon contains large amounts of Cr (Contreras et al., 2004). In Mexico, however, wastwater sludge often contains pathogens that restrict its use in agricultural practices (Franco-Hernández et al., 2003). For instance, wastewater sludge obtained from the treatment plant in Lerma contained 30×10^3 viable eggs of helminthes. Consequently, the sludge can not be applied to arable land, but it can be applied to soil that is not used for agricultural practices, e.g. remediation of contaminated soil (USEPA 1994, 1999). This study reports on the effect wastewater sludge has on the removal of hydrocarbons from soil. Anthracene, phenanthrene or benzo(a)pyrene, recalcitrant polycyclic aromatic hydrocarbon, (PAHs), that are toxic to humans (Cai et al., 2007) were used as models in this study.

2. Materials and methods

2.1 Sampling sites, collection and characteristics of the different soils used

The soils used in the experiments reported here were collected from different arable lands or from the former lake Texcoco in the State of Mexico, Mexico, (N.L. 19o42', W.L. 98o49'; 2349 m above sea level). The climate is sub-humid temperate with a mean annual temperature of 14.8 oC and average annual precipitation of 577 mm mainly from June through August (http://www.inegi.gob.mx). The arable soils are generally low in organic matter and N depleted. The area is mainly cultivated with maize and common bean, receiving a minimum amount of inorganic fertilizer without being irrigated (http://www.inegi.gob.mx). The soil of Texcoco is characterized by a high pH and salinity. Details of the arable Acolman soil used in the experiment can be found in Betancur - Galviset al. (2006) and of the Texcoco soil in Dendooven et al. (2010). Soil was sampled at random by augering the top 0-15 cm soil-layer of three plots of approximately 0.5 ha. The soil from each plot was pooled and as such a total three soil samples was obtained.

2.2 Wastewater sludge

The wastewater sludge used in the experiments reported here was obtained from Reciclagua (Sistema Ecológico de Regeneración de Aguas Residuales Ind., S.A. de C.V.) in Lerma, State of Mexico (Mexico). Details of the wastewater sludge can be found in Franco-Hernández et al. (2003). Briefly, Reciclagua treats wastewater from different sources. Ninety percent of the sewage biosolids were from different industrial origin mainly from textile industries and the rest from households. The waste from each company must comply with the following guidelines: biological oxygen demand (BOD) less than 1000 mg dm^{-3}, lipids content less than 150 mg dm^{-3}, phenol content less than 1 mg dm^{-3} and not containing organic contaminants. The wastewater is aerobically digested in a reactor and the biosolids obtained after the addition of a flocculant is passed trough a belt filter. Ten kg of aerobically digested industrial biosolids were sampled three times aseptically in plastic bags after passing through the belt filter.

2.3 Aerobic incubation experiment, soil characterization and determination of PAHs

All the reported data were obtained from aerobic incubation experiments. The details of the experimental design and the methods used to characterize the soil can be found in each of the mentioned manuscripts. The amounts of PAHs added to soil varied although they were generally high so as to facilitate the study of the dynamics and the possible effects of the treatments.

2.4 Extraction of PAHs from soil

The amounts of Anthra, Phen and BaP in soil were measured as described by Song et al. (1995). A sample of 1.5 g of soil was weighted into a 15 ml Pyrex tube and 10 ml acetone was added, shaked in vortex and sonicated for 20 min. The PAHs extracted with acetone were separated from the soil by centrifugation at 13700 × g for 15 min, the supernatant was added to 20 ml glass flasks and the acetone used to extract PAHs was left to evaporate. The same procedure was repeated twice more and the extracts were added to a 20 ml flask. The extracts were passed through a 0.45 μm syringe filter, the filtered extracts were concentrated to 1 ml and then analyzed by GC.

3. Results and discussion

3.1 Characteristics of the wastewater sludge and vermicompost

The pH of the sludge sampled at different times ranged from 6.4 to 8.1, while the most important nutrients, such as NH_4^+ ranged from 221 to 702 mg N kg^{-1} soil and extractable P from 11 to 600 mg P kg^{-1} dry sludge (Table 1). The high total N content, which ranged from 28 to 42 g kg^{-1} dry sludge, will provide more mineral N upon mineralization of organic N, when the wastewater sludge is added to soil (Castillo et al., 2010).

Characteristics	A	B	C	D	E
pH$_{H_2O}$	7.1 [a]	6	7.5	6.4	8.1
Conductivity (mS m^{-1})	2.6	NM [b]	5.7	5.7	7.9
Organic carbon (g kg^{-1})	499	NM	350	509	288
Inorganic C (g kg $^{-1}$)	3.9	NM	NM	NM	NM
Total N (g kg^{-1})	41	NM	33	28	42
Total P (mg kg^{-1})	5.1	NM	6.8	1.7	NM
NH$_4^+$ (mg kg^{-1})	221	3071	702	500	13000
NO$_3^-$ (mg kg^{-1})	29	NM	NM	86	122
NO$_2^-$ (mg kg^{-1})	41	NM	NM	8	8
Extractable PO$_4^{3-}$ (mg kg^{-1})	11	400	112	600	NM
Cation exchange capacity (cmol$_c$ kg^{-1})	1.6	NM	1.4	NM	NM
Cl$^-$ (g kg^{-1})	1.67	NM	NM	NM	NM
Ash (kg^{-1})	327	NM	NM	NM	NM
Na$^+$ (mg kg)	ND	NM	4792	NM	NM
Water content (g kg^{-1})	820	660	805	793	847

A: Franco-Hernandez et al. (2003) B: Betancur-Galvis et al. (2006), C: Contreras-Ramos et al. (2007), D: Fernandez-Luqueno et al. (2008), E: Lopez-Valdez et al. (2010). [a] mean of four replicates, [b] NM: Not measured. All values are on a dry matter base.

Table 1. Physicochemical characteristics of the wastewater sludge.

Heavy metal concentrations in the wastewater sludge are generally low (Franco-Hernández et al., 2003) making this wastewater sludge of excellent quality (USEPA, 1994) (Table 2). Additionally, concentrations of toxic organic compounds are also low (Reciclagua, Personal communication).

The wastewater sludge can be classified as a class "B" wastewater sludge (Franco-Hernández et al., 2003) considering its pathogen content (USEPA, 1994) (Table 3). One of the problems of the wastewater sludge was its large number of eggs of Helminthes detected. Generally, the number of pathogens is one of the main limitations in the use of this kind of sludge in agricultural practices. Addition of lime to pH 12, which is a simply and unexpensive treatment, strongly reduced the number of pathogens. However, even with liming, the sludge can be applied to soil that is not used for agricultural practices, e.g. remediation of contaminated soil. Another possible disadvantage is the large EC or salt content, which ranges from 2.6 to 7.9 dS m^{-1}. Consequently long-term application of the wastewater sludge to arable land might inhibit plant growth (Mer et al., 2000). The concentrations of Na$^+$ are also high and might inhibit microbial activity and plant growth upon frequent application (Finocchiaro & Kremer, 2010).

| Metal | A | B | USEPA | |
			Excelent	Acceptable
Pb	19 [a]	ND	300	800
Mn	13	NM	NG	NG
Ni	63	NM	420	420
Co	63	NM	NG	NG
Cu	29	7.5	1500	4300
Cr	298	73	1200	3000
Zn	162	163	2800	7500
Cd	8	NM	39	85
Ag	ND	NM	NG	NG

A: Franco-Hernandez et al. (2003), B: Contreras-Ramos et al. (2007).
[a] mean of four replicates, [b] ND: Not detectable, [c] NM: Not measured, [c] NG: not given

Table 2. Concentration of heavy metals in the biosolids and USEPA norms (1994) for excellent and acceptable biosolids.

| | | | USEPA (1994) maximum acceptable limits | |
	A	B	Class A	Class B
Fungi (CFU [a] g^{-1} dry biosolids)	950 [b]	NM	ND [c]	ND
Total coliforms (CFU g^{-1} dry biosolids)	66×10^3	2×10^6	ND	ND
Faecal coliforms (CFU g^{-1} dry biosolids)	1200	NM [d]	< 1000	$< 20\times10^5$
Shigella spp. (CFU g^{-1} dry biosolids)	ND	ND	ND	ND
Salmonella spp. (CFU g^{-1} dry biosolids)	250	2	< 3	< 300
Viable eggs of Helminthes (eggs kg^{-1} dry biosolids)	30×10^3	ND	$< 10\times10^3$	$< 35\times10^3$

A: Franco-Hernandez et al. (2003), B: Contreras-Ramos et al. (2005).
[a] CFU: colony forming units, [b] mean of four replicates, [c] ND: not detectable, [d] NM: not measured

Table 3. Microorganisms in the wastewater sludge and maximum allowed limits of them (USEPA, 1994).

3.2 Dynamics of polycyclic aromatic hydrocarbons in soil

In all of the experiments done, abiotic factors had only a small effect on the concentrations of phenanthrene, anthracene or benzo(a)pyrene in soil (Table 4). On average, 81% of the Anthra added to soil was extracted from soil immediately. For BaP the mean amount extracted from soil immediately was 78% and for Phen 73%. Similar results were reported by Song et al. (2002). They found recoveries of 93% for Anthra, 74% for Phen, and 71% for BaP from soil with 98% sand.

The amount of Anthr that was not extractable from sterilized soil between day 0 and the end of the experiment, i.e. varying between 70 and 112 days, was on the average 5%, while it was 4% for BaP and Phen. Consequently, the sequestration of the studied PAHs was low in the agricultural soil. Some authors reported an increased sequestration and a decreasing

	Anthracene			Benzo(a)pyrene			Phenanthrene		
	Ext [a]	Seq [b]	Bio [c]	Ext	Seq	Biol	Ext	Seq	Biol
References				(%) Acolman soil					
Contreras-Ramos et al. (2006)	14	11	18	7	8	11	27	11	50
Betancur-Galvis et al. (2006)	28	0	39	35	5	31	17	6	38
Alvarez-Bernal et al. (2006)	31	5	63	31	5	46	33	0	66
Rivera-Espinoza and Dendooven (2007)	ND	4	25	39	0	58	ND	1	36
Contreras-Ramos et al. (2006)	0	6	35	0	2	14	25	2	70
Fernandez-Luqueno et al. (2008)	24	ND	ND	ND	ND	ND	32	ND	ND
Mean	19	5	36	22	4	32	27	4	52
				Texcoco soil					
Betancur et al. (2006)	18	8	12	26	10	4	5	16	18

[a] Ext: Difference between the amount of PAHs added to soil and extracted immediately after expressed as a percentage of the total amount added, [b] Seq: Difference between the amount of PAHs added to the sterilized soil and extracted at the end of the incubation expressed as a percentage of the total amount added, [c] Biol: Difference between the amount of PAHs added to the unsterilized soil and extracted at the end of the incubation expressed as a percentage of the total amount added.

Table 4. Percentage of anthracene, phenanthrene and benzo(a)pyrene removed from the soil due to abiotic processes, i.e. the amount that was not extractable (Ext) and sequestered (Seq), and the amount removed biologically (Bio) from the Acolman and Texcoco soil.

extractability of PAHs, with aging of contaminated soil (Nam and Alexander, 2001). Northcott and Jones (1999) found that extraction of BaP decreased 17% after 525 days aging. Most of the PAHs that was not extractable from soil was biologically removed. Approximately 36% of the Anthra added was biologically removed, 32% of BaP and 52% of Phen. It is well known that soil microorganisms can remove hydrocarbons from soil and numerous bacteria and fungi have been reported that can degrade PAHs (Fernández-Luqueño et al., On line).

3.2 The effect of wastewater sludge on removal of anthracene, BaP and phenanthrene from soil

Application of sewage sludge accelerated and reduced the final concentrations of PAHs in soil. In the agricultural soil 39% of the Anthra and 38% of the Phen was removed after 112 days, but 54% and 73%, respectively, when wastewater sludge was added (Table 4). The effect of wastewater sludge on the removal of BaP in the agricultural soil was smaller. Thirty one % of BaP was removed from soil and 35% when wastewater sludge was added after 112 days. The

application of wastewater sludge had an even larger effect on the removal of PAHs from the Texcoco soil. The biological removal of Anthr increased approximately 3.5 times, BaP 6 times and Phen 3 times in the Texcoco soil when added with wastewater sludge.

Different factors in the sludge might have contributed to the accelerated removal of PAHs from an agricultural soil. First, sludge is rich in N and P, which are important nutrients to sustain microbial activity. The agricultural soil of Acolman is N depleted, which can inhibit microbial activity and thus removal of PAHs from soil (Betancur-Galvis et al., 2006). In the Acolman soil, application of an equal amount of inorganic N and P as was applied with the sludge resulted in a similar removal of PAHs from soil (Table 4). As such, the N and P in sewage sludge stimulated removal of PAHs from soil. However, in the alkaline saline soil of Texcoco, the removal of PAHs from soil amended with sludge was higher than when applied with inorganic N and P. The removal of Anthra was 31% when inorganic N+P was added and 43% when sludge was added. The effect of the sludge was less outspoken with BaP, but larger for Phen as 32% was abiotic removed when inorganic N+P was added, but 52% when sludge was added. The pH in the alkaline saline Texcoco soil is high so it can be argued that changes in pH due to the application of the sludge accounted for the higher removal of the PAHs from the soil. However, adjusting the pH in the soil amended with sludge to the same pH as in the unamended soil did not affect removal of PAHs from soil (Fernández-Luqueño et al., 2008). Another factor that might have contributed to the accelerated removal of the PAHs when sludge was added to soil were the microorganisms in the sludge. Survival of microorganisms added to soil is normally low as competition for resources, i.e. C substrate, is strong and autochthonous microorganisms are better adapted to soil conditions. However, in the Texcoco soil microorganisms added with the sludge might contribute to the removal of PAHs from soil. For instance, in soil amended with 1200 mg Phen kg^{-1}, 109 mg was extracted when sludge was added, 218 mg in the unamended soil and 316 mg in soil amended with sterilized sludge (LSD=195 mg). The micronutrients in the wastewater sludge might also have stimulated microbial activity and thus removal of PAHs from soil.

Application of wastewater sludge often accelerates removal of PAHs from soil, but not always, even when using the same soil. Rivera-Espinoza et al. (2006) added wastewater sludge to soil contaminated with anthracene, benzo(a)pyrene and phenanthrene and found no significant effect on their removal.

4. Conclusion

It was found that application of wastewater sludge stimulated removal of PAHs from soil, but not always. The nutrients in the sewage sludge are important for this increased removal, although the microorganisms in the sludge might contribute to the increased dissipation especially in an alkaline saline soil. Additionally, the organic material in the sludge will improve the soil structure and aeration, thereby further improving the removal of contaminants from soil.

5. Acknowledgements

6. References

Álvarez-Bernal, D.; Contreras-Ramos, S.; Marsch, R. & Dendooven, L. (2007). Influence of catclaw *Mimosa monancistra* on the dissipation of soil PAHs. *International Journal of Phytoremediation* 9, 79-90.

Alvarez-Bernal, D.; Garcia-Diaz, E.L.; Contreras-Ramos, S.M. &Dendooven L (2006). Dissipation of polycyclic hydrocarbons from soil added with manure or vermicompost.Chemosphere 65, 1642-1651.

Barea, J.M.; Pozo, M.J.; Azcon, R.& Azcon-Aguilar, C. (2005). Microbial co-operation in the rhizosphere. *Journal of Experimental Botany* 56, 1761-1778.

Betancur-Galvis, L.A.; Alvarez-Bernal, D.; Ramos-Valdivia, A.C. & Dendooven, L. (2006). Bioremediation of polycyclic aromatic hydrocarbon-contaminated saline-alkaline soils of the former Lake Texcoco. *Chemosphere* 62, 11, 1749-1760.

Bouchez, N.; Rakatozafy, M.H.; Marchal, R.; Leveau, J.Y. & Vandecasteele, J.P. (1999). Diversity of bacterial strains degrading hexadecane in relation to the mode of substrate uptake. Journalof Applied Microbiology 86, 421-428.

Cai, Q.Y.; Mo, C.H.; Li, Y.H.; Zeng, Q.Y.; Katsoyiannis, A.; Wu, Q.T. & Férard, J.F. (2007). Occurrence and assessment of polycyclic aromatic hydrocarbons in soils from vegetable fields of the Pearl River Delta, South China. *Chemosphere* 68, 159-168. doi: 10.1016/j.chemosphere.2006.12.015.

Castillo, M.S.; Sollenberger, L.E.; Vendramini, J.M.B.; Woodard, K.R.; Gilmour, J.T.; O'Connor, G.A.; Newman, Y.C.; Silveira, M.L. & Sartain, J.B. (2010). Municipal Biosolids as an Alternative Nutrient Source for Bioenergy Crops: II. Decomposition and Organic Nitrogen Mineralization. Agronomy Journal 102 (4), 1314-1320.

Contreras-Ramos, S. M.; Alvarez Bernal, D. & Dendooven, L. (2006). *Eisenia fetida* increased removal of polycyclic aromatic hydrocarbons from soil. *Environmental Pollution* 141, 396-401.

Contreras-Ramos, S.M.; Álvarez-Bernal D. &. Dendooven L. (2007). Dynamics of nitrogen in soil contaminated with polycyclic aromatic hydrocarbons amended with biosolid and vermicompost in the presence of *Eiseniafetida.* Chemosphere 67, 2072-2081.

Contreras-Ramos, S.M.; Alvarez-Bernal, D.; Trujillo-Tapia, N. & Dendooven, L. (2004). Composting of tannery effluent with cow manure and wheat straw. *Bioresource Technology* 89, 223-228.

Contreras-Ramos, S.M.; Escamilla-Silva, E.M. &Dendooven, L., 2005. Vermicomposting of biosolids with cow manure and oat straw.Biology and Fertility of Soils 41, 190-198.

De Lorenzo, V. (2008). Systems biology approaches to bioremediation. *Current Opinions in Biotechnology* 19, 579-589. doi: 10.1016/j.copbio.2008.10.004.

Dendooven, L.; Alcántara-Hernández, R.J.; Valenzuela-Encinas, C.; Luna-Guido, M.; Perez, F. & Marsch R. (2010). Dynamics of carbon and nitrogen in an 'extreme' alkaline saline soil: a review. *Soil Biology & Biochemistry* 42, 865-877.

Fernández-Luqueño, F.; Valenzuela-Encinas, C.; Marsch, R.; Martínez-Suárez, C.;Vázquez-Núñez, E.& Dendooven, L. (2010). Microbial communities to mitigate contamination of PAHsin soil—possibilities and challenges: a review. *Environment Science Pollution Research*.On line

Fernández-Luqueño, F.; Marsch, R.; Espinosa-Victoria, D.; Thalasso, F.; Hidalgo Lara, M.E.; Munive, A.; Luna-Guido, M.L. & Dendooven L. (2008). Remediation of PAHs in saline-alkaline soils amended with wastewater sludge. *Science of the Total Environment* 402, 18-28.

Finocchiaro, R.G. & Kremer, R.J. (2010). Effect of Municipal Wastewater as a Wetland Water Source on Soil Microbial Activity. Communications in Soil Science and Plant Analysis 41 (16), 1974-1985.

Franco-Hernández O.; Mckelligan-González A.N.; Lopez-Olguin A.M.; Espinosa-Ceron F.; Escamilla-Silva, E. &Dendooven, L. (2003). Dynamics of carbon, nitrogen and phosphorus in soil amended with irradiated, pasteurized and limed biosolids. *Bioresource Technology,* 87, 93-102.

Grant, R.J., Muckian, L.M., Clipson, N.J.W., Doyle, E.M. (2007).Microbialcommunity changes during the bioremediation ofcreosote-contaminated soil. *Letters in Applied Microbiology* 44, 293–300.

López-Valdez, F.; Fernández-Luqueño, F.; Luna-Guido, M.L.; Marsch, R.; Olalde-Portugal, V. & Dendooven L. (2010). Microorganisms in wastewater sludge contributed to rapid immobilization of inorganic nitrogen when addedto an extreme alkaline saline soil. Applied Soil Ecology 45, 225–231.

Mer, R.K.; Prajith, P.K.; Pandya, D.H. & Pandey, A.N. (2000). Effect of salts on germination of seeds and growth of young plants of *Hordeum vulgare*, *Triticum aestivum*, *Cicer arietinum* and *Brassica juncea*. Journal of Agronomy and Crop Science – Zeitschrift fur Acker und Pflanzenbau 185 (4), 209-217.

Nam, K. & Alexander, M. (2001). Relationship between biodegradation rate and percentage of a compound that becomes sequestered in soil. *Soil Biology and Biochemistry*33, 787-792.

Northcott, G.L. & Jones, K.C.(1999). Partitioning, extractability, and formation of nonextractable PAH residues in soil. 1. Compound differences in aging and sequestration.*Environmental Science & Technology*159, 52-64.

Scullion, J. (2006). Remediating polluted soils. *Naturwissenschaften* 93, 51-65. doi: 10.1007/s00114-005-0079-5.

Rivera-Espinoza, Y. & Dendooven L. (2007). Dynamics of carbon and nitrogen in a mixture of polycyclic aromatic hydrocarbons contaminated soil amended with organic residues. *Environmental Technology*28, 883-893.

Scullion, J. (2006). Remediating polluted soils. *Naturwissenschaften* 93, 51-65. doi: 10.1007/s00114-005-0079-5.

Song, Y.F.; Jing X.; Fleischmann S. & Wilke B.M. (2002).Comparative study of extraction methods for the determination of PAHs from contaminated soils and sediments. *Chemosphere* 48, 993-1001.

Song, Y.F.; Ou, Z.Q.; Sun, T.H.; Yediler, A.; Lorinci, G. & Kettrup, A. (1995). Analytical method for polycyclic aromatic hydrocarbons (PAHs) in soil and plants samples. *Chinese Journal of Applied Ecology* 6, 92-96.

Teng, Y.; Lou, Y.; Sun, M.; Liu, Z.; Li, Z. & Christie, P. (2010). Effect of bioaugmentation by *Paracoccus* sp. strain HPD-2 on the soil microbial community and removal of polycyclic aromatic hydrocarbons from an aged contaminated soil. Bioresource Technol 101:3437-3443. doi: 10.1016/j.biortech.2009.12.088

The Economist (2009). *Pocket world in figures.* Profile Books Ltd, London UK.

USEPA (1994). *A plain English guide to the EPA Part 503 biosolids rule U.S.EPA/832/r-93/003*. Environmental Protection Agency Office of Wastewater Management. Washington D. C.

USEPA (1999). *Environmental regulations and technology*. Control of pathogens and Vector attraction in sewage sludge. (including domestic septage). Under 40 CFR Part 503. Appendix F, G, and I. EPA/625/R-92-013. U.S. Environmental Protection Agency Office of Research and Development. National Risk Management Research.

Waste-Water Use in Energy Crops Production

Cecilia Rebora, Horacio Lelio, Luciana Gómez and Leandra Ibarguren
Facultad de Ciencias Agrarias - Universidad Nacional de Cuyo
Argentina

1. Introduction

1.1 Waste water use in irrigation

Water supply and water quality degradation are global concerns that will intensify with increasing water demand; for this reason, worldwide, marginal-quality water will become an increasingly important component of agricultural water supplies, particularly in water-scarce regions. The status of severe water resource shortage determines that new water source must be developed to cope with the deficiency of water sources for agriculture irrigation. One of the major types of marginal-quality water is the wastewater from urban and peri-urban areas (Pedrero *et al.*, 2010). The municipal wastewater is a potential water resource with stability of water quantity and reliable supply. Irrigation with reclaimed municipal wastewater that is properly treated and satisfied with the agricultural recycling standards has huge benefits and profound social effects (Shi *et al.*, 2008).

In recent years wastewater use has gained importance in water-scarce regions. In Pakistan 26% of national vegetable production is irrigated with wastewater (Ensink *et al.*, 2004). In Ghana, informal irrigation involving diluted wastewater from rivers and streams occurs on an estimated 11,500 hectares, an area larger than the reported extent of formal irrigation in the country (Keraita and Drechsel, 2004). In Mexico about 260,000 hectares are irrigated with wastewater, mostly untreated (Mexico CAN, 2004).

Wastewater reuse in agriculture is an ancient practice that has been generally implemented worldwide. Agricultural deployment of wastewater for irrigation is based on the value of its constituents, which are used as fertilizers. However, crop irrigation with insufficiently treated wastewater may result in health risks. The use of sewage effluent for irrigation exposes the public to the dangers of infection with a variety of pathogens such as bacteria, viruses, protozoa and helminths. Thus the benefit of wastewater reuse is limited by its potential health hazards associated with the transmission of pathogenic organisms from the irrigated soil to crops, to grazing animals and humans (Gupta *et al.*, 2009). Human health risks from wastewater irrigation include firstly farmers' and consumers' exposure to pathogens including helminth infections, and secondly, organic and inorganic trace elements. Protective measures such as wearing boots and gloves, and changing irrigation methods can reduce farmer exposure (Qadir *et al.*, 2010).

1.2 Energy crops and biofuels

Energy crops, also called "bioenergy crops", are grown for the specific purpose of producing energy (electricity or liquid fuels). As these crops are not grown for the purpose of producing food, there are no health risks implicated for the consumers.

The possibility of using biomass as a source of energy in reducing green-house gas emissions is a matter of great interest. In particular, biomass from agriculture represent one of the largest and most diversified sources to be exploited and more specifically, ethanol and diesel deriving from biomass have the potential to be a sustainable means of replacing fossil fuels for transportation (Singh *et al.*, 2008; Dalla Marta *et al.*, 2010).

These liquid biofuels are bioethanol (gasoline-equivalent) and biodiesel (diesel-equivalent).

Bioethanol is used as an additive or substitute for gasoline, and biodiesel, alone or combined with diesel for diesel engines. The first is obtained from fermentation of grains such as maize starch-, sugar cane or reserve organs rich in carbohydrates (Jerusalem artichoke, sugar beet, among others). Biodiesel comes from vegetable oils through a chemical process called "transesterification" (Huergo, 2001).

Bioethanol is by far the most common biofuel in use worldwide. Global bioethanol production increased from 4.4 billion litres in 1980 to 46.2 billion litres in 2005 (Fig. 1). The largest producers of ethanol are United States, Brazil and China. Bioethanol is produced from the fermentation of starch or sugar-rich crops. Bioethanol can also be produced from cellulosic materials, such as trees, grasses, and agriculture residues. However, cellulosic ethanol is not yet commercially viable due to high production costs (Fulton *et al.*, 2004; de Vries *et al.*, 2010).

Global biodiesel production increased from 11.4 million litres in 1991 to 3.9 billion litres in 2005. Germany, France, United States, and Italy are the leading producers of biodiesel. This biofuel can be produced from vegetable oil, used frying oil, or animal fat through a transesterification process in which oil molecules react with an alcohol and a catalyst to form fatty acid- methyl esters (FAME or biodiesel) and glycerol (Pin Koh and Ghazoul, 2008).
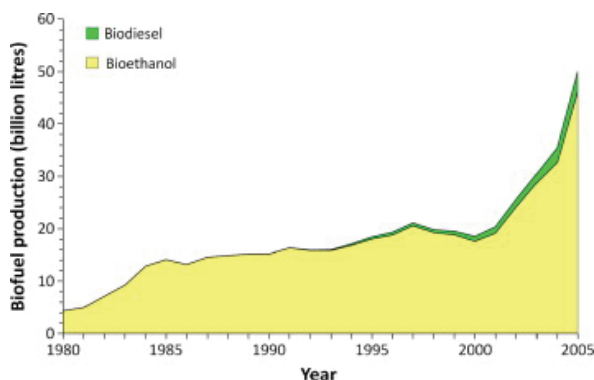
Fig. 1. Increase in global production of bioethanol and biodiesel between 1980 and 2005. Taken from Pin Koh and Ghazoul, 2008.

Argentina is today the fourth largest producer of biodiesel after the European Union, United States and Brazil. Most of Argentina's biodiesel is already destined to foreign markets. The Argentine biodiesel industry is mainly based on the use of soybean as feedstock. The ethanol production complex in Argentina is mainly comprised by sugar mills in the northwestern part of the country. However, the ethanol produced by these firms is not exclusively meant for fuel usage. In 2006, a large ethanol distillery was inaugurated in the Tucumán province, aimed at producing ethanol fuel for the domestic and export markets[1].

---

[1] http://www.argentina.gov.ar/argentina/portal/papups/biofuels-opportunities.pdf

2. Waste water use in energy crops production in Mendoza, Argentina: research experience

In Argentina we have no available data of wastewater use for irrigation; but information from Mendoza province is the following: 3.2 m³/s of domestic efluents are generated; it is estimated that 10,300 hectares are irrigated with urban waste water with different treatment level (G. Fasciolo, personal communication, 2010).

Mendoza weather conditions may be labeled 'warm-arid'. Annual rainfall ranges from 100 mm in the north, up to 400 mm in the south, with a mean annual temperature varying from 13°C in the south to 20°C in the north (Guevara, 1997). Irrigation is essential for crops production. The main species grown in Mendoza province are wine-grape, some fruit trees, and vegetables such as garlic, onion, potato and tomato.

In order not to compete for water with these traditional species, we studied energy crops production using waste water irrigation. Jerusalem artichoke (*Helianthus tuberosus* L.) and rape (*Brassica napus* L.) were selected for this study.

Photo 1. Horacio Lelio (one of the authors of this chapter) between the two energy crops tryed in our research, "rape" in the left and "Jerusalem artichoke" in the right, december 2008.

Jerusalem artichoke is a potentially useful crop for bioetanol production (Kays and Nottingham, 2008). Some studies indicate that 4,500 l of ethanol can be produced from 50 tons of tubers. Rape oil can be used as raw material to produce biodiesel (de Vries, 2010).

2.1 Brief characterization of the energy crops studied

Brassica napus L. ("rape" or "canola") is a cultivated plant of the Brassica family. It is an annual plant that reaches 0.3 to 1 m tall, leaves are 5 to 40 cm long, flowering occurs in early spring with yellow flowers, the fruit is a siliqua from 5 to 7 cm with several seeds 1.5 mm in diameter.

Canola is the name given to certain varieties of oilseed rape. This name is a trademark for a hybrid variety of rape initially bred in Canada.

Photo 2. Rape in flower, spring 2008.

Photo 3. Jerusalem artichoke in flower, March 2008.

Rape is cultivated worldwide for forage, vegetable oil for human consumption and biodiesel. The major producers are the European Union, Canada, United States, Australia, China and India.

According to the United States Agriculture Department, rapeseed was the third largest source of vegetable oil in 2009, after soybean and palm[2].

The main use of rapeseed oil is biodiesel production. This biofuel may be used in pure form in newer engines without damage, and is frequently combined with fossil-fuel diesel in ratios varying from 2% to 20% biodiesel. Rapeseed oil is the preferred oil stock for biodiesel

---

[2] http://es.wikipedia.org/wiki/Brassica_napus

production in most of Europe, partly because rapeseed produces more oil per unit of land area compared to other oil sources, such as soy beans[3].

Helianthus tuberosus L. ("Jerusalem artichoke", "sunroot", "sunchoke" or "topinambur") is a species of sunflower native to North America, and long used by the American Indian for food. It has been introduced and became naturalized in all temperate regions in the Northern and Southern Hemispheres. It is also cultivated widely across the temperate zone for its tubers, which are used as root vegetable (Duke J., 1983).

It is an herbaceous perennial plant growing to 1.5–3 m tall. The flowers are yellow, produced in capitate flowerheads which are 5–10 cm in diameter. The tubers are elongated and uneven, typically 7.5–10 cm long and 3–5 cm thick, and vaguely resembling ginger root, with a crisp texture when raw. They vary in color from pale brown to white, red or purple (Huxley, *et al.*, 1992).

The main uses of Jerusalem artichoke are: horticulture, forage and industry (inulin extraction and ethanol production).

2.2 Waste-water use in energy crops production: our experiences

We conducted a trial in which yield and potential to produce ethanol of Jerusalem artichoke and yield and potential to produce biodiesel of a winter rape cultivar were compared. Two types of irrigation: urban waste water (UWW) and ground water (GW) were used (Table 1).

Both researches were conducted in the Urban Waste Water Treatment Plant of Obras Sanitarias Mendoza in Tunuyán (33°32'89'' S and 69°00'80'' W). The characteristics of the soil of the trial are shown in table 2.

Photo 4. Urban Waste Water Treatment Plant of Obras Sanitarias Mendoza in Tunuyán; the treatment pools are behind the trees.

---

[3] http://www.openmarket.org/2007/11/12/biofuel-mandates-cause-global-warming-scientists-say/

Parameter	GW	UWW
Electrical conductivity (dS/M)	0.42	1.10
Total nitrogen (mg/l)	5.6	28.7
Mineral nitrogen, $NH_4 + NO_3$ (mg/l)	1.05	14.7
Phosphorus, P (mg/l)	0.13	11.51
Phosphorus, PO_4^{-3} (mg/l)	0.39	35.3
Potassium, K (mg/l)	11	20
Potassium, K_2O (mg/l)	13.2	24
Organic matter (mg/l)	73.4	236

Table 1. Characterization of irrigation waters, ground water (GW) and urban waste water (UWW)

Photo 5. Appearance of the waste water used for irrigation.

Variable	Soil Condition	
Depht (cm)	0-10	10-30
pH	6.63	6.76
Electrical conductivity (dS/M)	19.80	12.20
Saturation percentage (g%g)	35	49.8
sedimentation volume (ml%g)	116	124
Total nitrogen (mg/kg)	5570	3780
Phosphorus (1:10) (mg/kg)	26.2	13.3
Exchangeable Potassium (mg/kg)	1149	740
Organic matter (g%g)	9.2	6.2
C/N Relationship	9.6	9.5

Table 2. Soil characterization

2.3 Jerusalem artichoke trial
2.3.1 Materials y methods

Two cultivars of Jerusalem artichoke were tryed (red tubers, **R**, and white tubers, **W**), and two kinds of waters were used for irrigation (urban waste water, **UWW**, an ground water, **GW**).

Photo 6. Tubers of the two Jerusalem artichoke cultivars tryed in this experience. R, with red tubers, in the left; and W, with white tubers, in the right.

The experimental test had a random plot design, with 3 repetitions per treatment (each combination of cultivar and kind of water). The planting density was 25,000 plantas/hectares; 0.8 m between rows and 0.5 m between plants in the row. The tubers seed weight was around 50 g, and planting depth was 10 cm. It was carried out manual weed control and we did weekly irrigations with 22 mm of water (35 applications in total = 767 mm). We harvested individual crop plants and in each one, the following parameters were determined:

• Performance of tubers per plant (kg)
• Number of tubers per plant
• Height (m)
• Number of main stems
• Performance of dry biomass (kg). On a sample of biomass combustion heat was determined, with a calorimeter bomb.

In laboratory, we estimated the potential to produce bioethanol from tubers, taking into account the following relationship: for each kg of fermentable carbohydrates, 0.5563 l of ethanol is obtained[4].

2.3.2 Results

Jerusalem artichoke tuber yield showed differences between type of water treatment, being 177,750 kg/hectares in UWW and 144,000 kg/hectares in GW.

---

[4] http://journeytoforever.org/biofuel_library/ethanol_motherearth/meCh2.html

Varieties	UWW	GW
R	206,250	154,000
W	149,500	134,250
Average	177,750	144,000

Table 3. Tuber yield per hectare (kg) for each irrigation treatment (ground water GW and urban waste water UWW) and for two varieties (R and W).

In both varieties yield was higher when UWW was used for irrigation. R had higher yield than W variety. Yields in this trial were bigger than those got in Australia when Jerusalem artichoke was irrigated using UWW; Parameswaran (1999) in that country had 120,000 kg tubers/ hectare.

Number of tubers produced per plant was significantly higher in those urban waste water irrigated. Besides, plants belonging to W variety had significantly more tubers than R plants. Results can be seen in the following table.

Varieties	UWW	GW
R	94.27 b	66.08 b
W	122.53 a	113.08 a
Average	108.4 a	89.58 b

Table 4. Number of tubers per plant for each irrigation treatment (ground water GW and urban waste water UWW) and for two varieties (R and W).
Different letters indicate significant differences at P = 0.05

Plant height significantly differed between irrigation treatments (P= 0,00001), but did not between varieties (P= 0.1257). Results are shown in table 5.

Varieties	UWW	GW
R	3.07 a	2.56 a
W	2.87 a	2.86 a
Average	2.97 a	2.71 b

Table 5. Plant height (m) for each irrigation treatment (ground water GW and urban waste water UWW) and for two varieties (R and W).
Different letters indicate significant differences at P = 0.05

The number of main stems per plant differed significantly betwen kind of irrigation water (p= 0.0013), but did not differ between varieties (p= 0.5207). Plants irrigated with urban waste water had more stems than those ground water irrigated (table 6).

Varieties	UWW	GW
R	1.47 a	1.39 a
W	1.62 a	1.32 a
Average	1.54 a	1.35 b

Table 6. Number of main stems per plant for each irrigation treatment (ground water GW and urban waste water UWW) and for two varieties (R and W).
Different letters indicate significant differences at P = 0.05

Dry aerial biomass per plant differed between irrigation treatments (P= 0.00001) and between varieties (P= 0.0125). It was higher in plots irrigated with UWW and in R variety, as can be seen in table 7.

Varieties	UWW	GW
R	0.87 a	0.58 a
W	0.71 b	0.62 a
Average	0.79 a	0.60 b

Table 7. Aerial dry biomass per plant (kg) for each irrigation treatment (ground water GW and urban waste water UWW) and for two varieties (R and W).
Different letters indicate significant differences at P = 0.05

The remanent dry aerial biomass of the crop per ha was 23,250 kg in UWW and 17,750 kg in GW. The combustion heat of it was 3,668 kcal/kg, representing an important energy contribution that can be usefull in the industrial process for obtaining ethanol.

The potential to produce ethanol was 15,000 l/ha in plots irrigated with UWW and 13,000 l/ha in the GW irrigated. Ethanol potential production was estimated from the amount of fermentable carbohydrates in the tubers. To produce 1 l of ethanol from tubers, 11 kg were needed, considering that soluble solids in tubers were about 16% (Lelio *et al.*, 2009).

Tuber yield of both varieties of Jerusalem artichoke urban wastewater irrigated is higher of that found when the crop is ground water irrigated. This high yield is related to more tubers per plant, higher plants, more stems per plant, and higher aerial biomass per plant.

2.4 Rape trial
In this work yield and potential to produce biodiesel of a winter rape cultivar under two irrigation treatments (urban waste water (UWW) and ground water (GW)) were compared.

2.4.1 Materials and methods
The experimental test had a random plot design, with 3 repetitions per treatment (each kind of irrigation water, UWW and GW). "Gospel" winter rape cultivar was grown. Sowing date was February 28th, 2008, and a density of 8 kg/ hectare was sown, with a distance of 0.4 m between rows. Each plot had 7 rows of 5 m long. It was carried out manual weed control and we did weekly irrigations (32 applications in total = 700 mm). At the end of November, 2008, the plots were harvested and the following parameters were determined:
- Number of plants per square meter.
- Number of siliqua per plant, on 30 plants randomly taken in each plot.
- Number of seed per siliqua, on 150 siliqua randomly taken in each plot.
- One thousand seeds weight, on five groups of 1000 seeds per experimental plot.
- Seed yield per unit surface. Cut in farm and laboratory threshing.
- Oil in seeds, Soxlhet methodology.

Variance tests were performed to compare the previous parameters.

2.4.2 Results
In the following table results of yield components for each irrigation system (UWW and GW) are shown.

Yield component	Kind of irrigation water		Significant differences at 5 % level
	UWW	GW	
N° plants/ m²	27.5 ± 4.33	33.32± 8.77	No, p=0.3603
N° siliqua/ plant	692.3± 16.80	533.7± 16.62	Yes, p= 0.0003
N° seeds/ siliqua	23.07± 0.83	20.48 ± 0.38	Yes, p= 0.0048
1000 seeds weight	3.60± 0.10	2.43 ± 0.35	Yes, p=0.0050
% oil in seeds	36.7	36.2	-

Table 8. Number of plants/m², number of siliqua/plant, number of seeds/siliqua, 1.000 seeds weight, oil percentage in seeds in each irrigation treatment (UWW y GW) of rape grown in Tunuyán, 2008.

Photo 7. Rape crop before harvest.

As it can be seen in table 8, number of plants per unit surface did not show significant differences, average was 30.41 plants/m²; that is between the range recommended for winter cultivars, from 20 to 60 plants/m² (Iriarte and Apella, 2007).

The number of siliqua per plant significantly differed between irrigation treatments. We found 692.3 siliqua per plant in UWW plots and 533.7 in GW plots; both higher than values indicated by other authors (Iriarte y Valetti, 2008, Tamagno *et al.*, 1999).

The number of seeds per siliqua differed between UWW and GW irrigation treatments. Siliqua from UWW plots had 23.07 seeds average, while GW siliqua had 20.48 seeds.

One thousand seeds weight presented significant differences. Bigger seeds were produced in UWW compared with GW.

Rape yield can be estimated from yield componentes: number of plants per unit surface, number of siliqua per plant, number of seeds per siliqua, and seeds weight (Gómez and Miralles, 2006). In our trial, yield estimations were 15,811 kg/ hectare in UWW and 8,851 kg/ hectare in GW treatment.

Harvest plots yield results

In UWW plots yield was higher (7,690 kg/ hectare) than in GW plots (3,886 kg/ hectare). These values of yield are very high; probably associated to the high level of nutrients in the irrigation UWW (Rebora *et al.*, 2010).

Photo 8. Rape harvest, december 2008.

Photo 9. Final dry of siliqua in laboratory.

Oil

Oil percentage found in seeds of both treatments was lower than that indicated for Gospel cultivar (47%). It was 36.7 in UWW and 36.2% in GW seeds. Usually, seed yields are associated with low oil percentage in seeds. Besides, high levels of nitrogen fertilization tend to reduce oil content in seeds.

Variable	Kind of irrigation water	
	UWW	GW
Seed yield (kg/ha)	7,690	3,886
Oil (%)	36.7	36.2
Oil yield (kg/ha)	**2,822**	**1,406**

Table 9. Oil yield of rape grown under two irrigation treatments (UWW, urban waste water, and GW, ground water) in Tunuyán, Mendoza, 2008.

Biodiesel production

Every 100 litres oil, 100 litres biodiesel can be obtained (Muñoz, 2005). According to the previous relation, the oil that could be obtained represents the ammount of biodiesel that could be produced per unit surface; this is 2,822 l biodiesel/hectare when rape is irrigated with urban waste-water and 1,406 litres biodiesel/ha when it is irrigated with ground water. From our results we are able to say that the use of urban waste water in rape irrigation allows to reach very high yields, both of seeds and biodiesel per unit surface.

3. Conclusions

In recent years waste-water use has gained importance in water-scarce regions. Waste-water reuse in agriculture is an old practice that has been generally implemented worldwide. Agricultural deployment of wastewater for irrigation is based on the value of its water content and its constituents, which are used as fertilizers. However, crop irrigation with insufficiently treated wastewater may result in health risks. Energy crops, not grown for the purpose of producing food, have no health risks implicated for the consumers. Many crops can be used as energy crops for biofuels (bioethanol and biodiesel) production.

Mendoza province generates 3.2 m^3/s of domestic efluents. It is estimated that 10,300 hectare are irrigated today with urban waste water with different treatment level. There are still many ha that could be used for energy crops using remanent urban waste-water.

Both "rape" and "Jerusalem artichoke" have shown to be interesting energy crops under urban waste-water irrigation in Mendoza, Argentina, For biodiesel and bioethanol production, respectively.

To conclude, urban waste-water could be used to enlarge oasis in Mendoza, and energy crops such us rape and Jerusalem artichoke present higher yields when they are irrigated with this type of water compared to the yields of those crops using ground water irrigation.

4. Acknowledgement

5. References

Dalla Marta, A., Mancini, M., Ferrise, R., Bindi, M., Orlandini, S. 2010. Energy crops for biofuel production: Analysis of the potential in Tuscany. B i oma s s and b i o e n e rgy 3 4: 1 0 4 1 – 1 0 5 2.

de Vries, S. C., van de Ven, G. W. J., van Ittersum, M. K., Giller, K. E. 2010. Resource use efficiency and environmental performance of nine major biofuel crops, processed by first-generation conversion techniques. B i o m a s s and b i o energy 3 4: 5 8 8 – 6 0 1.

Duke, J. A. 1983. Handbook of Energy Crops. http://www.hort.purdue.edu/newcrop/duke_energy/Helianthus_tuberosus.html

Ensink, H.H., Mehmood, T., Vand der Hoeck, W., Raschid-Sally, L., Amerasinghe, F.P., 2004. A nation-wide assessment of wastewater use in Pakistan: an obscure activity or a vitally important one? Water Policy 6, 197–206.

Fulton, L., Howes, T., Hardy, J. 2004. Biofuels for transport: an international perspective. International Energy Agency, Paris, France. In: http://www.iea.org/textbase/nppdf/free/2004/biofuels2004.pdf

Gómez, N., Miralles, D. 2006. Colza. Capítulo 2.4, en: Cultivos industriales. Editorial Facultad de Agronomía. UBA.

Guevara, J. C., Cavagnaro, J. B., Estevez, O. R., Le Houérouf, H. N. and C. R. Stasi. 1997. Productivity, management and development problems in the arid rangelands of the central Mendoza plains (Argentina). Journal of Arid Environments Volume 35, Issue 4, 575-600.

Gupta, N., Khan, D.K., Santra, S.C. 2009. Prevalence of intestinal helminth eggs on vegetables grown in wastewater-irrigated areas of Titagarh, West Bengal, India. Food Control 20: 942–945.

Huergo, H. 2001. El biodiesel, una contribución de agro para mejorar el medio ambiente. Bolsa de Cereales 3026: 3-5.

Huxley, A. J., Griffiths, M. and M. Levy. 1992. The New Royal Horticultural Society dictionary of gardening. London: Macmillan Publishers. ISBN 0333474945. OCLC 29360744.

Iriarte, L., C. Appella. 2007. Densidad de siembra en cultivares invernales. Campaña 2007. Chacra Experimental Integrada Barrow. Capítulo 7: Tecnología del cultivo. Cultivo de colza. Editores Iriarte L., y O. Valetti. Chacra Experimental Integrada Barrow. Convenio MAAyP- INTA.

Iriarte, L., Valetti, O., 2008. Cultivo de colza. Editores Iriarte L., y O. Valetti. Chacra Experimental Integrada Barrow. Convenio MAAyP- INTA.

Kays, S. J. & Nottingham, S. F. 2008. Biology and Chemistry of Jerusalem Artichoke Helianthus tuberosus L. Ed. CRC Press.

Keraita, B.N., Drechsel, P., 2004. Agricultural use of untreated urban wastewater in Ghana. In: Scott, C.A., Faruqui, N.I., Raschid-Sally, L. (Eds.), Wastewater Use in Irrigated Agriculture. CABI Publishing, Wallingford, UK.

Lelio, H., Rebora, C., Gómez, L. 2009. Ethanol potential production from Jerusalem artichoke (*Helianthus tuberosus* L.) irrigated with urban waste water. Revista FCA- UNCuyo. Tomo XLI (1): 123-133.

Mexico CAN (Comision Nacional del Agua), 2004. Water Statistics. National Water Commission, Mexico City.

Muñoz, C. M. 2005. El biodiesel como solución energética. Revista Agromercado 248, pág. 6-8.

Parameswaran, M. 1999. Urban wastewater use in plant biomass production. Resourses, Conservation and Recycling, 27: 39-56.

Pedrero, F., Kalavrouziotis, I., Alarcón, J. J., Koukoulakis, P. , Asano, T. 2010. Use of treated municipal wastewater in irrigated agriculture. Review of some practices in Spain and Greece. Agricultural Water Management 97: 1233–1241.

Pin Koh, L., Ghazoul, J. 2008. Biofuels, biodiversity, and people: Understanding the conflicts and finding opportunities. B I O LO G I CA L C O NS E RVAT IO N 1 4: 2 4 5 0 –2 4 6 0.

Qadir, M., Wichelns, D., Raschid-Sally, L., McCornick, P. G., P. Drechsel, P., Bahri, A., Minhas, P. S. 2010. The challenges of wastewater irrigation in developing countries. Agricultural Water Management 97 (2010) 561–568.

Rebora, C., Lelio, H., Gómez, L. 2010. Use of urban waste water in rape (*Brassica napus* L.)production destinated to biofuel. Revista FCA- UNCuyo, Tomo 42. Nº 1, 207-212.

Shi R., Peng S., Wang Y., Zhang H., Zhao Y., Liu F. and Zhou Q. 2008. Countermeasures of Reclaimed Municipal Wastewater for Safety of Agricultural Use in China. Agricultural Sciences in China, 7(11): 1365-1373.

Singh J, Panesar BS, Sharma SK. 2008. Energy potential through agricultural biomass using geographical information system –a case study of Punjab. Biomass and Bioenergy; 32:301–7.

Tamagno, L.. N., Chamorro, A. M., S. J. Sarandón. 1999. Aplicación fraccionada de nitrógeno en colza (*Brassica napus* L.): efectos sobre el rendimiento y la calidad de la semilla. Revista de la Facultad de Agronomía de La Plata, 104 (1): 25-34.

Using Wastewater as a Source of N in Agriculture: Emissions of Gases and Reuse of Sludge on Soil Fertility

Dr. Mora Ravelo Sandra Grisell and Dr. Gavi Reyes Francisco
Colegio de Postgraduados
Mexico

1. Introduction

Nitrogen is one of the essential elements most required by plants and, for this reason, large amounts are applied for agricultural production; as consequence, N is one of the nutrients that most impacts the environment. The use of nitrogenated fertilizers and the use of residual waters as sources of nutrients for crops have increased production remarkably; however, a large part of the N supplied by fertilizers or residual waters is not recuperated in the harvest, primarily due to losses through filtration to the ground, although there are also losses to the atmosphere that have an impact on the stratosphere and participate in the greenhouse effect (Bergstrom *et al.*, 2001; Oron, *et al.*, 1999).

The continuous growth of the world population, together with industrial and agricultural activities to increase the food supply, as well as consecutive drought during the last years, have caused the consumption of existing water resources; a phenomenon that reaches its greatest expression in arid and semiarid regions.

Therefore, any source of water that can be utilized and is financially profitable must be taken into account to promote a greater development in regions with limited sources of water. It is worth mentioning that treated residual water can be used for agriculture. However, the residual water supply is not always treated (Wang *et al.*, 2007, Kiziloglu *et al.*, 2007). independently of the nutrient contribution to crops, where N is one of the main ones.

2. Nitrogen transformations

Recently, a growing concern has come up regarding the ever more popular use of nitrogenated fertilizers, both chemical or organic, since they both (along with residual waters) are used for agricultural activities, significantly contributing to environmental pollution.

Nitrogen in the soil solution is subject to a series of transformations; part of that N is consumed by the crop, while another part suffers a series of loss processes outside the soil-plant system. In agro-ecosystems without erosion, the loss of N to the atmosphere occurs through the processes of denitrification and volatilization, while lixiviation is associated with contamination of water tables. The magnitude of each of these losses will depend on the environmental and crop management conditions in place.

The environment (soil, climate, among others) is not very changeable, but crop management, especially the nutrients added through residual waters, can be optimized with the goal of maximizing their utilization (Kiziloglu *et al.*, 2007; Duxbury *et al.*, 1993).

3. Residual waters as a source of nitrogen

Residual waters are a product, fundamentally, of a population's water supply, after being made impure through various uses. From the point of view of their origin, these waters are the combination of liquids or waste dragged by the water, from houses, commercial and institutional buildings, from industrial establishments, and from underground, superficial or precipitation water that may be added (DSEUA, 2000).

Residual water contains various pollutants: total and suspended solids, biodegradable organic material (OM) (animal fats, minerals and oils), non-biodegradable OM (detergents, pesticide and solvents), toxic substances (heavy metals), nutrients (N, P and K), and various types of chemical products and pathogenic agents (bacteria, virus and protozoans) (Domínguez-Mariana *et al.*, 2004).

3.1 Nitrogen content in residual waters

Residual waters contain considerable amounts of N, which represents a benefit for agricultural activities and which can contribute to soils that are not very fertile (Agin *et al.*, 2005). It is necessary to take into consideration this contribution in N for the fertilization plan of a crop, in order to avoid excess quantities of N in the soil, since this excess can decrease production or quality in crops such as cotton, tomato for conserve, beet, potato, melon, apple and grapes (Bowder and Idelovitch, 1987).

Taking into account that residual water can have an N content of 20 to 40 mg L^{-1}, a crop that through irrigation is applied a total of 5000 m^3 ha^{-1}, receives 100 to 200 kg of N ha^{-1}. These quantities can cover the N needs of a crop in many cases (Ramos, 1998).

In Saudi Arabia, Hussain *et al.* (1996) carried out applications of 300 kg N ha^{-1} to the soil in wheat crops, from residual water with an N content of 207 mg L^{-1}. Other N contents applied on the soil from residual water were 30 to 200 mg L^{-1} (Oron *et al.*, 1991; Zekri and Koo, 1994). Hussain and Al-Jaloud (1998) carried out applications, by using waste water from aquaculture, equivalent to 150 kg ha^{-1} of N.

In Mexico, the use of residual water in Valle del Mezquital constitutes a regular practice; the volumes applied annually are between 10 000 and 20 000 m^3 ha^{-1} with concentrations of 20 to 40 mg L^{-1}, these applications represent dosages of 200 to 800 kg N ha^{-1} $year^{-1}$.

An additional problem caused by the N in residual waters is that the demand of the nutrient and water can possibly not coincide in time: in most crops, the N demand is low during the initial phase of cultivation, increases during the growth phase and is low again in the final phase of cultivation, once the plant has completed its development. An excess of N, in addition to being damaging to the plants, increases the NO_3^- lixiviation and the pollution of underground waters (Ramos, 1998).

3.1.2 The use of residual water in agriculture

The use of residual water in agriculture arose from the competition there is between cities and agriculture over the resource. The way to solve this situation was, initially, the use of water by cities, and later, its use in agriculture (Bouwer, 1992).

For Zekri and Koo (1994), the need to preserve the vital liquid, as well as the safe and economical disposal of residual water, are the factors responsible for the use of this water in agriculture, and its utilization is considered a viable option, with the advantages of being able to reduce the application of fertilizers and decrease the costs of production.

The use of water without treatment for irrigation is a popular practice in Mexico, where there are nearly 165,000 ha that are irrigated with 51 $m^3 s^{-1}$ of residual waters from the main cities (Alfaro, 1998).

According to data from the National Statistics and Information Institute (INEGI, Instituto Nacional de Estadística Geografía e Informática), the volume of residual water of urban origin was 239 $m^3 s^{-1}$ in 1002, out of which 187 $m^3 s^{-1}$ were channeled through drainage. On the other hand, in 2001, industries generated residual waters equivalent to 5.39 km^3 annually (171 $m^3 s^{-1}$).

Currently, it is estimated that out of the 145 605 L s^{-1} of residual waters (urban and industrial) generated in the country, 41 495 correspond to Mexico City's metropolitan area, 7135 L s^{-1} to Monterrey's metropolitan area and 5658 L s^{-1} to Guadalajara's.

In Mexico, the use of urban residual water for agriculture has existed since more than 100 years ago in Valle del Mezquital, located in the state of Hidalgo, the place where the world's largest (100 000 ha) and most ancient agricultural area irrigated with residual water is located (DFID, 1998). Water from Mexico City and surrounding areas constitute the main source for agricultural/livestock development in the valley, which has a limited availability of first-use water (Flores et al., 1997).

As was mentioned before, the total irrigated area in Valle del Mezquital is approximately 100 000 ha, and these are supplied with residual water (50 000 000 m^3 year^{-1}) or a mixture of residual waters and rainwater. The total water application varies from 1500 to 2000 mm ha^{-1} year^{-1}, depending on the requirements of the crops, the soil texture, the depth and the availability of water throughout the year (Gutiérrez et al., 1994).

In countries like Israel, the lack of drinking water has fostered the use of residual water in agriculture, making it one of the countries with the greatest use of residual waters to supply crops with the vital liquid. According to Harrosh (1993), two thirds of the residual water produced is recycled and 50% of the total volume of water is used for agriculture supply. The author mentions that in this country, they decided to develop an irrigation system of residual water onto soil, in order to cultivate. In the case of Australia, an increase of 100% has been registered for the use of residual water for irrigation of fruit trees in only 5 years (Snow et al., 1999).

Research about the use of residual water in different countries in the world has produced different observations. For example, Vázquez-Montiel et al. (1995) indicate that the response of soy and corn to application of residual water is favorable, yet differences are observed in grain production and N absorption. The difference was due to the time and amount of water applied, and it was observed that the decrease in residual water application during the early growing stage stimulates N absorption.

Sawwam (1992), working with chrysanthemum, found a greater number of inflorescences in plants irrigated with residual water, and an increase in the content of chlorophyll, Fe and Zn; however, the content of other nutrients (K, Mn and Cu), was not affected. In corn, it has been found that the concentration of P in plants irrigated with residual water is greater, as are those of N, Ca, Mg, Na and K (Al-Nakshabandi et al., 1997).

Studies by Hussain et al. (1996) have proven that the high production in treatments with high dosages of N can be attributed to a better physiological growth and a greater utilization

of nutrients, as compared with the control. When evaluating wheat yield, they found a response between 6.19 and 6.87 Mg ha^{-1} with the application of residual water, indicating that the nutrients present in water can be enough for an optimal growth of the crop.

Al-Nakshabandi *et al*. (1997) and Oron *et al*. (1991) also observed an increase in yields when applying residual waters, indicating that the production is favored with the sole application of waste water.

Kiziloglu *et al*. (2007) reported an N increase of 0.18% in the soil, at a depth of 30 cm, and a greater yield in the cultivation of cabbage irrigated with residual water, as compared to the yield obtained with irrigation water.

When evaluating the efficiency in N use (ENU) of residual water, Hussain *et al*. (1996) found that it is favored when N is not applied to the soil, and that it decreases with the application of nitrogenous fertilizer; they also mentioned that estimating EUN is important in order to determine the relationship between the input and the output and to save in the use of inorganic fertilizer. Oron *et al.* (1999) found that the efficiencies vary from 35 to 64%; the highest values correspond to treatments irrigated with treated residual water, due to the quantity of P, K and other lesser elements contained in the water.

With this information, we can clearly see that the agronomic and economic benefits of using residual waters in irrigation are evident, for they increase productivity (Al-Nakshabandi *et al*., 1997), thanks to the high levels of N, P and K (Pescod, 1992), and therefore, can be applied for agricultural production (Magesan *et al*., 1998). According to Jenssen and Vant (1991), the use of N and P from residual water in agriculture can reduce the use of fertilizers in 15%.

In addition to what has been described, it has been observed that mineralization of N in the soil irrigated with residual waters is a fast process, with the liberation of the greater part of the N applied, which remains available for absorption by the plant. Also, the OM in residual water has the capacity of retaining water and giving the soil structure (Oron *et. al*., 1999).

3.1.3 Economic value of residual waters

As has been discussed, residual waters constitute an alternative to be used in agriculture because of the nutrient content present, in available forms, for crops; an important factor of its use is the possibility of reducing the production costs because of the decrease in inputs.

Assuming a cost of N equivalent to urea ($1675 MX pesos Mg[-1]), the application of urban residual water for crop production represents savings, as is indicated by the following cases: in Saudi Arabia, the 300 kg N ha^{-1} applied to wheat crops by Hussain *et al*. (1996), represent $ 502.5, the 200 kg N ha^{-1} applied by Oron *et al*. (1991), correspond to $ 335, and the applications done by Hussain and Al-Jaloud (1998, represent USD $ 251.25 (for the 150 kg N ha^{-1}).

The application of residual water in Valle del Mezquital represents an investment per hectare that varies from $335.00 MX pesos, for a dosage of 200 kg N, to $1340.00 MX pesos with applications of 800 kg N ha^{-1} (Hernández *et al*., 1993).

3.1.4 Disadvantages and environmental impact of residual waters

As has been seen, the use of residual waters in agriculture is a common practice, since the OM present improves soil conditions and plant productivity. However, it contributes in a parallel manner to the contamination of soil, plants and the environment, putting human health, in general, at risk (Cuenca, 2000).

In spite of these advantages, their use can be restricted by the high content of salts, heavy metals, bacteria and virus that can be present in residual waters (Zekri and Koo, 1994), reason why developed and developing countries have decided to establish rules for their use.

The use of residential waters for crop irrigation has increased in several communities, although some factors that limit the use of residual waters for irrigation include the following (Bhatnagar *et al.*, 1992:

1. water availability at the time of irrigation
2. water quality according to the standards of use
3. disease transmission potential
4. accumulation of toxic substances

This is demonstrated by Cortés (1989), who points out that residual waters can be considered unhealthy at the time they reach the parcel, because they exceed the limits of microbe contamination suggested in Engelberg, Switzerland (1995) which should be of no more than 1000 fecal coliforms per 100 ml of water, and should not have more than one helminth L^{-1} of water (WHO, 1989).

The presence of these microorganisms in residual waters, soils and fruits, as is the case of coliforms (*Escherichia coli* and *Klebsiella pneumoniae*), *Pseudomonas* spp, and helminth eggs (*Ascaris lumbricoides* and *Trichuris trichuria*), among others,which cause real and potential risks to public health.

In Mexico, the specific and non-specific sources of residual water discharges that come from population centers, industry and agriculture, exercise a heavy pressure over most of the superficial bodies of water; 29 monitored hydrologic regions, out of a total of 37, reach an acceptable category of water quality. Out of the total load of oxygen biochemical demand (OBD), 89% is concentrated in just 15 basins, and almost 50% specifically in the Pánuco, Lerma, San Juan and Balsas rivers, causing heavy contamination in them (INEGI, 2001).

Organochloride pesticides stand out since 1948, because of the application of considerable amounts of these on crops in the region. Due to their intense use, they are widely distributed in the high region of the Gulf of California.

4. Denitrication: N$_2$O emission in wheat irrigated with residual water

Denitrification is considered the most important mechanism for N, No and N$_2$O volatilization during the N cycle in agro-ecosystems (Mosier, 2001; Oenema *et al.*, 2001; Aulakh *et al.*, 1998). Bouwman (1990) has estimated that N$_2$O emissions from the soil are approximately 90% of the total of this gas' emissions. N$_2$O is produced by microorganisms' biological activity.

The efficient use of urban residual waters for crops is an agronomic, economic and environmental necessity (Yadav *et al.*, 2003; Toze. 2006). The nitrogen applied to crops as fertilizer is not completely taken up by them. One of the mechanisms through which N is lost and its efficiency decreases, when applied to crops, is denitrification, which consists of the liberation of N oxides from the soil to the atmosphere. The latter negatively affects the producer's economy and can also affect the environment. One of the gases released is N$_2$O. This is a gas that increases the greenhouse effect with concentrations of 0.6 - 0.9 µLm_3/-year (Prinn *et al*. 2000) and contributes to the ozone layer's thinning (Aulakh *et al*., 1998). The International Panel on Climate Change (IPCC, 2001) reports that 44% of the global emission of 16.2 Tg N$_2$O N yr^{-1} is anthropogenic; out of this fraction, it is estimated that 46% comes from agricultural activities.

Magesan *et al*. (1998) indicate that approximately 2 kg N ha^{-1} from residual water are lost to denitrification, data that differ from those presented by Zheng *et al*. (1994), who estimate that approximately 16% of the nitrified N can be converted to N$_2$O. For Barton *et al*. (1999), based on the rates of denitrification in New Zealand soils that are irrigated with residual water, losses over denitrification are 2.4 kg N ha^{-1} year^{-1}, which corresponds to less than 1% of the N supplied by residual water. The same authors point out that under lab conditions, the denitrification potential can be of 13.4 kg N ha^{-1} year^{-1}; when comparing the results, they mention that the low emission is due mainly to the soil conditions, which do not favor the process, indicating that emissions to the environment can be higher than 200 kg N ha^{-1} yr^{-1}.

Similarly, the combination of muds from residual waters and nitrogenated fertilizer can make the emission of N$_2$O increase, when the NO$_3^-$ and C applied are available (Rochette *et al*., 2000; van Groeningen *et al*., 2004).

For the soils in Valle del Mezquital, Vivanco *et al*. (2001) reported amounts of N released through denitrification of 158 a 231 kg N$_2$O ha^{-1} año^{-1}.

Mora-Ravelo *et al*. (2007) reported that the N$_2$O emission was 279 kg ha^{-1} in wheat irrigated with residual waters, taking into consideration that in greenhouse conditions, N losses in gas form have been 5 to 10 times greater than those generally reported in the field, in agricultural soils (Daum and Schenk 1998), Así Likewise, Jianwen *et al.* (2005) point out that the N$_2$O emissions in wheat crops depend on the degree of development of the plant. This is generally accepted from two mechanisms for the flow of this gas in plants: N$_2$O derived from the soil that is transported by plants and N$_2$O that is directly produced by plants during N assimilation. In this study, losses because of denitrification were high, which can also be due to the phenological stages of wheat.

In face of the data exposed, we consider necessary the development of appropriate management and monitoring practices that allow a better control of the resource (Bouwer, 1992). According to Snow *et al*. (1999), it is necessary to predict and measure the concentration and distribution of elements applied in residual water, depending on the depth of the soil, since the application of waste water increases the concentration of NO$_3^-$ in the profile.

From the environmental point of view, reutilization of residual waters offers positive aspects such as the more rational utilization of the water resource and irrigation in areas where water resources are scarce, favoring the recuperation of desert lands (Crook, 1984). However, it is important to mention that until today there is only information of the damaging effect on health of microorganisms present in residual water (Zekri and Koo, 1994; DSEUA, 2000), and that the efficiency of N use is restricted to plants taking it up from NH$_3^+$ oxidation, which must be oxidized through nitrifying bacteria to NO$_3^-$ (Luna *et al.*, 2002). Therefore, it is necessary to establish the importance of microorganisms present in the residual water on the efficient use of N.

5. Biosolids as improvers of agricultural soils

Biosolids are the subproduct of the activity of purification of residual waters, which is a combination of physical, chemical and biological processes that generates huge volumes of highly decomposable organic muds. In order to ease their management, they are subjected to processes for thickening, digestion and dehydration, thus acquiring the category of biosolids: muds that are rich in organic matter, nutrients, microorganisms, water and heavy metals (Cuevas *et al*., 2006; Vélez, 2007).

Biosolid production from the treatment of residual waters is not new in the world, for reports are known from the 19th Century, and by 1921, there were commercial options from the transformation of biosolids in agricultural fertilizers. The elimination of muds in a treatment plant constitutes a problem of utmost importance in our days, which is why there is the general tendency to reduce, recycle or reuse them rationally in order to protect the environment (Seoanez, M and Angúlo, I.1999).

The tendency in organic residue management is recycling, and therefore, during the last years it has been promoted, taking into account its agricultural value as fertilizer or rectifier in the soil, for there is a general consensus among experts that many of the problems that affect soils (erosion, the dependency on chemical products and organic, mineral and microbe shortages) could decrease to a great extent with the recycling of these compounds (Ceccanti and Masciandaro, 1999; Garcia *et al.,* 1999; Masciandaro *et al.*, 2006).

The benefits of mud utilization from treatment plants in agricultural activities is due to various components, such as humic acid, microorganisms and nutrients (N, P, K), which can be employed as agricultural fertilizers. However, the agricultural use of muds can be limited by the presence of substances that are potentially toxic, such as heavy metals, pathogens and residual chemical molecules.

During the last decades, the production of urban muds has increased remarkably. The reutilization and disposal of residual muds has become an issue of great interest throughout the world. In an attempt to improve its acceptance, systems have been developed to transform residual muds into a substance similar to humus ("humification" or transformation of residual muds).

Although many of the traditional cleaning technologies for contaminated soils and water have proven to be efficient, they are usually very expensive and of intensive labor. In the case of contaminated soils, they normally require specific *in situ* techniques to minimize the secondary environmental effects; in the case of residual water, the cost-efficacy relation is always a problem in decision making. Phytoremediation offers a cost-effective option that is non-intrusive, respectful of the environment and a safe alternative to conventional cleaning techniques. This technique was widely used in artificial wetlands for residual water treatment, as a promising field in China (Zhang et al., 2007).

Recently, research has revealed the advantages of bioremediation and particularly phytoremediation, as very promising, in view of its low costs. With this, technological options keep increasing, allowing us to think that the use of biosolids in agricultural lands could become a sustainable alternative if they are managed in a responsible manner.

Biodegradation contributes to recycling in soils, in water and in the atmosphere, of different nutrients and minerals that sustain life. Thus, carbon and nitrogen cycles are essential in nature. In the last years it has been recognized that biodegradation can also be applied to potentially toxic residues, and the technique has been developed to detect and increase the natural *in situ* biorecuperation.

Phytoremediation, for example, builds wetlands that can be a respectful alternative for the environment, in cleaning residual waters, based on solid scientific research. Using different trees, shrubs and grass species to cancel, degrade or immobilize harmful chemical products can reduce the risk of contaminated water at a low cost (Weis and Weis, 2004; Shankers *et al*., 2005). There are reports that indicate that some species can accumulate certain heavy metals, although the plant species vary in their capacity to eliminate and accumulate heavy metals (Rai *et al*., 1995).

In fact, biorecuperation or bioremediation, and particularly rhizofiltration or phytoremediation, could be a good solution for the feared metals, to convert them into less toxic forms, or simply recuperate them to recycle them.

Bioremediation includes the utilization of biological systems, enzymatic complexes, microorganisms or plants, to produce ruptures or molecular changes of toxic elements, contaminants and substances of environmental importance in soils, waters and air, and to generate compounds of lesser or no environmental impact. These degradations or changes usually occur in nature, although the speed of these changes is low. Through an adequate manipulation, these biological systems can be optimized to increase the speed of change and, thus, use them in sites with a high concentration of contaminants.

Recently, phytoremediation has been imposed as an interesting technology that can be used to bioremediate sites with a high level of contamination. Basically, phytoremediation is the use of plants to "clean" or "remediate" polluted environments, due in great measure to the physiological capacity and biochemical characteristics that some plants have to absorb and retain contaminants such as metals, organic complexes, radioactive compounds, petrochemical elements and others.

As an alternative, in Italy, experiments have been performed with natural technologies for mud treatment, with the goal of reducing costs of investment and eliminating the practical maintenance costs of the system, through stabilization of muds by the process of phytomineralization and biological conditioning when preparing tecnosuoli for agricultural and environmental use (Ceccanti and Masciandaro, 2006).

For example, with the use of Phragmites australis, a rhizomatose plant from the Poaceae family that has interesting characteristics for its use in phytoremediation or phytostabilization of nitrogen, phosphorous, organic compounds and heavy metals in water (Marrs and Walbot, 1997; Peruzzi *et a*l., 2010).

6. Conclusions

Research on the relationship between the wastewater and bacteria involved in N dynamics have been conducted separately. Some studies have reported on an individual crop nutrition with nitrogen fertilizer or the N contributed by wastewater highlighting the advantages and disadvantages of using them.

However, these studies do not consider the microbiological, which has a role based in the cycle of N. Each of these variables properly can provide important information which could help in future studies to handling the dynamics of N increasing agricultural productivity and minimize environmental impact by deepening the interaction between employment and bacteria wastewater participants N. losses

The fitotratamiento phytotreatment sludge process by opening the door to a kind of new concept of intervention, ensuring close the cycle of sludge directly to purification.

The product obtained with this treatment is pre-humified and therefore fit to be subjected to a composting process to develop a matrix to be addressed in different uses (agricultural and environmental).

The process has enabled a reduction in the average volume of over 90%, thus significantly reducing the cost of sludge management.

The final product is found to comply with the legal parameters for the production of compost soil mixed.

7. References

Angin, I., Yaganoglu, A. V., Turan, M. 2005: Effects of long-term wastewater irrigation on soil properties. *J.Sust. Agric.* 26, 31–42.

Alfaro, J. 1998. Uso de agua y energía para riego en América Latina. Alfaro & Associates. P. O. Box 4267, Salinas, CA 93912, U. S. A.

Al-Nakshabandi, G., M. Saqqar, M. Shatanawi, M. Fallad y H. Al-Horani, 1997. Some environmental problems associated whit the use of treated wastewater for irrigation in Jordan. Agricultural Water Management. 34: 81-94.

Aulakh, M. S., J. W. Doran y A. R. Monsier. 1998. Soil denitrification significance, measurement and effects of management. Adv. Soil Sci. 18: 2-42.

Barton, L., C. McLay, L. Schipper y C. Smith. 1999. Denitrification rates in a wastewater irrigated forest soil in New Zealand. J. Environ. Qual. 28: 2008-2014.

Bergstrom, D. W., M. Tenuta y E. G. Beauchamp. 2001. Nitrous oxide production and flux from soil under sod following application of different nitrogen fertilizers. Commun. Soil. Sci. Plant. Anal. 32: 553-570.

Bhatnaga, V., M. Degen, W. Jonson, H. Bailey y D. Rigby. 1992. The use of reclaimed municipal wastewater for agricultural irrigation. ICID 3er Pan American regional conference, Mazatlán, México.

Bouwman, A. F. 1990. Exchange of greenhouse gases between terrestrial ecosystem and the atmosphere. Soils and the greenhouse effect. John Wiley. Chicheste, New York. U. S. A. pp. 723.

Bouwer, H. 1992. Agricultural and municipal use of wastewater. Water Science and Technology. 26: 7-8.

Bouwer, H. y E. Idelovitch. 1987. Quality requirements for irrigation with sewage water. J. Irrig. & Drainage Eng. 113: 516-535.

Ceccanti B. and Masciandaro G. 1999. Researchers study vermicomposting of municipal and papermill sludges. Biocycle, vol. 40, No. 6, pp. 71-72.

Ceccanti B. e Masciandaro G. 2006. Canne palustri per la depurazione di fanghi urbani. In: Italian Applications: Progetti e competenze della Ricerca Italiana da valorizzare e da sviluppare" (Pedrocchi F., ed.), Hublab editino s.r.l., Milano, pp. 124-125.

Cortés, M. E. J. 1989. Informe final del proyecto microbiológico del agua en la agricultura. Instituto Mexicano de Tecnología del Agua, México. pp 80.

Crook, J. 1984. Health and regulatory considerations. Pettygrove, G., y T. Asano (eds.). Irrigation with reclaimed municipal wastewater. California state water resources control board. Sacramento, California, U.S.A.

Cuenca, A. E. 2000. Efecto del agua residual e los cultivos de cebolla (*Allium* cepa L.) y tomate de cáscara (*Physalis* ixiocarpa Brot.) Epidiomiologia y control de microorganismos perjudiciales al hombre. Tesis de Doctor Ciencias. UNAM, México.

Daum D. y Schenk M. 1998. Influence of nutrient solution pH on N_2O and N_2 emissions from a soilless culture system. Plant and Soil. 203, 279-287.

DFID (Departament for Internacional Development). 1998. Impact of wastewater reuse on groundwater in the Mezquital Valley, Hidalgo State, Mexico. CAN, BGS, LSHTM and UB.

DSEUA (Departamento de Salud de los Estados Unidos de América). 2000. Manual de tratamiento de aguas negras. Limusa, Noriega Editores. México. pp. 150.

Domínguez-Mariana E, Carrillo-Chávez A, Ortega A. 2004. Wastewater reuse in valsequillo agricultural area, Mexico: environmental impact on groundwater[J]. Water Air and Soil Pollution, 155: 251–267.

Duxbury, J. M., L. A. Harper, y A. R. Monsier. 1993. Contribution of agroecosystems to global change. pp. 1-18. *In* Agricultural ecosystem effects on trace gases and global climate change. ASA Spec. Publ. 55. ASA, CSSA, y SSA, Madison, New York, U.S.A.

Flores, L., G. Hernández, R. Alcala y M. Maples. 1992. Total contents of cadmium, copper, manganese and zinc in agricultural soils irrigated with wastewater from Hidalgo, Mexico City. Rev. Int. Contam. Ambient. 8: 37-46.

Gutiérrez, M., C. Siebe y I. Sommer. 1994. Effects of land application of water from México city on soil fertility and heavy metal accumulation: a bibliographical review. Environmental Review. 3: 318-330.

Harrosh, J. 1993. Recycling wastewater for environmental protection and farm water supply. International Water and Irrigation Review. 13: 12-13.

Hernández, S. G., D. L. Flores, V. M. Maples, M. G. Solorio, M. R. Alcala y S. D. Hernández. 1993. Actas del XII Congreso Latinoamericano de la Ciencia del Suelo. Salamanca España.

Hussain, G., A. Al-Jaloud y S. Karimulla. 1996. Effect of treated effluent irrigation and nitrogen on yield and nitrogen use efficiency of wheat. Agricultural Water Management 30: 175-184.

Hussain, G. y A. Al-Jaloud. 1998. Effect of irrigation and nitrogen on yield, yield components and water use efficiency of barley in Saudi Arabia. Agricultural Water Management. 36: 55-70.

INEGI (Instituto Nacional de Estadística, Geografía e Informatica). 2001. informe del uso de aguas residuales. México

IPCC. 2001. Atmospheric chemistry and greenhouse gases. pp. 251-253. *In*: Houghton *et a*l. Climate Change: the   Scientific Basis (eds). Cambridge University Press, Cambridge.

Jenssen, P. y A. Vant. 1991. Ecological sound wastewater treatment: concepts and implementation. *In E*cological Engineering for Wastewater Treatment. Proceedings of the international conference held at Stensund Folk College, Sweden, March 24-28.

Jianwen Z., Huan Y., Sun W., Zheng X. y Wang Y. 2005. Contribution of plants to N_2O emissions in soil-winter wheat ecosystem: pot and field experiments. . Plant and Soil. 269, 205-211.

Kiziloglu M, F., Turan, M., Sahin, U., Angin, I., Anapali O. y Okuroglu M. 2007. (Effects of wastewater irrigation on soil and cabbage-plant (*brassicaolerecea* var. capitate cv. yalova-1) chemical properties. Nutr de *j. Plant. Suelo SCI. 170:* 166–172.

Luna Guido, M. L; C. V. Jarquín, M. O. F. Hernández, S. V. Murrieta, N. T. Topa, E. R. Fuentes y L. Dendooven. 2002 Actividad microbiana en el suelo. Avances y Perspectivas. 21: 328-332.

Magesan, G., C. Mclay y V. Lal. 1998. Nitrate leaching from a free-draining volcanic soil irrigated whit municipal sewage effluent in New Zealand. Agricultural Water Management 70: 181-187.

Marrs K A, Walbot V. 1997. Expression and RNA splicing of the maize glutathione S-transferase *Bronze*2 gene is regulated by cadmium and other stresses. J. Plant Physiol, 113: 93–102.

Masciandaro G., Ceccanti B., Macci C., Doni S., Peruzzi E., Viglianti A., Montanelli T. 2006. Chiusura del ciclo di depurazione delle acque reflue civili mediante trattamento di fitostabilizzazione dei fanghi. VIII Simpòsio Ìtalo Brasileiro de Engenharia Sanitària e Ambiental. Fortaleza CE (Brasile), 17-22 Settembre.

Mosier A.R. 2001. Exchange of gaseous nitrogen compounds between agricultural systems and the atmosphere. Plant Soil. 228: 17–27.

Mora-Ravelo, S.G., Gavi, R. F., Peña, C. J. J.,Pérz, M. J., Tijerina, C. L., Vaquera, H. H. 2007. Desnitrificación de un fertilizante de lenta liberación y urea+fosfato monoamónico aplicados a trigo irrigado con agua residual o de pozo. Rev. Int. Contam. Ambient. 23 (1) 25-33

MUÑOZ, F. 2004. Biorremediación. [online]. Chile : Universidad de Santiago de Chile, s.f. [Citado en Julio de 2004]. Disponible en: <http://lauca.usach.cl/ima/bio1.htm>

Oenema, O., Velthof, G., Kuikman, P., 2001. Technical and policy aspects of strategies to decrease greenhouse gas emissions from agriculture. Nutr. Cycl. Agroecosys. 60, 301–315.

Oron, G., J. DeMalach, Z. Hoffman y R. Cibotaru. 1991. Subsurface microirrigation whit effluent. Journal of Irrigation and Drainage Engineering. 117: 25-36.

Oron, G., C. Campos, L. Guillerman y M. Salgot. 1999. Wastewater treatment, renovation and reuse for agricultural irrigation in small communities. Agricultural Water Management. 38: 223-234.

Peruzzi; E., Masciandaro, G. Macci, C., Doni S., Mora-Ravelo, S. G., Peruzzi P., Ceccanti B. 2010. Heavy metal fractionation and organic matter stabilization in sewage sludge treatment wetlands. J. Ecological Engineering.

Pescod, M. 1992. Wastewater treatment and use in agriculture. FAO Irrig. & Drain. paper No. 47, Roma.

Pescod, M. 1992. The urban water cycle including wastewater use in agriculture. Outlook in Agricultura. 21: 263-270.

Pettygrove, G. y T. Asano. 1984. Manual práctico de riego con agua residual municipal regenerada. Ediciones de la Universitat Politécnica de Cataluña, Barcelona, España.

Prinn R. G., R. F. Weiss, P. J. Fraser, P. G. Siimmonds, D. M. Cunnold, F. N. Alyea, S. O´Doherty, P. Salameth, B. R. Miller, J. Huang, R. H. J. Wang, D. E. Harthey C. Harth, L. P. Steele, G. Sturrock, P. M. Midgley y A. McCulloch. 2000. A history of chemically and radioactively important gases in air deduced from ALE/GAGE/AGAGE. J. Geophys. Res. 105(D14):17751-17792.

Rai U N, Sinha S, Tripathi R D. 1995. Wastewater treatability potential of some aqutic macrophytes: Removal of heavy metals. J. Ecol Eng, 5: 5–12.

Ramos, C. 1998. El uso de aguas residuales en riegos localizados y en cultivos hidropónicos. Instituto Valenciano de Investigaciones Agrarias. Apdo. Oficial, 46113 Moncada, España.

Rochette P., E. van Bochove, D. Prevóst, D.A.Angers, D. Coté y N. Bertrand. 2000. Soil carbon and nitrogen dynamics following application of pig slurry for 19th consecutive year: nitrous oxide fluxes and mineral nitrogen. Soil Sc. Soc. Am. J. 64:1396-1403.

Sawwan, J. 1992. Response of *Chrysanthemum morifolium* Ramatto to drip irrigation with treated wastewater and fresh water at different planting densities. Pure and Applied Science. 19: 279-295.

Sepúlveda, H. 1998. Treatment of Industrial Wastewaters. Roundtable on Municipal Water. Vancouver, Canada, March 15-17.

Seoanez, M. y Angúlo, I. 1999. . Aguas residuales urbanas. Madrid: Ediciones mundi-prensa, 368 p.

Shankers A K, Cervantes C, Losa-Tavera H. 2005. Chromium toxicity in plants. J. Environ Int, 31(5): 739–753.

Snow, V., W. Bond, B. Myers, S. Theiveyanathan, C. Smith y R. Benyon. 1999. Modelling the water balance of effluent-irrigated tress. Agricultural Water Management 39: 47-67.

Toze S. 2006. Reuse of effluent water-benefits and risks. Agricultural water managament. 80, 147-150.

van Groenigen J. W., G. J. Kasper, G. L. Velthof, A. van den Pol-van Dasselaar y P. J. Kuikman. 2004. Nitrous oxide emissions from silage Maite fields under different mineral nitrogen fertilizer and slurry applications. Plant and Soil. 263: 101-111.

Vélez-Zuluaga, J. F. 2007. Los biosólidos:¿una solución o un problema?. Producción + Limpia. 2(2): 57-71.

Vivanco-Estrada R. A., F. Gavi-Reyes, J. J. Peña-Cabriales y J. de J. Martínez-Hernández. 2001. Flujos de nitrógeno en un suelo cultivados con forrajes y regado con agua residual urbana. Terra Latinoamericana. 19(4): 301-308.

WANG Jun-feng, WANG Gen-xu, WANYAN Hua. 2007. Treated wastewater irrigation e_ect on soil, crop and environment: Wastewater recycling in the loess area of China. J. Environ Sci. 19:1093–1099.

Weis J S, Weis P. 2004. Metal uptake, transport and release by wetland plants: implications for phytoremediation and restoration. J. Environ Int, 30(5): 685–700.

WHO (Wordl Health Organitation). 1989. Health guidelines for the use of wastewater in agricultural and aquaculture. WHO Technical Report Senes 778 Geneva, Switzerland.

Yadav R.K., Chaturvedj R.K., Dubey S.K. Joshi P.K. y Minhas P.S. 2003. Potentials and hazards associated with sewage irrigation in Haryana. Agricult. Sci. Indian.

Zhang Xiao-bin, Liu P., Yang, Yue-suo, Chen, Wen-ren. 2007. Phytoremediation of urban wastewater by model wetlands with ornamental hydrophytes. J. of Environ. Sci.19:902–909.

Zerki, M. y R. Koo. 1994. Treated municipal wastewater for citrus irrigation. Journal of Plant Nutrition. 17: 693-708.

Zheng, H., K. Hanaki, T. Matsuo y D. Ballay. 1994. Production of nitrous oxide gas during nitrification of wastewater. Water Science and Technology. 30: 133-141.

Biotechnology in Textiles –
an Opportunity of Saving Water

Petra Forte Tavčer
University of Ljubljana, Faculty of Natural Sciences and Engineering
Slovenia

1. Introduction

In the last few years biotechnology has been making its way into many areas of industry. Biotechnology is the application of life organisms and their components into industrial processes and products (Warke & Chandratre, 2003). The biological systems that have traditionally been used are organisms such as yeasts, fungi and bacteria. The progress of industrial biotechnology in the last twenty years, especially in molecular biology, protein engineering and fermentation technology, enhanced the development of new uses of enzymes in the food industry, the use spread into the areas of detergents, paper and leather industry, natural polymer modification, organic chemical synthesis, diagnostics … The use of enzymes experienced an increase in the textile industry as well.

Amylases were the first enzymes applied in textile processing to remove starch-based sizes from fabrics after weaving. Later proteases were introduced into detergent formulations to remove organic protein-based stains from textile garments and cellulases to remove fibrillation in multiple washes. Further applications have been found for these enzymes to produce the aged look of denim and other garments (Gübitz & Cavaco-Paulo, 2001).

Today enzymes offer a wide variety of alternative, environment and fibre friendly procedures which are replacing or improving the existing classical technological procedures. Cellulases, proteases, amylases, catalases, pectinases, peroxidases and lactases are the enzymes that can replace aggressive chemicals (Cavaco-Paulo & Gübitz, 2003).

Researchers have tried to apply enzymes into every step of textile wet processing, ranging from pretreatment, bleaching, dyeing to finishing, and even effluent treatment. Some applications have become well established and routine, while some have not yet been successfully industrialized due to technical or cost constraints. A famous example is bioscouring or biopreparation, a process that specifically targets noncellulosic impurities within the textile fabrics, with pectinases (Lu, 2005).

1.1 Cotton fibre

A mature cotton fibre is composed of several concentric layers and a central area called lumen. A cuticle, a primary cell wall, intermediary wall as well as secondary cell wall follow each other from the outer to the inner part of the fibre. The whole cotton fibre contains 88 to 96.5% of cellulose, the rest are uncellulosic substances, called incrusts (Karmakar, 1999). Pectins, waxes, proteins, minerals and other organic substances are classified as uncellulosic substances. The larger part of these substances is found in the cuticle and the primary cell

wall. During the growth of the fibres uncellulosic substances, especially waxes, protect them against the loss of water, insects and other outside influences that might damage the fibres. Furthermore, they also protect them against mechanical damage that can occur as a result of processing.

Row cotton fibres have to go through several chemical processes to obtain properties suitable for use. With scouring, non-cellulose substances (wax, pectin, proteins, hemicelluloses…) that surround the fibre cellulose core are removed, and as a result, fibres become hydrophilic and suitable for bleaching, dyeing and other processing.

Pectin, there is 0.4 to 1.2% of pectin in cotton fibres, acts as an adhesive, a glue between the cellulose and uncellulosic substances. By removing pectin, it is easier to remove all other uncellulosic substances. The processes of bioscouring that are in use today are based on the decomposition of pectin by the enzymes called pectinases.

1.2 Pectin substances

Pectin substances are generically called the complex polysaccharide macromolecules with high and varying molecular mass (Ridley et al., 2001). They are negatively charged and acidic. The primary chain is composed with α-(1,4) linked molecules of α-D-galacturonic acid. The side chains also contain molecules of L-rhamnose, arabinose, galactose and xylose that are connected to the main chain through their first and the second carbon atom. The structural formula of the primary chain of pectin- the polygalacturonic acid is shown in Figure 1.
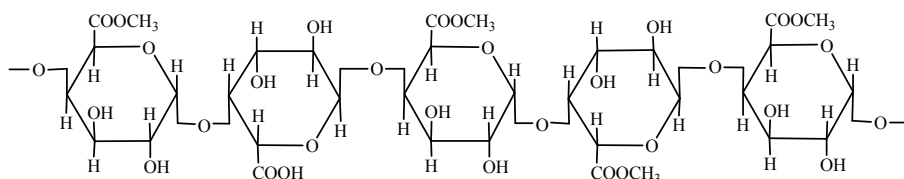

Fig. 1. Structural formula of the polygalacturonic acid.

The carboxyl groups of galacturonic acid are partially esterified by methyl groups and partially or completely neutralized by calcium, potassium, magnesium, iron, ammonium or other ions. Some of the hydroxyl groups on the second and the third carbon atom can be acetylated (Jayani et al., 2005; Kashyap et al., 2001; Gamble, 2003). With the help of electrostatic interactions unesterified or slightly esterified galacturonic groups with negative charge and calcium ions with positive charge form bonds. A calcium ion also bonds pectin with other polysaccharides. It forms a coordination bond between the hydroxyl group of the polysaccharide and an ionic bond with the carboxyl group of pectin. The removal of the calcium ion enhances the decomposition of the pectin substances rich in calcium (Losonczi et al., 2005).

1.3 Enzymes

Enzymes are biological catalysts that accelerate the rate of chemical reactions (Cavaco-Paulo & Gübitz, 2003). The reaction happens with lower activation energy which is reached by forming an intermediate enzyme – substrate. In the reaction itself the enzymes are not used up, they do not become a part of the final product of the reaction, but only change the chemical bonds of other compounds. At the end of the reaction they are released and can participate again in the next biochemical reaction.

All known enzymes are proteins. They therefore consist of one ore more polypeptide chains and display properties that are typical of proteins. Some enzymes require small non-protein molecules, known as cofactors, in order to function as catalysts (Jenkins, 2003).

Generally they are active at mild temperatures. Above certain temperature the enzyme is denaturated. Enzymes have a characteristic pH at which their activity is maximal. Extreme pH values influence on the electrostatic interactions within the enzyme, leading to inactivation of enzyme. Other important factors that influence the effect of enzymatic processes are the concentration of enzyme, the time of treatment, additives like surfactants and chelators and mechanical stress.

Most enzymes are highly specific. They only catalyse a single reaction on a limited number of substrates. Enzymes are distinguished according to the form of the molecule and the charge distribution of the active side. The active side is an area where catalyses occurs and is just a small part of the enzyme. It must provide an environment where the substrate can bond and other molecules do not interfere with catalyses. The specific enzyme action has become known as the 'lock and key' model. The active side of the enzyme, the lock, with an accurately defined rigid structure can only suit a substrate, the key, which is adapted only to it.

Enzymes differ from chemical catalysts in several important characteristics (Cavaco-Paulo & Gübitz, 2003). Enzyme catalysed reactions are several times faster than chemically catalysed ones. Compared to the non-catalysed reaction the rates is from 10^8 to 10^{10} higher (Faber, 1995 15). Enzymes have far greater reaction specificity than chemically catalysed reactions and rarely form byproducts. Enzymes catalyse a reaction under mild reaction conditions: the temperature is below 100°C, the atmospheric pressure and a pH of around 7 are needed.

1.4 Pectinases

The pectinolyic enzymes or pectinases are a heterogeneous group of related enzymes that hydrolise pectin substances present mainly in plants (Jayani et al., 2005). According to an international nomenclature they are classified into the third group (EC3 – hydrolases due to the specifics of the reactions (Holme, 2004).

The pectinases are produced by numerous microorganisms such as bacteria and fungi. Almost all of the commercial products of the pectinases are extracted from fungi, in industrial production of pectinolized enzymes fungi *Aspergillus niger* (Jayani et al., 2005) are most commonly used. This type of microorganism has a GRAS (Generally Regarded As Safe) status meaning that the produced metabolites are safe for use. Numerous types of pectinases can be produced from them including polymethylgalacturonases, polygalacturonases and pectinesterases. They can also be produced from other types of microorganisms, such as *Penicillium frequentans, Mucur pusilus* and others. Their stability is best in the pH range between 5 and 6. With the help of genetic changed microorganisms the alkaline pectinases were produced, they are active in the pH range between 8 and 9. The leading producers of the commercial products of pectinases are Novozymes (Netherlands), Novartis (Switzerland), Roche (Germany) and Biocon (India) (Gummadi & Panda, 2003 16). Products of pectinases are found under different names. Acid pectinases are marketed under the following commercial names: Forylase KL – Cognis, Viscozyme 120 L – Novozymes, Pectinase P9179, Pectinase p3026 – Sigma Chemical Co., Pectinase 62L – Biocatalysts, Multifect pectinase PL – Genencor International; and alkaline pectinases under the following commercial names: Bioprep 3000L, Pulpzyme HC, Scourzyme L – Novozymes, Baylase EVO – Bayer, Unizim PEC – Color-Center SA as well as numerous other names.

Pectinases are today among the enzymes with the best perspective for further application. They play an important role in the production of juices in food industry, in processing of the waste waters, the fermentation of coffee and tea, the preparation of animal forage and extraction of citric oil, in paper industry and have other biotechnological applications (Jayani et al., 2005). In the textile industry pectinases are used as agents in cotton scouring and in the biopreparation of bast fibers such as flax, ramie and jute (Holme, 2004).

1.5 Scouring
1.5.1 Alkaline scouring
The most commonly used procedure for removing noncellulosic material from cotton is the procedure of scouring with sodium hydroxide (classical or alkaline scouring). The procedure is performed at a high temperature in a bath that contains up to 4 % NaOH. Several auxiliary agents, such as wetting agents, emulsifiers and complexants, which improve the efficiency of scouring and reduce the damage of fibres, are also added to the scouring bath. Waxes, pectins, hemicellulose and proteins from the cuticle and the primary wall of the cotton fibres are efficiently removed in this procedure. Dust, different metal salts, chemical and processing impurities are also removed from the surface of the fibres, and partly also immature fibres and seed husks. Besides all the advantages mentioned, the procedure has some disadvantages. In the alkaline medium in contact with oxygen from the air oxycellulose can be formed on fibres. In cases when the concentration of the solution is irregular, the scouring is unequal since mercerisation of the cotton fibre can occur randomly. Having concluded the procedure, the fabric needs to be thoroughly rinsed and neutralised, with a considerable amount of water used in the process. Salts formed in neutralisation needs special procedures of cleaning. Due to high temperature a lot of energy is consumed in the process.

The efficiency of scouring is evaluated by determining residues of the different types of impurities, especially waxes and pectin that are found on the fibres (Preša & Tavčer, 2008a). Cracks are formed on the fibres, cuticle and the primary cell are removed. The fine structure of the fibre does not change, only the degree of crystallinity of cotton is slightly changed. The most noticeable change in the cotton fabric is the loss of mass. The lenght of the fabric shortens during boiling due to shrinking, causing the increasing of density and the tearing force. The most important change is the increased wettability which is a necessary property for a successful and even bleaching, dyeing and final treatment. The wettability needs to be good not only in spaces between the fibres but in the inner parts of the fibre as well (Lewin & Sello, 1983).

1.5.2 Bioscouring
The disadvantages of scouring with sodium hydroxide have motivated textile industry to introduce more enhanced biologic agents which would be as effective in removing non-cellulose substances as sodium hydroxide but would not have damaging effects on cellulose and would be less energy and water consuming. Favourable effects of scouring have been obtained with the enzymes pectinases (Etters, 1999; Hartzell & Hsieh, 1998; Li & Hardin, 1998; Csiszar e tal., 2001, Anis & Eren, 2001; Buchert et al., 2000), that catalyse the hydrolysis of pectin substances. Three main types of enzymes are used to break down pectin substances (Jayani, 2005): pectin esterases, polygalacturonases and pectin lyases. Considering the type of pectinases the bath may be slightly acidic or alkaline. It is recommendable to add the non-ionic surfactant into the bath and, depending on the type of

the pectinases, a sequestering agent. The procedure is based on a fact that pectin acts as a type of cement or glue that stabilises the primary cell of the cotton fibres. When the pectinases are active a complex is formed between the pectinase and the pectin which causes the hydrolysis of the pectin substances. The result of this hydrolysis is a split of the bond between the cuticle and the cellulose body (Li & Hardin, 1998). The outer layers are destabilised and removed in the following procedures of rinsing. The enzymes are released and bond again with the pectin. The procedure is repeated until the enzyme is not destroyed chemically, with the change in pH or in the temperature (Etters et al., 1999). By removing pectin, other noncellulose substances are removed. The procedure of bioscouring gives softer fibres than conventional scouring, however the degree of whiteness is lower and the procedure is not appropriate for removing seed-coat fragments. The potencial advantages that make the enzyme scouring commercially appealing, are a higher quality of the fibres (softer to the touch and better strength), less waste waters, economy of energy and compatibility with other procedures, equipment and materials (Cavaco-Paulo & Gübitz, 2003).

1.5.2.1 The development and conditions of bioscouring

The starting studies of enzyme treatment for scouring that is, cleaning of cotton fibres, were carried out by German researchers (Schacht et al., 1995; Rößner, 1995), and they included pectinases, proteases and lipases that act upon impurities and cellulases which hydrolyse the cellulose chain. Many other researchers followed in their path. They established that cellulases and pectinases are the most effective ones, lipases less with proteases being the least effective. On the basis of their studies they concluded that a simple procedure with pectinases in presence of non-ionic surfactant is sufficient to attain good absorbency (Li & Hardin, 1998; Hartzell & Hsieh, 1998; Buchert et al., 2000; Traore & Buschle-Diller, 2000; Galante & Formantici, 2003).

The first researches including pectinases as agents for scouring cotton were carried out to optimise the conditions of their activity. The concentration of the enzymes in the bath as well as time and temperature of treatment, pH of the bath, additives in the bath and the mechanical treatment all influence on the activity of the enzymes.

Due to a wide variety of enzymes, the added amount of pectinases strongly differs from research to research. The concentrations are usually low, from 0,05 to 2 % according to the weight of the fibres. The increase of concentration above the optimal value neither enhances nor improves the efficacy of the treatment.

The temperature of bioscouring is much lower compared to classic scouring, the optimal temperature is from 40 to 60 °C (Li & Hardin, 1998). Above the mentioned temperature the pectinases lose their activity since a higher temperature destroys the enzymes. However, a temperature that is too low does not suffice for removing the waxes, which have a melting point above 70 °C. A raise in temperature of the bath after completing the scouring is recommended for a better removal of the noncelullulosic material. A second reason for raising the temperature is also the deactivating of the enzymes. The pectinases alone are not harmful to the cellulose fibres, however, enzyme preparations often contain traces of cellulases which could be damaging to the fibres.

Beside the temperature, the pH of the environment is crucial for the activity and stability of the enzyme. The majority of enzymes are active in the pH range between 5 and 9. They are active in a wider pH range, however, at extreme values the three-dimensional form of the enzymes collapses and the enzymes lose their catalytic behaviour. Alkaline or acidic

environment depends on the type of pectinases. Acidic pectinases that function in a slightly acidic medium (pH between 4 and 6), as well as alkaline pectinases that function in a slightly alkaline medium (pH between 7 and 9) are known, both types have similar effects on cotton (Aly et al., 2004, Tzanov et al., 2001; Yachmenev at al., 2001). In acidic medium the pectin structure degrades without adding the pectinases which is often the reason for a better functioning of the acidic pectinases over the alkaline pectinases (Preša & Tavčer, 2008b).

In the starting researches, longer times of treatment were pointed out as the main disadvantage of the enzyme scouring (Sawada et al., 1998). By developing new pectinases, the times of treatment have shortened. Thus, the present forms of pectinases need 30 to 60 minutes for their functioning (Aly et al., 2004; Hartzell-Lawson & Durant, 2000).

Added surfactants also have a big influence on removing noncellulose impurities, however, caution is advised when adding surfactant. Anionic surfactants can form complexes with proteins and influence the structure. Cationic surfactants have a similar influence on proteins, however, with a lower affinity. Enzymes usually retain their catalytic activity in a solution with non-ionic surfactants, unless the concentration of the surfactants in the solution exceeds the critical micelle concentration (Li & Hardin, 1998). Non-ionic surfactants are compatible with enzymes and do not break their three-dimensional structure. They accelerate the effects of scouring due to lowering the surface tension of the fibres and an easier penetration of the enzyme into micropores and cracks of the fibres. Ultimately, the surfactants pull the enzyme back into the bath where it is available for further catalytic activity (). Surfactants take an active part in removing waxes and grease (Li & Hardin, 1998; Tzanov et al., 2001; Durden et al., 2001).

Enzyme inhibitors such as heavy metals and ionic detergents as well as product on the basis of formaldehyde need to be avoided since they deactivate the enzyme (Cavaco-Paulo & Gübitz, 2003; Li & Hardin, 1998).

One of the possibilities of improving the degradation of pectin is also the addition of the chelating agent. It is well known that calcium ions play an important part in the structure of the pectin, the Ca^{2+} ions bond the nonestrificated molecules of pectin. By removing the ion, the structure of the pectin is destabilised which enables the pectinases an easier access to the areas of attack.

Despite the good results in simultaneous activity of the chelating agent and the pectinases, caution is advisable in choosing the chelating agent. Chelating agents that are too strong also bond the metal ion, which is present in some types of enzymes, the so called metalo enzymes. The removal of this metal ion destroys the structure of the enzyme which causes a deactivation of the enzyme. Therefore, the use of weaker chelating agents, such as phosphate, silicate and carbon chelating agents, is recommended (Durden et al., 2001; Preša & Tavčer, 2008b).

The pectinases penetrate into the fibres through the cuticle in places where there are cracks and micropores, and catalyse the reaction of hydrolysis of the pectin molecules. The mixing loosens the bonds between the primary and the secondary wall of the cotton causing more micropores and cracks to appear on the surface of the fibres (Li & Hardin, 1998). This enables the enzyme to penetrate more easily into the inner part of the fibres. Introducing agitation into the procedure of scouring with the pectinases strongly enhances the absorption of the cotton fabric. The time of treatment is shortened and the amount of pectinases needed to attain good absorption of the fabric is lowered (Hartzel-Lawson & Durant, 2000).

1.5.2.2 Influence of bioscouring on further finishing procedures

After the bioscouring the cotton fibres are darker than after alkaline scouring (Preša & Tavčer, 2009; Tavčer, 2008). In further bleaching with hydrogen peroxide, it was established that a better degree of whiteness can be attained on alkaline scoured sample than on the bioscoured one, however, it need to be taken into account that alkaline scoured fibred are very sensitive to oxidative damage during bleaching. More significant damage occures compared to the samples scoured with pectinases (Buschle-Diller et al., 1998).

Several researchers examined the possibilities of combining bioscouring with previous and following procedure. They achieved an adequate wettability by combining enzyme desizing and bioscouring (Lenting & Warmoeskerken, 2004; Yachmenev et al., 2001). Tzanov (Tzanov et al., 2001) used a desizing bath for scouring and it proved to be an important source of glucose in the following procedure with the glucose oxidases. The glucose oxidases produce hydrogen peroxide in water solutions in the presence of glucose from oxygen dissolved in water. The degree of whiteness attained in this procedure is lower than the degree of whiteness of the fibres bleached in a classic procedure with hydrogen peroxide.

Dyeing with direct and reactive dyes was efficient and equal on fabrics that were differently scoured (Canal et al., 2004; Preša & Tavčer, 2009). Etters (Etters et al., 2001) did not notice any statistically significant difference between the rate of uptake, equilibrium exhaustion, or colour depth on the cotton substrate between the two fabrics that were either alkaline scoured or bioscoured. On the contrary Losonczi and colleges (Loszonci et al., 2004) claim that classically scoured fabric compared to bioscoured fabric has a lighter colour. After previous bleaching of differently scoured fabric, no differences can be noticed in lighter dyeing. Treatments with or without the enzyme do not affect the evenness of the dyeing.
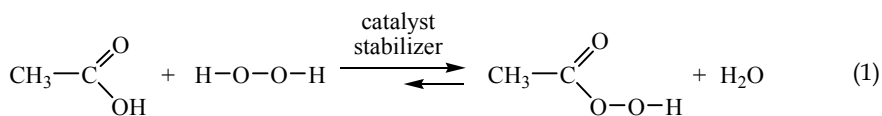
1.6 Bleaching

Scouring is regularly followed by a bleaching process, which removes the natural pigments of cotton fibres. Cellulose fibres are most frequently bleached with hydrogen peroxide (HP) resulting in high and uniform degrees of whiteness. The water absorbency also increases, however, during the decomposition of hydrogen peroxide, radicals that can damage the fibres are formed. For this reason, organic and inorganic stabilizers and chelators are added to the treatment bath.

Hydrogen peroxide (redox potential is 1.78 eV) (1) is not ecologically disputable. The large amount of water used to rinse and neutralize the alkaline scoured and peroxide bleached textiles is ecologically disputable. Namely, the bleaching process is conducted in an alkaline bath at pH 10 to 12 and at temperatures up to 120°C. Due to high working temperature, a large amount of energy is consumed. Auxiliary chemicals added into the bath increase the TOC and COD values of effluents. Upon neutralization of highly alkaline waste baths, large amounts of salts are produced. Consequently, the textile industry is considered one of the biggest water, energy and chemical consumers (Alaton et al., 2006).

Bleaching with peracetic acid (PAA) is an alternative to bleaching with hydrogen peroxide (Gürsoy & Daioglu, 2000; Križman et al., 2005, Hickman, 2002; Prabaharan et al., 2000, Tavčer, 2008; Tavčer, 2010). It is a powerful oxidizing agent (redox potential: 1.81 eV) (Preša & Tavčer, 2009) with excellent antimicrobial and bleaching properties. It is efficient at low concentrations, temperatures and in neutral to slightly alkaline medium. Its products of decomposition are biologically degradable. In the past, it was prepared in situ from acetic acid anhydride and hydrogen peroxide (Rucker, 1989; Wurster, 1992). However, the risk of

explosion during the synthesis reaction prevented affirmation of PAA as a bleaching agent in industry. In recent years, PAA has become interesting (Hickman, 2002). Several commercial products are available as balanced mixtures of PAA, acetic acid and hydrogen peroxide (Equation 1). They are stabilized with a minimum amount of chelating agent. Today, PAA products available in the market are safe, simple to use, and price-effective. PAA induces epoxidation of coloured substances in fibres. Good bleaching results are obtained with low concentrations of PAA at the temperature 40 °C – 80 °C and the pH value 7 - 8. During bleaching, acetic acid is released from peracetic acid and the pH of the bleaching bath decreases. At the end of the process, the bleaching bath is slightly acidic and neutralisation is not necessary. Rinsing is needed only to remove wetting agents. PAA does not damage fibres. It decomposes to oxygen and acetic acid and is therefore environmentally safe (Križman et al., 2005; Križman et al., 2007, Preša & Tavčer, 2008b).

$$CH_3-C\!\!\begin{array}{c}O\\ \\OH\end{array} \; + \; H-O-O-H \; \underset{}{\overset{\text{catalyst}\;\text{stabilizer}}{\rightleftharpoons}} \; CH_3-C\!\!\begin{array}{c}O\\ \\O-O-H\end{array} \; + \; H_2O \qquad (1)$$

Equation 2 shows the reaction that occurs when PAA is used for bleaching.

$$CH_3COOOH + \text{impurities} \longrightarrow CH_3COOH + \text{oxidised impurities} \qquad (2)$$
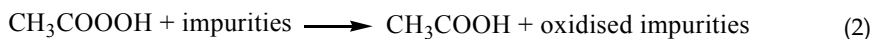
1.7 Aim of research

Both processes, scouring with pectinases and bleaching with PAA, are conducted at temperatures of 50–60°C for 40–60 minutes and pH 5–8. If both processes could be combined into one process, huge amounts of water, energy, time, and auxiliary agents can be saved. In a previous study (Preša & Tavčer, 2008b), it was confirmed using a viscosimetric method that pectinases retain their activity in the presence of PAA and that combined processes are feasible.

The objective of our work was to compare the properties of enzymatically-scoured and PAA-bleached cotton fabrics treated by two-bath and one-bath scouring/bleaching methods, with respect to conventionally-treated fabrics (alkaline scoured and bleached with hydrogen peroxide). The degree of whiteness, water absorbency, fiber damage, and dyeability of woven fabrics were evaluated.

In addition, after all these treatments, pH, TOC, COD and BOD_5 values of the remaining baths were measured. The amount of water and heating energy used during the treatments and rinsing were measured as well.

2. Experimental

2.1 Materials

Desized cotton fabric, 100 g/m², was obtained from Tekstina, Slovenia. Acid pectinases Forylase KL (AP) was supplied from Cognis, Germany, and alkaline pectinases Bioprep 3000L (BP) from Novozymes, Denmark. Cotoblanc HTD-N (anionic wetting and dispersing agent, alkansulphonate with chelator) was supplied from CHT, Germany. H_2O_2 35% (HP) and peracetic acid (PAA) as a 15% equilibrium solution in the commercial bleaching agent Persan S15 were obtained from Belinka, Slovenia. Foryl JA (nonionic wetting agent) and

Locanit S (ionic-nonionic dispersing agent) were obtained from Cognis, Germany and Lawotan RWS (nonionic wetting agent) was obtained from CHT, Germany. Sodium hydroxide was supplied from Šampionka, Slovenia, and acetic acid and sodium carbonate were supplied from Riedel-de Haen, Germany.

2.2 Treatment methods

The cotton fabric was scoured according to three different procedures using sodium hydroxide, acid pectinases or alkaline pectinases. The scoured fabrics were bleached with two bleaching agents: hydrogen peroxide and Persan S15. The abbreviation of processes and treatment conditions are displayed in Table 1. Enzymatic scouring and one-step treatments were performed 60 minutes at 55 °C, than the temperature of the bath was increased to 80 °C to for 10 minutes to deactivate the enzymes. To activate PAA in AP/PAA treatment, the pH was adjusted to 8 after 30 minutes. Demineralised water was used in all processes. The treatments were performed on the Jet JFL apparatus manufactured by Werner Mathis AG loaded with 50 g of fabric at a liquor ratio of 1:20. After all treatments, the bath was discharged and the jet was filled sequentially with fresh water heated to 80 °C, 60 °C and 25 °C to rinse the fabric. After alkaline scouring and peroxide bleaching, the fabrics were neutralised with a neutralizing bath containing acetic acid and rinsed with cold water.

Process	Conditions
AS - Alkaline scouring	3 g/l NaOH, 2 g/l Cotoblanc HTD-N, 95°C, 40 minutes
AP - Scouring with acid pectinases	5 ml/l Forylase KL, 0,75 ml/l Foryl JA, 2 ml/l Locanit S and CH_3COOH to pH 5 - 5,5
BP - Scouring with alkaline pectinases	0,05 % Bioprep, 0,5 g/l Lawotan RWS, Na_2CO_3 to pH 8
HP - bleaching with hydrogen peroxide	7 g/l H_2O_2 35%, 1 g/l Cottoblanc HTD-N, 4 g/l NaOH 100%, 95 °C, 45 min
PAA - bleaching with peracetic acid	15 ml/l Persan S15, 55 ml/l Na_2CO_3 0,5 M, 0,1g/l Lawotan RWS, pH 8, 55 °C, 40 min
AP+PAA - one step scouring with acid pectinase and bleaching	5 ml /l Forylase KL, 0.75 ml/l Foryl JA, 2 ml/l LocanitS, 15 ml/l Persan S15
BP+PAA - one step scouring with alkaline pectinase and bleaching	0.05 % Bioprep 3000L, 0.1 mL/L Lawotan RWS, 15 mL/L Persan S15, pH 8 with NaOH

Table 1. The abbreviation of processes and treatment conditions

2.3 Analytical methods

Prior to the measurements, fabrics were conditioned 24 hours at 20 °C and 65% relative humidity. The degree of whiteness and the colour values were measured on the Spectraflash SF600 Plus using the CIE method according to EN ISO 105-J02:1997(E) standard and EN ISO 105-J01:1997(E), respectively. Weight loss due to the pretreatments was determined by weighing the fabric samples before and after pretreatment and was expressed in percent. Water absorbency was measured according to DIN 53 924 (velocity of soaking water of textile fabrics, method for determining the rising height). Measurements of tenacity at maximum load were performed on Instron Tensile Tester Model 5567. The mean degree of polymerisation (DP) was determined with the viscosimetric method in cuoxam.

Samples of remaining bleaching and scouring baths were collected after all treatments. Their ecological parameters, such as pH, total organic carbon (TOC), chemical oxygen demand (COD) and biological oxygen demand (BOD_5), were measured. TOC was measured on a Shimadzu TOC-5000A according to ISO 8245. COD was performed according to SIST ISO 6060, BOD_5 according to SIST ISO 5815, and biological degradation as a ratio of BOD_5 and COD.

The consumption of water for treatments was estimated by adding up all the sequential fillings of the jet apparatus with treatment and rinsing baths and the total consumption of 1 kg of fabrics was recalculated. The energy consumption was expressed with the amount of steam required to heat water to treat and rinse baths. The amount of steam required for heating one litter of water from certain starting temperatures to a defined final temperature was obtained from the technical documentation of the textile dyeing plant.

3. Results and discussion

3.1 Fabric properties

Table 2 represents the whiteness values, the loss of mass, rising height in warp direction, tenacity at maximum load and degree of polymerisation of differently pretreated cotton fabric samples.

	W	Mass loss (%)	Rising height (cm)	Tenacity (cN/tex)	DP
D	11.1		0	18.47	2482
AS	19.5	1.27	2.9	18.45	2432
AP	8.2	0.30	2.7	16.96	2451
BP	8.4	0.89	2.5	17.95	2385
AS+HP	84.1	1.52	3.0	16.65	1774
AP+HP	85.6	1.51	3.0	17.12	1947
BP+HP	85.1	1.62	2.8	16.83	2004
AS+PAA	72.7	1.30	2.8	16.94	2278
AP+PAA	57.7	0.65	2.9	18.12	2318
BP+PAA	57.3	0.95	2.9	13.75	2399
AP/PAA	68.7	0.40	2.7	16.94	2438
BP/PAA	69.6	0.60	2.8	18.84	2300

Table 2. Whiteness (W), the loss of mass, rising height in warp direction, tenacity at maximum load, degree of differently pretreated and desized only (D) cotton fabric samples.

Alkaline scoured samples are whiter than enzymaticaly scoured ones. The degree of whiteness increased significantly after HP bleaching and the differences in whiteness from previous scouring disappeared. With PAA bleaching, a high degree of whiteness was not achieved and the differences in whiteness from the previous scouring remained visible. This occurs because bleaching with PAA proceeds at a low temperature and pH, where the impurities remaining after scouring could not be fully oxidised. Bioscoured fibres, which were not treated at high temperature and high pH, contained more waxes and other impurities that hindered the successful oxidation with PAA at mild conditions. Bleaching

the alkaline scoured fabrics with PAA is more effective since the impurities were removed from cotton fibers to a higher extent in the previous process and the pigments within fibers were more exposed to the oxidant's influence.

The degrees of whiteness after a one-bath treatment were higher than those after two-bath bioscouring and bleaching with PAA and close to the whiteness achieved after alkaline scouring and bleaching with PAA. The one-step process, namely ended with rising of temperature to 80 °C and this temperature activate the presented hydrogen peroxide, which improves the whiteness of fabric.

The loss of mass demonstrates that scouring with NaOH is more intensive and removes more incrusts than enzymatic scouring. In the following bleaching HP removed a large portion of compounds, which remained on fibers after scouring. The total mass loss after scouring and HP bleaching was similar for all samples.

PAA bleaching also removed a certain part of the noncellulosic substances, which remained on fibers after scouring, but the quantity was lower relative to HP bleaching. Bleaching with PAA did not equalize the differences in the loss of mass, which is in agreement with the whiteness results. We can conclude that high temperature and high pH are conditions that contribute decisively to the removal of non-cellulosic impurities. Specifically, waxes cannot be removed completely when all processes are conducted at low temperatures and neutral pH, as is the case for bioscouring and PAA bleaching. The remained substances influence on the water absorbency and consequently alkaline scoured samples had the highest absorbency. Bleaching improved the absorbency of the scoured fabrics, particularly of enzymatically scoured ones. However, the difference in rising height was so small, that all the samples could be considered absorbent.

There were no higher differences in tenacity at maximum load between the de-sized and differently treated samples. On the other hand, the results of DP demonstrate, that bleaching with HP decreased the degree of polymerisation significantly, while other processes preserved the DP values close to the starting value. The bioscouring and bleaching with PAA in a one bath or two bath process causes no damage to fibers and this is one of the benefits of such processes.

3.2 Ecological parameters

Figures 2 to 5 present the final pH values of the remaining baths from different processes, total organic carbon (TOC), chemical oxygen demand (COD), biological oxygen demand (BOD_5) and biological degradability of remaining baths (BOD_5/COD ratio), respectively.
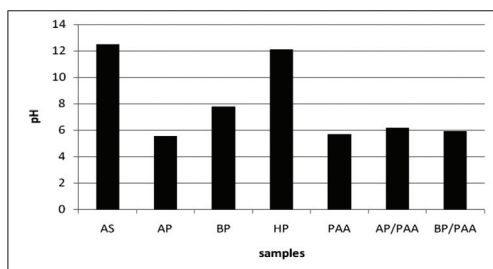

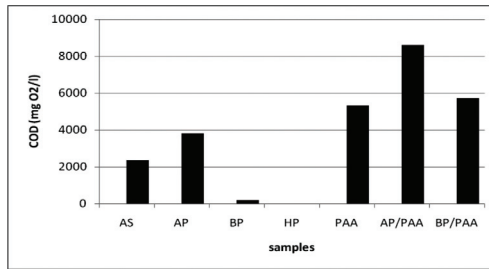Fig. 2. Final pH of scouring, bleaching and scouring/bleaching baths.

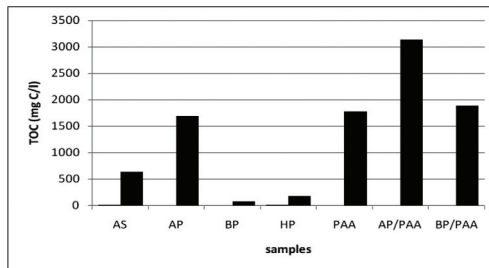Fig. 3. COD values of scouring, bleaching and scouring/bleaching baths.

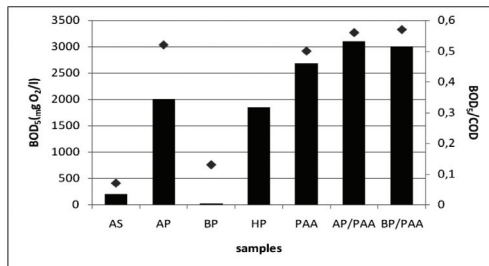Fig. 4. TOC values of scouring, bleaching and scouring/bleaching baths.

Fig. 5. BOD$_5$ values (column) and BOD5/COD (♦) of scouring, bleaching and scouring/bleaching baths.

Conventional treatment of cotton fibres was conducted in an alkaline environment: final pH at alkaline scouring and at bleaching with hydrogen peroxide was around 12.5. Such alkaline baths should be neutralized prior to drainage into the sewage system. At neutralization, salts that additionally load wastewaters are produced.

The processes of bioscouring and bleaching with PAA occurred between pH 5.5 and 8. The final pH value of the bath was 5.5 while scouring with acidic pectinases, and 7.5 while scouring with alkaline pectinases. While bleaching with PAA and at both combined processes, the final pH value of the bath was near 6. Since neither of these processes requires neutralization of fibres, the treatment process can be shorter and less expensive. Additionally, the remaining baths do not require the neutralization step prior to drainage into the sewage system, which also reduces the cost of processes.

TOC, COD and BOD$_5$ values show similar relations. The scouring bath with alkaline pectinases exhibited the lowest TOC and COD values. These values were so low that they did not exceed the limit values (TOC 60 mg C/L and COD 200 mg O$_2$/L) for direct drainage into the sewage system (Decree, 1996). However, the scouring bath with acidic pectinases had high TOC and COD values that were even higher than alkaline scouring. The reason lies in the initial composition of the bath, which was prepared according to the producer's instructions and contained more auxiliary agents than the bath with alkaline pectinases, which contained only enzyme and wetting agent. We anticipate that the optimisation of the recipe of scouring with acid pectinases would improve its ecological parameters.

Among bleaching baths, the baths with PAA had higher TOC and COD values. PAA is an organic compound, which contributes to higher TOC and COD values, as well as acetic acid, which is present in the balanced mixture. Peracetic acid is decomposed in the waste bath to acetic acid and oxygen. Acetic acid, as such, is not ecologically disputable, and does not cause any problems in wastewaters in which it appears in the diluted state. Its biodegradability is 51 – 99% (Howard, 1990).

After bleaching with hydrogen peroxide, a certain amount of the non-used hydrogen peroxide remained in the bath. For that reason, we could not determine the real COD value, such that it is not presented in the diagram.

The BOD$_5$ values (columns of Figure 5) are high with the bioscouring baths with acidic pectinases (2000 mg O$_2$/l) and the baths containing PAA (between 2680 and 3100 mg O$_2$/l). The lowest BOD$_5$ value (25 mg O$_2$/l) belongs to the bath with alkaline pectinases.

The baths with enzymes and PAA were biodegradable, while the bath was non-degradable after alkaline scouring. Biological degradability of the peroxide bleaching bath could not be determined in this manner.

3.3 Consumption of water and energy

Figure 6 presents the amount of water and energy required for the treatment of 1 kg of material at a liquor ratio 1:20 for different processes.

The amount of water consumed for alkaline scouring and bleaching with HP was higher than the amount of water consumed for bioscouring and bleaching with PAA. After alkaline scouring and bleaching with hydrogen peroxide, the fabric must be neutralized. Neutralization is not required after bioscouring and bleaching with PAA because the pH value is only slightly acidic and is neutralized during the first rinsing. The process of bioscouring and bleaching with PAA consumed only 66.6% of water relative to alkaline scouring and bleaching with HP. During the one-bath treatment, the consumption of water was still lower, i.e. only 50% in comparison with two-bath process, and only 33% in comparison with conventional pre-treatment process.

While scouring with pectinases and bleaching with PAA, the consumption of energy required to heat the bath was also lower. Conventional processes of scouring and bleaching were performed at temperatures near the boiling point, whereas bioscouring and bleaching with PAA were conducted at a temperature of 55 °C. Due to the lower temperature, less energy was required, which is presented in Figure 4. Only 63.3% of the steam, which was required during alkaline scouring, was consumed at bioscouring, and only 30.5 % of the steam, which was required at bleaching with hydrogen peroxide, was consumed at bleaching with PAA. The lowest amount of energy was consumed by the one-bath process, i.e. 67.4% of steam was consumed by the two-bath process, while only 31.6% of the steam was required for alkaline scouring and bleaching with hydrogen peroxide.
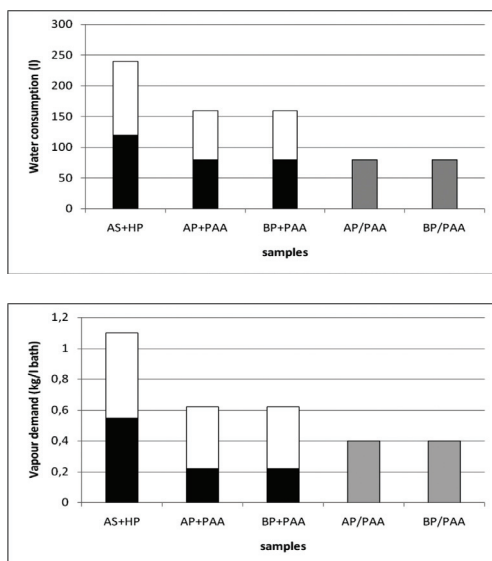
Fig. 6. Water (above) and energy (below) consumption for alkaline scouring and bleaching with hydrogen peroxide (AS+HP), for scouring with acid or alkaline pectinases and bleaching with PAA (AP+PAA, BP+PAA) and for combined bioscouring and bleaching with PAA (AP/PAA, BP/PAA) for treatment of 1 kg of fabric at liquor ratio of 1:20 (scouring ■, bleaching □, combined treatment ▨).

4. Conclusions

Bioscouring can be recommended as an adequate procedure for scouring of cotton. It is a simple, repeatable and safe procedure. The removal of pectin components from cotton adequately improves the water absorbencies of the fibres and facilitates the penetration of the dye and other substances into the fibre. Natural qualities of the cotton fibre are preserved, the fabric is softer to the touch than after classic scouring. Fibres are also less damaged. Biouscouring can also be used for mixtures of cotton and silk, wool and cashmere; in severe alkaline conditions of classic scouring, damage occurs on these fibres.

Sodium hydroxide is removed from the textile treatment procedures or its use is considerably lowered. Due to a lower pH of the bath, less rinsing is needed, what results in shorter times of treatment and lower use of water. Energy is economised as well, since the bioscouring occurs at a lower temperature. Direct dyeing without the intermediary bleaching is possible in the case of dyeing dark shades.

Waste waters are less polluted, the COD values of the scouring baths are thus lower due to the economised use of chemicals as well as BOD_5 values due to a smaller loss of the fibre weight.

However, bioscouring has a few disadvantages. Due to a relatively low treatment temperature, the waxes are not entirely removed. The attained degree of whiteness is lower compared to alkaline scoured or even desized fabric. Due to a lower pH the seed-coat fragments do not swell and are not so decolorized in bleaching.

Peracid bleaching can substitute the hydrogen peroxide bleaching when medium degree of whiteness is demanded. Cotton fibers, bleached with peracetic acid have appropriate water absorbancy and are not damaged. When bleaching with PAA, less water and energy is consumed, and the bleaching baths are biodegradable.

The consumption of water and energy is the lowest at one-bath processes of scouring/bleaching with pectinases and PAA. The degree of whiteness of fabrics is higher than at two-step scouring and bleaching with PAA, but lower than at bleaching with HP. The fabrics have good water absorbency, the fibres are not damaged and the remaining baths are biodegradable.

5. References

Alaton, I. A., Insel, G., Eremektar, G., Babuna, F. G., & Orhon, D. (2006). Effect of textile auxiliaries on biodegradation of dyehouse effluent in activated sludge. *Chemosphere*, Vol. 62, No. 9, 1549–1557, ISSN 0045 - 6535

Aly, A. S., Moustafa, A. B., Hebeish, A. (2004). Bio-technological treatment of cellulosic textiles. *Journal of Cleaner Production*, Vol. 12, No. 7, 697–705, ISSN 0959 - 6526

Anis, P., & Eren, H. A. (2002). Comparison of alkaline scouring of cotton vs. alkaline pectinase preparation. *AATCC Review*, Vol. 2, No. 12, 22–26, ISSN 1532-8813

Buchert, J., Pere, J., Puolakka, A., & Pertti, N. (2000). Scouring of cotton with pectinases, proteases, and lipases. *Textile Chemist and Colorist*, Vol. 32, No. 5, 48–52, ISSN 0040-490X

Buschle-Diller, G., El Mogashzy, Y., Inglesby, M. K. & Zeronian, S. H. (1998). Effects of scouring with enzymes, organic solvents, and caustic soda on the properties of hydrogen peroxide bleached cotton yarn. *Textile Research Journal*, Vol. 68, No. 12, 920–929, ISSN 0040-5175

Canal, J. M., Navarro, A., Calafell, M., Rodriguez, C., Caballero, G., Vega, B., Canal, C., & Paul, R. (2004). Effect of various bioscouring systems on the accessibility of dyes into cotton. *Coloration Technology*, Vol.120, No.6, 311–315, ISSN 1472 - 3581

Cavaco-Paulo A. & Gübitz G. M. (2003). Cambridge: Woodhead Publishing, *Textile processing with enzyme*. 17–18, 30–34, 51–52, 90–95, 110, 124–125, 129–131, 158–169, ISBN 18557366101

Csiszar, E., Losonczi, A., Szakacs, G., Rusznak, I., Bezur, L. & Reichar, J. (2001). Enzymes and chelating agent in cotton pretreatment. *Journal of Biotechnology*, Vol. 89, No. 2 – 3, 271–279, ISSN 0168 - 1656

Durden, D. K., Etters, J. N., Sarkar, A. K., Henderson, L. A. & Hill, J. E. (2001). Advances in commercial biopreparation of cotton with alkaline pectinase. *AATCC Rewiew*, Vol. 1, No. 8, 28–31, ISSN 1532-8813

Etters, J. N. (1999). Cotton preparation with alkaline pectinase: an environmental advance. *Textile Chemist and Colorist*, Vol.1, No.3, 33–36, ISSN 0040-490X

Etters, J. N., Condon, B. D., Husain, P. A. & Lange, N. K. (1999). Alkaline pectinase: key to cost-effective, environmentally friendly preparation. *American Dyestuff Reporter*, Vol. 88, No. 6, 19–23, ISSN 0002 - 8266

Faber, K., Springer – Verlag (1995). *Biotransformations in organic chemistry : a textbook*. 2nd edition. Berlin (etc.) : Vol. 2, No. 10, ISBN 978-3-540-20097-0

Gürsoy, N. Ç., & Dayioğlu, H. (2000). Evaluating peracetic acid bleaching of cotton as an environmentally safe alternative to hypochloride bleaching. *Textile Research Journal*, Vol. 70, No. 6, 475–480, ISSN 0040 - 5175

Galante, Y. M., & Formantici, C. (2003). Enzyme applications in detergency and in manufacturing industries. *Current Organic Chemistry*, Vol. 7, No. 13, 1399–1422, ISSN 1385 - 2728

Gamble, G. R. (2003). Effects of elevated temperatures on the chemical propeties of cotton fiber pectin. *Textile Research Journal*, Vol. 73, No. 2, 157–160 ISSN 0040-5175

Gummadi, S. N., & Panda, T. (2003). Purification and biochemical properties of microbial pectinases, a review: *Process biochemistry*, Vol. 38, No. 7, 987–996, ISSN 1359 - 5113

Hartzell, M. M. & Hsieh, Y. (1998). Enzymatic scouring to improve cotton fabric wettability. *Textile Research Journal*, Vol. 68, no. 4, 233–241, ISSN 0040 - 5175

Hickman, W. S. (2002). Peracetic acid and its use in fiber bleaching. *Review of Progress in Coloration*, Vol. 32, 13–27, ISSN 0557-9325

Howard, P. H. (1990). Handbook of environmental fate and exposure data for organic chemicals, CRC press

Holme, I. (2004). Enzymes for innovative textile treatments. *Textiles magazine*, Vol. 31, No. 3, 8–14, ISSN 1367-1308

Jayani, R. S., Saxena, S., & Gupta, R. (2005). Microbial pectinolytic enzymes: a review. *Process Biochemistry*, Vol. 40, No. 9, 2931–2944, ISSN 1359 - 5113

Jenkins R. O. (2003). in: Textile Processing with Enzymes, Edited by Cavaco-Paulo A. & Gübitz GM, Woodhead publishing Ltd., CRC Press, Boca Raton, ISBN 18557366101

Kashyap, D. R., Vohra, P. K., Chopra, S., & Tewari, R. (2001). Applications of pectinases in the commercial sector: a review, *Bioresource Technology*, Vol. 77, No. 3, 215–227, ISSN 0960 - 8524

Karmakar, S. R. (1999). Textile Science and Technology 12 : Chemical Technology in the Pretreatment processes of textiles. Elsavier: Amsterdam, 3–8, 72–75, 86–89, 160, 168–173, 188–190, ISBN 0-444-50060-X

Križman, P., Kovač, F., & Tavčer, P. F. (2005). Bleaching of cotton fabric with peracetic acid in the presence of different activators. *Coloration Technology*, Vol. 121, No. 6, 304–309, ISSN 1472 - 3581

Križman Lavrič, P., Kovač, F., Tavčer, P. F., Hauser, P., & Hinks, D. (2007). Enhanced PAA bleaching of cotton by incorporating a cationic bleach activator. *Coloration Technology*, Vol. 123, No. 4, 230-236, ISSN 1472 - 3581

Dekker, M., (1983). Chemical processing of fibers and fabrics : fundamentals and preparation : part A. New York ; Basel : Marcel Dekker, In: Handbook of fiber science and technology, Edited by M. Lewin and S.B. Sello. Vol. I : 111–125. ISBN 0-8247-7010-2

Lenting, H. B. M. & Warmoeskerkern, M. M. C. G. (2004). A fast, continuous enzyme-based pretreatment process concept for cotton containing textiles. *Biocatalysis and Biotransformation*, Vol. 22, No. 56, 361–368, ISSN 10242422

Li, Y., & Hardin, I. R. (1998). Enzymatic scouring of cotton – surfactants, agitation and selection of enzymes. *Textile Chemist and Colorist*, Vol. 30, No. 9, 23–29, ISSN 0040-490X

Losonczi, A., Csiszár, E., & Szakács, G. (2004). Bleachability and Dyeing Properties of Biopretreated and Conventionally Scoured Cotton Fabrics. *Textile Research Journal*, Vol. 74, No. 6, 501–508, ISSN 0040 - 5175

Losonczi, A., Csiszár, E., Szakács, G., & Bezúr, L. (2005). Role of the EDTA chelating agent in bioscouring of cotton. *Textile Research Journal*, Vol. 75, No. 5, 411–417, ISSN 0040 - 5175

Lu, H. (2005) : Insights into Cotton Enzymatic Pretreatment. *International Dyer*, No.4 10-13, ISSN 0020 – 658X

Prabaharan, M., Nayae, R. C., & Rao, J. V., (2000). Process optimization in peracetic acid bleaching of cotton. *Textile Research Journal*, Vol. 70, No. 8, 657–661, ISSN 0040 - 5175

Preša, P, Tavčer, P. F. (2008a). Pretreated cotton fiber characterization. *AATCC Review*, Vol. 8, No. 11, (Nov. 2008) 37-48, ISSN 1532-8813

Preša, P, Tavčer, P. F. (2008b). Bioscouring and bleaching of cotton with pectinase enzyme and peracetic acid in one bath. *Coloration Technology*, Vol. 124, No. 1, 36-42, ISSN 1472 - 3581

Preša, P, Tavčer, P. F. (2009). Low water and energy saving process for cotton pretreatment. *Textile Research Journal*, Vol. 79, No. 1, 76-88, ISSN 0040 - 5175

Ridley, B.L., O'neill M.A. in Mohnen, D. (2001). Pectins: structure, biosynthesis, and oligogalacturonide-related signaling. *Phytochemistry*, Vol. 57, No. 6, 929–967, ISSN 0031 - 9422

Rößner, U. (1995). Enzyme in der Baumwollvorbehandlung. *Textilveredlung*, Vol. 30, No. 3–4, 82–88, ISSN 0040 - 5310

Rucker, J. W. (1989). Low temperature bleaching of cotton with peracetic acid, *Text. Chem. Color.*, Vol. 21, No. 5, 19–25, ISSN 0040-490X

Sawada, K., Tokino, S., Ueda, M., & Wang, X. Y. (1998). Bioscouring of cotton with pectinse enzyme. *Journal of the Society of Dyers and Colourists*, Vol. 114, No. 11, 333–336, ISSN 0037-9859

Schacht, H., Kesting, W. & Schollmeyer, E. (1995). Perspectiven Enzymatiscer Prozesse in der Textilveredlung. *Textilveredlung*, 1995, Vol. 30, 237–243, ISSN 0040 – 5310

Tavčer, P. F. (2008) The influence of different pretreatments on the quantity of seed-coat fragments in cotton fibres. *Fibres & Textiles in Eastern Europe*, Vol. 16, No. 1 (66), 19-23, ISSN 1230 - 3666

Tavčer, P. F. (2010). Impregnation and exhaustion bleaching of cotton with peracetic acid. *Textile Research Journal*, Vol. 80, No. 1, 3-11, ISSN 0040 - 5175

Traore, M.K. & Buschle-Diller, G. (2000). Environmentally friendly scouring processes. *Textile Chemist and Colorist*, Vol. 32, No. 12, 40–43, ISSN 0040-490X

Tzanov, T., Calafell, M., Guebitz, G. M., & Cavaco-Paulo, A. (2001). Bio-preparation of cotton fabrics. *Enzyme Microb. Technol.*, Vol. 29, No. 6–7, 357–362, ISSN 0141 - 0229

Warke, V. V., & Chandratre, P. R. (2003). Application of biotechnology in textiles. *Man-made Textiles in India*, No. 4, XLVI, 142–146, ISSN 0377-7537

Wurster, P. (1992). Peracetic Acid bleach an alternative to bleaching processes using halogenated oxidizers. *Textil praxis int. Sonderdruck*, Vol. 10, 960–965, ISSN 0340-5028

Yachmenev, V.G., Bertoniere, N.R. & Blanchard, E.J. (2001). Effect of sonication on cotton preparation with alkaline pectinase. *Textile Research Journal*, Vol. 71, No. 6, 527–533, ISSN 0040 - 5175

Decree on the emission of substances in the drainage of wastewater from facilities and plants for the production, processing and treatment of textile fibres. Official Gazette of the Republic of Slovenia No. 35/96

Wastewater Minimization in a Chlor-Alkali Complex

Zuwei Liao, Jingdai Wang and Yongrong Yang
Department of Chemical and Biological Engineering, Zhejiang University
P. R. China

1. Introduction

Water network integration is one of the most efficient technologies for wastewater reduction [1]. During the past two decades, both the water pinch technology and the mathematical programming method have been frequently discussed and widely applied in the industry.

The water pinch technology divides the water network integration into two steps: targeting and design. This technology was initiated by Wang and Smith [2] in 1994. They treat the water using operation as a mass transfer unit and use concentration vs mass load coordinate to obtain the minimum freshwater consumption of the whole system. Based on this coordinate system, the targets of wastewater reuse and regeneration reuse are established. The methods of Wang and Smith [2, 3] have been well supplemented by many authors in recent years.

The first supplement is on the model of the water using operation. It is obvious that not all the water using operations are the mass transfer type. Typical water using units like cooling tower, boiler and reactor are not this kind. Actually, these units are flow rate fixed operations. To treat operations in this category, targeting methods in different coordinates were developed. Dhole et al.[5] obtained the composite curve in concentration vs flow rate coordinate, which has been supplemented by several works [6-9]. Hallale [6] introduced a water surplus diagram and obtained the real target. El-Halwagi et al. [8] and Prakash and Shenoy[9] developed a mass load vs flow rate composite by analogy to the heat integration system. In addition, Agrawal and Shenoy[10] achieved the freshwater target in the concentration vs mass load coordinate; Bandyopadhyay et al.[11, 12] calculated the wastewater target in the same coordinate. Recently, Pillai and Bandyopadhyay [13] established a simple and more effective algebraic method for wastewater targeting. The above mentioned four methods are the most efficient methods for fixed flow rate operations, and they can be extended to cases of multiple water sources [14-16]. The targeting concept is also applicable to process changes [11, 17] and threshold problems [18].

The second supplement is on the regeneration target. The regeneration has two cases: regeneration reuse and regeneration recycle. For regeneration reuse, Wang and Smith [2] proposed that the regeneration concentration should be at the pinch concentration. Latter, Mann and Liu [19] pointed that the optimum regeneration concentration can be above the pinch. Feng et al. [20] introduced a targeting method for regeneration recycle, which has been extended to the regeneration reuse system [21] and the zero discharge system [22]. On the other hand, the regeneration problem for fixed flow rate problems are more complicated than the fixed mass load problems, because the regeneration flow rate is constrained by

water sources. Agrawal and Shenoy [10] adopted the method of Wang and Smith [2] to treat this problem. Bandyopadhyay et al. [23] considered the regeneration recycle problem. Ng and Foo et al. [24, 25] divided the system into two blocks: the regeneration block and the freshwater block where the final targets are obtained.

The third supplement is on the wastewater treatment minimization. After the freshwater and regeneration water targets are determined, Kuo and Smith [26, 27] addressed the wastewater treatment problem by constructing the wastewater composite curve. Bandyopadhyay et al. [12] established the wastewater and wastewater treatment targets simultaneously in their source composite curve. Ng and Foo [28, 29] obtained the target by determining the wastewater flows.

The earliest design method for the water network is the "grid diagram" proposed by Wang and Smith [2]. To avoid the tedious steps of the method, Olesen and Polley [30, 31] developed the load table method. Subsequently, design rules based on "water main" [27, 32], "internal water main" [33] and other heuristic rules [34] are introduced. All these methods are focused on fixed mass load problems.

According to the necessary condition proved by Savelski and Bagajewicz [35], the methods for fixed flow rate problems are also suitable for fixed mass load problems. El-Halwagi [36] first designed the fixed flow rate problem by "source-sink" method. Prakash and Shenoy [9] introduced the nearest neighborhood algorithm, and proved its optimality. Later, they [37] reduced the number of connections by matrix operating. Ng and Foo [38] got the same target via a "water using path". Bandyopadhyay [13] proved that there is no cross pinch matches between water sources and demands under the optimal condition. Recently, Alwi and Manan[39] distributed the sources in the light of the source-sink composite curve. Moreover, total annual cost based design [40], retrofit design [41-43] and optimizing software [44] are becoming the next hot topic of this area.

The well developed water network integration technology has been widely applied in the industry. The most successful application should be in the refinery and petrochemical industry [45-47]. In 1980, Takama [48] reported the first refinery application which reduced 24% of the freshwater consumption. Wang and Smith [2] proposed 47.6% of further reduction by regeneration reuse. In 1997, Liu [19] increased the water reuse percentage from 18.6% to 37% in some petrochemical complex of Taiwan. In addition, the water integration technology has also been applied to the pulp and paper plant [41, 49, 50], sugar plant [51], pesticide [52], textile [53]、electroplate [49, 54]、clean agent [55]、fuel [56], catalyst [57] and steel industry [58].

We will use the well developed water pinch technology to the chlor-alkali industry. The chlor-alkali industry consumes huge amount of freshwater. Some large chlor-alkali complex takes dozens of million tons of freshwater every year. In certain area, the chlor-alkali industry occupies 1/4 to 1/3 of the total water consumption of the area, which causes the shortage of the freshwater supply. On the other hand, the chlor-alkali industry also discharge large amount of wastewater, while the environmental regulation is getting stricter. Therefore, it is very urgent for the chlor-alkali industry to improve their water using efficiency and carry out wastewater minimization.

2. The chlor-alkali complex and its water system

2.1 Complex description

The chlor-alkali complex processes brine and produces 40 kt caustic soda, 10 kt chlorine liquid, 20 kt hydrochloride, 8000 t bleaching powder every year. The complex includes 5

plants in which there are many subsections. The schematic flow sheet of the complex is shown in figure 1. Plant 1 is composed of one salt dissolving section, two evaporation sections, one solid caustic soda section and a boiler section. Plant 2 mainly includes chlorine drying section and the sections of various chlorine by products. The chlorine by products are chlorine liquid, hydrochloride, perchloravinyl, chlorinated paraffin, sodium hypochlorite. Plant 3 is the electrostenolysis plant which involves three set of electrostenolysis equipments. The hydrogen and chlorine products from this plant are sent to plant 1 and plant 2 respectively. Plant 4 is the bleaching powder plant while plant 5 is the utility plant. The utility plant has seven set of circulating cooling water systems and one set of pure water producing system. With all these processes and products, the whole system consumes huge amount of water as shown in table 1. In order to find the full range of water saving space, the water balance of the existing system should be addressed first, and this is implemented in the next section.
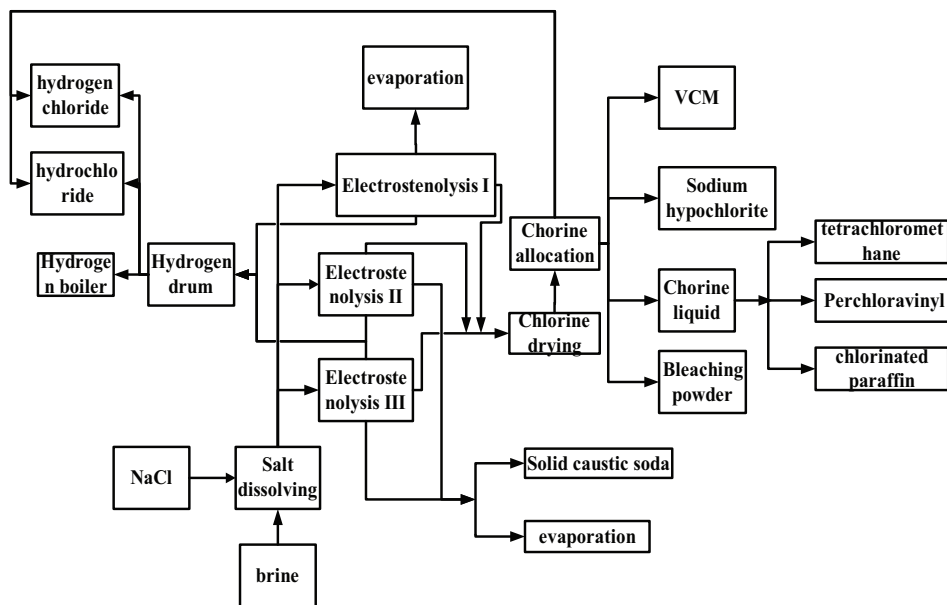

Fig. 1. Schematic flow sheet of the chlor-alkali complex

Plants	Water comsumption(t/d)
1	9683
2	25176
3	21303
5	1076

Table 1. Freshwater consumption of the chlor-alkali complex

2.2 The balanced water system of the complex
2.2.1 Plant 1

The balanced water system of plant 1 is shown in figure 2. Now, let's analysis the plant section by section.

Salt dissolving section

This section consumes freshwater (39m³/h), steam condensate (68.5m³/h) and resin washing water (15m³/h). These water sources are used to prepare refining agent, flocculants, to wash brine sludge, to cool pump. While all the discharged water is sent to dissolve the salt. The main constraint contaminant is the organic content which is represented by COD.

Electrostenolysis section

Water is used for hydrogen washing in this section. The washing unit consumes 50m³/h freshwater. The effluent from the washing unit is COD free, but contains trace amount of caustic soda. Therefore, it suggested to be used in the cooling water system.

Evaporation section

The evaporation section involves triple-effect distillation and double-effect distillation whose products are 30% and 48% alkali liquid respectively. The triple-effect distillation yields 80 m³/h steam condensate. Some condensate is sent to the cooling water system, which cause additional cooling load. Others are used in dissolving salt and washing the evaporator. Moreover, this section needs 10 m³/h pump cooling water. The double-effect distillation produces 25 m³/h steam condensate. 16 m³/h of the condensate is utilized as boiler feed water, while 9 m³/h of the condensate is sent to salt dissolving. In summary, the evaporation section produces 105 m³/h condensates. The condensates are used in salt dissolving, boiler feed, washing and cooling system. The reuse in dissolving and boiler feed recovers both the energy and water quality well. But the condensate used in cooling system is on the contrary. Therefore, they should be reused in other units.

Solid caustic soda

This section discharges 6 m³/h steam condensate.

2.2.2 Plant 2

Hydrochloride and high purity hydrochloride section

The HCl is absorbed by freshwater and the discharge water from the chlorinated paraffin section. The hydrochloride process welcomes water of weak acid. Also note that COD is the control contaminant. Thus, some acid wastewater might be reused here. On the other hand, the high purity hydrochloride process only consumes pure water.

Perchloroethylene section

This section consumes 140m³/h freshwater and discharges 135m³/h wastewater, where wastewater of 133 m³/h is cooling water discharge. This cooling water should be recycled in the cooling water system or reused in other units. The remaining freshwater are used in dissolving solid caustic soda (5m³/h) and washing (2m³/h).

Chlorinated paraffin section

The chlorinated paraffin section discharges

In this section, the flow rate of cooling water discharge is 48 m³/h. This discharge should be recycled. The freshwater is also used in tail gas absorption, and the discharge water has been reused in the hydrochloride process.

White carbon black section

The freshwater consumption of the white carbon black section is 27m³/h. The freshwater is mainly used in absorbing and cooling. Air absorber cooling consumes 5m³/h, while the consumption of tail gas absorber, acid gas absorber and discharge absorber are 6, 6, 10 m³/h respectively.
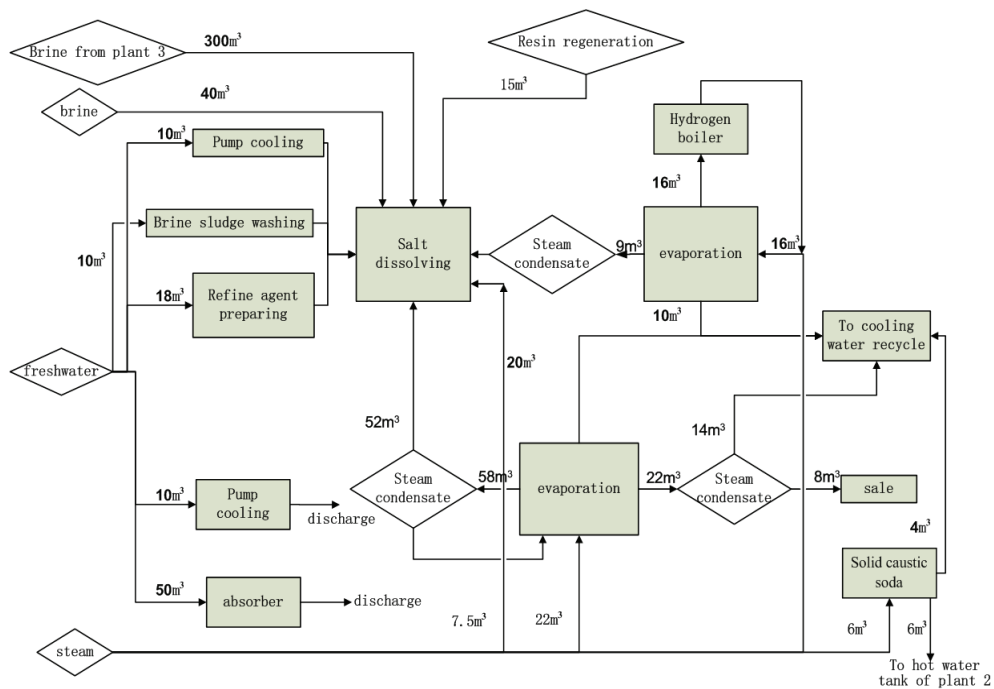
Fig. 2. Balanced water system of plant 1

Sodium hypochlorite section

This section has two streams of cooling water that are not recycled. They are the cooling water of the absorber and cooler whose flow rates are 16m³/h and 43m³/h respectively.

Chlorine drying section

The freshwater consumption is totally direct discharge cooling water. The discharged cooling water includes the tail gas column cooling, chlorine water cooling and the chlorine cooling.

Chlorine liquid section

Despite of direct discharging water, the freshwater are also used for bottle washing and hot water tank supplement.
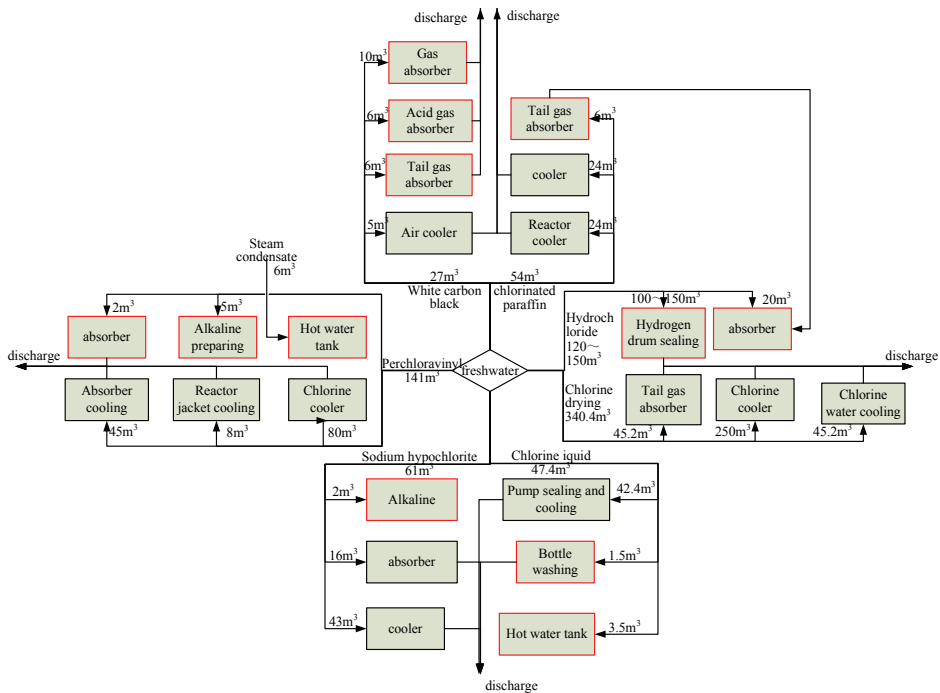
Fig. 3. Balanced water system of plant 2

2.2.3 Plant 3

Plant 3 only consumes pure water, and the pure water flow rate is 55 m³/h. The pure water is used in the electrolyzer feed and pump sealing. The discharge of pump sealing water could be reused in the resin regeneration. In addition, the batch process of filter washing and resin regeneration consume 360 m³ pure water per day, while the discharge is sent to dissolving salt.

2.2.4 Plant 5 utility plant

This plant is composed of the pure water production process and the cooling towers. The capacity of the cooling towers is 9000 m³/h, and the makeup freshwater is 145 m³/h and the discharge water is 72 m³/h. The pure water is produced from the freshwater, and the production rate is 80 m³/h. The cooling towers are divided into six separate systems. Current, only the cooling system for chlorine liquid has some spare capacity.

3. Evaluate and design of the water system

The whole water system of the complex is composed of the process water allocation system and the cooling water system. The interactions of these two systems are presented in figure 5. The freshwater are supplied to the process units. After mass transfer and reaction processes, wastewater is discharged. Since the quality of the cooling water is not degenerated during the

heat transfer process, most of them can be recycled. The recycling of the cooling water is mainly constrained by the capacity of the cooling tower. Therefore, we design the system in two steps: first determine the cooling water network, second the un-recycled cooling water are involved in the next design step of process water allocation system.
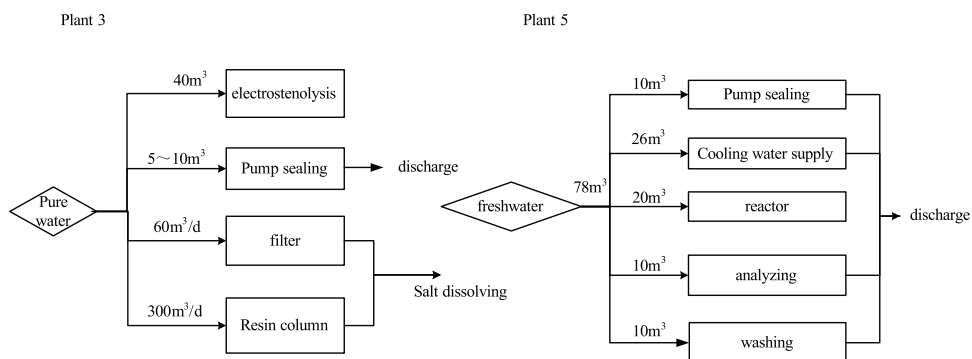
Plant 3   Plant 5

	40m³	electrostenolysis	10m³	Pump sealing
	5~10m³	Pump sealing → discharge	26m³	Cooling water supply
Pure water	60m³/d	filter	78m³	20m³ reactor → discharge
	300m³/d	Resin column	10m³	analyzing
		Salt dissolving	10m³	washing

freshwater

Fig. 4. Balanced water system of plant 3 and 5

Process water system → Steam condensate → Cooling water system
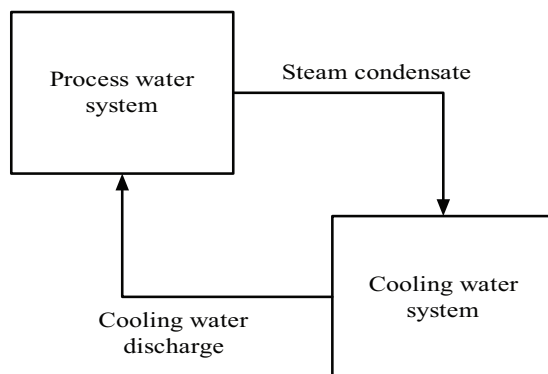
Cooling water discharge

Fig. 5. Schematic figure of the total water system

3.1 Retrofit of cooling water system

At present, 6 out of 8 cooling water recycle is overburdened at summer season, while the other 2 are not at their maximum capacity. Meanwhile, the cooling load should be enlarged because several direct discharge cooling water will be recycled. Moreover, additional cooling load of 450t/h is required for a new process. Consequently, the capacity of the current cooling system should be checked.

Table 2 illustrates the direct discharge cooling water that can be recycled. The cooling loads are mainly distributed in plant 2. From Table 2, only the items in bold are allowed using circulating cooling water, because process safety and other practical constraints.

Plant/process	Unit
Plant 1 Electrostenolysis section	Hydrogen washing
Plant 2 chlorine drying section	**Chlorine cooler**
Plant 2 chlorine drying section	Tail gas cooler
Plant 2 chlorine drying section	Chlorine water cooler
Plant 2 Perchloroethylene section	**Perchloroethylene cooler**
Plant 2 Sodium hypochlorite section	cooler
Plant 2 new chlorinated paraffin section	**cooler**

Table 2. List of direct discharge cooling water

Heat load(kkcal/h)	1450.18	126.983
Cooling water flow rate(t/h)	45.2	250
Cooling water initial temperature (°C)	28	28
Cooling water end temperature (°C)	60.08	28.51

Table 3. Parameters for the cooling of the chlorine drying process

Table 4 presents the parameters of the cooling water in the perchloravinyl section, the new chlorinated paraffin section and the chlorine water section. Table 5 and 6 show the current conditions for the cooling water system and the cooling tower of the chlorine liquid system. Since the cooling range of the cooling tower lies between 32°C and 42°C, the difference of these cooling streams should be adjusted. Table 7 illustrates the adjusted condition where the heat load is unchanged.

process	Perchloroethylene	Chlorine water cooling	Chlorinated paraffin
Inlet temperature (°C)	28	28	32
Outlet temperature (°C)	53	60	37
Heat load (KW)	3208.3	1687.5	2625
flow rate (m³/h)	110	45.2	450

Table 4. Cooling water temperature and its heat load

	York units	Water chilling units
Inlet temperature (°C)	32	32
Outlet temperature (°C)	42	34
flow rate (m³/h)	1072.5	450

Table 5. Condition of the circulating cooling water for the chlorine liquid process

item	value	Air volume flow rate(m³/h)	505000
		Air mass flow rate(kg/m²s)	3.07
Thermal property function	N=1.747×(λ0.4675)	Water flow rate(kg/h)	2.1×106
Filling type	Double taper thin film	water-spraying density (m³/m²h)	13.5
Filling shape	TX- II	Vapour/water ratio	0.82
Filling height (m)	1.5	Inlet temperature(°C)	42
Cross sectional area (m²)	51.84	Outlet temperature(°C)	32
wet-bulb temperature (°C)	28	Temperature difference(°C)	10

Table 6. Parameter for the cooling tower for chlorine liquid section

	Perchloroethylene	Chlorine water cooling	Chlorinated paraffin
Inlet temperature (°C)	32	32	32
Outlet temperature (°C)	42	42	37
flow rate (m³/h)	275	145	450

Table 7. Circulating cooling water conditions

If the cooling units are arranged in parallel mode as shown in figure 6, then the cooling outlet parameters are illustrated in table 8.

	at present	after retrofit
Outlet temperature	39.64°C	39.50°C
flow rate of circulating water	1522.5 m³/h	2392.5 m³/h
heat load of circulating water	13562kw	21087kw

Table 8. The cooling water outlet parameter under parallel condition

Combining the outlet condition in table 8 with the cooling tower parameters in table 6, one can obtain the performance of the cooling tower by running the cooling tower model[59]. The calculated result is shown in figure 6. From the figure, we can see that the outlet temperature of the cooling tower is higher than the required process cooling water inlet temperature. The heat load of cooling water system (21087KW) is larger than that of the cooling tower. Therefore, the cooling tower is overburdened. There is a bottleneck inside the system.

To eliminate the bottleneck, both the cooling tower and cooling water network should be modified. First, the cooling water inlet and outlet temperature of each process units are increased to their maximum value. This is because increasing the water inlet temperature will improve the heat load of the cooling tower. The limiting temperatures are presented in table 9.

	Perchloroethylene	Chlorine water cooling	Chlorinated paraffin
Inlet temperature (°C)	37	37	32
Outlet temperature (°C)	52	50	37
flow rate (m³/h)	183.3	111.5	450
	York units	Water chilling units	
Inlet temperature (°C)	32	32	
Outlet temperature (°C)	42	34	
flow rate (m³/h)	1072.5	450	

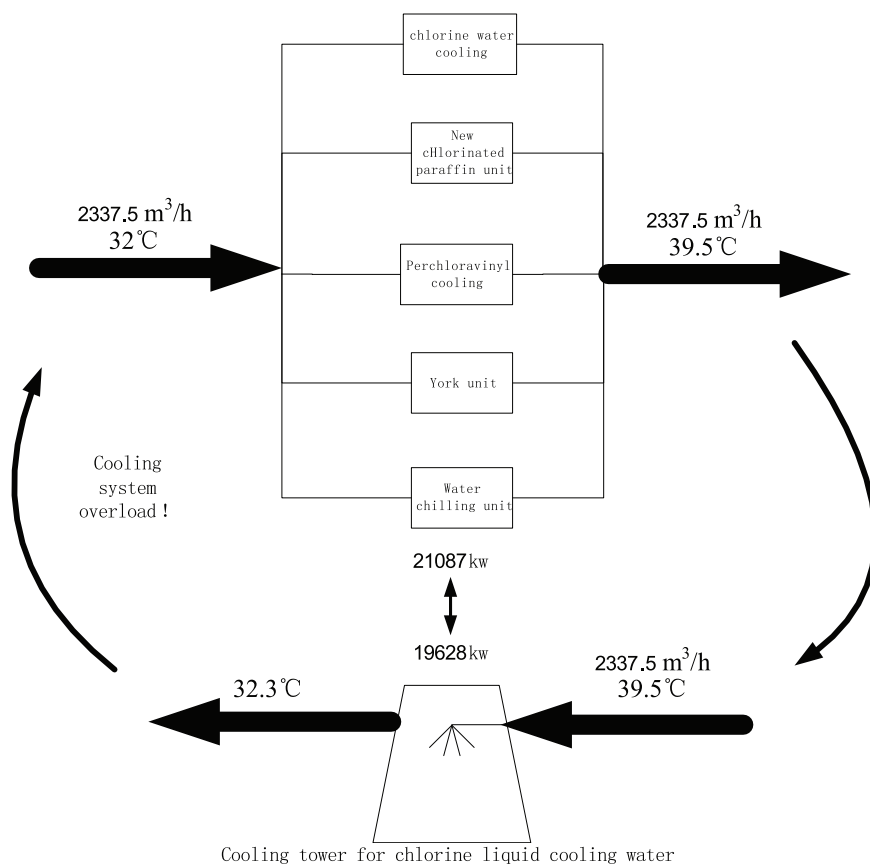Table 9. Cooling water operating parameter under limiting temperature condition

Fig. 6. The relationship between the cooling water network and cooling tower under the parallel condition

If the cooling water from one unit could be reused in another unit, then the total flow rate will be further decreased. The minimum cooling water flow rate can be determined by pinch analysis [59]. The "temperature vs enthalpy" diagram of the system is shown in figure 7. This composite curve is similar to the "contaminant vs mass load" diagram in water allocation networks, and the minimum cooling water flow rate is obtained as 1972.5m³/h.
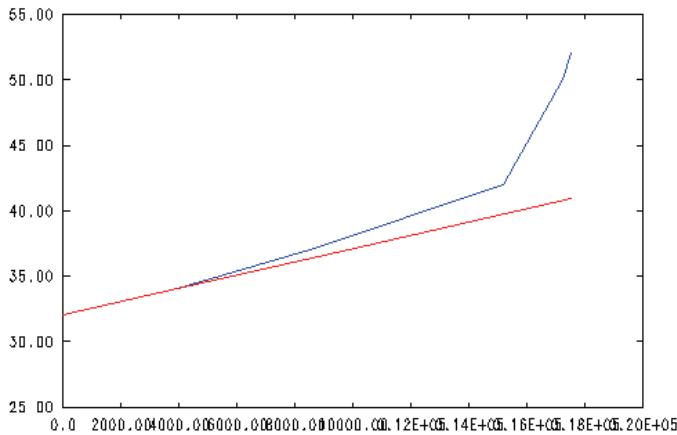

Fig. 7. Cooling water composite curve

To achieve the minimum cooling water consumption, sequential structures should be introduced to the cooling water network. On the other hand, the maximum cooling water flow rate is achieved by completely parallel structure. Both the maximum and minimum cooling water supply lines are presented in figure 8. Consequently, the region between these two lines is the feasible supply region, which is shown in shadow.
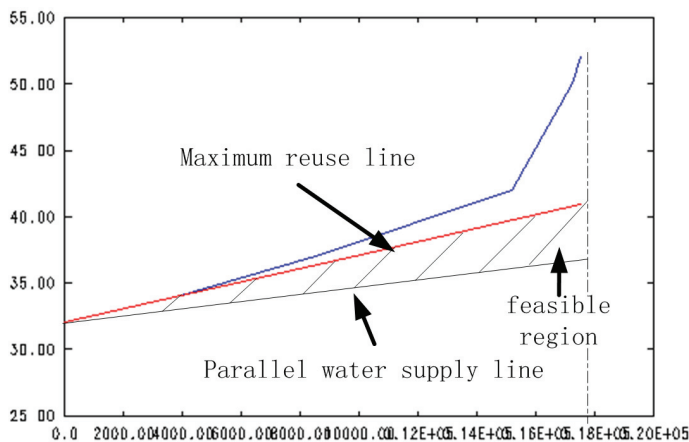

Fig. 8. The range of cooling water supply

It should be noted that all the supply lines inside the feasible region have the same heat load: 21087 kw. But the outlet temperatures and flow rate are different. This will lead to the

change of cooling tower heat load. In addition, the design of cooling water network must satisfy the following requirements: (1) the heat load of cooling water network matches the heat load of cooling tower; (2) the inlet temperature of cooling water network cannot exceed 32°C.
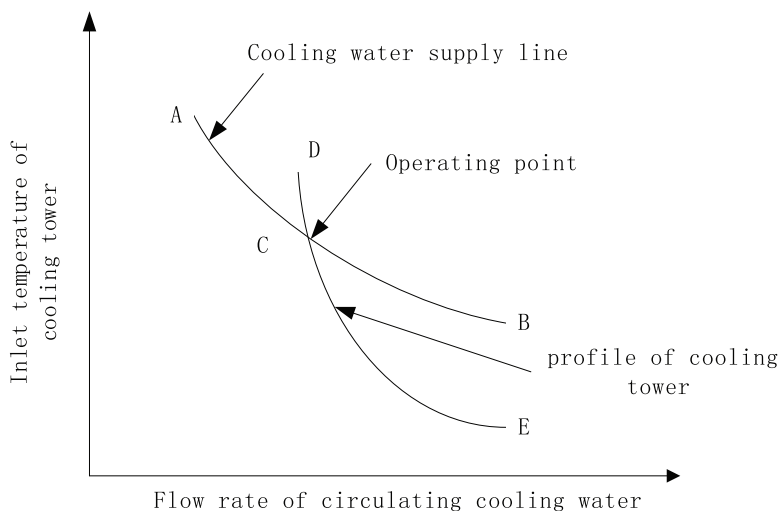

Fig. 9. Cooling tower profile and the cooling water supply line

To achieve the first requirement, we should find an operating point that satisfies both the network and the cooling tower. The operating point will be obtained via figure 9. In the figure, the vertical and horizontal axes are cooling tower inlet temperature and flow rate respectively. Under the same heat load, we can draw a cooling water supply line and a cooling tower working profile in this coordinate system. As shown in figure 9, the curve ACB is the cooling water supply line which represents the relationship between the outlet temperature of the cooling water network and the flow rate of cooling water. The curve DCE is the profile of cooling tower, which is obtained by cooling tower simulation under the fixed air flow rate (505000m³/h) and outlet temperature (32°C). At the intersection point C of the curve ACB and DCE, the outlet temperature of the cooling water network equals the inlet temperature of the cooling tower. Moreover, the flow rate and heat load of the two systems are also identical. Therefore, point C satisfies all the requirements, it is the operating point. In this case, the cross sectional point C is at temperature 41.146°C and flow rate 1972.5 m³/h which is the minimum cooling water flow rate.

The next step is to design the cooling water network under the determined temperature and flow rate. The network design procedure is similar to that of the process water network, and is not repeated here. Applying the design method, two final network structures are obtained as shown in figure 10 and 11.

The first solution shown in figure 10 includes the following reuse scheme: the outlet flow of water chilling units is sent to the chlorine water cooling and perchloroethylene cooling units. As shown in figure 11, the reuse source is shifted to the cooling water from new chlorinated paraffin unit in solution 2.
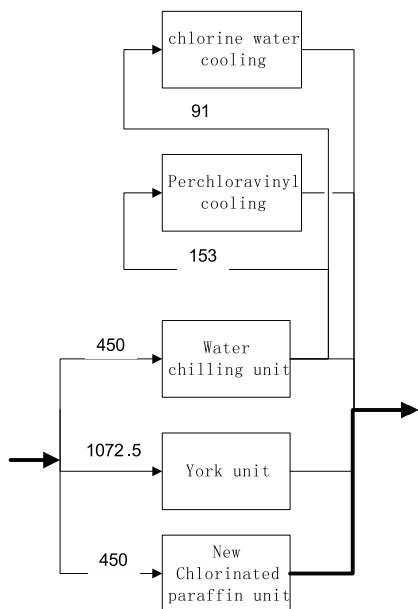
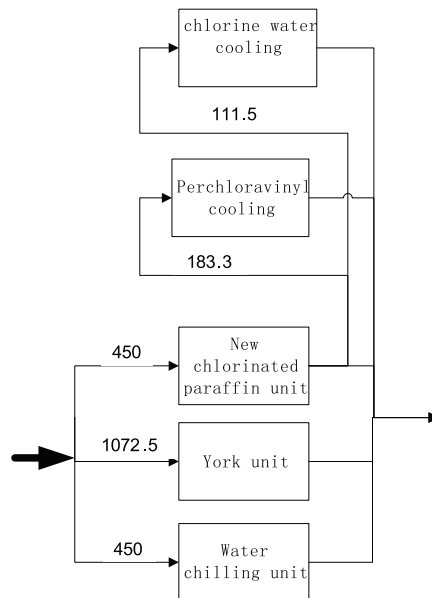Fig. 10. Cooling water system retrofit solution 1

Fig. 11. Cooling water system retrofit solution 2

3.2 Optimization of the process water allocation system

After determining the cooling water network system, it is term for optimizing the process water allocation network. The optimal design will be carried out via both pinch technology and mathematical methods. As this is a practical case, the procedure includes four steps: evaluate the existing system, determine water sources and sinks and the required flow rate, complement the limiting water using data, and finally the network design.

Step 1. evaluate the existing water system

The direct reuse choices within single units are considered in this step. Based on the introduction in the previous section, three choices are selected in this step:

In white carbon black section, the gas cooling water can be used to absorb the tail gas. This direct reuse of cooling water avoids the pumping cost of cooling water recycle system. 5 m3/h of freshwater can be saved, and it is no additional cost.

In the utility plant, the pump seal water can be reused as the supplement water for the cooling tower.

In the utility plant, the resin regeneration water can be reused for reverse washing.

Step 2. determine water sources and sinks and the required flow rate

The water using operations of the whole chlor-alkali complex are listed in table 10.

Step 3. complement limiting process data

In this step the contaminants and their limiting concentration will be provided via analysis, comparison and assumption.

For the whole complex, most of the processes are inorganic chemicals except the perchloravinyl and chlorinated paraffin section in plant 2. Normally, the wastewater from these inorganic sections does not have organic composition. Therefore, organic

Process	unit	limiting flow rate (m³/h)	Current source
Perchloravinyl	Alkali solution preparation	5	freshwater
	Hot water tank	6	freshwater
	Absorber	2	freshwater
Sodium hypochlorite	Alkali solution preparation	2	freshwater
Chlorine liquid	Bottle washing	1.5	freshwater
	Hot water tank	3.5	freshwater
hydrochloride	absorber	20	freshwater
chlorinated paraffin	Tail gas absorption	6	freshwater
White carbon black	absorber	10	freshwater
	Acid gas absorption	6	freshwater
	Tail gas absorption	6	freshwater
	Gas cooling	5	freshwater
electrostenolysis	Electrostenolysis tank	40	Pure water
	Resin regeneration	15	Pure water
	Pump sealing	7.5	Pure water
Bleaching powder	Pump sealing	10	freshwater
	Recycle supplement	20	freshwater
Utility	Cooling tower supply	26	freshwater
	washing	10	freshwater
Salt dissolving	brine sludge washing	10	freshwater
	Salt dissolving	15	Resin regeneration
	Pump cooling	10	freshwater
	Refining agent preparing	18	freshwater
Solid caustic soda	Steam condensate	6	
evaporation	Pump cooling	10	freshwater
	Steam condensate	14	

Table 10. Water using operations

process	operation	Flow rate	Current water source	Limiting inlet concentration (mg/l)	Limiting outlet concentration (mg/l)	range of PH value
perchloravinyl	Alkali solution preparation	5	freshwater	1000	3000	6~9
	Absorber	2	freshwater	600	3000	6~9
Sodium hypochlorite	Alkali solution preparation	2	freshwater	600	3000	6~9
chlorine liquid	Bottle washing	1.5	freshwater	600	3000	6~9
	Hot water tank	3.5	freshwater	450	3000	6~9
hydrochloride	absorber	20	freshwater	600	3000	<=7
chlorinated paraffin	Tail gas absorption	6	freshwater	600	3000	PH>=6
White carbon black	absorber	10	freshwater	450	600	PH>=6
	Acid gas absorption	6	freshwater	450	600	PH>=6
	Tail gas absorption	6	freshwater	450	600	PH>=6
	Gas cooling	5	freshwater	450	460	6~9
electrostenolysis	Electrostenolysis tank	40	Pure water	0	3000	7
	Resin regeneration	15	Pure water	0	1000	7
	Pump sealing	7.5	Pure water	0	50	6~9
Bleaching powder	Pump sealing	10	freshwater	450	600	6~9
	Recycle supplement	20	freshwater	1000	3000	6~9
	Cooling tower supply	26	freshwater	500	3000	6~9
	washing	10	freshwater			6~9
Salt dissolving	brine sludge washing	10	freshwater	450	3000	6~9
	Salt dissolving	15	Resin regeneration	100	3000	6~9
	Pump cooling	10	freshwater	450	460	6~9
	refining agent preparing	18	freshwater	100	3000	6~9
Evaporation	Pump cooling	10	freshwater	450	460	6~9
	Steam condensate	14		0	1	7

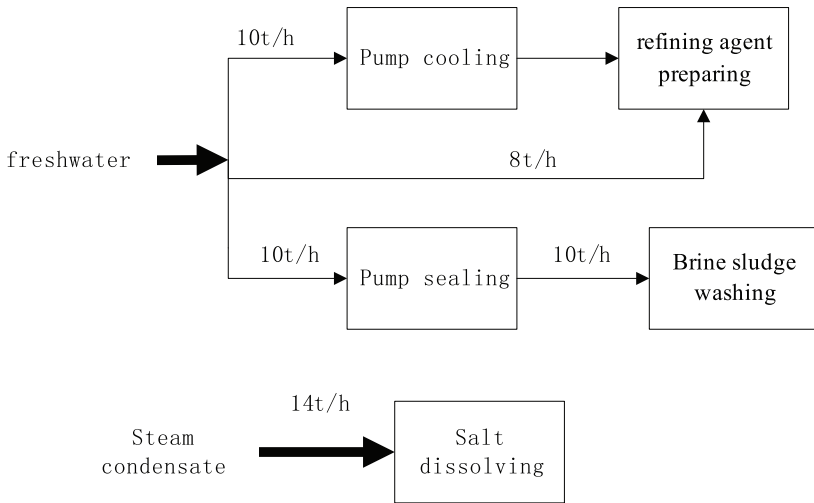Table 11. Limiting water operating data
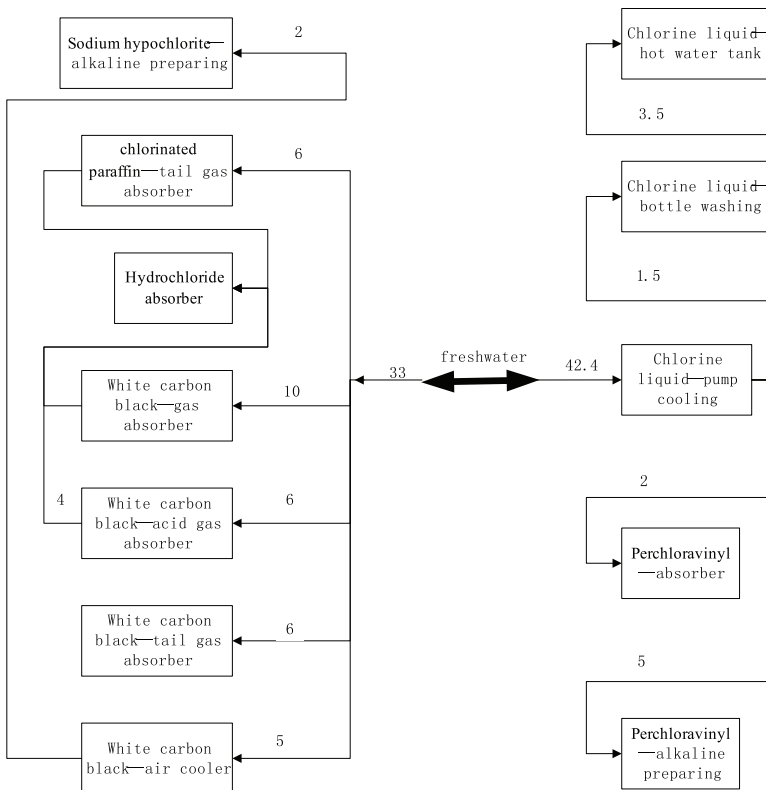
Fig. 12. Water reuse schemes in plant 1

Fig. 13. Water reuse scheme in plant 2

contaminants can be excluded. Analyzing the quality control items, the water using operations are sensitive to the PH value and the concentration of Ca^{2+} and Mg^{2+} (total hardness). For example, the water used in hydrochloride absorption cannot be alkaline, and the salt dissolving unit require low concentration of $Ca2+$ and $Mg2+$. On the other hand, the wastewater discharge of the operations mainly contains H^+, Ca^{2+} and Mg^{2+}. Consequently, total hardness is chosen as the chief contaminant that constraints water reuse. PH value is the assistant constraint. The limiting data is shown in table 11.

Step 4. network design

We analyze and optimize the existing system in two aspects: intra-plant integration and inter-plant integration. The design methodology is adopted from Liao et al.[60], and the detailed procedure is omitted here. Figures 12 to 14 represent the obtained intra- and inter-plant network structures. Note that no reuse happens in plant 3, because plant 3 only consumes pure water which cannot be replaced by freshwater.
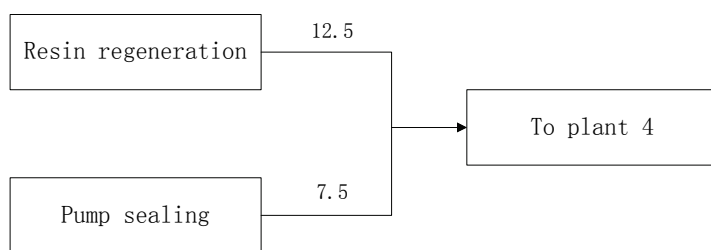

Fig. 14. Cross plant water reuse scheme

4. Conclusion

Due to the water shortage and environmental concerns, it is very important to improve the water using efficiency in traditional chemical industries. We take an chlor-alkali complex as example to show the applicability and effectiveness of the pinch based water integration technology. Based on the balanced system water consumption data, evaluation of the existing system has been established. The analysis and optimization of the whole system are carried out in cooling water system and process water system respectively.

For the cooling water system, the current cooling tower bottleneck has been relaxed by sequential arrangement of the coolers. For the process water allocation system, a number of 13 measures has been proposed (as shown in table 12) to save 88 t/h freshwater.

If the following freshwater and wastewater related cost are adopted:

Freshwater cost:	0.4 RMB/t
Pure water cost:	10.00 RMB/t
Circulating cooling water cost:	0.5 RMB/t
Water pumping cost:	0.06 RMB/t
Wastewater discharge cost:	1.20 RMB/t

Then the profit obtained from water saving can be calculated as follows:

1. Circulating cooling water system. The heat load of the cooling tower for chlorine liquid section has been enlarged by sequential arrangement of the cooling system. This enlargement breaks down the cooling water bottleneck of the system. Therefore, 208 t/h of the original direct discharge cooling water is now recycled.

Water saving profit:

$$208 \times (1.2 + 0.06 + 0.4 - 0.5) \times 8000 = 1930(\text{kRMB/Y})$$

2. Process water allocation system. The proposed 12 projects save freshwater in the amount of 88t/h. Water saving profit:

$$88 \times (1.2 + 0.06 + 0.4) \times 8000 = 1169(\text{kRMB/Y})$$

In conclusion, the total saving is 3,099 kRMB per year.

Process (section)	Water flow rate(t/h)	measures	Water saving amount(t/h)
pump cooling(salt dissolving)	10	sent to refining agent preparing	10
pump cooling(evaporation)	10	sent to brine sludge washing	10
Steam condensate (evaporation)	14	sent to salt dissolving	14
absorber(white carbon black)	10	sent to hydrochloride absorber	10
Acid gas absorber(white carbon black)	6	sent to hydrochloride absorber	4
Gas cooling (white carbon black)	5	sent to sodium hypochlorite section	2
pump cooling (chlorine liquid)	42.4	sent to bottle washing	1.5
		sent to hot water tank	3.5
		sent to the absorber in perchloravinyl section	2
		sent to the alkali solution preparation in perchloravinyl section	5
Resin regeneration(electrostenolysis)	15	sent to the bleaching powder section	12.5
Pump sealing(electrostenolysis)	7.5	sent to the bleaching powder section	7.5
Steam condensate (Solid caustic soda)	6	Sent to the hot water tank in the perchloravinyl section	6
total			88

Table 12. List of the retrofit projects

5. References

[1] Bagajewicz, M. A review of recent design procedures for water networks in refineries and process plants *Computers & Chemical Engineering* 2000 24(9-10) 2093-2113

[2] Wang, Y.; Smith, R. Wastewater Minimization *Chemical Engineering Science* 1994 49(7) 981-1006

[3] El-Halwagi, M. M.; Manousiouthakis, V. Synthesis of mass exchange networks *AIChE Journal* 1989 35(8) 1233-1243

[4] Wang, Y.; Smith, R. Wastewater minimisation with flow rate constraints *Chemical Engineering Research & Design* 1995 73 889-904

[5] Dhole, V.; Ramchandani, N.; Tainsh, R.; Wasilewski, M. Make Your Process Water Pay for Itself *Chemical Engineering* 1996 (103) 100-103

[6] Hallale, N. A new graphical targeting method for water minimisation *Advances in Environmental Research* 2002 6(3) 377-390

[7] Manan, Z.; Tan, Y.; Foo, D. Targeting the minimum water flow rate using water cascade analysis technique *AIChE Journal* 2004 50(12) 3169-3183

[8] El-Halwagi, M.; Gabriel, F.; Harell, D. Rigorous graphical targeting for resource conservation via material recycle/reuse networks *Industrial & Engineering Chemistry Research* 2003 42(19) 4319-4328

[9] Prakash, R.; Shenoy, U. Targeting and design of water networks for fixed flowrate and fixed contaminant load operations *Chemical Engineering Science* 2005 60(1) 255-268

[10] Agrawal, V.; Shenoy, U. V. Unified conceptual approach to targeting and design of water and hydrogen networks *AIChE Journal* 2006 52(3) 1071-1082

[11] Bandyopadhyay, S. Source composite curve for waste reduction *Chemical Engineering Journal* 2006 125(2) 99-110

[12] Bandyopadhyay, S.; Ghanekar, M. D.; Pillai, H. K. Process water management *Industrial & Engineering Chemistry Research* 2006 45(15) 5287-5297

[13] Pillai, H. K.; Bandyopadhyay, S. A rigorous targeting algorithm for resource allocation networks *Chemical Engineering Science* 2007 62(22) 6212-6221

[14] Alwi, S. R. W.; Manan, Z. A. Targeting multiple water utilities using composite curves *Industrial & Engineering Chemistry Research* 2007 46(18) 5968-5976

[15] Foo, D. C. Y. Water Cascade Analysis for Single and Multiple Impure Fresh Water Feed *Chemical Engineering Research & Design* 2007 85(8) 1169-1177

[16] Shenoy, U. V.; Bandyopadhyay, S. Targeting for multiple resources *Industrial & Engineering Chemistry Research* 2007 46(11) 3698-3708

[17] Alwi, S. R. W.; Manan, Z. A. SHARPS: A new cost-screening technique to attain gost-effective minimum water network *AIChE Journal* 2006 52(11) 3981-3988

[18] Foo, D. C. Y. Flowrate targeting for threshold problems and plant-wide integration for water network synthesis *Journal of Environmental Management* 2008 88(2) 253-274

[19] Mann, J.; Liu, Y., *Industrial water reuse and wastewater minimization*. McGraw Hill: New York, 1999.

[20] Feng, X.; Bai, J.; Zheng, X. S. On the use of graphical method to determine the targets of single-contaminant regeneration recycling water systems *Chemical Engineering Science* 2007 62(8) 2127-2138

[21] Bai, J.; Feng, X.; Deng, C. Graphically based optimization of single-contaminant regeneration reuse water systems *Chemical Engineering Research & Design* 2007 85(A8) 1178-1187

[22] Deng, C.; Feng, X.; Bai, J. Graphically based analysis of water system with zero liquid discharge *Chemical Engineering Research & Design* 2008 86(A2) 165-171

[23] Bandyopadhyay, S.; Cormos, C. C. Water management in process industries incorporating regeneration and recycle through a single treatment unit *Industrial & Engineering Chemistry Research* 2008 47(4) 1111-1119

[24] Ng, D. K. S.; Foo, D. C. Y.; Tan, R. R.; Tan, Y. L. Ultimate flowrate targeting with regeneration placement *Chemical Engineering Research & Design* 2007 85(A9) 1253-1267

[25] Ng, D. K. S.; Foo, D. C. Y.; Tan, R. R.; Tan, Y. L. Extension of targeting procedure for "Ultimate Flowrate Targeting with Regeneration Placement" by Ng et al., Chem. Eng. Res. Des., 85 (A9): 1253-1267 *Chemical Engineering Research & Design* 2008 86(10) 1182-1186

[26] Kuo, W.; Smith, R. Effluent treatment system design *Chemical Engineering Science* 1997 52(23) 4273-4290

[27] Kuo, W.; Smith, R. Designing for the interactions between water-use and effluent treatment *Chemical Engineering Research & Design*1998 76(A3) 287-301

[28] Ng, D. K. S.; Foo, D. C. Y.; Tan, R. R. Targeting for total water network. 1. Waste stream identification *Industrial & Engineering Chemistry Research* 2007 46(26) 9107-9113

[29] Ng, D. K. S.; Foo, D. C. Y.; Tan, R. R. Targeting for total water network. 2. Waste treatment targeting and interactions with water system elements *Industrial & Engineering Chemistry Research* 2007 46(26) 9114-9125

[30] Olesen, S. G.; Polley, G. T. Dealing with plant geography and piping constraints in water network design *Process Safety and Environmental Protection* 1996 74(B4) 273-276

[31] Olesen, S. G.; Polley, G. T. A simple methodology for the design of water networks handling single contaminants *Chemical Engineering Research & Design* 1997 75(A4) 420-426

[32] Castro, P.; Matos, H.; Fernandes, M.; Nunes, C. Improvements for mass-exchange networks design *Chemical Engineering Science* 1999 54(11) 1649-1665

[33] Ma, H.; Feng, X.; Cao, K. A rule-based design methodology for water networks with internal water mains *Chemical Engineering Research & Design* 2007 85(A4) 431-444

[34] Gomes, J. F. S.; Queiroz, E. M.; Pessoa, F. L. P. Design procedure for water/wastewater minimization: single contaminant *Journal of Cleaner Production* 2007 15(5) 474-485

[35] Savelski, M.; Bagajewicz, M. On the optimality conditions of water utilization systems in process plants with single contaminants *Chemical Engineering Science* 2000 55(21) 5035-5048

[36] El-Halwagi, M. M., *Pollution Prevention Through Process Integration:Systematic Design Tools*. Academic Press: San Diego, 1997.

[37] Prakash, R.; Shenoy, U. V. Design and evolution of water networks by source shifts *Chemical Engineering Science* 2005 60(7) 2089-2093

[38] Ng, D. K. S.; Foo, D. C. Y. Evolution of water network using improved source shift algorithm and water path analysis *Industrial & Engineering Chemistry Research* 2006 45(24) 8095-8104

[39] Alwi, S. R. W.; Manan, Z. A. Generic graphical technique for simultaneous targeting and design of water networks *Industrial & Engineering Chemistry Research* 2008 47(8) 2762-2777

[40] Alwi, S. R. W.; Manan, Z. A.; Samingin, M. H.; Misran, N. A holistic framework for design of cost-effective minimum water utilization network *Journal of Environmental Management* 2008 88(2) 219-252

[41] Tan, Y. L.; Manan, Z. A. Retrofit of water network with optimization of existing regeneration units *Industrial & Engineering Chemistry Research* 2006 45(22) 7592-7602

[42] Tan, Y. L.; Manan, Z. A. A new systematic technique for retrofit of water network *International Journal of Environment and Pollution* 2008 32(4) 519-526

[43] Tan, Y. L.; Manan, Z. A.; Foo, D. C. Y. Retrofit of water network with regeneration using water pinch analysis *Process Safety and Environmental Protection* 2007 85(B4) 305-317

[45] Alva-Argaez, A.; Kokossis, A. C.; Smith, R. The design of water-using systems in petroleum refining using a water-pinch decomposition *Chemical Engineering Journal* 2007 128(1) 33-46

[46] Koppol, A. R.; Bagajewicz, M. J.; Dericks, B. J.; Savelski, M. J. On zero water discharge solutions in the process industry *Advances in Environmental Research* 2004 8(2) 151-171

[47] Zbontar, L.; Glavic, P. Total site: wastewater minimization - Wastewater reuse and regeneration reuse *Resources Conservation and Recycling* 2000 30(4) 261-275

[48] Takama, N.; Kuriyama, T.; Shiroko, K.; Umeda, T. Optimal water allocation in a petroleum refinery *Computers & Chemical Engineering* 1980 4 251-258

[49] Yang, Y. H.; Lou, H. H.; Huang, Y. L. Synthesis of an optimal wastewater reuse network *Waste Management* 2000 20(4) 311-319

[50] Jacob, J.; Kaipe, H.; Couderc, F.; Paris, J. Water network analysis in pulp and paper processes by pinch and linear programming techniques *Chemical Engineering Communications* 2002 189(2) 184-206

[51] Dilek, F. B.; Yetis, U.; Gokcay, C. F. Water savings and sludge minimization in a beet-sugar factory through re-design of the wastewater treatment facility *Journal of Cleaner Production* 2003 11(3) 327-331

[52] Majozi, T.; Brouckaert, C. J.; Buckley, C. A. A graphical technique for wastewater minimisation in batch processes *Journal of Environmental Management* 2006 78(4) 317-329

[53] Ujang, Z.; Wong, C. L.; Manan, Z. A. Industrial wastewater minimization using water pinch analysis: a case study on an old textile plant *Water Science and Technology* 2002 46(11-12) 77-84

[54] Zhou, Q.; Lou, H. H.; Huang, Y. L. Design of a switchable water allocation network based on process dynamics *Industrial & Engineering Chemistry Research* 2001 40(22) 4866-4873

[55] Forstmeier, M.; Goers, B.; Wozny, G. Water network optimisation in the process industry - case study of a liquid detergent plant *Journal of Cleaner Production* 2005 13(5) 495-498

[56] Noureldin, M. B.; El-Halwagi, M. M. Interval-based targeting for pollution prevention via mass integration *Computers & Chemical Engineering* 1999 23(10) 1527-1543

[57] Feng, X.; Wang, N.; Chen, E. Water system integration in a catalyst plant *Chemical Engineering Research & Design* 2006 84(A8) 645-651

[58] Tian, J. R.; Zhou, P. J.; Lv, B. A process integration approach to industrial water conservation: A case study for a Chinese steel plant *Journal of Environmental Management* 2008 86(4) 682-687

[59] Jin-Kuk Kim, Robin Smith. Cooling water system design. Chemical Engineering Science, 2001,56: 3641–3658

[60] Z. W. Liao, J. T. Wu, B. B. Jiang, J. D. Wang, and Y. R. Yang, Design Methodology for Flexible Multiple Plant Water Networks, Ind. Eng. Chem. Res. 2007, 46, 4954-4963

Using Seawater to Remove SO$_2$ in a FGD System

Jia-Twu Lee and Ming-Chu Chen
Department of Environmental Engineering and Science
National Pingtung University of Science and Technology
Taiwan

1.Introduction

1.1 Introduction

Sea water contains significant amounts of HCO$_3$- and other alkaline compounds that help sulfur dioxide in flue gas dissolve in water. Flue gas desulphurization (FGD) achieves the goals of this system, for sea-water FGD systems. This study conducts a series of simulations or experiments using sea-water at a flue gas combustion plant to identify the advantages and disadvantages of, and related parameters for designing and operating FGD in the future.

1.2 Research objectives

1. Flue gas from a combustion plant is used in a series of experiments. The pre-water method has both advantages and disadvantages associated with relevant parameters.
2. To estimate the amount of tail water and solve the problem of disposing of large amounts of tail-water. To further tail water recycling research and development, one must simultaneously achieve the dual objectives of FGD and the creation of water resources.

2. Literature review

2.1 Flue gas desulfurization processes

Flue Gas Desulphurization is divided into wet, dry, and semi-dry methods (2). The wet method is the most efficient and most commonly used method. The wet method uses absorbent desulfurization processes that differ from other processes, which typically use lime, limestone, magnesium hydroxide, sodium carbonate, water, and double-base.

2.1.1 The seawater method uses sea-water that contains some Trona and SO$^-_2$ flue gas

The alkalinity of seawater is primarily influenced by calcium, magnesium, carbonate, and other related compounds. The pH of sea-water was 7.5 and 8.5. It can be neutralized with SO$_2$ during a reaction.

During seawater desulfurization, water is the primary absorber. Adding a small amount of NaOH or Mg (OH)$_2$ increases the effect, or alters the process than the final pH of sulfur water. The activity of pure water is as follows.

a.   Absorption reaction

Flue gas of SO_2 and water vapor from liquid dissolves into sulfite and hydrogen ions, resulting in fluid absorption at a pH of roughly 3.
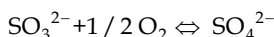
$$SO_2(g) \Leftrightarrow SO_2(L) \tag{1}$$

$$SO_2 + H_2O \Leftrightarrow HSO_3^- + H^+ \tag{2}$$

$$HSO_3^- \Leftrightarrow SO_3^{2-} + H^+ \tag{3}$$

b.   Neutralization reaction

 Bicarbonate ions in seawater and hydrogen ions in the carbon dioxide and water reaction, increase the pH of.

$$HCO_3^- + H^+ \Leftrightarrow CO_2 + H_2O$$

c.   Oxidation

$$SO_3^{2-} + 1/2\,O_2 \Leftrightarrow SO_4^{2-}$$
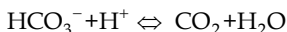
Although the oxidation reaction at low pH values (roughly $\leqq 4.5$) of the low efficiency of water requirement, yet the pH can increase to roughly 5.6. Additionally, aeration functions can eliminate CO_2 from the water, thereby increasing pH during the neutralization reaction.

d.   Total reaction

$$SO_2 + H_2O + 1/2O_2 \rightarrow SO_4^{2-} + 2H^+$$

$$HCO^{3-} + H^+ \rightarrow CO_2 + H_2O$$
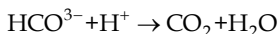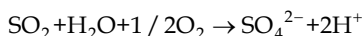
The seawater treatment process resembles the conventional wet process in that water and smoke are in contact in the reverse direction. The kinds of the process are filled with different types, such as the spray-type and layer different types of absorber plate. As water absorbs SO_2 after the acidic ($pH \rightleftharpoons 3$), adding large amounts of water before increasing the pH facilitates the following aeration reaction: SO_3^{2-} is oxidized to SO_4^{2-}, and discharge the dissolution of $CO_2.$

3. Seawater desulphurization process assessment

3.1 Business transfer performance

In the 1970s, the University of California at Berkeley first used seawater to remove SO_2 from flue gas . In 1978, Fujikasui, a Japanese researcher, used seawater to in an FGD system at a chemical plant . In 1988, ABB, a company, used seawater in an FGD system at an oil refinery in Norway(4).

3.2 System evaluation

Packing and orifice-plate systems in a field simulation test verified that pure seawater can remove up to 90% of SO_2 flue gas from combustion-fired units. The two sulfur tower designs have different advantages and disadvantages. For example, a packing system requires an absorber tower with a large volume.

Although the packing system clogs easily happen, the amount of seawater needed is reduced, resulting in energy savings; conversely, the orifice uses an absorber tower with a smaller volume and does not clog easily, however, this requires more seawater (4).

4. Experimental method: The seawater FGD process

4.1 The selection of a seawater FGD system simulation
According to the assessment of in Section 3.2, the processes that use different water desulfurization have both advantages and disadvantages. In this study, the selection of a seawater FGD orifice plate depends on the following factors.

Although the FGD system electrostatic precipitators (ESP), a small amount of fly ash flows into the desulfurization tower, such that the desulfurization tower can clog after long-term operation.

4.2 The orifice-plate type seawater FGD simulation system
The primary component of the system is a desulfurization tower tank, which is divided into a demisting zone, an SO$_2$ absorption zone (spray zone), and water oxidation zone. Water from a pump in the water tank tower into the desulfurization tower at the top of the absorption zone, and flue gas driven by a fan enters the bottom of the desulphurization tower tank. Gas from the bottom up, seawater from the top down, Seawater and gas in the orifice of the perforated plate then contact and SO$_2$ is absorbed by the seawater, such that the treated flue gas is emitted from the top side of the demister zone.

4.3 Desulfurization tests results
The concentration of flue gas SO$_2$ is controlled at 50-250ppm, The tested seawater is seawater from the first condenser. Figure 1 shows the simulation device. Figure 2 shows the absorption area in the orifice-plate. During the test, the flue gas flow rate is 1-3 m^3 / min: the water flow rate is 10-40 ft^3 / min; and the gas-to-liquid G/L ratio is controlled at 5 and 20.
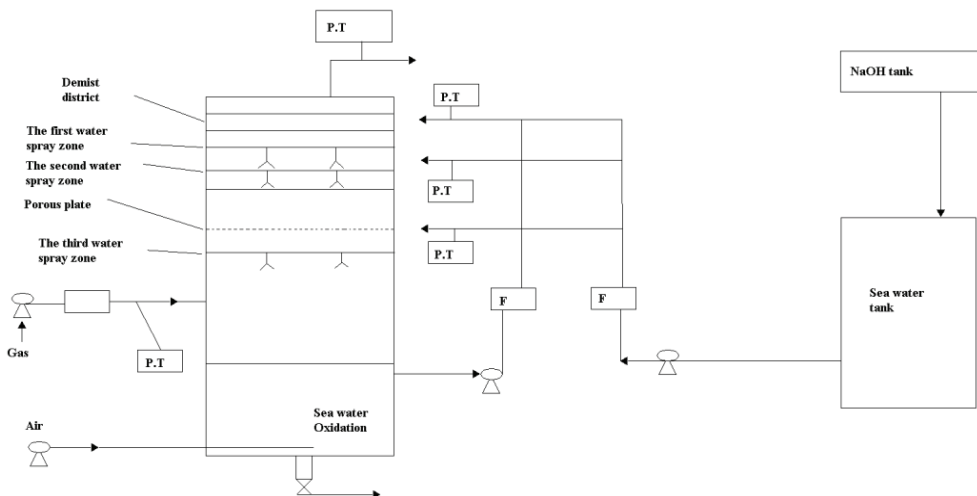

Fig. 1. The orifice-plate style seawater flue gas desulphurization simulation system
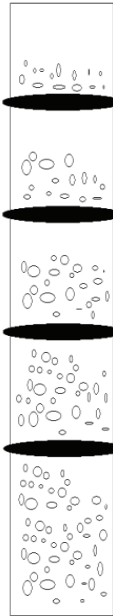
Fig. 2. The situation of gas-liquid mixture in the simulation test of desulfurization tower

4.3.1 Batch seawater desulphurization results

To reduce the amount of seawater used (and reduce pumping energy and the amount of waste-water), some seawater can be reused. The design cycle typically depends on the change in seawater pH and desulphurization efficiency. Via the seawater desulfurization circulation test (a batch test was adopted, and no seawater was discharged), one can identify the relationship between changes in seawater pH and desulphurization efficiency. Figure 4 and 5 list experimental results from two desulfurization tests (G/L ratio = 10-20). Experimental results show that desulfurization efficiency and the pH of exiting seawater decreased as reaction time increased. Experimental results also show that the amount of alkaline compounds in seawater decreased as reaction time increased. The alkalinity of the exiting sea-water convert to Fig. 3. Desulfurization efficiency and water pH are positively correlated. This experimental result indicates that a high residual water pH and large amounts of alkaline compounds lead to higher desulfurization efficiency. The exiting seawater can keep desulfurization efficiency at ≥ 90% under a seawater pH ≥ 6.0(Fig. 3).

4.3.2 Test results of continuous seawater desulphurization

When the system is operated continuously, the reflux ratio (reflux ratio R = (water flow recovery / raw water flow) can explain returning water usage. Figure 6 and 7 show the control loop volume from test results. Experimental results show that as the reflux ratio increased, the pH of exiting seawater decreased, and the amount of alkaline compounds in seawater decreased during the reaction. Adding a relatively smaller amount of fresh seawater reduced desulfurization efficiency; thus, the reflux ratio should not be > during operation. When the reflux ratio was controlled at ≦ 1 (inclusive) (Figure 6 and 7), the pH of

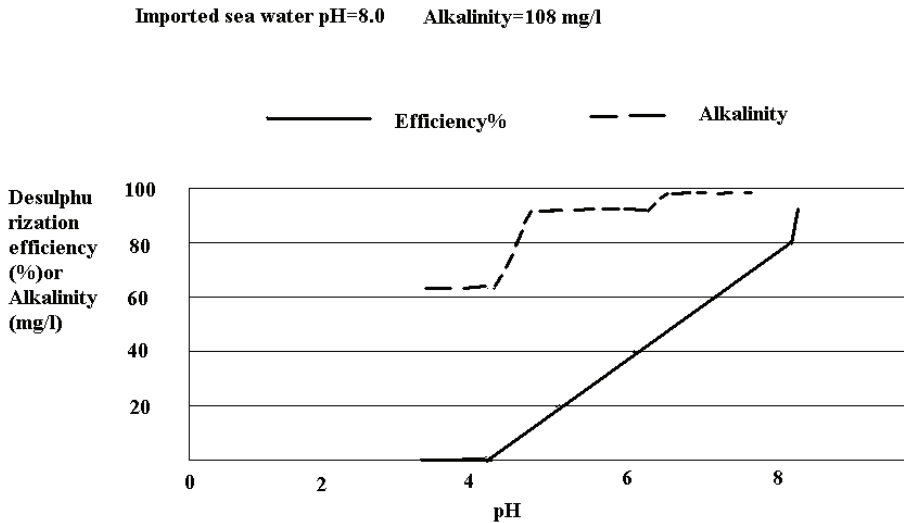Imported sea water pH=8.0   Alkalinity=108 mg/l

Fig. 3. The pH and alkalinity of exit seawater and desulphurization efficiency diagram
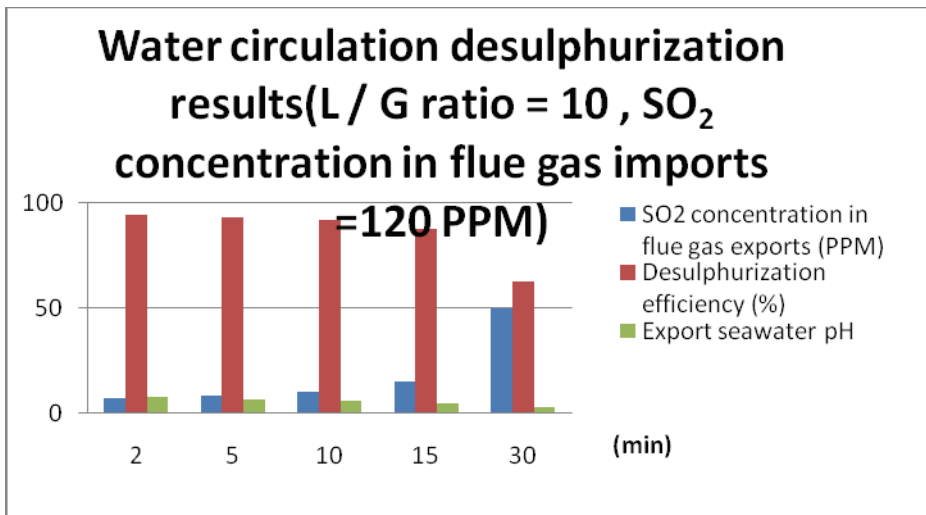

Fig. 4. The seawater circulation desulphurization test results

exiting seawater was kept at > 6.0, resulting in a desulphurization efficiency of ≥ 90%. However, the reflux ratio should be < to reduce seawater usage (which can reduce pump energy and the amount of wastewater used). In summary, the orifice-plate seawater FGD system is an effective system.
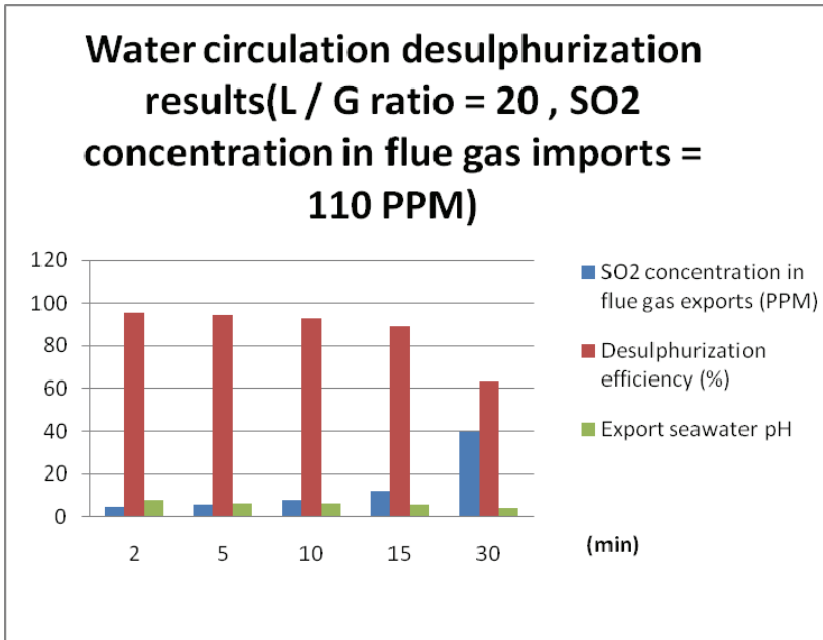
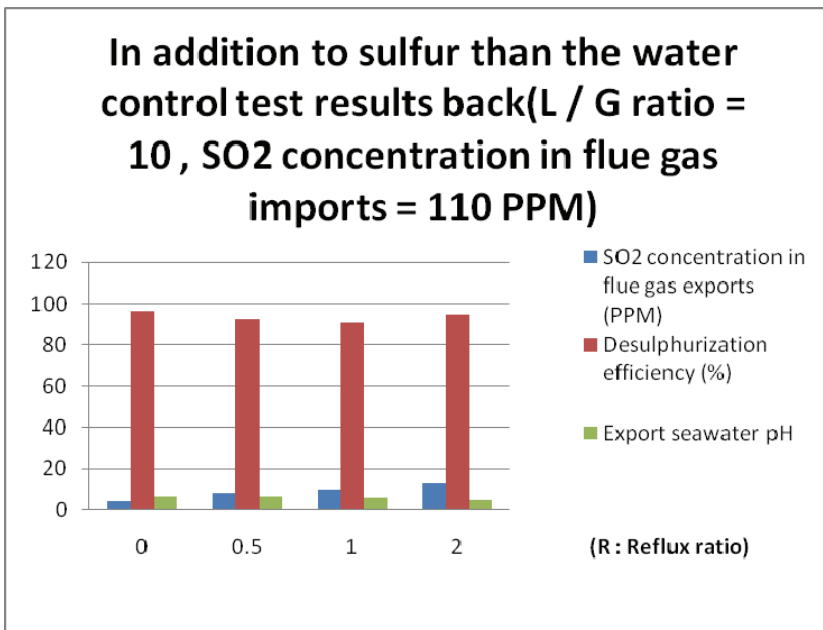Fig. 5. The seawater circulation desulphurization test results

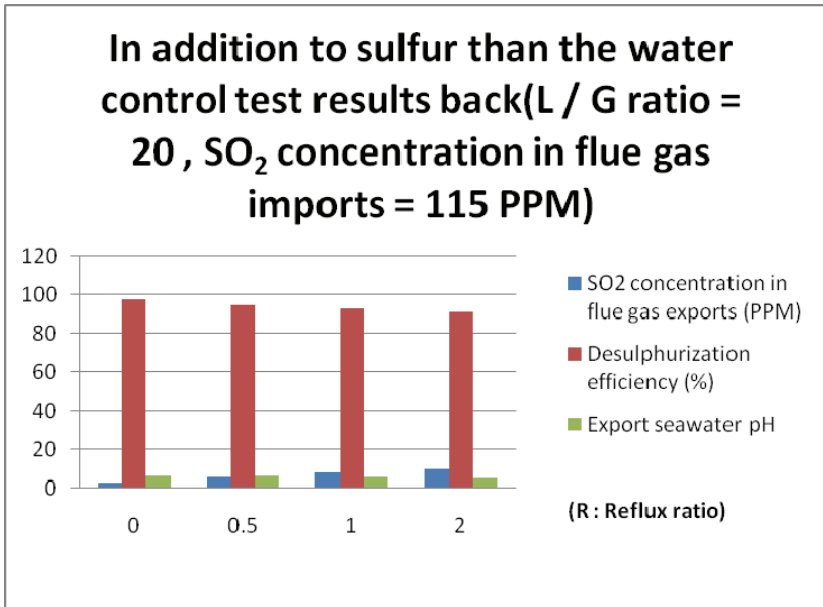Fig. 6. The results of controlling seawater reflux ratio desulfurization test

Fig. 7. The results of controlling seawater reflux ratio desulfurization test

4.3.3 Tubular seawater desulphurization results

In the tubular (one-through) seawater desulphurization process, original seawater passes directly through the desulfurization tower instead of being recycled. As the tubular process is used for fresh seawater desulphurization, all alkaline compounds in seawater are in the highest state; thus, a good desulfurization result is expected. Table 1 shows simulation test results. Experimental results confirm that the tubular (one-through) seawater desulphurization process yields excellent desulphurization results. With a G/L ratio > 13, the desulphurization rate exceeded 99%. General designs of often recycle seawater, have G/L ratios of 20 and desulphurization efficiency > 90%.

The entrance flue gas SO2 PPM concentration	L / G ratio	The exit flue gas SO2 PPM concentration	Desulphurization efficiency %	The pH of exit seawater
150	10	5	96.6	6.5
150	13	1	99	6.4
150	17	< 1	> 99	6.5
150	20	< 1	> 99	6.4

Table 1. The seawater desulphurization tubular (one-through) test results listed as follows

4.3.4 Evaluation and selection of a seawater desulphurization system

The best seawater desulphurization process is orifice-plate type. According to test results, desulfurization rate of the orifice-plate-type easily reached as high as 99%. However, the

tubular (one-through) system has a higher desulfurization efficiency, is easier to design, and has a lower installation cost than other designs. The G/L ratio depends on desulphurization efficiency. When the G/L ratio was 10, was 95%; conversely, when the G/L ratio was 15, desulphurization efficiency exceeded 99%.

5. Conclusions

1. The orifice-plate type simulated seawater desulphurization equipment, toward a coal-fired (EP) unit exit flue gas, proceeding the field simulation tests for seawater desulphurization. The G/L ratio, desulfurization seawater reflux ratio, number of porous plate boards, area of the perforated plate, the porous plate before and after changes in gas pressure, and the influence of changes in the height of the gas-liquid mixing layer are discussed. After appropriate adjustments, the design achieved a desulphurization efficiency of 99%. This experimental result can be used as the basis for designing and seawater desulphurization systems in power plants.
2. According to test results, the orifice-plate desulphurization system clogs less, has a better desulfurization efficiency, and requires a smaller desulfurization tower than the filling. Based on its economic advantages and limited plant area, the orifice-type is the best seawater desulphurization process for combustion power plants.

6. Acknowledgements

7. References

[1] Intellectual Resources, "FGD Water Recycling Feasibility Study", Taiwan Power Company report, Republic of China on December 92.
[2] Hermine N Sound, Mitsuru Takeshita "FGD Handbook",IEA Coal Research,1994 .2. Hermine N Sound, Mitsuru Takeshita "FGD Handbook", IEA Coal Research, 1994
[3] Xu gold, "Power Plant Flue Gas Desulfurization Project Description", Engineering, 2000.
[4] Katsuo Olikawa, Chaturong yongsiri, Kazuo Takeda Tayoshi Harimoto, "Seawater Flue Gas Desulfurization: It's Technical Implications and Performance Results", Environmental Progress, Vol. 22, No. 1, April 2003.